JOURNAL AerospaceLab

ONERA
THE FRENCH AEROSPACE LAB

Issue 14
September 2018

DOI: 10.12762/2018.AL14

Aeroelasticity and Structural Dynamics

Produced by
ONERA - BP 80100
Chemin de la Hunière
et des Joncherettes
91123 PALAISEAU CEDEX
France
www.onera.fr

ISSN: 2107-6596

Aeroelasticity and Structural Dynamics

Cédric LIAUZUN
(ONERA)
Senior Scientist

Nicolas PIET-LAHANIER
(ONERA)
Senior Scientist

DOI: 10.12762/2018.AL14-00

The fourteenth issue of AerospaceLab Journal is dedicated to aeroelasticity and structural dynamics. Aeroelasticity can be briefly defined as the study of the low frequency dynamic behavior of a structure (aircraft, turbomachine, helicopter rotor, etc.) in an aerodynamic flow. It focuses on the interactions between, on the one hand, the static or vibrational deformations of the structure and, on the other hand, the modifications or fluctuations of the aerodynamic flow field.

Aeroelastic phenomena have a strong influence on stability and therefore on the integrity of aeronautical structures, as well as on their performance and durability. In the current context, in which a reduction of the footprint of aeronautics on the environment is sought, in particular by reducing the mass and fuel consumption of aircraft, aeroelasticity problems must be taken into account as early as possible in the design of such structures, whether they are conventional or innovative concepts. It is therefore necessary to develop increasingly efficient and accurate numerical and experimental methods and tools, allowing additional complex physical phenomena to be taken into account. On the other hand, the development of larger and lighter aeronautical structures entails the need to determine the dynamic characteristics of such highly flexible structures, taking into account their possibly non-linear behavior (large displacements, for example), and optimizing them by, for example, taking advantage of the particular properties of new materials (in particular, composite materials).

This issue of AerospaceLab Journal presents the current situation regarding numerical calculation and simulation methods specific to aeroelasticity and structural dynamics for several applications: fan damping computation and flutter prediction, static and dynamic aeroelasticity of aircraft and gust response. Moreover, articles present results on smart morphing structures for airplanes. Other papers present the latest progress in terms of structure design and critical load assessment. Finally, articles present recent results relating to structural damping modelling and the non-linear behavior of structural assemblies, to the development of structure optimization algorithms taking into account uncertainties, to the development of vibration control devices and to the crashworthiness of aeronautical composite structures.

Structural dynamics is a wide scientific domain covering a very large range of applications such as structure vibrations, crash and impact, structure damping, vibroacoustics and so on. Aeroelasticity is strongly linked to the subdomain of the structural dynamics dedicated to the low frequencies. It can be briefly defined as the study of the dynamic behavior of a structure (aircraft, turbomachine, helicopter rotor, etc.) in an aerodynamic flow, or, according to the author of the famous aeroelastic triangle [3] (Figure 1), as "*the study of the mutual interaction that takes place within the triangle of the inertial, elastic and aerodynamic forces acting on structural members exposed to an airstream, and the influence of this study on design*" (A. R. Collar, 1947). Though Dutch windmill manufacturers empirically solved blade aeroelastic problems four centuries ago by moving the front spar from the mid-chord to the quarter-chord position [5], aeroelasticity is a rather recent discipline that arose with the first flight attempts (e.g. the second attempt of S. Langley in 1903 failed probably due to a static torsional divergence instability) [5]. After the success of the Wright flight, it was mainly biplanes that were developed in order to ensure a high torsional stiffness of the wings, but some aircraft as the Handley Page 0/400 bomber and the DH-9 still experienced tail flutter instabilities. One of the earliest documented cases mentioning failure resulting from the static interaction between the air flow and the wing deformation is that of the monoplane Fokker D-8, developed for its superior performance compared to biplanes during World War 1.

The aeroelasticity scientific domain has grown up alongside the aviation boom, especially during and after World War 2, with the increasing flight speed of the aircraft. It now concerns all aeronautical applications (aircraft, turbomachines, helicopters, launchers, missiles) as well as others such as wind turbines, bridges and buildings [4].

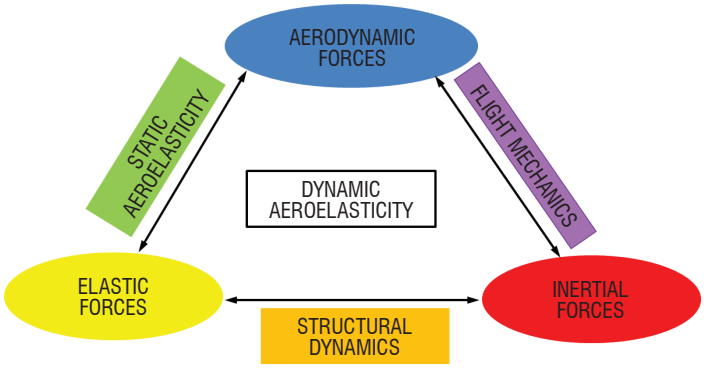

Figure 1 – Collar's representation of forces occurring in aeroelastic phenomena

Aeroelasticity used to be taken into account at a late stage of an airplane design, to check its stability. But today aeronautics has to drastically reduce its impact on the environment. One way to reach this goal is to decrease fuel consumption. For this purpose, a considerable effort is made to decrease the weight of the structures, which thereby tend to become more flexible. Furthermore, numerous new concepts of aircraft such as low sweep angle and high aspect ratio wing, laminar wing, highly flexible wing and strut braced wing, to mention just a few, are being developed to improve aerodynamic performance. But these new concepts tend toward lighter and more flexible wings. Therefore today aeroelasticity has an increasing influence on the design and has to be taken into account at earlier or even preliminary stages, not only to check the stability of the airplane design but also to compute its actual aerodynamic performance, the control surface effectiveness, and so prevent its reversal, and of course to verify both the static (static divergence) and dynamic (flutter) stabilities. Multi-disciplinary design and optimization methods are currently being developed to simultaneously determine the aerodynamic shape and the structural stiffness taking into account interactions between the aerodynamic flows and the structure [8] [1]. Garrigues *et al.* (AL14-09) presents a review of the aeroelastic practices at Dassault Aviation and shows the evolution of the role of aeroelasticity in aircraft design.

This issue of the AerospaceLab Journal presents a global overview of different activities required for aeroelastic analyses. Since aero-elasticity implies fluid-structure coupling, it is necessary first of all to be able to model and analyze the dynamic behavior of structures. The modelling of linear structure using finite element approaches is today of common practice for aeroelastic analyses. But aeronautical structures are most often non-linear owing to clearance and impact or friction for example. Kehr-Candille (AL14-04) is interested in the sources of non-linearities that result from a junction of two substructures, and proposes a numerical model of the damping occurring at such a junction. Stephan *et al.* (AL14-08) develops a new technology of nonlinear energy absorber aimed at mitigating the vibrations of real-life structures, and at thereby improv-ing their behavior in terms of lifetime, stability and user comfort. The last structural aspect addressed by this issue is the growing use of composite material in aeronautics over the last few years.

Such materials imply a different dynamic behavior due to their orthotropic constitutive laws and their low density, than that of structures made of metallic isotropic materials. Deletombe *et al.* (AL14-11) presents a bibliographic review on the crashworthiness of aircraft and helicop-ters made of composite material. This article deals with both numeri-cal and experimental studies.

Aeroelasticity is also concerned with the assessment of loads that apply to an airplane during the different flight phases. The article by Krueger *et al.* (AL14-01) presents the current situation regarding load computations aimed at structure design and certification. The process of identifying and assessing the different loads is complex but necessary to identify those which are critical for the structure sizing. These loads essentially result from flight or ground manoeuvers and from gust or air turbulence. They have to be assessed using numerical simulations and experimental ground and flight tests.

Aeroelastic analyses imply fluid-structure coupling simulations. Most often, in the case of aircraft design, such simulations used to be carried out using a loose coupling formulation: A reduced model of aerodynamic forces is first built from responses to harmonic motions, responses usually computed using low fidelity aerodynamic solvers. This aerodynamic model is then used to compute and update the aerodynamic forces that apply to the structure within the structural equation resolution process. Most of the theories about the aerodynamics of a wing were based on linear or potential flows [2]. However, current aircraft cruise speeds are subsonic but close to Mach 1, a flight regime for which the aerodynamic flows are non linear (transonic regime with shocks on the wing). Therefore, a higher fidelity of aerodynamic modeling is required to capture non-linear phenomena such as shock and flow separation. Fluid-structure coupling is nowadays performed using CFD (Computational Fluid Dynamics) methods and tools for aerodynamic force evaluation. Furthermore, CFD has led to the solving of the coupling in the time domain (also called "strong" coupling), *i.e.* a balance between the structure deformation and the aerodynamic forces is computed within each time step of a time consistent resolution. Dugeai *et al.* (AL14-03) presents a review of aeroelastic simulation methods based on CFD applied to turbomachines. Huvelin *et al.* (AL14-06) describes gust response and gust load alleviation simulations using CFD methods with comparisons with wind tunnel experiments.

Current research is focused on the development of more robust aeroelastic methods aimed at taking into account uncertainties in aeroelastic simulations or optimizations. The origins of these uncertainties may be of a structural nature, for example the manufacturing tolerance or the dispersion of the mechanical characteristics of composite materials, or they may be of an aerodynamic nature (flight angle of attack, velocity or altitude). Chassaing *et al.* (AL14-07) presents advances in the development of aeroelastic stochastic solvers to improve the robustness of the flutter critical velocity evaluation. Poirion *et al.* (AL14-05) proposes a stochastic method for gradient computations aimed at aeroelastic optimization, and thereby at improving the robustness of aeroelastic design.

The last topic addressed in this issue of AerospaceLab Journal concerns the morphing of aeronautical structures. One of the main challenges of the aeronautical community is to reduce its impact on the environment and on climate change. One idea therefore is to imitate birds, and consists in adapting the shape of the structure to the flight

conditions and to the aerodynamic load in order to improve the aerodynamic performance for the whole mission and to decrease the structure weight, thus allowing a reduction of the consumption and the release of polluting gases. Liauzun *et al.* (AL14-10) presents an assessment of morphing winglet concepts aimed at decreasing the aerodynamic load that applies to the wings and thereby at improving the aeroelastic behavior of the aircraft. Botez *et al.* (AL14-02) shows recent advances concerning the development of morphing wings with the objective of improving aerodynamic performance.

Only some aspects of aeroelasticity have been addressed in this issue. Although aeroelasticity started with observations that structures sometimes collapsed and mechanical engineers then reinforced their stiffness, it has become a multi disciplinary science that nowadays benefits from advances in numerous scientific domains: aerodynamics, numerical simulations, high performance computing, material and structure modelling, as well as experimental facilities and methods (e.g. large high speed wind tunnels, ground vibration tests [6]) and measurements [7] [9]) as can be seen in Aerospacelab Journal issue 12. All these advances are currently leading and will lead in the future to the identification, understanding and a better knowledge of more complex phenomena resulting from fluid-structure interactions. Notable examples are Limit Cycle Oscillation (LCO), which has an impact on the fatigue of structures, interactions in buffet conditions and structure behavior in a laminar-turbulent transitional flow that occurs on laminar wings, which is studied in order to decrease drag and consumption. On another hand, advances in composite materials allow the aeroelastic tailoring, or in other words the possibility of taking advantage of the structure flexibility instead of fighting it, in order to improve the structure behavior. All these scientific advances will lead to a more optimized aircraft design for the whole flight envelope, especially close to its boundaries ■

References

[1] T. ACHARD, C. BLONDEAU - *High-Fidelity Aerostructural Gradient Computation Techniques with Application to a Realistic Wing Sizing*. to appear in AIAA Journal, doi:10.2514/1.J056736.

[2] R. L. BISPLINGHOFF, H. ASHLEY, R. L. HALFMAN - *Aeroelasticity*. Dover Publications Inc, 1996.

[3] A. R. COLLAR - *The First Fifty Years of Aeroelasticity*. Aerospace 2.5 pp. 12-20, February 1978.

[4] E.L H. DOWELL, R. CLARK, D. COX, H. C. CURTISS JR, J. W. EDWARDS, K.C. HALL, D. A. PETERS, R. SCANLAN, E. SIMIU, F. SISTO, T. STRGANAC - *A Modern Course in Aeroelasticity Fourth Revised and Enlarged Edition*. Kluwer Academic Publishers, 2004.

[5] I. E. GARRICK, W. H. REED III - *Historical Development of Aircraft Flutter*. AIAA Journal of Aircraft vol. 18 no. 11, November 1981.

[6] S. GICLAIS, P. LUBRINA, C. STEPHAN - *Aircraft Ground Vibration Testing at ONERA*. AerospaceLab Journal 12, www.aerospacelab-journal.org, dec2016.

[7] L. JACQUIN, V. BRION, P. MOLTON, D. SIPP, J. DANDOIS, S. DECK, F. SARTOR, E. COUSTOLS, D. CARUANA - *Testing in Aerodynamics Research at ONERA : the Example of the Transonic Buffet*. AerospaceLab Journal 12, www.aerospacelab-journal.org, dec2016.

[8] G. KENWAY, J.R.R.A. MARTINS - *Multi-point High-fidelity Aerostructural Optimization of a Transport Aircraft Configuration*. Journal of Aircraft 51(1) pp. 144-160, 2015, doi:10.2514/1.C032150.

[9] B. LECLAIRE, C. BROSARD, R. COURTIER, F. DAVID, S. DAVOUST, A. GILLIOT, L. JACQUIN, J-M. JOURDAN, O. LEON, S. MASSEBOEUF, J-C. MONNIER, S. MOUTON, E. PIOT, A. RISTORI, D. SEBBANE, F. SIMON - *Planar Particle Image Velocimetry for Aerospace Research at ONERA*. AerospaceLab Journal 12, www.aerospacelab-journal.org, dec2016.

W. R. Krüger, P. D. Ciampa, M. Geier, T. Kier, T. Klimmek, D. Kohlgrüber, P. Ohme, K. Risse, J. Schwinn
German Aerospace Center (DLR)

E-mail: wolf.krueger@dlr.de

DOI: 10.12762/2018.AL14-01

A Comprehensive Load Process at the DLR – Definition, Analysis, and Experimental Evaluation

The determination of loads acting on the aircraft is one of the main tasks during aircraft development. The knowledge of loads is important for aircraft design, e.g., for the sizing of the airframe structure, as well as for certification. The definition of realistic load assumptions is important, as well as the generation of loads from simulation and experiment. The DLR is involved in a large number of aircraft design activities, and operates a fleet of research aircraft; thus, the DLR requires in-depth expertise for the definition and the determination of relevant and crucial load cases.

The aim of the iLOADS project is the development of an internal DLR load process, comprising expertise from various DLR institutes. The goal of the process is to strengthen the assessment capabilities of the DLR with respect to the influence of loads on new aircraft configurations, and to support certification capabilities for the DLR aircraft fleet. The load process is investigated with regard to the influence of various analysis approaches on aircraft structural design, and it is subject to verification and validation on different aircraft configurations.

The paper will give an overview of the background of the iLOADS project, as well as of the work performed in the project. The definition of the load process, as well as the implementations for different applications investigated in the project, will be presented in more detail.

iLOADS: a Comprehensive Load Process for DLR Needs

Background

To determine the loads acting upon the aircraft is one of the main tasks during aircraft design. Wright and Cooper, [1], summarize the task as follows: "Aircraft are subject to a range of static and dynamic loads resulting from flight maneuvers, ground maneuvers and gust/turbulence encounters. These load cases are responsible for the critical design loads over the aircraft structure and thus influence the structural design." Knowledge of the loads is thus required for design and structural sizing, and for prediction of the performance, as well as for certification. The definition of realistic load cases and the determination of loads during simulation and experiment are important.

The DLR carries out a great number of activities in aircraft preliminary design and in the operation of a fleet of research aircraft, and thus requires in-depth expertise for the analysis of relevant and crucial load cases. Thus, the DLR needs an established comprehensive and well-founded load process. At the same time, the various DLR institutes have extensive knowledge regarding numerous aspects of the field of load analysis. This expertise covers pragmatic approaches to high-end methods for both simulation and testing.

The DLR project iLOADS, "integrated LOADS at the DLR", answers to those requirements. The expertise in load analysis is combined and integrated into a comprehensive load process. Such a process has been formally defined in the project, and global rules for analysis and documentation have been set. Selected numerical methods for load analysis have been evaluated, and the load process has been used

to investigate the influence of various analysis approaches to aircraft structural design. Finally, the process has been subjected to verification and validation on different aircraft configurations, both numerically and experimentally.

Project Goals and Technical Content

Two main goals of the iLOADS projects were defined:

- the definition, implementation and validation of a load process tailored to DLR needs, and
- the support of the certification activities of the DLR aircraft fleet.

The project was structured into four work packages. In the first work package, the load process was defined and documented with respect to the DLR requirements. In the second work package, numerical simulation methods of varying complexity were compared, with a focus on aerodynamic methods, as well as on methods for the analysis of discrete gusts and for man oeuvre loads. In the third work package, various approaches for the sizing of fuselage structures have been compared and validated with experimental data. In the fourth work package, implementations of the load process have been applied to different use cases – these applications were the generation of preliminary design loads for a transport aircraft configuration, the numerical analysis of loads for an existing long-range aircraft, and the measurement of loads during flight testing on two aircraft, first on the structure of a sailplane, and second on the outer store of a high-altitude research aircraft. The current article follows the outline given in [2]. The work of Work Packages 2, 3 and 4 is summarized further down in the paper and described in detail in separate papers, see [3], [4], [5], [6], [7] and [8].

Related Activities

Load analysis plays a role in a number of running activities, both for the application of load analysis and for the development of selected load analysis methods.

At the DLR, a load process for conceptual design has been established and used in the VAMP and FrEACs projects [9]. The validation and application of approaches for gust load analysis have been part of the iGREEN [10] and ALLEGRA projects, including both numerical investigations and wind tunnel experiments on a transonic gust generator in the transonic wind tunnel Göttingen, TWG-DNW [11]. The DLR-project Digital-X has focused on the application of CFD and complex structural models in aircraft design loops, as well as on implementing an iterative process for loads and sizing [12]. Several projects of the German National Aeronautics Research Program (Lufo), e.g., the Lufo 4 projects M-FLY and FTEG, covered improvement and validation of load analysis methods in an industrial context. Within the framework of EU projects, the FP7 project Smart Fixed Wing Aircraft (SFWA) included a work package dedicated to load analysis on passive and active wings, including load alleviation strategies [13]. Reduced order methods and CFD-based gust analysis is the topic of the FP8-H2020 project AEROGUST [14].

Most of the projects mentioned concentrate on specific details of the load analysis, on the application of design aspects, or on the automation of a load process for MDO purposes. The DLR project iLOADS focuses in addition on the completeness and the quality of the load process as such.

Load Process

Definitions

The term "loads" is used in a wide context and with a variety of meanings, thus requiring the definition of the term as it will be used within the context of the paper.

"Loads" will be used to describe forces and moments acting on the aircraft structure, resulting from air pressure (lift, pressurization), mass forces (inertia, gravity), structural forces (elasticity) and other forces, such as landing impact or thrust.

The term "load process" will be used as follows:

- for given boundary conditions (e.g., operating conditions, or certification requirements),
- for a given configuration (aircraft or component),
- loads on the structure shall be determined,
- with methods of adequate fidelity,
- the loads will be used for structural design, configuration assessment, or aircraft certification.

Frequently, the term load is also used in the sense of cargo or additional equipment. While freight, of course, also inflicts mass forces on the aircraft, we will try not to mix these connotations. Furthermore, the paper will concentrate on mechanical (structural) loads, electric loads will not be addressed; they are an important topic when designing an aircraft, but with little direct impact on the structural load process.

"Classes" of loads are often combined in categories. A common classification differentiates between flight loads (man oeuvre loads, gust loads), ground loads (landing loads, ground maneuvers), inertial loads (oscillations, vibrations), and special load cases (pressurization, bird strike, crash/ditching, fatigue).

A complete load loop will consist of a large number of single analyses, potentially thousands. This, consequently, requires a well-structured data management and a careful and thorough evaluation, condensation and interpretation of the results, in order to be able to perform reliable assessments.

Standard Literature

A number of publications cover the load process and load analysis methods. The books by Lomax [15], concerning structural load analysis, and by Hoblit [16], covering gust analysis, are considered standard literature, as well as the book by Howe [17]. The textbook by Wright and Cooper [1] concerns the representation of the underlying physical effects. Important boundary conditions arise from certification and the respective specifications [18], [19]. The standard tasks of a load process are well described in the often-cited article by Neubauer and Günther [20].

Requirements

Approaches for industrial load analysis are dependent on aircraft size and type, regulations (CS-22 / CS-23 / CS-25), company size and company design philosophy. The DLR load process is defined to address specific DLR requirements. Criteria for the process are derived from the application scenarios. All tasks have in common that

a great number of analyses must be performed in a limited amount of time. Thus, the process has to be comprehensive for a given task, and performed with adequate fidelity. The process must be subjected to quality management under the following key topics – it must be possible to understand the approach, to reproduce all results, and to document and review the process and results. The process has to be maintained; availability of methods as well as of operators educated in the process is important.

The core process defined in the project consists of the following phases, see Figure 1:

- *Load case definition phase*
  i.e., the definition of relevant load cases for analysis, and of requirements for the models to be used.

- *Load analysis phase*
  i.e., the analysis of maneuver loads, gust loads, landing loads, special load cases, etc.

- *Load post-processing phase*
  The creation of a load database that can be processed according to the quantities needed; e.g., cut loads (cross-section loads) for evaluation or maximum nodal loads for sizing.

Specifications for the necessary analyses result from the operational requirements, like the projected flight speeds and altitudes of the aircraft. A catalogue of load cases is defined depending on those boundary conditions. Load cases defined in this catalogue will then be addressed subsequently.

The calculation of loads is a wide field, and the use of many different simulation tools depending on the load cases (maneuvers, gusts, landing, bird strike, etc.) might be necessary. Agreement on a common nomenclature and on common interfaces for model data and result data is therefore essential, and was part of the project.

The results of the analyses will be collected and used for the design and evaluation of configurations; for example, for structural sizing and aircraft mass estimation. For quick representation and comparability of project results, section loads defined on load reference axes were used. For wing structure sizing purposes, nodal loads were also available.

The load transfer from analysis to sizing and structural optimization includes two steps. First, load analyses are performed, where the number of load cases depends on the task. For the generation of a representative aircraft mass in the early design stages, less than 20 cases have shown to be sufficient. For the sizing of the wing and empennage, control points on the wings are defined, the so called "stations", at which section loads are monitored. For each station, load envelopes are created, see Figure 1, right. In the DLR process, structural sizing is usually performed as a structural optimization task, for which all load cases lying on the border of any envelope are provided to the structural optimization solution; see also [10] and [12]. Experience shows that with the current automated approach, about 100 flight load cases are activated for the sizing of a wing structure.

It should be noted that the selection of load cases considered in the project has been driven by the DLR requirements, in the sense of applications, as described in Section "Project Goals and Technical Content" above. First, the DLR interest is mainly on the numerical investigation of global loads to assess aircraft configurations in design studies with various levels of complexity. Second, there is the necessity to support experimental activities on test rigs or on research aircraft, where modifications of the aircraft are often at the component level, e.g., very often the installation of large antennas or sensor equipment. Thus, not all load analyses that are obligatory for the development and certification of a new aircraft on an industrial scale have been included in the DLR load loop in the course of the iLOADS project. Temperature loads have not been taken into consideration. Also, loads resulting from internal systems and equipment are not part of the standard approach and are only calculated as standalone investigations when specifically requested, for example, for the certification of a flight test modification.

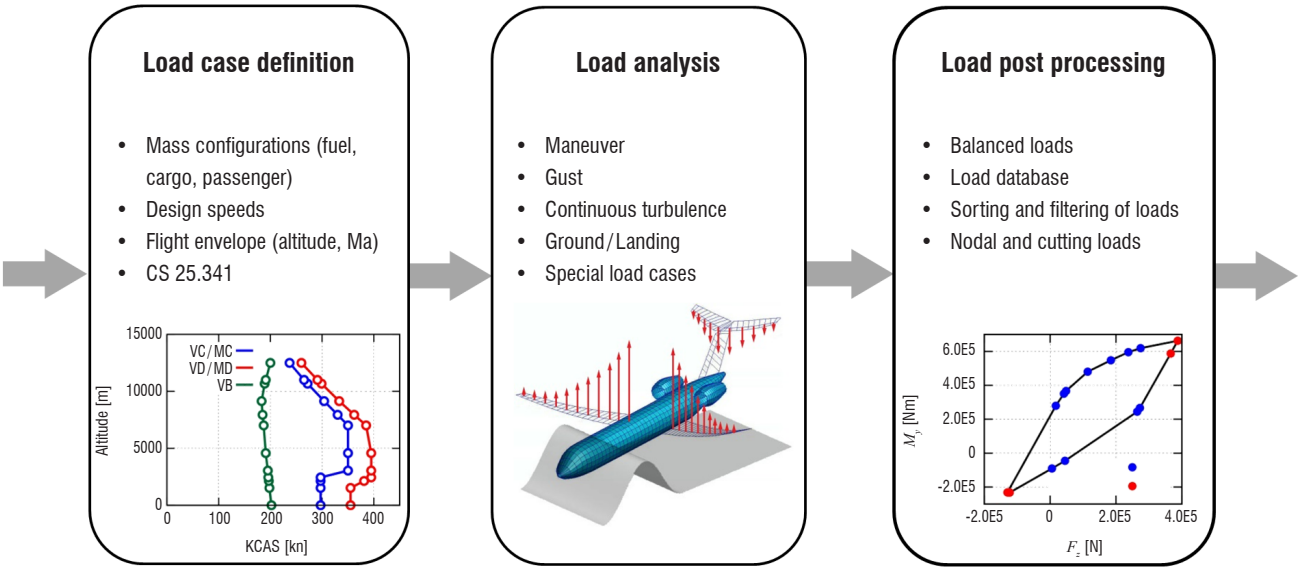

Figure 1 – Phases of the DLR load process

Aircraft Configurations

At the beginning of the project it was agreed to perform as many analyses as possible on a common reference configuration. For this purpose, the so-called DLR D150 configuration was available; that is, an aircraft design similar to an A320 in size, see Figures 2 and 4 below. For the D150, data was available from previous DLR projects [21]. A structural design, as well as aerodynamic data, both in the form of a Doublet Lattice Model (DLM) and CFD data, could be used. The wing geometry used for CFD meshes corresponds to the DLR F-6 configuration [22]. The experimental structural investigations (see Section "Loads and Structural Design") were also based on the geometry and loads calculated for the D150 aircraft.

Furthermore, design load data from two production aircraft could be used for comparison in the iLOADS project, the first data being taken from the VFW 614 design documentation, and the second data being provided by Gulfstream Aerospace in the course of the certification of the HALO atmospheric research aircraft, operated by the DLR [23].

Tools and Data Format

A number of different analysis tools have been used in the iLOADS project, depending on the application. Where necessary, details will be provided in the respective sections below. Commercial software packages used were the finite element codes ANSYS [24] and MSC.NASTRAN [25]. For CFD analysis, the DLR TAU code was used [26]. Load analysis was performed using MSC.NASTRAN and the DLR/Airbus development VARLOADS [27]. The DLR tool MONA (ModGen & NASTRAN) [10] was used for parametric modelling (ModGen) and sizing using the structural optimization routines of NASTRAN. For ANSYS, finite element models were set up by the DLR tools DELiS [28] and TRAFUMO [29], while sizing was performed using the commercial tool HyperSizer [30] or the DLR development S-BOT [28]. As much as possible, model definition and data exchange was performed in the CPACS format [33].

Analysis of Dynamic Loads

In this work package, simulation methods for load analysis were investigated. Focus was on the evaluation of different modelling levels-of-detail for aerodynamic analysis, and also for the analysis of maneuver loads, gust loads and landing loads. For those load classes, a comparison of load levels coming from dynamic analyses with loads derived from equivalent static load cases has been performed. Section "Analysis of Dynamic Loads" gives a summary of the activities in the work package. A comprehensive overview can be found in [3].

Aerodynamic Loads

Aerodynamic analyses in this work package were performed by the Institute of Aerodynamics and Flow Technology. Work was initially planned to be executed on the D150 configuration. It quickly showed that the wing geometry resulting from the preliminary design phase of that aircraft, and stored in the CPACS data, was not suitable for CFD analysis, since standard subsonic profiles have been used in that phase. It was thus agreed to use the geometry of the DLR F-6 configuration, which is very similar to that of the pre-design wing but with a transonic profile, as the reference for aerodynamic investigations, see Figure 2.

The following aerodynamic tools were taken into consideration for the comparison of methods:

- LIFTING_LINE (a multi lifting-line approach, DLR) [34]
- VSAERO (3D-Panel Method, commercial) [35]
- TAU (3D-Navier-Stokes-Solver, DLR) [26]

It should be noted that the LIFTING_LINE and VSAERO-interfaces are currently restricted to configurations with wing and empennage only, consequently neglecting the fuselage. This fact was acknowledged in the discussion of the results.

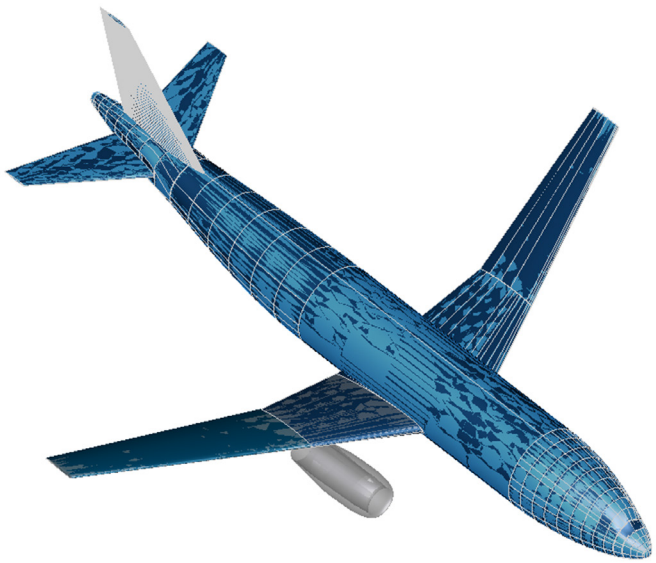

Figure 2 – Comparison of geometrical representations of the DLR-F6-D150 configuration using CATIA and CPACS

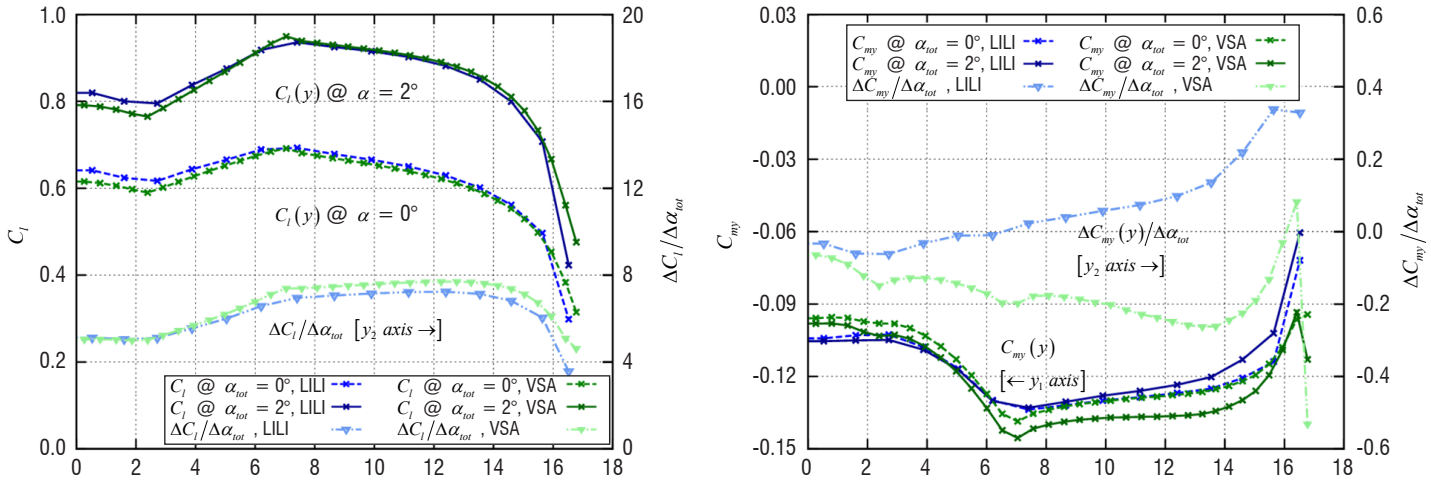

Figure 3 – Comparison of C_l and C_m distributions between LIFTING_LINE (LILI) and VSAERO (VSA)

An important step was the definition of assessment criteria for the calculation of aerodynamic parameters for load analysis. The following quantities were selected as relevant:

- global aerodynamic coefficients, especially the lift coefficient C_l and moment coefficient C_{My},
- distribution of local aerodynamic coefficients, especially of C_l and C_{My},
- gradients of aerodynamic coefficients with respect to angle of attack, especially $\Delta C_l/\Delta\alpha_{tot}$ and $\Delta C_{my}/\Delta\alpha$.

As an example, Figure 3 shows the span-wise distribution of the lift C_l and moment C_m, as well as the local gradients with respect to the total angle of attack α_{tot} at the transonic Mach number of $M = 0.75$. The small absolute deviations also confirm the agreement of the (subsonic) compressibility corrections implemented in both tools. The good agreement for the C_l gradients could also be shown for wing-tail configurations. While the span-wise distribution of C_{My} in Figure 3, right, shows deviations in the absolute values, but still with similar trends, very significant deviations are observed for the gradients with respect to α_{tot}, which is due to different sensitivities of the center of pressure between the multiple lifting-line method and the panel method.

This must be carefully checked during tool selection, when being applied for load analysis and prediction, as well as in the context of trimming of the overall aircraft configuration.

Gust Loads

For the definition of discrete gust loads, two approaches are common: the so-called 1-cosine-gust, solved by dynamic analysis, and the so-called Pratt gust, a steady approximation of the dynamic gust phenomenon. While dynamic simulations are required for transport aircraft certified according to CS-25, the Pratt gust is still much in use in conceptual and preliminary aircraft design and can be used for aircraft certification according to CS-23.

The goal of the activity was to assess the fidelity and achieve understanding of the differences between the approaches. The investigations described in the following paragraphs have been undertaken by the Institute of Aeroelasticity, using MSC.NASTRAN.

The Pratt equation is based on the following assumptions:

- the aircraft is rigid,
- the flight speed remains constant,
- the aircraft flies in a steady and trimmed state before hitting the gust,
- the only degree of freedom is the heave,
- lift is generated by the wings; the lift generated by the fuselage and empennage can be neglected,
- the gust speed is constant over the wing span and parallel to the vertical axis.

Pratt derived his equation for a gust length of 25 times the chord length. For a simple wing example performed in iLOADS, the load factor generated by the Pratt equation proved indeed to be identical to the maximum load factor of a 1-cosine-gust.

For a complete aircraft, the result of such a comparison depends on the gust length. For the D150 configuration, the maximum load factor of all gust lengths fits the Pratt assumption well, see Figure 4 for the example of a vertical gust. However, when the gust length excites a

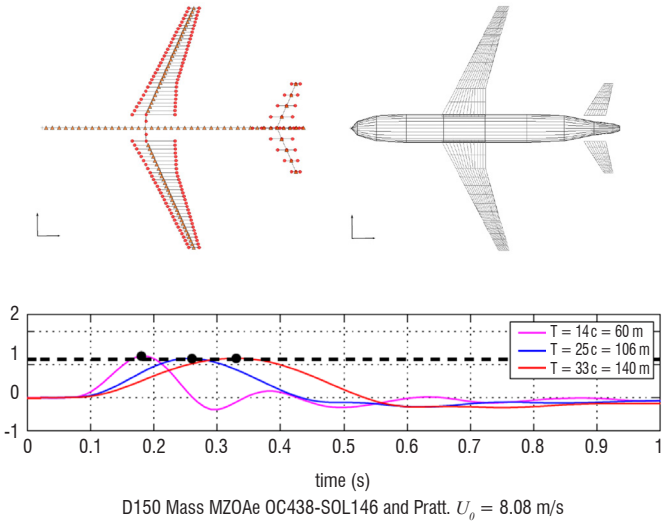

D150 Mass MZOAe OC438-SOL146 and Pratt. $U_0 = 8.08$ m/s

Figure 4 – Top: condensed structural model and DLM model of DLR-D150 used for gust analysis; bottom: comparison of the Pratt gust and 1-cos-gusts for different gust lengths

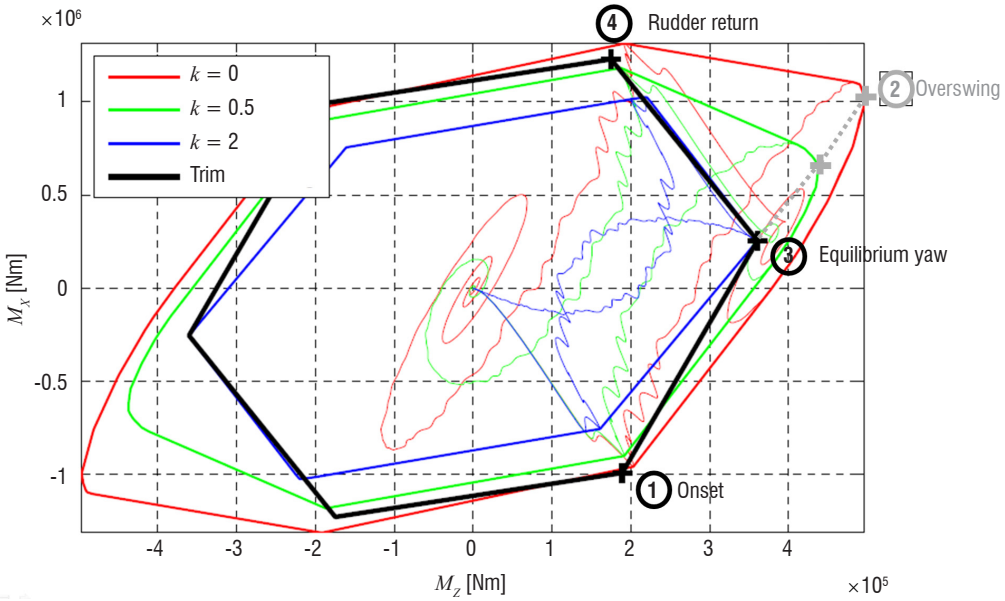

Figure 5 – Yaw maneuver: resulting loads (at the root of the vertical tail plane) for dynamic simulation and representative static analyses

natural frequency of the aircraft, e.g., the first wing bending mode, maximum load factors can be higher than predicted by the Pratt equation. Such an effect could be seen on the D150 configuration for lateral gust loads.

Manoeuvre Loads and the Effect of a Flight-Control System on Aircraft Dynamic Loads

Many manoeuver loads can be represented as so-called trim cases. One question is whether a (steady) trim case can correctly represent all loads arising in a dynamic manoeuver. In the work package, a dynamic yaw and dynamic roll manoeuver have been investigated by the Institute of System Dynamics and Control.

Dynamic yaw

According to Paragraph CS 25.351, the dynamic yaw manoeuver is defined in four phases:

1. In the cockpit, the rudder is rapidly pushed to the limit stop while the aircraft is in horizontal flight.
2. The aircraft yaws and will overswing into a maximum yaw angle.
3. After the transient is damped out, the aircraft will fly in steady slip with full rudder.
4. From this condition, the rudder is rapidly brought into the normal position.

A flight-control system has to be considered.

Rather than performing a dynamic simulation, representative trim calculations can be performed. Phases 1, 3 and 4 can be well represented by a trim calculation. Phase 2 is highly dynamic, and loads from overswing can only be calculated correctly by a dynamic simulation, see Figure 5. The figure shows bending and torsional moment at the root of the vertical tail plane [3]. If a yaw damper is used, it has a significant influence on the overswing loads, as can be seen in Figure 5, where different colors represent different yaw damper (k) settings.

Dynamic Roll

Maximum loads from a dynamic roll manoeuver heavily depend on the pilot model used. A pilot model is necessary, since a constant load factor during the manoeuver, as required by the regulations, cannot be obtained without such a model.

The steady roll and the two accelerated roll conditions can be specified as trim conditions. The resulting correlated load envelopes, for bending and torsional moment at a wing station just inboard of the aileron, for right and left roll, are depicted in Figure 6. The trim results compare well to the dynamic solution, except for the onset condition. This can be attributed to the "structural" dynamic overswing during the abrupt initialization of the roll maneuver. The resulting sharp peaks for the accelerated rolling conditions 1 and 3 are due to the very aggressive application of the ailerons. The remaining differences are a consequence of the inability to hold the appropriate load factor.

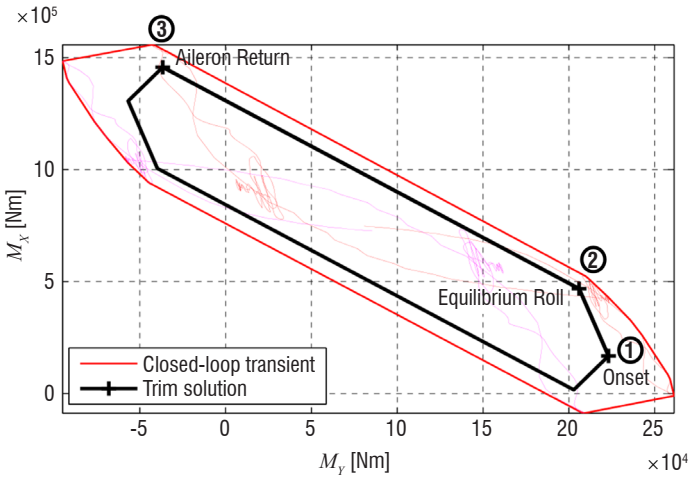

Figure 6 – Roll maneuver: correlated loads (just inboard of the aileron) for dynamic simulation compared to trim results

Ground Loads

There are two widely used approaches for the calculation of aircraft ground loads, empirical methods and simulation-based methods. Empirical methods are statistical approaches, based on data of existing aircraft. There are three major formulations for this method, which are given by Lomax [15], Howe [17] and Roskam [36]. These formulations determine the ground loads on each landing gear by first calculating equivalent dynamic loads from empirical equations and then multiplying those equivalent ground loads on each landing gear by load factors according to certification requirements, usually 1.5.

More realistic dynamic landing loads (sometimes called "rational loads") can be calculated by time domain simulation of landing impacts [37]. Cases frequently used are the so-called "3-Wheel Level Landing Case" according to CS 25.479 and the "2-Wheel Tail-Down Landing Case" (CS 25.481). Multibody models of aircraft and landing gear are used for simulation.

In the work package, results from the empirical approaches and from the simulation have been compared by the Institute of Aeroelasticity to design data from the VFW 614 aircraft, as used by DLR until 2012, see Figure 7. Results of interest for the validation are the main landing gear landing (MLG) loads.

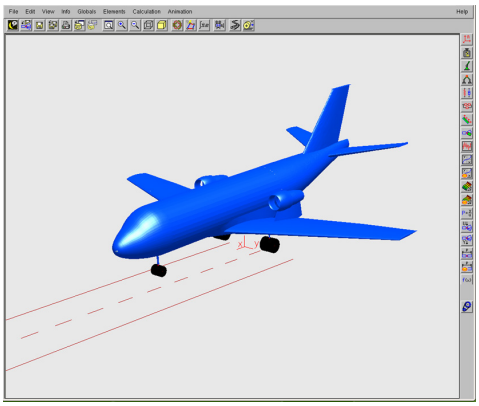

Figure 7 – Multibody model of VFW 614 aircraft used for ground load analysis

For the 2-wheel landing case, the estimated loads from all empirical methods vary no more than 5% from the values calculated by the aircraft manufacturer. The difference between the multibody simulation and the industrial data was in the same range. While a typical handbook method estimates the main landing gear attachment loads to be 6% higher than the industrial reference data, the multibody simulation result from the project is 4% lower than the reference data.

For the 3-wheel landing case, however, the empirical methods either cannot be applied or they give loads that are considerably off. The 2-wheel landing (not taking the nose landing gear into consideration) gives higher loads than the 3-wheel landing case. In addition, the VFW 614 has a conventional landing gear configuration. It may thus be concluded that the empirical methods investigated are capable of giving good estimates for maximum vertical landing loads, whereas for more realistic cases, time domain simulation, e.g., using multibody simulation, yields more reliable results. The same is true for unconventional landing gear or aircraft configurations, where statistical methods cannot yield reliable results because of the missing data base.

Loads and Structural Design

The goal of the work concerning loads and structural design was the use of results from the load analysis for the design for aircraft structures, and the assessment with respect to strength, stability, crash behavior and fatigue. A more detailed description of the work can be found in [4] and [5].

Realistic Load Assumptions for the Design of Aircraft Structures

In the project, the capabilities for the design of structures, here focused on fuselage design, were improved. For the D150 configuration, loads and a global structural design were available. However, those loads were defined on the load reference axis, thus, questions concerning a valid use of those loads for sizing of fuselage structures arise.

The geometry of the fuselage model, as well as the loads, are given in the CPACS format. The definition of the structure includes the skin with discrete reinforcements (stringers, frames), pressure bulkheads, PAX and cargo floor structure, structural coupling regions to wing and empennage models. Further considerations include material data (isotropic, orthotropic), layered compositions, as well as arbitrary profile cross-sections with arbitrary wall thickness.

Some load cases deliver local loads to the structure. One example are loads from the landing impact. Here, the global structural model has to include, e.g., a detailed representation of the wing-fuselage intersection, as well as the supporting structure of the landing gears, in order to allow a realistic load application and distribution. The Institute of Composite Structures and Adaptive Systems extended its model generator DELiS to create representative finite-element models of those areas, see Figure 8.

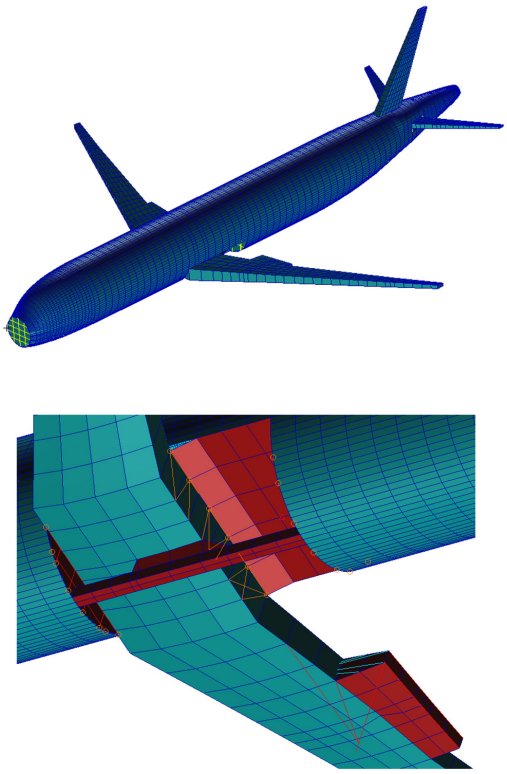

Figure 8 – Full aircraft finite-element model and detailed coupling region of the wing-fuselage intersection

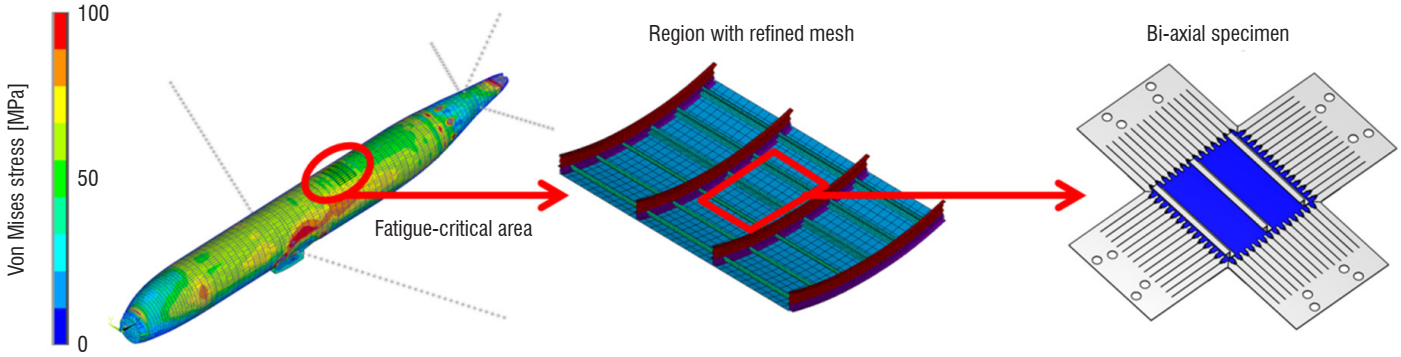

Figure 9 – Stress distribution in top fuselage at +1g flight case; red circle: fatigue-critical area

In addition, different structural sizings using either equivalent static load cases or the corresponding dynamic load cases (as described in Section "Analysis of Dynamic Loads" for gust loads, landing loads and maneuver loads) were performed and compared.

Realistic Load Assumptions for Component Design

The goal of this work package was the development of a procedure to calculate realistic loads for a fuselage panel on a full aircraft model and to use those loads for experimental investigations on test panels.

As stated above, loads given for the D150 configuration were defined on the load reference axis. Thus, different methods for the transfer of global loads, *i.e.*, shear, moment and torque given for selected points, to the distributed fuselage structure, *i.e.* the panels, have been developed and compared. The Institute of Structures and Design calculated such loads on an airframe model in the classical metallic stringer/frame design for ANYSY, built up using the DLR TRAFUMO tool, and sized by S-BOT+ as the sizing engine. For a 1g flight point, the resulting loads in a fatigue-critical area on the top of the fuselage have been derived, see Figure 9.

These loads were then passed on to the Institute of Materials Research, where the test on a bi-axial test rig was performed.

Realistic Load Assumptions for Testing Structures and Materials

The next step in the investigation was the experimental study of crack propagation for a representative fuselage section in a bi-axial test rig at the Institute of Materials Research.

The results of the load analysis described above (see Figure 9) were evaluated for the definition of test-rig loads. The stress from the simulation was taken as the maximum stress for the experiment. A load ratio of $R = \sigma_{min} / \sigma_{max} = 0.1$ was assumed for the fatigue test. This load ratio leads to fast fatigue crack propagation and represents ground-air-ground cycles.

The design of the bi-axial test specimen and of the forces to be applied in the experiment was performed using finite-element (FE) simulations, see Figure 10, with the software ANSYS. In the FE model, a crack can be included in order to determine stress intensity factors.

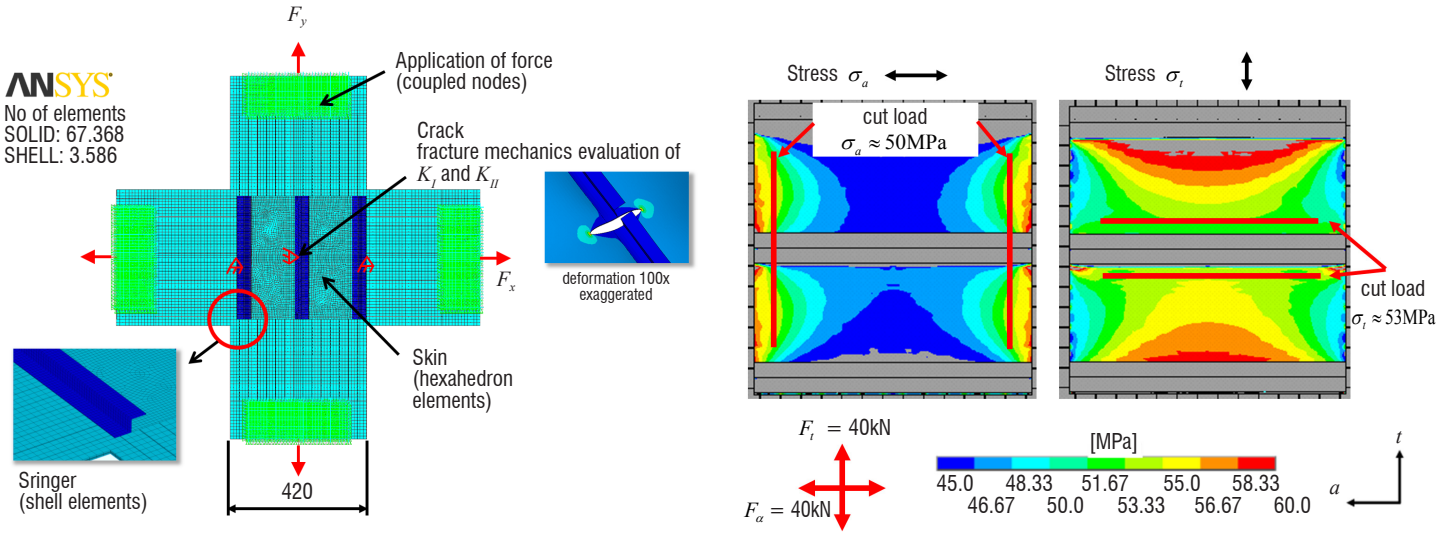

Figure 10 – FE-Model and cut loads for a bi-axial test specimen

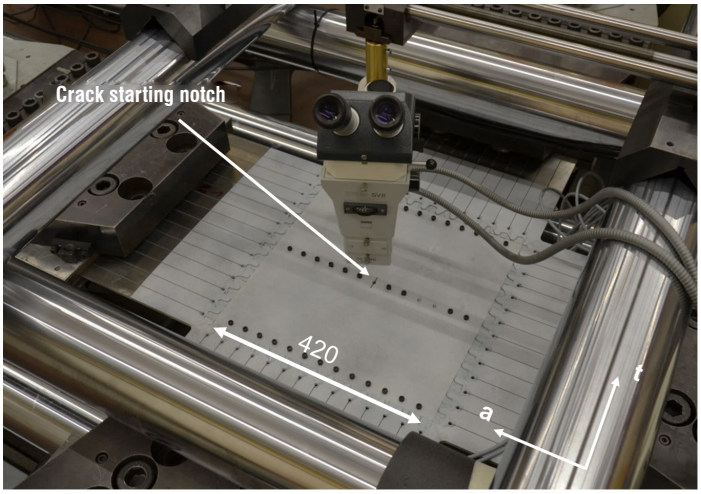

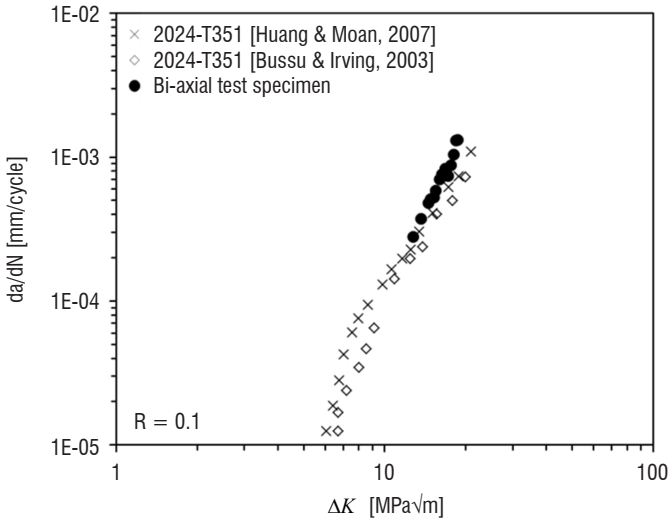

Figure 11 – Left: Test specimen in bi-axial test rig. Right: Crack growth rate for bi-axial specimen in comparison with data from literature [31], [32].

The test specimen was equipped with strain gauges in XY directions; furthermore, an optical system for deformation measurements was used. In a first experiment, the specimen was tested without a crack with different load ratios and forces up to 80 kN along both axes, see Figure 11, left. Optical measurements were employed at different force levels to compare simulation to test results.

In a second step, a notch was introduced across the riveted stringer and skin in the middle of the panel. During cyclic loading, a crack developed, which was monitored to observe the crack propagation rate (Figure 11, right) and the direction of the crack growth.

It could be shown that FE simulation can be used for the analysis of complex structures. In the future, the procedure can be performed "backwards" – with standard test-specimen crack-propagation data and numerical simulation, the resulting life time of complex structures can be predicted.

In a second test, the Institute of Composite Structures and Adaptive Systems used a panel of the fuselage section above the front door to validate their structural optimization process. This area is often sized by a braking load case leading to a compression load on the panel. Therefore, the optimization and test were focused on the prediction of the buckling behavior under uniaxial compression loads.

The panel test was performed on the Institute buckling test rig, see Figure 12. Next to strain gauges, two deflection sensors and two optical measurement systems (ARAMIS) were used for data acquisition. The ARAMIS systems covered the complete front side and most of the back side of the panel.

The respective FE simulation model is implemented using the Software Abaqus. It consists of 6-mm linear shell elements for the skin and the stringers. The top and bottom of the panel have fixed boundary conditions and the sides have free boundary conditions.

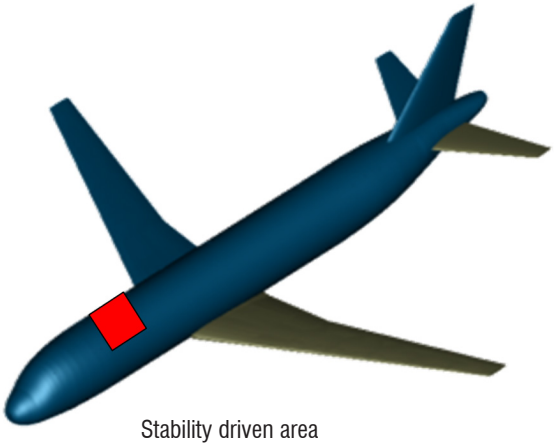

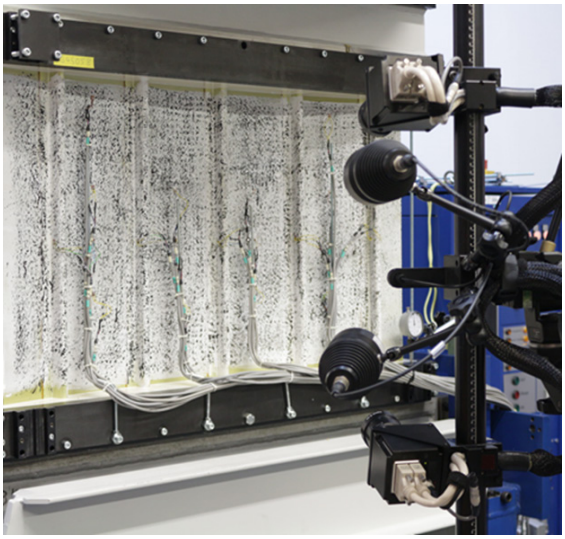

Figure 12 – Region of interest on the aircraft fuselage, and test setup for the buckling test of the panel

The experiment buckling loads are well represented in the simulation. The differences between simulation and experiment were 6.6% for the first and 3.4% for the second mode. For all modes, the buckling patterns and the global stiffness distribution of the numerical model fit the experimental result well, see Figure 13.

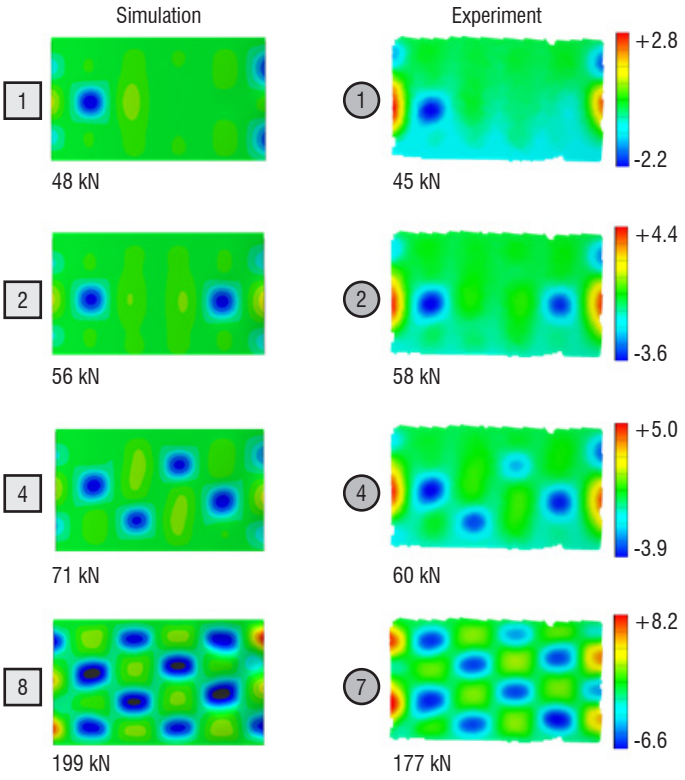

Figure 13 – Radial displacement and loads for different buckling patterns

Use Cases: from Conceptual Design to Flight Testing

The different implementations of the load process were applied to four different applications: so-called "use cases" – a pre-design study; the generation of a load envelope for a large long-range business jet; numerical analysis and test flight of an outer wing store; and load measurements on a sailplane. Details of the activities can be found in [5], [7], and [8].

Load Analysis Process in Pre-design

The first use case was the implementation of a load process for overall aircraft pre-design applications. A load loop for pre-design was implemented in the RCE environment by DLR Air Transportation Systems. Focus was on an automated process for early design and on robustness of the process. All modules were based on CPACS, and the TiGL geometrical kernel; any valid CPACS file can be analyzed, and the main physics effects captured.

The target of these activities was to be able to perform large trade studies. Since they are needed for coupling purposes, e.g., for fluid.-structure-coupling, multiple coupling schemes for mismatching topologies were evaluated. In iLOADS, the influence of aero-structural effects on sizing aircraft flexibility, and thus on performance, were of central interest.

Investigations were performed on the D150 model, see Figure 14. The overall aircraft design, including all dimensions of the aircraft geometry, results from a classical preceding conceptual design process and is taken as given for the loads and sizing loop. Analysis starts from an initial overall aircraft design (OAD) synthesis model, where the aircraft parameters are described in the CPACS format. The loads are calculated for the sizing of the airframe; a resulting deformation of the aircraft is calculated and used as input for a new load loop. After convergence, a performance analysis is performed.

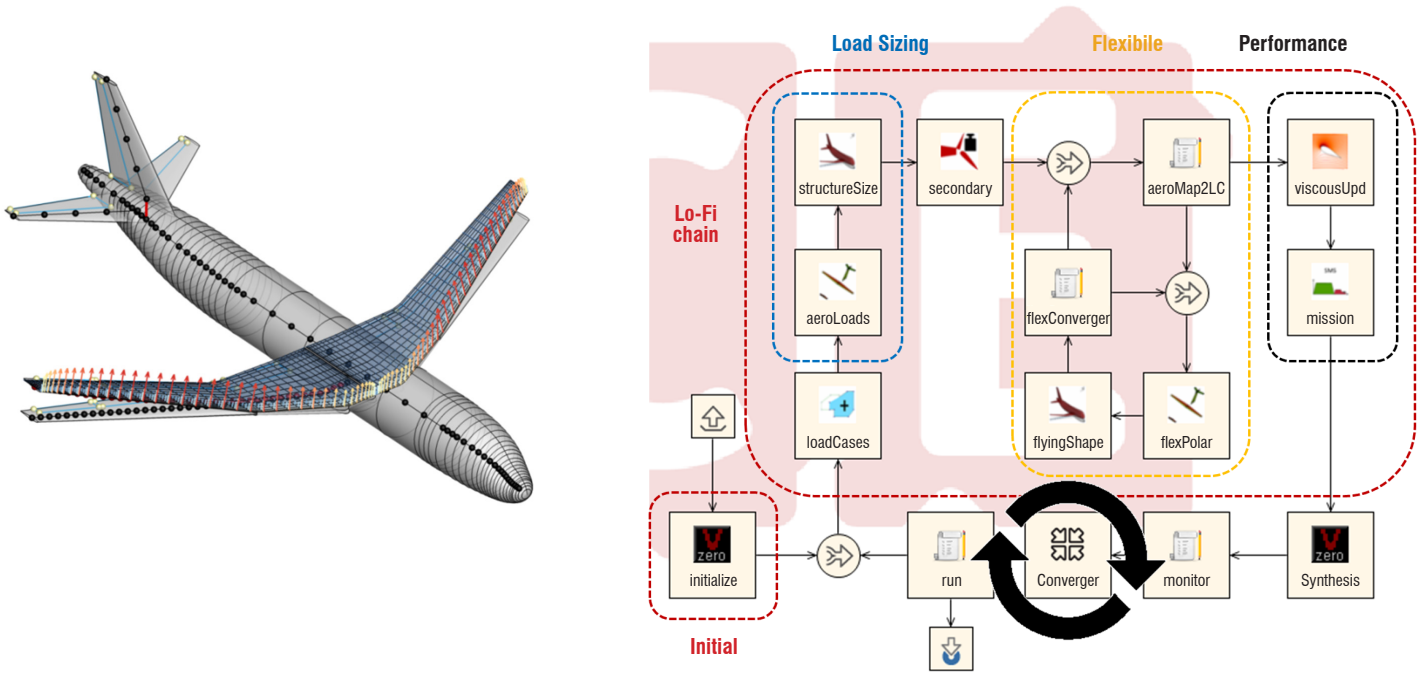

Figure 14 – D150 pre-design model and RCE-based analysis loop

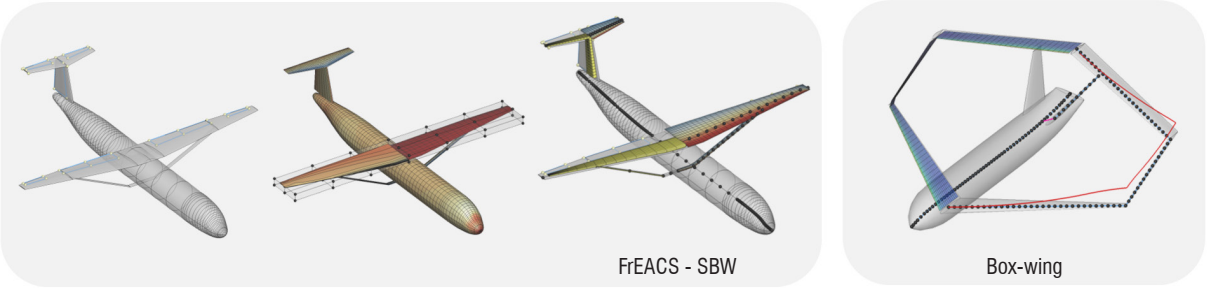

Figure 15 – Goal: reliable loads for unconventional configurations at the preliminary design stage

While the loop was tested for a conventional aircraft configuration, the final goal is to establish such a process for unconventional configurations, e.g., strut-braced wings or box-wing configurations, see Figure 15, where design trends can only be reliably predicted when taking elastic deformations into account.

Load Analysis on a High-Altitude Research Aircraft

The high-altitude research aircraft HALO, a Gulfstream G550, is operated by the DLR to provide a high-performance vehicle for atmospheric research. Test equipment can be placed in stores attached to the wings or fuselage. The DLR has to implement and certify these modifications depending on the specific mission. From aircraft certification activities for use with outer-wing stores, the DLR was provided by Gulfstream Aerospace (GAC) with load envelopes relevant for the placement of those attachments.

The second use case in iLOADS was the task of simulating those load cases with the DLR load process and with an aircraft model resulting from the DLR parametric design process. The design process used by the Institute of Aeroelasticity was the so-called MONA process, where a parameterized aircraft model with global structural representation (finite-element model), aerodynamic (DLM) model, and mass model including various mass configurations was set up. The aim of such a design is a simulation model that represents global aircraft dynamics well for load analysis and aeroelastic stability analysis. Depending on the community, such a model is known as a "Dynamic Master Model" or a "GFEM/dynamic". The modelling process is described in [12]. Contrary to the example given in [12], however, here sizing loads were not calculated by the DLR, but rather came from the data provided by the GAC. The task of the project was to compare the loads from the DLR process with those provided by the aircraft manufacturer.

A condensed model of the aircraft was used for load analysis, see Figure 16.

Loads on wings, fuselage and empennage were compared to the values given by the GAC. First evaluations showed good agreement for most parts of the aircraft structure; differences can be seen mainly for the empennage, where the modelling should be improved, e.g., by updating the model with information gathered from ground vibration testing performed by the DLR on the HALO in 2010.

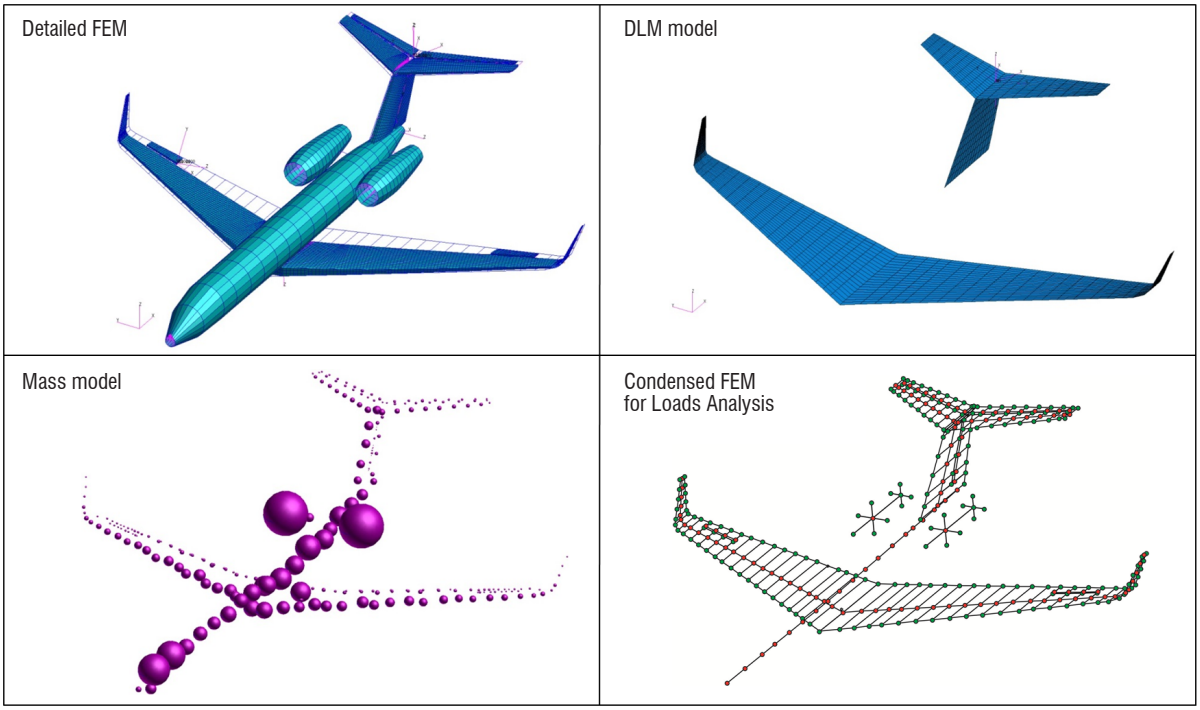

Figure 16 – Aircraft model of G550 HALO from the MONA process used for load analysis

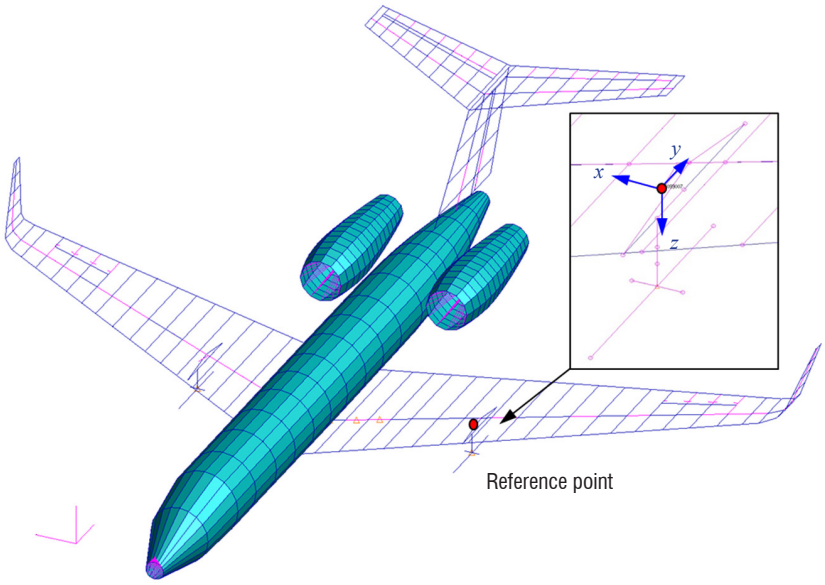

Figure 17 – Simulation of loads at the PMS attachment point

The HALO model was then used to generate realistic loads for the outer wings store, the so-called PMS (particle measurement system) - carrier, see Figure 17. For typical gust cases at Ma=0.85 and at an altitude of 8500 m, displacements and accelerations of the attachment point of the PMS carrier were generated. These values were later used for the hardware test of the PMS on the MAVIS vibration table at the Institute of Aeroelasticity.

Load Measurements on the HALO PMS-Carrier in Flight Tests

The PMS carrier tested is a DLR development for carrying large measurement equipment for atmospheric research under the wings of the HALO aircraft. For certification, it must be ensured that the maximum attachment loads of the carrier to the wing specified by the GAC will not be exceeded under any loading conditions or the PMS carrier. A numerical model of aircraft and carrier has been built, which must be validated through in-flight load measurements.

First, loads were calculated for the carrier, for a representative gust, by the Institute of Aeroelasticity. The PMS carrier was equipped with strain gauges and accelerometers to measure vibrations and cross-section loads close to the attachment points. The set-up was first tested on the MAVIS vibration table of the institute [38] and later installed on the HALO aircraft, see Figure 18. For the data acquisition, a de-centralized system, fitting into the central tube of the PMS carrier, was qualified for the flight tests.

In five flights, a large number of maneuvers could be flown, and an extensive amount of data was recorded. First evaluations showed promising agreement between numerical and experimental data, see [38], however, the greatest part of the evaluation is yet to be done and is part of follow-on projects. The same data set was used for online identification of the aeroelastic model of the aircraft, see [7], [38] and [39].

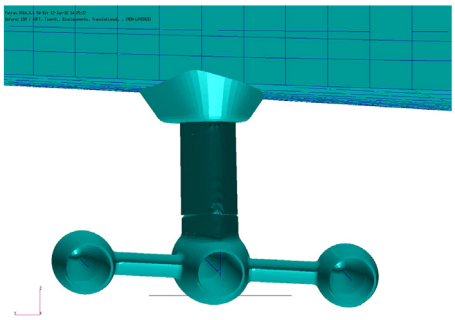

Figure 18 – PMS carrier, simulation model and hardware

In-Flight Measurements of Loads on the Discus-2c Sailplane

The Discus-2c is a research aircraft used at the DLR as a reference aircraft to validate new in-flight identification methods and to benchmark the performance of new glider designs. A special feature of the Discus-2c of the DLR is its generous storage space for measurement electronics. The fuselage and the wings are fitted with over a dozen

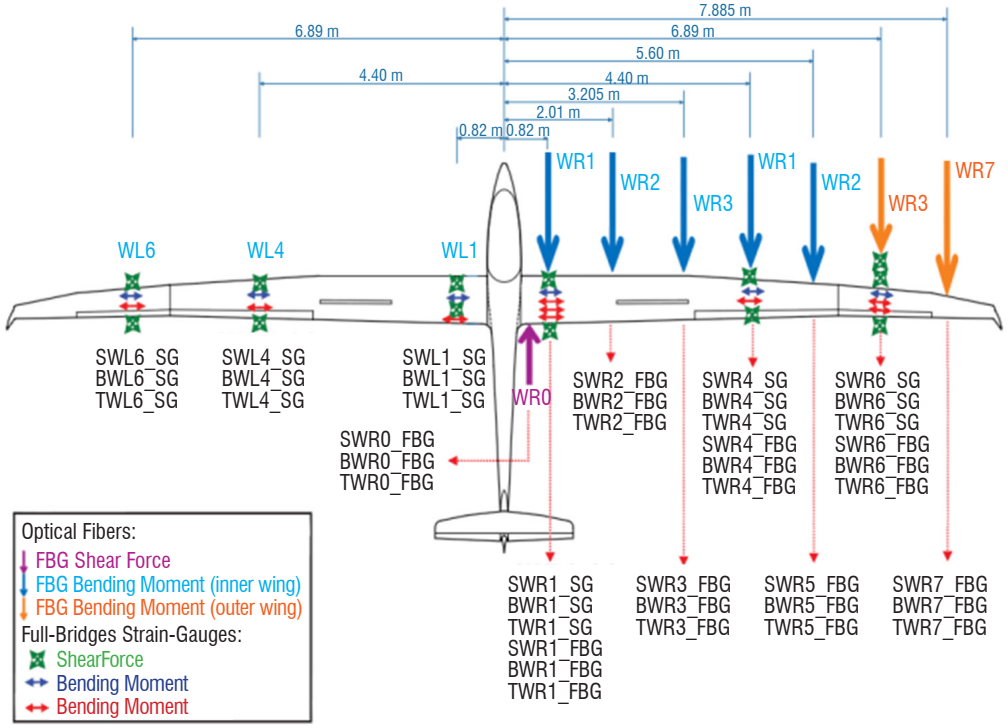

Figure 19 – Discus-2c in flight and positions of calibrated sensors for load measurements

strain gauges, designed to measure the load exerted under various flight conditions. The starboard wing also houses a fiber Bragg grating with glass fiber running along the spar. This system is used to make extremely precise wing-deflection measurements, see [40] and Figure 19.

Within the iLOADS project, an approach for in-flight load measurements has been developed by the Institute of Flight System Technology. An extensive calibration and flight-testing program was carried out. On the ground, the deflection of the wings and empennage under loads was measured with laser-interferometers at selected points. The strain gauges and Bragg grating were calibrated. In subsequent flight tests, maneuvers for longitudinal and lateral motion were performed at 396 test points in 22 flights.

With the experimental data, a real-time model for flight simulation was identified and approaches for the estimation of flight loads were developed. An integrated modelling approach takes the interaction between the rigid-body flight mechanics and structural dynamics into consideration. Simulations with the identified model show the quality of the identified model and can clearly illustrate the influence of elastic vibration modes on the quality of the simulated aircraft response. A close description of the flight tests and the results can be found in [8], [41] and [42].

Summary and Outlook

In the iLOADS project, a comprehensive DLR internal load loop was established. The load loop profits from the extensive know-how of the DLR institutes in various load analysis fields, from numerical simulation and experimental validation to flight testing. In the project, numerical methods were investigated, experiments on test rigs were performed, and in-flight load measurements were conducted.

Work continues on several DLR projects, with a focus on component loads including high lift, an automated load loop for multidisciplinary analysis using high-fidelity methods, and applications of the load process for various conventional and unconventional configurations. Other areas of interest for future activities are a dedicated process for component loads and the introduction of fatigue loads in the aircraft design assessment ■

Acknowledgements

The authors would like to thank all members of the project team for their dedication and commitment, and namely Sunpeth Cumnuantip, Gabriel Pinho Chiozzotto, Vega Handojo, Carsten Liersch, Martin Hepperle, Eric Breitbarth, Michael Besel, Marcus Vinicius Preisighe Viana, Julian Scherer, Martin Leitner and Reiko Müller for contributions to this paper. The authors explicitly refer to the papers describing all activities in more detail. Those publications have been mentioned in the text and are included in the list of references below. The authors also thank the DLR flight-test department and the program directorate for supporting the project, and specifically the flight-test campaigns.

References

[1] J. R. WRIGHT, J. E. COOPER - *Introduction to Aircraft Aeroelasticity and Loads.* 2nd edition, Wiley Aerospace Series, 2015.

[2] W. R KRÜGER, T. KLIMMEK - *Definition of a Comprehensive Loads Process in the DLR Project iLOADS.* Deutscher Luft und Raumfahrtkongress 2016, Paper ID 420105. Braunschweig, 2016. urn:nbn:de:101:1-201611183243.

[3] S. CUMNUANTIP, T. KIER, K. RISSE, G. PINHO CHIOZZOTTO - *Methods for the Quantification of Aircraft Loads in the DLR Project iLOADS.* Deutscher Luft und Raumfahrtkongress 2016, Paper ID 420145. Braunschweig, 2016. urn:nbn:de:101:1-201612161818.

[4] M. GEIER, D. KOHLGRÜBER, J. SCHWINN, E. BREITBARTH - *Definition und Anwendung eines Lastenprozesses zur Ableitung realistischer Bauteiltests im DLR-Projekt iLOADS.* Deutscher Luft und Raumfahrtkongress 2016, Paper ID 420219, Braunschweig, 2016. urn:nbn:de:101:1-201610075554.

[5] J. SCHWINN, D. KOHLGRÜBER, E. BREITBARTH, M. BESEL - *Biaxiale Versuche an rumpfstrukturnahen Proben mit realistischen Lastannahmen.* Deutscher Luft- und Raumfahrtkongress 2016, Paper ID 420154, Braunschweig, 2016. urn:nbn:de:101:1-201609303582.

[6] T. KLIMMEK, P. D. CIAMPA, V. HANDOJO, P. OHME, M.V. PREISIGHE VIANA - *Aircraft Loads - An Important Task from Pre-Design to Loads Flight Testing.* Deutscher Luft- und Raumfahrtkongress 2016, Paper ID 420223, Braunschweig, 2016. urn:nbn:de:101:1-201703036117.

[7] J. SINSKE, Y. GOVERS, V. HANDOJO, W.R. KRÜGER - *HALO Flugtest mit instrumentierten Außenlasten für Aeroelastik- und Lastmessungen im DLR Projekt iLOADS*. Deutscher Luft und Raumfahrtkongress 2016, Paper ID 420276. Braunschweig, 2016. urn:nbn:de:101:1-201609303750.

[8] P. OHME, C. RAAB, M. V. PREISIGHE VIANA - *Lastenmessung im Flugversuch und Entwicklung echtzeitfähiger Simulationsmodelle.* Deutscher Luft- und Raumfahrtkongress 2016, Paper Nr. 0052, Braunschweig, 2016.

[9] T. PFEIFFER, E. MOERLAND, D. BÖHNKE, B. NAGEL, V. GOLLNICK - *Aircraft Configuration Analysis Using a Low-Fidelity, Physics Based Aerospace Framework under Uncertainty Considerations*. Proc. 29th Congress for the Aeronautical Sciences, St. Petersburg, Russia, 2014.

[10] W.R. KRÜGER, T. KLIMMEK, R. LIEPELT, H. SCHMIDT, S. WAITZ, S. CUMNUANTIP - *Design and Aeroelastic Assessment of a Forward-Swept Wing Aircraft.* CEAS Aeronautical Journal, 5 (4), pp. 419-433. Springer Vienna, 2014. DOI: 10.1007/s13272-014-0117-0.

[11] J. NEUMANN, H. MAI - *Gust Response: Simulation of an Aeroelastic Experiment by a Fluid-Structure Interaction Method.* Journal of Fluids and Structures 38, pp. 290-302, April 2013. DOI: 10.1016/j.jfluidstructs.2012.12.007.

[12] M. LEITNER, R. LIEPELT, T. KIER, T. KLIMMEK, R. MÜLLER, M. SCHULZE - *A Fully Automatic Structural Optimization Framework to Determine Critical Design Loads.* Deutscher Luft- und Raumfahrtkongress 2016, Paper ID 420186, Braunschweig. urn:nbn:de:101:1-201611041880.

[13] W. R. KRÜGER, A. BERARD, R. DE BREUKER, K. HAYDN, M. REYES - *Adaptive Wing: Investigations of Passive Wing Technologies for Loads Reduction in the CleanSky Smart Fixed Wing Aircraft (SFWA) Project.* GREENER AVIATION 2016, Brussels, Belgium, 11-13 Oct., 2016.

[14] AeroGust (Aeroelastic Gust Modelling). http://www.aerogust.eu. Last visited 20-04-2018.

[15] T. L. LOMAX - *Structural Loads Analysis Theory and Practice for Commercial Aircraft Structural Loads Analysis: Theory and Practice for Commercial Aircraft.* AIAA Education Series, Washington, 1996.

[16] F. M. HOBLIT - *Gust Loads on Aircraft: Concepts and Applications.* AIAA Education Series, Washington, 2001.

[17] H. HOWE - *Aircraft Loading and Structural Layout.* AIAA Education Series, Washington, 2004.

[18] Federal Aviation Administration, Airworthiness standards - Transport category airplanes, FAA, 14 CFR Part 25, 2010.

[19] European Aviation Safety Agency, Certification Specifications for Large Airplanes CS-25, ED Decision 2010/013/R (2010).

[20] M. NEUBAUER, G. GÜNTHER - *Aircraft Loads.* RTO/AVT Lecture Series on "Aging Aircraft Fleets: Structural and Other Subsystem Aspects". RTO-EN-015-09, 2000.

[21] E. MOERLAND, T. ZILL, B. NAGEL, H. SPANGENBERG, H. SCHUMANN, P. ZAMOV - *Application of a Distributed MDAO Framework to the Design of a Short- to Medium-Range Aircraft.* 61th German Aerospace Congress (DLRK), Berlin, Germany, 2012.

[22] O. BRODERSEN - *Drag Prediction of Engine-Airframe Interference Effects Using Unstructured Navier-Stokes Calculations.* Journal of Aircraft, Vol. 39, No. 6, 2002.

[23] DLR-Aircraft Fleet: http://www.dlr.de/dlr/en/desktopdefault.aspx/tabid-10203/. Last visited 20-04-2018.

[24] ANSYS: http://www.ansys.com/Products/Structures. Last visited 20-04-2018.

[25] MSC.NASTRAN: http://www.mscsoftware.com/de/product/msc-nastran. Last visited 20-04-2018.

[26] T. GERHOLD - *Overview of the Hybrid RANS Code TAU.* MEGAFLOW-Numerical Flow Simulation for Aircraft Design, edited by Kroll, N. and Fassbender, J. K., Vol. 89 of Notes on Numerical Fluid Mechanics and Multidisciplinary Design, Springer, Berlin and Heidelberg, Germany, pp. 81-92, 2005.

[27] J. HOFSTEE, T. KIER, C. CERULLI, G. LOOYE - *A Variable, Fully Flexible Dynamic Response Tool for Special Investigations (VarLoads).* International Forum on Aeroelasticity and Structural Dynamics, 2003.

[28] T. FÜHRER, C. WILLBERG, S. FREUND, F. HEINECKE - *Automated Model Generation and Sizing of Aircraft Structures.* Aircraft Engineering and Aerospace Technology: An International Journal, Vol. 88, Iss: 2, pp. 268-276, 2016. DOI: 10.1108/AEAT-02-2015-0057.

[29] J. SCHERER, D. KOHLGRÜBER, F. DORBATH, M. SOROUR - *A Finite Element based Tool Chain for Structural Sizing of Transport Aircraft in Preliminary Aircraft Design*. Deutscher Luft- und Raumfahrtkongress 2013, Stuttgart, DocumentID: 301327.

[30] HyperSizer: http://hypersizer.com/. Last visited 20-04-2018.

[31] X. HUANG, T. MOAN - *Improved Modeling of the Effect of R-Ratio on Crack Growth Rate.* International Journal of Fatigue, 29, pp. 591-602, 2007.

[32] G. BUSSU, P. IRVING - *The Role of Residual Stress and Heat Affected Zone Properties on Fatigue Crack Propagation in Friction Stir Welded 2024-T351 aluminium joints.* International Journal of Fatigue, 25, 77-88, 2003.

[33] German Aerospace Center (DLR): *CPACS – A Common Language for Aircraft Design*. https://software.dlr.de/p/cpacs/home/. Last visited 20-04-2018.

[34] K.-H. HORSTMANN - *Ein Mehrfach-Traglinienverfahren und seine Verwendung für Entwurf und Nachrechnung nichtplanarer Flügelanordnungen.* Ph.D. Dissertation, Technical University of Braunschweig, Braunschweig, Germany, 1987; see also: Tech. Rep. FB 87-51, DFVLR, Braunschweig, Germany, 1987.

[35] VSAERO: http://www.ami.aero/software-computing/amis-computational-fluid-dynamics-tools/vsaero/ Last visited 20-04-2018.

[36] J. ROSKAM - *Airplane Design Part IV: Layout Design of Landing Gear and Systems.* Roskam Aviation and Engineering Corporation, Kansas, 1986.

[37] W. KRÜGER, M. MORANDINI - *Recent Developments at the Numerical Simulation of Landing Gear Dynamics.* CEAS Aeronautical Journal, 1 / 2011 (1-4), pp. 55-68, Springer, 2011.

[38] W. R. KRÜGER, V. HANDOJO, T. KLIMMEK - *Flight Loads Analysis and Measurements of External Stores on an Atmospheric Research Aircraft.* 58th AIAA/ASCE/AHS/ASC Structures, Structural Dynamics, and Materials Conference. AIAA SciTech Forum and Exhibition 2017, 9-13 January 2017, Grapevine, Texas. DOI: 10.2514/6.2017-1828.

[39] G. JELICIC, J. SCHWOCHOW, Y. GOVERS, J. SINSKE, R. BUCHBACH, J. SPRINGER - *Online Monitoring of Aircraft Modal Parameters during Flight Test based on permanent Output-only Modal Analysis.* 58th AIAA/ASCE/AHS/ASC Structures, Structural Dynamics, and Materials Conference. AIAA SciTech Forum and Exhibition 2017, 9-13 January 2017, Grapevine, Texas, USA. DOI: 10.2514/6.2017-1825.

[40] Discus-2C DLR: http://www.dlr.de/dlr/en/desktopdefault.aspx/tabid-10203/339_read-9181/#/gallery/8791. Last visited 20-04-2018.

[41] M. V. PREISIGHE VIANA - *Time-Domain System Identification of Rigid-Body Multipoint Loads Model.* American Institute of Aeronautics and Astronautics (AIAA). Atmospheric Flight Mechanics Conference. Paper AIAA-2016-3706, Washington D.C., United States of America, June 2016. http://dx.doi.org/10.2514/6.2016-3706.

[42] M. V. PREISIGHE VIANA - *Sensor Calibration for Calculation of Loads on a Flexible Aircraft*. International Forum on Aeroelasticity and Structural Dynamics (IFASD), Paper No IFASD-2015-042, Saint Petersburg, Russia, 2015.

AUTHOR

Wolf Krüger obtained the Engineering degree in mechanical engineering from the Technical University of Braunschweig, Germany. From 1994 to 2004 he worked at the German Aerospace Center (DLR) at the Department for Vehicle Dynamics in Oberpfaffenhofen. In 2000, he received his Ph.D. degree in Aerospace Engineering at the University of Stuttgart, Germany. Since 2004, Wolf Krüger works at the DLR Institute of Aeroelasticity in Göttingen, where he is heading the Department for Loads Analysis and Aeroelastic Design. He is a professor for Multibody Dynamics in Aerospace at the Technical University of Berlin where he also teaches Aeroelasticity. Wolf Krüger's research interests include multibody dynamics, aircraft loads analysis, aircraft ground dynamics and multidisciplinary simulation.

Pier Davide Ciampa works as a research assistant at the DLR Institute of System Architectures in Aeronautics in Hamburg, Germany.

Martin Geier received his Diploma degree in mechanical engineering with specialization in the field of aerospace engineering from the TU Braunschweig, Germany in 2011. He is currently a research assistant at the German Aerospace Center (DLR) in Braunschweig working on lightweight structure design within the preliminary aircraft design process.

Thiemo Kier: After receiving a Master's degree from the University of Washington, Seattle, USA and a Dipl.-Ing. degree from University of Stuttgart, Germany, Thiemo Kier worked for Fairchild Dornier GmbH in the loads department on the 728 aircraft development program. In 2002 he joined the German Aerospace Center (DLR). Currently, he holds the position as a group leader of the Flight Dynamics and Loads team at the Institute of System Dynamics and Control. His research interests focus on Multidisciplinary Aircraft Model Integration for Loads Analysis and Flight Dynamics Simulations.

Thomas Klimmek is research scientist and team leader at DLR Institute of Aeroelasticity in Göttingen. He received his Diploma in Mechanical Engineering in from the University of Siegen in 1997 and his Ph.D. from the Technical University of Braunschweig in 2016. He research is focused on aeroelastic design using structural and multidisciplinary optimization methods and the loads analysis for aircraft configurations.

Dieter Kohlgrüber graduated from University of Stuttgart in 1993 and got the diploma degree in aeronautical engineering. He joined DLR Institute of Structures and Design (BT) with the focus on crash research on aircraft structures and later also on predesign of aircraft structures. Currently he is team leader on aircraft predesign and deputy head of the department "Structural Integrity" of the Institute BT.

Per Ohme graduated in Aerospace Engineering from TU Berlin in 2006 and joined the DLR Institute of Flight Systems in the same year. He worked as research engineer in the fields of flight mechanics, aircraft performance, flight data analysis, aircraft system identification, modelling and simulation. In 2010 he became leader of the modelling and simulation team and gathered experience as manager of several research cooperations with industry and other scientific institutions. From 2011 to 2016 he was manager of two comprehensive research projects related to aircraft icing. Since 2017 he is acting head of the flight dynamics and simulation department.

Kristof Risse studied aerospace engineering at RWTH Aachen University. In 2016, he received the Ph.D. degree for his dissertation on overall aircraft design with hybrid laminar flow control. After his work in a joint contract between the German Aerospace Center (DLR) and Airbus on the design of wing and movables, he is now in charge of the DLR Virtual Product House in Bremen and coordinates the field "digitisation in aeronautics" for the DLR executive board.

Julian Schwinn joined the Institute of Materials Research at the German Aerospace Center (DLR) in Cologne in 2011. His research interests focus on fracture mechanics, mechanical testing with supporting finite element simulation, especially biaxial testing of aluminium alloys and fibre metal laminates for aerospace applications. He received the diploma degree of mechanical engineering at the University of Paderborn.

R. M. Botez
ETS-Research Laboratory in Active Controls, Avionics and Aeroservoelasticity (LARCASE)

E-mail: ruxandra.botez@etsmtl.ca

DOI: 10.12762/2018.AL14-02

Morphing Wing, UAV and Aircraft Multidisciplinary Studies at the Laboratory of Applied Research in Active Controls, Avionics and AeroServoElasticity LARCASE

Several large-scale projects were carried out at the LARCASE at ÉTS in numerical studies and experimental tests for morphing aircraft using three equipments. In this article, these projects are explained. First, two projects have been carried out at LARCASE on morphing wing studies in collaboration with industrial and research institutes teams. The first project was carried out in collaboration with aerospace companies, such as Bombardier Aerospace, Thales Canada, the Institute of Aerospace Research – National Research Council of Canada IAR-NRC, and École Polytechnique. The second project was carried out internationally as it took place with the same Canadian partners as those involved in the first project, but it also took place in collaboration with Italian partners of Alenia, CIRA and University of Naples – Frederico II. In these two projects, two morphing wings were designed, and then manufactured and equipped with several actuators and pressure sensors. These morphing wings designed to improve their aerodynamic performance were then tested in the IAR-NRC wind tunnel. The LARCASE Price-Païdoussis wind tunnel was used for the design and experimental testing of the ATR-42 model aircraft morphing wing models. Numerical results have been obtained following morphing studies of autonomous aerial systems UAS-S4 or S-45. Other morphing type concepts were also applied to the wings and horizontal tail of the Cessna Citation X business aircraft in order to reduce fuel consumption and flight distance.

Introduction

Research programs have been launched, and continue to be conducted in Europe (such as Clean Sky, CleanSky2, Smart Intelligent Aircraft Structures SARISTU [1] - [7]), Canada (the Green Aviation Research and Development Business-Led Network of Centres of Excellence (GARDN BL-NCE), Japan, USA with the aim to achieve the most efficient green aircraft technologies possible in terms of minimum fuel or bio-fuel consumption, lower emissions, reduced noise, etc.

The LARCASE at the ETS is equipped with the following three major research equipments shown in Figure 1: 1. the Price-Païdoussis subsonic blown wind tunnel from McGill University (on the upper left hand side of Figure 1), 2. the Research Aircraft Flight Simulator (RAFS) for the Cessna Citation X business aircraft from CAE Inc. (on the upper right hand side of Figure 1), and 3. the Research Aerial System (RAS) from Hydra Technologies (on the bottom side of Figure 1). These equipments were and continue to be used in the morphing aircraft numerical and experimental research. The LARCASE website can be consulted at https://en.etsmtl.ca/Unites-de-recherche/LARCASE/Accueil?lang=en-CA.

The Price-Païdoussis subsonic blow down wind tunnel is powered by a 40 HP, 67 Amps electrical engine, from North Western Electric Co. and is fitted with a double impeller centrifugal fan. The test chambers

Figure 1 – Illustration of the LARCASE equipment

are manufactured from wood, with Plexiglas removable doors on each side, for greater accessibility to the models installed inside. The biggest test chamber has dimensions of 0.62 x 0.91 x 1.83 m (H x W x L), and the maximum speed that can be obtained is of 40 m/s, equivalent to a Mach number of 0.12, with a maximum Reynolds number of 2.4 million. The smallest of the two test chambers has the dimensions of 0.31 x 0.61 x 1.22 m (H x W x L), and the maximum speed is of 61 m/s. equivalent to a Mach number of 0.18 at a Reynolds number of 3.5 million. Reynolds numbers were calculated using a chord of 0.8 m, which is the maximum chord that a model can have, in order to be tested in either of these two test chambers. The wind tunnel's turbulence level is approximately 0.3, that corresponds to a critical amplification factor of 5.5 for the XFoil solver analysis.

The second equipment is the Research Aircraft Flight Simulator (RAFS) that was designed and manufactured by the well-known aircraft modeling and simulation company CAE Inc. for the research needs of the LARCASE. The RAFS is equipped with the highest level of certification D flight dynamics toolbox for the Cessna Citation X business aircraft. The RAFS and the third equipment UAS-S4 were both acquired with research funds from the MDEIE and NSERC.

The third equipment is called the Research Aerial System (RAS), and is composed of an Unmanned Aerial Vehicle (UAV) aircraft, an UAV airframe/trainer aircraft, a fully portable ground control station, autopilot hardware and software and a replacement parts kit. The RAS is in fact a modified version of an existing manufactured UAS-S4 called God of Winds. The RAS has an approximate fuselage length of 9.84 ft and a wingspan of 14.76 ft. It may fly at a maximum speed of 90 knots at an altitude of 15,000 ft, and has a maximum take-off weight of 132 lbs. Hydra Technologies, a private Mexican company specialized in the development of unmanned aerial systems for military, police and civil applications, has built the RAS accordingly to the research needs of the LARCASE.

Different major projects took place at the LARCASE in the area of morphing aircraft numerical and experimental studies by use of the three equipments above mentioned. In this paper, these projects will be explained. Firstly, two major projects took place at the LARCASE at the ETS on morphing wing studies in collaboration with industrial and research institutes partners since 2016. The first project took place in collaboration with teams from major Aerospace companies: Bombardier Aerospace, Thales Canada, the Institute of Aerospace Research – National Research Council of Canada IAR-NRC, École Polytechnique. The second project was international as it took place with same partners as the ones mentioned in the first project, but in addition, took place in collaboration with Italian partners from Alenia, CIRA and Federico II – University of Naples. In both projects, two different morphing wings were equipped with various actuators and pressure sensors. These wings were designed, manufactured, and further they were tested using experimental wind tunnel tests at the IAR-NRC with the aim to improve their aerodynamic performances.

In the frame of the Canada Research Chair in Aircraft Modeling and Simulation Technologies, other projects took place. For example, the Price-Païdoussis subsonic blow down wind tunnel was used for design, manufacturing and testing of reduced scale morphing wing models, such as the ATR-42 model. At this time, numerical results were obtained for other reduced wing scale models of the UAS-S4 or S-45. In addition, morphing concepts were applied also on the Cessna Citation X business aircraft wing and horizontal stabilizer with the aim to reduce fuel consumption and the distance.

Explanation of projects at the LARCASE

As mentioned in the Introduction, the LARCASE is equipped with 3 infrastructures shown in Figure 1 and explained above. All these equipments are used for the morphing wing technologies development projects explained next.

Project 1. CRIAQ 7.1 – Laminar flow improvement on an aeroelastic research wing (Morphing Wing equipped with Smart Material Actuators and Pressure Sensors)

In this project, presented in [8], the analyzed wing had its dimensions of 0.5 m x 0.9 m, and its reference airfoil was chosen to be that of a laminar Wing Trailing Edge Airfoil (WTEA). The aerodynamic characteristics and performance were analyzed in transonic regime in a previous project and published (Khalid 1993; Khalid and Jones 1993). Three different teams worked on this project in the areas of aerodynamics, structures and controls. The project took place during a period of three years: 1. design, 2. manufacturing, 3. wind tunnel testing.

During the first year period, the aerodynamics and structures teams worked together to find the optimized shapes of the wing airfoil for aerodynamic performance improvement, thus for flow transition towards the airfoil trailing edge. The reference airfoil modified its shape for different flow cases in two specific points of actuation located at 25.3% and 47.6% of the chord with respect to the leading edge of the airfoil. These flow cases were expressed by 7 angles of attack between -1˚and 2˚, and five Mach numbers, between 0.2 and 0.3, thus 35 optimized airfoils were defined [9]. As shown in Figure 2, the morphing wing consisted of two main parts: 1. one fixed part and 2. one morphing part. The morphing part was manufactured from a flexible skin that was installed on the wing upper surface, and was equipped with two lines of nickel-titanium shape memory alloys actuators (SMA) that were located at the positions mentioned above, at 25.3% and 47.6% of the chord. The flexible skin had a thickness of 1.3 mm, a Young modulus of

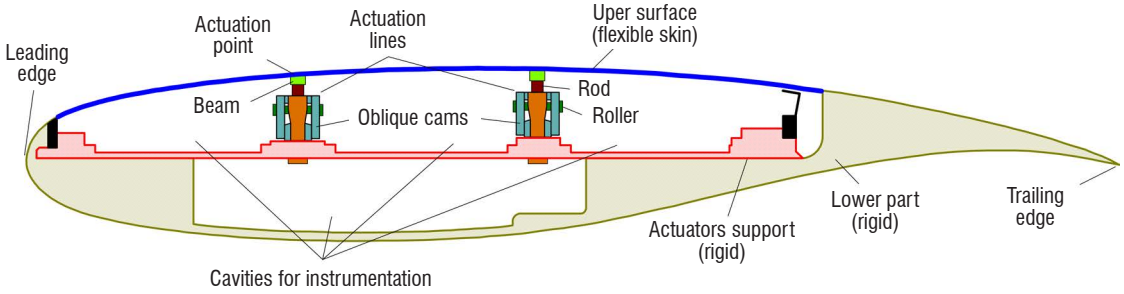

Figure 2 – Morphing wing model – cross section

60 GPa and the Poisson's ratios of 0.12 for the carbon/Kevlar® hybrid and 0.25 for the unidirectional carbon [10].

The horizontal motion that took place along the wing span was converted by the actuation system into vertical motion that was perpendicular to the chord. Therefore, as shown in Figure 3, the actuation system comprised two oblique cams with sliding rods, span-wise positioned.

Each actuator could move up or down with a certain distance smaller than 8 mm with respect to its original position in order to obtain each one of the 35 optimized airfoils. This actuation distance for each airfoil (obtained in two points) was given by the mechanical equilibrium between the SMA wires and the gas springs; the SMAs pulled the sliding rod in one direction, while the gas pulled the springs in the opposite direction. Three parallel SMA wires were connected to a power supply, and thus used to actuate each sliding rod.

The morphing wing control system has an open loop, and a closed loop architecture. In the open loop, the SMA system of actuation was controlled, while in the closed loop, the open loop architecture was included as an internal loop, and the transition region was controlled based on the 32 pressure sensors measurements. These 32 pressure sensors were actually of two types: optical and kulite sensors, and they were of course installed on the upper surface morphing wing skin with the aim to measure the pressures on the morphing wing. In fact, the flow transition was detected at frequencies between 3 kHz and 5 kHz by kulite sensors while the optical sensors were unable to detect it [10]. The Root Mean Square (RMS) method was used to visualize the transition from the laminar to turbulent flow because of the fact that is based on the pressure fluctuation increase in turbulent flow, while in the laminar flow they are of the order of 5e-4 Pa. The occurrence of a spike in the RMS plot in the array of sensors indicates the occurrence of the turbulence in that sensor location, and thus in the location of the transition between that sensor and the previous one in the array.

A second method to measure the flow transition used infrared measurements instead of pressure sensors measurements. An example of transition flow measurement is shown for one optimized airfoil with respect to the reference airfoil for one of the 35 flow cases, and is expressed in change of colours as seen on Figures 4.a, and 4.b. While the flow transition was found at the location of 26% of the chord ($x/c = 26\%$) for the reference airfoil (Figure 4.a), the flow transition was found for the optimized airfoil at the $x/c = 58\%$; thus, the transition was moved by up to 32% of the chord over the reference case for the optimized airfoil (Figure 4.b).

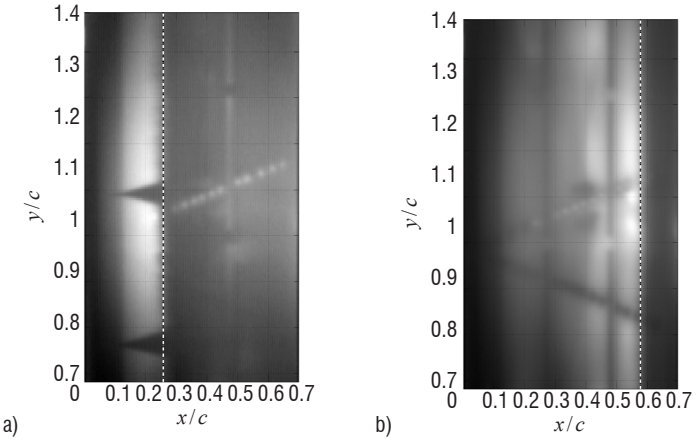

Figure 4 – Infrared results obtained at $M = 0.25$ and $\alpha = 0.5$ deg in a) reference, and b) after optimization

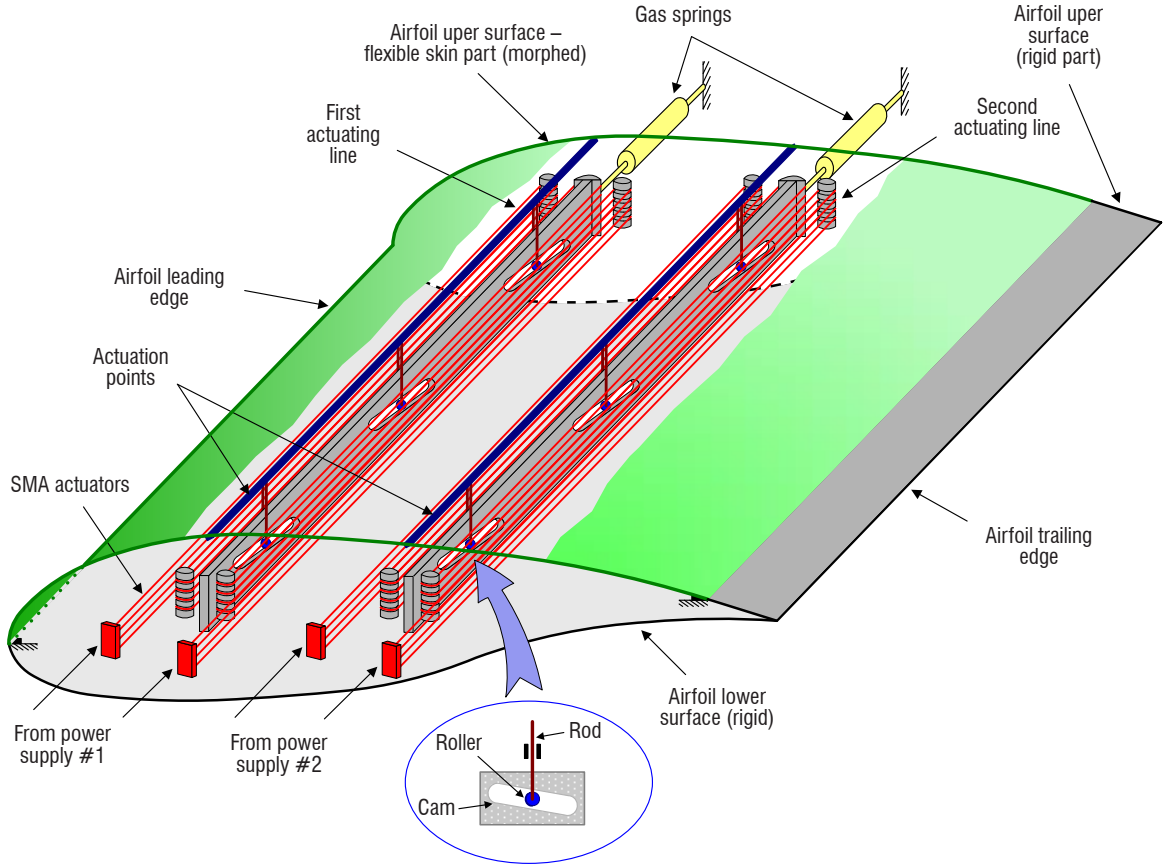

Figure 3 – Actuation system of the morphing wing

The same types of results were obtained for all the other 34 cases corresponding to optimized airfoils in terms of transition location moving closer to the airfoil trailing edge by a maximum of 40% of the chord. This transition delay will result evidently in drag, and thus, in fuel consumption reduction ([9], [11]-[14]).

Numerical simulations, bench tests and wind tunnel tests were performed to design, improve and validate experimentally the morphing wing control system ([11]-[19]). A high number of control methodologies were developed and applied in this project for the open loop and closed loop, based on Adaptive Neuro-Fuzzy Inference System ANFIS ([19]), Hybrid Fuzzy Logic Proportional Integral Derivative and Conventional On-Off Controller ([17],[18]), On-Off and Proportional-Integral Controller ([15],[16]), and Real Time Optimization ([9]). The aeroelastic analysis of the flexible wing upper skin was performed using MSC/Nastran software. This analysis showed that flutter has occurred at the Mach number of 0.55 higher than the Mach number of 0.3, the maximum Mach number allowed in the IAR-NRC wind tunnel. For this reason, the wind tunnel tests were performed safely [20].

The smart material actuators had low frequencies and high operating temperatures which make them difficult to be considered for their implementation on an aircraft ([15]-[19], ([21],[22]). For this reason, the Canadian industrial teams from Bombardier and Thales have launched a second major project at the LARCASE in which electrical actuators were considered instead of smart material actuators; the electrical actuators can be implemented on aircraft as they do not present the disadvantages of the smart material actuators.

Project 2. CRIAQ MDO 505 - Morphing architectures and related technologies for wing efficiency improvement

While in project 1, a morphing wing box concept was developed, in project 2, an existing aircraft wing-tip was developed with the aim to increase the Technical Readiness Level (TRL) of such type of device. Both multidisciplinary projects 1 and 2 required interactions between aerodynamic, structural and controls teams. The full-size wing-tip structure was formed by a morphing wing and two types of ailerons: a conventional rigid aileron and a morphing aileron.

The full-scale morphing wing model had a span of 1.5 m and a root chord of 1.5 m, a taper ratio of 0.72, and leading and trailing edges sweep angles of 8°. The chord distribution of the wing model followed the distribution of the wing-tip section, while the sweep angle and the span-wise twist distribution were modified in order to reduce the 3D flow effects. The wing box and its internal structure (spars, ribs, and lower skin) were manufactured from aluminum alloy, while the adaptive upper surface, which was located between 20% and 65% of the wing chord, was manufactured from carbon fibre composite materials.

The upper skin shape morphing, driven by actuators placed inside the wing box structure was a function of the flight condition (defined in terms of Mach number, Reynolds number and angle of attack). These actuators were specifically designed and manufactured in-house to meet the project requirements. Four electrical actuators were installed on two actuation lines; two actuators each, placed at 37% and 75% of the wing span, were fixed to the ribs and to the composite skin. Each actuator has the ability to operate independently from the others, and has a displacement range between ± 3.5 mm. On each actuation line, the actuators were positioned at 32% and 48% of the local wing chord.

The aileron hinge articulation was located at 72% of the chord. As mentioned above, two ailerons were designed and manufactured. One aileron was structurally rigid, while the other one represented a new morphing aileron concept. Both ailerons were designed to be attached to the same hinge axis of the wing box, and both were able to undergo a controlled deflection between -7° and +7°. This interval was more restricted than the normal deflection range of an aileron, but it was considered sufficient to demonstrate the proof of concept for the morphing aileron. This restriction was determined by the available space inside the NRC wind tunnel and by the load limits of the wind tunnel balance.

The aerodynamic objectives of the optimized shapes of the upper surface of the morphing wing and the rigid aileron assembly were to delay the onset of the flow transition region, and to reduce the drag coefficients. The objectives of the optimized shapes of the upper surface of the morphing wing and the morphing aileron had the aim to improve the lift coefficient, and thus the behavior of the boundary layer.

The optimized shapes were found through a 2D (airfoil) aerodynamic analysis because of the fact that in the beginning of the project bi-dimensional characteristics of the flow were expected to occur in the morphing upper surface skin of the wing located between the central ribs. The skin was clamped on all sides of the wing, and had the dimensions of 60 cm along the span and 55 cm along the chord; the first actuation line was installed at 56 cm from the wing root, while the second actuation line was installed at approximately 117 cm from the root.

An in-house Genetic Algorithm GA was developed as function of morphing wing structure and aileron (rigid and morphing) constraints or requirements with the aim to obtain the optimized airfoils. Following the comparison of the results obtained with the GA with the results obtained with both the Artificial Bee Colony (ABC) algorithms and the Gradient Method, the GA was selected due to the fact that results were better. Then, a coupling of the GA with a cubic spline reconstruction routine and the 2D XFoil solver was done in order to evaluate the model aerodynamic performances. Thus, optimized airfoils were obtained for a high number of different airspeeds (Mach numbers), angles of attack and aileron deflection angles. The results showed a flow transition onset improved by up to 10% of the chord, a lift improvement by up to 50% on average, and a maximum of 70% by using a morphing aileron ([23],[24]).

In addition to the 2D analysis, a 3D analysis was performed using ANSYS Fluent after establishing the wind tunnel matrix cases with the aim to compare the 2D with the 3D results. The analysis used the numerical wing for the first analyses, and after the first set of wind tunnel tests, its scanned shapes were used, and so on. Following the comparison of the 2D with 3D results, it was found that the transition region was over-estimated by XFoil (2D) solver with 2-3% of the chord [25].

A delay of the flow transition from the laminar to the turbulent state of up to 5% of the chord was found experimentally during wind tunnel tests, which resulted in drag reduction by up to 2%. In addition, drag reduction was found also where transition was not observed.

An example is the over-estimation of the transition region by the numerical optimization for almost all cases (146 cases for all three sets of wind tunnel tests).

The experimental pressures measured by kulite sensors had the same values as the numerically-calculated pressures by XFoil or ANSYS solvers, and the aerodynamic performances were therefore improved.

The design and manufacturing of the composite upper surface of the morphing wing, of the rigid and morphing ailerons was one of the structural work objectives. This composite skin had specific elastic properties on its both chord and span directions, which ensured the flexibility needed by the morphing upper surface, while respecting the design, manufacturing and structural requirements demanded by the industrial partners. Another achieved objective was closely related to the design, manufacturing and testing of the internal morphing system. This system included actuators and sensors needed for the structural bench testing, and for the wind tunnel tests ([26], [27], [31]).

The structural and the aerodynamic teams needed to interact closely during the project for the design, and mainly for the optimization of the morphing skin. The optimization gave the number, thickness and distribution of plies/fibres that were chosen for the composite morphing skin modeling. The main result of this optimization was quantified in terms of the composite skin flexibility that was tested through morphing by both structural and controls teams. Therefore, control bench testing was performed at the LARCASE in the absence of the wing to ensure obtaining the morphed required shapes.

In addition, 1 g loads tests were performed to test the behavior of the wing under static conditions. These 1 g loads corresponded to in-flight loadings that a wing structure would encounter, and allowed the observation of the static behaviour of the actively morphing wing under loading; the 1 g load tests were successful, as the wing tip structure passed these tests under both morphed and un-morphed conditions. The scans performed during the tests have shown that no bending deformations were detected beyond the ones considered as expected and safe.

The wing-tip internal and external structure were slightly modified to accommodate the actuation and pressure sensors systems, and to correspond to the wind tunnel dimensions. The maximum dimensions of the wing model were determined also as function of the length, width and height of the wind tunnel. Since the wind tunnel chamber dimensions were fixed, if there were any inconsistencies between the wind tunnel and the model, then the model was designed to fit within the wind tunnel dimensions. Any modification of the geometry was slight, not something radical or necessary visible in any way. The wing tip was manufactured at the IAR-NRC in Ottawa. For the wing manufacturing, the requirements regarding the precision of manufacturing techniques were provided by Bombardier.

Furthermore, the optimization of the upper surface composite skin led to a gain of approximately 2 kg on the total wing tip weight (without the actuation system installed). Overall, the wing tip equipped with the composite upper surface, internal actuation system and aileron had its weight similar to the original base aluminium wing tip. The fully equipped morphing wing without aileron weighted approximately 60 kg, while the aileron weighted approximately 18 kg.

In addition, due to the displacements and forces requirements, the actuation system was developed (design and manufacturing) from the beginning of the project. In the beginning of the project, the actuators displacements were set at +/- 10 mm. After performance of preliminary analyses, the displacements were lowered to 5 mm in order to reduce the forces needed to displace the skin. Finally, the requirements for the actuators were: to have a displacement of +/- 5 mm (a total of 10 mm), to develop forces of up to 2,000 N and to have dimensions that would allow them to fit inside the wing box. In project 1, the actuators have the maximum displacements of +/- 8 mm. An analysis of the "off-the-shelf" actuator market has shown that this type of actuator was not on the market ([28],[29]).

Therefore, four electrical actuators were designed and manufactured in-house at the ETS, and they have met the constraints of size, displacements, forces and safety as required by the project team. The displacement targets resulted from the aerodynamic optimization, and the associated force magnitudes resulted from the structural analysis of the wing with its upper surface morphed with the maximum allowed displacements.

The maximum values of the actuators displacements were chosen in the beginning of the project (the 10 mm values) following aerodynamic optimization, and the subsequent values (smaller than 10 mm) were established by structural analysis and manufactured wing capabilities. Therefore, since the actuators had to respect security requirements, the values determined by the structural analysis were considered as the maximum allowed displacements.

A rigid aileron was also designed and manufactured by the NRC team. The aileron met the constraints set by Bombardier, and was activated by using an external actuation system. The external actuator was mounted on the wing's mounting block. This actuator was constrained to perform limited deflections, between 7 degrees down and 7 degrees up with a step of 1 degree, because of the limited available space inside the wind tunnel testing chamber.

From control systems point of view, the objectives were the design and implementation of an integrated control system that connected the wing tip pressure sensors, electrical actuators and aileron external actuator. The control system was developed using the data calculated from the aerodynamic optimization. The control system developed during this project respected all the constraints for safety and certification requirements demanded by the Thales Canada team.

The control system implemented four (4) interchangeable controllers for the actuator displacements control. The four controllers were based on Proportional Integral Derivative (PID), Fuzzy-Logic and Neural Network control algorithms. All these controllers used both external and internal data from the skin and the actuators to calibrate the system to the desired precision of 0.2 mm. Scans performed at the NRC and LARCASE wind tunnel facilities after each wind tunnel test showed that the controllers achieved the desired actuators displacements and their precisions for each studied flight case.

The main controller (part of the integrated communication and control system) was developed as a PID controller, as per Thales Canada recommendations. The integration of controllers on the whole National Instruments (NI) system was a step forward to an embedded system for morphing wing as required by Thales. Therefore, the control and communication systems were developed following Thales requirements, and in collaboration with NI, that pushed the high morphing technology to a high TRL. In addition, different other linear and nonlinear algorithms were developed (as mentioned at the ETS previously) to analyze the obtained results – for comparison purposes, and they were integrated also on the NI system.

It is also important to understand that the controller has to operate in wind tunnel conditions so it needed to be robust, easy, automatic and safe to manipulate. The controller had to solve (minimize or eliminate) the uncertainties of all other disciplines. The controllers were tested

in wind tunnel, and on a wing model based on a real aircraft wing tip. The results obtained by different methodologies, and their performance were compared with those obtained by the PID controller.

The controllers and the full control system were bench tested using an aluminium skin in the design phase, and a composite skin (identical to the one installed on the wing tip demonstrator) in the final phases of the design and development of the morphing wing. For the development of the control system, "off-the-shelf" and "user-defined" designed parts were used, as well as commercial and "in-house" software.

The control system was validated using the wind tunnel tests results, which showed that it was fast, reliable and robust. The precision of the controllers was validated with static high precision scans of the upper-surface composite skin after each of the three sets of wind tunnel tests. Figure 5 and Figure 6 show the morphing upper surface and ailerons integration that can achieve the desired shapes obtained during numerical optimization. No winglet is considered in this project.

From the point of view of the morphing aileron system, the objective was the design, manufacture and testing of an aileron capable of changing its shape while deflecting with certain angles in order to improve the lift performances of the wing. The morphing aileron had to respect geometrical and deflection requirements. The deflection angles were provided by the Canadian team along with the aileron shapes to the Italian team. The Italian team developed an aileron that respected the geometrical and wing box installation requirements, and this aileron was capable of morphing during tests ([30], [32]).

Figure 7 presents the morphing wing model concept as it was mounted and tested in the NRC subsonic wind tunnel. Figure 8 presents an overview of the morphing wing control system. The wing was equipped with 32 kulite pressure sensors installed on two parallel staggered lines at 60 cm from the root of the wing. Three accelerometers were installed on the wing: on the wing box, aileron and balance shaft, for safety purposes, by monitoring the vibration behaviour of

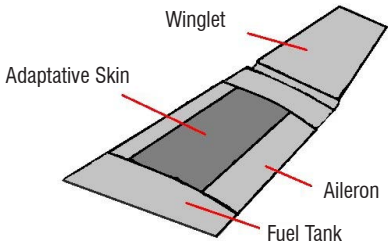

Figure 5 – The layout of the morphing skin on the aircraft wing

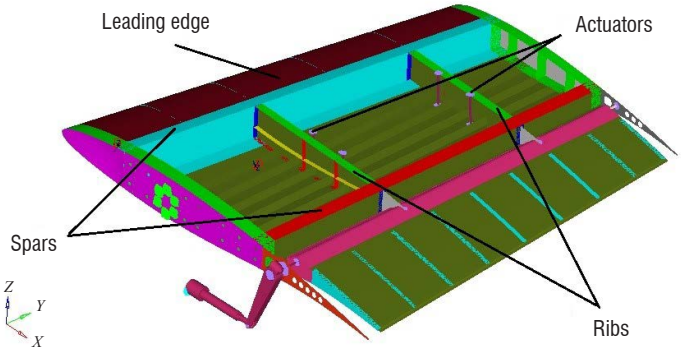

Figure 6 – The structural elements of the CRIAQ MDO 505 morphing wing box (the morphing skin is not shown in the figure)

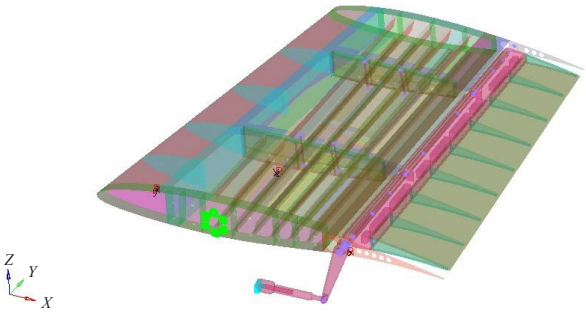

Figure 7 – CRIAQ MDO 505 morphing wing model

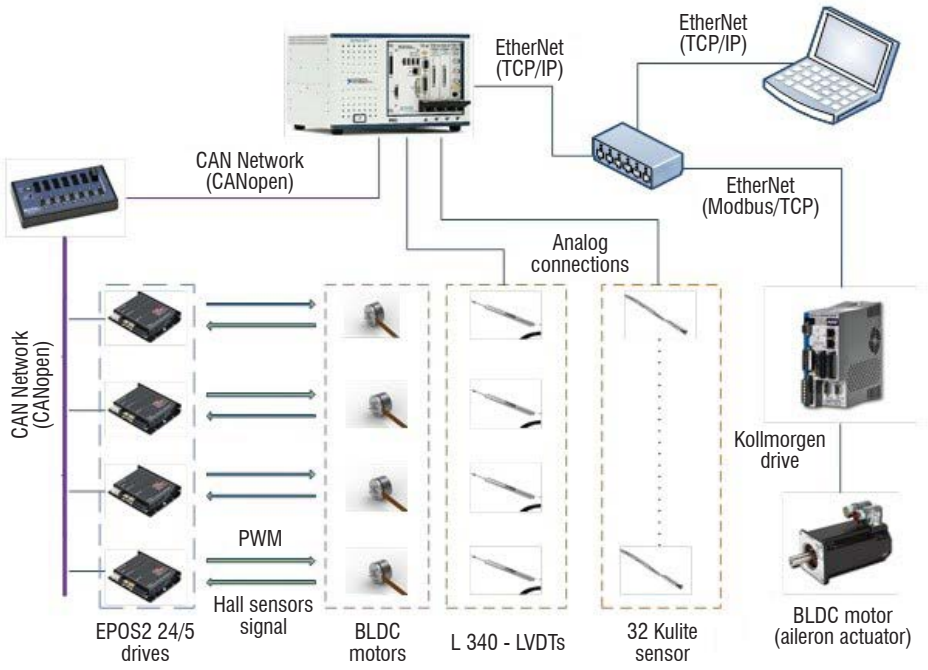

Figure 8 – Overview of the morphing wing control system

the wing during wind tunnel tests. The wing tip was manufactured, and complied with the technological requirements demanded by the industrial partners. Aeroelastic studies were performed in [27]. In this reference, two finite element models are analyzed; the first model corresponds to a traditional aluminium upper surface skin of constant thickness and the second model corresponds to a composite optimized upper surface skin for morphing capabilities. The two models were analyzed for flutter occurrence, and effects on the aeroelastic behaviour of the wing were studied by replacing the aluminium upper surface skin of the wing with a specially developed composite version. The morphing wing model with composite upper surface was manufactured and fitted with three accelerometers to record the amplitudes and frequencies during tests at the subsonic wind tunnel facility at the National Research Council. The results presented showed that no aeroelastic phenomenon occurred at the speeds, angles of attack and aileron deflections studied in the wind tunnel and confirmed the prediction of the flutter analysis on the frequencies and modal displacements.

Project 3. ATR-42 Optimized Wing Geometry for Laminar Flow Improvement Validation using the Price-Païdoussis Subsonic Wind Tunnel

This project took place at the LARCASE in the time frame between projects 1 and 2. An experimental validation of optimized wing geometry in the Price-Païdoussis subsonic wind tunnel was presented in [33].

In this project, two reduced scale wing models based on the ATR-42 aircraft airfoil were designed. The first model was based on the original airfoil shape while the second model was based on the optimized airfoil shape for one flight condition expressed by the Mach number of 0.1 and the angle of attack of 0°. Then, these models were manufactured using optimized glass fiber composite, and were further tested in the wind tunnel at three wind speeds and various angles of attack at which the model was optimized. Figure 9 shows the installation of the model in the test chamber of the Price-Païdoussis subsonic wind tunnel.

An "in-house" genetic algorithm was coupled with a cubic spline reconstruction routine to design the optimized airfoils. Then, the XFoil aerodynamic solver was used to obtain the pressure coefficients for the optimized airfoils in 14 points on the upper surface of the wing, and these numerically calculated data were compared with the experimental pressure data obtained experimentally in the wind tunnel. The transition region was calculated with a second derivative methodology from the experimental pressure data obtained in the wind tunnel, and was validated with the transition region predicted by XFoil code. This methodology was also used in the project 1 [34].

Two DC motors were used to rotate two eccentric shafts which morphed the flexible skin located between 10% and 70% of the chord along two parallel actuation lines. A Proportional-Derivative control algorithm was used to control and validate the morphing wing model using Matlab/Simulink in-house codes [35].

The transition region moved from 2% to 18% of the chord, thus giving an improvement of the laminar flow, and a drag coefficient reduction from 3% to 10.5% of its initial value. LabView software was used for controlling the reduced models in the wind tunnel, which were simulated using Matlab/Simulink program.

Project 4. UAS-S4 and UAS-S5 Morphing Studies

Within the Canada Research Chair in Aircraft Modeling and Simulation Technologies (website: http://www.chairs-chaires.gc.ca/chair-holders-titulaires/profile-eng.aspx?profileId=2744), various projects were performed by the LARCASE team by using a reduced scale UAS-S4 or UAS-S45 morphing wing model to be tested in the Price-Païdousssis subsonic wind tunnel at the ÉTS. Most of these morphing configurations were already aerodynamically and structurally designed and analysed, as explained in this section.

Figure 9 – Installation of the model in the wind tunnel

In [36], an in-house optimization methodology was developed with the aim to reduce drag coefficients on the **UAS-S4** morphing wing. This methodology was based on the Artificial Bee Colony (ABC), and the Broyden-Fletcher-Goldfarb-Shanno (BFGS) algorithms, and was applied for various flight conditions given in terms of Reynolds numbers, airspeeds and angles of attack; the optimized airfoils were obtained for their displacements of 2.5 mm, and for various flight cases. Then, reductions of drag coefficients up to 14% were obtained using a 2D linear panel method, coupled with an incompressible boundary layer model and a transition estimation criterion.

In [37], the ABC and BFGS algorithms were coupled as explained in [36] and [38] with the aim to delay the boundary layer separation and to increase the maximum lift coefficient. Validation of the coupling of these algorithm results were validated with an advanced commercially optimized tool. The 2D linear panel method was coupled with an incompressible boundary layer model and a transition estimation criterion, and was used to calculate the lift and drag coefficients. Lift coefficients increased by up to 18%, drag coefficients decreased, and boundary layer separated at high angles of attack for airfoil displacements smaller than 2.5 mm, as the ones in [36].

In [38], the ABC and BFGS algorithms used in [36] were applied with Non-Uniform Rational B-Splines in the optimization methodology with the aim to increase the lift-to-drag ratio, and to reduce the drag. The lift-to-drag ratios and the drag coefficients were calculated for four flight cases expressed by angles of attack between -40 and 80, by using a rapid, nonlinear lifting line method, coupled with a two-dimensional viscous flow solver, as well as a Navier-Stokes 3D solver. The comparison of aerodynamic coefficients obtained in the 2D flow with those obtained in the 3D flow conducted to the conclusion that the 2D new nonlinear lifting line method could be successfully used, as it gave close results to the 3D Navier-Stokes solver, and was also faster. It was found that the lift-to-drag ratio increased with a maximum of 4%.

The UAS-S4 wing design was modified by decreasing its sweep and increasing of its aspect ratio. Shape optimization was added to this redesign, and resulted in reductions of drag coefficients of up to 5% in the cruise regime [39].

An adaptive leading edge system was designed numerically for the **UAS-S45**, for which aero-structural studies were already performed. At this time, the structural analysis of the model aims to validate the structural integrity of the adaptive leading edge wing model proposed. Figure 10 shows the wing equipped with leading edge system designed using ANSYS / Fluent code. Structural studies were also performed using the Hypermesh code.

A new morphing wing system was designed and manufactured at the LARCASE, and had the aim to reduce the drag, and therefore the fuel consumption. The morphing wing allowed the change of its trailing edge shape, and it was found that the aileron could be replaced on the wing by the morphing trailing edge in order to reduce the drag following experimental tests in the Price-Païdoussis subsonic blow down wind tunnel.

Project 5. Cessna Citation X Business Aircraft Morphing Studies through its Performance Optimization

The LARCASE is equipped with the Research Aircraft Flight Simulator (RAFS) that has the flight dynamics tests data of the Cessna Citation X business aircraft validated, and therefore certified to their highest level D by the FAA. Thus, it is possible to use the flight test data of the RAFS to validate the research proposed in this project; the RAFS is presented in Figure 1, as one of the LARCASE equipments, and is further used in this project for morphing wing and horizontal tail design of the Cessna Citation X.

Although the LARCASE team has several accurate performance models of the Cessna Citation X that can predict its behavior during a flight, this project requires designing and validating a new model specially composed of an aerodynamic model of the Cessna Citation X horizontal stabilizer made from geometrical data. To design this model, the horizontal stabilizer airfoil of the aircraft was found from a Genetic Algorithm (GA) coupled to a level D flight simulator data and a Bezier-Parsec parameterization curve.

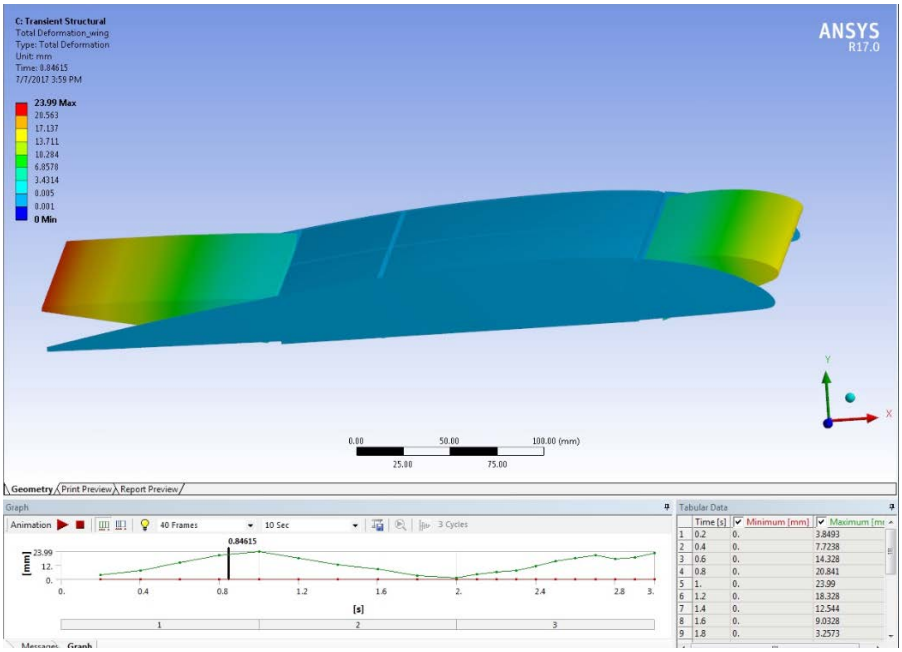

Figure 10 – Wing equipped with leading edge system design with ANSYS / Fluent code

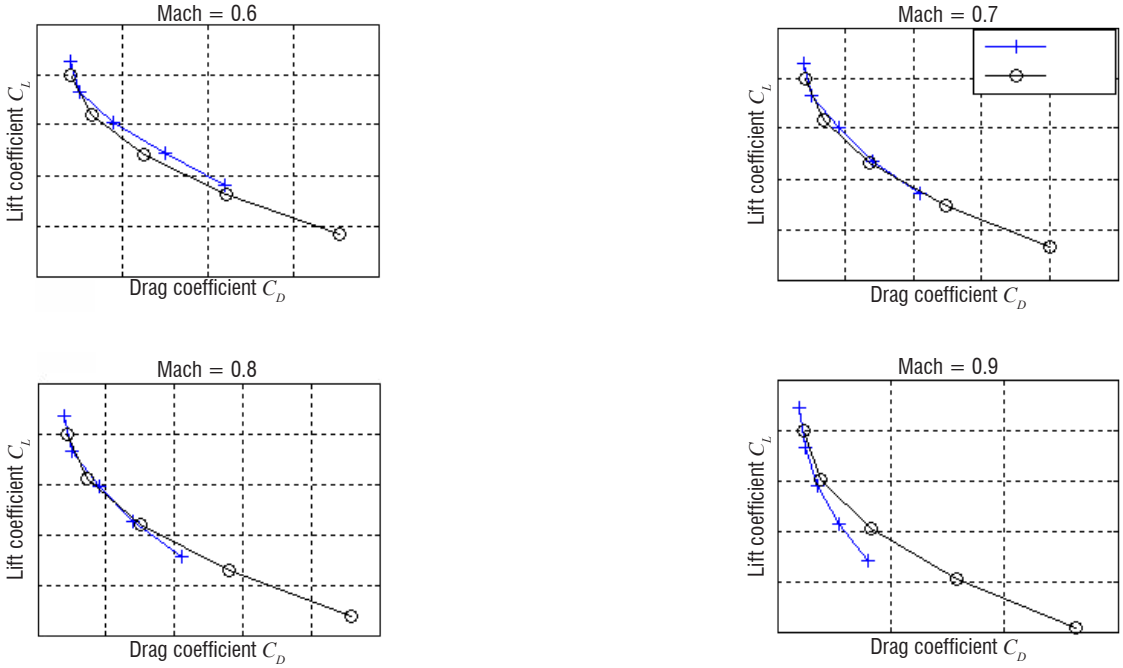

Figure 11 – Horizontal Tail aerodynamic polar comparison between results obtained by the modeled wing equipped with the average airfoil (Model) and experimental reference data obtained from the Flight Simulator (RAFS)

Figure 11 shows a comparison between aerodynamic polar of the wing equipped with the average airfoil founded and aerodynamic polar given by the Research Aircraft Flight Simulator (RAFS) that is constitute a relevant reference. For Mach numbers of 0.6, 0.7 and 0.8, aerodynamic coefficients, for angle of attack between 0 to -6 degrees, are very well estimated with a maximum difference of 0.15 on the lift coefficient and 0.006 on the drag coefficient (for angle of attack equal to -6 degrees and Mach = 0.8). For Mach number 0.9, coefficients seem to be well estimates only for angle of attack close between 0 to -4 degrees. From results obtained in Figure 11, the horizontal tail model geometry is validated [40].

In this project, the Cessna Citation X Business Aircraft performances (fuel consumption, distance) were optimized due to morphing technologies. The two surfaces of the aircraft: stabilizer and wing were morphed, one at a time, with the aim to reduce the fuel consumption in cruise. Thus, the morphing stabilizer benefits were studied separately of the morphing wing benefits. However, the horizontal stabilizer of the Cessna Citation X turns around the span axis of horizontal tail with an angle between -8 to 2 degrees. With this range of angle, the horizontal stabilizer generates for sure some unwanted drag. To cancel this drag, the LARCASE proposes to balance the aircraft by a horizontal stabilizer equipped by a morphing wing that can generate enough lift on the tail to balance the aircraft.

It can be concluded that all the five above projects are interesting and that the LARCASE team continues to work on these projects related to morphing technologies in the aeronautical field, and produce interesting results ■

Acknowledgements

We would like to thank to Dr Cedric Liauzun from ONERA for the invitation to write this article. We would also like to thank for their support in projects 1 and 2 to our Canadian partners from Bombardier, Thales, IAR-NRC, École Polytechnique, and our Italian partners from Federico II University of Naples, CIRA and Alenia. Thanks are dues also to the Hydra Technologies team for their support on project 4, and to CAE Inc. for their support on project 5. We would also like to thank to Professors Michael Paidoussis and Stuart Price for the donation of the Price-Païdoussis wind tunnel to the LARCASE, that make possible the realisation of project 3 and many other projects. Many thanks are dues to the government support from the NSERC, MDEIE, CFI, and the Canada Research Chairs Secretariat, as well as to the LARCASE team, and to Mrs Odette Lacasse from ÉTS.

Acronyms

ABC	(Artificial Bee Colony)
ANFIS	(Adaptive Neuro-Fuzzy Inference System)
BFGS	(Broyden-Fletcher-Goldfarb-Shanno)
GA	(Genetic Algorithm)
GARDN BL-NCE	(Green Aviation Research and Development Business-Led Network of Centres of Excellence)
LARCASE	(Research Laboratory in Active Controls, Avionics and Aeroservoelasticity)

NI	(National Instruments)
PID	(Proportional Integral Derivative)
RAFS	(Research Aircraft Flight Simulator)
RAS	(Research Aerial System)
RMS	(Root Mean Square)
SARISTU	(Smart Intelligent Aircraft Structures)
SMA	(Smart Material Alloys)
TRL	(Technical Readiness Level)
UAV	(Unmanned Aerial Vehicle)
WTEA	(Wing Trailing Edge Airfoil)

References

[1] G. M. CAROSSA, S. RICCI, A. DE GASPARI, C. LIAUZUN, A. DUMONT, M. STEINBUCH - *Adaptive Trailing Edge: Specifications, Aerodynamics and Exploitation.* Chapter in the book: Smart Intelligent Aircraft Structures (SARISTU), Edition: 1, Publisher: Springer International Publishing, Editors: Piet Christof Wölcken, Michael Papadopoulos, pp.143-158, 2015.

[2] M. ARENA, R. PECORA, F. AMOROSO, M. C. NOVIELLO, F. REA, A. CONCILIO - *Aeroelastic Analysis of an Adaptive Trailing Edge with a Smart Elastic Skin*. The 2nd International Conference on Energy Engineering and Smart Materials: ICEESM 2017, AIP Conference Proceedings 1884(1):040002, DOI 10.1063/1.5002521, 2017.

[3] F. REA, R. PECORA, F. AMOROSO, M. REA, M. C. NOVIELLO, G. AMENDOLA - *Aeroelastic Stability Analysis of a Wind Tunnel Wing Model Equipped with a True Scale Morphing Aileron*. International Journal of Mechanical Engineering and Robotics Research, Vol. 6, No. 6, November 2017.

[4] G. AMENDOLA, I. DIMINO, A. CONCILIO, R. PECORA, F. AMOROSO, M. ARENA - *Morphing Aileron*. DOI: 10.1016/B978-0-08-100964-2.00018-6, Morphing Wing Technologies, 2018.

[5] A. CONCILIO, I. DIMINO, M. CIMINELLO, R. PECORA, F. AMOROSO, M. MAGNIFICO - *An Adaptive Trailing Edge.* DOI: 10.1016/B978-0-08-100964-2.00017-4, Morphing Wing Technologies, 2018.

[6] I. DIMINO, M. CIMINELLO, A. CONCILIO, A. GRATIAS, M. SCHUELLER, R. PECORA - *Control System Design for a Morphing Wing Trailing Edge*. DOI: 10.1007/978-3-319-44507-6_9, Smart Structures and Materials, 2017.

[7] I. DIMINO, M. CIMINELLO, A. CONCILIO, R. PECORA, F. AMOROSO, M. MAGNIFICO, M. SCHUELLER, A. GRATIAS, A. VOLOVICK, L. ZIVAN - *Distributed Actuation and Control of a Morphing Wing Trailing Edge*. DOI: 10.1007/978-3-319-22413-8_9, Smart Intelligent Aircraft Structures (SARISTU), 2016.

[8] R. M. BOTEZ, P. MOLARET, E. LAURENDEAU - *Laminar Flow Control on a Research Wing Project Presentation Covering a Three Years Period*. Canadian Aeronautics and Space Institute Annual General Meeting, Toronto, Ont., Canada, May 16-18, 2007.

[9] A. V. POPOV, T. L. GRIGORIE, R. M. BOTEZ, M. MAMOU, Y. MEBARKI - *Real Time Morphing Wing Optimization Validation Using Wind-Tunnel Tests*. Journal of Aircraft, Vol. 47, no 4, pp. 1346-1355, 2010.

[10] C. SAINMONT, I., PARASCHIVOIU, D. COUTU - *Multidisciplinary Approach for the Optimization of a Laminar Airfoil Equipped with a Morphing Upper Surface*. NATO VT-168 Symposium on Morphing Vehicles, Evora, Portugal, 2009.

[11] A. V. POPOV, R. M. BOTEZ, M. MAMOU, T. L. GRIGORIE - *Variations in Optical Sensor Pressure Measurements Due to Temperature in Wind-Tunnel Testing*. Journal of Aircraft, Vol. 46, no 4, pp. 1314-1318, 2009.

[12] A. V. POPOV, T. L. GRIGORIE, R. M. BOTEZ, M. MAMOU, Y. MEBARKI - *Controller Optimization in Real Time for a Morphing Wing in a Wind Tunnel*. 15th IEEE Mediterranean Electro-technical Conference (MELECON 2010), Malta, pp. 107-112, 2010.

[13] A. V. POPOV, T. L. GRIGORIE, R. M. BOTEZ, M. MAMOU, Y. MEBARKI - *Modeling and Testing of a Morphing Wing in Open-Loop Architecture*. Journal of Aircraft, Vol. 47, no 3, pp. 917-923, 2010.

[14] A. V. POPOV, T. L. GRIGORIE, R. M. BOTEZ, M. MAMOU, Y. MEBARKI - *Closed-Loop Control Validation of a Morphing Wing Using Wind Tunnel Tests*. Journal of Aircraft, Vol. 47, no 4, pp. 1309-1317, 2010.

[15] T. L. GRIGORIE, A. V. POPOV, R. M. BOTEZ, M. MAMOU, Y. MEBARKI - *On-Off and Proportional-Integral Controller for a Morphing Wing. Part 1: Actuation Mechanism and Control Design*. Proceedings of the Institution of Mechanical Engineers, Part G: Journal of Aerospace Engineering, Vol. 226, no 2, pp. 131-145, 2012.

[16] T. L. GRIGORIE, A. V. POPOV, R. M. BOTEZ, M. MAMOU, Y. MEBARKI - *On-Off and Proportional-Integral Controller for a Morphing Wing. Part 2: Control Validation - Numerical Simulations and Experimental Tests*. Proceedings of the Institution of Mechanical Engineers, Part G: Journal of Aerospace Engineering, Vol. 226, no 2, pp. 146-162, 2012.

[17] T. L. GRIGORIE, A. V. POPOV, R. M. BOTEZ, M. MAMOU, Y. MEBARKI - *A Hybrid Fuzzy Logic Proportional-Integral-Derivative and Conventional On-Off Controller for Morphing Wing Actuation Using Shape Memory Alloy Part 1: Morphing System Mechanisms and Controller Architecture Design*. The Aeronautical Journal, Vol. 116, pp. 433-449, 2012.

[18] T. L. GRIGORIE, A. V. POPOV, R. M. BOTEZ, M. MAMOU, Y. MEBARKI - *A Hybrid Fuzzy Logic Proportional-Integral-Derivative and Conventional On-Off Controller for Morphing Wing Actuation Using Shape Memory Alloy Part 2: Controller Implementation and Validation*. The Aeronautical Journal, Vol. 116, pp. 451-465, 2012.

[19] T. L. GRIGORIE, R. M. BOTEZ - *Adaptive Neuro-Fuzzy Inference System-Based Controllers for Smart Material Actuator Modeling*. Proceedings of the Institution of Mechanical Engineers Part G: Journal of Aerospace Engineering, Vol. 223, no 6, pp. 655-668, 2009.

[20] S. COURCHESNE, A. V. POPOV, R. M. BOTEZ - *New Aeroelastic Studies for a Morphing Wing*. INCAS Bulletin, Vol. 4, no 2, pp. 19-28, 2012.

[21] T. L. GRIGORIE, R. M. BOTEZ, A. V. POPOV - *Adaptive Neuro-Fuzzy Controllers for an Open-Loop Morphing Wing System*. Proceedings of the Institution of Mechanical Engineers, Part G: Journal of Aerospace Engineering, Vol. 223, no 7, pp. 965-975, 2009.

[22] T. L. GRIGORIE, R. M. BOTEZ - *New Adaptive Controller Method for SMA Hysteresis Modelling of a Morphing Wing*. The Aeronautical Journal, Vol. 114, pp. 1-13, 2010.

[23] A. KOREANSCHI, O. SUGAR GABOR, J. ACOTTO, G. BRIANCHON, G. PORTIER, R. M. BOTEZ, M. MAMOU, Y. MEBARKI - *Optimization of a Morphing Wing Tip Aircraft Demonstrator for Drag Reduction at Low Speeds, Part I - Numerical Analysis Using 3 Algorithms: Genetic, Artificial Bee Colony and Gradient Descent*. Chinese Journal of Aeronautics, Vol. 30, no 1, pp. 149-163, 2017.

[24] A. KOREANSCHI, O. SUGAR GABOR, J. ACOTTO, G. BRIANCHON, G. PORTIER, R. M. BOTEZ, M. MAMOU, Y. MEBARKI - *Optimization of a Morphing Wing Tip Aircraft Demonstrator for Drag Reduction at Low Speeds, Part II - Experimental Validation Using Infra-Red Transition Measurements During Wind Tunnel Tests*. Chinese Journal of Aeronautics, Vol. 30, no 1, pp. 164-174, 2017.

[25] O. SUGAR GABOR, A. KOREANSCHI, R. M. BOTEZ, M. MAMOU, Y. MEBARKI - *Numerical Simulation and Wind Tunnel Tests Investigation and Validation of a Morphing Wing-Tip Demonstrator Aerodynamic Performance*. Aerospace Science and Technology, Vol. 53, pp. 136-153, 2016.

[26] F. MICHAUD, S. JONCAS, R. M. BOTEZ - *Design, Manufacturing and Testing of a Small-Scale Composite Morphing Wing*. Proceedings of the 19th International Conference on Composite Materials ICCM19, Montréal, Québec, Canada, July 28-Aug. 2, 2013.

[27] A. KOREANSCHI, M. B. HENIA, O. GUILLEMETTE, F. MICHAUD, Y. TONDJI, O. SUGAR-GABOR, M. FLORES-SALINAS - *Flutter Analysis of a Morphing Wing Technology Demonstrator: Numerical Simulation and Wind Tunnel Testing*. INCAS Bulletin, Vol. 8, no 1, pp. 99-124, 2016.

[28] M. J. TCHATCHUENG KAMMEGNE, D. H. NGUYEN, R. M. BOTEZ, T. L. GRIGORIE - *Control Validation of a Morphing Wing in an Open Loop Architecture*. AIAA Modeling and Simulation Technologies Conference, Dallas, TX, USA, June 22-25, 2015.

[29] M. J. TCHATCHUENG KAMMEGNE, H. BELHADJ, D. H. NGUYEN, R. M. BOTEZ - *Nonlinear Control Logic for an Actuator to Morph a Wing: Design and Experimental Validation*. The 34th IASTED International Conference on Modelling, Identification and Control MIC, February 16-18, 2015.

[30] R. M. BOTEZ, A. KOREANSCHI, O. SUGAR GABOR, Y. MEBARKI, M. MAMOU, Y. TONDJI, G. BRIANCHON, F. AMOROSO, R. PECORA, L. LECCE, G. AMENDOLA, I. DIMINO, A. CONCILIO - *Innovative Wing Tip Equipped with Morphing Upper Surface and Morphing Aileron for Greener Aviation*. Greener Aviation Conference, Brussels, Belgium, June 11-13, 2016.

[31] F. MICHAUD - *Design and Optimization of a Composite Skin for an Adaptive Wing*. Master of Science Thesis, ÉTS, Montreal, Canada, 2014.

[32] R. M. BOTEZ, A. KOREANSCHI, O. SUGAR GABOR, Y. MEBARKI, M. MAMOU, Y. TONDJI, F. AMOROSO, R. PECORA, L. LECCE, G. AMENDOLA, I. DIMINO, A. CONCILIO - *Numerical and Experimental Testing of a Morphing Upper Surface Wing Equipped with Conventional and Morphing Ailerons*. AIAA SciTech Forum – 55th AIAA Aerospace Sciences Meeting, Grapevine, USA, AIAA Paper nr. 2017-1425, 2017.

[33] A. KOREANSCHI, O. SUGAR-GABOR, R. M. BOTEZ - *Numerical and Experimental Validation of a Morphed Wing Geometry Using Price-Païdoussis Wind Tunnel Testing*. The Aeronautical Journal, Vol. 120, no 1227, pp. 757-795, 2016.

[34] A. V. POPOV, R. M. BOTEZ, M. LABIB - *Transition Point Detection from the Surface Pressure Distribution for Controller Design*. Journal of Aircraft 45 (1), pp. 23-28, 2008.

[35] M. J. TCHATCHUENG KAMMEGNE, T. L. GRIGORIE, R. M. BOTEZ, A. KOREANSCHI - *Design and Wind Tunnel Experimental Validation of a Controlled New Rotary Actuation System for A Morphing Wing Application*. Proceedings of the Institution of Mechanical Engineers, Part G: Journal of Aerospace Engineering, Vol. 230, no 1, pp. 132-145, 2015.

[36] O. SUGAR GABOR, A. SIMON, A. KOREANSCHI, R. M. BOTEZ - *Aerodynamic Performance Improvement of the UAS-S4 Éhecatl Morphing Airfoil Using Novel Optimization Techniques*. Proceedings of the Institution of Mechanical Engineers, Part G: Journal of Aerospace Engineering, Vol. 230, no 7, 2015.

[37] O. SUGAR GABOR, A. SIMON, A. KOREANSCHI, R. M. BOTEZ - *Improving the UAS-S4 Éhecatl Airfoil High Angles-of-Attack Performance Characteristics Using a Morphing Wing Approach*. Proceedings of the Institution of Mechanical Engineers, Part G: Journal of Aerospace Engineering, Vol 230, no 1, pp. 118-131, 2016.

[38] O. SUGAR GABOR, A. KOREANSCHI, R. M. BOTEZ - *Analysis of UAS-S4 Éhecatl Aerodynamic Performance Improvement Using Several Configurations of a Morphing Wing Technology*. The Aeronautical Journal, Vol. 120, no 1231, pp. 1337-1364, 2016.

[39] O. SUGAR GABOR, A. KOREANSCHI, R. M. BOTEZ - *A New Non-Linear Vortex Lattice Method: Applications to Wing Aerodynamic Optimizations*. Chinese Journal of Aeronautics, Vol. 29, no 5, pp. 1178-1195, 2016.

[40] M. SEGUI, M. MANTILLA, R. M. BOTEZ - *Conception and Validation of an Aerodynamic Model of the Cessna Citation X Horizontal Stabilizer Using OpenVSP and Digital Datcom Software*. 20th International Conference on Engineering Education and Research ICEER-2018, Innsbruck, Austria, 2018.

AUTHOR

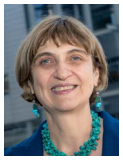

Ruxandra Botez is Full Professor at the ÉTS since 1998, and Canada Research Chair Tier 1 Holder in Aircraft Modelling and Simulation Technologies since 2011. Dr Botez is also the Founder and Head of the Laboratory of Applied Research in Active Controls, Avionics and Simulation LARCASE since 2003. Dr Botez has published 106 journal papers, 247 conference papers and 7 invited book chapters. She and her team obtained 35 awards and recognitions. Dr Botez also graduated 202 Bachelor's, 85 Master's students, and 11 PhD students who worked on various research projects in collaboration with Aerospace Engineering companies. Dr Botez is also Editor-in-Chief of the National Institute for Aerospace Research "Elie Carafoli" INCAS Bulletin.

A. Dugeai, Y. Mauffrey,
A. Placzek, S. Verley
(ONERA)

E-mail: alain.dugeai@onera.fr

DOI: 10.12762/2018.AL14-03

Overview of the Aeroelastic Capabilities of the *elsA* Solver within the Context of Aeronautical Engines

This paper presents the status of current development and research activities conducted at ONERA concerning the numerical modelling of aeroelastic phenomena of rotating machines. Three different topics are detailed after a short reminder of some features of ONERA's CFD solver *elsA*. The first one addresses the development of methodologies for taking into account geometrical non-linear structural behavior in the modelling of the static aeroelasticity of large fan blades. The second one presents the current capabilities available for aeroelastic stability analyses of rotating machines conducted within the frame of stage and multi-stage configurations. The third point concerns the resolution of aeroelastic forced response problems. An overview of recent applications in the field of turbomachinery aeroelasticity will finally be drawn before giving some perspectives of new activities.

Introduction

The Aeroelasticity Modeling and Simulation research unit of ONERA develops and validates numerical methods for the prediction of the aeroelastic behavior of aeronautical structures. This activity covers various applicative purposes, such as military and civil aircraft, aeronautical engines, and helicopters. This paper presents recent developments and applications conducted at ONERA, related to the prediction of the aeroelastic behavior of aeronautical rotating machines, such as fans, contra-fans, and open-rotors.

Over the last decades, a great effort has been made by several academic teams in the development of numerical methods for modelling the unsteady aerodynamics generated by fan blades vibrations, for the purpose of the prediction of dynamic aeroelastic stability (flutter) and forced response. Due to the complexity of unsteady flows occurring in industrial turbomachines, including compressibility, turbulence and separation effects in a large region of the operating domains, as well as rotor-stator interaction effects, aeroelastic stability in the field of turbomachines was studied using simplified formulations, such as linearized potential flow [1]. In the 90s, linearized Euler and Navier-Stokes formulations were then developed [2, 3, 4, 5] for the resolution of time-harmonic unsteady aerodynamic problems, introducing new numerical prediction methods for transonic flows in cascades. Since then, sector reduction techniques have been developed, assuming space-time periodicity properties in order to improve efficiency and face large 3D problems [6, 7, 8, 9, 10, 11, 12].

With increasing computational power, non-linear Euler and Navier-Stokes equations formulations in the time domain, including mesh deformation algorithms, have been also evaluated and developed since the mid-90s [13, 14, 15, 16, 17, 18, 19]. More recently, vibration problems have been addressed using a non-linear aeroelastic approach implementing a harmonic balance formulation. In this approach, the non-linear response of the fluid is modeled using a Fourier decomposition in the time domain of the periodic flow response to vibration [20, 21, 22, 23, 24].

The development of these unsteady aerodynamic numerical tools, using decoupled or fully coupled time-marching methods, has been a key player in the study of aeroelastic phenomena like stall and acoustic flutter [25, 26, 27], or flutter in the presence of distortion [28, 29] with applications to low-speed fans [30] and counter-rotating open rotor CROR [31, 32], as well as for the investigation of the forced-response phenomenon induced by blade passage effects in single-stage [19, 33] or multi-stage configurations [34, 35] and, more recently, by inlet distortion effects [36, 37, 29, 38]. Recent investigations have also been carried out to study the impact of structural non-linearities on the static aeroelastic behavior of large fan blades. Due to the dimension increase of fan and propeller blades for efficiency purposes, non-linear effects are indeed more likely to impact deformations and, in particular, centrifugal following forces have to be taken into account for the proper evaluation of hot blade shapes [39, 40].

All of these efforts contribute to the improvement of engine design, in order to face the current environmental challenges. In the trend of global reduction of the impact of aeronautical systems on the environment, very stringent constraints are indeed placed on Aircraft and Engine manufacturers to meet ACARE 2020 objectives, in order to reduce noise emission and drastically improve energetic efficiency. Compared to the figures for 2005, the emission reduction target levels are as high as 50% for CO_2, 80% for NO_x and 50% in terms of noise emission. Within this context, the external dimensions of aeronautical engines are becoming larger and larger, in order to achieve higher bypass ratios and thus higher efficiencies. To this end, the blade radii of fans and open-rotors are increasing and new materials like composites are being used, resulting in more flexible structures prone to aeroelastic phenomena.

These new requirements are leading to new challenges for the prediction of the aeroelastic behavior of fan blades, due to larger sizes and greater flexibilities. Consequently, a new need emerges on the one hand to take into account the non-linear modelling of the blade structure to surpass the classical linear blade structural models. On the other hand, the need for a better modelling of the complex turbomachinery environment for aeroelasticity arises, in particular when it comes to considering the effects induced by adjacent blade rows in (multi-)stage configurations involving unsteady coupled interactions due to rotation and vibration, which are neglected in isolated blade row models usually considered for flutter, although they can be significant [41, 42].

In this paper, a first section will be devoted to the presentation of some details concerning the aerodynamic and aeroelastic solver *elsA*, developed by ONERA, which has been implemented in the presently discussed studies. A first point will focus on the coupling features developed within the aeroelastic module, in order to couple the aerodynamic solver *elsA* with the structural solver MSC Nastran, enabling fully non-linear static aeroelastic simulations. Then, specific insight will be given into specific sector-reduction techniques used in the case of the aeroelastic modelling of turbomachines, implementing phase-lagged and multiple-frequency phase-lagged boundary conditions. Eventually, a discussion on available methods for forced response problems will be given. The last section of the paper will present some applications of these features and techniques.

Aerodynamic Solver *elsA*

The present work has been conducted with the *elsA* solver, developed at ONERA (ONERA-Airbus-SAFRAN property). This project started in 1997 within ONERA's aerodynamics department, and is now being developed by a large number of contributors from several departments within ONERA, as well as by industrial or academic partners, such as AIRBUS, SAFRAN, CERFACS, ECL/LMFA and CENAERO. *elsA* is a multipurpose aerodynamic software dedicated to the simulations of external and internal flows for aircraft, turbomachinery, helicopter and propellers, among other applications [43].

elsA Aerodynamic Solver Features

elsA allows aerodynamic computations for compressible viscous and inviscid flows. It handles RANS and URANS equations with a large set of turbulence models, ranging from algebraic to turbulent transport equations, including Reynolds Stress Models, Detached or Large Eddy Simulation (DES, LES) models, which are now being implemented for some applications. Laminar-turbulent transition criteria are also available, including the Menter transport equation model. Considering the meshing strategy, *elsA* was initially developed as a multiblock structured grid solver. However, incoming developments have gradually been made to increase its capabilities, in order, first to take into account partially or non-coincident block joins, and then to handle Chimera overset grids. Patched grid and overset Chimera grid techniques can be implemented to overcome multiblock structured grid meshing issues for complex geometrical configurations. Moreover, hybrid structured/unstructured mesh capabilities are now available, which have been extensively validated in particular for taking into account turbomachinery complex geometries, including technological effects (cavities, injections, cooling devices, and trenches). The use of Cartesian grids is available.

Motion and deformations of bodies can be taken into account for steady/unsteady applications. The finite-volume approach is used for spatial discretization in connection with centered or upwind schemes (Jameson, Roe, Van Leer). High-order schemes are available or under development in *elsA* (k-exact schemes), and Runge-Kutta or backward Euler time schemes are available. Local, global, dual and Gear time stepping schemes are implemented. Convergence can be accelerated using implicit techniques and/or multigrid resolution schemes. For unsteady time-accurate simulations, Dual Time Stepping and Gear schemes are available. For rotating machinery problems, relative frame with either relative or absolute variable formulations can be used for turbomachinery, helicopters and propellers. Parallelization is achieved through the distribution of mesh blocks over a set of processors. As far as unsteady computations are concerned, *elsA* is able to handle mesh deformation using an Arbitrary Lagrangian Eulerian (ALE) formulation of flow equations.

elsA/Ael Aeroelastic Module

The Aeroelasticity Modelling and Simulation research unit of ONERA has been developing, within the *elsA* solver, a specific module for solving aeroelastic problems, either static or dynamic. A general framework has been developed in the optional "Ael" module of *elsA* over the last few years [44, 45, 46, 47], in order to extend *elsA* to different kinds of static or unsteady aeroelastic simulations (Figure 1).

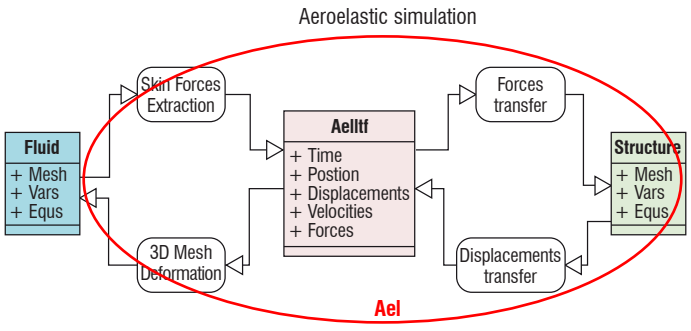

Figure 1 – Connections between the fluid and structural solver within the elsA/*Ael* aeroelastic module

The purpose of these simulations is the prediction of the in-flight static or dynamic behavior of flexible aerodynamic structures and their aeroelastic stability. This "Ael" subsystem gives access, in a unified formulation, to different types of aeroelastic simulations, compatible with the flow solver features. The available simulations include non-linear and linearized harmonic forced motion computations, static coupling and consistent dynamic coupling simulations in

the time-domain. The harmonic balance method is also implemented for periodic forced motion simulations.

In the AeI module, however, only a simple linear structural behavior is assumed and implemented. Various kinds of linear structural modelling are available ("reduced flexibility matrix" for static coupling, modal approach, or full-finite-element structural model). In addition to the specific aeroelastic simulation driver, the *elsA*/AeI module basically integrates three main subsystems: a module for data transfer between the fluid and structure solvers (including load and displacement components), an integrated static and dynamic linear structural solver and a 3D fluid mesh deformation tool.

Transfer of displacements and loads between the structure and the fluid are based on the exchange of generalized coordinates and forces in the case of the modal approach, whereas it uses specific interpolation or smoothing techniques, the nearest neighbor or virtual-work-principle-based techniques for the finite-element approach. With regard to the important issue of 3D fluid mesh deformation, several techniques are also implemented in the AeI module. A first technique is based on the resolution of an equivalent linear elastic continuous medium problem, whose boundary conditions prescribe the displacement of the aerodynamic grid at the aeroelastic interfaces. An 8-node hexahedral finite-element approach is used to discretize the aerodynamic grid mesh deformation problem. The local stiffness matrix is computed approximately, using a one-point Gauss integration procedure, specifically corrected for Hour-glass spurious mode treatment. The static equilibrium of the discretized system leads to the following linear system:

$$K_{ii} q_i = -K_{if} q_f \tag{1}$$

where K_{ii} and K_{if} are stiffness matrices resulting from the discretization of the structural analogy problem, and where q_i and q_f are respectively the computed and boundary prescribed displacement vectors. Given that the stiffness matrix is positive definite, the system is solved using a pre-conditioned conjugated gradient method. For *elsA,* the technique is implemented in the case of multi-block structured grids. The full-mesh deformation is defined as a sequence of individual block deformations.

Boundary conditions are set to impose zero or prescribed displacement values, to move on a plane, on the local surface boundary, or along or normally to a prescribed vector, and to achieve deformation continuity through block interfaces. In order to fulfil the boundary conditions, the conjugated gradient algorithm is modified.

The resolution procedure is kept compatible with the boundary conditions by iteratively projecting the solution and search direction vectors in the proper linear subspace. However, performing structural static deformation computations on the full aerodynamic grid is expensive, and reduction techniques are implemented to solve the structural problem on a coarse grid, by packing cells, especially in the boundary layer regions, where the aerodynamic discretization is extremely dense.

The structural analogy method is very versatile and is used for a wide range of applications, including turbomachines, aircrafts, helicopters, propellers and CRORs (see Figure 2). The mesh deformation procedure implemented has been validated for use with Chimera grids, and is now being fully parallelized in the current *elsA* version.

An alternate mesh deformation method based on a mixture of the Inverse Distance Weighting (IDW) method and TransFinite Interpolation (TFI) is also available in the case of multiblock structured configurations. IDW is implemented in order to prescribe displacements on block boundaries, and the displacements of internal block nodes are obtained from the boundaries using the TFI algorithm. New developments are currently being made, in order to implement a Quaternion-based mesh deformation method in a robust and efficient way, using a Fast-Multipole Method accelerated IDW algorithm.

The time-consistent unsteady aeroelastic simulations discussed in this paper are performed using dual time stepping or Gear methods. These simulations allow for the evaluation of the aeroelastic stability of aeronautical structures, either in a weakly-coupled or strongly-coupled strategy. In the weak coupling case, the motion of the structural model is prescribed as a single harmonic motion, or a combination of harmonic motions, which can be rigid or can follow its natural vibration modes Φ. The structure is indeed classically considered as a linear elastic medium for aeroelastic stability analyses and the structural displacement field x of the vibrating structure subjected to aerodynamic forces F_A satisfies the discretized equations of motion:

$$M\ddot{x} + D\dot{x} + Kx = F_A(x,t) \tag{2}$$

Assuming a linear behavior of the structural model, the displacement field is approximated as a linear combination of the first structural mode shapes $x \approx \Phi q$ and the following reduced system is obtained after projection on the modal basis:

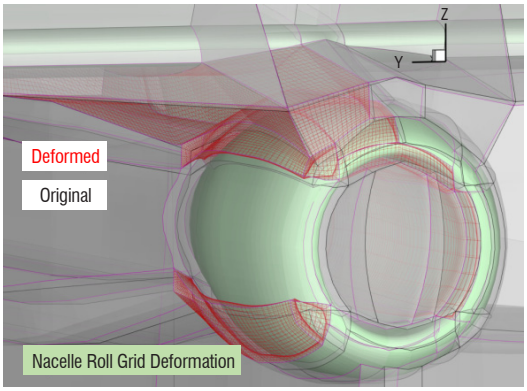

(a) oscillating nacelle

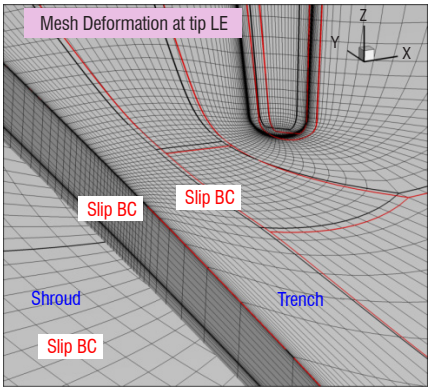

(b) axial compressor with trench clearance at shroud

Figure 2 – Mesh deformation examples using structural elastic analogy

$$\mu\ddot{q} + \beta\dot{q} + \gamma q = GAF(q,t) \quad (3)$$

where

$$\mu = \Phi^t M \Phi \quad \beta = \Phi^t D \Phi \quad \gamma = \Phi^t K \Phi \quad GAF(q,t) = \Phi^t F_A(x,t) \quad (4)$$

are respectively the generalized mass, damping and stiffness matrices and the generalized aerodynamic force. Weakly-coupled aeroelastic computations are run over several periods of vibration, in order to obtain the unsteady aerodynamic response to a forced motion of the structure prescribed with the modal shapes Φ. The aerodynamic temporal response of the fluid gives access to unsteady pressure distributions on the model surface, and may be integrated to obtain unsteady aerodynamic loads over the structure. With the purpose of performing a linear stability analysis for flutter, these pressure load distributions $F_A(t) = -pn$ are projected onto the structural modal basis shapes Φ, to obtain the unsteady Generalized Aerodynamic Forces $GAF(t) = \Phi^t F_A(t)$, which are involved in the right hand side of the modal structural dynamics equation (3).

A first harmonic analysis of the unsteady forces is performed to study, in the frequency domain, the aeroelastic stability of the fluid-structure coupled system. Flutter response is classically analyzed using the $p-k$ stability method [49], Karpel's minimum state smoothing method [50] or energy considerations [48].

In the strong coupling case, the structural dynamics equation is directly solved in the time domain during the unsteady aerodynamic computation, using a Newmark resolution scheme. At each physical time step, aerodynamic forces and elastic forces are balanced using an additional coupling loop, usually requiring 3 steps for the proper convergence of the fluid-structure equilibrium. The procedure then gives access to the unsteady evolutions of the structural variables, and of the aerodynamic field as well.

Resolution of Static Aeroelastic Equilibrium within a Non-Linear structural Context

In many aeroelasticity problems, the structure can be classically assumed to behave linearly. However, in some cases, the linear structure assumption is no longer valid. This is the case when geometric non-linearities, such as large displacements, are to be considered, for example for highly flexible wings, or in the turbomachine case, for rotating blades of large dimensions, such as large propellers, open-rotors or UHBR fan blades.

Therefore, new solutions for coupling non-linear aerodynamics and non-linear structural models are to be considered. The fluid-structure problem can be formulated as a coupled-field problem, where the solutions are coupled only at the boundary interfaces between the fluid and the structure [51]. It is then possible to run separate solvers for the flow computation and the structure computation, and to reach a coupled solution by exchanging information at the common fluid-structure boundaries.

The currently implemented mechanism used for coupling *elsA* and an external Computational Structural Mechanics (CSM) solver basically relies on the exchange of data at the aeroelastic interface, using a CGNS standard compliant interface. The aeroelastic module features of *elsA* are used, except for the internal structural model resolution, which is externalized. The standard aeroelastic simulation is interrupted at each coupling step, and aerodynamic forces relative to an embedded reduced structural model (either modal or finite element) are computed using the *elsA*/Ael aeroelastic module integrated force transfer methods. This data is extracted and provided to the CGNS memory database, which in turn is processed by an external Python coupling script in charge of the communication with the external structural solver. The CSM solver Nastran is run in non-linear mode with the dedicated SOL400 solution, taking into account the following forces for the prescription of aerodynamic forces at each time step. At the end of the structural solver step, displacements on the reduced structural model are sent back to *elsA* and transferred to the aeroelastic interface. 3D aerodynamic mesh deformation is then performed, before continuing with new fluid resolution iterations.

This architecture has been developed for the purpose of running aeroelastic simulations coupling *elsA* with the non-linear commercial structural solver MSC NASTRAN. To this end, a specific interface written in C language and based on the use of the OpenFSI module of Nastran has been developed and coupled with a Python interface (Figure 3).

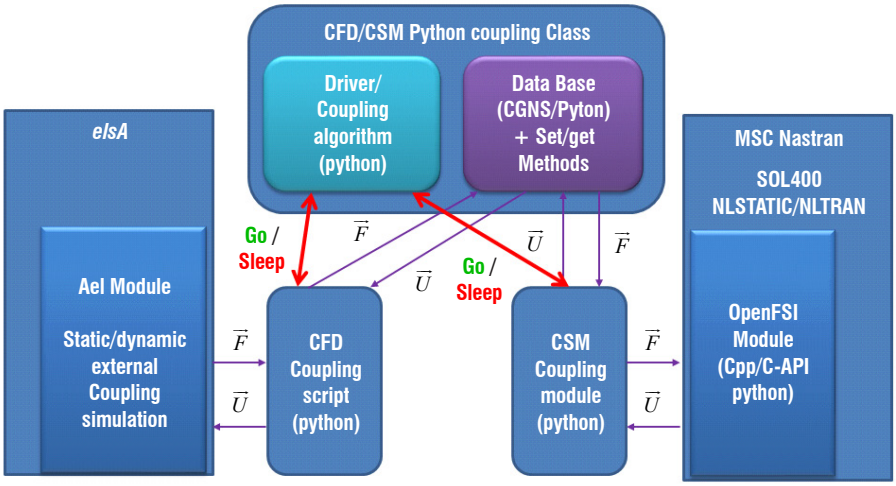

Figure 3 – Current coupling architecture between elsA aerodynamic solver and MSC Nastran SOL 400 non-linear structural solver

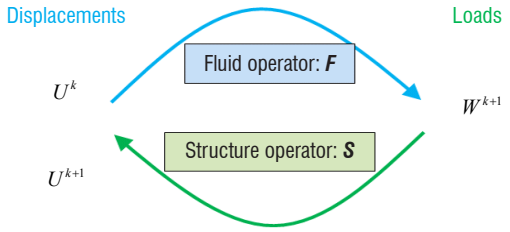

$$X^k = \begin{bmatrix} u^k \\ w^k \end{bmatrix}$$

$$X^{k+1} = \begin{bmatrix} u^{k+1} = S(w^{k+1}) \\ w^{k+1} = F(u^k) \end{bmatrix}$$

$$X^{k+1} = X^k + \alpha\left(SF(X^k) - X^k\right)$$

Figure 4 – Fluid-structure fixed-point algorithm

The coupling strategy is basically a fixed-point method, potentially requiring the use of a relaxation procedure to ensure convergence (Figure 4). This mechanism has been implemented in the case of static hot shape predictions of UHBR and open-rotor fan blades. In this case, the nonlinear structural modelling is mandatory, due to effect of high-speed rotation inducing additional stiffness terms and centrifugal forces.

Dynamic Aeroelasticity Features for Stage/Multistage Turbomachine Configurations

Reductions for Dynamic Aeroelastic Stability Problems for Cyclic Periodic Configurations

The aeroelastic module of *elsA* can be used for the study of the aeroelastic stability of aeronautical structures, using the weakly-coupled approach described previously. In this case harmonic forced motion simulations are performed, in order to obtain the generalized aerodynamic forces $GAF(t)$ giving access to the aerodynamic damping.

The stability of an aeroelastic coupled system is analyzed from the behavior of the structural linear dynamic system governed by Equation 2 or by Equation 3, when the system is projected onto the structural mode shapes of interest. In this latter case, the knowledge of the generalized aerodynamic forces $GAF(t)$ resulting from the projection of the aerodynamic forces $F_A(x)$ onto the structural mode shapes is necessary to perform the stability analysis and weakly coupled simulations are run for that purpose.

The stability analysis is aimed at evaluating whether the coupling of the aerodynamic flow with the modal vibrations produces additional damping or amplification of the motion, which is likely to lead to the destruction of the structure, through the so-called flutter phenomenon. Consequently, the linear stability analysis of the modal equation (3) is performed, in order to seek complex exponential solutions of the system in the form

$$q(t) = q^* e^{pt} \quad \text{with} \quad p = j\omega(1 + j\alpha) \tag{5}$$

The solution may be damped or amplified, whether the real part of the eigenvalue p is negative or not. ω is the pulsation and α is the particular solution damping. Therefore, the substitution of the particular solution (5) in the structural dynamics equation (3) leads to:

$$\left(p^2\mu + p\beta + \gamma\right)q^* e^{pt} = GAF(q,t) \tag{6}$$

Assuming then that the vibration-induced generalized aerodynamic forces are linear with respect to the structural motion (included in phase and out-of-phase components), leads to:

$$GAF(q,t) \approx Aq + B\dot{q} \tag{7}$$

Finally, the stability of the coupled system is conditioned by the eigenvalues of the homogeneous problem:

$$\left(p^2\mu + p(\beta - B) + (\gamma - A)\right)q^* = 0 \tag{8}$$

The aerodynamic stiffness A and damping B for the various mode shapes of interest are obtained via harmonic forced motion simulations, which lead to the identification of the generalized aerodynamic force matrix in the frequency domain. The stability of the system then depends solely on the value of the aerodynamic damping B.

In the case of perfectly tuned turbomachine configurations, the geometry and the mechanical solution fields are assumed to exhibit a cyclic symmetry periodicity. This property satisfied by the structural and aerodynamic flow fields allows for channel reduction formulations, which are described in the following subsections.

Phase-Lagged Boundary Conditions

The phase-lagged boundary condition holds in the case of a single purely time-periodic phenomenon. This is basically the case in harmonic forced motion simulations implemented for the purpose of an aeroelastic stability analysis of a perfectly tuned isolated blade row, as described in the previous section.

In the case of cyclic symmetric structures, the deformation of the structure may be represented in the linear case as a combination of nodal diameter mode shapes, for which successive blades vibrate at a specific inter-blade phase angle. The vibration of the row can be described by the duplication of a reference sector, taking into account the phase shift induced by a specific inter-blade phase angle. This property allows for the single-sector reduction of the aeroelastic harmonic forced motion simulation, where only the reference sector is modeled. Specific boundary conditions at the limits of the computational domain are to be used to take into account a specific value of the inter-blade modal vibration phase-shift.

Due to the azimuthal periodicity of the deformation, a generic displacement field can be represented as a Fourier series in azimuth , and taking into account the cyclic symmetry of the row (made up of N identical sectors), it can be expressed as the sum of so-called diameter modes u_n as written below:

$$u(r,\theta,z,t) = \Re\left\{\sum_{n=0}^{N-1} u_n(r,\theta,z,t)\right\} \tag{9}$$

Each nodal diameter component exhibits a boundary condition between the values of u_n at the upper and lower azimuthal boundaries

of the sector, associated with a specific value of inter blade phase angle σ_n, which can be expressed as follows:

$$u_n(r,\theta+\beta,z,t) = u_n(r,\theta,z,t)e^{i\sigma_n} \text{ with } \sigma_n = n\beta \quad (10)$$

where $\beta = 2\pi / N$ is the azimuthal extension of the sector.

In the case of an aeroelastic simulation with a prescribed harmonic motion following an -nodal diameter mode of vibration Φ_n inheriting the same phase-shift property, the temporal evolution of the reference sector displacements can be expressed as:

$$u_n(r,\theta,z,t) = \Phi_n(r,\theta,z)q^* e^{i\omega t} \quad (11)$$

The phase-lagged boundary conditions (10) expressed with the phase angle σ_n can be reformulated for a harmonic motion, in such a way that the displacement fields on both azimuthal boundaries are connected by the time-shift of duration $\tau = \sigma_n / \omega$, corresponding to the propagation time of the deformation/unsteady flow component rotating wave through the sector boundaries:

$$\begin{aligned} u_n(r,\theta+\beta,z,t) &= \Phi_n(r,\theta,z)e^{i\omega t}e^{i\sigma_n} \\ &= \Phi_n(r,\theta,z)e^{i\omega\left(t+\frac{\sigma_n}{\omega}\right)} \\ &= u_n\left(r,\theta,z,t+\frac{\sigma_n}{\omega}\right) \end{aligned} \quad (12)$$

These properties extend to the flow field induced by the structural motion, which also exhibits the same n-nodal diameter azimuthal periodicity at the convergence of the process:

$$w_n(r,\theta+\beta,z,t) = w_n(r,\theta,z,t)e^{i\sigma_n} = w_n\left(r,\theta,z,t+\frac{\sigma_n}{\omega}\right) \quad (13)$$

This condition is implemented in *elsA* for aeroelastic simulations with a prescribed harmonic motion as the so-called "chorochronic" boundary condition, using a moving-average Fourier decomposition process in the time domain that is relevant because of the time-periodic features of the phenomenon. This Fourier analysis is conducted at each time step at upper and lower boundaries of the sector, and characteristic relations are used to establish the equilibrium with the flow reconstructed at a shifted time on the other boundary using the current Fourier coefficients [8] [10].

Extension of the Phaselagged Boundary Conditions in the Case of Stage Aeroelastic Simulations

In the case of harmonic forced motion simulations conducted on a turbomachine stage configuration, two different periodic phenomena are superimposed. The first is the effect of a periodic blade passage of the opposite row, and the second is the rotating wave of deformation induced by the propagation wave of the considered n-nodal deformation mode shape. Since both phenomena are driven by non-commensurable fundamental frequencies in the general case, the resulting unsteady flow field is basically not periodic in time. Using an assumption of small perturbations, the unsteady flow field can be represented as a summation of rotating perturbation waves due to both phenomena. Following Tyler and Soffrin [52] and He [9], the unsteady flow can be approximated as:

$$w(r,\theta,z,t) \approx w_0(r,\theta,z) + \sum_{p=0}^{N_{sp}-1} w_p(r,\theta,z,t) \quad (14)$$

where w_p is a rotating wave associated with a specific phenomenon, whose characteristics are a specific wave number κ_p (or nodal diameter) and a specific pulsation ω_p. Each rotating wave exhibits a specific rotation speed $c_p = \omega_p / \kappa_p$, and phase-lagged boundary conditions like (10) can be applied at the upper and lower boundaries of the considered row sector distant from the sector angle $\beta = 2\pi / N$, with specific phase and/or time shift for each rotating wave, as described in Table 1 [53]. The same approximation based on the superposition principle can also be considered for multistage configurations [54] [12], in which case the rotating waves correspond to the blade passage effects of the two adjacent rows.

	Wave number	Pulsation	Phase shift	Time shift
	κ_p	ω_p	$\sigma = \kappa_p\beta$	$\tau = \frac{\kappa_p}{\omega_p}\beta$
Blade passing	Number of opposite blades N_{opp}	Pulsation of blade passing $N_{opp}\Delta\Omega$	$N_{opp}\beta$	$\frac{\beta}{\Delta\Omega}$
Vibration	Nodal diameter n	Vibration pulsation ω	$n\beta$	$\frac{n\beta}{\omega}$

Table 1 – Frequency-time relationships for a rotating wave component

The moving average Fourier decomposition/reconstruction process at the sector boundaries, as well as on the blade row stage interfaces, is applied here separately for each rotating wave component, in order to prescribe the proper boundary conditions. For better robustness, a relaxation procedure is applied at each time step on the Fourier coefficients of each rotating wave included in the simulation. These boundary conditions are implemented in the following unsteady simulations presented hereafter in the applicative section.

Forced Response in the Turbomachinery Stage

Forced response is a dynamic aeroelastic phenomenon. It corresponds to the dynamic response of a structure due to impinging unsteady aerodynamic forces. Contrary to flutter, the excitation forces are assumed to be independent from the system vibration. However, the excitation forces induce vibration, which in turn adds vibration-induced aerodynamic forces. This phenomenon is likely to occur when upstream wakes are striking a downstream located structure, which is subject to unsteady aerodynamic forces, and therefore starts to vibrate. The level of vibration depends on the mechanical characteristics of the structure (in particular, structural damping) and on the amplitude and frequency of the excitation. This phenomenon can also arise in the case of external flows, for example, when an unsteady wake develops from the main wing surface to the horizontal tail plane of an aircraft, thus creating vibrations, or in the case of turbomachinery flows, where the excitation source may come from the upstream wakes of an adjacent blade row in (multi-)stage configurations or from non-uniformities in the inlet flow breathed by the engine, which can be induced by inlet geometry, a cross-wind generating flow separation or the ingestion of a boundary layer, for example.

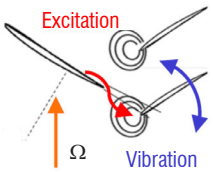

Figure 5 – Illustration of the load sources involved in the forced-response phenomenon for a rotor/stator stage.

Forced Response in the Turbomachinery Stages

In the case of a turbomachinery engine stage, let us say for a rotor/stator configuration like the one described in Figure 5, the flow field of the rotor is seen at each rotation by the stator blades as an unsteady perturbation, due to the differential rotation between both row frames. This effect generates an excitation of the stator blades whose frequency is a multiple of the rotation speed. Potentially dangerous forced-response levels may occur when there is coincidence between the excitation frequency and the natural frequency of the excited system. When this frequency is close to one of the blade eigenmodes, the blade oscillates and the vibration amplitude may be large depending on the system damping. A high vibration level may lead to material fatigue, or even destruction of the blade row.

In the turbomachinery case, frequency coincidences are likely to occur between rotation speed harmonics and natural frequencies of the different mode shapes of the excited row, especially during low to high regime of rotation modifications for operating condition transitions of the engine (acceleration or deceleration). Therefore, the potential coincidences are usually plotted in the classical Campbell diagram, as shown by the intersections of curves in Figure 6.

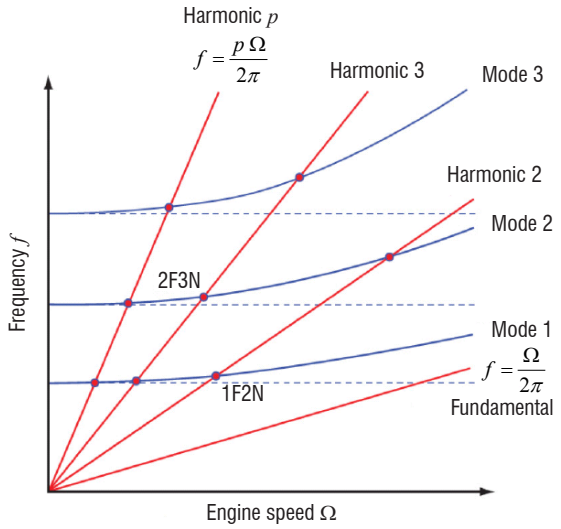

Figure 6 – Campbell diagram representing the structural mode frequencies as a function of the rotation speed in blue, and the different engine harmonics in red. Crossings between both types of curve may lead to a high level of vibration.

Forced Response of a Linear Structure

As for the weakly-coupled aeroelastic simulations performed for flutter analyses, a linear elastic model of the structure can be considered and the projection of the dynamic equations of motion on the mode shapes of interest leads to the reduced system of Equation 3 already considered for flutter in the previous section. The analysis of the forced-response phenomenon is, however, different from that of the aeroelastic stability of the system, since the purpose is to study the system response to an excitation field, in order to find the amplitude and phase of the induced vibration. The aeroelastic forced response is due to the combination of two kinds of generalized aerodynamic forces $GAF(t) = F_{exc}(t) + F_{vib}(t)$:

- the excitation generalized force F_{exc} (assumed to be motion independent) due to an external force,

$$F_{exc}(t) = \Phi^t F_{Aexc}(t) \tag{15}$$

- the aeroelastic generalized force F_{vib} generated by the structure vibration due to the excitation,

$$F_{vib}(q,t) = \Phi^t F_{Avib}(x,t) \tag{16}$$

Under the assumption of force linear superposition, which is standard in classical linear aeroelasticity, the contribution due to the vibration F_{vib} can be approximated as in Equation 7 for flutter analysis, as:

$$F_{vib}(q,t) \approx Aq + B\dot{q} \tag{17}$$

Substituting the previous expression in the dynamic equation of motion (3) results in:

$$\mu\ddot{q} + (\beta - B)\dot{q} + (\gamma - A)q = F_{exc}(t) \tag{18}$$

The effect of the aerodynamic forces due to the vibration is double:

- Induce additional stiffness (A coefficient),
- Induce additional positive or negative damping (B coefficient).

This aerodynamic damping B is likely to influence the level of forced response of the system. As is well known, near resonance, the level of vibration of a linear structural dynamic system is, roughly speaking, inverse proportional to the damping coefficient. Therefore, in order to properly predict aeroelastic forced response levels, it is mandatory to correctly evaluate the total aeroelastic damping $\beta - B$ and, consequently, of the aerodynamic damping B. The situation is all the more critical in the case of small values of the structural damping β, which may be small compared to aerodynamic damping B.

Classical Numerical Approaches for the Resolution of Forced-Response Problems

Several numerical approaches are available for the resolution of aeroelastic forced response problems.

The first one is the classical linear superposition method. In this approach, both the excitation and vibration phenomena are handled separately. The corresponding aerodynamic forces F_{exc} and F_{vib} are then summed, following a linear superposition assumption whose relevance has been investigated [34] [55]. Therefore, two numerical simulations are performed, the first taking into account the excitation only (no vibration), and the second with vibration and no excitation. The vibration simulation gives access to the aerodynamic stiffness and damping, but a linear assumption is made. Moreover, no coupling between excitation and vibration can be represented. This time domain approach may be expensive, because two fully-converged simulations are necessary, but frequency-domain approaches can help to reduce these costs [34].

The second approach is the fully-coupled fluid/structure dynamic simulation [34] [35]. This brute force approach does not make any assumption of linearity or superposition. The fully-coupled fluid-structure system is solved in the time domain. Aerodynamic non-linearities are taken into account, and excitation and vibration forces are fully represented and coupled. However, for low damping values, the simulation may be very expensive, due to the large transient needed to reach the stabilized periodic solution, which is characteristic of the forced-response phenomenon.

The extension of the method to non-linear structures is not considered here, but may be addressed either in the case of lal non-linearities using

the Craig and Bampton approach including additional degrees of freedom, and non-linear force terms or, in a more general framework, using specific methods for the resolution of the non-linear structural dynamics, such as the harmonic balance method for structures (see [56]).

Twin Approach

A third approach has been proposed by Mesbah [57], and evaluated at ONERA [58], which is referred to as the twin approach. In this approach, both vibration and excitation phenomena are included in the same single simulation, which is the so-called "twin" simulation. No linearization of the aerodynamic forces (as in the decoupled approach) is introduced here, but there is no need to solve for a long transient either, until forced response levels convergence (as in the time domain coupled approach), which may be extremely expensive, especially for low damping values. Indeed, the simulation is not coupled in the sense that a forced vibration motion is prescribed at the excitation frequency and at a specific amplitude and phase angle with respect to the excitation. These amplitude and phase angles are tuned during the simulation, in order to reach the proper values matching the forced-response phenomenon. To this end, the equilibrium of the structural dynamic system (3) subject to the combined aerodynamic forces $GAF(t)=F_{exc}(t)+F_{vib}(t)$ is solved and the characteristic of the (multi)harmonic motion is iteratively corrected until convergence.

The corresponding procedure is described as follows. At forced response, the aerodynamic forces and motion are periodic and the structural dynamics equations (3) are considered. The generalized modal coordinate q associated with the mode shape Φ of interest for the forced response is assumed to have the following complex harmonic form:

$$q = q^* e^{j\omega t} \text{, with } q^* \text{ complex.} \tag{19}$$

Seeking a harmonic response in terms of generalized forces (linear aerodynamic behavior assumption), the generalized aerodynamic forces can be approximated as:

$$GAF(t)=\Phi^t F_A(t) \approx F^* e^{j\omega t} \text{, with } F^* \text{ complex.} \tag{20}$$

In the frequency domain, the structural dynamic equation (3) projected onto the modal basis is now written as:

$$\left(-\omega^2\mu + j\omega\beta + \gamma\right)q^* = F^* \tag{21}$$

and the corresponding frequency response function

$$H = \frac{q^*}{F^*} = \frac{1}{\gamma - \omega^2\mu + j\omega\beta} \tag{22}$$

gives access to the amplitude of the harmonic motion response due to the combined aerodynamic force, and to the phase angle between force and motion. This equation can be extended to the periodic, multi-harmonic problem and gives, in this case, access to the fundamental and harmonic components of the motion.

A non-linear iterative procedure is needed to simultaneously converge motion and aerodynamic force components. This can be a fixed-point procedure, with or without smoothing, or a Newton procedure, which needs to evaluate the Jacobian matrix of a residual term. In any case, proper convergence of the aerodynamic forces due to vibration is mandatory, in order to correctly evaluate the aerodynamic damping of the involved vibration mode, which is of prominent importance for an accurate prediction of the forced response amplitude.

Applications

This section presents an overview of several application activities implementing the previously detailed aeroelastic capabilities of *elsA*. Two applications concern the CFD-CSM coupling procedure presented in Section 0which has been used within the framework of the ENOVAL and ADEC European projects. Two other items are presented concerning the use of the phase-lagged and multiple frequency phase-lagged sector reduction capabilities detailed previously for stage and multi-stage configurations, during the COBRA Europe-Russia collaboration and within the framework of the *elsA*-ASO development program with SAFRAN. Finally, some results relative to the forced-response twin methodology are presented. Caution: Due to the confidential features of the presented industrial applications, figures have been suppressed from specific plots.

ENOVAL UHBR Fan Flexible Operating Map Prediction

An application of the developed simulation tools based on the coupling of *elsA*/Ael and MSC/Nastran has been performed for the purpose of computing the hot-shape of a UHBR fan blade within the framework of the European project ENOVAL.

The implemented fan model is shown in Figure 7. On the left side, a view of the aerodynamic sector domain is displayed. The middle plot presents the selected reduced structural model nodes defining the

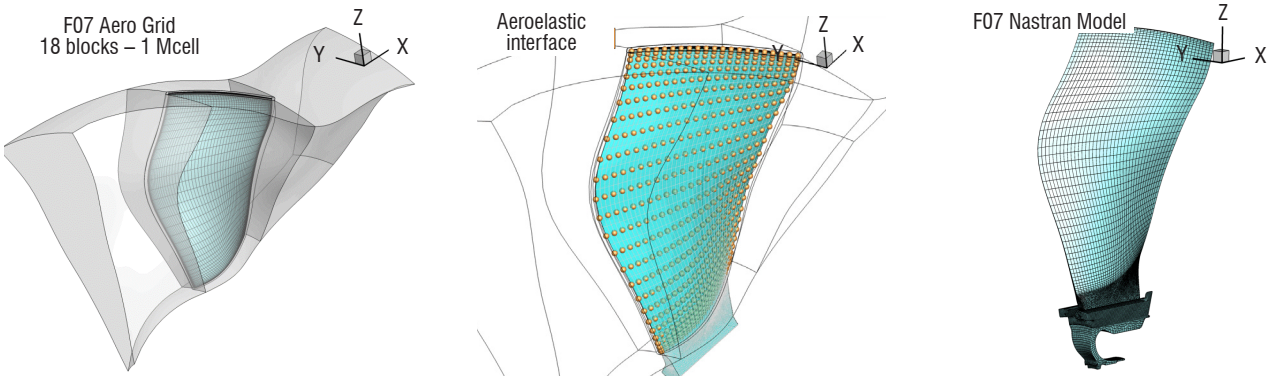

(a) Single-passage aerodynamic computational domain

(b) Interface nodes of the fan blade for the aeroelastic transfer of data

(c) Structural Finite-Element grid including the disk

Figure 7 – ENOVAL fan aeroelastic model

aeroelastic transfer model. On the right, the full Finite-Element model used for static non-linear large displacement structural simulations with Nastran is plotted.

The present fully non-linear coupling algorithm has been put to the test for the computation of the massflow to pressure ratio characteristic map of the fan for 100% of the nominal speed line. Contrary to the standard procedure, where a single shape (computed on the nominal operating line) is used for the evaluation of the performance of the fan, the coupled fluid-structure equilibrium is evaluated at each point of the characteristic line, which means that a specific shape is computed at each point of the map, due to modification of the pressure loads.

The *elsA* solver is implemented using the Smith $k-\ell$ turbulence model, on an aerodynamic grid including the Outlet Guide Vane (OGV),

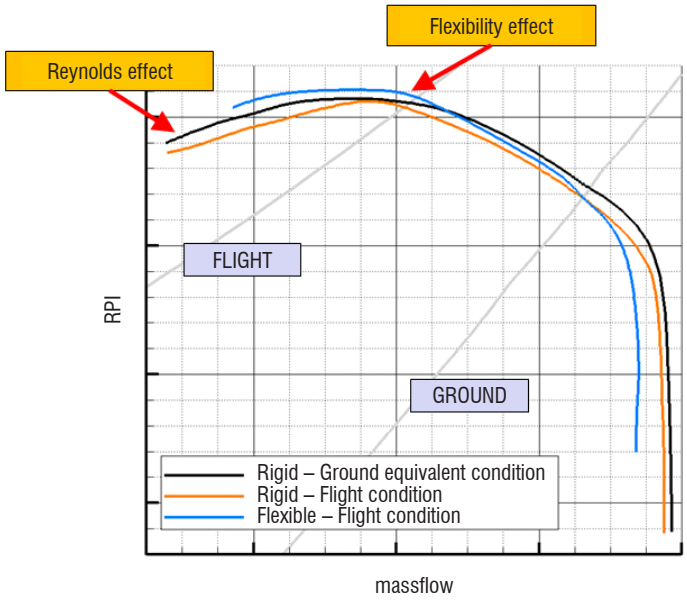

Figure 8 – Influence of the aeroelastic flexibility effect on the characteristic line at 100% Nn

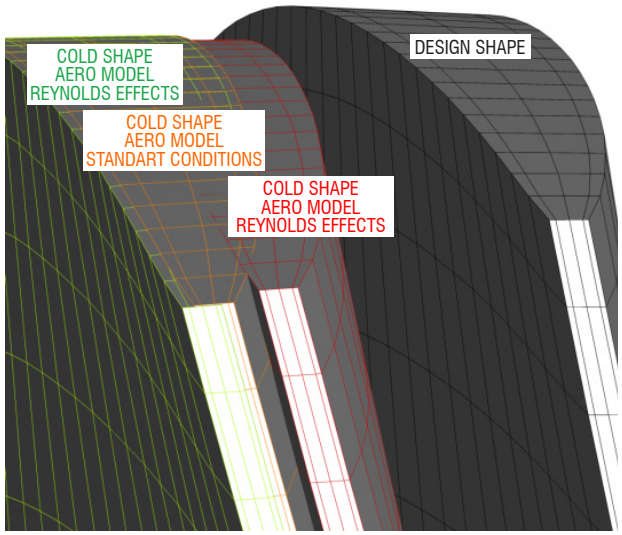

Figure 9 – Blade tip deformations with respect to the rigid design shape.

of 1.6 Mio cells. The fan performance for ground conditions computed with flexible shapes is compared in Figure 8 to those obtained with a single rigid shape for all operating points of the speed line.

Reynolds effects are taken into account in comparing aerodynamic loads classically obtained with flight conditions and extrapolated to ground conditions in the rigid blade case (Figure 9 in orange and black) and that obtained with the present coupling method, in the flexible blade case, with flight conditions (in blue).

The impact of taking into account flexibility is visible in Figure 8 (orange line: rigid computation, blue line: flexible computation). Differences in terms of maximum pressure ratio and blocking massflow occur, which are related to the variation in blade shape due to flexibility. In particular, blade twist evolves with the pressure ratio in the case of a flexible computation, whereas it remains fixed at its design value in the rigid computation. In the flexible case, an increase in the twist angle under blocking conditions induces a channel section reduction responsible for massflow reduction with respect to the rigid simulation. For high-loaded conditions, flexibility induces a tip gap reduction, leading to better blade efficiency and a higher maximum pressure ratio.

However, one bottleneck for the generalization of the procedure for the entire fan map is the robustness of the mesh deformation process, due to the large variations in the fan shape, especially considering the fan tip gap region, which may vary considerably, inducing large mesh stretching (Figure 9). One clue for the extension of the procedure will be the improvement of mesh deformation technique robustness and efficiency.

CleanSky II / ADEC CROR Non-Linear Hot Shape Prediction

The present CFD-CSM coupling procedure has also been implemented within the framework of the CleanSky 2 ADEC European project, for the purpose of predicting fan blade hot shapes of the AIPX7 Airbus CROR model shown in Figure 10, tested at the Z49 rig in the S2Ma ONERA wind-tunnel facility [32][59].

For this study, non-linear structural modelling has been implemented in coupling *elsA* using the solution SOL400 of MSC/NASTRAN, in order to take into account geometric non-linear large displacement

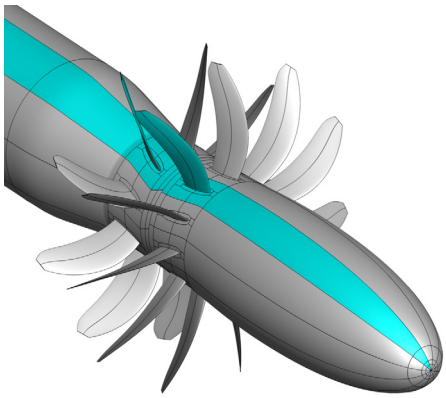

Figure 10 – Full AIPX7 CROR model and single sector model highlighted in cyan

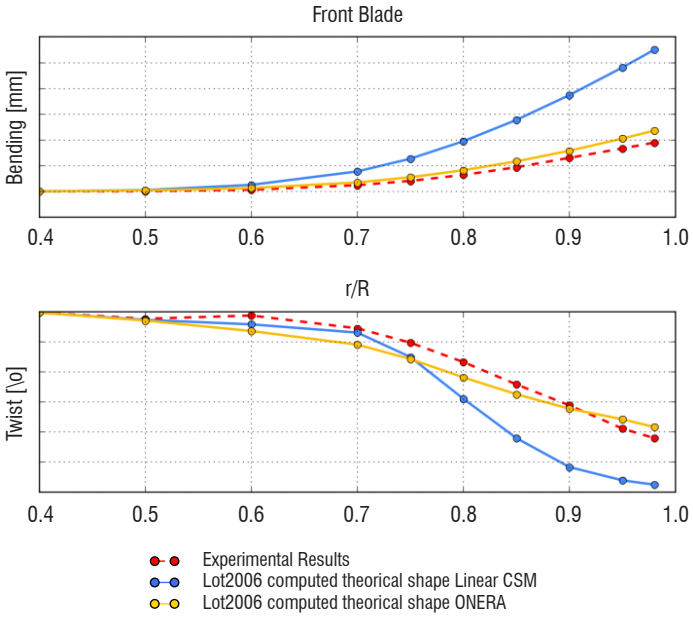

Figure 11 – Comparison between CFD-CSM coupling simulation and experimental results for the AIXP7 front blade at Z49 rig @ cruise conditions $Ma = 0.75$

effects. In order to highlight the need for non-linear structural modeling in hot shape predictions in this case, Figure 11 shows a comparison between the blade displacements, in terms of bending (top) and twist angle (bottom), obtained using linear CSM (in blue) and nonlinear CSM (in orange) during hot shape computations for the front rotor blade, in comparison with the experimental data in dashed red lines. The selected operating point for this comparison is located at $Ma = 0.75$, for a rotation speed of 4510 rpm, at 0° angle of attack. The linear approach overestimates both the blade bending and blade twist by a factor 2. In comparison, non-linear results fit the experimental data very well.

During this study, manufactured blade shape measurements were performed by Airbus using the Z49 test facility. Part of the work was dedicated to evaluating the consequences of manufacturing uncertainties on numerical hot shape prediction. Figure 12 (a) shows blade deformation comparison, in terms of bending (top) and twist (bottom) versus blade span for the front rotor blade.

The blue and orange curves respectively depict the computed deflection using the CAD shape and the experimental shape. Although fair agreement with the experimental data is observed for both models, taking into account the real manufactured shapes improves the results for twist angle in the blade tip region. Results for the rear blade are shown in Figure 12 (b). Experimental and numerical results are in good agreement with regard to the bending, but major discrepancies are observed with regard to the twist. It seems that a physical phenomenon is missed by the numerical simulations. First investigations tend to show that the blade vortex interaction may have an impact on the blade displacements, but the mixing plane boundary conditions prescribed at the front and rear rotor interface, which forces a steady solution in the CFD computations, does not allow this unsteady interaction to be taken into account.

Work is now ongoing in order to take into account this phenomenon using 360° simulations, and to perform numerical restitutions of unsteady blade deformations for experimental operating points with nonzero angle of attack.

COBRA Contrafan Aeroelastic Stability Analysis

ONERA is a partner in the COBRA Europe-Russia cooperative research project, in collaboration with SAFRAN, DLR, CIAM and COMOTI. The purpose of COBRA is to design a high by-pass ratio (15-25) contra-fan resulting in much lower blade tip speed and blade count, able to improve aerodynamic and acoustic efficiency. This section presents the activity carried out as part of the work package WP4 of COBRA to assess the aeroelastic stability of Version V4bis of the VITAL contrafan designed during the project. Figure 13 presents the geometries of the structure and aerodynamic models. Both front and aft fans are fully metallic and made of titanium.

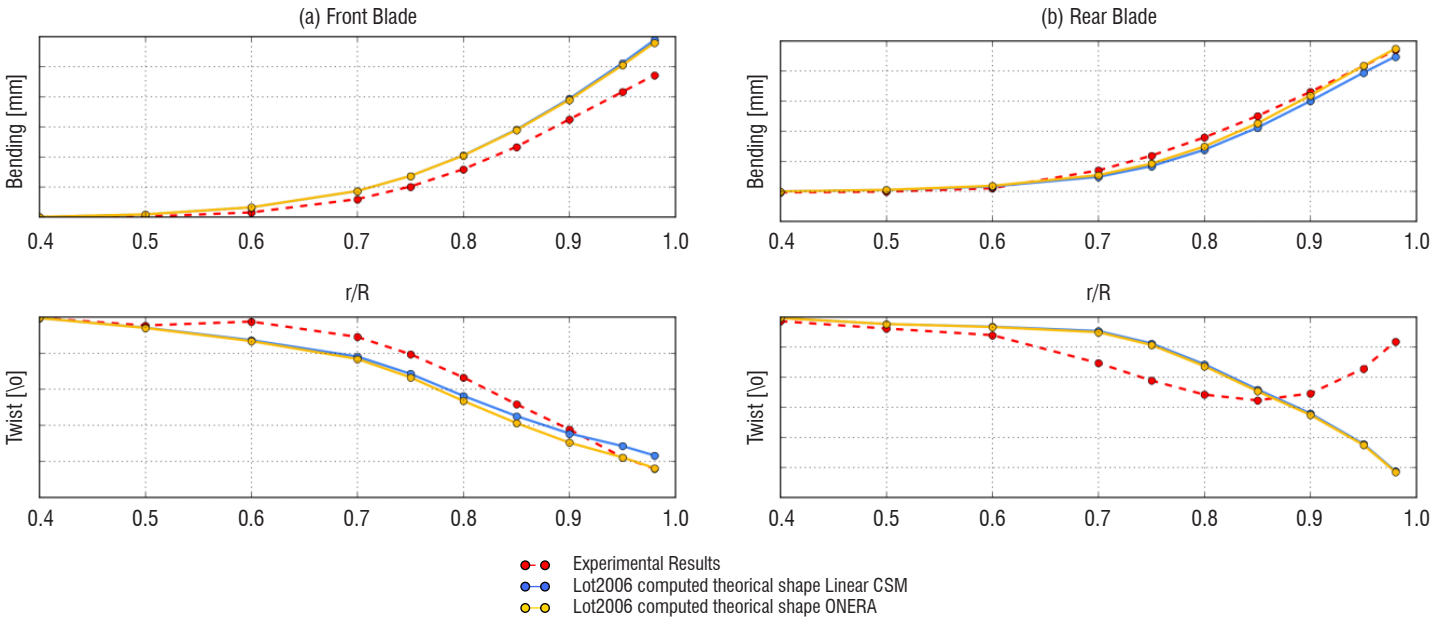

Figure 12 – AIXP7 at Z49 rig – CFD-CSM coupling simulation @ cruise conditions $Ma = 0.75$. Comparison between manufactured shape and CAD shape blade deflections

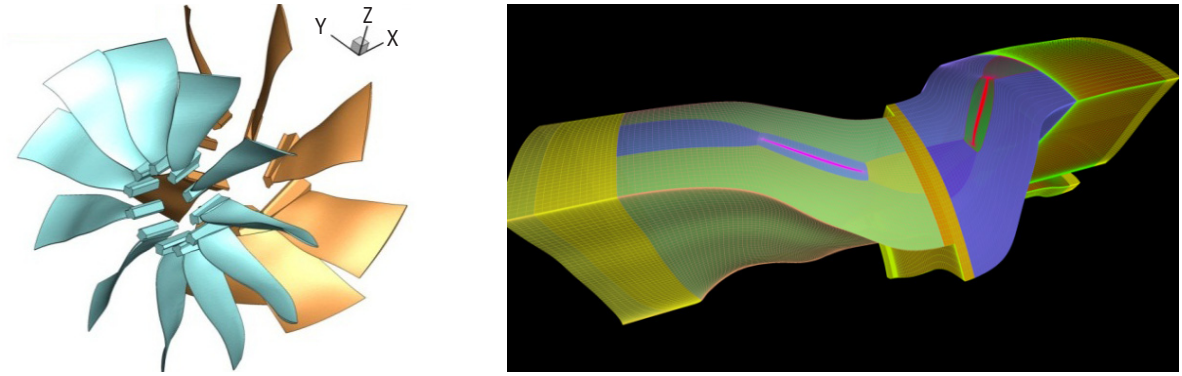

(a) Structural model of front and rear fan

(b) Single-passage aerodynamic computational domain

Figure 13 – COBRA contrafan structural and aerodynamic models

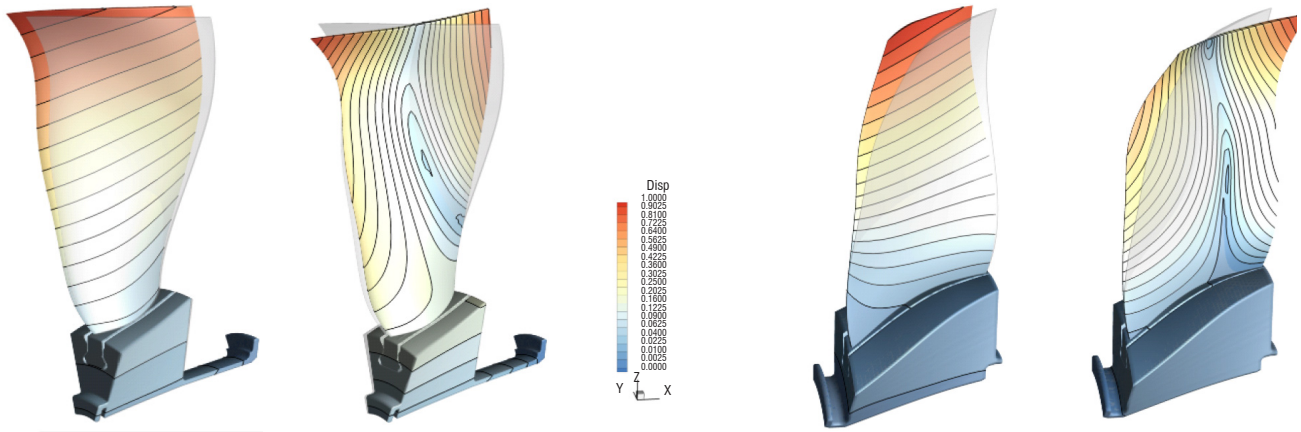

(a) Front blade

(b) Aft blade

Figure 14 – 1F, 1T structural modes @ design point for the nodal diameter 0

For aeroelastic simulations, finite-element grids have been generated for both blades using an in-house software, and connected to blade disk models provided by COMOTI. NASTRAN SOL106 non-linear static analysis, followed by a normal mode analysis, is performed to obtain the eigenmode basis relative to the non-linear deformed shape, including large displacement effects. Figure 14 illustrates the obtained mode shapes at nodal diameter 0, at the aerodynamic design point, for the front blade model (a) and for the aft one (b).

Aerodynamic steady computations have been performed using *elsA* and compared to equivalent results obtained by the DLR. Some discrepancies have been observed in terms of max massflow values, as well as max pressure ratio near stall, which may be due to different design evolutions between both models (Figure 15).

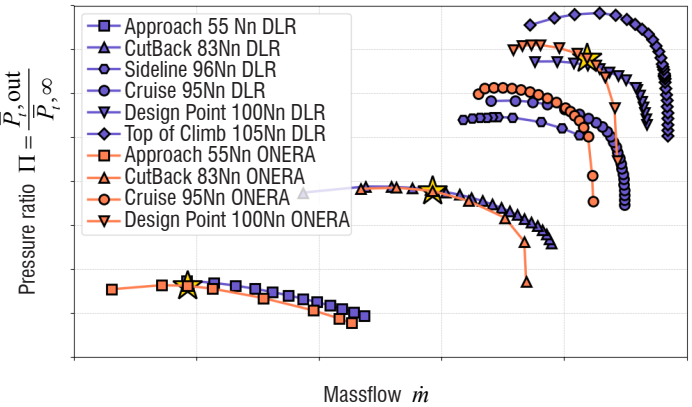

Figure 15 – COBRA contrafan operating map for a different rotation speed

Numerical simulations were then performed using *elsA,* in order to study the aeroelastic stability of the contrafan. In this case, sector reduction was implemented, with classical phase-lagged boundary conditions, assuming no unsteady aerodynamic interactions between both fans. Therefore, an azimuthal average mixing plane boundary condition based on characteristic relations was applied at the row interface, and a single aeroelastic rotating wave was taken into account in each row domain. No provision was made here for rotor-stator unsteady interactions, which was addressed using the multi-chorochronic approach previously detailed.

Aeroelastic simulations have been conducted for 3 operating points indicated by the yellow stars in Figure 15. The Dual Time Stepping scheme has been used for the time-consistent resolution of the aerodynamic response to a harmonic forced motion following modal vibrations of each blade row. 26 vibration periods have been computed, in order to reach a conveniently converged periodic solution. First and second bending and first torsion modes have been investigated for each blade row, along with inter-blade dephasing patterns matching 7 (resp., 6) values of nodal diameter over the 11 (resp., 8) possible values for the front (resp., aft) blade. A set of 117 non-linear deformable unsteady aeroelastic URANS simulations requiring the use of phase-lagged boundary conditions have thus been run on 32 cores, each of them corresponding to a typical wall clock computation time of 13 hours.

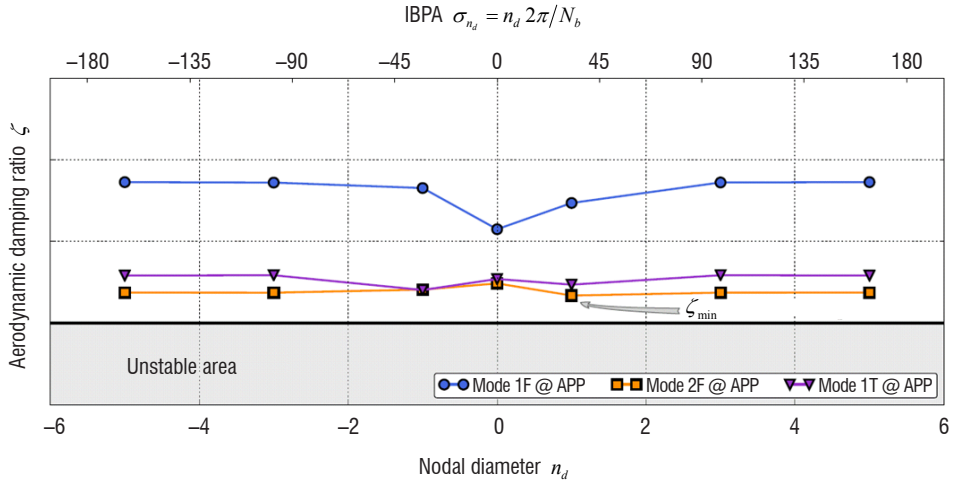

Figure 16 – Approach case – Row 1: aerodynamic damping evolution *vs.* nodal diameter for 1F, 2F and 1T modes

The harmonic analysis of the generalized aerodynamic forces leads to the extraction of the corresponding damping values, which are plotted in Figure 16, for the Approach operating point, and for the three selected mode shapes (namely the first and second bending and first torsion). The minimal value of aerodynamic damping is obtained in this case for the second bending at nodal diameter 1. However, the full configuration stays clear of flutter in any case investigated here.

ASTEC2 Multi-Stage Compressor Analysis with Multiple Frequency Phase-Lagged Boundary Conditions

Multiple-frequency phase-lagged boundary conditions have been put to the test (Placzek & Castillon, Aeroelastic Response of a Contrafan Stage Using Full Annulus and Single Passage Models, 2014) (Placzek, Aeroelastic damping predictions for multistage turbomachinery applications, 2014) in the case of the multi-stage axial compressor configuration provided by SAFRAN HE, composed of 6 rows, including a structural strut row R1, an inlet guide vane (IGV) R2 and two rotor/stator stages R3/R4 and R5/R6. Due to the high number of blades of the full 360° configuration (131 blades), a single passage modelling approach is considered for aeroelastic unsteady configurations, in order to keep within acceptable CPU time resources. Aerodynamic interactions between adjacent rows are taken into account with the implementation of the multiple-frequency phase-lagged boundary condition detailed previously.

Several models have been considered to validate the proper use of interface boundary conditions between Rows 1 and 2 and the multiple-frequency phase-lagged boundary condition setup. A full 360° annulus slice model (blue geometry in Figure 17, with 6.5 Mio cells) and the corresponding single passage reduction model (0.54 Mio cells) were first built, in order to cross-validate at a lower cost the implementation of the multiple-frequency phase-lagged boundary conditions. For the 3D configuration (grey geometry in Figure 17), only a single-passage model was used, including 164 blocks and roughly 16 Mio cells.

The steady operating map for the 3D model is presented in Figure 18, with the pressure fields for 3 different operating points. A reference unsteady simulation is then performed with the full 360° annulus slice multi-stage configuration, using 64 processors. The simulation is run for 14.4 revolutions, so that a periodic state can be reached for a total wall-clock time of about 10 days. This simulation is compared to the equivalent single passage simulation performed using multiple frequency phase-lagged boundary conditions to allow for the propagation of blade passage perturbation rotating waves. In this case, a maximum of two spinning modes is considered, corresponding to the rotating waves produced by the blade-passing of the two adjacent rows with nonzero relative speed. For all spinning modes, 48 harmonics are computed with a low value of the relaxation coefficient to

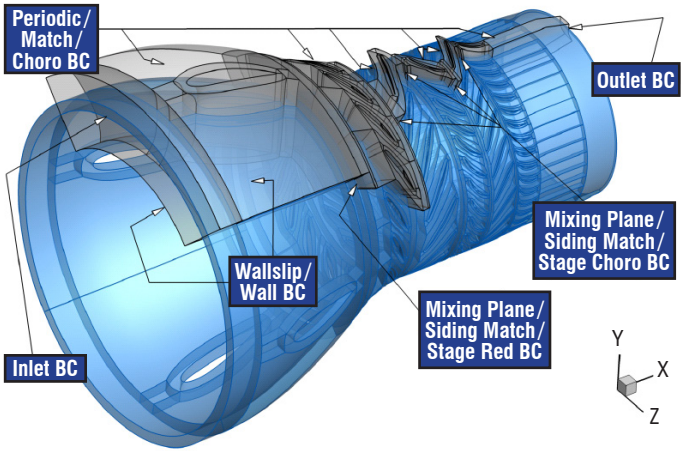

Figure 17 – SAFRAN HE multistage compressor configuration: single passage reduction (grey) vs. 360° full annulus slice model (blue)

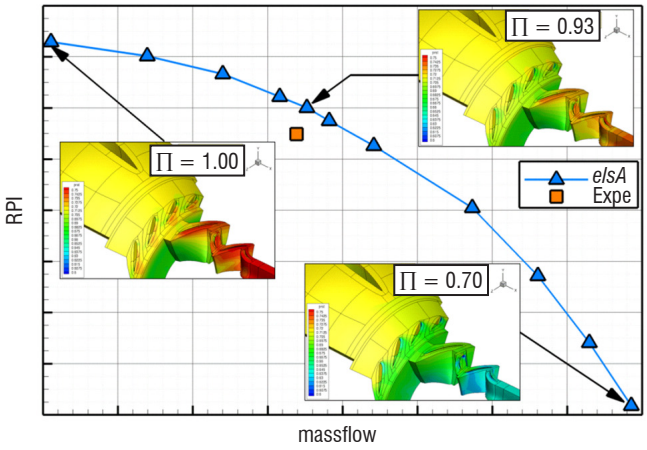

Figure 18 – Compressor operating map of the 3D single-passage model

ensure proper convergence. Due to the small value of the relaxation coefficient, the transient is longer than for the full annulus simulation, but a periodic state is reached before the end of the 14.4 revolutions. The computation is run on only 14 processors, for a global wall-clock time of 2 days and 8 hours.

Figure 19 presents, at the pressure time, histories recorded on numerical pressure sensors located at the mid chord of each blade (#04 on R1, #10 on R2, #18 on R3, #26 on R4, #34 on R5 and #42 on R6). The results from the full 360° annulus slice model are compared as a reference to the single-passage reduction solution using the multiple-frequency phase-lagged boundary conditions involving two different values of the relaxation parameter α .

The agreement between both solutions is satisfactory in terms of global frequency content and, to a lesser extent, in terms of amplitude, see Figure 20. The blue curve corresponds to the multiple frequency phase-lagged case, with the highest value of relaxation coefficient $\alpha = 0.5$, which however leads to a divergence of the simulation. The spectral analyses of the time histories at the bottom reveal that, apart from an unexpected asynchronous frequency observed at 7.5 Engine Order ($EO = f / \Omega$) with the 360° simulation in the first 4 rows, the spectral content is driven by the blade passage frequencies in the different blade rows, with the main contribution of the 16th EO and its first harmonic (32nd EO) in R1 and R2, because of the blade-passage effect of the first rotor R3 made up of 16 blades. In blade row R3 the 16th EO due to the passage of R2>R3 and the 29th EO due to the passage of R4>R3 are dominant, with the additional 45th EO induced by the combination of the 16th and 29th EO. The blade passages of R3>R4 and R5>R4 induce significant levels of pressure fluctuations at the 16th and 23rd EO, respectively, in blade row R4 and, finally, in blade row R5, the 29th and 43rd EO induced by the blade passage of R4>R5 and R6>R5 contribute mainly, whereas only the 23rd EO due to the passage of R5>R6 is visible in blade row R6.

It must be pointed out that a small relaxation factor ($\alpha = 0.1$) is necessary to ensure the robustness of the multiple-frequency phase-lagged approximation for long-time simulations and to avoid the apparition of spurious frequencies. Moreover, the full 360° annulus model response exhibits an asynchronous frequency generated by a separated flow area downstream from R2 that cannot be captured by the multiple-frequency phase-lagged approximation.

The unsteady rigid simulation has also been performed in the case of the 3D single passage model for the intermediate operating point

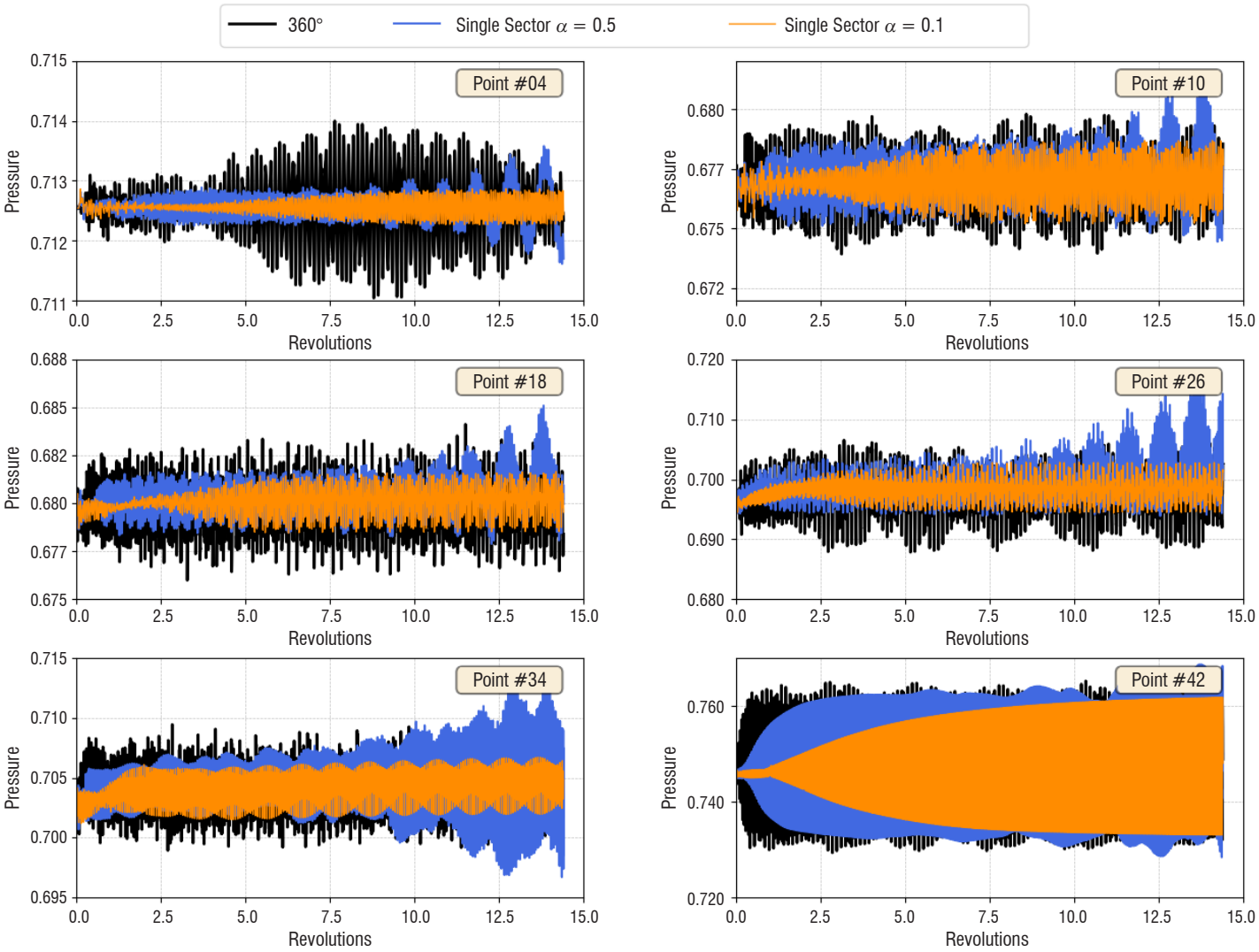

Figure 19 – Pressure-time histories of blade skin sensors for the full 360° annulus slice model vs. the single-passage slice model with different values of the relaxation parameter

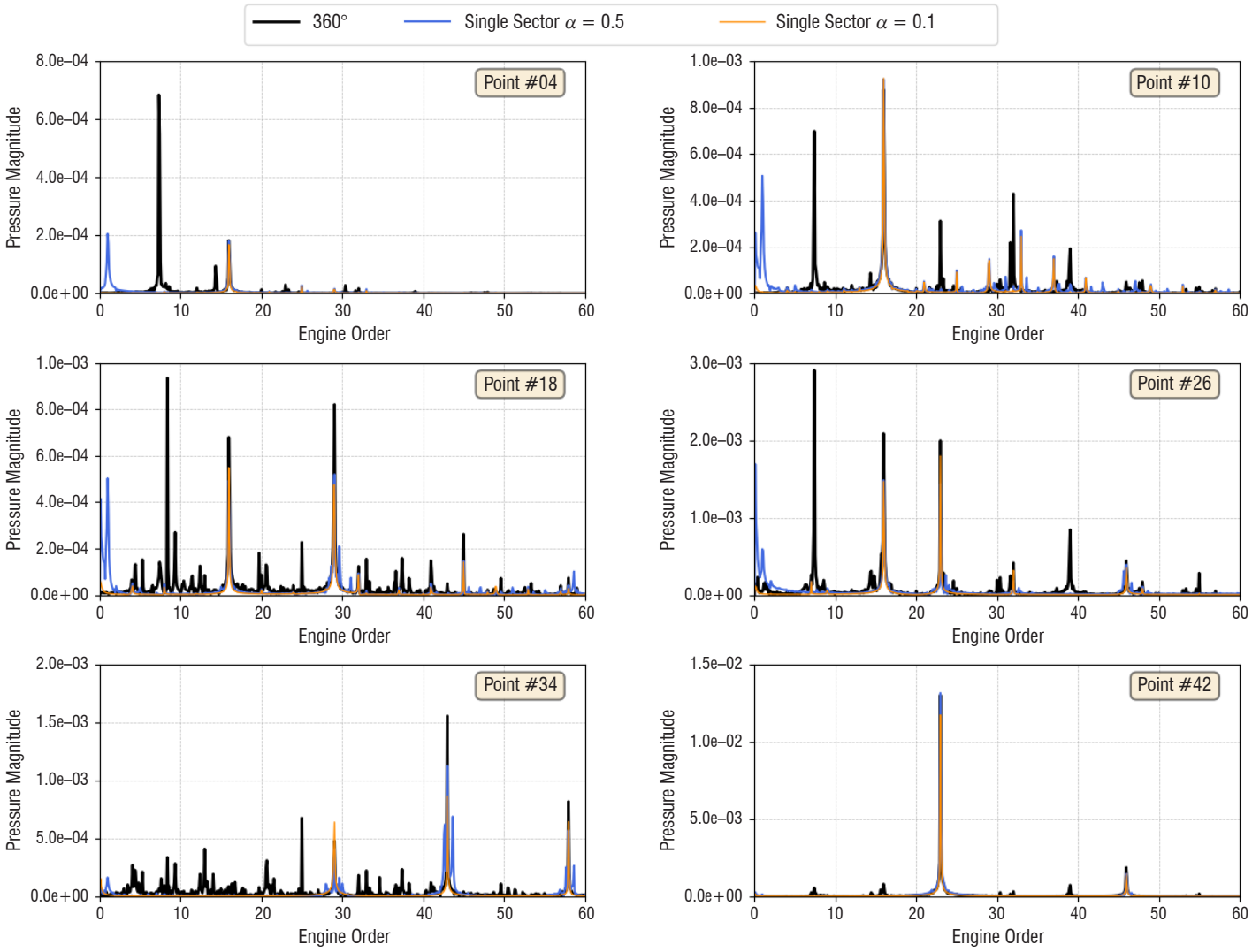

Figure 20 – Frequency content of the pressure blade skin sensors for the full 360° annulus slice model vs. the single-passage slice model with different values of the relaxation parameter

on the speedline shown in Figure 18. Figure 21 and Figure 22 present, respectively, the time histories and spectral analyses recorded by the same pressure sensors as those monitored with the 360° slice model. These simulations, however, have not been validated against the full 360° 3D configuration equivalent results, for clear CPU cost reasons. The simulation for the single-passage model run with 90 processors indeed requires a total wallclock time of 20 days to cover 30 revolutions.

The use of the multiple-frequency phased-lagged boundary condition approach for a multi-stage compressor configuration has been validated on a slice reduction of the machine against full 360° annulus model results. This validation, however, has been made for the rigid case, due to the lack of data for a proper aeroelastic validation setup. Moreover, a demonstration of the capability of the multiple frequency phase-lagged approach has also been made on the 3D single-passage model.

A fully-aeroelastic validation implementing a modal vibration of a row, although already conducted on the simpler VITAL contrafan stage configuration [53], has still to be conducted on the ASTEC2 case, in order to fully validate the approach for aero-structure problems of multi-stage configurations.

Forced-Response Problems

The twin method presented in the previous section has been tested in the case of a transonic gust-generator experimental system [37], developed within the framework of the SFWA European project, implementing a basic forced-response problem.

Figure 23 presents the experimental device that consists of an aeroelastic model (foreground), comprising an OAT15A airfoil placed on a mechanical suspension system, and a gust generator (background), comprising a set of two NACA airfoils oscillating in phase. The arrow shows the propagation of the gust. The system is located in the ONERA S3Ch transonic wind-tunnel. The two front airfoils of the Gust Generator device synchronously oscillate in pitch to generate a gust flow that excites the aft profile. This airfoil is free to move according to its mechanical suspension system properties, allowing a pitch and heave motion. The aerodynamic excitation due to the wake thus leads to a periodical forced response motion of the OAT airfoil.

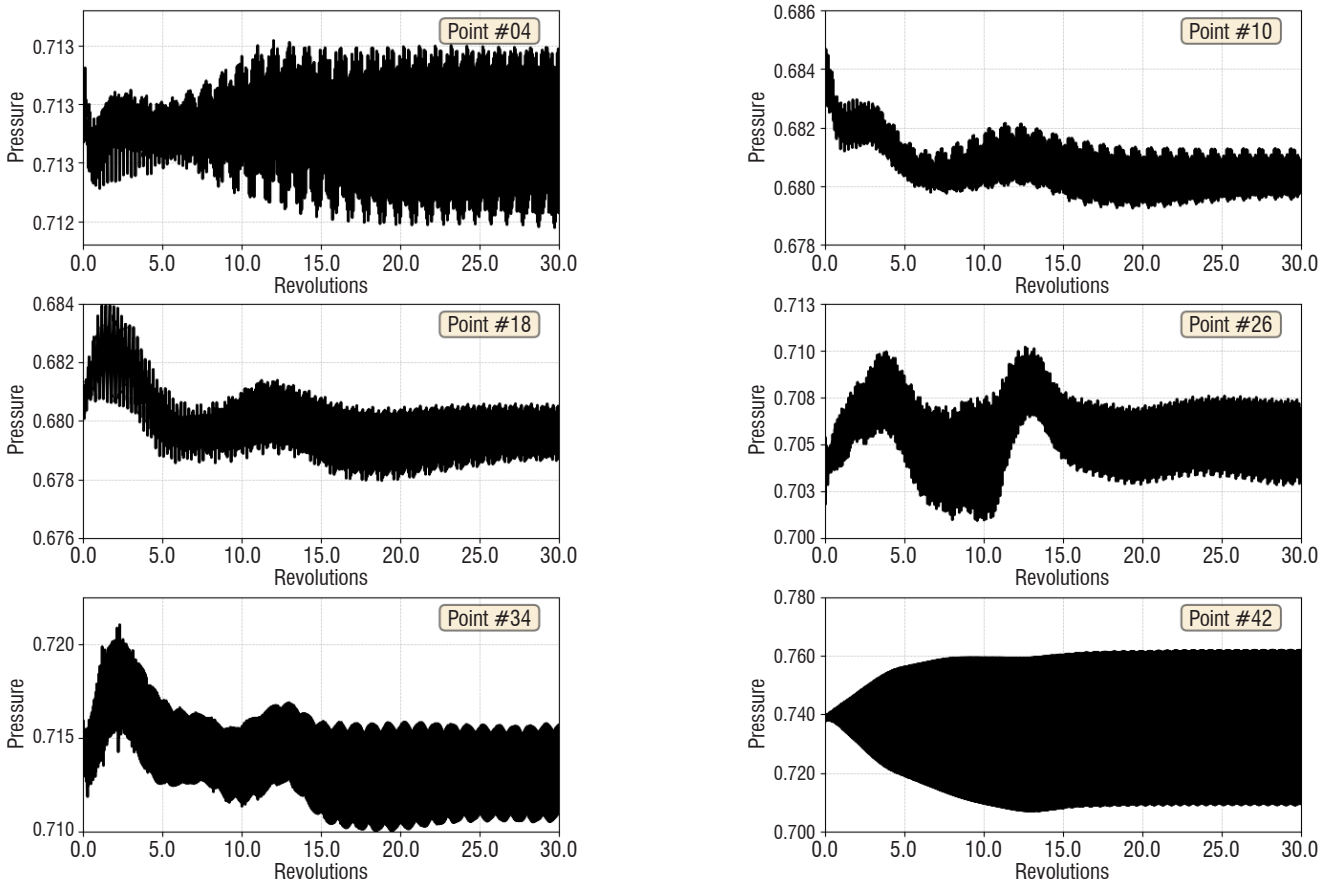

Figure 21 – Pressure time histories of blade skins sensors for the 3D single passage model with $\alpha = 0.1$

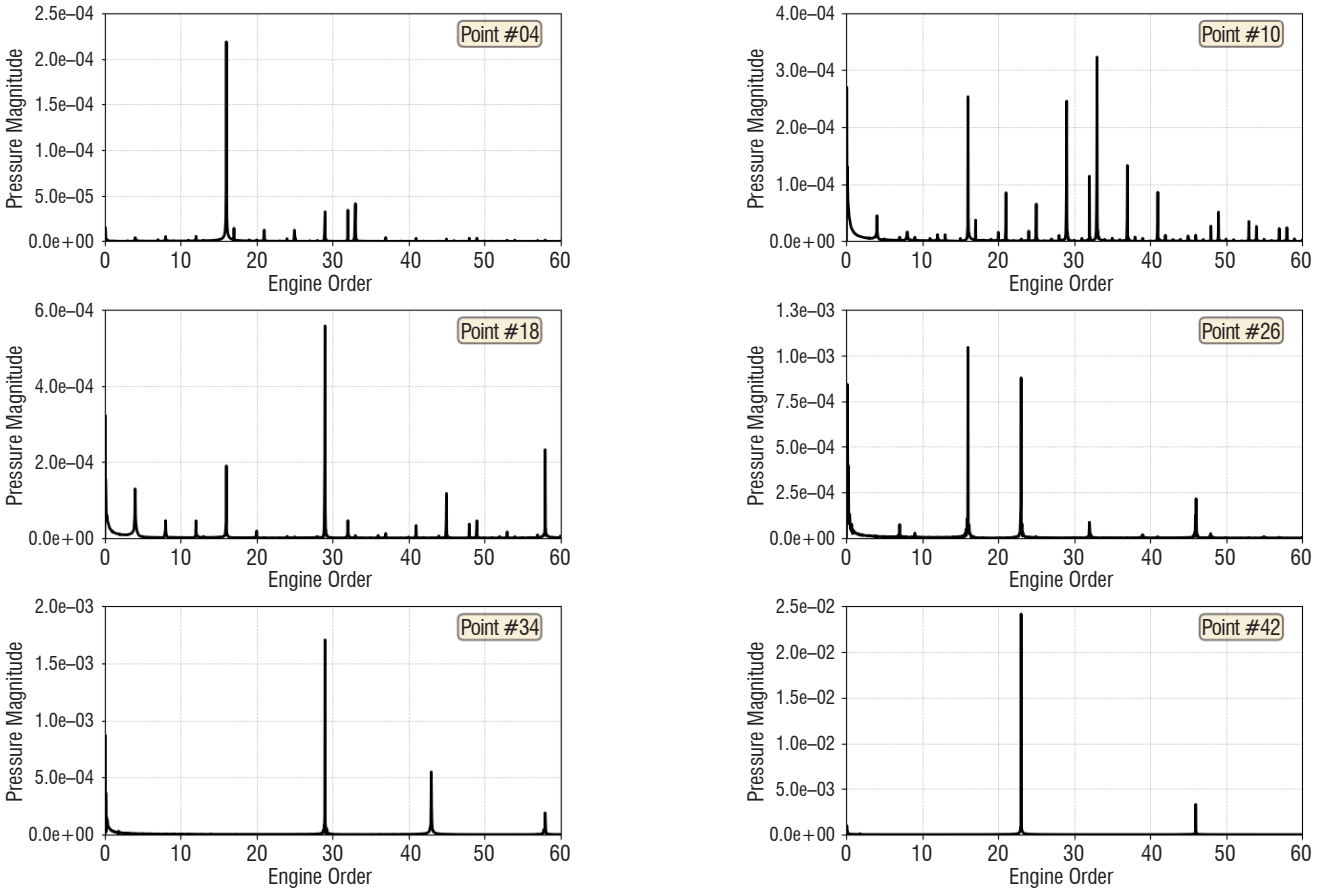

Figure 22 – Frequency content of the pressure blade skin sensors for the 3D single-passage model with $\alpha = 0.1$

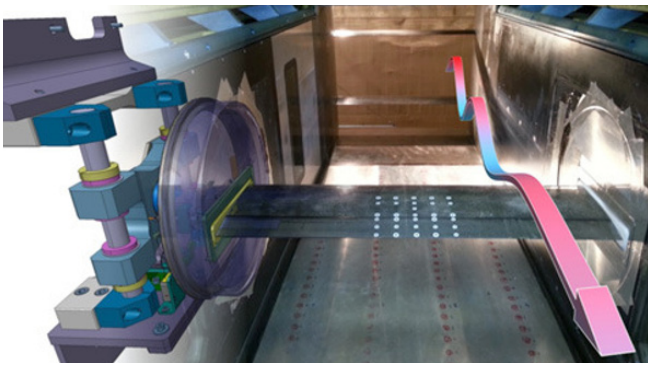

Figure 23 – SFWA Gust-generator experimental setup

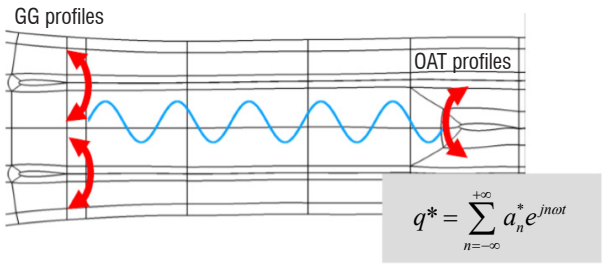

Figure 24 – Twin forced-response procedure implementing gust excitation and prescribed forced motion of the excited profile

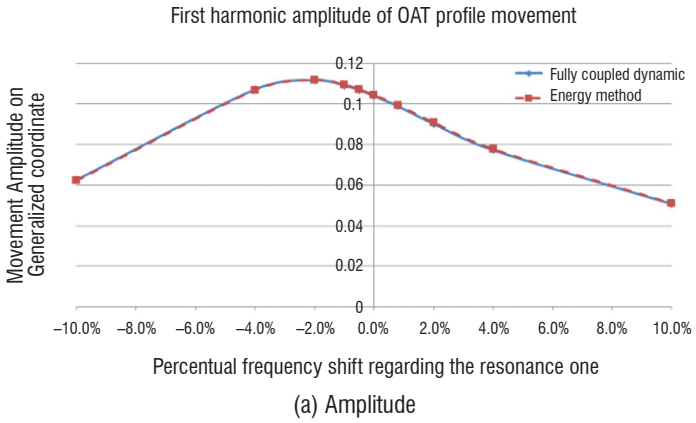

(a) Amplitude

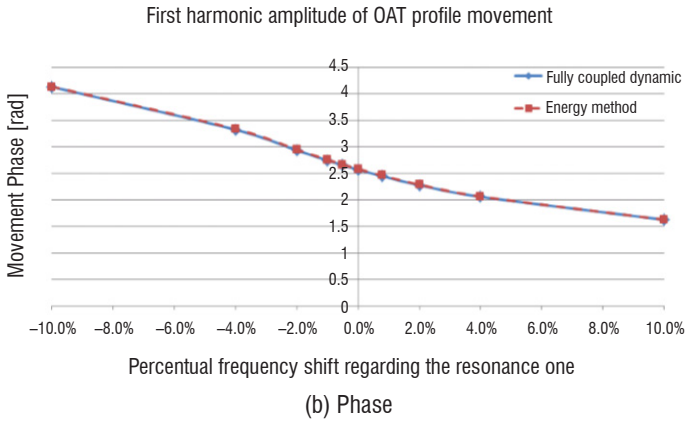

(b) Phase

Figure 25 – Forced response close to the coincidence frequency

The effect of gust fields on the aerodynamic and aeroelastic behavior of the model was analyzed and the experimental data was delivered to ONERA's main partners (Airbus and Dassault Aviation) for the validation of their numerical methods.

A twin simulation is conducted on this configuration, including a harmonic forced motion of the gust generator airfoil doublet, as well as a periodic forced motion of the OAT profile, whose harmonic content is periodically updated to balance the dynamic system forced-response equations (Figure 24). The gust generator is excited at frequency 25 Hz and amplitude 3°, for a Mach number of 0.7294. The values of the generalized mass, damping and stiffness for the excited heave mode are: $\mu = 0.01$, $\beta = 0.115$, $\gamma = 242.94$.

Figure 25 presents the results of the twin simulation (in red) compared to those obtained with the fully-coupled direct method in time domain (in blue). Amplitude levels (a) and phase (b) of the first harmonic component of motion are given, for various excitation frequencies, close to the heave modal frequency (–10% to +10% range). The maximum amplitude is obtained, as expected, near the modal frequency, but a slight deviation is observed due to the impact of the aerodynamic stiffness, which induces a small offset. The agreement with the fully coupled method is excellent.

It must be noticed, however, that the convergence of the method is made all the more difficult if the structural damping is small, which leads to high levels of forced response. This point must be improved for a robust use of the method in the case of turbomachinery forced-response problems, such as rotor stator interaction, inlet distortion or crosswind-induced response.

Perspectives

Several activities are currently being carried out in the Aeroelasticity Modelling and Simulation research unit of ONERA to address new topics concerning the aeroelastic behavior of turbomachines. One main issue concerns the prediction of the aeroelastic stability and of the forced response of turbomachines, especially fans, facing distorted inlet conditions. In particular, due to inhomogeneous total pressure and velocity at the inlet, large levels of structural forced response may be observed, which must be studied for safety reasons. These conditions may occur, in various circumstances, such as crosswind conditions, impinging wakes, boundary layer ingestion (BLI), or even interactions with ground-induced vortices (Figure 26). In these cases, the basic assumption of cyclic symmetry retained for sector reduction modelling is questionable, and 360° modelling may be mandatory.

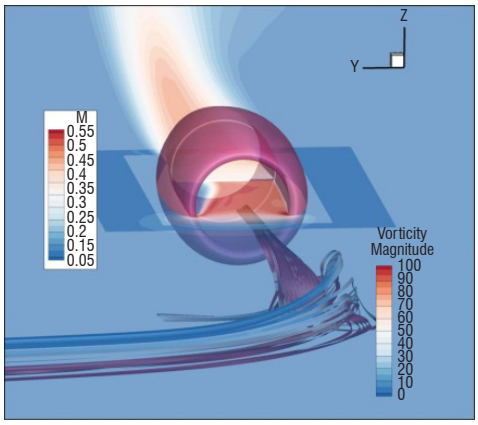

Figure 26 – Current activities on fan-vortex interaction [38]

On the other hand, new activities are currently being conducted, in order to build a modular aeroelastic simulation environment, whose objective is to deliver new simulation capabilities in coupling several individual modules for the resolution of aeroelastic problems. This work is intended to provide a tool versatile enough to extend the coupling solution currently available with *elsA* to other non-linear aerodynamic solvers (newly developed CFD2030 aerodynamic codes) and non-linear structural solvers. Such a tool will potentially provide access to an aerodynamic modeling alternative to URANS, such as LES, or Lattice-Boltzmann, and to innovative techniques such as the Immersed Boundary Method for aeroelasticity. Moreover, this modular architecture will allow new innovative algorithms for fluid-structure transfers and mesh deformation strategy to be implemented more easily, without costly additional *elsA* C++ Kernel development. This architecture will rely on a CGNS compliant data model, specifically extended to fluid-structure coupling, and modular extensions using Python interfaces (Figure 27).

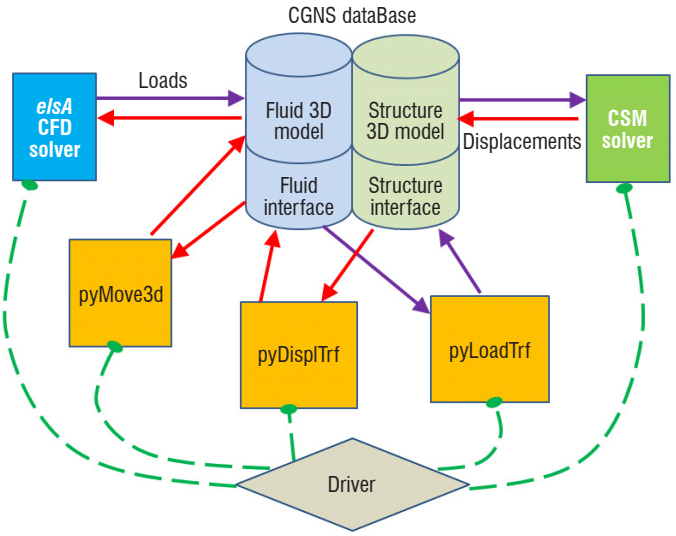

Figure 27 – Targeted fluid-structure modular architecture for the communications between fluid and structural solvers

Conclusion

The aim of this paper was to present the current development status and research activities concerning the modelling of aeroelastic phenomena of rotating machines recently conducted at ONERA. In the second part, we have presented some basic capabilities of the *elsA* ONERA aerodynamic solver, and then those of the specific aeroelastic extension of *elsA*, AeI.

Next, we have first described specific capabilities recently implemented for the non-linear coupling of the *elsA* non-linear aerodynamic solver and MSC/Nastran, allowing for the resolution of non-linear large-displacement static problems. Then, dynamic functionalities for unsteady weak coupling aeroelastic simulations, in the case of stage and multi-stage turbomachine configurations and for forced response problems, have been presented. These functionalities have been implemented in several European and national projects, such as COBRA, ENOVAL, CS2-ADEC and *elsA*/ASO.

One perspective for future work within the framework of turbomachine aeroelastic problems concerns the taking into account of the impact of distorted inflow on the aeroelasticity of fans and open-rotors, especially with regard to forced response. This topic will be addressed within the framework of the ENOVAL European project in particular. Secondly, the extension of aeroelastic coupling capabilities to fully non-linear fluid-structure modelling is currently under construction and will provide larger modelling capabilities for aeroelastic problems ■

Acknowledgements

The studies presented in this article have been partially funded by Airbus, Safran and ONERA, which are co-owners of the software.

Nomenclature

θ	(azimuth angle)
N	(number of sectors of the row)
Φ	(deformation mode shapes)
M, D, K	(structural mass, damping, stiffness matrices)
q	(generalized coordinates)
$F_A(t)$	(aerodynamic force)
α	(relaxation coefficient)
u	(structural displacements)
w	(aerodynamic field)
σ_n	(inter-blade phase angle)
$X = \begin{bmatrix} u \\ w \end{bmatrix}$	(fluid-structure variables)

References

[1] A. GROLET, F. THOUVEREZ - *On a New Harmonic Selection Technique for Harmonic Balance Method*. Mechanical Systems an Signal Processing, Vol. 30, pp. 43-60, 2012.

[2] M. A. BAKHLE, T. S. REDDY, R. CORONEOS, J. B. MIN, A. J. PROVENZA, K. P. DUFFY, G. S. HEINLEIN - *Aeromechanics Analysis of a Distortion-Tolerant Fan with Boundary Layer Ingestion*. AIAA Aerospace Sciences Meeting, 2018.

[3] M. A. BAKHLE, T. S. REDDY, M. RULA, M. CORONEOS - *Forced Response Analysis of a Fan with Boundary Layer Inlet Distortion*. 50th AIAA/ASME/SAE/ASEE Joint Propulsion Conference, 2014.

[4] M. A. BAKHLE, R. SRIVASTAVA, T. G. KEITH, G. L. STEFKO, & J. JANUS - *Development of an Aeroelastic Code Based on an Euler/Navier-Stokes Aerodynamic Solver*. NASA Technical Memorendum, NASA, November 1996.

[5] T. BERTHELON, A. DUGEAI, J. LANGRIDGE, F. THOUVEREZ - *Fan Forced Response due to Inlet Ground Vortex Ingestion*. 53rd 3AF International Conference on Applied Aerodynamics. Salon de Provence, France, 2018.

[6] C. BRÉARD, M. VAHDATI, A. I. SAYMA, M. IMREGUN - *An Integrated Time-Domain Aeroelasticity Model for the Prediction of Fan Forced Response Due to Inlet Distortion*. ASME Turbo Expo 2000: Power for Land, Sea, and Air, 2000.

[7] L. CAMBIER, S. HEIB, S. PLOT - *The ONERA elsA CFD Software: Input from Research and Feedback from Industry*. Mechanics & Industry, 14(3), 159-174. Retrieved from dx.doi.org/10.1051/meca/2013056, 2013.

[8] V. CARSTENS - *Computations of Unsteady Transonic 3D-Flow in Oscillating Turbomachinery Bladings by an Euler Algorithm with Deformaing Grids*. 7th International Symposium on Unsteady Aerodynamics and Aeroelasticity of Tubomachines. Fukuoka, Japan, 25-29 September 1994.

[9] F. O. CARTA - *Coupled Blade-Disk-Shroud Flutter Instabilities in Turbojet Engine Rotors*. Journal of Engineering for Gas Turbines and Power, 89(3), 419-426. Retrieved from dx.doi.org/10.1115/1.3616708, 1967.

[10] L. CASTILLON, N. GOURDAIN, X. OTTAVY - *Multiple-Frequency Phase-Lagged Unsteady Simulations of Experimental Axial Compressor*. Journal of Propulsion and Power, 31(1), 444-455. Retrieved from dx.doi.org/10.2514/1.B35247, January 2015.

[11] W. S. CLARK, K. C. HALL - *A Time-Linearized Navier-Stokes Analysis of Stall Flutter.* ASME Journal of Turbomachinery, 122, 467-476, 2000.

[12] A. DUGEAI - *Turbomachinaery Aeroelastic Developments and Validations using ONERA elsA Solver.* International Forum on Aeroelasticity and Structural Dynamics. Stockholm, Sweden, 18-20 June 2007.

[13] A. DUGEAI, S. VERLEY - *Numerical Evaluation of CRORs Dynamic Loads Induced by Whirl Flutter*. 3AF CEAS Greener Aviation. Brussels, Belgium, 2014.

[14] A. DUGEAI, A. MADEC, A. S. SENS - *Numerical Unsteady Aerodynamics for Turbomachinery Aeroelasticity.* 9th International Symposium on Unsteady Aerodynamics, Aeroacoustics and Aeroelasticity of Turbomachines. Lyon, 4-7 Septembre 2000.

[15] A. DUGEAI, Y. MAUFFREY, F. SICOT - *Aeroelastic Capabilities of the elsA Solver for Rotating Machines Applications*. International Forum on Aeroelasticity and Structural Dynamics. Paris, France, June 2011.

[16] K. EKICI, K. C. HALL - *Nonlinear Analysis of Unsteady Flows in Multistage Turbomachines using Harmonic Balance*. AIAA Journal, 45(5), 1047-1057, 2007.

[17] J. I. ERDOS, E. ALZNER, W. MCNALLY - *Numerical Solution of Periodic Transonic Flow through a Fan Stage.* AIAA Journal, 15(11), 1559-1568, 1977.

[18] M. ERRERA, A. DUGEAI, P. GIRODROUX-LAVIGNE, J. GARAUD, M. POINOT, S. CERQUEIRA, G. CHAINERAY - *Multi-Physics Coupling Approaches for Aerospace Numerical Simulations*. AerospaceLab, 2(2), 1-16, 2011.

[19] G. A. GEROLYMOS - *Filtered Chorochronic Interface as a Capability for 3-D Unsteady Throughflow Analysis of Multistage Turbomachinery*. International Journal of Computational Fluid Dynamics, 27(2), 100-117, 2013.

[20] G. A. GEROLYMOS, G. J. MICHON, J. NEUBAUER - *Analysis and Application of Chorochronic Periodicity in Turbomachinery Rotor/Stator Interaction Computations*. AIAA Journal, 18(6), 1139-1152, 2002.

[21] G. GEROLYMOS, I. VALLET - *Validation of 3-D Euler Methods for Vibrating Cascade Aerodynamics*. ASME Turbo Expo, 1994.

[22] M. B. GILES - *Calculation of Unsteady Wake/Rotor Interaction*. Journal of Propulsion and Power, 4(4), 356-362, 1988.

[23] P. GIRODROUX-LAVIGNE, A. DUGEAI - *Fluid-Structure Coupling Using Chimera Grids*. International Forum on Aeroelasticity and Structural Dynamics. Seattle, USA, 21-25 June 2009.

[24] K. C. HALL, E. F. CRAWLEY - *Calculation of Unsteady Flows in Turbomachinery using the Linearized Euler Equations*. AIAA Journal, 27(6), 777-787, 1989.

[25] K. C. HALL, B. LORENCE - *Calculation of Three-Dimensional Unsteady Flows in Turbomachinery Using the Linearized Harmonic Euler Equations*. Journal of Turbomachinery, 115(4), 800-809, October 1993.

[26] K. C. HALL, P. D. SILKOWSKI - *The Influence of Neighboring Blade Rows on the Unsteady Aerodynamic Response of Cascades*. Journal of Turbomachinery, 119(1), 85-93, 1997.

[27] K. C. HALL, J. P. THOMAS, W. S. CLARK - *Computation of Unsteady Nonlinear Flows in Cascades using a Harmonic Balance Technique*. AIAA Journal, 40(5), 879-886, 2002.

[28] H. J. HASSIG - *An Approximate True Damping Solution of the Flutter Equation by Determinant Iteration.* Journal of Aircraft, 8(11), 885-889, 1971.

[29] L. HE - *An Euler Solution for Unsteady Flows Around Oscillating Blades.* Journal of Turbomachinery, 112(4), 714-722, 1990.

[30] L. HE - *Method of Simulating Unsteady Turbomachinery Flows with Multiple Perturbations*. AIAA Journal, 30(11), 2730-2735, 1992.

[31] L. HE, W. Ning - *Efficient Approach for Analysis of Unsteady Viscous Flows in Turbomachines*. AIAA Journal, 36(11), 2005-2012. Retrieved from https://doi.org/10.2514/2.328, November 1998.

[32] G. P. HERRICK - *Assessing Fan Flutter Stability in Presence of Inlet Distortion Using One-way and Two-way Coupled Methods*. 50th AIAA/ASME/SAE/ASEE Joint Propulsion Conference, 2014.

[33] X. Q. HUANG, L. HE, D. L. BELL - *Influence of Upstream Stator on Rotor Flutter Stability in a Low Pressure Steam Turbine Stage*. Journal of Power and Energy, 220(1), 25-35, 2006.

[34] M. KARPEL - *Design for Active Flutter Suppression and Gust Alleviation Using State-Space Aeroelastic Modeling*. AIAA Journal of Aircraft, 19, 221-227, 1982.

[35] R. E. KIELB - *Forced Response Design Analysis.* Aeroelasticity in Axial-Flow Turbomachines. Rhode-Saint-Genese, Belgium: von Karman Institute for Fluid Dynamics, 1999.

[36] K. LEE, M. WILSON, M. VAHDATI - *Numerical Study on Aeroelastic Instability for a Low-Speed Fan*. Journal of Turbomachinery, 139(7), 2017.

[37] A. LEPAGE, Y. AMOSSE, D. LEBIHAN, C. POUSSOT-VASSAL, V. BRION, E. RANTET - *A Complete Experimental Investigation of Gust Load from Generation to Active Control*. International Forum on Aeroelasticity and Structural Dynamics. Saint Petersburg, Russia, 2015.

[38] J. G. MARSHALL, M. IMREGUN - *A Review of Aeroelasticity Methods with Emphasis on Turbomachinery Applications*. Journal of Fluids and Structures, 10(3), 237-267, 1996.

[39] Y. MAUFFREY, A. GEERAERT - *CROR Blade Deformation, part 2: Aeroelastic Computations and Comparison with Experiments*. International Forum on Aeroelasticity and Structural Dynamics. Saint Petersburg, Russia, June 28-July 2 2015.

[40] M. MESBAH, J.-F. THOMAS, F. THIRIFAY, A. NAERT, S. HIERNAUX - *Investigation of Forced Response Sensitivity of Low Pressure Compressor With Respect to Variation in Tip Clearance Size*. Journal of Turbomachinery, 137(9), 2015.

[41] S. MOFFAT, W. NING, Y. LI, R. G. WELLS, L. HE - *Blade Forced Response Prediction for Industrial Gas Turbine*. Journal of Propulsion and Power, 21(4), 707-714, July-August 2005.

[42] R. MORETTI - *Direct Method to Predict the Forced Response in Turbomachinery Compressor.* MSc Thesis, Politecnico di Torino, October 2016.

[43] A. PLACZEK - *Aeroelastic Damping Predictions for Multistage Turbomachinery Applications*. 29th Congress of the International Council of the Aeronautical Sciences. Saint Petersburg. Retrieved from hal-onera.archives-ouvertes.fr/hal-01078504/, 7-12 September 2014.

[44] A. PLACZEK, L. CASTILLON - *Aeroelastic Response of a Contrafan Stage Using Full Annulus and Single Passage Models.* Journal of Aeroelasticity and Structural Dynamics, 3(2), 1-30. Retrieved from dx.doi.org/10.3293/asdj.2014.30, May 2014.

[45] A. PLACZEK, A. DUGEAI - *Numerical Prediction of the Aeroelastic Damping using Multi-Modal Dynamically Coupled Simulations on a 360° fan configuration*. International Forum on Aeroelasticity and Structural Dynamics. Paris, 27-30 juin 2011.

[46] A. I. SAYMA, M. VAHDATI, M. IMREGUN - *An Integrated Nonlinear Approach for Turbomachinery Forced Response Prediction*. Part I: Formulation. Journal of Fluids and Structures, 14(1), 87-101, 2000.

[47] S. SCHMITT, D. NÜRNBERGER, V. CARSTENS - *Evaluation of the Principle of Aerodynamic Superposition in Forced Response Calculations*. 10th International Symposium on Aerodynamics, Aeroacoustics and Aeroelasticity in Turbomachines. Durham (NC), 2003.

[48] M. SCHUFF, T. LENGYEL-KAMPMANN, N. FORSTHOFER - *Influence of the Steady Deformation on Numerical Flutter Prediction for Highly Loaded and Flexible Fan Blades*. ASME Turbo Expo. Charlotte, North Carolina, USA, 26-30 June 2017.

[49] F. SICOT, T. GUÉDENEY, G. DUFOUR - *Time-Domain Harmonic Balance Method for Aerodynamic and Aeroelastic Simulations of Turbomachinery Flows*. International Journal of Computational Fluid Dynamics, 27(2), 68-78, 2012.

[50] S. C. STAPELFELDT, L. DI MARE - *A Method for Modelling Flow Past Non-Axisymmetric Configurations on Reduced Passage Counts*. 13th International Symposium on Unsteady Aerodynamics, Aeroacoustics and Aeroelasticity of Turbomachines. Tokyo, 11-14 Septembre 2012.

[51] S. C. STAPELFELDT, A. PARRY, M. VAHDATI - *Investigation of Flutter Mechanisms of a Contra-Rotating Open Rotor*. Journal of Turbomachinery, 138(5), 2016.

[52] D.-M. TRAN, C. LIAUZUN, C. LABASTE - *Methods of Fluid-Structure Coupling in Frequency and Time Domains using Linearized Aerodynamics for Turbomachinery.* Journal of Fluids and Structures, 17(8), 1161-1180. Retrieved from dx.doi.org/10.1016/S0889-9746(03)00068-9, 2003.

[53] J. M. TYLER, T. G. SOFFRIN - *Axial Flow Compressor Noise Studies*. SAE Transactions, 70(620532), 309-332. Retrieved from dx.doi.org/10.4271/620532, 1962.

[54] M. VAHDATI, A. I. SAYMA, M. IMREGUN - *An Integrated Nonlinear Approach for Turbomachinery Forced Response Prediction. Part II: Case Studies*. Journal of Fluids and Structures, 14(1), 103-125, 2000.

[55] M. VAHDATI, A. SAYMA, M. IMREGUN, G. SIMPSON - *Multibladerow Forced Response Modeling in Axial-Flow Core Compressors*. Journal of Turbomachinery, 129(2), 412-420, 2005.

[56] M. VAHDATI, A. SAYMA, J. G. MARSHALL, M. IMREGUN - *Mechanisms and Prediction Methods for Fan Blade Stall Flutter.* Journal of Propulsion and Power, 17(5), 1100-1108. Retrieved from https://arc.aiaa.org/doi/abs/10.2514/2.5850, September-October 2001.

[57] M. VAHDATI, G. SIMPSON, M. IMREGUN - *Mechanisms for Wide-Chord Fan Blade Flutter*. Journal of Turbomachinery, 133(4), 2011.

[58] M. VAHDATI, N. SMITH, F. ZHAO - *Influence of Intake on Fan Blade Flutter.* ASME Turbo Expo: Power for Land, Sea, and Air. Düsseldorf, Germany, 16-20 June 2015.

[59] E. VAN DER WEIDE, A. K. GOPINATH, A. JAMESON - *Turbomachinery Applications with the Time Spectral Method*. 35th AIAA Fluid Dynamics Conference and Exhibit. Toronto, 6-9 Juin 2005.

[60] J. M. VERDON - *Review of Unsteady Aerodynamic Methods for Turbomachinery Aeroelastic and Aeroacoustic Applications*. AIAA Journal, 31, 235-250, 1993.

[61] S. WANG, S. LI, X. SONG - *Investigations on Static Aeroelastic Problems of Transonic Fans Based on Fuid–Structure Interaction Method*. Proceedings of the Institution of Mechanical Engineers, Part A: Journal of Power and Energy, 230(7), 685-695, September 2016.

Alain Dugeai graduated from the "*Ecole Centrale de Paris*" in 1985. He received a specialty degree in "Aerospace Mechanics" from the "*Ecole Nationale de l'Aéronautique et de l'Espace*" in Toulouse in 1986. Alain Dugeai has been working as a research engineer at ONERA's Structural Department in Chatillon, FRANCE since 1988. He has been involved in several development topics dealing with numerical aeroelasticity, such as: supersonic linearized numerical aeroelasticity methods, unstructured grid formulations for aeroelasticity, and mesh deformation techniques. He has been involved in the development of the aeroelastic module of ONERA's non-linear aerodynamic solver *elsA* since 2000, and was in charge of the development of numerical aeroelasticity and fluid-structure coupling methods for turbomachine and propeller applications. He is involved in several cooperation programs with industrial and academic partners, concerning civil aircraft and turbomachinery aeroelasticity, within both national and European collaboration contexts. He is now head of the Aeroelastic Modeling and Simulation unit (MSAE) of the Aerodynamics, Aeroelasticity and Acoustics Department (DAAA) of ONERA.

Yann Mauffrey is a research engineer in the Aeroelastic Modeling and Simulation unit (MSAE) of the Aerodynamics, Aeroelasticity and Acoustics Department (DAAA) of ONERA.

Antoine Placzek graduated from the mechanical engineering school Supmeca and obtained a Master's Degree from the University of La Rochelle. He received his PhD in Mechanics from the CNAM in 2009 and has since been working at Onera, where he is currently in charge of numerical developments for turbomachinery aeroelasticity.

Simon Verley is a scientist researcher in aeroelasticity of rotating bodies. He obtained his engineering diploma from ESTACA Paris in 2008 and his PhD in aerodynamics from the University of Orleans in 2012, on the topic of the evaluation of "Far-field" torque of a helicopter rotor during hover. Since then, he has been studying aeroelasticty of turbomachinery, CROR and helicopters. His main topics of research are the study of the whirl-flutter of CROR engines, the non-linear coupling between the elsA CFD software and the MSC Nastran CSM software and the coupling between *elsA* and the helicopter comprehensive code HOST.

V. Kehr-Candille
(ONERA)

E-mail: veronique.kehr-candille@onera.fr

DOI: 10.12762/2018.AL14-04

Modelling the Damping at the Junction between Two Substructures by Non-Linear Meta-Models

We are interested in the modelling of the damping at the junction between two substructures. We model the connection by a meta-model, which takes into account both dissipative and non-linear aspects of the connection. We use the Bouc-Wen meta-model. This model is adapted for insertion into a finite-element model. We obtained a non-linear dynamical system, which can be solved in the time domain with a Runge-Kutta algorithm. A software tool corresponding to this method is developed. To decrease calculation costs, we reduce the size of the system by a Craig-Bampton method. We present an application on an academic test-case, and also a comparison with experimental results.

Introduction

In structural dynamics, vibratory levels depend directly on damping. Therefore, it is necessary to have, from the design phase, tools and models that allow the damping to be correctly represented.

The origin of the energy dissipation in the aeronautical structures is double: on the one hand, material intrinsic damping and, on the other hand, dissipation generated by the friction phenomena at the interfaces between the sub-structures. We are interested here in the representation of this second source of dissipation. For the metallic structures, the dissipation generated at the interfaces is the main damping source.

Modelling friction and interface contact has been the subject of numerous studies (for instance, [1, 2, 3]). Most finite-element software contains contact-modelling modules (Nastran, Abaqus, Aster). However, these approaches, used for the calculation of dynamic responses, lead to extremely long calculation times, which become prohibitive for industrial structures. Our objective is to propose a relatively simplified modelling (meta-model) of the junction between two sub-structures, which allows dissipative and non-linear aspects to be correctly represented, without leading to an excessively long time in the calculations of the dynamic response.

Junction model

Single-degree-of-freedom model

Numerous non-linear dissipation models can be found in literature: we are mainly interested in the Bouc-Wen model [4], which allows the modelling of various dissipation phenomena.

For a single-degree-of-freedom system, the differential equations of this model are:

$$\begin{cases} m\ddot{x} + k_{\text{linear}}\, x + z = f_e(t) \\ \dot{z} = \alpha\left[A\dot{x} - \beta|\dot{x}|\,|z|^{n-1} z - \gamma\dot{x}|z|^n \right] \end{cases} \quad (1)$$

The Bouc-Wen model introduces an additional degree of freedom z. The mass of the system is m, the excitation force is denoted by $f_e(t)$. The variable z comprises both non-linear stiffness and non-linear damping aspects.

This model is described by 5 parameters: α, β, γ, A and n (n is not necessarily an integer).

We present Figure 1 to illustrate an example of a response of a single-degree-of-freedom system ($m=1$, $k_{linear}=200$, $f_e(t)=2.\sin(4\pi t)$, $\alpha=200$, $A=1$ and $n=1$, for two sets of parameter values β and γ. For dissipative systems, the most representative curve is the hysteresis curve (hysteresis cycle): displacement x / force z.

Use in a finite-element model

The models presented above are well known. The originality of our approach is in their inclusion in finite-element models.

We consider a Bouc-Wen model inserted between two degrees of freedom of nodes A and B.

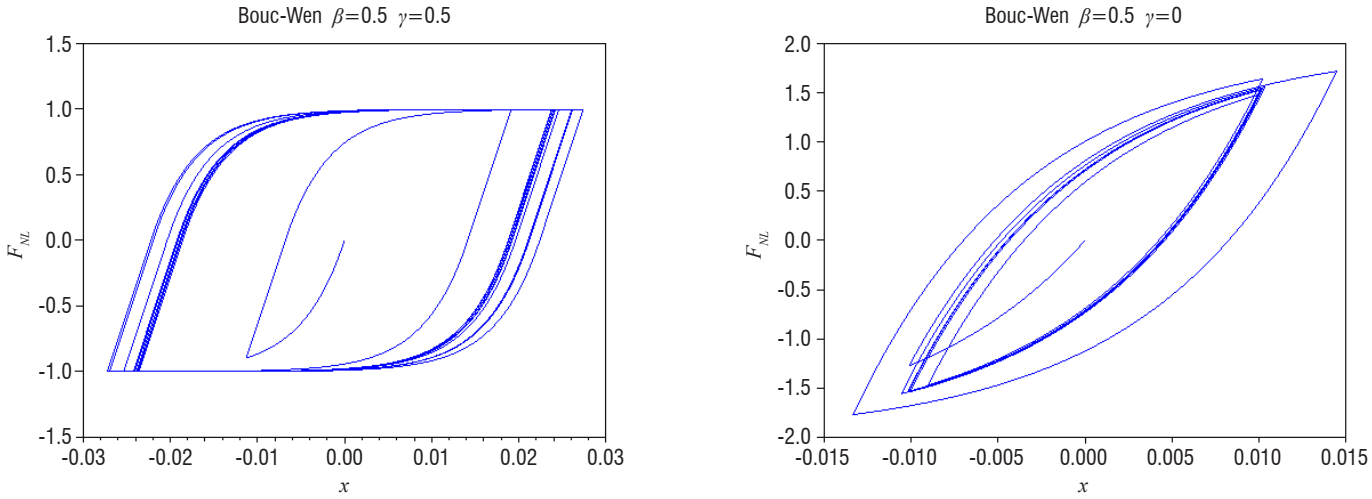

Figure 1 – Hysteresis cycle for a one degree of freedom model

It should be noted that this system is introduced between two degrees of freedom, and not between two nodes. For instance, one can choose to link only the x degree of freedom of node A and the x degree of freedom of node B by a Bouc-Wen model, without linking the y and z degrees of freedom for these two nodes.

Figure 2 – Diagram of the integration of the Bouc-Wen model between two sub-structures

The differential system is written as follows:

$$\begin{cases} \mathrm{M}\ddot{\mathrm{X}} + \mathrm{C}\dot{\mathrm{X}} + \mathrm{KX} + \mathrm{F}_{NL}(z) = \mathrm{F}_e(t) \\ \dot{z} = \alpha\left[A\dot{x} - \beta|\dot{x}|\,|z|^{n-1} z - \gamma\dot{x}|z|^n \right] \end{cases} \tag{2}$$

where

$$\begin{cases} \mathrm{F}_{NL}(i_A) = -z \quad \mathrm{F}_{NL}(i_B) = +z \quad \mathrm{F}_{NL} = 0 \text{ elsewhere} \\ x = x_B - x_A = \mathrm{X}(i_B) - \mathrm{X}(i_A) \\ i_A = n^o \mathrm{ddl}\, x_A \quad i_B = n^o\, \mathrm{ddl}\, x_B \end{cases} \tag{3}$$

The Bouc-Wen model introduces an additional degree of freedom z in the initial system. The non-linear force F_{NL} depends on this additional degree of freedom.

This model can be easily extended to several Bouc-Model models. We introduce as many additional degrees of freedom as Bouc-Wen models.

Resolution

System resolution

The system described above is a time-domain non-linear system, which is well adapted to a resolution by the classical Runge-Kutta method of order 4.

The Runge-Kutta algorithm requires the system to be expressed in the form of a 1st order differential system:

$$\dot{\mathrm{Y}} = f(\mathrm{Y}) \quad \text{avec } \mathrm{Y} = \begin{cases} \mathrm{Y}_1 = \dot{\mathrm{X}} \\ \mathrm{Y}_2 = \mathrm{X} \\ \mathrm{Y}_3 = z \end{cases} \tag{4}$$

The function f is defined by:

$$\begin{cases} \dot{\mathrm{Y}}_1 = -\mathrm{M}^{-1}\mathrm{K}\,\mathrm{Y}_2 - \mathrm{M}^{-1}\mathrm{C}\,\mathrm{Y}_1 - \mathrm{M}^{-1}\mathrm{F}_{NL} + \mathrm{M}^{-1}\mathrm{F}_e(t) \\ \dot{\mathrm{Y}}_2 = \mathrm{Y}_1 \\ \dot{\mathrm{Y}}_3 = \alpha\left[A\dot{x} - \beta|\dot{x}|\,|z|^{n-1} z - \gamma\dot{x}|z|^n \right] \end{cases} \tag{5}$$

where $z = \mathrm{Y}_3 = +\mathrm{F}_{NL}(i_B) = -\mathrm{F}_{NL}(i_A)$ and $\dot{x} = \mathrm{Y}_1(i_B) - \mathrm{Y}_1(i_A)$

For several Bouc-Wen models, the last equation is modified:

$$\dot{\mathrm{Y}}_3(j) = \alpha_j\left[A_j\dot{x}_j - \beta_j|\dot{x}_j|\,|z_j|^{n-1} z_j - \gamma_j\,\dot{x}_j|z_j|^n \right] \tag{6}$$

where $\mathrm{Y}_3(j) = z_j = +\mathrm{F}_{NL}(i_{Bj}) = -\mathrm{F}_{NL}(i_{Aj})$ and $\dot{x}_j = \mathrm{Y}_1(i_{Bj}) - \mathrm{Y}_1(i_{Aj})$, for j varying from 1 to the number of Bouc-Wen models.

We use the Nastran ® software. We have developed in the internal language of Nastran ® (DMAP) a module that allows several Bouc-Wen models to be inserted between some degrees of freedom of the system (chosen by the user). We also developed in DMAP language the Runge-Kutta algorithm. This module has been implemented in SOL 109 (direct linear transient method).

Reduction method

The previous numerical resolution is directly performed from the initial finite-element system (physical degrees of freedom). This can lead to a prohibitive calculation time for industrial applications.

For linear problems, several model-reduction methods are available to reduce the calculation time. The problem is different for non-linear systems, and it is necessary to develop specific methods (see [5]).

However, in our case, we are dealing with a non-linear system where non-linearities are spatially localized. Therefore, we choose a classical method for a linear system: the Craig-Bampton method.

We briefly recall the different stages of this method:

- the degrees of freedom of the finite-element model are separated into two groups: internal degrees of freedom and boundary degrees of freedom,
- the eigenmodes with clamped boundary degrees of freedom are calculated: modes Φ_m,
- constrained modes are calculated: static response to a unitary imposed displacement of one boundary degree of freedom, with the other boundary degrees of freedom clamped: modes Φ_l,
- the initial finite-element system is projected on the base $\Phi=[\Phi_m\ \Phi_l]$.

The degrees of freedom involved in the Bouc-Wen models are considered as boundary degrees of freedom: the value of these degrees of freedom can be accessed directly during the non-linear transient resolution.

The second software version, which uses the Craig-Bampton reduction method, includes two stages:

- in the first stage, we use Nastran to calculate clamped eigenmodes Φ_m and constrained modes Φ_l, and to carry out the projection on the basis $\Phi=[\Phi_m\ \Phi_l]$,
- in a second stage, we carry out the time domain calculation, on the reduced system, with a Runge-Kutta algorithm. This second phase is computed in Fortran (this stage is independent from the Nastran software).

Academic application

Computing transient response

The above method is applied to a simple academic system, including masses and springs (see Figure 3). This model is the assembly of two sub-structures, and each sub-structure includes 4 masses ($m=10$kg) and 3 springs ($k=10^5$N/m). substructure 1 is clamped at one end. The excitation force is applied to substructure 2 at the other end: $F_e(t)=\cos(2\pi f_0 t)$, where $f_0=2$Hz. A Bouc-Wen model (without linear elasticity $k_{\text{linear}}=0$) links the two substructures.

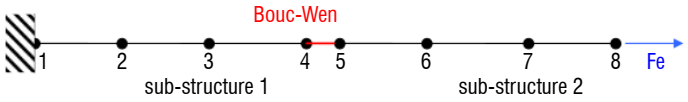

Figure 3 – Mass/spring system

First, in order to validate the software, we consider a non-dissipative and linear case: if we take the values of the Bouc-Wen model parameters $\beta=\gamma=0$, $A=0$, $n=1$, $\alpha=10^5$, the junction is equivalent to a simple spring (non-dissipative and linear), whose stiffness is $k=\alpha A$. We can check that the result is the same as that obtained for a classical linear case, replacing the Bouc-Wen model by a spring.

Then, we calculate the transient response of the system for various parameter values. All of the calculations are performed on the time interval $0-5s$, with a constant time step $\Delta t=10^{-3}s$.

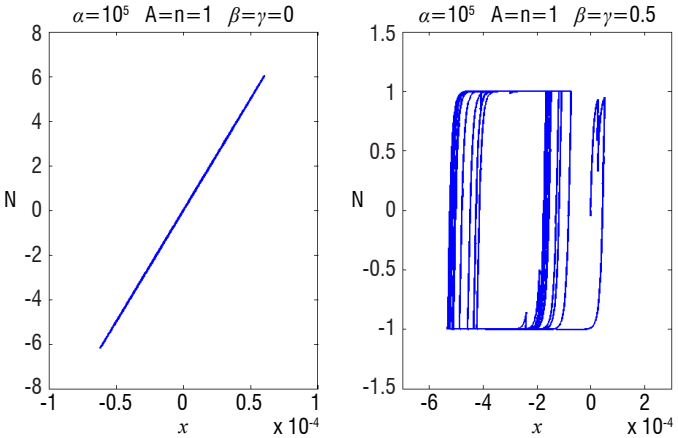

Figure 4 – Hysteresis cycle for the mass/spring system

Craig-Bampton reduction method

We verify, on the academic model, the Craig-Bampton reduction method. Indeed, the validity and efficiency of this method are well known for linear systems. The use of the Bouc-Wen model leads to a non-linear system. However, the non-linearities are localized and only concern the boundary degrees of freedom; therefore, clamped eigenmodes and constrained modes are calculated for the linear part.

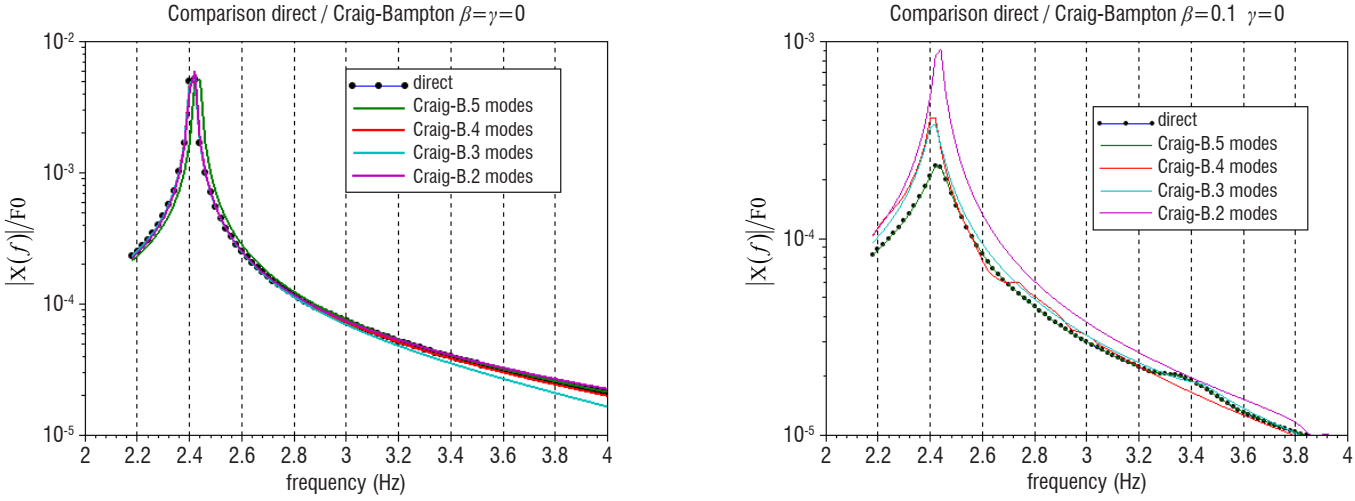

Figure 5 – Comparison of direct responses and responses with the Craig-Bampton method for a linear case (on the left) and a non-linear case (on the right)

We use the transient excitation force $f_e(t) = F_0 \dfrac{\sin(2\pi f_0 t)}{t}$ with $f_0 = 20$ Hz, which allows the two first eigenmodes (2.4 Hz and 7.2 Hz) to be caught. In Figure 5, we compare the direct response (reference response) and the response obtained by the Craig-Bampton method, with various numbers of clamped modes.

We note that convergence is reached for this non-linear system, but for a higher number of modes than for linear systems.

Thus, we can consider that the use of the Craig-Bampton method is valid for non-linear systems with localized non-linearities. However, without general mathematical results, a convergence study is essential.

Comparison with experiment

Description of the mock-up

Within the framework of the MAIAS project, a mock-up, representative of an aeronautic structure, has been built. It is composed of a long part and a short part, linked by a bracket junction (see Figure 6). A detailed description of the mock-up can be found in [7]. We are especially interested in the modelling of this junction.

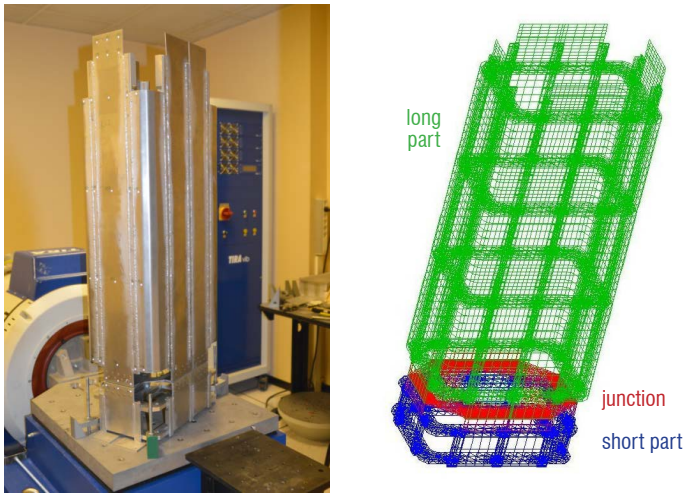

Figure 6 – Mock-up: experimental test (left) and finite-element mesh (right)

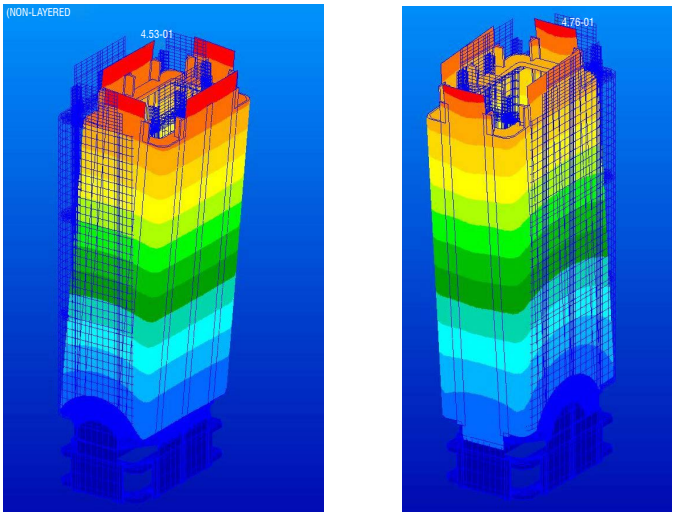

Figure 7 – Eigenmodes (on the left Mode 1: 37.9 Hz simulation, 35 Hz experiment; on the right Mode 2: 72.7 Hz simulation, 69 Hz experiment)

This mock-up has been used for experiments (see [7] and [8]). The experiments performed in [7] allowed he initial finite-element model to be improved, comparing experimental and computed eigenmodes.

We are interested in the experiment performed in [8] (see Figure 6): acceleration is applied at the base of the mock-up, and the response is measured at various points, for several excitation levels. In Reference [8], experimental curves clearly show a non-linear behavior (the frequency response functions depend on the excitation level).

Comparison: experimental and numerical results

In Reference [7], a detailed representation of the bracket junction has been used. Our purpose is to replace this refined junction model by a Bouc-Wen meta-model, and to compare the results thus obtained with experimental results [8].

We considered the finite-element model of [7], and then we removed the finite-element part corresponding to the junction and replaced it by springs and Bouc-Wen models. We introduced 8 springs on each small face, and 13 springs on each large face (42 springs in total), in the three directions x, y and z. At the center of each small face and

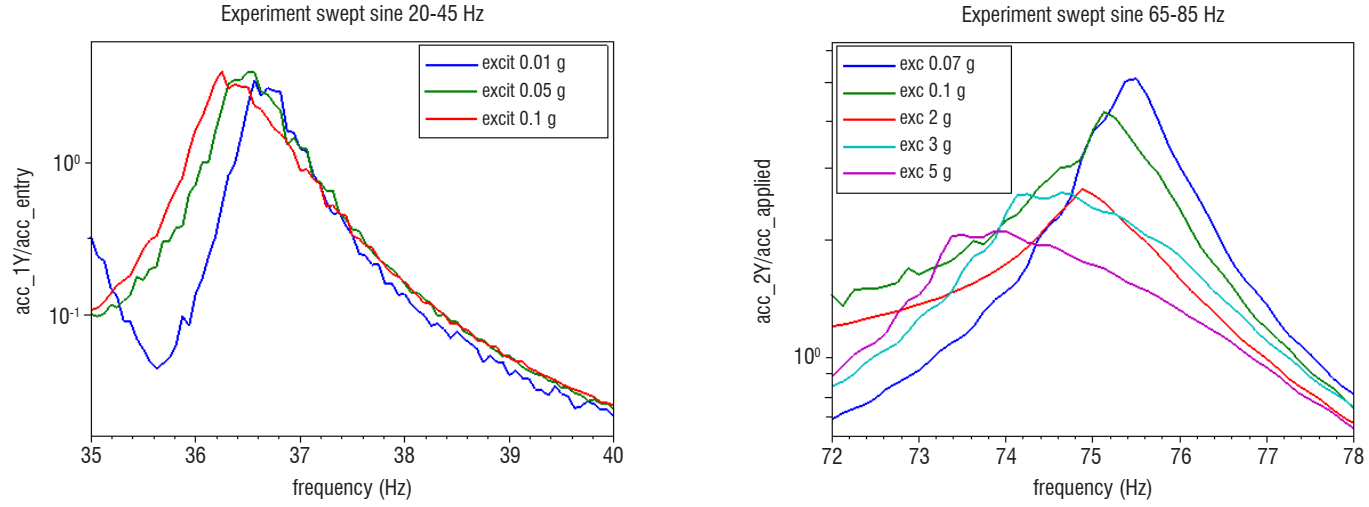

Figure 8 – Experimental responses of the mock-up (in the neighborhood of resonance peaks)

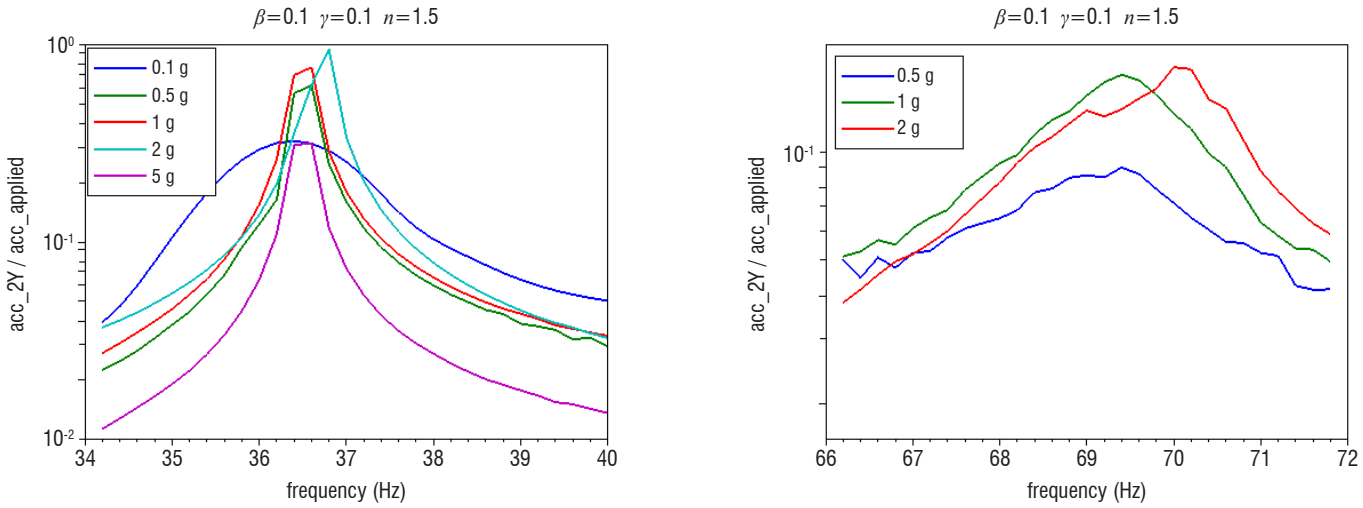

Figure 9 – Simulated responses of the mock-up

each large face, we introduced a mixed junction: a Bouc-Wen model in the vertical direction z, and springs in the two other directions.

In a first stage, the spring stiffness values were modified, in order to use the same values as in the experiment for the first two eigenmodes (see Figure 7).

In a second stage, we included in the finite-element system the 4 Bouc-Wen models, and we performed transient dynamic response calculations, using the Craig-Bampton method. Simulations were performed for several levels of the acceleration applied.

We present below the frequency response curves: experimental (Figure 8) and simulated (Figure 9). These curves are shown separately, because they do not correspond exactly to the same excitations. In fact, experimental excitations are swept sines; the numerical simulation of swept sines leads to very high calculation times. Moreover, numerical problems (divergence of the numerical scheme) occur after a certain period. Thus, for the numerical simulations, we have used the time excitation $A_0 \dfrac{\sin(2\pi f_0 t)}{t}$ with $f_0 = 200\,\text{Hz}$, which allows the first bending modes to be excited, for reasonable time calculations.

Comments

At first sight, the comparison between the simulation and experimental results is not very good. First, one can note significant differences for resonance frequencies. Moreover, on experimental curves, the resonance frequency decreases and the damping increases when the excitation amplitude increases, while the opposite seems to occur on simulation curves (however, the trend is not obvious).

With regard to the resonance frequency, as a first step, the conservative finite-element model was adapted to fit the experimental eigenvalues. Then, the introduction of damping and non-linear aspects through the Bouc-Wen model leads to a discrepancy between the initial conservative eigenfrequencies and the resonance peak frequencies.

For the second point, for the Bouc-Wen model, the evolution of a resonance frequency and damping rate with the excitation amplitude is not very clear (this fact has been checked in many other examples).

However, despite these differences between experiment and simulation, this test case shows that the Bouc-Wen model allows both the dissipative and the non-linear aspects of the junction to be represented, with a much simpler model of the junction, and lower computation time.

Of course, the approach has to be improved. In particular, a rigorous method to identify the Bouc-Wen parameters must be developed. Moreover, this experimental mock-up was certainly too complicated for a first application.

Conclusion

We have presented a method to model the junctions in structural dynamics with meta-models. This approach allows both the dissipative aspect and the non-linear aspect of the junction to be taken into account.

This approach could be completed by the development of a method for identifying the values of the meta-model parameters *a priori*. Methods to identify Bouc-Wen parameters from experimental hysteric loops are under investigation.

The resolution method itself could be improved, on the one hand by improving the time domain non-linear algorithm and, on the other hand, by using the latest research developments concerning reduction methods in non-linear cases ■

Acknowledgements

This work was carried out within the framework of the collaborative project MAIAS (*Maîtrise de l'Amortissement Induit dans les ASsemblages*, *i.e.*, induced damping control in assemblies), under FUI financing (French government).

References

[1] S. BOGRAD, P. REUSS, A. SCHMIDT, L. GAUL - *Modeling the Dynamics of Mechanical Joints*. Mechanical Systems and Signal Processing 25, 2801–2826 (2011).

[2] H. FESTJENS - *Contribution à la caractérisation et à la modélisation du comportement dynamique des structures assemblées*. LISMMA Supmeca doctoral thesis (2014).

[3] A. CAIGNOT - *Prédiction par essais virtuels de l'amortissement dans les structures spatiales*. LMT ENS Cachan doctoral thesis (2009).

[4] M. ISMAIL, F. IKHOUANE, J. RODELLAR - *The Hysteresis Bouc-Wen Model, a Survey*. Archives of Computational Methods in Engineering 16,161-188 (2009).

[5] F. A. LÜLF, D.M. TRAN, R. OHAYON - *Reduced Bases for Nonlinear Structural Dynamic Systems: a Comparative Study*. Journal of Sound and Vibration 332, 3897-3921 (2013).

[6] C. HAMMAMI, E. BALMES, M. GUSKOV - *Conception et validation d'une liaison boulonnée dissipative*. 11ème Colloque National en Calcul des Structures (Giens), 13-17 May 2013.

[7] C. HAMMAMI - *Intégration de modèles de jonctions dissipatives dans la conception vibratoire de structures amorties*. ENSAM doctoral thesis (2014).

[8] A. SÉNÉCHAL - *Présentation du projet MAIAS*. colloque Aero'Nov Connection, 28 and 29 January 2014.

AUTHOR

Véronique Kehr-Candille graduated from ECL Ecole Centrale de Lyon in 1987. She joined ONERA in 1988, first in the Structure Department, and then in the Structural Dynamics Department. She carried out scientific studies in various fields of structural dynamic simulation: vibroacoustic, acoustic materials, viscoelascity and rotor dynamics. Her current main research interests are damping models and nonlinear structural dynamic response.

F. Poirion, Q. Mercier
(ONERA)

E-mail: fabrice.poirion@onera.fr

DOI: 10.12762/2018.AL14-05

Descent Methods for Design Optimization under Uncertainty

This paper is about optimization under uncertainty, when the uncertain parameters are modeled through random variables. Contrary to traditional robust approaches, which deal with a deterministic problem through a worst-case scenario formulation, the stochastic algorithms presented introduce the distribution of the random variables modeling the uncertainty. For single-objective problems such methods are currently classical, based on the Robbins-Monro algorithm. When several objectives are involved, the optimization problem becomes much more difficult and the few available methods in the literature are based on a genetic approach coupled with Monte-Carlo approaches, which are numerically very expensive. We present a new algorithm for solving the expectation formulation of stochastic smooth or non-smooth multi-objective optimization problems. The proposed method is an extension of the classical stochastic gradient algorithm to multi-objective optimization, using the properties of a common descent vector. The mean square and the almost-certain convergence of the algorithm are proven. The algorithm efficiency is illustrated and assessed on an academic example.

Introduction

Manufacturers are ever looking for designing products with better performance, and higher reliability at lower cost and risk. One way to address these antagonistic objectives is to use multi-objective optimization approaches. However, real-world problems are rarely described through a collection of fixed parameters and uncertainty has to be taken into account, whether it appears in the system description itself, or in the environment and operational conditions. Indeed, the system behavior can be very sensitive to modifications in some parameters [1, 2, 3]. This is why uncertainty has to be introduced in the design process from the start. Optimization under uncertainty has undergone important advances since the second half of the 20th century [4, 5] and various approaches have been proposed, including robust optimization, where only the bounds of the uncertain parameters are used, and stochastic optimization where uncertain parameters are modeled through random variables with a given distribution and where the probabilistic information is directly introduced into the numerical approaches. In that context, the uncertain multi-objective problems are written in terms of the expectation of each objective. Considering single objective stochastic optimization problems, a large variety of numerical approaches [6, 7] can be found in the literature, with the first results appearing in the late 50's [4, 8, 5]. With regard to aerospace applications, optimization problems under uncertainty are either considered as robust optimization problems or as reliability ones. In both cases, the numerical procedures that are the most frequently used are purely deterministic ones: this is indeed the case for robust optimization, since it is written as a "worst case" deterministic optimization problem, but it is also true when reliability is addressed. In this last situation, the chance constraint is transformed into a deterministic constraint using FORM or SORM approximations [9]. In both cases classical deterministic algorithms, such as the SQP algorithm [10], are eventually used to numerically solve the optimization problem. There is another route: it uses the probabilistic distribution of the random variables modeling the uncertainty [11, 12, 13]. There are two main approaches: the stochastic gradient algorithm, based on stochastic approximations such as the Robbins Monro algorithm [14, 15, 16], which is a descent method, and a second one based on scenario approaches [17, 18], the latter being more frequently applied for chance-constrained problems.

After briefly presenting the now-classical stochastic gradient algorithm, we illustrate its potential for being used in structural optimization on a reliability optimization problem in aeroelasticity. We pursue this by presenting the problem of optimizing several objective functions when uncertainty, modeled through random variables,

is introduced in part of the objective function. After providing some necessary mathematical elements for comprehension of the method, we present a general algorithm based on the existence of a descent vector common to each objective, which can be used in a broad context: for regular or non-regular, convex or non-convex objectives, with or without constraints. An illustration on the optimal design of a sandwich will highlight the efficiency of the proposed approach compared to that of classical genetic algorithms.

Single-Objective Stochastic Optimization

The following deterministic optimization problem

$$\text{Argmin}\left\{f(x)\,|\,g(x)\geq 0, x\in X\right\};\ f,g:\mathbb{R}^n\to\mathbb{R};\ X\subset\mathbb{R}^n \quad (1)$$

is a classical problem for any regular objective function f and constraint function g. However, when random parameters $\xi(\omega)=(\xi_1(\omega),...,\xi_d(\omega))\in\mathbb{R}^d$ defined on a probability space $(\Omega,\mathcal{T},\mathbb{P})$ are introduced into either one or both functions f and g, the meaning given to the random problem must be specified:

$$\text{Argmin}\left\{f(x,\xi(\omega))\,|\,g(x,\xi(\omega))\geq 0, x\in X\right\} \quad (2)$$

Depending on the nature of the practical applications considered, there are several approaches to deal with stochastic optimization problems. For instance, without being limited to these options, one can consider working with either:

- a mean value description:
$$\text{Argmin}\left\{\mathbb{E}\left[f(x,\xi(\omega))\right]\,|\,\mathbb{E}\left[g(x,\xi(\omega))\right]\geq 0\right\}$$
- a worst case scenario:
$$\text{Argmin}\left\{\mathbb{E}\left[f(x,\xi(\omega))\right]\,|\,g(x,\xi(\omega))\geq 0,\forall\omega\in\Omega\right\}$$
- a robust context:
$$\text{Argmin}\left\{\mathbb{E}\left[f(x,\xi(\omega))\right]\,|\,g(x,\xi(\omega))\geq 0,\forall\omega\in F\subset\Omega,\mathbb{P}(F)=p_0,p_0\in[0,1]\right\}$$
- or a chance-constraint formulation:
$$\text{Argmin}\left\{\mathbb{E}\left[f(x,\xi(\omega))\right]\,|\,\mathbb{P}\left[g(x,\xi(\omega))\geq 0\right]\geq p_0\right\}$$

denoting the mathematical expectation as $\mathbb{E}$.

The Stochastic Gradient Approach

Let $(\Omega,\mathcal{A},\mathbb{P})$ be an abstract probabilistic space, and $\xi:\Omega\to\mathbb{R}^d$ a random vector. We denote as μ the distribution of the random variable ξ, and as $\mathcal{W}$ its image space $\xi(\Omega)$. Let $\xi_1,...,\xi_k,...$ be independent copies of the random variable ξ, which will be used to generate independent random samples with the distribution μ. We consider the case where the constraints and the optimization parameters are deterministic. In the stochastic optimization problem (the objective function is defined as the mathematical expectation of the random quantity $f(x,\xi(\omega))$):

$$x^*=\underset{x\in X^{\text{ad}}}{\text{Argmin}}\ J(x);\ J(x)=\mathbb{E}\left[f(x,\xi(\omega))\right] \quad (3)$$

X^{ad} denotes the admissible space. There exists a stochastic extension of the standard deterministic gradient method that is particularly suited to this problem: it does not necessitate the estimation of the expectation in relation (3) to be built at each optimization step.

The algorithm of the stochastic gradient method uses optimization iteration instead, in order to build an estimate of the gradient expectation:

- Choose $x_0\in X$ and $\gamma_k>0$ for $k\in\mathbb{N}$.
- Draw ξ_{n+1} under the law of ξ independently from ξ_k for $k\leq n$.
- Update

$$X_{n+1}=x_n-\gamma_n\left(f'_x(x_n,\xi_{n+1})\right) \quad (4)$$

- Project over the feasible space X^{ad}

$$x_{n+1}=\Pi_{X^{\text{ad}}}(X_{n+1}) \quad (5)$$

$\Pi_{X^{\text{ad}}}$ defines the projection operator on the feasible space X^{ad}. The series (γ_n) must be divergent, and the series (γ_n^2) convergent. Typically, $\gamma_n=a/(n^\alpha+b)$, $\alpha\in]0.5,1]$. Like its deterministic version, the sequence (x_n) converges to the solution x^* of the problem under the Robbins-Monroe assumptions applied to f'_x [14]. When the gradient is easily available the method is very efficient (see the discussion section and Figure 10). Some results on convergence speed and enhancements can be found in the book [19].

An Aeroelasticity Illustration

Flutter Equation

We consider the classical context of aeroelasticity, where the aerodynamic forces are calculated using a linearized assumption together with a doublet-lattice method [20], where the airplane structure is described through a finite-element model, and when uncertainty is introduced in the mass and stiffness matrices through a vector valued random variable ξ. The finite-element discretization for the aeroelastic analysis can be formulated in the frequency domain as follows:

$$L(\xi)^T\quad\left[p^2\Phi^T(\xi)M(\xi)\Phi(\xi)+\Phi^T(\xi)K(\xi)\Phi(\xi)+\frac{1}{2}\rho V^2\Phi^T(\xi)A(p/V)\Phi(\xi)\right]R(\xi)=0 \quad (6)$$

where M and K are the structural mass and stiffness matrices, ρ is the air density, V is the flow speed, A is the aerodynamic load matrix and Φ is the modal basis of the structure (M, K). Assuming the airflow speed V to be constant, the solution $p\in\mathbb{C}$ of the flutter equation depends on the aerodynamic parameter ρ and on the uncertain parameters ξ. The sign of the real part $\Re(p)$ specifies the stability of the coupled system. We define the critical pressure q_c as the smallest pressure value q such that $\Re(p(q))=0$, if any. The critical pressure depends on the uncertain parameters ξ and, therefore, is itself a random variable. The vectors L and R are the associated pseudo left and right eigenvectors. The dimension of Problem (6) is equal to the number of eigenmodes retained for the aeroelastic analysis.

Gradient Calculation

We shall address the problem of optimizing the mass distribution of a given number of concentrated masses $m_i, i=1,q$ of the finite element model, in order to maximize the critical pressure value. We shall denote by m the vector $m=(m_1,...,m_q)$. Therefore, we shall need to

evaluate the gradients $\frac{\partial p}{\partial m_i}$ and $\frac{\partial p}{\partial q}$. The derivation of such quantities is classical [21, 22]; they are obtained by differentiating Equation (6):

$$\frac{\partial p}{\partial m_i} = -\frac{p^2 L^T \Phi^T \frac{\partial M}{\partial m_i} \Phi R}{L^T \Phi^T \left(2pM + \frac{1}{2} q V^2 A'(p/V) \right) \Phi R'} \tag{7}$$

$$\frac{\partial p}{\partial q} = -\frac{\frac{1}{2} L^T \Phi^T V^2 A(p/V) \Phi R}{L^T \Phi^T \left(2pM + \frac{1}{2} q V^2 A'(p/V) \right) \Phi R'} \tag{8}$$

where A' stands for the derivative of A. These two relations will allow the derivation of the critical pressure gradient expression. For each mass distribution m, the critical pressure is defined by $\Re\left(p(m, q_c)\right) = 0$. Using the implicit function theorem in the neighborhood of a point $\left(m^0, q_c^0\right)$, under the assumption that p is a regular function, there exists a function ϕ such that $\phi(m) = q_c$ (with $q_c^0 = \phi\left(m^0\right)$). Moreover, in the neighborhood of $\left(m^0, q_c^0\right)$, we have, for each mass point m_i:

$$\frac{\partial \phi}{\partial m_i}\left(m^0\right) = \frac{\partial q_c}{\partial m_i}\left(m^0\right) = -\frac{\Re\left(\frac{\partial p}{\partial m_i}\left(m^0, q_c^0\right) \right)}{\Re\left(\frac{\partial p}{\partial q}\left(m^0, q_c^0\right) \right)} \tag{9}$$

The aerodynamic load matrix is modeled by a matrix-valued rational function using the "Minimum State" approach [23]. The analytical expression of the aerodynamic matrix gradients can then be readily derived, since their calculation involves rational function differentiation.

Wing Model

The goal of this section is to show numerically the applicability of these two algorithms to an aeroelastic optimization problem. We shall consider a finite-element model of a simple wing and introduce uncertainty in several structural parameters. We consider then two different optimization problems: the first one involving a probabilistic objective function and deterministic constraints, which will be solved using the stochastic gradient algorithm, and the second one, which is a chance constraint optimization problem, and which will be solved using the stochastic Arrow-Hurwicz algorithm.

Description of the Model

We consider a wing model that was defined as a wind-tunnel model similar to a heavy-carrier airplane wing, in order to evaluate and compare different CFD codes among various partners in the late '80s [24]: Aerospatiale, ONERA, DLR and MBB. The structural model is given in Figure 1. It is a stick model with concentrated masses. This model has the advantage of being numerically more tractable for testing stochastic algorithms. During the design and optimization stages, stick models are, in fact, used by manufacturers because they give a clear and synthetic overview of the structure properties. The stick model, including the super element modelling the mounting bracket, is defined with 93 beams and 97 concentrated masses m_i.

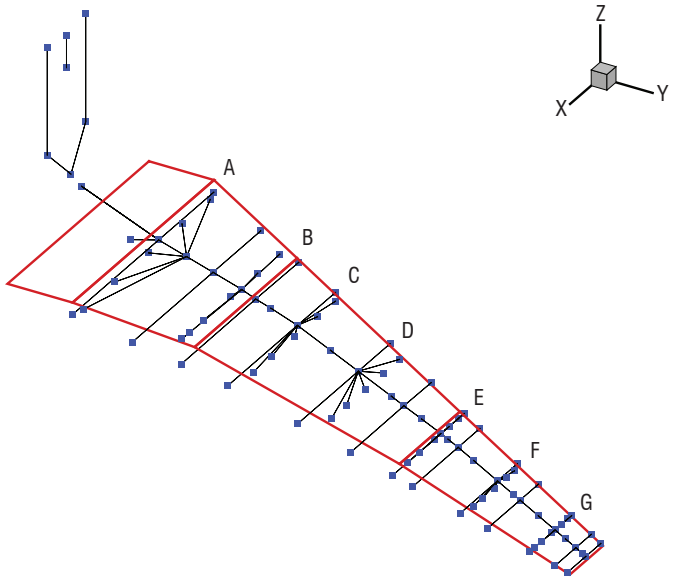

Figure 1 – AMP stick model

The root and tip chord lengths are, respectively, equal to 0.42 m and 0.10 m. The sweep angle is equal to 32 degrees, and the span length is equal to 1 m.

A flutter analysis is performed using a doublet-lattice method for computing the aerodynamic matrix. In Figure 2, the frequency and damping evolution of the first bending mode (23.4 Hz) and first torsion mode (31.85 Hz) with respect to the pressure are shown. The first torsion mode becomes unstable for $q_c \approx 12 \times 10^4$.

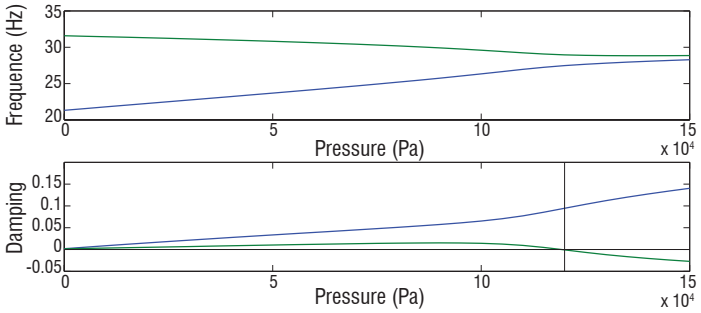

Figure 2 – Flutter diagram for the AMP wing

Optimization of the Critical Pressure

The illustration goal is to test and assess the gradient-based method applied to our simple stick model. The optimization problem purpose is to modify the value of each of the 89 mass points lying on the wing, in order to increase the value of the critical pressure. The mass points defining the mounting bracket are not considered. Several constraints are introduced. The first one is to keep the global mass of the model constant. The other set of constraints is related to the range of variation of each mass point: their value must stay within a bounded interval in order to avoid physical aberration (negative or null mass). The optimization problem is then written as:

$$\text{Argmax}\left\{ \mathbb{E}\left[q_c\left(m, \xi(\omega)\right) \right] \middle| \sum_{j=1}^{N} m_j = c \,;\, m_i \in [a_i, b_i], \forall i \right\} \tag{10}$$

The feasible space

$$X^{\text{ad}} = \left\{ m = (m_1,...,m_N) \in \mathbb{R}^N \,|\, \sum_{j=1}^{N} m_j = c \,;\, m_i \in [a_i, b_i], \forall i \right\}$$

is convex. The gradient-based algorithm iterates on the values of vector m and is written:

$$m^{n+1} = \Pi_{X^{\text{ad}}} \left(m^n + \gamma_n \frac{\partial q_c}{\partial m}(m^n, \xi_{n+1}) \right) \tag{11}$$

The divergent series (γ_n) is chosen as: $\frac{K_1}{K_2 + n}$, where K_1 and K_2 are parameters that need to be tuned. Indeed, these two parameters have an impact on the convergence speed. For this particular application, only a couple of tests were necessary to obtain an acceptable convergence speed. More precisely, we have taken $K_1 = 0.01$ and $K_2 = 100$. Under classical assumptions [19], the gradient-based algorithm converges to the best solution, either almost surely or as a mean square for the norm $\mathbb{L}^2(\Omega)$.

In the numerical experiment, seven regions of the stick model have been considered, for which a random stiffness coefficient ξ_i is introduced in order to model the stiffness uncertainty of each region. Those seven regions (indicated in Figure 1 by the letters A through G) contain the beams connecting the mass points lying on a same chord. The uncertainty is modeled as a uniform random variable over $[0.75 \times \xi_{i,0}, 1.25 \times \xi_{i,0}]$, where $\xi_{i,0}$ are the stiffness nominal values for each region. Eighty nine grid mass points m_j are chosen as optimization parameters, and a maximum variation of 25% of the initial values: $m_j \in [0.75 \times m_{j,0}, 1.25 \times m_{j,0}]$ is allowed.

Five hundred iterations of the stochastic gradient algorithm have been considered. In order to illustrate the quality of the optimization result, we have performed an uncertainty propagation study by drawing 1000 random stiffness realizations for the initial and final mass configurations and by constructing the critical pressure histogram.

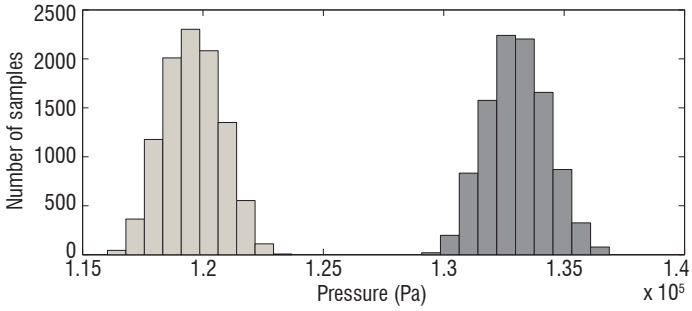

Figure 3 – Random critical pressure distribution before and after optimization

The critical pressure histogram corresponding to the initial values of the optimization parameters is represented on the left in Figure 3, and that corresponding to the final values is on the right. The gain obtained is clearly visible. This result shows that the critical pressure of the wing can be significantly increased by modifying the mass distribution, without modifying the total weight. Such a result can be interesting for updating the numerical model of a wing with uncertain parameters, in order to match an experimental critical speed value for a wind tunnel mockup.

The locus of the wing centers has hardly been modified by the optimization procedure.

Multi-Criteria Stochastic Optimization

Let m functions f_i: $\mathbb{R}^n \times \mathcal{W} \to \mathbb{R}$, $i=1,...m$ depending on uncertain parameters be modeled trough a random vector $W(\omega)$. We consider the following stochastic optimization problem:

$$\min_{x \in \mathbb{R}^n} \left\{ \mathbb{E}\left[f_1(x, W(\omega)) \right], \mathbb{E}\left[f_2(x, W(\omega)) \right], ..., \mathbb{E}\left[f_m(x, W(\omega)) \right] \right\} \tag{12}$$

More precisely, we want to construct the associated Pareto set: multi-objective optimization is based on the notion of Pareto-optimal and weak Pareto-optimal solutions. Consider m convex functions f_i: $\mathbb{R}^n \to \mathbb{R}$, $i=1,... m$ and the unconstrained optimization problem

$$\min_{x \in \mathbb{R}^n} \left\{ f_1(x), ..., f_m(x) \right\} \tag{13}$$

A solution x^* of Problem (13) is Pareto-optimal if no point x such that $f_i(x) \le f_i(x^*)\ \forall i = 1,...,m$ and $f_j(x) < f_j(x^*)$ for an index $j \in \{1,...,m\}$ exists. It is weakly Pareto-optimal if no point x such that $f_i(x) < f_i(x^*)\ \forall i = 1,...,m$ exists. A complete review of multi-objective optimization can be found in [25]. Before continuing with the algorithm description that will be used to solve the previous problem, we shall recall definitions of some notions appearing in the context of non-smooth analysis and multi-objective optimization. Throughout the paper, the standard inner product on $\mathbb{R}^n$ will be used and denoted as $\langle \cdot, \cdot \rangle$, with the norm being denoted as $\| \cdot \|$.

Some Definitions and Results in Convex Analysis

Definition 1 – *A function $f : \mathbb{R}^n \to \mathbb{R}$ is locally Lipschitz-continuous at point x if there exists scalars $K > 0$ and $\varepsilon > 0$ such that, for all $y, z \in B(x, \varepsilon)$*

$$|f(y) - f(x)| \le K \|y - z\|$$

where $B(x, \varepsilon)$ denotes the open ball of center x and radius ε.

Definition 2 – *A function $f : \mathbb{R}^n \to \mathbb{R}$ is convex if for all $x, y \in \mathbb{R}^n$ and $\lambda \in [0,1]$ the following inequality holds:*

$$f(\lambda x + (1-\lambda) y) \le \lambda f(x) + (1-\lambda) f(y)$$

Definition 3 – *The directional derivative at x along the direction $v \in \mathbb{R}^n$ of a function $f : \mathbb{R}^n \to \mathbb{R}$ is defined by the limit:*

$$f'(x; v) = \lim_{t \downarrow 0} \frac{f(x + tv) - f(x)}{t}$$

Any convex function f is continuous and differentiable almost everywhere. Moreover, there exists at each point x a lower affine function that is identical to f at x. This affine function defines the equation of a plane called a tangent plane. When the function f is differentiable at x, there is only one tangent plane characterized by the gradient $\nabla f(x)$. When f is non-differentiable at x, there exists an infinity of tangent planes that define the subdifferential.

Definition 4 – *The subdifferential of a function $f : \mathbb{R}^n \to \mathbb{R}$ at x is the set*

$$\partial f(x) = \left\{ s \in \mathbb{R}^n : f(y) \ge f(x) + \langle s, y - x \rangle \ \forall y \in \mathbb{R}^n \right\} \tag{14}$$

This set is non-empty, convex, closed and reduced to $\nabla f(x)$ when f is differentiable. The following result allows the notion of subdifferential to be used for characterizing the optima of convex functions.

Theorem 1 ([26]) – *Let $f:\mathbb{R}^n \to \mathbb{R}$ a convex function. The following statements are equivalent*

- *f is minimized at x^*: $f(y) \geq f(x^*)\ \forall y \in \mathbb{R}^n$,*
- *$0 \in \partial f(x^*)$,*
- *$f'(x^*, d) \geq 0\ \forall d \in \mathbb{R}^n$.*

When the function is no longer convex, but is locally Lipschitz-continuous, the directional derivative defined in Definition 3 does not necessarily exist and a generalized directional derivative must be considered. Moreover, the notion of subdifferential has to be replaced by the notion of Clarke subdifferential [27]. The Clarke subdifferential at point x is the set containing all of the convex combinations of limits of gradients at points located in the neighborhood of x:

$$\partial f(x) = conv\left\{\lim_{i\to\infty} \nabla f(x_i) ; x_i \to x \text{ and } \nabla f(x_i) \text{ exists}\right\} \quad (15)$$

In order to define the Clarke subdifferential more formally, we give the definition of a generalized directional derivative in a first step:

Definition 5 – *Let $f:\mathbb{R}^n \to \mathbb{R}$ be a locally Lipschitz-continuous function. The generalized directional derivative of f at x in the direction $v \in \mathbb{R}^n$ is defined by:*

$$f^o(x;v) = \limsup_{y\to x; t\downarrow 0} \frac{f(y+tv) - f(y)}{t}$$

Definition 6 – *Let $f:\mathbb{R}^n \to \mathbb{R}$ be a locally Lipschitz-continuous function. The Clarke subdifferential of f at x is the set $\partial f(x)$ of vectors defined by:*

$$\partial f(x) = \left\{s \in \mathbb{R}^n : f^o(x;v) \geq s^T v\ \forall v \in \mathbb{R}^n\right\} \quad (16)$$

Theorem 1 cannot be generalized to arbitrary non-convex functions: a locally Lipschitz continuous function f has a local minimum at x^* if $0 \in \partial f(x^*)$, but it is not a sufficient condition. There exist, however, classes of functions for which the result still holds, it is the case, for instance, of f^0-pseudoconvex functions, which are defined by:

Definition 7 – *A locally Lipschitz-continuous function $f:\mathbb{R}^n \to \mathbb{R}$ is f^0-pseudoconvex if*

$$\forall x, y \in \mathbb{R}^n,\ f(y) < f(x) \Rightarrow f^o(x; y-x) < 0 \quad (17)$$

Common Descent Direction

The algorithm presented in the next section is based on the existence and construction of a descent direction. We first recall its definition.

Definition 8 – *A vector d is called a descent direction if $\exists t_0 > 0$, such that $f(x+td) < f(x)$ for all $t \in [0, t_0]$.*

For smooth functions it is well known that the opposite direction of the gradient is a descent vector. In the non-smooth convex or non-convex context, not all elements of the subdifferential are a descent vector.

There are several techniques to construct such a descent vector: proximal bundle methods [28, 29, 30], quasisecant methods [31], or gradient sampling methods [32, 33]. Considering now m functions $f_1, ..., f_m$, we show that there exists a vector d that is a descent direction for each function. Its construction is based on properties of the following convex set C:

Lemma 1 ([36]) – *Let C be the convex hull of either*

- *the gradients $\nabla f_i(x)$ of the objective functions when they are differentiable,*
- *or the union of the subdifferentials $\partial f_i(x)$, $i = 1, ..., m$ when they are non-differentiable but convex, or*
- *the union of the Clarke subdifferentials $\partial f_i(x)$, $i = 1, ..., m$ if they are non-convex.*

Then, there exists a unique vector $p^* = \text{Argmin}_{p\in C} \|p\|$ such that

$$\forall p \in C : p^T p^* \geq p^{*T} p^* = \|p^*\|^2$$

The existence of the common direction d and its construction is given by the following theorem:

Theorem 2 ([36]) – *Let C be the convex set defined in Lemma 1 and let p^* be its minimum norm element. Then, either we have*

- *$p^* = 0$ and the point x is Pareto-stationary or*
- *$p^* \neq 0$ and the vector $-p^*$ is a common descent direction for every objective function.*

We now have sufficient elements to present the SMGDA (Stochastic Multi-Gradient Descent Algorithm) algorithm.

The SMGDA Algorithm

As written problem (12) is a deterministic problem, but the objective function expectations are seldom known. A classical approach, the sample average approximation (SAA) method, is to replace each expectancy by an estimator built using independent samples w_k of the random variable W, [34, 35]. The algorithm that we propose does not need the objective function expectancy to be calculated, and is based only on the construction of a common descent vector. Let ω be given in Ω, and consider the deterministic multi-objective optimization problem:

$$\min_{x\in\mathbb{R}^n} \left\{f_1(x, W(\omega)), f_2(x, W(\omega)), ..., f_m(x, W(\omega))\right\} \quad (18)$$

Pursuant to Theorem 2 there exists a descent vector common to each objective function $f_k(x, W(\omega)), k = 1, ..., m$ at point x.

The common descent vector depends on x and ω, and therefore will be considered as a random vector denoted by $d(\omega)$ defined on the probability space $(\Omega, \mathcal{A}, \mathbb{P})$.

The Algorithm

We now list the successive steps of the algorithm that we propose.

1. Choose an initial point x_0 in the design space, a number N of iterations and a σ-sequence $t_k : \sum t_k = \infty ; \sum t_k^2 < \infty$,

2. At each step k, draw a sample w_k of the random variable $W_k(\omega)$,

3. Construct the common descent vector $d(w_k)$ using Theorem 2 and the gradient sampling approximation method,

4. Update the current point : $x_k = x_{k-1} + t_k d(w_k)$.

The last step of the algorithm defines a sequence of random variables on the probability space $(\Omega, \mathcal{A}, \mathbb{P})$ through the relation

$$X_k(\omega) = X_{k-1}(\omega) - t_k d\left(X_{k-1}(\omega), W_k(\omega)\right) \tag{19}$$

Initializing the algorithm with different points in the admissible space, for instance using a random or quasi-random distribution, allows different points located on the Pareto front to be constructed. This procedure is entirely parallelizable.

Theorem 3 ([36]) – *Under a set of assumptions,*

1. *The sequence of random variables $X_k(\omega)$ defined by Relation (19) converges in a mean square towards a point X^* of the Pareto set:*

$$\lim_{k \to +\infty} \mathbb{E}\left[\left\| X_k(\omega) - X^\star \right\|^2 \right] = 0$$

2. *The sequence converges almost surely towards X^*.*

$$\mathbb{P}\left(\left\{ \omega \in \Omega, \lim_{k \to \infty} X_k(\omega) = X^\star \right\} \right) = 1$$

Illustration: Optimal Designs of a Sandwich Plate with Uncertainties

We consider a sandwich panel whose constitutive materials are given but their mechanical properties are uncertain: solid foams present random, disordered micro-structure, while a honeycomb core may present uncertain geometrical characteristics, which may result in a distinct scatter and unpredictability of the macroscopic material properties. These uncertainties will be introduced into the optimization problem by means of random variables.

More precisely, in this application we consider a three-layer non-symmetric sandwich panel with aluminum skins and a regular hexagonal honeycomb core. The mechanical properties of the plate are described by the Young modulus $E_{(.)}$, the elastic resistance $\sigma_{(.)}$ and the mass density $\rho_{(.)}$ of the upper and bottom skin and of the core constitutive material. We introduce the honeycomb wall thickness/length ratio $\mathrm{R} = t/\ell$.

The relations yielding the honeycomb core material properties from its geometrical description and from its constitutive material properties are given in [37] and are recalled in Table 1.

R	=	t/l
ρ_{R}	=	$\dfrac{3}{2\cos(\tilde{\theta})\left(1+\sin(\tilde{\theta})\right)} \rho_c \mathrm{R}$
E_{R}	=	$\rho_{\mathrm{R}E_c} / \rho_c$
σ_{R}	=	$5.6(\mathrm{R})^{\frac{5}{3}} \sigma_c$

Table 1: Core material property function of R

Two objectives are considered in the design process:

- Minimization of the mass per unit of surface

$$M = \rho_u \mathrm{t}_u + \rho_c \mathrm{t}_c + \rho_b \mathrm{t}_b \tag{20}$$

- Maximization of the critical force leading to a failure mode when two modes are introduced: Mode $F_{c,1}$ leading to the core indentation and Mode $F_{c,2}$ leading to the lower-skin plastic stretching. We shall then consider the failure mode F_c, which appears first:

$$F_c = \min_{i=(1,2)} \left\{ F_{c,i} \right\} \tag{21}$$

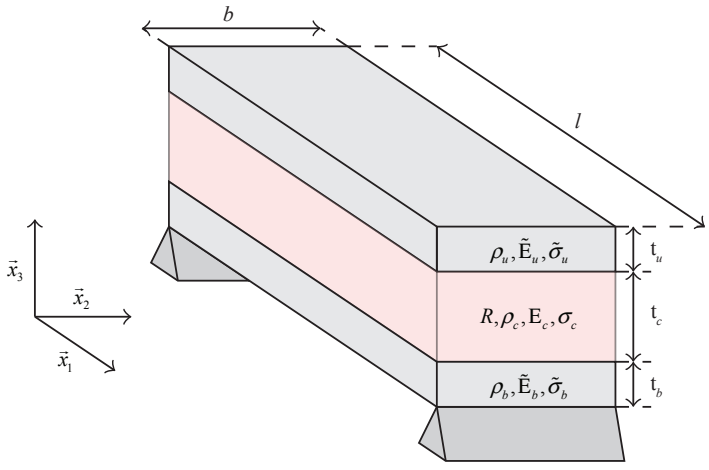

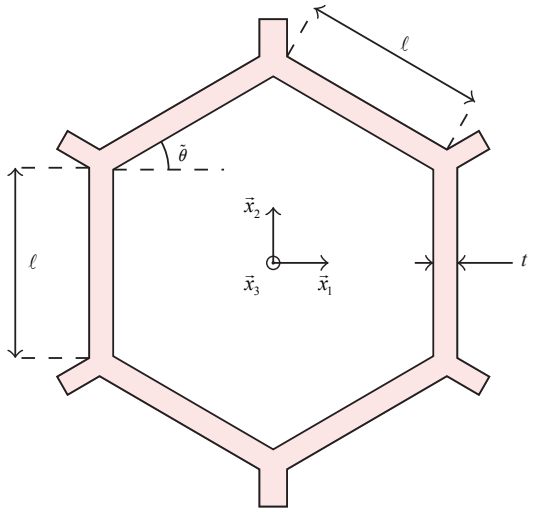

Figure 4 – Three-layer sandwich material beam

$$F_{c,1} = 2bt_u\sqrt{\sigma_c\tilde{\sigma}_u} + ab\sigma_c \; ; \; F_{c,2} = \frac{4bt_b\left(t_c + \left(t_u + t_b\right)/2\right)}{4}\tilde{\sigma}_b \qquad (22)$$

This last objective function is not differentiable, due to the presence of the minimum function.

Four design parameters are considered: the three thickness parameters of the sandwich plate $\left(t_u, t_b, t_c\right)$ and the honeycomb wall thickness/length ratio $\left(R = \frac{t}{\ell}\right)$. We shall denote by $x = \left(t_u, t_b, t_c, R\right)$ the vector containing the four design parameters. Two types of constraints are introduced into the problem, the first are bounding constraints on each design variable, which are handled using a projection method on the convex feasible set C defined by these constraints:

$$t_u, t_b \in [0.03, 14]\,\text{cm} \; ; \; t_c \in [0.05, 32]\,\text{cm} \; ; \; R \in [0.01, 0.2]$$

The second type is an inequality constraint for the total thickness e of the sandwich material:

$$e = t_u + t_b + t_c \le 0.25$$

In the following numerical application, this last constraint is handled by introducing the exact penalty term [26]

$$g(x) = r \times \min\{0, 1 - e/.25\} \qquad (23)$$

into each objective function, where r is a penalty term. Classically, an increasing sequence $r = p^q, q = 1, 2, \ldots$ is used, with q being the smallest integer for which the constraint is satisfied. For this application we have chosen $r = 10^q$.

We now introduce uncertainty in some parameters of the sandwich material. More precisely, 20% uncertainty is considered for the upper and bottom skin elastic resistance value:

$$\left(\tilde{\sigma}_u, \tilde{\sigma}_b\right) = \bar{\sigma}_{Alu} \times \left((1,1) + U_1\right) \qquad (24)$$

where U_1 is a uniform random variable on $[-.2,.2]\times[-.2,.2]$ and where $\bar{\sigma}_{Alu} = 350\,MPa$ is the nominal value. A second uncertain parameter is introduced: the value of the honeycomb angle $\tilde{\theta} = \bar{\theta}\left(1 + U_2\right)$, where U_2 is a uniform random variable on $[-.2,.2]$ and where $\bar{\theta} = \pi/6$. We shall denote by $\xi = [U_1, U_2]$ the vector containing the various random variables introduced in the problem, which are assumed to be independent. In order to take into account these uncertainties in the design process, the following stochastic multi-objective problem is considered:

$$\min_{x \in C}\left\{\mathbb{E}\left[M(x)\right], \mathbb{E}\left[-F_c(x)\right]\right\} \text{ subject to } e(x) \le 0.25 \qquad (25)$$

This problem is rewritten using the exact penalty formulation:

$$\min_{x \in C}\left\{\mathbb{E}\left[M(x)\right] - rg(x), \mathbb{E}\left[-F_c(x)\right] - rg(x)\right\} \qquad (26)$$

In order to compare the efficiency of the method assessed to the classical genetic algorithm NSGA-II, the expectancies appearing in Problem 12 are estimated, to be used in NSGA-II, through a sample-average method:

$$\mathbb{E}\left[f(x,\xi)\right] \approx \frac{1}{N}\sum_{i=1}^{N} f\left(w, \xi_i\right) \qquad (27)$$

where ξ_i are independent samples of the random variable ξ. The number N of samples plays a crucial role in the efficiency of the algorithm: an excessively small value will give a wide confidence interval and a poor estimate of the objective function, while an excessively high value will dramatically increase the computational cost (see Figure 5).

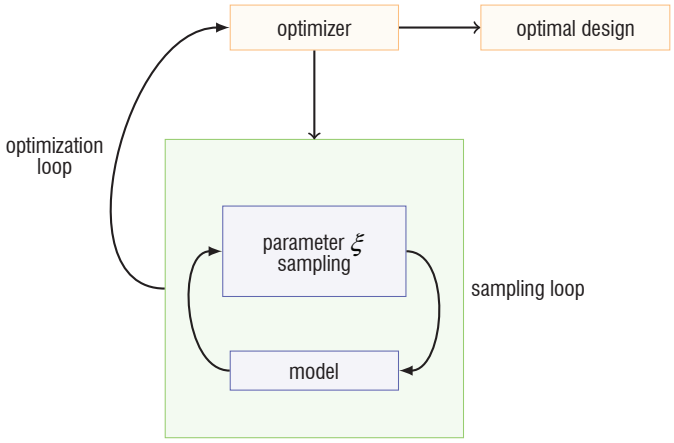

Figure 5 – Stochastic genetic optimization framework

In order to compare the two algorithms, we have chosen to compare results obtained for the same number of function calls $f\left(w, \xi_i\right)$. In the case of SMGDA, this number includes the number of starting points and the number of iterations per initial point. In the case of NSGA-II it includes the size of the initial population, the number N used for estimating the objective functions, and the number of generations.

In the numerical illustration, the SMGDA algorithm is initiated from 50 starting points in $\mathbb{R}^4$ and around 250 iterations were necessary to reach convergence. The same population number (50) is used for NSGA-II. The σ-sequence $t_k = .03/(3\times k + 10)$ is used in this illustration. Figures 6 and 7 illustrate the Pareto sets obtained by the two algorithms. The constraint is represented in the design space by a plane. Both methods give solutions that comply with the constraints. Variable R is represented in the figure by a variation of color according to the color scale in Figure 6. For a low number of function calls, NSGA-II coupled with a Monte Carlo estimator gives a less good result than SMGDA. It needs about one hundred times more calls to the objective functions to reach an identical Pareto set.

In order to evaluate the effect of uncertainty on the objective functions considered at optimal design points x^* located on the Pareto front, we have estimated the distribution of the random vector $\left(M\left(x^*, \xi(\omega)\right), -F_c\left(x^*, \xi(\omega)\right)\right)$ for two points x_1^* and x_2^*, by generating 10^5 samples of the random vector W. The corresponding probability distributions are drawn in Figure 8 and Figure 9, where the position of the chosen point x^* is indicated on the inner figure. The blue and red dots on the graph denote the mode of failure obtained for some of the samples used to estimate the distribution. A first result that can be drawn is that the distribution obtained is not a classical one, but there is no reason to obtain a classical distribution. The second observation is that the effect of the uncertainties is more important for the critical force objective than for the mass objective. Such a result could be valuable during the design stage of the material, knowing the high sensitivity of the critical force optimal value to uncertain parameters.

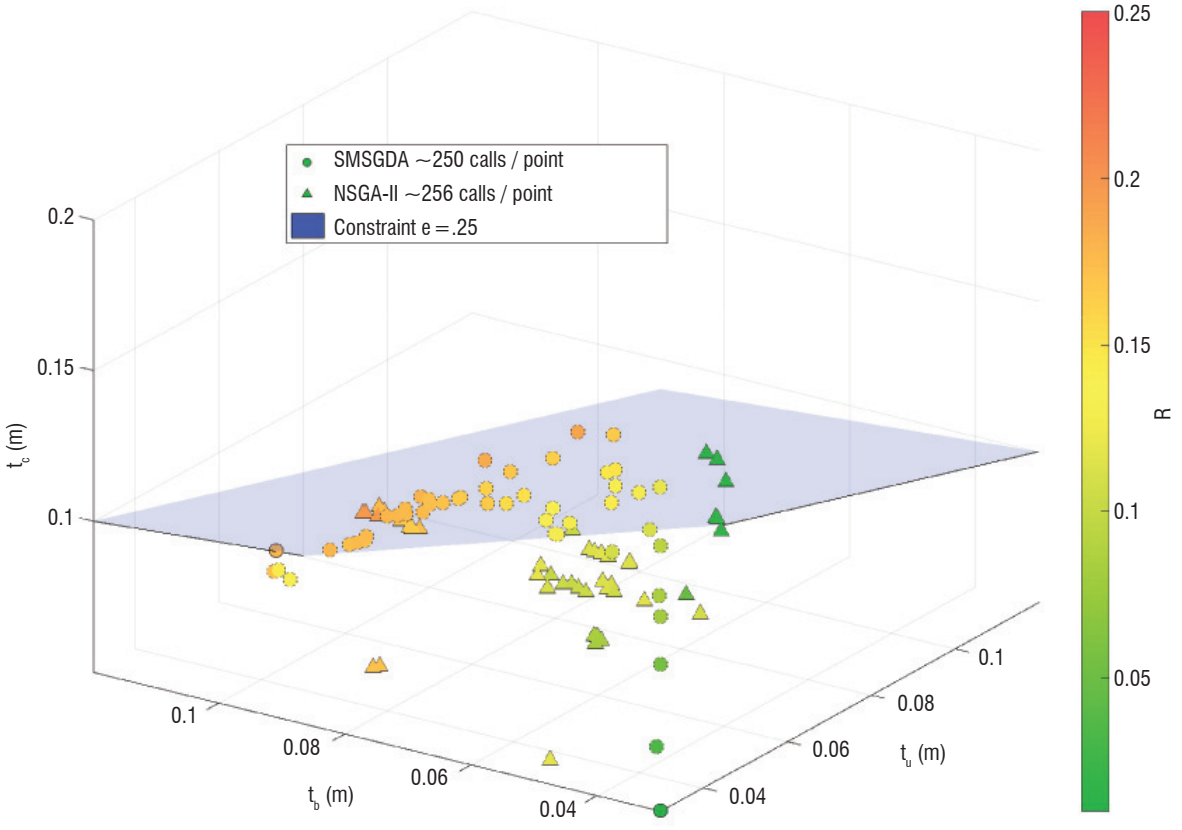

Figure 6 – Pareto set in the design space

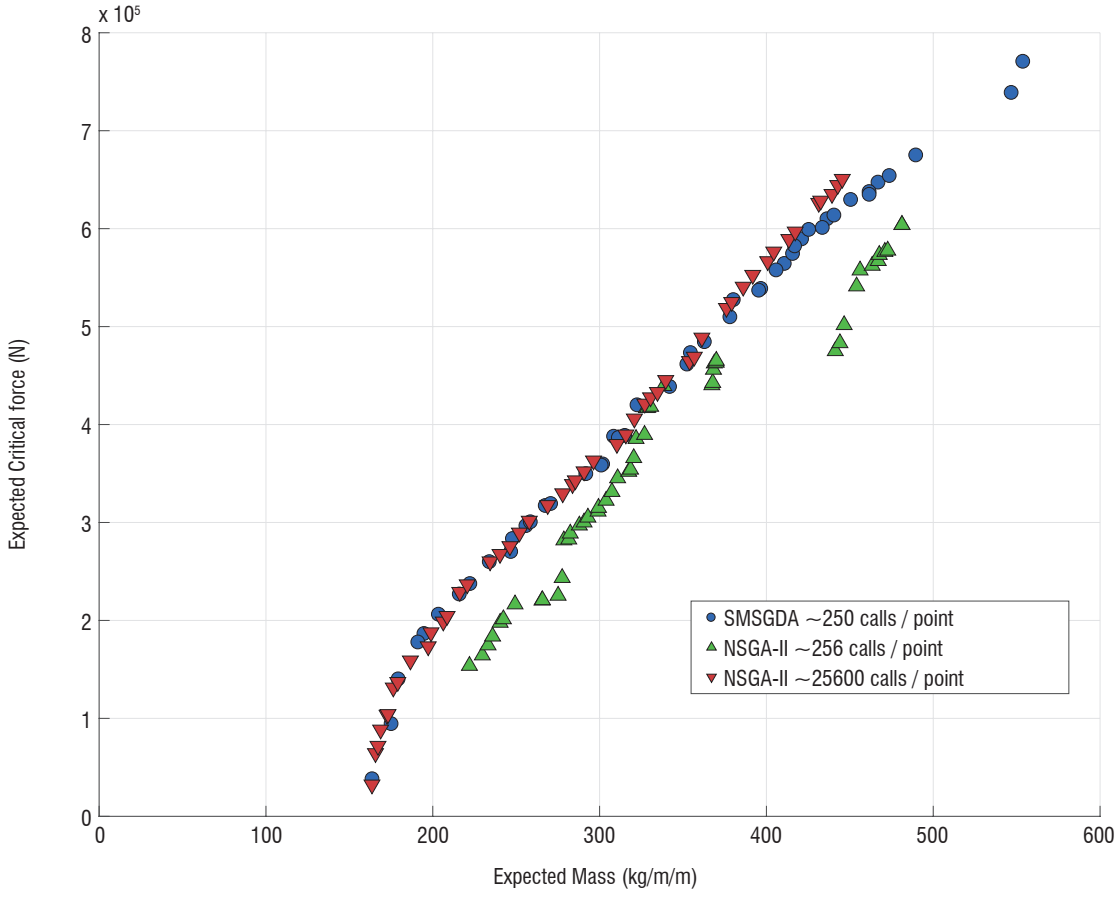

Figure 7 – Pareto set in the objective space

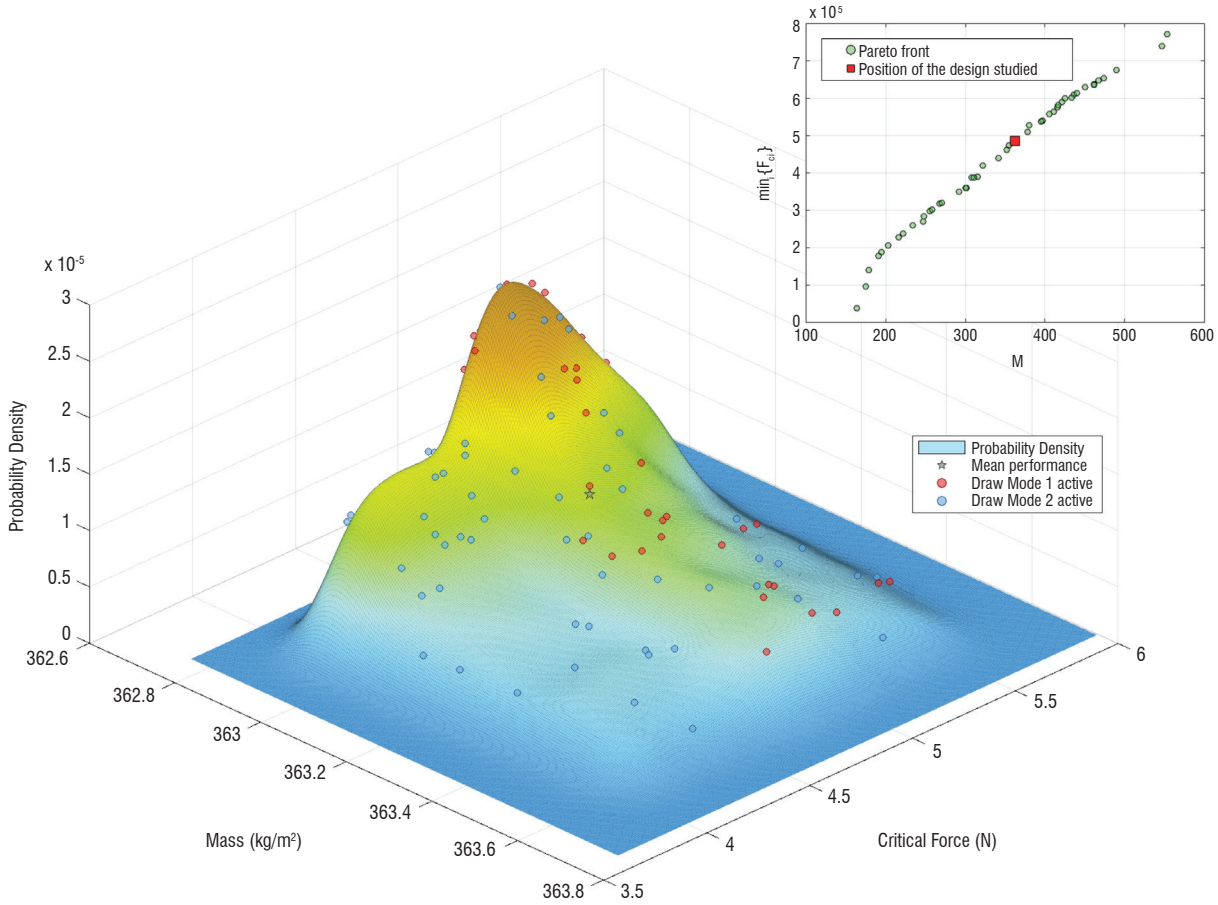

Figure 8 – Probability density of $M\left(x_1^*,W(\omega)\right),-F_c\left(x_1^*,W(\omega)\right)$

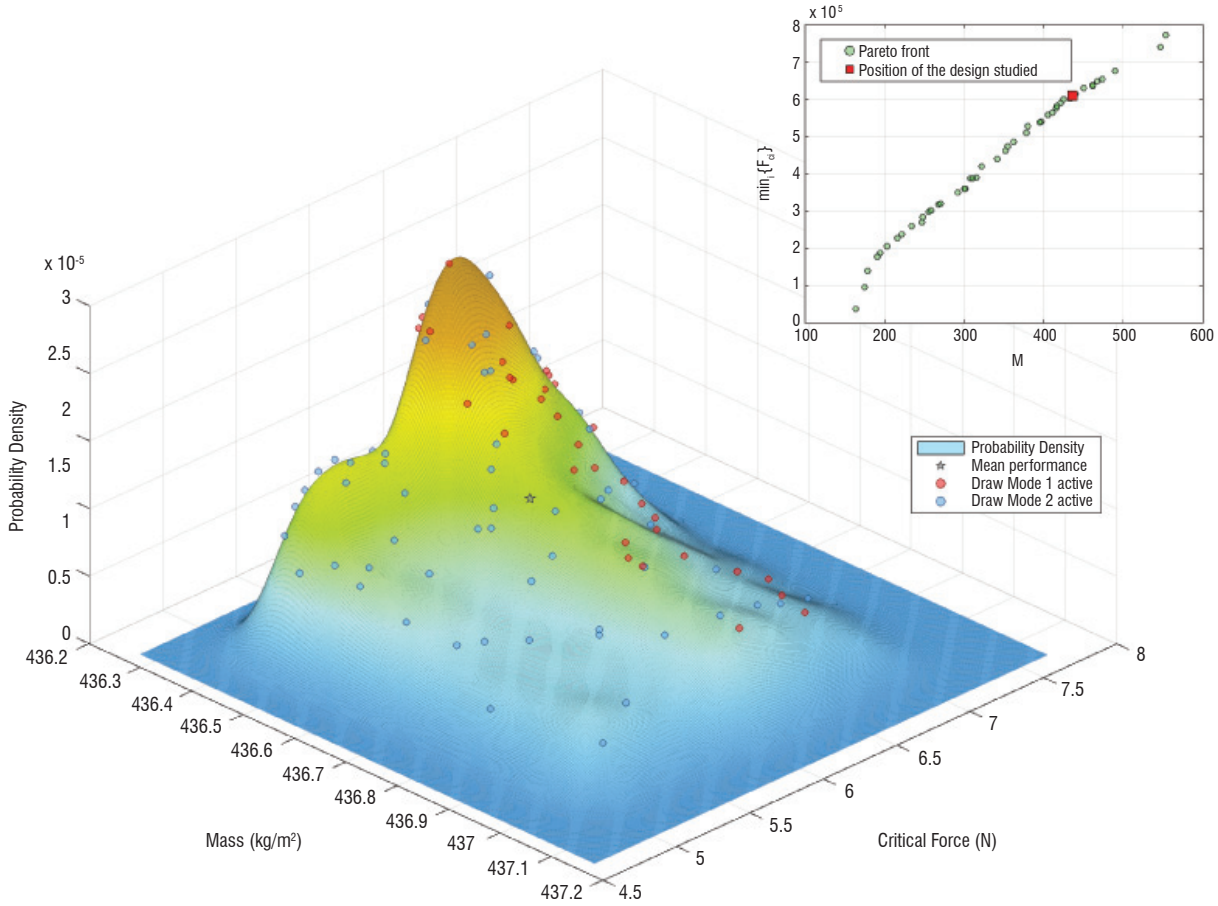

Figure 9 – Probability density of $M\left(x_2^*,W(\omega)\right),-F_c\left(x_2^*,W(\omega)\right)$

Conclusion

Although the stochastic gradient algorithm is now a classical approach to deal with uncertain single-objective design optimization problems, it is much more difficult to deal with multiple uncertain objectives. The most classical approaches are based on the use of genetic algorithms, such as NSGA coupled with a scenario method, to construct estimates of the objective expectations, but their usefulness is limited by the numerical cost induced by the estimator loop. Conversely, the SMGDA algorithm does not rely on the expectation estimation and converges relatively rapidly toward the Pareto boundary. It can, moreover, be entirely parallelizable. An illustration on the design optimization of a sandwich plate has shown its potential usefulness for engineering problems ■

References

[1] C. PAPADIMITRIOU, L. S. KATAFYGIOTIS, S.-K. AU - *Effects of Structural Uncertainties on tmd Design : A Reliability-Based Approach.* Journal of Structural Control, 4:65-88, 1997.

[2] H. G. MATTHIES, C. E. BRENNER, C. G. BUCHER, C. G. SOARES - *Uncertainties in Probabilistic Numerical Analysis of Structures and Solids-Stochastic Finite Elements*. Structural safety, 3:283-336, 1997.

[3] R. ARNAUD, F. POIRION - *Optimization of an Uncertain Aeroelastic System Using Stochastic Gradient Approaches.* Journal of Aircraft, doi: arc.aiaa.org/doi/abs/10.2514/1.C032142., 2014.

[4] B. G. DANTZIG - *Linear Programming Under Uncertainty.* Management Science, 1:197-206, 1955.

[5] R. E. BELLMAN, L. A. ZADEH - *Decision-Making in a Fuzzy Environment*. Management Science, 17:141-161, 1970.

[6] N. V. SAHINIDIS - *Optimization Under Uncertainty: State-of-the-Art and Opportunities*. Computers & Chemical Engineering, 28(6-7):971-983, 2004.

[7] R. ROY, S. HINDUJA, R. TETI - *Recent Advances in Engineering Design Optimisation: Challenges and Future Trends.* Manufacturing Technology, 57:697-715, 2008.

[8] R. E. BELLMAN - *Dynamic Programming*. Princeton University Press, 1957.

[9] A. D. KIUREGHIAN - *First and Second Order Reliability Methods.* Chapter 14, CRC Press, 2005.

[10] K. SCHITTKOWSKI - *A FORTRAN Subroutine for Solving Constrained Nonlinear Programming Problems.* Ann Operations Research, 5:485-500, 1985.

[11] B. AROUNA - *Robbins-Monro Algorithms and Variance Reduction in Finance.* The Journal of Computational Finance, 7(2), Winter 2003/2004., 7(2), Winter 2003/2004.

[12] P. GLASSERMAN - *Monte Carlo Methods in Financial Engineering.* Stochastic Modelling and Applied Probability, volume 53 of Applications of Mathematics (New York), Springer-Verlag, New York, 2004, 2004.

[13] J. LELONG - *Asymptotic Properties of Stochastic Algorithms and Pricing of Parisian Options.* PhD thesis, Ecole Nationale des Ponts et Chaussées, 2007.

[14] H. ROBBINS, S. MONRO - *A Stochastic Approximation Method.* Ann. Math. Statistics, 22:400-407, 1951.

[15] Y. ERMOLIEV - *Stochastic Quasigradient Methods and their Application to Systems Optimization.* Stochastics, 9:1-36, 1983.

[16] Y. ERMOLIEV, R. WETS - *Numerical Techniques for Stochastic Optimization*. Springer Verlag, 1988.

[17] J. DUPACOV - *Stochastic Programming: Approximation via Scenarios.* Proceedings of 3rd Caribbean Conference on Approximation and Optimization, Puebla, 1995.

[18] A. SHAPIRO - *Handbooks in OR & MS.* Vol. 10, chapter 6, Monte Carlo Sampling Methods, pp. 353-425. Elsevier Science B.V., 2003.

[19] M. DUFLO - *Random Iterative Models.* Springer-Verlag, 1997.

[20] E. ALBANO, W. RODDEN - *A Doublet Lattice Method for Calculating Lift Distributions on Surfaces in Subsonic Flows.* AIAA Journal, 7(2):279-285, Feb 1969. Errata vol 7, no. 11, Nov. 1969.

[21] R. L. FOX, M. P. KAPPOR - *Rates of Change of Eigenvalues and Eigenvectors.* AIAA Journal, 6(12):2427-2429, 1968.

[22] C. S. RUDISILL, K. BHATIA - *Optimization of Complex Structures to Safety Flutter Requirements.* AIAA Journal, 9(8):1487-1491, 1971.

[23] S. H. TIFFANY, M. KARPEL - *Aeroservoelastic Modeling and Applications Using Minimum-State Approximations of the Unsteady Aerodynamics.* Technical Report TM-101574, NASA, 1989.

[24] H. ZINGEL - *Measurement of Steady and Unsteady Airloads on a Stiffness Scaled Model of Modern Transport Aircraft Wing.* Proc. Int. Forum on Aeroelastcity Structural Dynamics, volume DGLR 91-06, pp. 120-131, 1991.

[25] K. MIETTINEN - *Nonlinear Multiobjective Optimization, Volume 12 of International Series in Operations Research & Management Science.* Springer US, 1998.

[26] A. BAGIROV, N. KARMITSA, M. M. MKEL - *Introduction to Nonsmooth Optimization: Theory, Practice and Software.* Springer, 2014.

[27] F. H. CLARKE - *Optimization and Nonsmooth Analysis.* Wiley, 1983.

[28] K. C. KIWIEL - *Methods of Descent for Nondifferentiable Optimization.* Number 1133 in Lecture Notes in Mathematics. Berlin edition, 1985.

[29] O. WILPPU, N. KARMITSA, M. M. MKEL - *New Multiple Subgradient Descent Bundle Method for Nonsmooth Multiobjective Optimization.* Technical Report, Turku Centre for Computer Science, 2014.

[30] M. M. MÄKELÄ, N. KARMITSA, O. WILPPU - *Mathematical Modeling and Optimization of Complex Structures.* Chapter Proximal Bundle Method for Nonsmooth and Nonconvex Multiobjective Optimization, pp. 191-204. Springer, 2016.

[31] A. BAGIROV, L. JIN, N. KARMITSA, A. AL NUIMAT, N. SULTANOVA - *Subgradient Method for Nonconvex Nonsmooth Optimization.* Journal of Optimization Theory and Applications, 157:416-435, 2013.

[32] J. V. BURKE, A. S. LEWIS, M. L. OVERTON - *Approximating Subdifferentials by Random Sampling of Gradients.* Mathematics of Operation Research, 27:567-584, 2002.

[33] J. V. BURKE, A. S. LEWIS, M. L. OVERTON - *A Robust Gradient Sampling Algorithm for Nonsmooth, Nonconvex Optimization.* SIAM J. Optim., 15:751-779, 2005.

[34] H. BONNEL, J. COLLONGE - *Stochastic Optimization Over a Pareto Set Associated with a Stochastic Multi-Objective Optimization Problem.* J. Optim. Theory Appl., 162:405-427, 2014.

[35] J. FLIEGE, H. XU - *Stochastic Multiobjective Optimization: Sample Average Approximation and Applications.* Journal of Optimization Theory and Applications, 151:135-162, 2011.

[36] F. POIRION, Q. MERCIER, J. A. DÉSIDÉRI - *Descent Algorithm for Nonsmooth Stochastic Multiobjective Optimization.* Computational Optimization and Applications, pp. 10.1007/s10589-017-9921-x, 2017.

[37] L. J. GIBSON, M. F. ASHBY - *Cellular Solids. Structure and Properties.* Cambridge University Press, 1997.

[38] J. A. DÉSIDÉRI - *Multiple-Gradient Descent Algorithm (MGDA) for Multiobjective Optimization.* CRAS Paris, Ser. I, 350:313-318, 2012.

AUTHORS

Fabrice Poirion has a PhD in Mathematics from the Pierre et Marie Curie University (Paris 6), and obtained the *Habilitation à Diriger des Recherches* (HDR) at the same University in 1999. He currently works in stochastic structural dynamics, and aeroelasticity, and manages an internal project on probability and statistics, at ONERA.

Quentin Mercier is a PhD student at ONERA and an ENS Cachan graduate.

F. Huvelin, S. Dequand, A. Lepage, C. Liauzun
(ONERA)

E-mail: fabien.huvelin@onera.fr

DOI: 10.12762/2018.AL14-06

On the Validation and Use of High-Fidelity Numerical Simulations for Gust Response Analysis

Specific gust response is considered as one of the most important loads encountered by an aircraft. The Certification Specification (CS) 25, defined by the European Aviation Safety Agency (EASA), and the Federal Aviation Regulations (FAR) 25, defined by the Federal Aviation Administration (FAA), describe the critical gusts that an aircraft must withstand. They must be analyzed for a large range of flight points (Altitude and Equivalent Air speed) and mass configurations. For some load cases, the standard tools could not be accurate enough to correctly predict the gust response and the use of high-fidelity computation could be required. Therefore, ONERA has implemented in its in-house Computational Fluid Dynamics (CFD) code *elsA* (ONERA-Airbus-Safran property) the capability to compute the high-fidelity aeroelastic gust response, directly in the time-domain, for different discrete gust shapes.

This paper presents some recent work achieved at ONERA concerning high-fidelity simulations for gust response. First, a physical validation of the gust response simulation is performed by comparing the results to those obtained experimentally on a scaled model. Second, numerical comparisons are performed using various techniques, in order to model the gust. Finally, an application for generic regional aircraft is shown.

Introduction

An important prerequisite for the certification of an aircraft design is to investigate the effects produced by atmospheric disturbances. In particular, the aircraft has to be designed to withstand loads resulting from gusts. One step to assess the aircraft gust response is to apply the criteria defined for certification [11], [12], [13]. One of these criteria, called "discrete gust design", considers that the airplane is subjected to symmetrical vertical and/or lateral gusts. Dynamic gust analyzes usually rely on linear techniques in the frequency domain, based on simple Doublet Lattice Methods (DLM) for the aerodynamic flow prediction [1]. These techniques are valid for subsonic flows, but could sometimes be not accurate enough to obtain realistic responses in the transonic regime, characterized by strong non-linearities, such as shocks and flow separation.

Consequently, a great effort has been made to use high-fidelity tools for gust response modelling. The most natural approach is then based on the implementation of gust models directly in the CFD code and on performing time-domain simulations [20]. However, due to the very high CPU time consumption of such an approach, alternative methods to pure unsteady CFD are necessary. A first idea consists in using CFD simulations to correct the DLM [34], [8] or to build reduced-order models (ROM) [31]. Some ROM allow the physical phenomena to be coupled by taking into account flow and flight dynamics [29], as well as structural mechanics [2], to obtain the gust response of an elastically trimmed aircraft. Another method consists in linearizing the unsteady Navier-Stokes equations with respect to the gust disturbance, which is assumed to be small. This leads to a faster resolution of the flow equations, but can provide less accurate results due to the linearization assumptions [3].

ONERA has implemented in the *elsA* software the capability to compute the high-fidelity aeroelastic response to gusts. In this paper, the so-called "Field Velocity Method" (FVM) and the corresponding linearized approach are first described. Secondly, the FVM is validated by comparison with experimental results on a scaled model. Thirdly, numerical benchmarks are performed, in order to validate both approaches. Finally, an application example for gust load alleviation is presented.

Gust Response Modeling

The certification of a new aircraft model requires the evaluation of its response to wind gusts. The FAA (with the FAR25) and the EASA (with the CS25) have defined both discrete and continuous gust velocity profiles, which are used for the certification of the aircraft [11], [12], [13]. Both vertical and lateral gusts need to be investigated. In the present study, only discrete gusts are considered. The "one-minus cosine" gust shape is defined by:

$$\begin{cases} U &= \dfrac{U_{ds}}{2}\left(1-\cos\left(\dfrac{\pi s}{H}\right)\right) \\ U_{ds} &= U_{ref} F_g \left(\dfrac{H}{350}\right)^{\frac{1}{6}} \end{cases} \quad (1)$$

where:

- H is the gust gradient (feet), defined as the distance parallel to the flight path of the airplane for the gust to reach its peak velocity, and has to be within the 30 feet to 350 feet range;
- s is the distance penetrated into the gust (feet) with the condition: $0 \leq s \leq 2H$;
- U_{ds} is the design gust velocity in equivalent airspeed;
- U_{ref} is the reference gust velocity in equivalent airspeed (feet/s);
- F_g is the flight profile alleviation factor.

The specification prescribes a reference gust velocity of 56 feet/s equivalent airspeed at sea level. The required reference gust velocity is reduced linearly to 44 feet/s equivalent airspeed at 15,000 feet. It can be further reduced linearly from 44 feet/s down to 26 feet/s equivalent airspeed at 50,000 feet. The flight profile alleviation factor increases linearly from the sea level value up to a value $F_g = 1$ at the maximum operating altitude. At sea level, the flight profile alleviation factor is computed as:

$$\begin{cases} F_g &= \dfrac{1}{2}\left(F_{gz} + F_{gm}\right) \\ F_{gz} &= 1 - \dfrac{Maximum\ operating\ Altitude}{25000} \\ F_{gm} &= \sqrt{R_2 \tan\left(\dfrac{\pi R_1}{4}\right)} \\ F_{gm} &= \sqrt{\dfrac{MZFW}{MTOW}\tan\left(\dfrac{\pi}{4}\dfrac{MLW}{MTOW}\right)} \end{cases} \quad (2)$$

where:

- MZFW is the Maximum Zero-Fuel Weight;
- MTOW is the Maximum Take-off Weight;
- MLW is the Maximum Landing Weight.

High-Fidelity Modeling

The high-fidelity simulation tool developed at ONERA for aeroelastic applications is based on the *elsA* CFD solver for the flow computation [5], [15]. Over the last decade, a general framework has been developed in the optional "***Ael***" subsystem of *elsA*, giving access in a unified formulation to several types of aeroelastic simulations, while minimizing the impact on the flow solver. The available simulations cover nonlinear and linearized harmonic forced motion, steady aeroelasticity and dynamic coupling simulations in the time-domain with various structural modelling approaches. The motivation of these developments, detailed in [10], [17], [18], is to provide a numerical tool for the prediction of various aeroelastic phenomena, such as flutter or LCO and aerodynamic phenomena involving complex nonlinear flows, such as shocks, vortex flow, and flow separation. An overview of the coupled simulation system is shown in Figure 1.

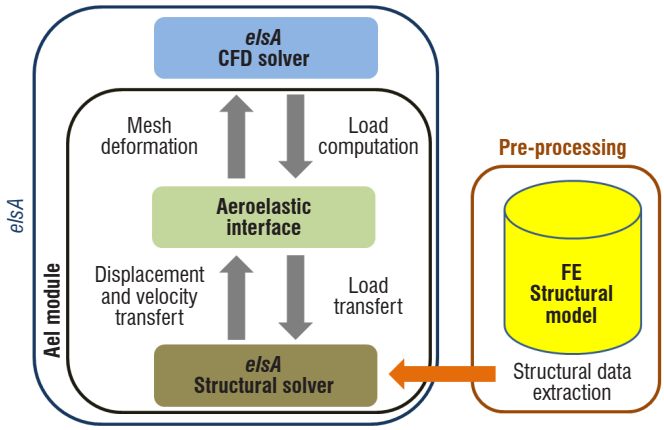

Figure 1 – Aeroelastic optional subsystem of *elsA* for aeroelastic simulations

Field Velocity Method

There are several possibilities to implement a gust response capability in CFD codes. One way consists in introducing the gust velocity into the far field boundary conditions of the computational domain. This approach would allow not only the effect of the gust on the aircraft to be taken into account, but also the reverse effect of the aircraft on the gust [21]. However, the main drawback of such an approach is that the gust must in this case be propagated from the boundaries of the computational domain to the aircraft location, without being damped by the numerical dissipation of the discretization schemes. This would require high-order schemes and also the use of fine grids in a large part of the computational domain. An alternative to this approach is to use the so-called "Field Velocity Approach" suggested by Sitaraman *et al.* [33]. This approach takes advantage of the Arbitrary Lagrangian Euler (ALE) formulation [9], which introduces a grid velocity in the Navier-Stokes equations to take into account in a consistent way the mesh deformation in the numerical simulation.

- Mass equation

$$\left.\frac{\partial}{\partial t}\right|_{\chi} \int_{V_t} \rho dV + \int_{S_t} \rho \boldsymbol{c}\cdot\boldsymbol{n} dS = 0 \quad (3)$$

- Momentum equation

$$\left.\frac{\partial}{\partial t}\right|_{\chi} \int_{V_t} \rho \boldsymbol{v} dV + \int_{S_t} \rho \boldsymbol{v}\boldsymbol{c}\cdot\boldsymbol{n} dS \int_{V_t} \left(\nabla\cdot\boldsymbol{\sigma} + \rho\boldsymbol{b}\right) dV \quad (4)$$

- Energy equation

$$\left.\frac{\partial}{\partial t}\right|_{\chi}\int_{V_t}\rho E dV+\int_{S_t}\rho E\boldsymbol{c}\cdot\boldsymbol{n}dS=\int_{V_t}\left(\nabla\cdot\left(\boldsymbol{\sigma}\cdot\boldsymbol{v}\right)+\boldsymbol{v}\cdot\rho\boldsymbol{b}\right)dV \qquad (5)$$

where t is the time, χ is the reference coordinate, V_t is an arbitrary volume with a surface boundary S_t, ρ is the density, $\boldsymbol{c}$ is the convective velocity, $\boldsymbol{n}$ is the normal to the boundary surface, $\rho\boldsymbol{v}$ is the momentum, ρE is the specific total energy, $\boldsymbol{\sigma}$ is the Cauchy tensor, $\boldsymbol{v}$ is the material velocity and $\boldsymbol{b}$ is the specific body force vector. The convective velocity is expressed by the material velocity and the grid velocity ($\boldsymbol{v}_{grid}$) as follows:

$$\mathrm{c}=\boldsymbol{v}-\boldsymbol{v}_{grid} \qquad (6)$$

The standard Eulerian formulation corresponds to a grid velocity equal to 0 ($\boldsymbol{v}_{grid}=0$), while the Lagrangian formulation corresponds to a convective velocity equal to 0 ($\boldsymbol{v}=\boldsymbol{v}_{grid}$). Due to the volume change in time, an extra conservation law has to be satisfied, the "geometric conservation law" (GCL), in order to maintain a conservative numerical scheme and to avoid additional numerical dissipation.

$$GCL:\ \left.\frac{\partial}{\partial t}\right|_{\chi}\int_{V_t}dV+\int_{S_t}\boldsymbol{v}_{grid}\cdot\boldsymbol{n}dS=0 \qquad (7)$$

According to the "Field Velocity Method", a prescribed gust velocity field, depending on both space and time, is added to the grid deformation velocity in each cell of the aerodynamic grid. All equations have to be corrected with this updated grid velocity.

$$\boldsymbol{v}_{grid}\left(\chi,t\right)\rightarrow\boldsymbol{v}_{grid}\left(\chi,t\right)+\boldsymbol{v}_{gust}\left(\chi,t\right) \qquad (8)$$

The field velocity approach has been implemented in the ONERA tool *elsA-Ael* [7], [22], [26] with three discrete gust models:

- the "sharp-edged gust";
- the "one-minus cosine" profile, often used for certification;
- the "sine" profile, which could be used for the simulation of the harmonic gust response.

Linearized Gust Response in the Frequency Domain

The high-fidelity nonlinear CFD method to compute the gust response consists in solving the URANS equations for rather long physical time durations. An alternative to this computationally expensive method is based on the linearization of the Navier-Stokes equations in the frequency domain with the fluid excited by a harmonic gust velocity. The latter derives from the linearized formulation to compute the response to a wall harmonic motion first written for turbomachinery [19] and then adapted to aircraft for load [27], [28], [30] and flutter prediction [25].

The approach implemented in the ONERA software *elsA* (LUR module, which stands for Linearized URans module) performs the linearization after having applied the space-discretization scheme. The semi-discrete URANS equations are then written using the ALE formulation to take into account the wall motion.

$$\begin{cases}\dfrac{d}{dt}\displaystyle\int_{\Omega(t)}\boldsymbol{W}d\Omega\int &= -\displaystyle\int_{S_t}\left(\begin{pmatrix}f(\boldsymbol{W})\\g(\boldsymbol{W})\\h(\boldsymbol{W})\end{pmatrix}-\boldsymbol{W}\boldsymbol{v}_{grid}\right)\cdot\boldsymbol{n}dS\\ &\quad+\displaystyle\int_{\Omega(t)}\boldsymbol{T}(\boldsymbol{W})d\Omega\\ \dfrac{d}{dt}\displaystyle\int_{\Omega(t)}d\Omega &= \displaystyle\int_{S_t}\boldsymbol{v}_{grid}\cdot\boldsymbol{n}dS\end{cases} \qquad (9)$$

where $\boldsymbol{W}$ represents the flow conservative variables (ρ, $\boldsymbol{v}$, E), Ω is the volume of the cell, $\boldsymbol{f}$, $\boldsymbol{g}$ and $\boldsymbol{h}$ are the convective and diffusive fluxes in the three space directions, $\boldsymbol{n}$ is the vector normal to the wall, $\boldsymbol{T}$ is the source term (null for the case of gust response), and $\boldsymbol{v}_{grid}$ is the grid deformation velocity vector. In the case of gust response simulation, no wall motion is considered. However, according to the Sitaraman approach [33], the gust velocity is introduced into the grid deformation velocity vector:

$$\boldsymbol{v}_{grid}\rightarrow\boldsymbol{v}_{grid}+\boldsymbol{V}_{gust}$$

The fluid variables are thereafter written as the sum of a steady or time constant part denoted by the subscript s and a perturbation part that is assumed to be harmonic of small complex amplitude:

$$\begin{cases}\boldsymbol{W} &= \boldsymbol{W}_s &+ &\boldsymbol{\delta W}e^{i\omega t}\\ \boldsymbol{f} &= \boldsymbol{f}_s &+ &\boldsymbol{\delta f}e^{i\omega t}\\ \boldsymbol{g} &= \boldsymbol{g}_s &+ &\boldsymbol{\delta g}e^{i\omega t}\\ \boldsymbol{h} &= \boldsymbol{h}_s &+ &\boldsymbol{\delta h}e^{i\omega t}\\ \boldsymbol{V}_{gust} &= & &e^{-i\boldsymbol{k}(\boldsymbol{X}-\boldsymbol{X}_0)}e^{i\omega t}\end{cases} \qquad (10)$$

where $\boldsymbol{k}$ is the wave number vector $\boldsymbol{k}=\dfrac{2\pi}{\lambda}\boldsymbol{u}_{Gust}$, $\boldsymbol{u}_{Gust}$ is the gust propagation unit vector, $\boldsymbol{X}$ represents the space coordinates of a point, $\lambda=\dfrac{2\pi U_\infty}{\omega}$ is the wavelength, U_∞ is the aircraft flight speed and ω is the gust angular frequency. Linearizing (10) using (11) yields the complex linear system in $\delta\boldsymbol{W}$:

$$\begin{cases}i\omega\Omega_s\delta\boldsymbol{W} &+ \displaystyle\sum_l\frac{1}{2}\begin{pmatrix}\delta f+\delta f_l\\ \delta g+\delta g_l\\ \delta h+\delta h_l\end{pmatrix}\cdot\boldsymbol{n}\\ &+ \displaystyle\sum_l\boldsymbol{V}_{gust}\cdot\boldsymbol{n}_{sl}\frac{1}{2}\left(\boldsymbol{W}_s+\boldsymbol{W}_{sl}\right) &= 0\end{cases} \qquad (11)$$

The metrics (volumes and normal vectors) remain indeed constant for the case of a gust response and the fluxes perturbations $\delta\boldsymbol{f}$, $\delta\boldsymbol{g}$, $\delta\boldsymbol{h}$ are linear in $\delta\boldsymbol{W}$. The linear system is solved using a pseudo time approach based on a backward Euler algorithm with an LU-SSOR implicit stage. All acceleration techniques usually used to obtain a steady CFD RANS solution as multi-grid or local time steps can be used.

Experimental Validation

Experimental Set-Up

In order to generate an experimental database for the validation of high-fidelity numerical codes, a test campaign was performed in the ONERA S3Ch facility (Figure 2). This closed return wind tunnel (WT) is a transonic continuous run facility with a 0.8 m x 0.8 m square test section operating at atmospheric stagnation pressure and stagnation temperature, and is equipped with deformable adaptive walls (top and bottom walls).

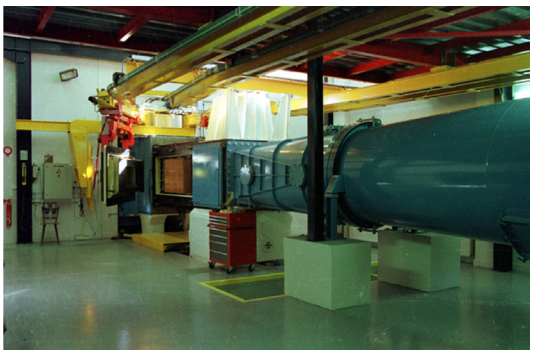

Figure 2 – The ONERA S3Ch transonic Wind Tunnel

The experimental set-up is composed of a gust generator and an aeroelastic model (Figure 3 and Figure 4). The purpose of the gust generator is to have an experimental tool able to generate relevant perturbations (gust load) for wind tunnel conditions, from the subsonic to the transonic range. The concept of the gust generator consists of two identical oscillating airfoils installed upstream of the wind tunnel test section and producing air flow deflections to generate a cylindrical gust field downstream. Its functioning is based on synchronous dynamic motions of the 2 airfoils (pitch motions) performed by 4 servo-hydraulic jacks with a frequency bandwidth of 100 Hz.

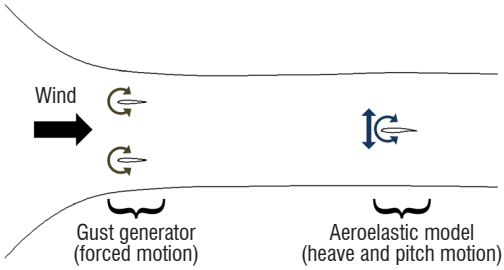

Figure 3 – Sketch of the experimental set-up

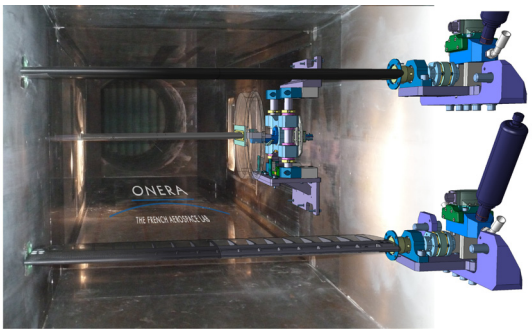

Figure 4 – "Inside Artist view" of the experimental set-up in the S3Ch facility: the gust generator (foreground) and the aeroelastic model (background)

The aeroelastic model is aimed at representing the behavior of a classical aeroelastic model with 2 degrees of freedom (dof), *i.e.*, a 2D model with heave and pitch motions. The aerodynamic part is based on the OAT15A airfoil (ONERA supercritical airfoil [32]) with a 0.25 m chord length. In order to preserve the 2D characteristic of the flow, the airfoil is designed as rigid as possible and is composed of a steel spar and 2 upper and lower carbon reinforced skins. A specific manufacturing process was defined to avoid any geometrical variations and to respect the aerodynamic shape of the airfoil (no cover, no access). The pitch and heave dof are driven by a couple of stiffness (flexible beams) and mass parameters, in addition to an arrangement of bearings in order to better "constrain/prescribe" the "rigid body" motions of the wing. In the WT test section, the mounting system is composed of 2 identical mounting parts located on each test section door. The model is equipped with a full span trailing edge control surface driven on either side by a high torque – high speed actuator allowing dynamic deflections up to 100 Hz. The instrumentation of the model is made of steady and unsteady pressure transducers, accelerometers and strain gages.

The experimental roadmap was split into several phases to correctly investigate gust load in a WT environment [24]. A first WT test campaign has been carried out to qualify the unsteady flow induced by the gust generator and its ability to generate a cylindrical gust field with significant and reproducible amplitudes in subsonic and transonic ranges [4]. Then, a second WT tests was devoted to the analysis of the gust effects on the test model behavior, *i.e.*, the aerodynamic and aeroelastic responses to an impacting gust. The final WT test objective was the demonstration in real time of gust load alleviation through the active control of the model aeroelastic response for a gust disturbance [23].

The achieved WT tests have provided a comprehensive and consistent database for the validation process of gust simulation capacities with the CFD/CSM HiFi tools.

Physical validation

The numerical simulation allows the Field Velocity Method implemented in the non-linear equation solver to be validated.

The OAT15A airfoil was modeled with far-field conditions and conditions of adherent wall on the airfoil. A C-mesh was built around the airfoil.

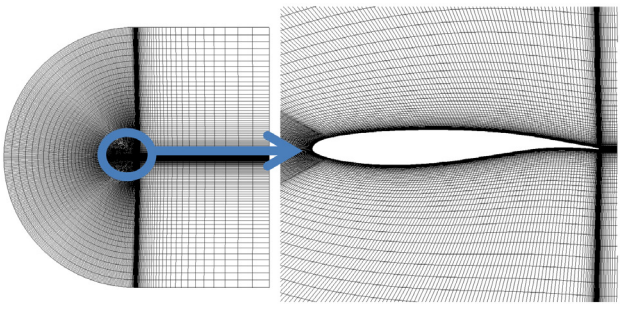

Figure 5 – Far-field mesh: overview and, OAT15 airfoil

Tests were performed at Mach number 0.73 with an angle of attack (AoA) of 2°. Numerical simulations were carried out by solving the non-linear Unsteady Reynolds-Averaged Navier-Stokes (URANS)

equations. Two kinds of gust response simulations were performed. For the first one, the physical validation was performed with a rigid airfoil (fully clamped model), in order to validate the flow around the profile. The gust frequency was set to 20 Hz. For the second one, the airfoil was able to move according to its heave and pitch degrees of freedom, thus allowing the assessment of its aeroelastic response and its comparison with experimental results. The gust frequency was set to 25 Hz (frequency of the heave mode). For both simulations, a steady state was first computed. The aerodynamic parameters were adjusted to fit the steady experimental results.

The numerical and experimental unsteady pressure distributions were compared using 38 unsteady pressure transducers located along the center line in the spanwise direction. The same Fourier analysis was applied to both the numerical and the experimental results, in order to avoid any additional or compensation errors.

For the rigid response, a good agreement between the numerical and experimental data can be observed for the magnitude of the pressure (Figure 6). The extrema are indeed correctly predicted. With regard to the phase, a good agreement is also noticed on the upper surface up to the shock. However, larger differences arise close to the trailing edge.

For the aeroelastic response, the aerodynamic flow around the airfoil is well predicted (Figure 7). The pressure magnitude peak is appropriately captured, thanks to the tuning of the FVM model. The latter model indeed avoids numerical dissipation and cannot take into account the physical dissipation of the flow perturbation generated by the gust generator. The numerical gust amplitude encountered by the airfoil must then be determined according to the flow velocity measurements provided by the probe located ahead of the leading edge. The unsteady pressure magnitude after the shock root and on the lower surface is less accurately predicted. A large difference appears in the phase around the trailing edge.

The numerical and experimental acceleration were compared using 4 accelerometers located along the chord.

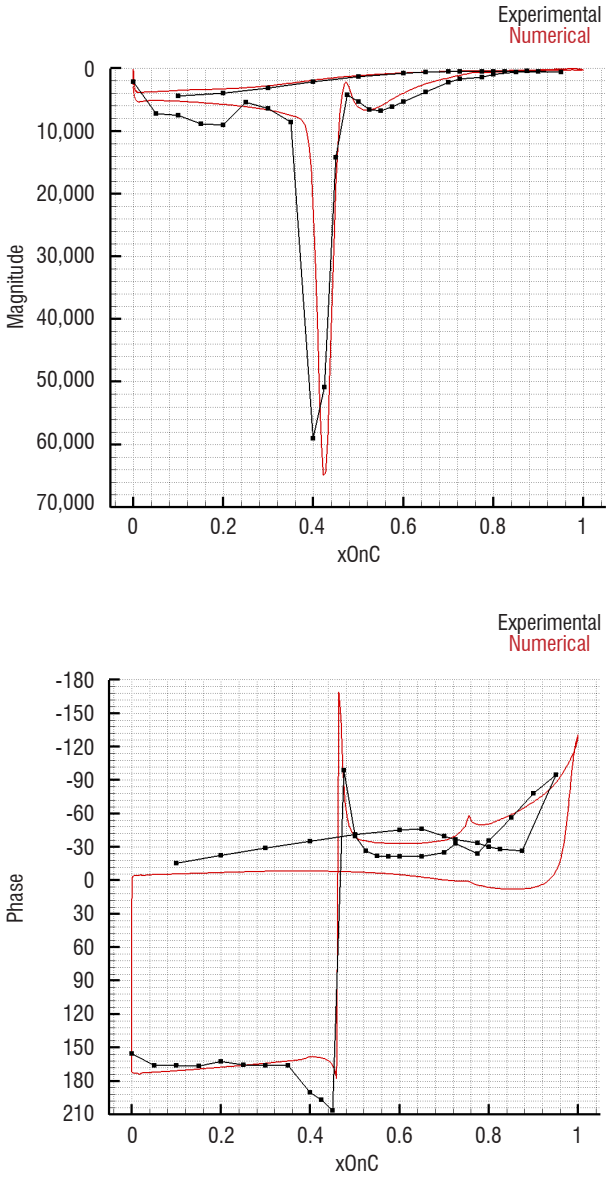

Figure 6 – Comparison between numerical and experimental unsteady pressure distributions – rigid airfoil

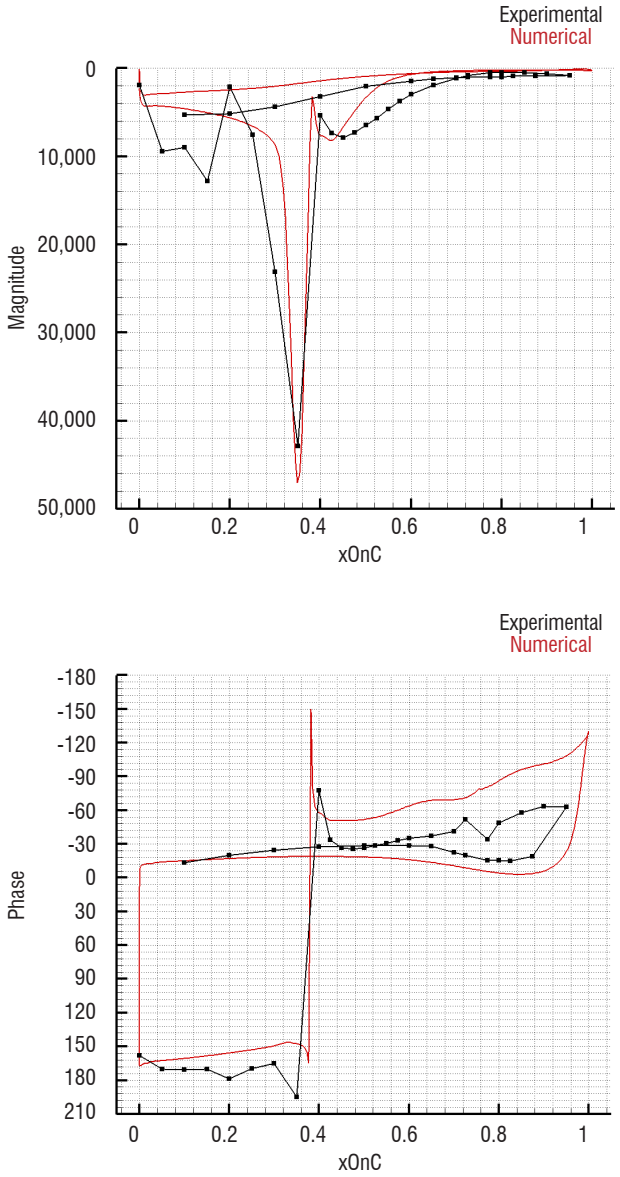

Figure 7 – Comparison between numerical and experimental unsteady pressure distributions – aeroelastic airfoil

The structural behavior is better predicted (Figure 8) than the pressure distribution. The magnitude of the acceleration is closer to the experimental result near the leading edge. A difference appears around the third probe due to the hinge of the control surface present in the mock-up. The hinge is not stiff and its flexibility is not taken into account in the computation. The phase is accurately predicted.

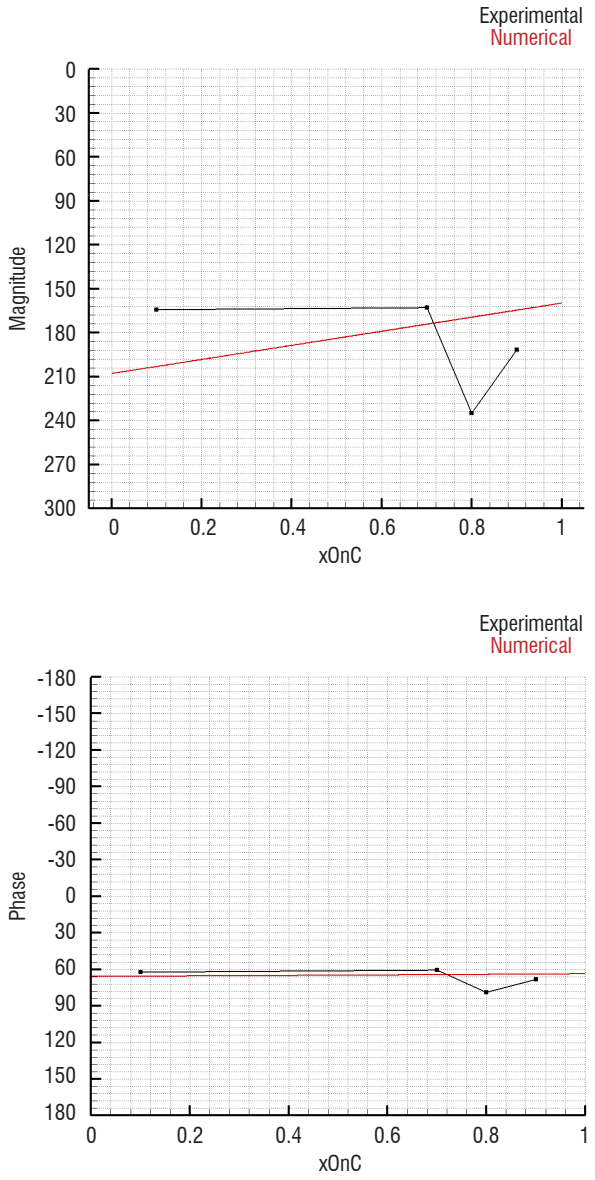

Figure 8 – Comparison of structural responses between numerical and experimental results – aeroelastic airfoil

Numerical validation

One-scale numerical benchmark for FVM

Dynamic gust analyzes usually rely on linear techniques in the frequency domain, based on simple Doublet Lattice Methods (DLM) for the aerodynamic flow prediction. These techniques are valid for subsonic flows, but could sometimes be not accurate enough to obtain realistic responses in the transonic regime, characterized by strong non-linearities such as shocks and flow separation. This method is compared to the high-fidelity approach using the Field Velocity Method on an industrial case. The Airbus XRF-1 transport aircraft configuration has been used for the benchmark. It is a generic research configuration representative of wide-body modern civil transport aircrafts.

The structured aerodynamic mesh was built around a cruise shape and includes about 7.47 million cells (Figure 9). The grid designed for URANS simulations, is thus rather coarse for a half-aircraft configuration. It is therefore not possible to accurately capture the viscous phenomena, especially around the nacelle, on which a wall slip condition was therefore applied. An adiabatic condition of adherent wall was applied everywhere else on the aircraft. All of the RANS and URANS simulations were performed using the Spalart-Allmaras turbulence modeling.

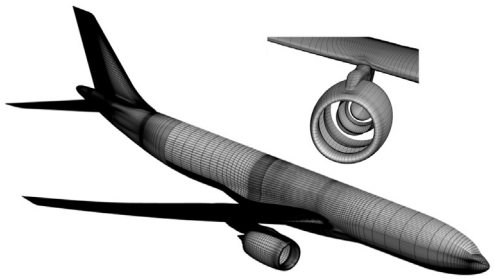

Figure 9 – Aerodynamic mesh

A simplified Nastran Finite-Element model of the whole aircraft was built, based on a detailed representation (solid, shell and bar elements) of the wings and the central part of the fuselage, and on condensed elements (super elements) for the front and rear parts of the fuselage and for the tail (Figure 10). For CFD and DLM aeroelastic simulations, a structural damping ratio equal to 2% of the critical damping was imposed.

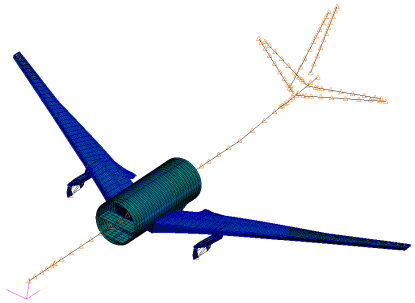

Figure 10 – Structural model

Case and benchmark description

The capability to predict the response to a gust has been assessed for typical cruise flight conditions (Mach = 0.86, Altitude = 35,000 ft, Mass = 230 tons and AoA = 2.3°). The applied discrete gust velocity corresponds to a "one-minus cosine" shape and the parameters of the gust were selected using the FAR25 rules. In particular, the gust gradient (H = 350 ft), and the design gust velocity (U_{ds} =9.82 m/s) were evaluated from the mass and altitude features of the aircraft. The gust induced angle of attack corresponds to $\Delta\alpha$ = 2.28° at the peak. A physical time duration of 4.0 s was simulated.

Several simulations were performed in order to study dynamic gust responses. Both rigid and flexible high-fidelity gust dynamic simulations were run with *elsA*, in order to quantify the effect of flexibility on the load distribution. A Nastran gust response simulation was also run using, as the high-fidelity approach, a restrained aircraft hypothesis. The objective of this computation is first to validate the high-fidelity approach, and also to investigate its benefits with respect to the linear aerodynamic Doublet Lattice Method approach used in Nastran.

Result comparison

Figure 11 shows the additional load factor (ΔN) for three computations, *i.e.*, CFD rigid (rigid load factor), CFD aeroelastic (aeroelastic load factor) and Nastran DLM (Nastran load factor), corresponding to the Maximum Take-Off Weight (MTOW) load case. The gust amplitude time history is also plotted.

elsA-Ael and Nastran simulations predict a similar maximum load factor, with a phase shift with respect to the gust input. After the first cycle, the two dynamic responses differ, with larger unsteady levels in the non-linear *elsA-Ael* simulation but a similar pseudo-frequency.

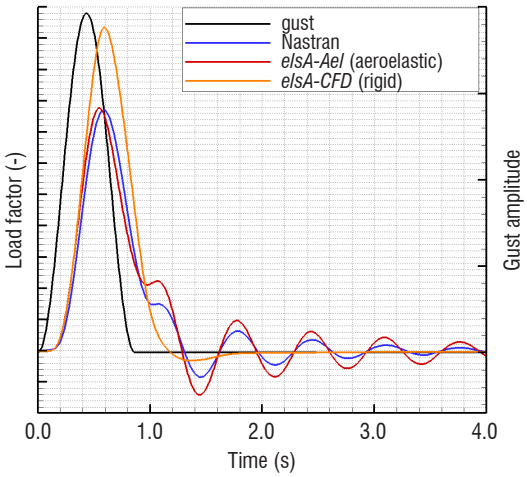

Figure 11 – Time evolution of additional gust load factor

The rigid computation predicts a higher maximum load factor with a greater delay than that of the aeroelastic simulations. The reason for this over-estimation is mainly due to the inertial forces, which are only taken into account in the aeroelastic simulations. Indeed, the inertia relief has a favorable effect on the load factor. To check this assumption, an aeroelastic Nastran computation for an OWE configuration has been achieved. OWE results lead to a higher maximum induced load factor than that of the rigid MTOW, showing the beneficial effect of inertia relief for the MTOW case. Figure 12 shows the maximum displacement and twist over time for the nonlinear *elsA-Ael* and Nastran MTOW computations.

The pseudo-frequencies predicted by both computations are roughly identical. Larger displacements are, however, observed in the case of the nonlinear aerodynamics of the *elsA-Ael* computation, leading to a difference of damping between the two computations.

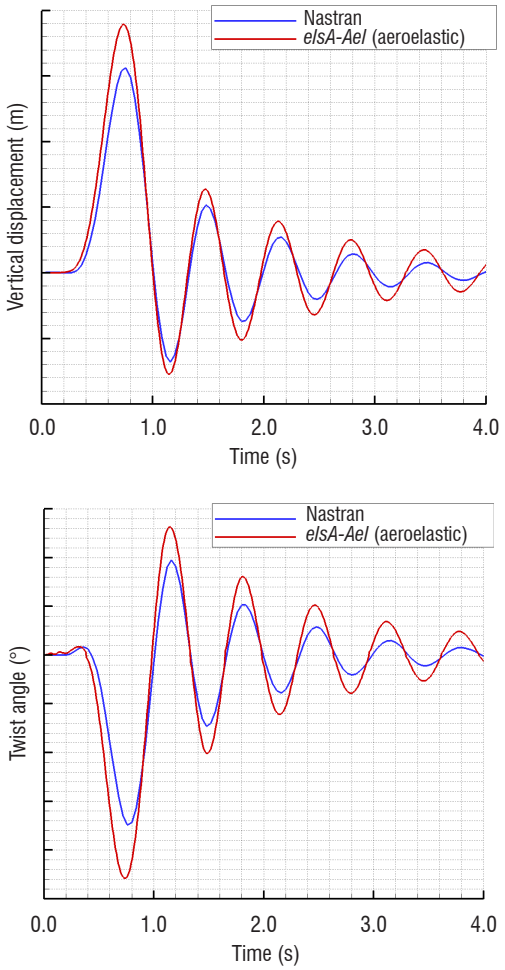

Figure 12 – Time-evolution of maximum vertical displacement (up) and twist (bottom)

The combined load diagram (Figure 13) shows that the maximum/minimum of the twisting moment corresponds to the maximum/minimum of the shear force for both rigid and aeroelastic computations. The rigid simulation exhibits a higher maximum shear force and twisting moment than the aeroelastic simulation. *elsA-Ael* and Nastran estimate a similar minimum and maximum transverse force, while the twisting moment is under-estimated by the Nastran calculation in comparison with *elsA-Ael*.

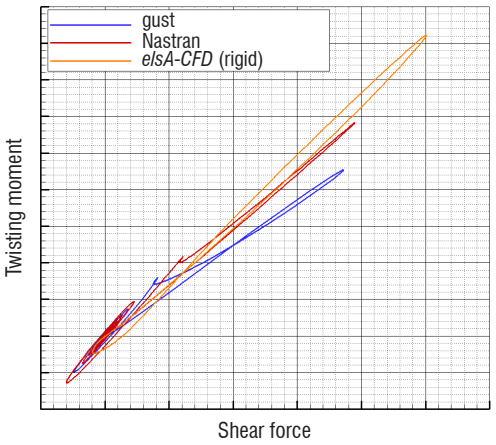

Figure 13 – Time-evolution of combined loads plot at the wing root for rigid, aeroelastic and NASTRAN computations

The gust has a large impact on the flow distribution around the wing (Figure 14). Before the gust encounter, the flow over the wing is rather two-dimensional. When the gust reaches the wing, a disturbance appears at the tip part and expands towards the wing root until a flow separation occurs. After the gust encounter, the flow returns to its initial state.

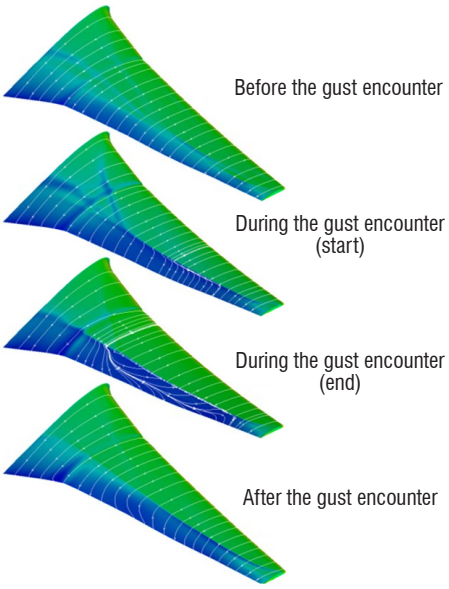

Figure 14 – Friction stream traces for the *elsA-Ael* simulation before, during and after the gust encounters the wing

Numerical 2D benchmark for the linearized approach

The linearized approach has been validated in an industrial context to compute gust loads in the subsonic regime [35]. This benchmarks is aimed at validating the approach for transonic flight conditions. Given that the Field velocity method has been validated by comparing experimental and numerical results, this method has been used as reference, in order to validate the linearized formulation.

This alternative method to compute the gust response has been assessed by comparisons with non-linear URANS simulations for two cases: the 2D airfoil NACA64A010 in a transonic viscous flow and a 3D wing in an inviscid flow.

Gust responses of the 2D symmetric airfoil have been computed for transonic conditions for which experiments have been carried out for both steady and harmonic pitching motion measurements [6].

$$\begin{cases} Mach &= 0.796 \\ P_i &= 203321\ Pa \\ T_i &= 310\ K \\ \alpha &= 0^o \end{cases}$$

As a first step, a steady simulation was performed using the Spalart-Allmaras turbulence model, and yielded a well-converging solution exhibiting, as expected, a strong shock (Figure 15).

Responses to harmonic gust excitations of a wavelength 25 times the chord matching a gust frequency of 21.17 Hz were computed using both the linearized and non-linear URANS solvers. The non-linear simulations were carried out for gust amplitudes $V_G = \frac{U_\infty}{60}$ matching an incidence variation of 0.955°, $V_G = \frac{U_\infty}{300}$ (0.191°) and $V_G = \frac{U_\infty}{1500}$ (0.0382°). They were run for physical time durations long enough to reach the harmonic regime, as can be seen in Figure 16.

Unlike the simulation with the lowest gust amplitude (25 times lower), the one with the largest amplitude exhibits a large shock motion inducing probably unsteady non-linear phenomena in the flow field

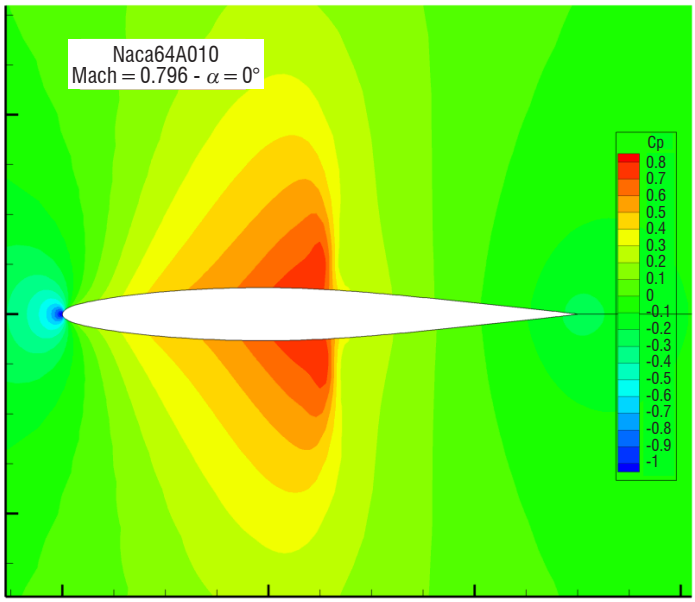

Figure 15 – Steady Cp distribution

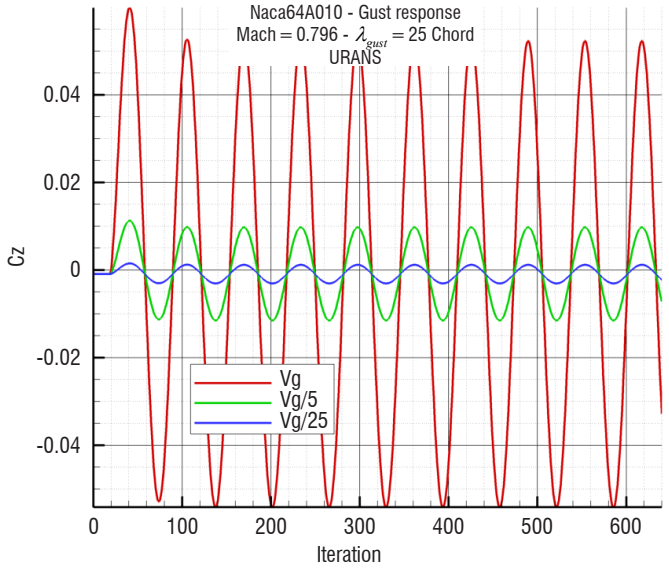

Figure 16 – Histories of Lift coefficient computed with the non-linear solver

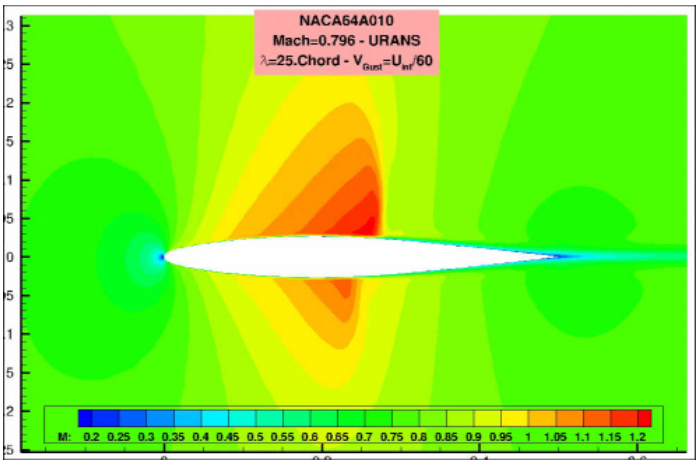

Video 1 – Mach distributions for a gust period (URANS simulation with the gust amplitude equal to U∞/60)

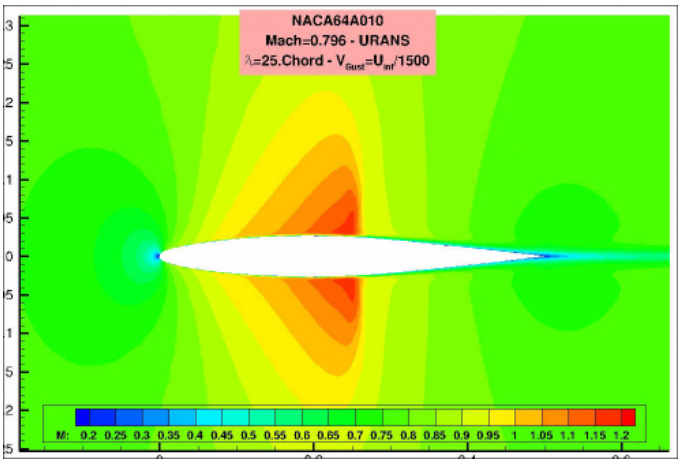

Video 2 – Mach distributions for a gust period (URANS simulation with the gust amplitude equal to U∞/1500)

(Video 1 and Video 2). Since the linearized solver actually provides the sensitivity of the unsteady pressure to the input excitation (here the gust amplitude), comparisons with the nonlinear solvers have been carried out on the first harmonic of the Fourier Series of the pressure coefficient time signal divided by the gust amplitude. Figure 17 shows these complex unsteady Cp distributions resulting from both linearized and URANS simulations. The distributions obtained with the non-linear solver indeed tends with decreasing gust amplitude to the distribution obtained using the linearized solver, which validates the linearized formulation for the 2D symmetric airfoils in transonic flows and confirms the nonlinear unsteady phenomena occurring with the largest gust amplitudes.

Numerical 3D benchmark for the linearized approach

This second test case is aimed at checking the validity of the linearized solver for 3D geometries in high subsonic inviscid flows. It concerns the M6 wing, for which a generic structural finite element model representing a standard spars/ribs/stiffener architecture has been built. This structural model has been used only to determine the steady state used to initialize unsteady simulations. This steady state results from a static fluid-structure coupling simulation carried out for the aerodynamic conditions defined below (Figure 18).

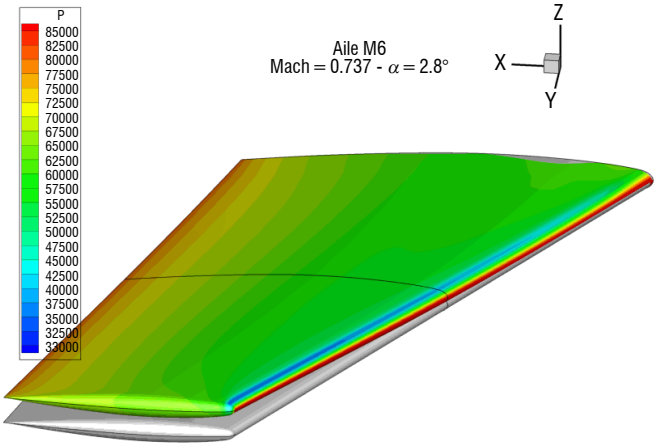

Figure 18 – Pressure distribution and wing deformations resulting from a static aeroelastic simulation

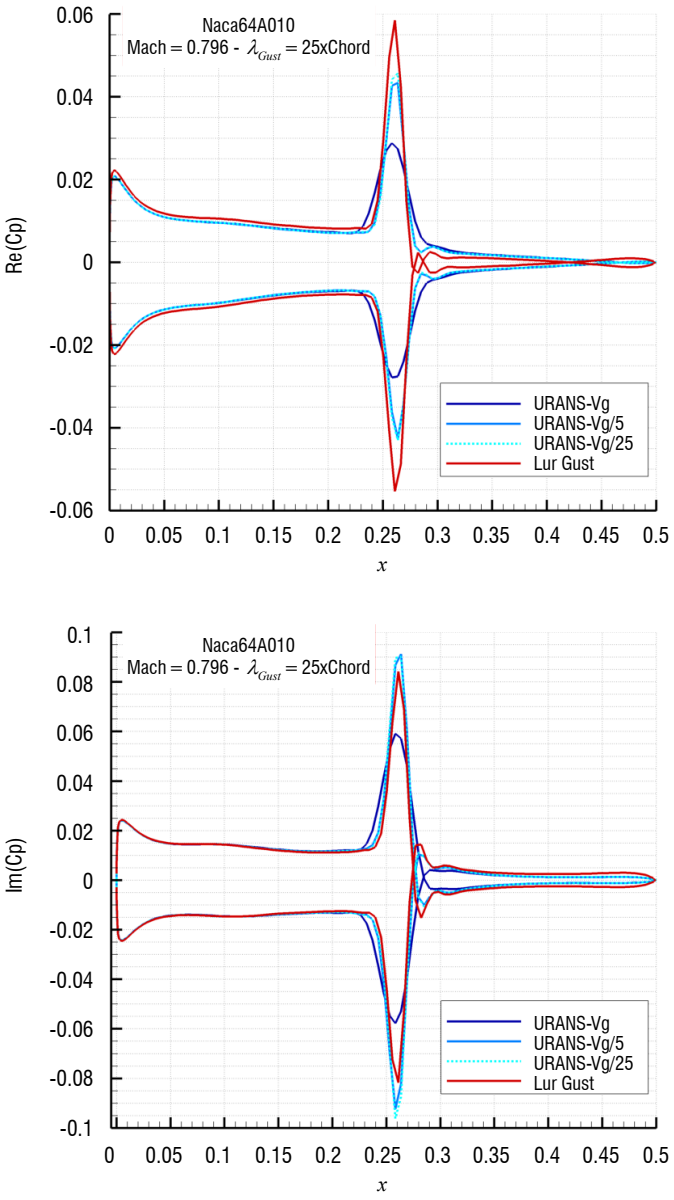

Figure 17 – Unsteady Cp distributions obtained with both the linearized solver (Lur) and the non-linear solver (URANS) (real part in the top figure, imaginary part in the bottom figure)

Unsteady simulations using both the non-linear and linearized solvers are performed to obtain the response to the harmonic gust defined in Table 1. Similar unsteady complex pressure (first harmonic) distributions were obtained, as can be seen in Figure 19 and Figure 20 showing the real and imaginary parts of Cp on the upper and lower surfaces. Figure 21 presents the Cp distributions on 2 span-wise sections obtained with the 2 solvers. The discrepancies, which are greater in the imaginary parts, can be explained by the amplitude of the applied gust in the non-linear simulation, which is an amplitude that is probably too high to remain in the domain of the linear unsteady perturbations.

$$\begin{cases} Mach = 0.734 \\ \alpha = 2.8° \\ P_i = 101325\,Pa \\ T_i = 300\,K \\ reference\,surface = 0.758\,m^2 \\ mean\,chord = 0.805\,m \end{cases}$$

$$\begin{cases} \text{gust wavelength} & \lambda = 25Chord \\ \text{gust frequency} & f = 12.02\,Hz \\ \text{gust amplitude} & V_g = \dfrac{U_\infty}{300} \\ \text{gust incidence variation} & \alpha_g = 0.191° \end{cases}$$

Table 1 – Flight conditions and gust characteristics applied to the M6 wing

As for the 2D case, there is a significant CPU time gain for the linearized simulations: one non-linear simulation requires about 30.000 s, whereas one linearized computation requires about 4.000 s. This CPU time gain is similar to that noticed by other authors [14] using similar numerical techniques, *i.e.*, the linear system is solved using a pseudo time method with a LUSSOR implicit formulation. Nevertheless, the numerical performances could be improved up to 2 orders of magnitude [3] when most recent resolution algorithms, such as a preconditioned flexible GMRES with deflated restarting [16], are used.

Application

Given that a gust is one of the most severe loads for an aircraft, an important issue is the gust load alleviation. The use of control laws is one way to reduce the load factor on an aircraft encountering a gust.

Control laws are built with dedicated tools using different levels of modeling for the fluid and the structure. Most often a design process uses low-fidelity aerodynamic models to synthetize control laws. However, it can be useful to check their behaviors with high-fidelity tools (efficiency, robustness and stability).

High-fidelity fluid-structure coupling simulations have thus been carried out in the case of a regional aircraft using the aileron to alleviate

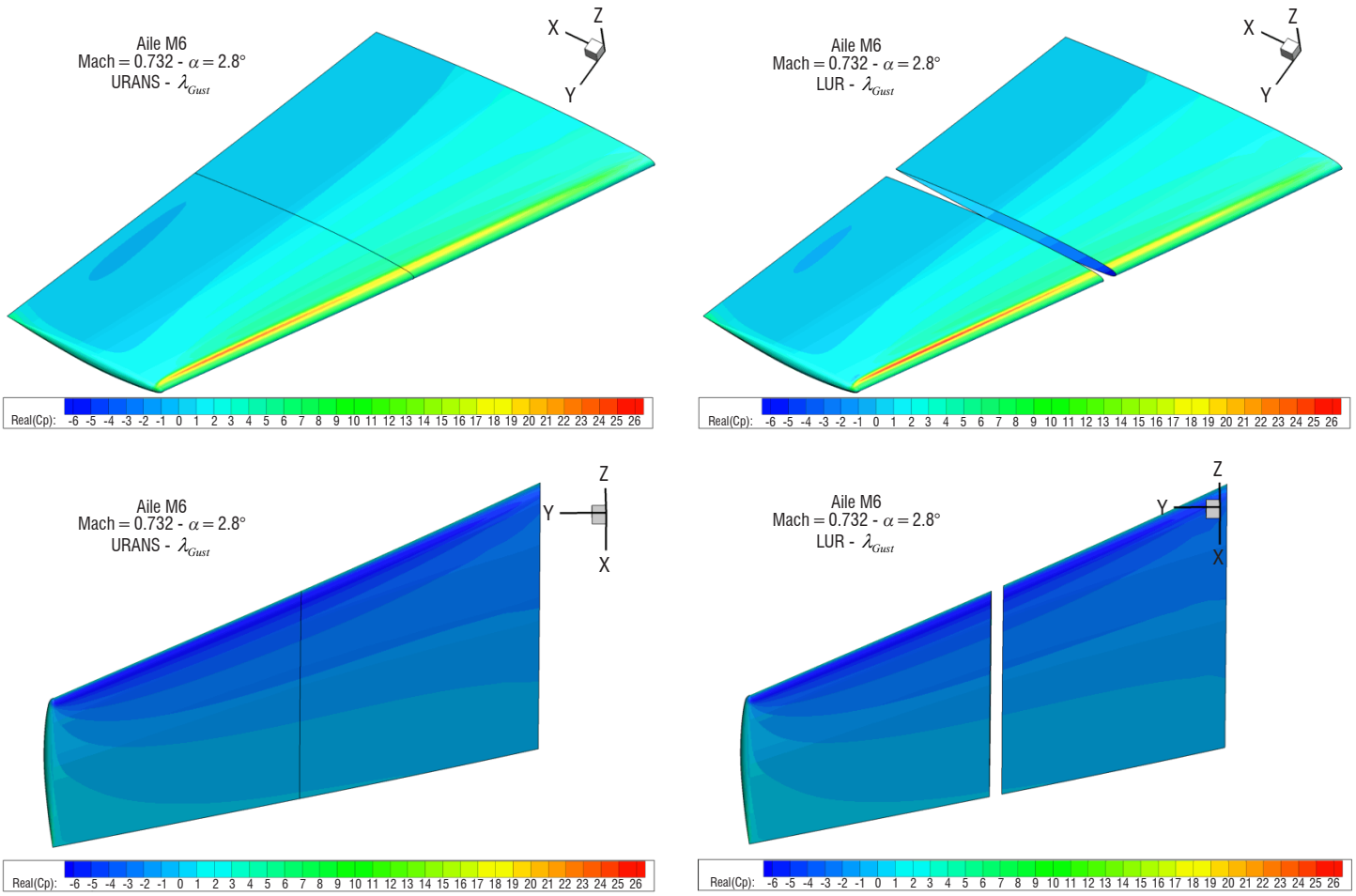

Figure 19 – M6 wing - Real part of unsteady Cp distributions resulting from a gust excitation (non-linear on the left, linearized on the right, upper surface at the top, lower surface at the bottom)

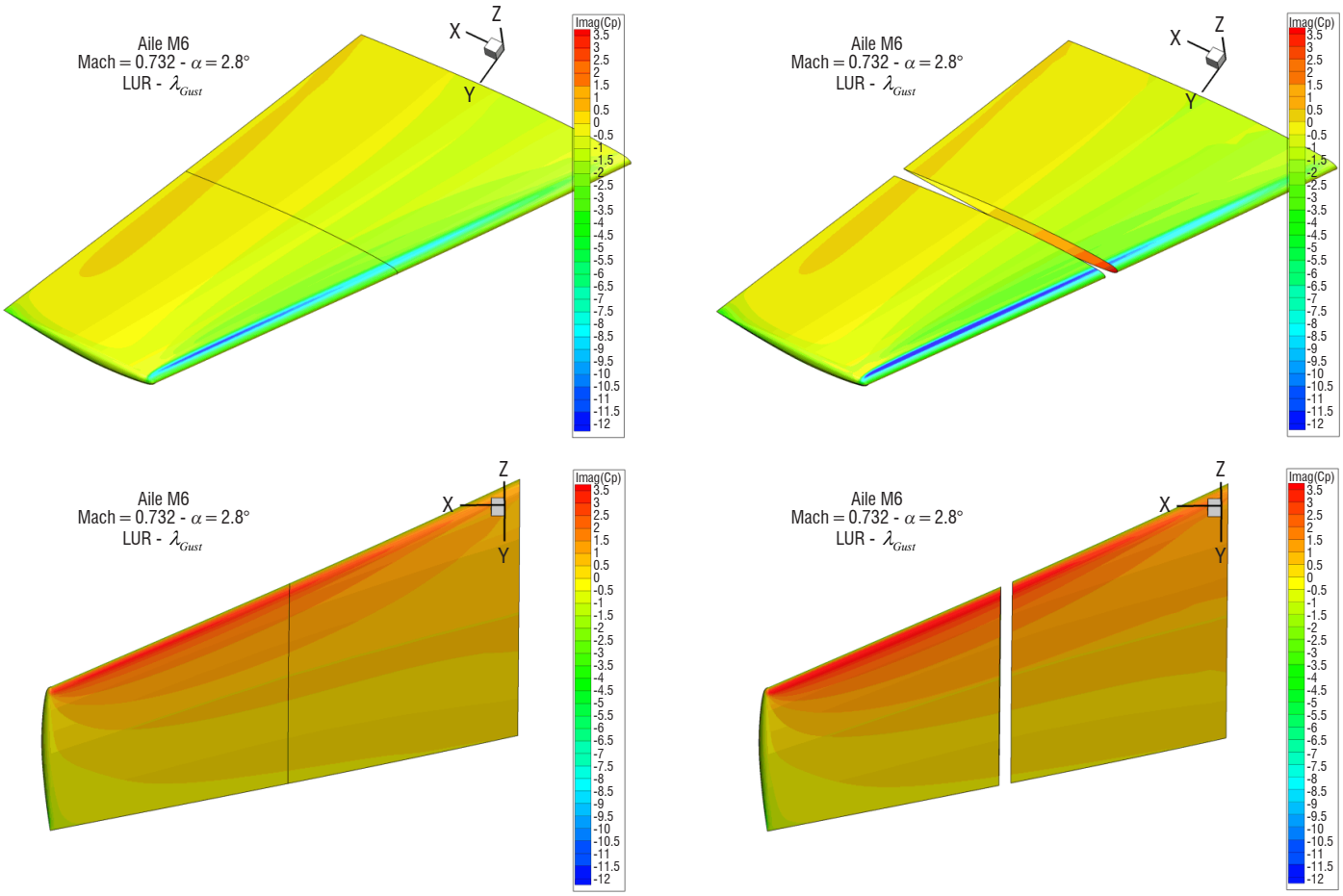

Figure 20 – M6 wing - Imaginary part of unsteady Cp distributions resulting from a gust excitation (non-linear on the left, linearized on the right, upper surface at the top, lower surface at the bottom)

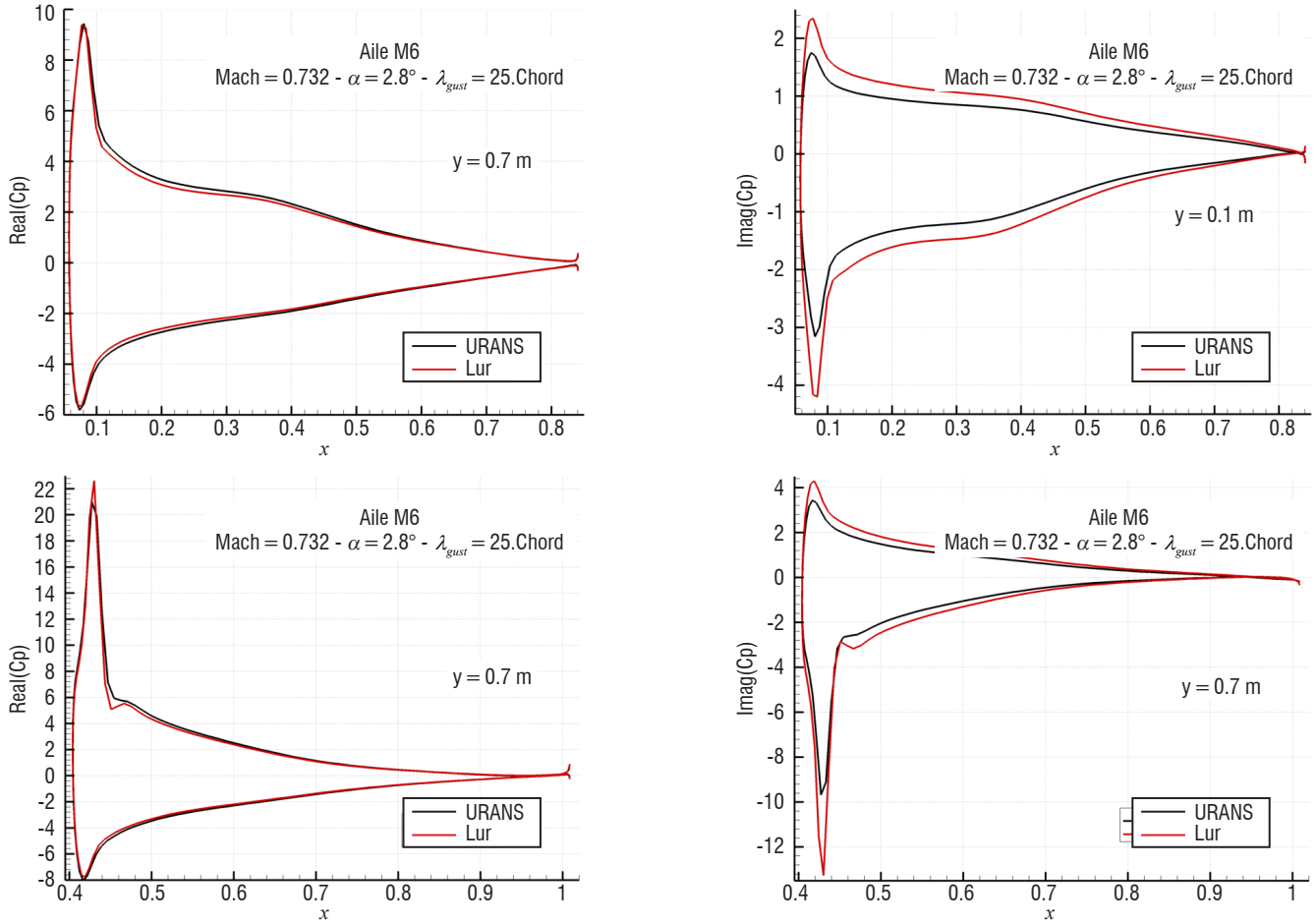

Figure 21 – Unsteady Cp distributions on 2 wing sections computed with the non-linear (URANS) and linearized (Lur) solvers

gust loads. The control surface has been modelled on the fluid interface, in order to obtain an interaction between the moving surface and the flow disturbance due to the gust (Figure 22).

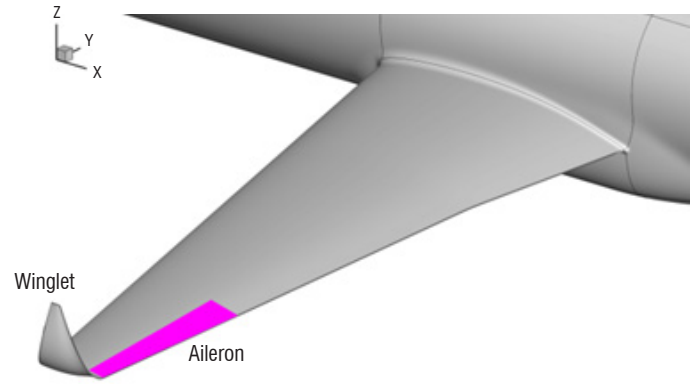

Figure 22 – Fluid interface with control surface

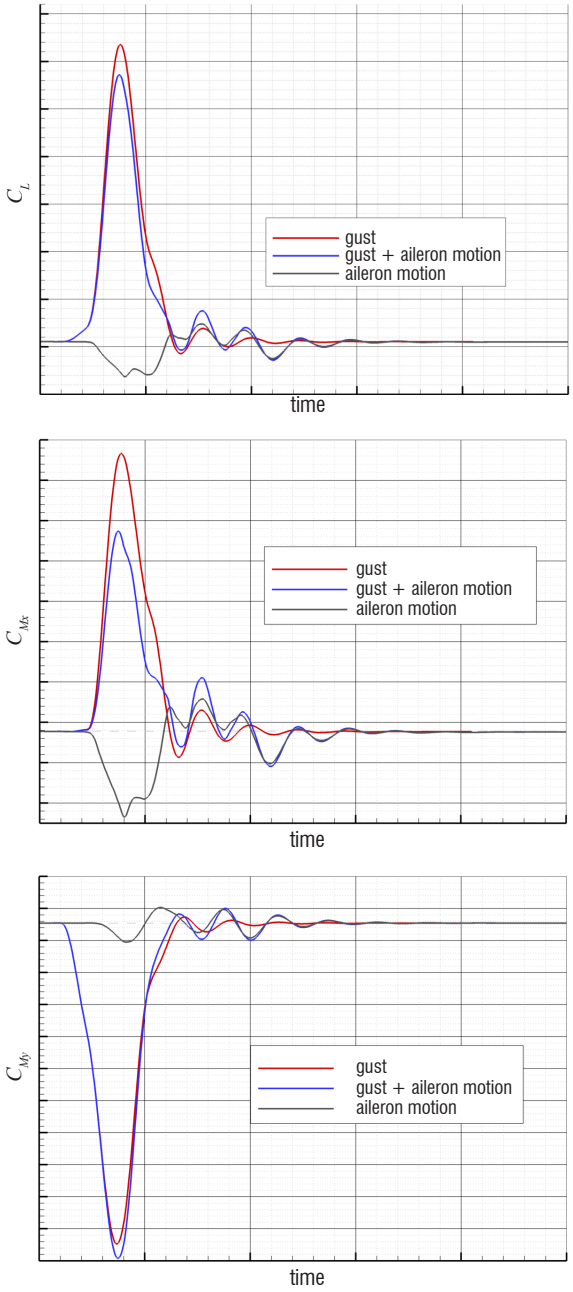

Figure 23 – Lift, rolling and pitching moment coefficient for tuned gust

A control law has been synthetized with low-fidelity tools to counteract a (1-cos) gust whose frequency is close to the first structural Eigen-frequency (first bending mode).

The gusts and corresponding control surface motions have been prescribed in a high-fidelity simulation modeling a fuselage and a wing.

Figure 23 shows the resulting time evolutions of the lift, rolling and pitching moment coefficients. An alleviation of the peak of 10.2 % due to the aileron deflection movement can then be noticed on lift, and 28 % on the rolling moment. However, a slight increase (-4.5 %) of the pitching moment is observed.

Figure 24 represents the time evolutions of the 1st (first bending mode) and 4th (first torsion mode) generalized coordinates.

The application of the aileron deflection law induces a great decrease of the main peak of the first generalized coordinate (55.8 %). The amplitude of the main peak then becomes of the same order as the amplitude of the post gust oscillations, which are strongly damped as soon as the aileron stops its deflection motion. Like this generalized coordinate, the vertical displacement of the leading edge of a wing section close to the wingtip (between the aileron and the winglet root) is 58 % alleviated by the action of the aileron motion. Indeed, this maximal displacement is equal to 0.51 m with no aileron deflection, and equal to 0.22 m with aileron motion.

The torsion modal coordinate has a time behavior similar to the generalized coordinate of the imposed aileron motion. However, the peak amplitude is almost twice that resulting from the simulation, with only

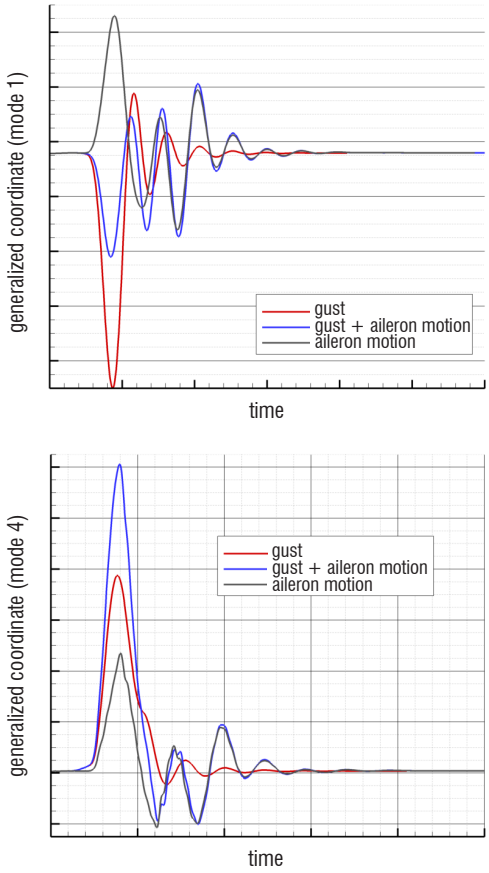

Figure 24 – Time evolutions of the 1st (1st bending) and 4th (1st torsion) modal coordinates (tuned gust)

the gust and without any aileron motion (-56.8 %). This 4th generalized coordinate seems to be highly sensitive to the aileron motion, and the first upward deflection of the aileron tends to amplify the peak due to the gust passage. Nevertheless, in order to obtain information from a more physical quantity about the wing deformation, the twist deformation time evolutions of the previously mentioned wing section have been extracted from the simulations. They are very different from the 4th generalized coordinates, as can be observed in Figure 25 (positive values meaning an increase in the apparent incidence of the section).

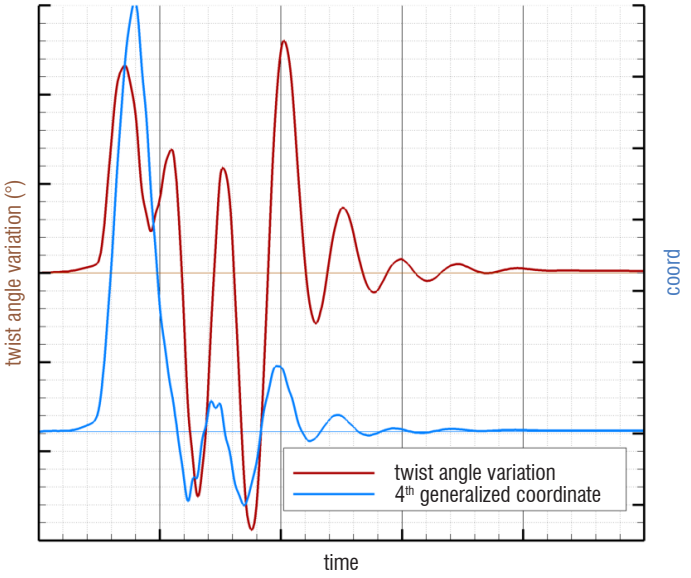

Figure 25 – Time evolutions of the twist angle variation for a wingtip section and of the 4th generalized coordinate in the case of a gust with aileron motion

This shows that the wing twist is highly influenced by modes other than the first torsion mode. Furthermore, a significant alleviation of this twist deformation due to the aileron motion is noticeable (Figure 26).

Post-gust oscillations are indeed in this case of greater amplitude than the first peak. Figure 27 shows the pressure distributions on the wing and its deformation at two different instants at which extreme

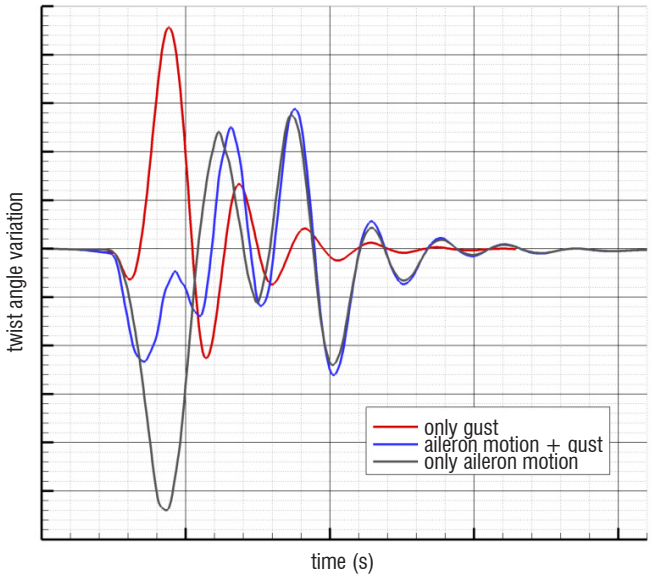

Figure 26 – Time evolutions of the twist angle variation for a section close to the wingtip

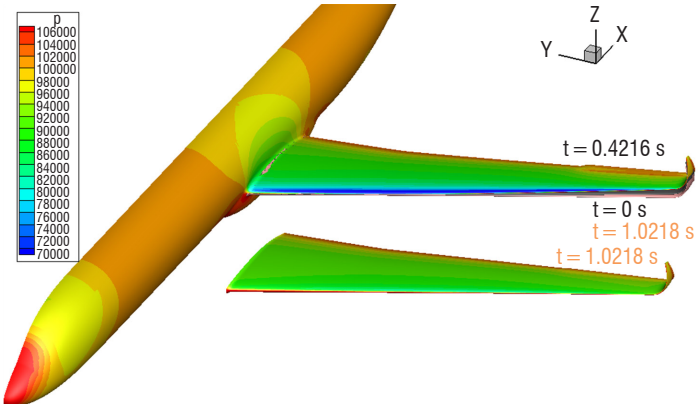

Figure 27 – Pressure distribution and wing deformation at two instants (highest upward deformation at t = 0.42 s and highest downward deformation at t = 1.02 s)

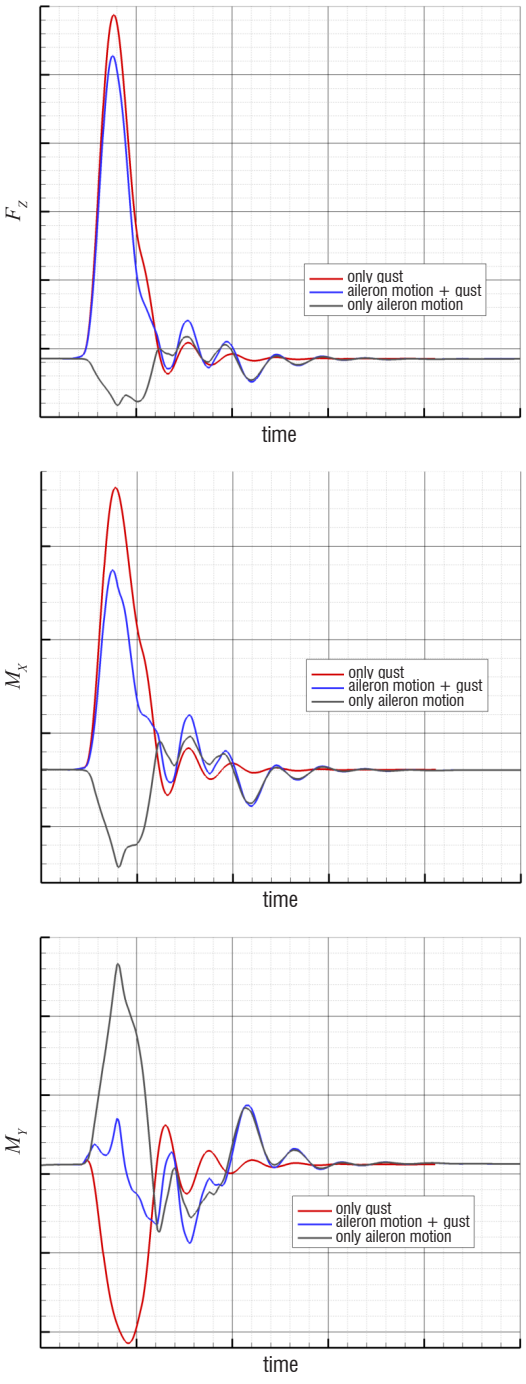

Figure 28 – Time evolution of the shear force, bending and torsion moments at the wing root

wing deformations occur. The first snapshot at $t = 0.42$ s matches the instant just after the gust peak, at which the maximal value of the first generalized coordinate is reached. The second snapshot ($t = 1.0218$ s) corresponds to the lowest value of the latter generalized coordinates and to the highest downward deflection angle of the aileron after the gust passage. Finally, integrated loads have been computed with respect to time for both gust responses (with and without aileron motion) and for the aileron motion response (without gust) (Figure 28). Similar time behavior can be noticed for both the shear force and bending moment. The aileron motion induces a significant alleviation of the peak due to the gust passage (11.9 % for the shear force and 29.2 % for the bending moment). From the torsion moment point of view, the aileron motion induces the peak removal, and resulting secondary oscillations are quickly damped as soon as the aileron motion stops (these oscillations vanish after 2 s).

Conclusion and Perspectives

Gusts encountered by airplanes induce loads that can be critical for some severe flight conditions, and therefore must be considered in the sizing in a structure design process. Furthermore, in the context of aircraft drag optimization and weight saving, airplane structures become increasingly flexible (large span, high wing aspect ratios). There is then a need to increase fidelity modelling to accurately assess gust loads. High-fidelity fluid-structure coupling methodologies and simulation tools have therefore been developed to compute the response of an aircraft to a discrete gust. The first consists in modelling the flow using the URANS formulation and in solving both the structure and fluid equations in a time-consistent coupling process. The gust has therefore been modelled as an added fluid velocity field according to the Sitaraman approach. Control surface motions according to prescribed laws have also been implemented, in order to assess load alleviation and law efficiency. Such a simulation approach has first been validated by comparisons with dynamic wind tunnel experiments. A specific gust generator was designed and implemented in the wind tunnel; this generator is able to provide different kinds of time function gusts. Gust load alleviation capacities were also assessed in the case of a wing-fuselage configuration equipped with an aileron for load control.

Nevertheless, since such fluid-structure coupling simulations are very time consuming, an alternative method has been developed to obtain the aircraft response to a harmonic gust. It is based on the linearization of the URANS equations in the frequency domain.

For perspective, the free flight effects have to be accounted for in gust response simulations. Current work deals with the coupling of *elsA-Ael* to a flight dynamics model. For gust alleviation, work is underway to couple this kind of simulation to a feedback function. An update of the control law parameter based on the flow history is performed at each time step of the computation ■

Acknowledgement

The research leading to these results has received funding from the European Union's Seventh Framework Program (FP7/2007-2013) for the Clean Sky Joint Technology Initiative, under grant agreements CSJU-GAM-SFWA-2008-001 and CSJU-GAM-GRA-2008-001.

The studies presented in this article have been (partially) funded by Airbus, Safran, and ONERA, which are co-owners of the software *elsA*.

The authors would also like to thank AIRBUS for having provided the XRF1 aerodynamic and structural models.

The authors would like to thank Leonardo Aircraft Division for having provided data for the JTI-GRA project.

References

[1] E. ALBANO, W. P. RODDEN - *A Doublet-Lattice Method for Calculating Lift Distributions on Oscillating Surfaces in Subsonic Flows*. AIAA Journal, 7(2):279–285, 1969.

[2] P. BEKEMEYER, R. THORMANN, S. TIMME - *Rapid Gust Response Simulation of Large Civil Aircraft Using Computational Fluid Dynamics*. The Aeronautical Journal Volume 121, issue 1246, pp. 1795-1807, December 2017.

[3] P. BEKEMEYER, R. THORMANN, S. TIMME - *Frequency-Domain Gust Response Simulation Using Computational Fluid Dynamics*. AIAA Journal, Vol. 55, No. 7 (2017), pp. 2174-2185.

[4] V. BRION, A. LEPAGE, Y. AMOSSE, D. SOULEVANT, P. SENECAT, J.-C. ABART, P. PAILLART - *Generation of Vertical Gusts in a Transonic Wind Tunnel*. Experiments in Fluid, (2015) 56: 145. https://doi.org/10.1007/s00348-015-2016-5.

[5] L. CAMBIER, S. HEIB, S. PLOT - *The ONERA elsA CFD Software: Input from Research and Feedback from Industry.* Mechanics & Industry, 14(3): 159-174, doi:10.1051/meca/2013056, 2013.

[6] S. S. DAVIS - *Compendium of Unsteady Aerodynamic Measurements*. AGARD Report No. 702 data set 2 NACA64A010 (NASA AMES MODEL) oscillatory pitching, 1982.

[7] S. DEQUAND, C. LIAUZUN, P. GIRODROUX-LAVIGNE, A. LEPAGE - *Transonic Response to a Gust*. International Forum on Aeroelasticity and Structural Dynamics, 26-30 June 2011, Paris, France.

[8] D. DIMITROV, R. THORMANN - *DLM-Correction Method for Aerodynamic Gust Response Prediction*. International Forum on Aeroelasticity and Structural Dynamics (IFASD), IFASD2013-24C, 24-26 June 2013, Bristol, UK.

[9] J. DONEA, A. HUERTA, J.-P. PONTHOT, A. RODRIGUEZ-FERRAN - *Encyclopedia of Computational Mechanics, Volume 1: Fundamentals, Chapter 14: Arbitrary Lagrangian-Eulerian Methods*". John Wiley & Sons, Ltd, 2004.

[10] A. DUGEAI - *Aeroelastic Developments in the elsA Code and Unsteady RANS Applications*. International Forum on Aeroelasticity and Structural Dynamics, 28 June – 1 July 2005, Munich, Germany.

[11] EUROPEAN AVIATION SAFETY AGENCY - *Certification Specifications for Large Aeroplanes CS-25*.

[12] FEDERAL AVIATION ADMINISTRATION - *Federal Aviation Regulations, Section 25.341, Gust and Turbulence Loads*.

[13] FEDERAL AVIATION ADMINISTRATION - *Federal Aviation Regulations, Appendix G, Continuous Gust Design Criteria*.

[14] M. FORSTER, C. BREITSAMTER - *Aeroelastic Prediction of Discrete Gust Loads Using Nonlinear and Time-Linearized CFD-Methods*. Aeroelasticity and Structural Dynamics Journal, Vol. 3, No. 3, 2015.

[15] M. GAZAIX, A. JOLLES, M. LAZAREFF - *The elsA Object-Oriented Computational Tool for Industrial Applications*. 23rd Congress of ICAS, Toronto, Canada, 8-13 September, 2002.

[16] L. GIRAUD, S. GRATTON, X. PINEL, X. VASSEUR - *Flexible GMRES with Deflated Restarting*. SIAM Journal on Scientific Computing, Vol. 32, No. 4, pp. 1858-1878, 2010.

[17] P. GIRODROUX-LAVIGNE - *Progress in Steady/Unsteady Fluid-Structure Coupling with Navier-Stokes Equations*. International Forum on Aeroelasticity and Structural Dynamics, 28 June – 1 July 2005, Munich, Germany.

[18] P. GIRODROUX-LAVIGNE - *Recent Navier-Stokes Aeroelastic Simulations Using the elsA Code for Aircraft Applications*. International Forum on Aeroelasticity and Structural Dynamics, 18-20 June 2007, Stockholm, Sweden.

[19] K. C. HALL, E. F. CRAWLEY - *Calculation of Unsteady Flows in Turbomachinery Using the Linearized Euler Equations*. AIAA Journal, Vol. 7, No. 6, pp. 777-787, 1989.

[20] R. HEINRICH - *Simulation of Interaction of Aircraft and Gust Using the TAU-Code*. In: A. DILLMANN, G. HELLER, E. KRAMER, H. P. KREPLIN, W. NITSCHE, U. RIST (eds) - *New Results in Numerical and Experimental Fluid Mechanics IX*. Notes on Numerical Fluid Mechanics and Multidisciplinary Design, Vol. 124, 2014, Springer, Cham.

[21] R. HEINRICH, L. REIMER - *Comparison of Different Approaches for Gust Modelling in the CFD Code TAU*. International Forum on Aeroelasticity and Structural Dynamics, 24-26 June 2013, Bristol, UK.

[22] F. HUVELIN, P. GIRODROUX-LAVIGNE, C. BLONDEAU - *High-Fidelity Numerical Simulations for Gust Response Analysis*. International Forum on Aeroelasticity and Structural Dynamics, 24-26 June 2013, Bristol, UK.

[23] A. LEPAGE, Y. AMOSSE, D. LEBIHAN, C. POUSSOT-VASSAL, V. BRION, E. RANTET - *A Complete Experimental Investigation of Gust Load from Generation to Active Control*. IFASD 2015, Saint Petersburg, Russia, 28 June - 2 July 2015.

[24] A. LEPAGE, F. HUVELIN, D. LE BIHAN, C. POUSSOT-VASSAL, V. BRION, P. NAUDIN, E. RANTET - *Experimental Investigation and Control of Gust Load Response in Transonic Flow*. Greener Aviation, Brussels, Belgium, 11-13 October 2016.

[25] C. LIAUZUN, E. CANONNE, G. D. MORTCHÉLÉWICZ - *Flutter Numerical Computations Using the Linearized Navier-Stokes Equations*. Proc Advanced Methods in Aeroelasticity, pp. 8-1-8-12, RTO-MP-AVT-154, Loen Norway, May 2008.

[26] C. LIAUZUN - *Aeroelastic Response to Gust Using CFD Techniques*. Proceedings of 3rd Joint US-European Fluids Engineering Summer Meeting and 8th International Conference on Nanochannels, Microchannels, and Minichannels, FEDSM2010-ICNMM2010, Montreal, Canada, August 2-4, 2010.

[27] G. D. MORTCHÉLÉWICZ - *Prediction of Aircraft Transonic Aeroelasticity by the Linearized Euler Equations*. 41st Israel Annual Conference on Aerospace Sciences, 2001.

[28] G. D. MORTCHÉLÉWICZ - *Aircraft Aeroelasticity Computed with Linearized Rans Equations*. 43rd Annual Conference on aerospace Sciences, Tel Aviv Haifa (Israel), February 2003

[29] G. PAGLIUCA, S. TIMME - *Model Reduction for Flight Dynamics Simulations Using Computational Fluid Dynamics*. Aerospace Science and Technology, Volume 69, pp. 15-26, October 2017.

[30] A. PECHLOFF, B. LASCHKA - *Small Disturbance Navier-Stokes Method: an Efficient Tool for Predicting Unsteady Air Loads*. Journal of Aircraft, Vol. 43, No. 1, 2006.

[31] D.E. RAVEH - *CFD-Based Models of Aerodynamic Gust Response*. Journal of Aircraft, Vol 44, No 3, May-June 2007.

[32] A. M. RODDE, J. P. ARCHAMBAUD - *OAT15A Airfoil Data*. AGARD advisory report N° 303: *A Selection of Experimental Test Cases for the Validation of CFD Codes*.

[33] J. SITARAMAN, V. S. IYENGAR, J. D. BAEDER - *On field velocity approach and geometric conservation law for unsteady flow simulations*. 16th AIAA Computational Fluid Dynamics Conference, Orlando FL, 2003.

[34] C. VALENTE, C. WALES, D. JONES, A. GAITONDE, J. E. COOPER, Y. LEMMENS - *A Doublet-Lattice Method Correction Approach for High Fidelity Gust Loads Analysis.* 58th AIAA/ASCE/AHS/ASC Structures, Structural Dynamics, and Materials Conference. Grapevine, Texas, 2017.

[35] W. WEIGOLD, B. STICKAN, I. TRAVIESO-ALVAREZ, C. KAISER, P. TEUFEL - *Linearized Unsteady CFD for Gust Loads with TAU*. IFASD 2017, Como, Italia, 25-28 June 2017.

Fabien Huvelin graduated from the National Engineering Institute for Electronics, Computing, Telecommunications, Mathematics and Mechanics ENSEIRB-MATMECA of Bordeaux in 2003 and obtained his PhD for his work on the fluid-structure interaction modeling by high-fidelity tool coupling in 2008. He joined the aeroelasticity department of ONERA in 2012. His main research activities are focused on the development and validation of aeroelastic modeling with high-fidelity tools.

Sylvie Dequand graduated from ISEN Lille and specialized in "Fundamental Acoustics" at the University of Le Mans in 1997. She then obtained a PhD degree in Fluid Mechanics from the Technological University of Eindhoven in 2001. She first worked as a research assistant in Aeroacoustics at the LMS in Leuven, and then in the Automotive Department of Loughborough University. Since 2004, she has been working at ONERA as an Aeroelasticity engineer. She was first involved, together with the experimental team, in ground vibration and wind tunnel tests. Since 2008, she has been working in the Aeroelastic Modeling and Simulation unit of the Aerodynamics, Aeroelasticity and Acoustics Department of ONERA, where she is mainly in charge of fluid-structure coupling simulations and aeroelastic stability studies for civil aircraft cooperation programs.

Arnaud Lepage graduated from the École Nationale Supérieure de Mécanique et des Microtechniques (ENSMM) of Besançon in 1998 and received a PhD degree from the University of Franche-Comté in 2002 for a thesis on experimental modal analysis in structural dynamics. Then, he joined the aeroelasticity department of ONERA as a research engineer, where he initially worked on active vibration control. Since 2006, his fields of interest have been the experimental investigation and control of fixed-wing aeroelasticity and unsteady aerodynamics (gust, buffet, and flutter).

Cédric Liauzun graduated from the École Nationale Supérieure de Mécanique et d'Aérotechniques (ENSMA) in 1996, and has about 20 years of experience as a member of the Numerical Aeroelasticity team at ONERA, where his activity is mainly devoted to the development of numerical simulation methods for aeroelasticity and fluid-structure coupling.

J.-C. Chassaing, C. T. Nitschke, A. Vincenti
(Sorbonne Université)

P. Cinnella
(Laboratoire DynFluid)

D. Lucor
(LIMSI-CNRS)

E-mail:
jean-camille.chassaing@sorbonne-universite.fr

DOI: 10.12762/2018.AL14-07

Advances in Parametric and Model-Form Uncertainty Quantification in Canonical Aeroelastic Systems

Uncertainty quantification is going to play a crucial role in the aeroelastic design and optimization of aircraft. Stochastic aeroelastic models are currently being considered to account for manufacturing tolerance in material properties, variability in flight conditions or uncertainty in the aeroelastic model itself. In this paper, some challenging issues in the development of efficient and robust stochastic solvers are reported within the framework of canonical aeroelastic systems. First, independent or correlated parametric uncertainties are propagated to compute the probability density function of the critical flutter velocity or the limit cycle oscillations in the presence of discontinuous responses. Secondly, inverse stochastic aeroelastic problems are addressed, in which experimental data are used to calibrate several stochastic aerodynamic models within a Bayesian framework. Studied configurations concern linear and non-linear pitching and plunging airfoils, and the stochastic flutter of a cantilevered straight composite wing subject to ply angle and thickness uncertainties.

Introduction

Aeroelasticity can be defined as the study of combined structural and aerodynamic effects on the vibratory behavior of aeronautical components, like panels, wings, rotorcraft or the whole aircraft itself. Aeroelastic effects result from the interaction of inertial, elastic and aerodynamic forces acting on aircraft components. Depending on the aeromechanical properties of the aircraft and the flight conditions, the aeroelastic response may exhibit some undesirable phenomena, ranging from the degradation of the aerodynamic performance of the aircraft to the apparition of self-sustained, possibly dramatic, oscillations of the structure, such as divergence and flutter. Due to the explosive nature of the flutter phenomenon, aircraft certification is mandatory to guarantee that no aeroelastic instability can be encountered inside the flight envelope. However, small variations in the aeromechanical parameters may strongly affect the aeroelastic response of the aircraft [12, 56, 84]. For instance, Thomas *et al.* [103] observed that a 0.10 Hz change in the structural natural frequencies or a 1 deg. change in the mean angle of attack reduce by approximately 10% the computed flutter onset Mach Number.

The study of aeroelasticity with uncertainties, which can be illustrated by using an extension of the classical Collar's aeroelastic triangle of forces (Figure 1), has become an extensive field of research over the last decades [6, 9, 10, 29, 84]. Based on state-of-the-art traditional aeroelasticity and computational aeroelasticity

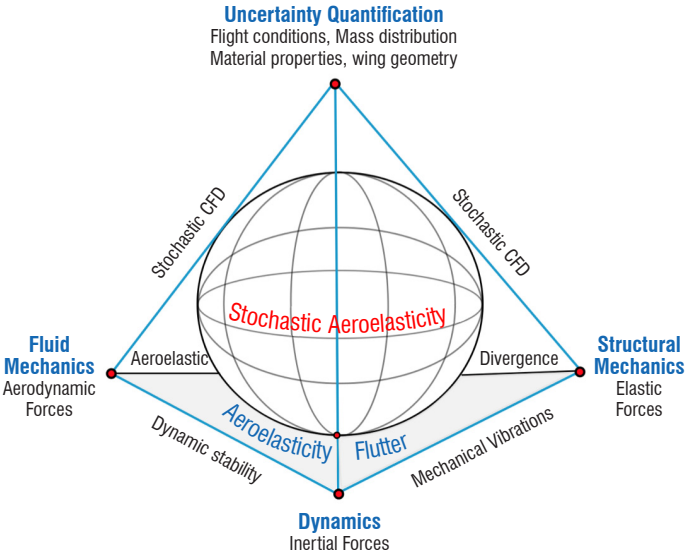

Figure 1 – Probabilistic interpretation of the Collar force triangle in aeroelasticity

approaches [6, 10] originally used within a deterministic framework, uncertainty quantification (UQ) will consist in studying the effect of both aleatory and epistemic uncertainties affecting the aeroelastic response of the aircraft. According to the taxonomy adopted by Melchers [64],any irreducible uncertainty in the system parameters is referred to as aleatory, whereas epistemic uncertainties result from the lack of knowledge about the physical aeroelastic model.

The identification of aeroelastic uncertainties was thoroughly discussed in the review by Pettit [84] on uncertainty quantification in aeroelasticity. Aleatory uncertainties may have various sources, such as, for example, manufacturing tolerance on aircraft geometry or material properties, and in-flight conditions (non-uniform and gusty winds). On the other hand, epistemic uncertainties are typically related to the choice of the physical aeroelastic model. A detailed description of uncertainty sources for physical parameters of aeroelastic configurations can be found in [29].

The study of aeroelasticity with parametric uncertainty can be performed using different approaches. Robust flutter aeroelastic analyses are conducted using non-probabilistic approaches, by studying the stability of the aeroelastic system for parameter variations within given uncertainty bounds. Such approaches, which do not require the probability distribution of the input uncertain aeromechanical parameters, consist in identifying the worst aeroelastic case in the uncertain parametric support [15, 30, 58, 59]. The corresponding methods and advances in the development of non-probabilistic robust aeroelasticity were recently reviewed in [29].

The second type of approach that can be considered to perform aeroelastic studies with uncertainties is referred to as probabilistic aeroelastic analysis. In such a stochastic representation, random input variables with known distributions are used to model the parametric aeroelastic uncertainties. Then, they are propagated using suitable probabilistic approaches, in order to compute the distributions of the aircraft aeroelastic response. The probabilistic collocation methods [5, 100, 124] and the stochastic spectral projection methods [40, 43, 115, 123] are two widely used approaches for the propagation of parametric uncertainty in computational structural dynamics (CSD) and in computational fluid dynamics (CFD). Boosted by the availability of open-source implementations of most popular stochastic solvers [1, 7, 38, 62], CFD-based computations of the stochastic aeroelastic response of elastic structures under uncertain flight conditions or structural variability have been widened substantially [6, 10, 12, 68].

Recently, Stanford and Massey [98] focused on the computation of the failure probabilities of the flexible Common Research Model [109] using a RANS-based CFD solver in the presence of atmospheric, structural and inertial parametric randomness, where up to 11 random variables were considered. In order to deal with a relatively moderate number of random dimensions, a sparse Polynomial Chaos Expansion method (PCE) [45] was used to compute the flutter probability. Although the probability that flutter appears within the commonly adopted 15% flutter margin [2] has been demonstrated at Mach 0.7, PCE fails to accurately compute the tail of the failure probability. It was shown that the lack of accuracy of the spectral projection approach is due to the presence of the physical nonlinearities associated with the transonic regime, which are reported in the random space.

Nowadays, uncertainty quantification in linear and nonlinear aeroelasticity faces several issues that cannot be addressed directly using stochastic approaches like standard PCE and Stochastic Collocation. To this end, there is a need to develop adaptive stochastic approaches in order to deal with a discontinuous response due to the presence of aeroelastic mode switching or subcritical Hopf bifurcations. Moreover, aeroelastic uncertainty quantification studies of realistic configurations involve a large number of random variables, like, for instance, in the case of aircraft components made of composite laminates with uncertain angles and thicknesses in their layup, making the use of adaptive methods more tricky [22]. In order to avoid the development of high-dimensional stochastic solvers, physical low-order modeling can be used to reduce the number of random variables to be propagated, such as, for instance, the use of lamination parameters for the case of the stochastic flutter of a composite wing [94]. However, the resulting uncertainty propagation step must account for correlated random variables, again in the context of possible discontinuity in the random space.

Another major difficulty in the computation of the aeroelastic instability boundary of aircraft is related to the inherent sensitivity of the numerical predictions to the choice of numerical model, as illustrated, for instance, by the difference obtained between the results of Delayed Detached Eddy Simulation and Unsteady Reynolds Averaged Navier-Stokes of the flutter boundary of the AGARD wing 445.6 [125]. In such a context, copying with both parametric and model-form uncertainties in aeroelasticity enables the calibration of uncertain model coefficients from experimental data and, at the same time, the construction of adjusted stochastic models with robust predictive capabilities.

The scope of this paper is to review some recent advances in the development of uncertainty quantification in probabilistic aeroelasticty. Both aleatory and epistemic uncertainties associated with linear and nonlinear canonical aeroelastic systems [21, 52, 77, 78] are considered. Emphasis is placed in Section "Stochastic limit cycle oscillations of the PAPA aeroelastic model" on the treatment of discontinuous response surfaces due to bifurcations in the aeroelastic response of nonlinear PAPA test-cases. The propagation of correlated random variables with arbitrary distributions is described in Section "Stochastic flutter of a composite wing" for the prediction of the stochastic flutter velocity of a composite plate wing.

Finally, the quantification of both model form and parametric uncertainties associated with two low-order aerodynamic models of a PAPA aeroelastic configuration is carried out by using a Bayesian Model Averaging framework.

Forward uncertainty quantification of parametric uncertainties

Stochastic limit cycle oscillations of the PAPA aeroelastic model

Limit cycle oscillations (LCO) can be observed in the presence of nonlinearities in the structural or aerodynamic operator of the aeroelastic system [27, 55, 56]. As illustrated by the typical bifurcation diagram of a PAPA model in Figure 2, the amplitude of these oscillations strongly depends on the subcritical or supercritical nature of the Hopf bifurcation corresponding to a change in the response from a stable solution to an oscillatory behavior [12, 57, 65].

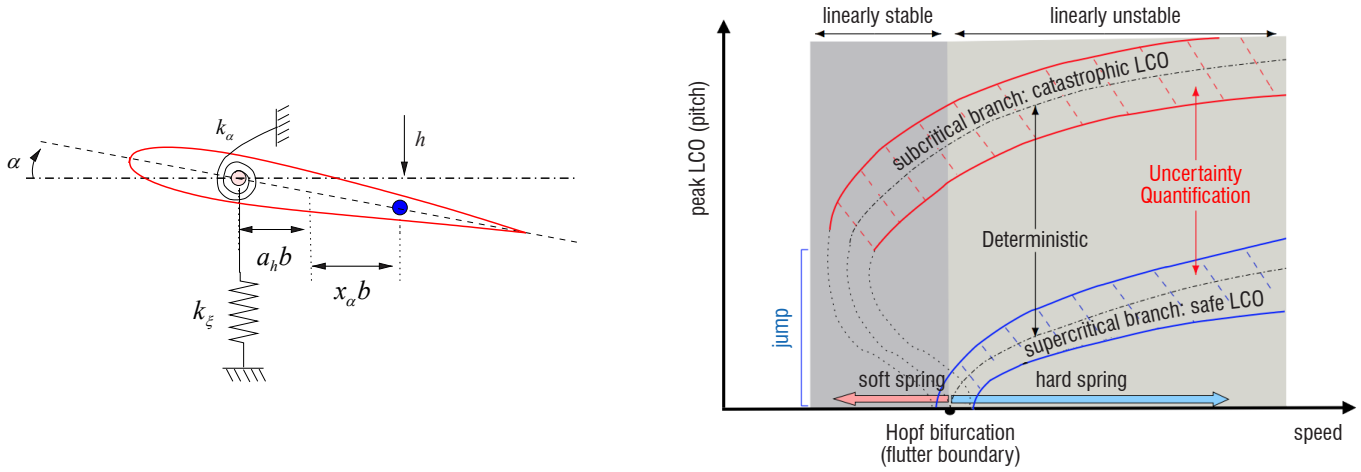

Figure 2 – Left: typical 2DOF pitch and plunge (PAPA) airfoil section problem. Right: Corresponding typical aeroelastic bifurcation diagram due to softening and hardening cubic stiffness restoring forces in pitch.

The onset of LCO of a typical airfoil section model in an incompressible flow with structural nonlinearities in pitch stiffness was studied in a stochastic framework by Pettit and Beran [85]. Subcritical bifurcations were investigated by means of a pentic pitch stiffness model and uncertain initial conditions with Gaussian normal distribution were propagated using Monte Carlo simulations to compute the corresponding stochastic bifurcation diagram. Later, uncertainty quantification in LCO of canonical aeroelastic problems were performed using cheaper stochastic solvers, such as probabilistic collocation methods based on polynomial chaos or Fourier chaos expansions [11, 12, 31, 44, 65, 66, 69, 72, 93, 101, 112], the unsteady adaptive stochastic finite-element approach [116-120] and the stochastic spectral projection [17, 21, 32, 52]. Stochastic LCO and bifurcation diagram of the PAPA canonical aeroelastic model were also investigated in [122] by means of bounded random variables with λ-pdf and in [12] using Wiener-Haar and Wiener-Hermite expansions.

Uncertainty quantification using adaptive spectral methods

The convergence rate of PCE methods with global support may be very slow in the presence of discontinuities in the random space [17, 25, 52, 113, 114, 123], due for instance to a jump from a stable to an unstable aeroelastic response. To circumvent this drawback, the capabilities of the adaptive multi-element generalized Polynomial Chaos (ME-gPC) method developed by Wan and Karniadakis [113] were investigated in [21, 52] for the case of stochastic bifurcation due to non-linear restoring forces in the aeroelastic model.

The first step in the application of the ME-gPC method relies on the definition of an $N-$element partition $\mathbf{D}$ of the random space with B_k elements ($k=1,2,...,N$).

Given a probability space $(\Omega,\mathcal{F},P)$, where Ω is the sample space, $\mathcal{F}$ is a subset of Ω and P is the probability measure, the ME-gPC approximation $u^r(\boldsymbol{\xi})$ of any space-time random field $u(\boldsymbol{x},t;\boldsymbol{\xi})\in L_2(\Omega,\mathcal{F},P)$ is written as [113]

$$u^r(\boldsymbol{\xi})=\sum_{k=1}^{N}\sum_{j=0}^{M}\hat{u}_{k,j}\Phi_{k,j}(\boldsymbol{\xi}_k)I_{B_k} \tag{1}$$

where $\boldsymbol{\xi}$ is a random variable defined over the global random space whose components are independent uniform random variables, $\hat{u}_k$ is the local polynomial chaos expansion in element B_k with new random variable $\boldsymbol{\xi}_k$. The value of the indicator random variable I_{B_k} is equal to 1 when the vector of random variables belongs to element k and is equal to zero otherwise.

The polynomial basis $\{\Phi_{k,j}\}$ is orthogonal in each element with respect to the local probability measure. Then, the gPC coefficients $\hat{u}_{k,j}$ are computed from the Galerkin projection of the stochastic solution onto each member of the local orthogonal basis. The total number of modes M is determined by the dimension d of $\boldsymbol{\xi}$ and the order of the local gPC expansion P is written as $M=((P+d)!)/(P!d!)-1$. Note that, when using uniform/Legendre discretization for the ME-gPC representation, the local polynomials, which must be considered with respect to the conditional probability density function (*pdf*) in each element, remain Legendre polynomials. Therefore, a simple scaling, resulting from the derivation of the conditional *pdf*, is required to map the local element to a standard element of reference.

Although this piecewise polynomial approximation is more appropriate to deal with nonlinear dynamics than the global gPC approach, it must be combined with an adaptive framework in order to avoid computational growth [21, 52, 113]. To this end, a sensitivity-based adaptivity procedure can be constructed starting from the local solution variance obtained from the gPC approximation with polynomial order P.

$$\sigma^2_{k,p}=\sum_{j=1}^{M_P}\hat{u}^2_{k,j}\mathbb{E}\left[\Phi^2_{k,j}\right] \tag{2}$$

Then, coefficients representing the decay rate and the sensitivity to the random dimension can be constructed [113]

$$\eta_k=\frac{\sum_{i=M_{P-1}+1}^{M_P}\hat{u}^2_{k,i}\mathbb{E}[\Phi^2_{k,i}]}{\sigma^2_{k,p}},\quad r_i=\frac{\hat{u}^2_{i,P}\mathbb{E}[\Phi^2_{i,P}]}{\sum_{j=M_{P-1}+1}^{M_P}\hat{u}^2_j\mathbb{E}[\Phi^2_j]},\quad i=1,2,\cdots,d \tag{3}$$

where subscript $\cdot_{i,P}$ denotes the mode consisting only of random dimension ξ_i with polynomial order P.

Finally, the refinement procedure is defined by the following criteria

$$\eta_k^\gamma\,\Pr\left(I_{B_k}=1\right)\geq\theta_1,\quad r_i\geq\theta_2\cdot\max_{l=1,\cdots,d}r_l \tag{4}$$

where γ, θ_1 and θ_2 are prescribed constant parameters controlling the adaptive procedure. When the first condition is satisfied for element B_k, an anisotropic splitting is performed based on the most sensitive random dimension according to coefficient r_i. Alternatives to this error criterion were proposed by Chouvion and Sarrouy [25], based on the residual error and the local variance discontinuity created by partitioning. In the following sections, the adaptive ME-gPC approach is used to predict the distribution of the LCO amplitude of nonlinear PAPA configurations for both incompressible [52] and supersonic [21] flows in the presence of uncertainties in the torsional restoring stiffness.

Stochastic limit cycle oscillations of a supersonic lifting surface

Lamorte *et al.* [51] used a stochastic collocation approach [36] to propagate variabilities in the pitch and plunge natural uncoupled frequencies of an elastically-mounted 2D supersonic lifting surface. The use of a 6th order expansion with Lagrange polynomials was sufficient to show that under uncertainties, linear flutter may be observed at critical speeds below those obtained under deterministic nominal conditions.

In the following, results obtained about the study of stochastic limit cycle oscillations of an elastically-mounted 2-D supersonic lifting surface (Figure 3) performed using a ME-gPC method [21] are reported.

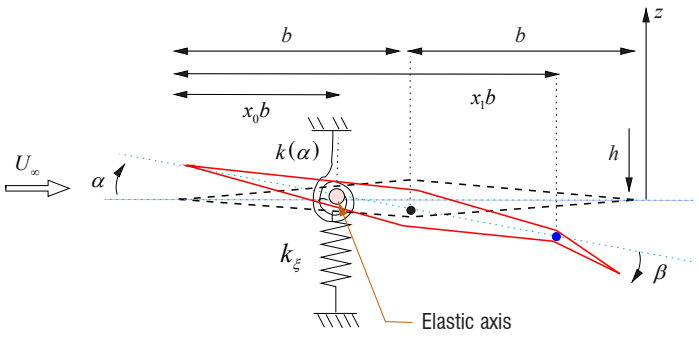

Figure 3 – Two-degree-of-freedom pitch-and-plunge supersonic lifting surface model, with b the half chord, x_α the dimensionless static unbalance and U_∞ the free-stream velocity

The pitch angle α and the dimensionless plunge displacement $\xi = h/b$ of the elastic axis are described by the following canonical aeroelastic equations [57]

$$\begin{aligned} \xi'' + x_\alpha \alpha'' + 2\zeta_h \frac{\overline{\omega}}{V}\xi' + \left(\frac{\overline{\omega}}{V}\right)^2 \xi = l_a(\tau) \\ \frac{x_\alpha}{r_\alpha^2}\xi'' + \alpha'' + 2\frac{\zeta_\alpha}{V}\alpha' + \left(\frac{1}{V}\right)^2 k(\alpha) = -m_a(\tau) \end{aligned} \quad (5)$$

The non-dimensional lift $l_a(\tau)$ and aerodynamic pitching moment $m_a(\tau)$, which account for the flap deflection angle β, are computed using an unsteady nonlinear aerodynamic model based on the piston theory in the third approximation [57]. The complete description of the dimensionless aero-mechanical parameters r_α, μ, ζ_α, ζ_ξ, $\overline{\omega}$, $k(\alpha)$ can be found in [54]. The nondimensional airspeed parameter is V and the primes refer to differentiation with respect to the nondimensional time $\tau = U_\infty t/b$ (Figure 3). The aeroelastic equations can be written in space-state form as [21]

$$\dot{\mathbf{x}} = \mathbf{A}\mathbf{x} + (\mathbf{p}_s + \mathbf{p}_a)\alpha^3 + \mathbf{f} \quad (6)$$

where the state vector $\mathbf{x} = [\xi \quad \alpha \quad \xi' \quad \alpha']^T$ is obtained using an explicit fourth-order Runge-Kutta time-integration scheme. [54]

As discussed in the introduction, it is well known that physical nonlinearities in the restoring forces may promote sharp and sudden flutter onset for small changes in the reduced velocity. The purely deterministic parametric investigations conducted in [86] were revisited within a stochastic framework using the ME-gPC approach in [21]. To this end, the structural damping coefficients ζ_h and ζ_α (Equation 6) are considered as input variables with an independent *uniform* random distribution:

$$\begin{aligned} \zeta_h &= \overline{\zeta}_h + \sigma_{\zeta_h}\Theta_1 \\ \zeta_\alpha &= \overline{\zeta}_\alpha + \sigma_{\zeta_\alpha}\Theta_2 \end{aligned} \quad (7)$$

where $\overline{\zeta}_h = \overline{\zeta}_\alpha = 0.005$ and $\sigma_{\zeta_h} = \sigma_{\zeta_\alpha} = 0.005$.

The response surface of the pitch amplitude obtained for a Mach number of 2.1 using a global gPC representation with a relatively high polynomial order $P = 14$ is shown in Figure 4-left.

Spurious oscillations of the response surface are clearly visible for both the stable state and the LCO branch. The global gPC response surface fails to clearly identify the discontinuity front in the random space, resulting in a poor representation of the stochastic response.

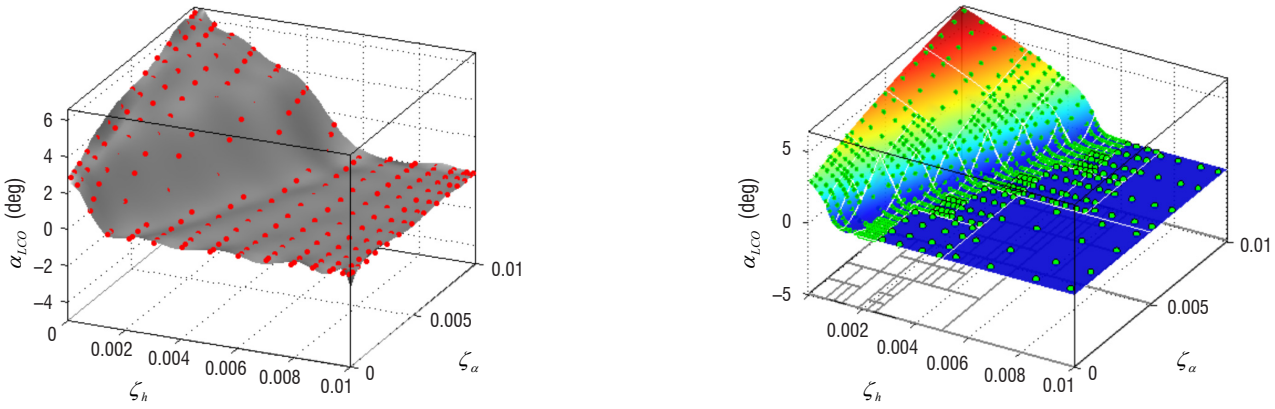

Figure 4 – Left: gPC response surface of α_{LCO} at $M = 2.1$ obtained using polynomial order $P = 14$. Right: ME-gPC results. The deterministic aeromechanical parameters are [21]: $x_\alpha = 0.25$, $r_\alpha = 0.5$, $b = 1.5$, $\overline{\omega} = 1$, $\mu = 50$, $x_0 = 0.5$, $\mu = 50$, $\gamma = 1.4$, $B = 5$

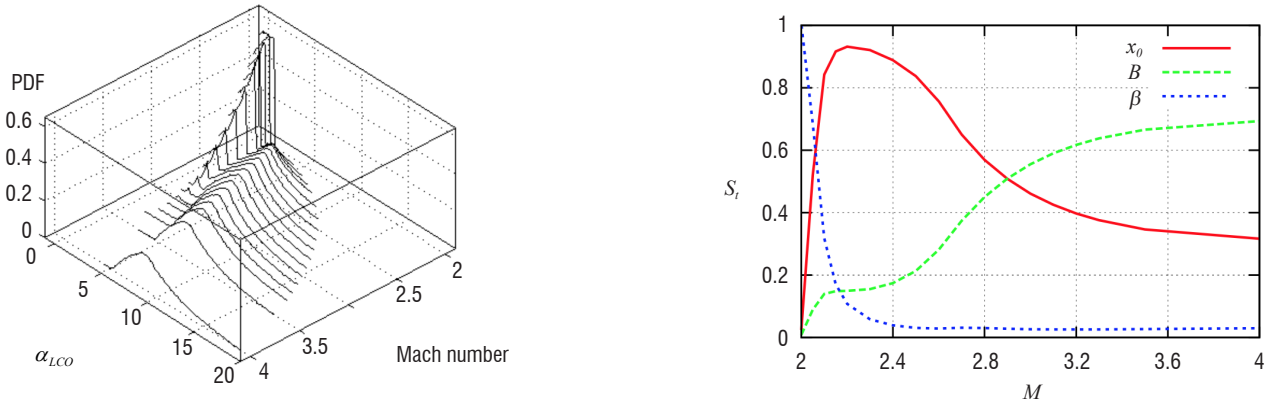

Figure 5 – Left: Distributions of the pitch LCO amplitude α_{LCO} obtained for $M=2$ up to $M=4$ for randomness due to the elastic axis location x_0, the nonlinear torsional stiffness parameter B and flap angle β. Right: Stochastic sensitivity study using Total Sobol indices in the case of three sources of randomness in x_0, B and β [21]

Due to a refinement process performed according to the most sensitive random dimensions (Equation 3), the ME-gPC expansion with $P=3$ succeeds in accurately capturing the steep front in the response, where 8 grid-levels were required to reach a resolution level set to $\varepsilon_1=10^{-3}$. The total number of cubature points required by the piecewise gPC solver is 1456 (encompassing 55 elements) compared to $(P+1)^2=225$ points for the global gPC representation.

In the following, parametric uncertainties in the elastic axis location, the nonlinear torsional stiffness parameter and flap angle are propagated using the ME-gPC approach. Figure 5-left shows the *pdf* of pitch LCO computed for operating conditions ranging from Mach number $M=2$ up to $M=4$. Each distribution is estimated from the ME-gPC expansions using 1 million samples. The bimodal shape of the distribution of the peak LCO, visible up to $M=2.8$, corresponds to the stochastic bifurcation region. The stable stationary branch is characterized by a *uniform*-like distribution with possible pitch amplitude ranging between 0 and 2 deg. We remark that the shape of the distribution is not strongly influenced by the Mach number in the post-bifurcation region defined by $M>3$. However, the upper limit of possible values of the peak pitch amplitude exhibits a nonlinear behavior according to the Mach number.

The analysis of the stochastic solution sensitivity to the uncertain parameters can be performed by means of the *total* Sobol indices [96], which are computed *a posteriori* using two independent MC sample sets drawn from the piecewise gPC expansion [21]. As shown in Figure 5-right, the most sensitive random variable differs depending on flow conditions. The lower bound of the Mach number range ($M<2.1$) is dominated by randomness in the flap angle. However, the stochastic solution in the bifurcation region ($M\in[2.1,2.9]$) is sensitive to inherent variations in the position of the elastic center. Conversely, uncertainties in both the nonlinear stiffness term and the location of the elastic axis mainly affect the stochastic response for high Mach numbers ($M>2.9$).

Subcritical stochastic bifurcation with random initial pitch angle and cubic spring term

The ME-gPC approach was successfully used in [52] to predict stochastic bifurcations with *uniformly* distributed random inputs in the linear torsional stiffness coefficient ($\bar{k}_{\alpha_1}=1$ and $\sigma_{k_{\alpha_1}}=0.1$) and the cubic torsional stiffness coefficient ($\bar{k}_{\alpha_3}=3$ and $\sigma_{k_{\alpha_3}}=0.75$) of a PAPA canonical model for incompressible flows. The pdf isocontours of the LCO amplitude in pitch α_A (Figure 6-right) reveal that three distinct regions can be identified in the stochastic aeroelastic response of the airfoil: (i) damped oscillations for $U^*<6.6$, (ii) a bi-modal response in the bifurcation region with both damped oscillations and LCO and (iii) a post-bifurcation region for $U^*>6.6$. Moreover, the error bars of the prediction of α_A (Fig. 6-left) show that, in the presence of combined uncertainties in k_{α_1} and k_{α_3}, the instability onset could appear before the nominal (deterministic) flutter conditions are reached.

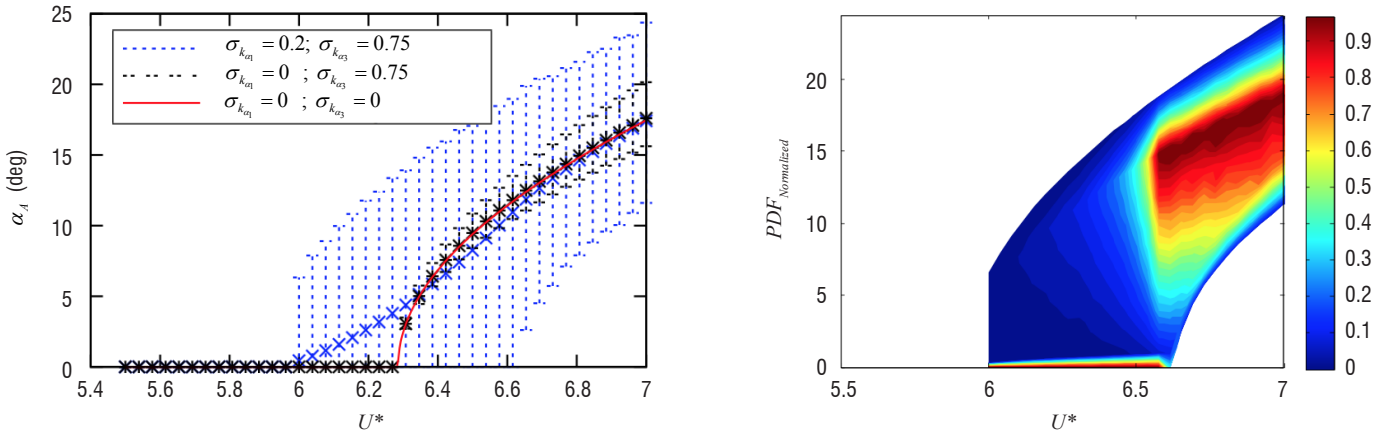

Figure 6 – Distribution of the amplitude LCO branch due to cubic hardening stiffness in pitch [52]

Figure 7 shows a subcritical stochastic bifurcation obtained for uncertainties in the initial pitch angle $\alpha(0)$ and cubic spring term k_{α_3}. The distribution of the peak pitch amplitude due to statistic of these uncertain variables defined by $\overline{\alpha}(0)=12.5$ deg, $\sigma_{\alpha}(0)=12.5$ deg, $\overline{k}_{\alpha_3}=-3$ and $\sigma_{k_{\alpha_3}}=0.75$ are presented in Figure 7-left. The stochastic bifurcation regime is studied for reduced velocities ranging from $U^*=5.8$ to $U^*=6.3$. The bimodal density response of the peak LCO amplitude in pitch corresponds to a sharp Dirac delta-like peak due to the zero-amplitude stable branch and a second peak corresponding to the probability to observe the stable large amplitude LCO branch, which results from the discontinuous shape of the response surface, as shown in Figure 7-mid for $U^*=6$.

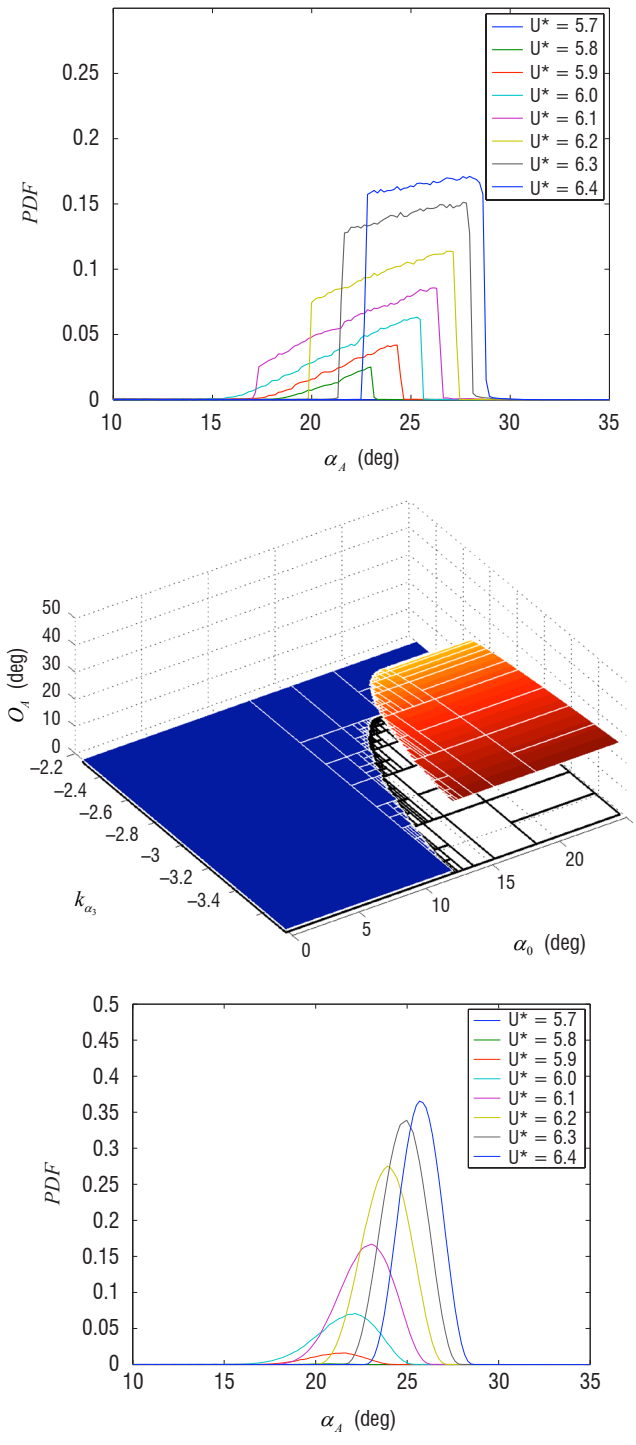

Figure 7 – Up: pdf of the stable large amplitude LCO branch due to uncertainties in $\alpha(0)$ and k_{α_3} described by uniform distributions. Mid: corresponding ME-gPC response surface computed for $U^*=6$. Bottom: distribution of α_{LCO} assuming the k_{α_3} and $\alpha(0)$ follow independent $Beta(\alpha=3,\beta=3)$ distributions [52]

Although the previous stochastic study was performed using *uniformly* distributed inputs, it is possible to compute the stochastic response due to different random input distributions defined on the same support of the probability space [52]. In this case, the statistics of the response can be readily obtained as a post-processing stage using Equation 1. As an example, Figure 7-right shows the shape of *pdf* of α_{LCO} obtained when both k_{α_3} and $\alpha(0)$ follow independent $Beta(\alpha=3,\beta=3)$ distributions. Although the resulting distributions of the peak pitch amplitude look similar to $Beta$ distributions, the tails of the distribution exhibits a longer left tail toward the zero-amplitude stable branch.

Stochastic flutter of a composite wing

Global-support-based Polynomial-Chaos expansions were used by Manan and Cooper [61] for the propagation of uncertain longitudinal Young modulus and shear modulus in the frequency response function of a composite wing. Recently, Scarth *et al.* [94] addressed the problem of uncertainty quantification in the ply angle uncertainty of a composite rectangular wing. To this end, the composite laminate layups were modeled using the lamination parameters [106], in order to reduce the number of random dimensions of the stochastic problem. Rosenblatt decomposition was applied to deal with correlations in the input random variables. Moreover, a convex-hull approach was considered in order to split the random domain, according to the discontinuity due to the presence of a mode switch in the aeroelastic response of the composite wing. This approach was successfully used to capture the multi-modal response of the distribution of the critical flutter velocity, whereas results obtained using a Polynomial Chaos Expansion with global support are not sufficiently accurate. However, the aeroelastic configurations of interest were concerned with uncertainties in ply angles only and the effects of membrane-bending coupling were neglected, thus introducing an artificial symmetrization of the material in the stochastic framework.

In this section, we consider the study of uncertainty propagation on the linear flutter speed of a composite cantilevered wing due to parametric variabilities in the angular ply placement and thickness for several laminate configurations [73, 78]. Since laminates with a dozen or more plies can be used in aeronautical components, the corresponding number of uncertain constitutive parameters is expected to be large compared to those of the stochastic study in Section "Stochastic limit cycle oscillations of the PAPA aeroelastic model". Therefore, we introduce the polar method [108, 111] as a possible way to reduce the random dimensional space. As a side effect, conventional spectral projection methods must be adapted to deal with correlated random variables and arbitrary input distributions.

Aeroelastic system

We aim to investigate the stochastic aeroelastic response of a flat cantilevered laminated composite plate [94, 99] depicted in Figure 8. The wing geometry is reported in Table 1.

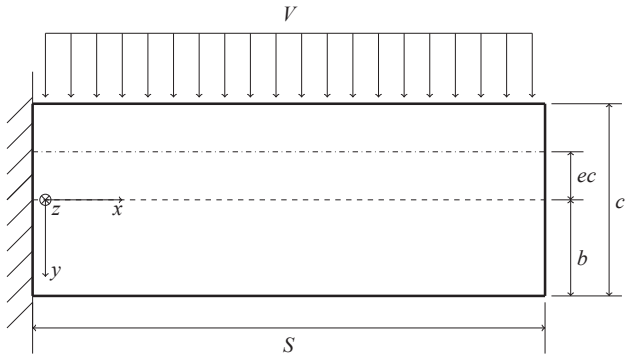

Figure 8 – Scheme of the studied cantilevered laminated plate wing [99]

Wing half span $S[m]$	Chord $c[m]$	Air density $\rho_a\left[kg/m^3\right]$	Lift excentricity e	Unsteady parameter $M_{\dot{\theta}}$
0.3048	0.0762	1.225	0.25	–1.2

Table 1 – Wing geometry and aeromechanical data [99]

Hereafter, we consider sixteen-layer layups based on AS4/3502 graphite/epoxy laminate [106, 107], and the engineering moduli of this base layer are summarized in Table 2.

$E_1[GPa]$	$E_2[GPa]$	$G_{12}[GPa]$	$\nu_{12}[-]$	$\rho\left[kg/m^3\right]$	Ply thickness $t[mm]$
138.0	8.96	7.1	0.3	1600	0.1

Table 2 – Material properties of AS4/3502 UD layer

In the absence of membrane forces, the bending moments m are related to the curvature $\boldsymbol{\kappa}=\left(-\frac{\partial^2 w}{\partial x^2},-\frac{\partial^2 w}{\partial y^2},-2\frac{\partial^2 w}{\partial x \partial y}\right)^T$ by

$$\mathbf{m}=\left(\mathbf{D}-\mathbf{B}\mathbf{A}^{-1}\mathbf{B}\right)\boldsymbol{\kappa}=\tilde{\mathbf{D}}\boldsymbol{\kappa} \tag{8}$$

where $\mathbf{A}$ denotes the membrane stiffness, $\mathbf{D}$ is the bending stiffness, $\mathbf{B}$ describes the coupling between the membrane and the bending forces, and $\tilde{\mathbf{D}}$ is the modified bending stiffness [67], which reduces to tensor $\mathbf{D}$ for uncoupled laminates.

The aeroelastic governing equations are obtained using the Lagrange equations for the generalized coordinates $\mathbf{q}$

$$\frac{d}{dt}\left(\frac{\partial T}{\partial \dot{\mathbf{q}}}\right)-\frac{\partial T}{\partial \mathbf{q}}+\frac{\partial U}{\partial \mathbf{q}}=\frac{\partial(\delta W)}{\partial(\delta \mathbf{q})} \tag{9}$$

where the potential energy U, the kinetic energy T and the virtual work of the aerodynamic forces are

$$\begin{aligned} U&=\frac{1}{2}\iint \boldsymbol{\kappa}^{\mathrm{T}}\tilde{\mathbf{D}}\boldsymbol{\kappa}dxdy \\ T&=\frac{1}{2}\rho d\iint \dot{w}^2 dxdy \\ \delta W&=\int l_a(-\delta w)dx+\int m_a\delta\theta dx \end{aligned} \tag{10}$$

As in the work by Stodieck *et al.* [99], the quasi-steady strip theory [121] was used to model the aerodynamic lift l_a and moment m_a [99].

The governing equations are solved using a Rayleigh-Ritz approximation of the displacements w, which are represented by a combination of algebraic polynomials. The resulting equations of motion are written as the following generalized eigenvalue problem [78] in terms of the vector $\hat{\mathbf{q}}$ of the $n_x \times n_y$ amplitude coefficients $\hat{q}_{(ij)}$

$$\begin{bmatrix} 0 & \mathbf{I} \\ \left(\mathbf{K}_{aero}-\mathbf{K}_{struct}\right) & \mathbf{D}_{aero} \end{bmatrix}\begin{bmatrix} \hat{\mathbf{q}} \\ \lambda\hat{\mathbf{q}} \end{bmatrix}=\begin{bmatrix} \mathbf{I} & 0 \\ 0 & \mathbf{M}_{struct} \end{bmatrix}\lambda\begin{bmatrix} \hat{\mathbf{q}} \\ \lambda\hat{\mathbf{q}} \end{bmatrix} \tag{11}$$

where $\mathbf{M}_{struct}$, $\mathbf{D}_{aero}$, $\mathbf{K}_{aero}$ and $\mathbf{K}_{struct}$ are respectively, the structural mass matrix, the aerodynamic damping matrix, the aerodynamic stiffness matrix and the elastic stiffness matrix.

The critical flutter conditions are defined by $\Re\mathfrak{e}(\lambda)=0$ with corresponding flutter speed V_f and circular frequency ω_f. Details about the aeroelastic solver can be found in [73].

Random variable reduction using the Polar Method

The concept of lamination parameters [106] and polar method [108, 111] are two widely used approaches for the analysis and design of composite laminates. They provide a smaller set of parameters to describe the behavior of a laminate instead of considering the entire set of constitutive parameters. Therefore, they are particularly suited for propagating uncertainties in layer thicknesses and angles due to the manufacturing process, by reducing the number of random variables, thus making possible the use of the Polynomial-Chaos-based spectral projection method, for instance. Due to its natural ability to deal with uncertainty in ply thickness and its natural physical meaning, the polar method, which is based on tensor invariants was recently used by Nitschke *et al.* [73, 78] in the context of aeroelastic UQ of composite plates.

The polar method consists in describing the modified bending tensor $\tilde{\mathbf{D}}$ by the polar constants $\boldsymbol{\theta}=\left\{T_0^{\tilde{D}},T_1^{\tilde{D}},R_0^{\tilde{D}},R_1^{\tilde{D}},\Phi_0^{\tilde{D}},\Phi_1^{\tilde{D}}\right\}$, such as [108, 111]

$$\begin{aligned} \tilde{D}_{xx}&=T_0+2T_1+R_0\cos\left(4\Phi_0\right)+4R_1\cos\left(2\Phi_1\right) \\ \tilde{D}_{xy}&=-T_0+2T_1-R_0\cos\left(4\Phi_0\right) \\ \tilde{D}_{xs}&=R_0\sin\left(4\Phi_0\right)+2R_1\sin\left(2\Phi_1\right) \\ \tilde{D}_{yy}&=T_0+2T_1+R_0\cos\left(4\Phi_0\right)-4R_1\cos\left(2\Phi_1\right) \\ \tilde{D}_{ys}&=-R_0\sin\left(4\Phi_0\right)+2R_1\sin\left(2\Phi_1\right) \\ \tilde{D}_{ss}&=T_0-R_0\cos\left(4\Phi_0\right) \end{aligned} \tag{12}$$

where quantities T_0,T_1,R_0,R_1 and $\left(\Phi_0-\Phi_1\right)$ are invariants. The isotropic part of the tensor is represented by parameters T_0 and T_1, coefficients R_0 and R_1 are the modules of the anisotropic part and Φ_0 and Φ_1 are the corresponding orientation angles.

Figure 9 presents the flutter response of the studied cantilevered wing (Table 1) over the polar domain of nominally orthotropic and uncoupled laminates and considering that the principal orthotropy axis of the laminate is aligned with the wing mid-chord axis.

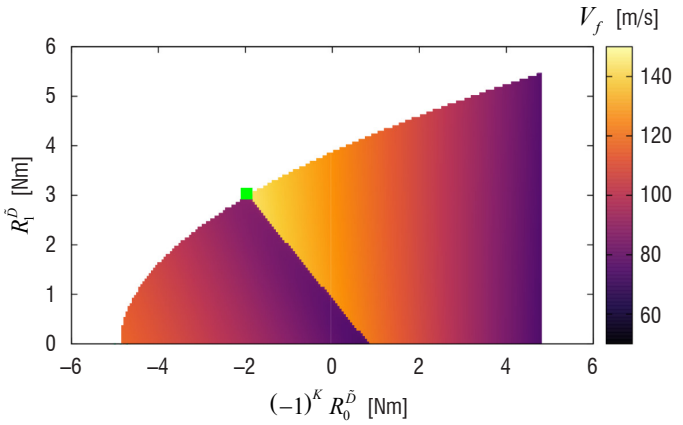

Figure 9 – Response surface of the critical flutter speed V_f defined in the polar domain for orthotropic laminates [78] for the cantilevered plate wing (Figure 8). The green dot corresponds to the configuration depicted in Table 3 and giving the maximum flutter speed.

We immediately remark a step in the critical flutter speed V_f, which separates the response surface into two sub-regions. This discontinuity illustrates the mode switch present in the aeroelastic instability mechanism of the studied configuration. We also note that the laminate configurations corresponding to the extreme values of V_f (V_f^{max}=148.5 m/s and V_f^{min} =76.3 m/s) are very close, approximately in the region close to the point $(-1)^K R_0^D = -1.948$ and $R_1^D = 3.032$ (green dot in Figure 9) apart from the step. This fact, clearly illustrates the need for considering uncertainties in the aeroelasticity analysis, since tolerance errors in the elastic stiffness of the composite laminate, due for instance to the manufacturing process, could lead to the worst flutter case, whereas it is designed to be the best flutter case within a deterministic framework.

In the following, we consider the layup configuration, which maximizes the flutter speed (see the green dot in Figure 9). The corresponding polar properties and stacking sequence are reported in Tables 3 and 4, respectively.

Next, we consider randomness in the ply angles and thicknesses, according to a Gaussian distribution with standard deviation of 1 [°] and 0.005 [mm] respectively. These parametric uncertainties in the sixteen-layer layup are propagated by Monte Carlo simulation, in order to characterize the *pdf* of the six polar constants (Equation 12). As illustrated by the scatter plot of $R_1^{\tilde{D}}$ against $T_0^{\tilde{D}}$ in Figure 10-left, the polar constants exhibit rather strong correlations depending on the configuration of the layup. Moreover, the resulting distributions no longer have a Gaussian shape, and they can be arbitrary symmetric or skew distributions, as shown in Figure 10-mid/right.

The fact that the random variables of the polar constants are not independent, with non-Gaussian distributions, is due to the nonlinear nature of the transformation in Equation 12. Therefore, the uncertainty quantification in the ply angles and thicknesses by means of polar constants requires conventional global-Polynomial-Chaos stochastic solvers to be adapted, in order to deal with (i) arbitrary input distributions, (ii) correlated random variables and (iii) discontinuity in the random space.

The first two points are addressed by using the arbitrary Polynomial Chaos method (aPC) presented in [70, 79, 82, 97, 120]. The latter point was treated by combining the aPC approach with machine-learning techniques, in order to identify clusters of points belonging to each sub-region of the response surface.

$T_0^{\tilde{D}}[Nm]$	$T_1^{\tilde{D}}[Nm]$	$(-1)^K R_0^{\tilde{D}}[Nm]$	$R_1^{\tilde{D}}[Nm]$	$\Phi_0^{\tilde{D}}[^\circ]$	$\Phi_1^{\tilde{D}}[^\circ]$	$V_f[m/s]$	$\omega_f\left[\frac{rad}{s}\right]$
7.288	6.538	–1.948	3.032	0	0	143.48	505.24

Table 3 – Polar properties and flutter response of the studied configuration, which corresponds to the maximum flutter speed $V_{f_{max}}$ in the response surface (Figure 9)

Stacking sequence	Property summary
$[28.4_2, -28.4_4, 28.4_2, -28.4_2, 28.4_4, -28.4_2]$	general orthotropic, $V_{f_{max}}$

Table 4 – Stacking sequence of the AS4/3502-based laminate corresponding to parameters given in Table 3

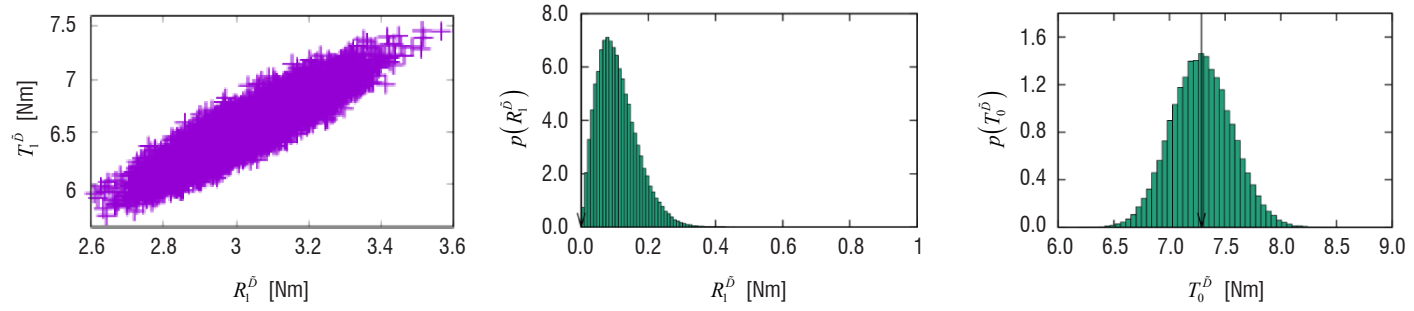

Figure 10 – Scatter plots and distributions of modified bending polar parameters $R_1^{\tilde{D}}$ and $T_0^{\tilde{D}}$ due to uncertainties in angular ply placement and thickness based on the nominal configuration of the composite laminates in Table 3 [78]

Dealing with correlations in the random polar parameters

As seen in Section "Uncertainty quantification using adaptive spectral methods", the spectral expansion in the stochastic space of the Polynomial Chaos methods relies on the use of the orthogonal polynomial basis Φ_i and expansion coefficients $\hat{u}_i$ (Equation 1). In order to be able to deal with arbitrary distributions and correlated variables, we follow the work by Navarro *et al.* [70, 120], in which a Gram-Schmidt algorithm is used to compute the coefficients of the polynomials based on the scalar product

$$\left\langle \phi_i, \phi_j \right\rangle = \int_{\boldsymbol{\Theta}} \phi_i(\boldsymbol{\theta}) \phi_j(\boldsymbol{\theta}) \, p(\boldsymbol{\theta}) d\boldsymbol{\theta} = \mathbb{E}\left\{ \phi_i(\boldsymbol{\theta})^2 \right\} \delta_{ij} \qquad (13)$$

Since no analytical representation of the joint distribution of the random polar constants is available, the integrals required for the computation of the coefficients of polynomials are derived from MC integration based on the analytical expression of the polar parameters in Equation 12. Moreover, a least-square fitting procedure is used to compute the expansion coefficients $\hat{u}_i$, based on MC draws in the random space. The extension of the aPC method to correlated random variables is detailed in [78].

UQ in the vicinity of the aeroelastic mode switch

In Section "Stochastic limit cycle oscillations of a supersonic lifting surface", the ME-gPC method was used to deal with discontinuities in the random space. Here, an alternative method is developed by combining the global support aPC solver with a machine learning-based filtering procedure in order to decompose the response surface according to different aeroelastic modal regimes. Note that Scarth *et al.* [94] have addressed the same aeroelastic problem by coupling the gPC method with the Rosenblatt transformation and convex hull identification for response surface splitting.

The present approach consists of two steps [73, 78]. First, the different modal regimes in the response surface are identified by applying the DBSCAN clustering algorithm [37] from a preliminary set of samples of the flutter speed V_f and frequency ω_f, requiring typically 10^3 calls to the aeroelastic solver.

Figure 11-left illustrates the identification step of the modal regimes due to the uncertainties defined in Section "Random variable reduction using the Polar Method", from the laminate presented in Table 3 and whose nominal configuration maximizes the flutter speed (green square symbol in Figure 9). Based on the preliminary sampling of V_f and ω_f, the DBSCAN algorithm succeeds in clustering the data as shown by the different colors of the clouds. The number of samples used in the aPC.

In the second step, a large set of samples of polar parameters, drawn from their analytical expression (Equation 12), are used (typically with size of 10^5), in conjunction with the training data from the clustering, by a neural network-type Multi-layer perceptron classifier [83], in order to generate filtered samples that are used for the construction of the polynomials in the aPC solver for each sub-region of the discontinuous response surface. Moreover, the fitting procedure in the aPC is performed using the clustered samples, thus avoiding any additional calls to the aeroelastic solver. Details about the implementation of the machine-learning approach used within the context of the aeroelastic aPC framework are given in [78].

The multi-modal aPC-machine learning classifier method was used to compute the distribution of the flutter speed shown in Figure 11-right for nominal conditions giving the maximum flutter speed. As expected, the bi-modal shape of the distribution relies on the mode switch as a consequence of randomness in the ply angles and thicknesses. The peak at high critical flutter speed is located near the nominal value $V_f = 143\, m/s$. The lower peak appears for a critical flutter speed around $V_f = 83\, m/s$. It is clear that, in the present case, the conventional flutter margin of $122\, m/s$, which corresponds to a 15% offset from the nominal value, fails to define a safety operational range, as confirmed by the computation of the 1% percentile (Figure 11-right).

Note that the comparison of the distribution of V_f with a Monte Carlo simulation shows that the present multi-modal aPC approach could be an interesting approach to propagate correlated parametric uncertainties with arbitrary input distribution in the presence of discontinuity in the random space.

Model-form uncertainty quantification in aeroelasticity

Although it was previously shown that parametric uncertainties can be efficiently propagated through an aeroelastic model to predict the stochastic response of the critical flutter speed or LCO amplitudes, epistemic uncertainties, which result from a lack of knowledge, may induce greater variability in the stochastic response than real physical randomness [103, 126]. Therefore, the quantification of model assumptions and predictive uncertainties [26, 81] should be taken into account in the prediction of the stochastic aeroelastic response.

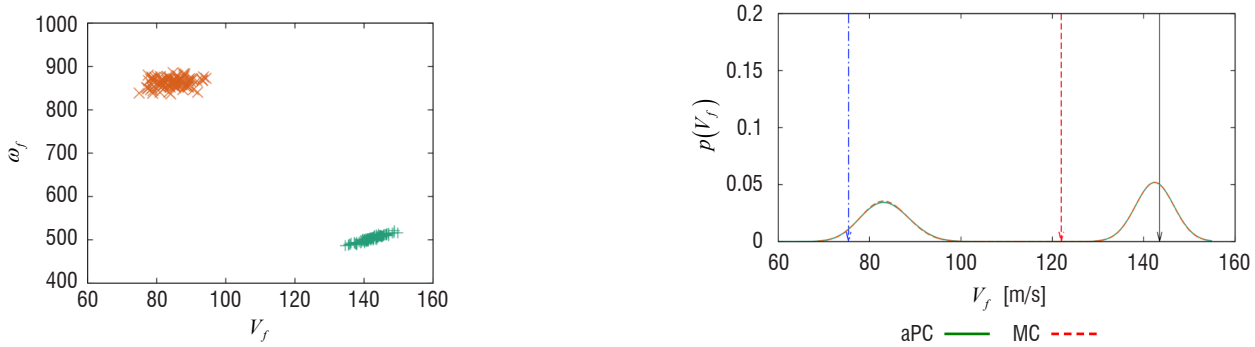

Figure 11 – Aeroelastic uncertainty propagation in ply angles and thicknesses of the sixteen-layer AS4/3502 graphite/epoxy laminate (Table 3). Left: Clouds of samples showing V_f plotted against ω_f and colored by the results of the DBSCAN clustering. Right: Multi-modal distribution of the flutter speed V_f computed using the machine learning augmented aPC method [79]. The solid black arrow indicates the nominal critical flutter speed, the red dashed arrow is the classical 15% flutter margin and the blue dash-dotted arrow indicates the 1% percentile for the occurrence of flutter.

Number of states	Reference	Function definition
Two states	Jones R.T [46]	$C(k) \approx 1.0 - \frac{0.165k}{k-0.0455i} - \frac{0.335k}{k-0.3i}$
	Jones W.P [47]	$C(k) \approx 1.0 - \frac{0.165k}{k-0.041i} - \frac{0.335k}{k-0.32i}$
	Riley [89]	$C(k) \approx \frac{(1.0+10.61ik)(1.0+1.774ik)}{(1.0+13.51ik)(1.0+2.745ik)}$
	Jones rounded [89]	$C(k) \approx \frac{0.015+0.3ik-0.5k^2}{0.015+0.35ik-k^2}$
Four states	Brunton [18]	$C(k) \approx \frac{0.5k^4-0.703ik^3-0.2393k^2+0.01894ik+2.32510^{-4}}{k^4-1.158ik^3-0.3052k^2+0.02028ik+2.32510^{-4}}$
	Vepa [110]	$C(k) \approx \frac{k^4-0.761ik^3-0.1021k^2+2.551i10^{-3}k+9.55710^{-6}}{2k^4-1.064ik^3-0.1134k^2+2.617i10^{-3}k+9.55710^{-6}}$

Table 5 – Approximations of the Theodorsen function used to construct the stochastic lift functions [75].

Typically, the choice of low- or high-fidelity structural and aerodynamic operators to be considered for aeroelastic simulations relies on model-form uncertainty, with possible uncertain parameters, which may strongly affect the prediction of the flutter boundary. Another important issue concerns the sensitivity of these models, which may strongly differ depending on the physical scenario of interest.

Such stochastic problems can be addressed using Bayesian inference methods for parameter calibration and model updating, as in [4, 16, 53]. First, a likelihood function must be built, based on prescribed prior distributions of model coefficients and observations of parameters of interest. Then, the Bayes theorem is applied to compute the joint posterior distribution of model parameters using Markov Chain Monte Carlo (MCMC) sampling. In this case, an adjusted stochastic model can be constructed using the Bayesian Model Averaging Approach (BMA) [42], where previously individual calibrated models are weighted using their posterior model probability.

A Bayesian estimation of structural uncertainties of the Goland wing was performed by Dwight *et al.* [35], in whose work the use of few observation data was sufficient to substantially reduce the variability in the parameters of the high-fidelity CFD/Finite Element aeroelastic solver. A BMA adjusted statistical model dedicated to the computation of the flutter margin of the 445.6 wing was deployed by Riley and Grandhi [88]. The same aeroelastic configuration was used by Riley [89] to predict both model-form and parametric uncertainties in the flutter margin, where the latter are propagated using the fast Fourier transform technique with a weighted-Stack Response Surface method.

Intensive research in the field of Bayesian parameter estimation for nonlinear aeroelasticity was carried out in a series of papers by Khalil *et al.* [48-50]. Initially, Markov Chain Monte Carlo (MCMC) algorithms were coupled to extended Kalman filter techniques to build the joint posterior distribution of LCO amplitude of a pitching NACA0012 airfoil in the presence of noisy experimental data. More computationally efficient methods were also considered, like parallel adaptive MCMC sampling algorithms [23, 90] and Bayesian Model Selection [49, 91, 92], for the calibration of a fully-unsteady nonlinear aerodynamic model using wind-tunnel test data. Finally, the Bayesian model averaging approach was used in [73-76] to build an adjusted PAPA-based aeroelastic model from different classes of stochastic aerodynamic operator.

Problem statement

The motivation of the work presented hereafter, relies on the existence of multiple approximations of the Theodorsen [104] lift function $C(k)$, which can be considered to evaluate the unsteady aerodynamic forces acting on the pitching and plunging flat plate in an incompressible flow [33, 39, 41, 121]. Some of these approximations are given by the general form [75, 77]

$$C(k) \approx 1 - \sum_{j=1}^{N} \frac{\alpha_j k}{k - \beta_j i} \tag{14}$$

where N is the number of states of the models.

As illustrated in Table 5 and in Figure 12, several approximations can be found in the literature, depending on the number of states and the values of coefficients α_j and β_j [18, 46, 47, 89, 110].

Table 6 summarizes the experimental data of V_f^* taken from [102] and obtained for four different values of the frequency ratio ω_h / ω_α of uncoupled natural frequencies in pitch and plunge.

scenario	A	B	C	D
ω_h/ω_α	0.33	0.5	0.83	1
V_f^*	10.67	9.19	6.41	7.30

Table 6 – Experimental dataset $\mathcal{D} = \{d_A, d_B, d_C, d_D\}$ for the critical flutter velocity V_f^*, corresponding to four values of ω_h/ω_α. The other aeroelastic parameters are considered to be fixed, namely r_α = 0.5, x_α = 0.2, a_h = –0.4, μ = 400 [102].

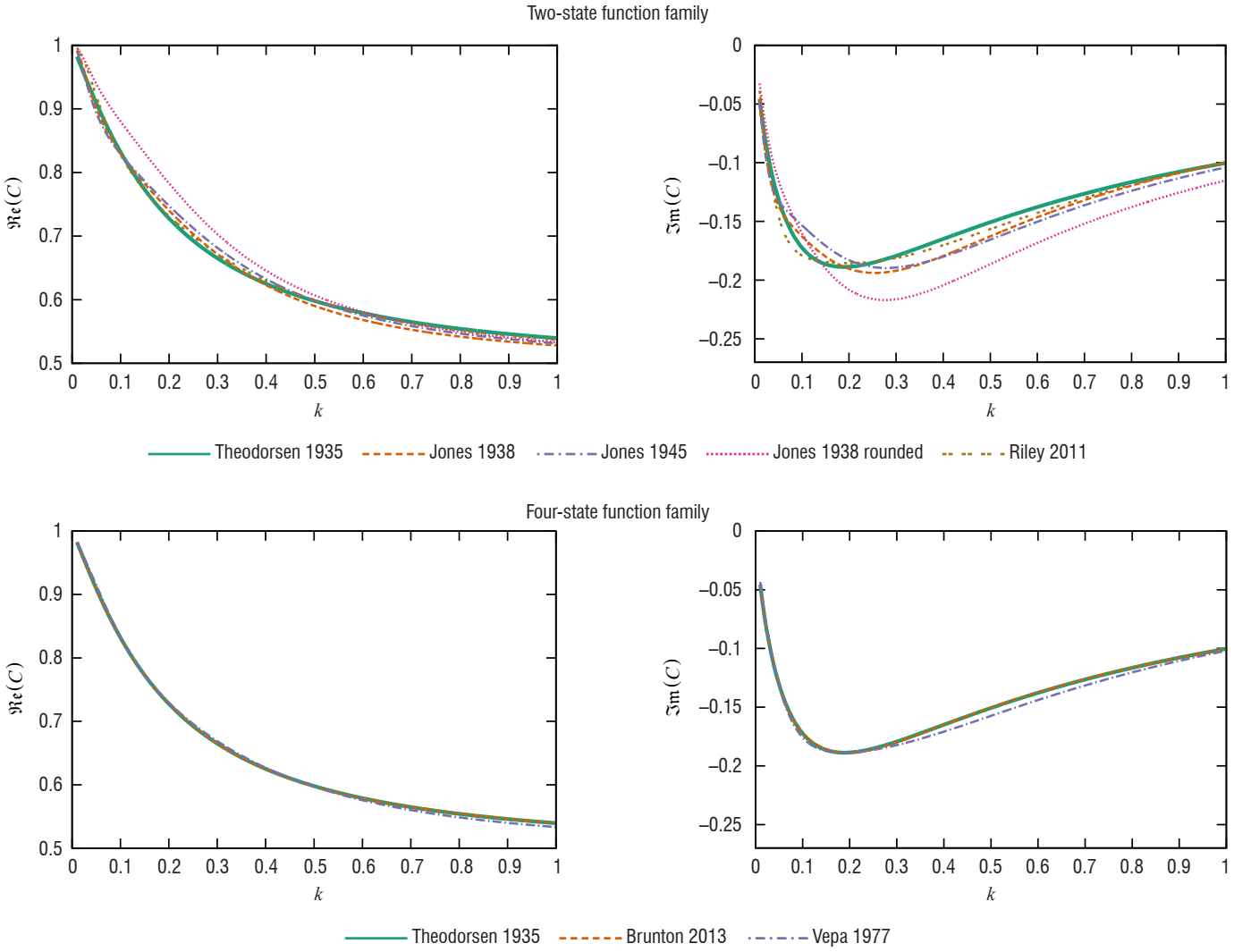

Figure 12 – Plots of typical approximations of the Theodorsen function $C(k)$ taken from [18, 75, 89] as described in Table 5.

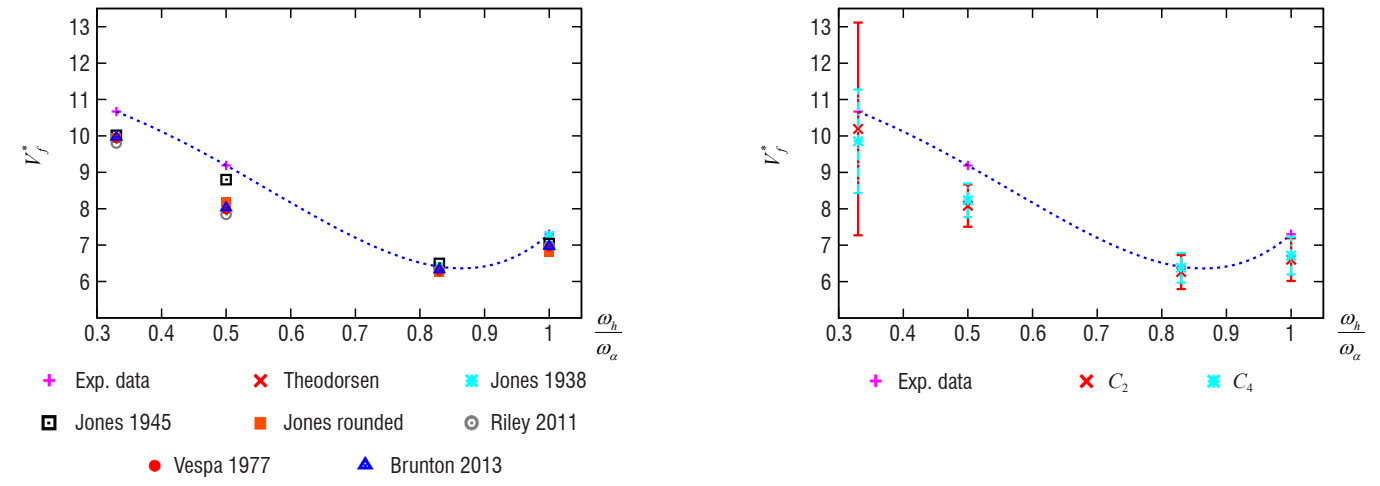

Figure 13 – Linear flutter boundary as a function of the ratio of uncoupled natural frequencies in pitch and plunge. Left: Comparison between experimental data [102] and values of the flutter speed V_f^* obtained from the approximations of the lift function $C(k)$ (Table 5). Right: Prior distributions of the model coefficients constructed according to Equation 15 using Monte Carlo sampling with 10^7 samples.

Figure 13-left shows the aeroelastic responses of a typical PAPA aeroelastic configuration, where the linear critical flutter velocity index V_f^* is computed using the iterative frequency-matching V-g method [13] for given parameters: $r_\alpha = 0.5$, $x_\alpha = 0.2$, $a_h = -0.4$, $\mu = 400$ [77]. Different spreads are observed, thus making the identification of the best approximation for all scenarios tricky.

Considering that the uncertainty associated with the choice of the more suitable model belongs to the family of epistemic model-form uncertainty, the Bayesian model averaging approach provides a theoretical framework to identify the most suited model of the lift function $C(k)$ and to calibrate its coefficients defined in Equation 14 within a stochastic framework. To this end, approximations shown in Table 5 are used to construct two stochastic models, depending on the number of states, by considering the following prior distributions for model coefficients $\tilde{\alpha}_j$ and β_j [73, 74]

$$\tilde{\alpha}_j \sim \mathcal{U}[0,1], \quad \beta_j \sim \mathcal{U}[0,0.9], \quad \tilde{\alpha}_j = \frac{\alpha_j}{\sum_{j=1}^{N} \alpha_j}, \quad j = 1,...,N \qquad (15)$$

Figure 13-right shows the mean and the 50% maximum credibility interval of the flutter speed obtained by Monte Carlo sampling of the two stochastic models C_2 and C_4, constructed respectively using 2 and 4 states in Equation 14 and according to the prior distributions of $\tilde{\alpha}_j$ and β_j in Equation 15. The two models are driven by extreme outliers, resulting in mean values possibly outside the 50% confidence intervals. The relatively large spread of the realizations suggests that calibrations of the stochastic model might be required.

Bayesian calibration using parameter inference

Bayesian inference techniques were considered in [74, 76, 77] for the reduction of the uncertainty associated with the choice of model parameters by calibrating model coefficients of model $M_1 = C_2$ and model $M_2 = C_4$, using the available experimental observations. Let y be the output of the deterministic aeroelastic model. The quantity of interest q, corresponding to the critical flutter velocity V_f^* in the present case, is modeled as the output of the deterministic aeroelastic model y plus a random error term ε due to model inadequacy or measurement error

$$q = y(\mathbf{x}, \boldsymbol{\theta}_i, M_i) + \varepsilon(\mu_i, \sigma_i, M_i) \qquad (16)$$

where $\mathbf{x}$ denotes the explicative aero-mechanical parameters and $\boldsymbol{\theta}_i$ represents the random model coefficients subject to epistemic uncertainties. The mean μ_i and the standard deviation σ_i are the hyperparameters that describe the error term ε, which is chosen to be Gaussian with zero mean [20]. Let $\mathcal{D}$ be the set of experimental data points $d_j\,(j = 1, n_d)$ of the flutter index V_f^*. The likelihood function, which corresponds to the probability of observing the data D given a model M_i, a set of parameters $\boldsymbol{\theta}_i$ and hyperparameters σ_i, is written as [8]

$$f_N(\mathcal{D}|\boldsymbol{\theta}_i, \sigma_i, M_i) = \Pi_{j=1}^{n_d} \frac{1}{\sqrt{2\pi\sigma_i^2}} \exp\left(-\frac{\left(d_j - y(\mathbf{x}_j, \boldsymbol{\theta}_i, M_i)\right)^2}{2\sigma_i^2} \right) \qquad (17)$$

The joint posterior distribution of the model parameters is computed using the Bayes rule as [8]

$$p(\boldsymbol{\theta}_i, \sigma_i | \mathcal{D}, M_i) \propto f_N(\mathcal{D}|\boldsymbol{\theta}_i, \sigma_i, M_i)\, p(\boldsymbol{\theta}_i, \sigma_i | M_i) \qquad (18)$$

where $p(\boldsymbol{\theta}_i, \sigma_i | M_i)$ is the joint prior probability density of the uncertain parameters and hyperparameters.

Figure 14-left presents the posterior distributions of hyperparameters whose prior distribution was taken as $p(\sigma_i | M_i) = \mathcal{U}[0.01, 0.7]$. Below values of $\sigma = 0.3$, the higher probability density values for model M_2 show that this model is able to yield more accurate results than model M_1.

Note that for $\sigma_i \to 0$, $p(\sigma|\mathcal{D}, \mathcal{M})$ vanishes, meaning that the models cannot reproduce the results without considering a discrepancy term. All computations are performed using hyperparameter inference [77], where the posterior parameter distributions for coefficient $\tilde{\beta}_1$ are presented in Figure 14-right. As expected, considering additional data leads to sharper distributions of the posterior *pdf* for the flutter speed.

Robust prediction of the stochastic models

Based on the posterior distribution of the random parameters $p(\boldsymbol{\theta}_i, \sigma_i | \mathcal{D}, M_i)$ in Equation 18, it is possible to predict an updated estimate of the quantity of interest, namely the marginal posterior predictive distribution for the critical flutter speed V_f [24]

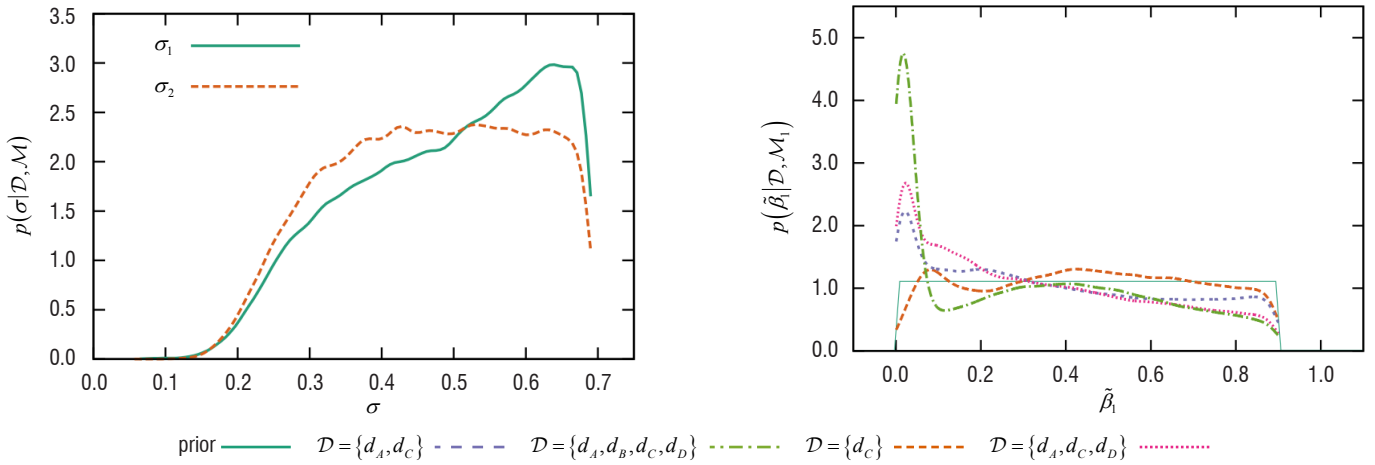

Figure 14 – Left: Kernel density estimations of the posterior distributions of σ_i for models M_1 and M_2. The prior distribution is $\sigma_i = \mathcal{U}[0.01, 0.7]$; Right: Influence of the size of the calibration dataset $\mathcal{D}$ (Table 6) on the posterior of model coefficients computed using hyperparameter inference with $\sigma_i \sim \mathcal{U}[0.01, 0.7]$.

$$p(q|\mathbf{x},\mathcal{D},M_i)=\int p(q|\mathbf{x},\boldsymbol{\theta}_i,\sigma_i,M_i)\,p(\boldsymbol{\theta}_i,\sigma_i|\mathcal{D},M_i)\,d\boldsymbol{\theta}_i d\sigma_i \quad (19)$$

$$\approx \frac{1}{n_s}\sum_{\ell=1}^{n_s} p(q|\mathbf{x},\boldsymbol{\theta}_i(\ell),\sigma_i(\ell),M_i) \quad (20)$$

where $\boldsymbol{\theta}_i(\ell)$ and $\sigma_i(\ell)$ are the ℓ-th sample of $p(\boldsymbol{\theta}_i,\sigma_i|\mathcal{D},M_i)$ used during the Monte Carlo integration procedure. The predictive distribution for a given set of parameters and hyperparameters $p(q|\mathbf{x},\boldsymbol{\theta}_i,\sigma_i,M_i)$ is defined by

$$p(q|\mathbf{x},\boldsymbol{\theta}_i,\sigma_i,M_i)=\frac{1}{\sqrt{2\pi\sigma_i^2}}\exp\left(-\frac{\left(q-y(\mathbf{x},\boldsymbol{\theta}_i,M_i)\right)^2}{2\sigma_i^2}\right) \quad (21)$$

Bayesian model averaging

Bayesian Model Averaging (BMA) is a statistical method [42] that accounts for the uncertainty in the selection of the model itself. The total predictive distribution $p(q|\mathbf{x},\mathcal{D})$ of the resulting BMA adjusted stochastic model is based on the average of the posterior predictive distributions of the two models, weighted by the posterior model probability of each individual model $\mathcal{M}_i$

$$p(q|\mathbf{x},\mathcal{D})=\sum_{i=1}^{m} p(q|\mathbf{x},\mathcal{D},M_i)P(M_i|\mathcal{D}) \quad (22)$$

where $p(q|\mathcal{D},\mathbf{x},M_i)$ is the robust or posterior predictive distribution of model M_i. The posterior model probability $P(M_i|\mathcal{D})$ is evaluated using Bayesian inference as

$$P(M_i|\mathcal{D})=\frac{P(\mathcal{D}|M_i)P(M_i)}{\sum_{j=1}^{m}P(\mathcal{D}|M_j)P(M_j)} \quad (23)$$

The prior model probability $P(M_i)$ is assumed to follow a uniform distribution. According to Cheung *et al.* [24], the marginal likelihood $P(\mathcal{D}|M_i)$ is given by

$$P(\mathcal{D}|M_i)=\int f_N(\mathcal{D}|\boldsymbol{\theta}_i,\sigma_i,M_i)\,p(\boldsymbol{\theta}_i|M_i)\,p(\sigma_i|M_i)\,d\boldsymbol{\theta}_i d\sigma_i \quad (24)$$

where the prior density $p(\boldsymbol{\theta}_i|M_i)$ is evaluated based on expert opinion.

Table 7 shows that the higher model probability is attributed to the four-state model M_2. The same conclusion holds when setting σ_i to a fixed deterministic value, or when including σ_i in the inference procedure, as described in Section "Bayesian calibration using parameter inference".

model error	$P(M_1\|\mathcal{D})$	$P(M_2\|\mathcal{D})$
$\sigma_i = 0.6$	0.3526	0.6474
$\sigma_i \sim \mathcal{U}[0.01,0.7]$	0.311	0.689

Table 7 – Posterior model probabilities $P(q|\mathbf{x},\mathcal{D},M_i)$ for calibration over $\mathcal{D}=\{d_A,d_C,d_D\}$ (Table 6) obtained from BMA with different modeling of the random error term $\varepsilon(\sigma_i,M_i)$ [77]

The total predictive distribution $p(q|\mathbf{x},\mathcal{D})_{determ.}$ for point d_B based on BMA of the deterministic (*e.g.,* non-calibrated) models, is presented in Figure 15. The most probable value for the flutter speed index is about $V_f^* \sim 8.1$, which is far from the experimental value given by $V_f^* \sim 9.19$. On the contrary, results obtained after individual

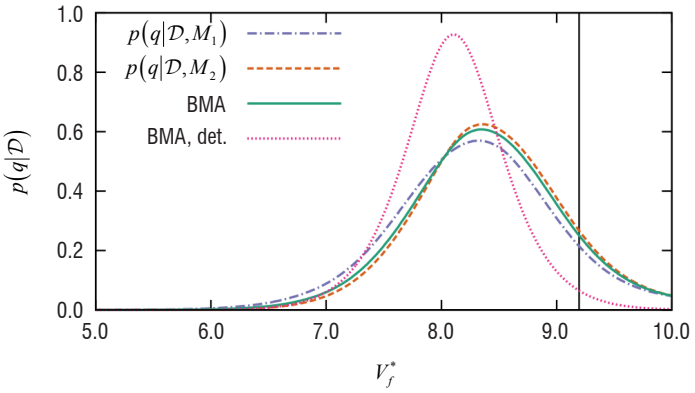

Figure 15 – Predictive distribution of the critical flutter velocity V_f^* for scenario d_B obtained by applying the BMA framework to model-form uncertainty in $C(k)$ with calibrated stochastic coefficients $\tilde{\alpha}_j$ and β_j in Equation 15 ($\mathcal{D}=\{d_A,d_C,d_D\}$ (Table 6) and $\sigma_i \sim \mathcal{U}[0.01,0.7]$ [78])

calibrations of models M_1 and M_2 over dataset $\mathcal{D}=\{d_A,d_C,d_D\}$ clearly show the benefit of calibrating the coefficients of the lift function $C(k)$, since their probability density values for the sought value of V_f^* are higher than those for the deterministic BMA.

The differences between the individual models after the Bayesian inference step are relatively small. Quite similar results are thus expected to be observed for the total predictive distribution given by BMA. Attempts were made in [77] to reduce the confidence intervals of the prediction of V_f^* by introducing a bias relative to the error term used in the Bayesian inference procedure.

Concluding remarks

This paper reviewed some recent development for the study of canonical aeroelastic systems under uncertainties. Forward stochastic analysis of parametric uncertainties in the aero-mechanical parameters were performed within the framework of Polynomial-Chaos-based approaches. Adaptive multi-element generalized Polynomial Chaos and machine learning-augmented arbitrary Polynomial Chaos were successfully used for capturing the multi-modal behavior of the stochastic critical flutter velocity or limit-cycle-oscillations. In particular, the study of variabilities in ply angles and thicknesses of composite laminate layups on the aeroelastic flutter of a cantilevered plate wing was performed. Due to the presence of a mode switch mechanism in the aeroelastic response, a dramatic reduction in the linear flutter speed was observed compared to values obtained from classical safety margins. Finally, the effects of model-form and predictive uncertainties on the flutter boundary of an elastically-mounted pitch and plunge airfoil were investigated within the framework of Bayesian uncertainty quantification. To this end, Bayesian inference was used for the stochastic calibration of the coefficients of two low-order aerodynamic models. Then, a Bayesian Model Averaging method was used to construct an adjusted stochastic model with robust predictive capabilities, where substantial reductions in the variability of the flutter boundary were obtained compared to the application of the BMA approach on deterministic aerodynamic models.

It is believed that forward uncertainty quantification in high-fidelity-based aeroelastic systems will quickly benefit from the development of advanced stochastic tools for the propagation of parametric

uncertainties in canonical aeroelastic problems with discontinuous response. In particular, improvement in the prediction of the stochastic flutter boundary of complete aeroelastic aircraft configuration in the transonic flight regime are expected, by combining CFD-based aeroelastic solvers with adaptive sparse stochastic solvers [14, 87]. Although probabilistic methods are not well-suited for the accurate estimation of quantiles and probability of failure, attempts to deal with the use of polynomial chaos for robust design and the computation of failure probabilities can be found in [34, 69, 80, 104] and could be considered for reliable aeroelastic stability analysis. Moreover, variable-fidelity and multi-fidelity surrogate modeling [6, 19, 71, 95] can be used to further reduce the computation cost by combining machine learning tools and Bayesian Inference steps for the calibration of low-order aeroelastic models and observations gained from possibly CFD-based higher-fidelity models.

Due to their ability to identify or verify parameter values in the presence of model-form uncertainties, Bayesian approaches could help in constructing an adjusted stochastic model for reliable predictions of the flutter boundary. However, several issues remain to be addressed. First, the considered data sets must be sufficiently large, in order to avoid strong sensitivity of the adjusted model to the calibration data ideally, the posterior distributions should no longer vary when additional observations are added. Thus, this would lead to the construction of specially-designed aeroelastic databases for a large range of realistic scenarios. Secondly, efficient methods will be required to overcome the computational burden due to the use of CFD-based aeroelastic analysis within the Bayesian framework. To this end, surrogates based on Polynomial Chaos or stochastic collocation could be incorporated into the Bayesian inference step [3, 28, 60, 63, 105] ■

References

[1] B. M. ADAMS, L. E. BAUMAN, W. J. BOHNHOFF , K. R. DALBEY, M. S. EBEIDA, J. P. EDDY, M. S. ELDRED, P. D. HOUGH, K. T. HU, J. D. JAKEMAN, L. P. SWILER, D. M. VIGIL - *Dakota, a Multilevel Parallel Object-Oriented Framework for Design Optimization, Parameter Estimation, Uncertainty Quantification, and Sensitivity Analysis: Version 5.4 User's Manual*. Sandia Technical Report SAND2010-2183, December 2009. Updated April 2013, 2013.

[2] FEDERAL AVIATION ADMINISTRATION. *Aeroelastic Stability Substantiation of Transport Category Airplanes*. Advisory Circular 25.629-1B, U.S. Department of Transportation, Federal Aviation Administration, Washington, D.C., October 2014.

[3] M. ARNST, R. GHANEM, C. SOIZE - *Identification of Bayesian Posteriors for Coefficients of Chaos Expansions*. Journal of Computational Physics, 229(9):3134-3154, 2010.

[4] R. ASTER, B. BORCHERS, C. THURBER - *Parameter Estimation and Inverse Problems*. Elsevier, second edition edition, 2012.

[5] I. BABUŠKA, F. NOBILE, R. TEMPONE - *A Stochastic Collocation Method for Elliptic Partial Differential Equations with Random Input Data*. SIAM Journal on Numerical Analysis, 45(3):1005-1034, 2007.

[6] K. J. BADCOCK, S. TIMME, S. MARQUES, H. KHODAPARAST, M. PRANDINA, J. E. MOTTERSHEAD, A. SWIFT, A. DA RONCH, M. A. WOODGATE - *Transonic Aeroelastic Simulation for Instability Searches and Uncertainty Analysis*. Progress in Aerospace Sciences, 47(5):392-423, 2011.

[7] M. BAUDIN, A. DUTFOY, B. IOOSS, A.-L. POPELIN - *OpenTURNS: An Industrial Software for Uncertainty Quantification in Simulation*. Pages 1-38, Springer International Publishing, Cham, 2016.

[8] J. L. BECK, L. S. KATAFYGIOTIS - *Updating Models and their Uncertainties. I: Bayesian Statistical Framework*. Journal of Engineering Mechanics, 124:455-461, 1998.

[9] P. BERAN, B. STANFORD - *Uncertainty Quantification in Aeroelasticity*. Lecture Notes in Computational Science and Engineering, 92:59-103, 2013.

[10] P. BERAN, B. STANFORD, C. SCHROCK - *Uncertainty Quantification in Aeroelasticity*. Annual Review of Fluid Mechanics, 49(1):361-386, 2017.

[11] P. S. BERAN, C. L. PETTIT - *A Direct Method for Quantifying Limit-Cycle Oscillation Response Characteristics in the Presence of Uncertainties*. AIAA Paper 2004-1695, 2004.

[12] P. S. BERAN, C. L. PETTIT, D. R. MILLMAN - *Uncertainty Quantification of Limit-Cyle Oscillations*. Journal of Computational Physics, 217:217-247, 2006.

[13] R. L. BISPLINGHOFF, H. ASHLEY, R. L. HALFMAN, editors - *Aeroelasticity*. Addison-Wesley, 1955.

[14] G. BLATMAN, B. SUDRET - *Sparse Polynomial Chaos Expansions and Adaptive Stochastic Finite Elements using a Regression Approach*. Comptes Rendus Mécanique, 336(6):518-523, 2008.

[15] D. BORGLUND - *The $\mu - k$ Method for Robust Flutter Solutions*. Journal of Aircraft, 41(5):1209-1216, 2004.

[16] G.E.P. Box, G. C. TIAO - *Bayesian Inference in Statistical Analysis*. Wiley, 1973.

[17] L. BRUNO, C. CANUTO, D. FRANSOS - *Stochastic Aerodynamics and Aeroelasticity of a Flat Plate via Generalised Polynomial Chaos*. Journal of Fluids and Structures, 25:1158-1176, 2009.

[18] S. L. BRUNTON, C. W. ROWLEY - *Empirical State-Space Representations for Theodorsen's Lift Model*. Journal of Fluids and Structures, 38:174-186, 2013.

[19] D. E. BRYSON, M. P. RUMPFKEIL - *Variable-Fidelity Surrogate Modeling of Lambda Wing Transonic Aerodynamic Performance*. AIAA Paper No. 2016- 0294.

[20] B. P. CARLIN, T. A. LOUIS - *Bayesian Methods for Data Analysis*. Number 78 in Chapman & Hall, CRC texts in statistical science series. CRC Press, Boca Raton, Fla., 3. ed edition, 2009.

[21] J.-C. CHASSAING, D. LUCOR, J. TRÉGON - *Stochastic Nonlinear Aeroelastic Analysis of a Supersonic Lifting Surface using an Adaptive Spectral Method*. Journal of Sound and Vibration, 331:394-411, 2012.

[22] X. CHEN, Z. QIU - *A Novel Uncertainty Analysis Method for Composite Structures with Mixed Uncertainties Including Random and Interval Variables*. Composite Structures, 184:400-410, 2018.

[23] S. H. CHEUNG, J. L. BECK - *Bayesian Model Updating using Hybrid Monte Carlo Simulation with Application to Structural Dynamic Models with many Uncertain Parameters*. Journal of Engineering Mechanics, 135:243-255, 2009.

[24] S. H. CHEUNG, T. A. OLIVER, E. E. PRUDENCIO, S. PRUDHOMME, R. D. MOSER - *Bayesian Uncertainty Analysis with Applications to Turbulence Modeling*. Reliability Engineering and System Safety, 96:1137-1149, 2011.

[25] B. CHOUVION, E. SARROUY - *Development of Error Criteria for Adaptive Multi-Element Polynomial Chaos Approaches*. Mechanical Systems and Signal Processing, 66-67:201-222, 2016.

[26] M. CLYDE, E. I. GEORGE - *Model Uncertainty*. Statistical Science, 19:81-94, 2004.

[27] B. D. COLLER, P. A. CHAMARA - *Structural Non-Linearities and the Failure of the Classic Flutter Instability*. Journal of sound and vibration, 277:711-739, 2004.

[28] A. A. CONTRERAS, O. P. LE MAÎTRE, W. AQUINO, O. M. KNIO - *Multi-Model Polynomial Chaos Surrogate Dictionary for Bayesian Inference in Elasticity Problems*. Probabilistic Engineering Mechanics, 46:107-119, 2016.

[29] Y. DAI, C. YANG - *Methods and Advances in the Study of Aeroelasticity with Uncertainties*. Chinese Journal of Aeronautics, 27(3):461-474, 2014.

[30] B. P. DANOWSKY, J. R. CHRSTOS, D. H. KLYDE, C. FARHAT, M. BRENNER - *Evaluation of Aeroelastic Uncertainty Analysis Methods*. Journal of Aircraft, 47(4), 2010.

[31] J. DENG, C. ANTON, Y.S. WONG - *Uncertainty Investigations in Nonlinear Aeroelastic Systems*. Journal of Computational and Applied Mathematics, 235(13):3910-3920, 2011. Engineering and Computational Mathematics: A Special Issue of the International Conference on Engineering and Computational Mathematics, 27-29 May 2009.

[32] A. DESAI, S. SARKAR - *Uncertainty Quantification and Bifurcation Behavior of an Aeroelastic System*. ASME 2010, Paper FEDSM-ICNMM2010-30050, August 1-5, 2010 Montréal, Quebec, Canada, 2010.

[33] E. H. DOWELL, E. F. CRAWLEY, H. C. CURTISS Jr, D. A PETERS, R. H. SCANLAN, F. SISTO - *A Modern Course in Aeroelasticity.* Kluwer academic publishers edition, 1995.

[34] V. DUBOURG, B. SUDRET, F. DEHEEGER - *Metamodel-Based Importance Sampling for Structural Reliability Analysis*. Probabilistic Engineering Mechanics, 33:47-57, 2013.

[35] R. DWIGHT., H. BIJL, S. MARQUES, K. BADCOCK - *Reducing Uncertainty in Aeroelastic Boundaries Using Experimental Data*. International Forum of Aeroelasticity and Structural Dynamics, 2011.

[36] M. S. ELDRED, J. BURKARDT - *Comparison of Non-Intrusive Polynomial Chaos and Stochastic Collocation Methods for Uncertainty Quantification.* AIAA Paper No. 2009-0976, 2009.

[37] M. ESTER, H.-P. KRIEGEL, J. SANDER, X. XU - *A Density-Based Algorithm for Discovering Clusters in Large Spatial Databases with Noise.* Proceedings of the Second International Conference on Knowledge Discovery and Data Mining, volume 96, pp. 226-231, 1996.

[38] J. FEINBERG, H. P. LANGTANGEN - *Chaospy: an Open Source Tool for Designing Methods of Uncertainty Quantification*. Journal of Computational Science, 11:46-57, 2015.

[39] Y. C. FUNG - *An Introduction to the Theory of Aeroelasticity*. Dover Publications, Inc., dover edition, 1993.

[40] R. GHANEM, P. D. SPANOS - *Stochastic Finite Elements: a Spectral Approach*. Springer-Verlag, New York, 1991.

[41] D. H. HODGES, G. A. PIERCE, editors - *Introduction to Structural Dynamics and Aeroelasticity.* Cambridge University Press, 2002.

[42] J. A. HOETING, D. MADIGAN, A. E. RAFTERY, C. T. VOLINSKY - *Bayesian Model Averaging: a Tutorial*. Statistical Science, 14:382-417, 1999.

[43] S. J. HOLLOWELL, J. DUGUNDJI - *Aeroelastic Flutter and Divergence of Stiffness Coupled, Graphite/Epoxy Cantilevered Plates*. Journal of Aircraft, 21(1):69-76, January 1984.

[44] S. HOSDER, R. W. WALTERS, R. PEREZ - *A Non-Intrusive Polynomial Chaos Method for Uncertainty Propagation in CFD Simulations*. AIAA Paper 2006-891, 2006.

[45] S. HOSDER, R. W. WALTERS, M. BALCH - *Point-Collocation Nonintrusive Polynomial Chaos Method for Stochastic Computational Fluid Dynamics.* AIAA Journal, 48(12):2721-2730, 2010.

[46] R. T. JONES - *Operational Treatment of the Nonuniform-Lift Theory in Airplane Dynamics*. Technical Report 667, National Advisory Committee for Aeronautics, 1938.

[47] W. P. JONES - *Aerodynamic Forces on Wings in Nonuniform Motion.* Technical Report 2117, Aeronautical Research Council, 1945.

[48] M. KHALIL, D. POIREL, A. SARKAR - *Probabilistic Parameter Estimation of a Fluttering Aeroelastic System in The Transitional Reynolds Number Regime*. Journal of Sound and Vibration, 332:3670-3691, 2013.

[49] M. KHALIL, D. POIREL, A. SARKAR - *Bayesian Analysis of the Flutter Margin Method in Aeroelasticity*. Journal of Sound and Vibration, 384:56-74, 2016.

[50] M. KHALIL, A. SARKAR, D. POIREL - *Application of Bayesian Inference to the Flutter Margin Method: New Developments.* ASME Conference Proceedings, FEDSM-ICNMM2010-30041, 2010.

[51] N. LAMORTE, B. GLAZ, P. P. FRIEDMANN, A. J. CULLER, A.R. CROWELL, J.J. MCNAMARA - *Uncertainty Propagation in Hypersonic Aerothermoelastic Analysis.* AIAA Paper 2010-2964, 2010.

[52] J. LE MEITOUR, D. LUCOR, J.-C. CHASSAING - *Prediction of Stochastic Limit Cycle Oscillations Using an Adaptive Polynomial Chaos Method.* Journal of Aeroelasticity and Structural Dynamics, 2(1):1-20, 2010.

[53] D. LEAMER, editor - *Specification Searches*. John Wiley & Sons, 1978.

[54] B. H. K. LEE, L. Y. JIANG, Y. S. WONG - *Flutter of an Airfoil with Cubic Restoring Force*. Journal of fluids and structures, 13:75-101, 1999.

[55] B. H. K. LEE, L. LIU, K. W. CHUNG - *Airfoil Motion in Subsonic Flow with Strong Cubic Nonlinear Restoring Forces*. Journal of Sound and Vibration, 281:699-717, 2005.

[56] B. H. K. LEE, S. J. PRICE, Y. S. WONG - *Nonlinear Aeroelastic Analysis of Airfoils: Bifurcation and Chaos*. Progress in aerospace sciences, 35:205-334, 1999.

[57] L. LIBRESCU, G. CHIOCCHIA, P. MARZOCCA - *Implications of Cubic Physical/Aerodynamic Non-Linearities on the Character of The Flutter Instability Boundary*. International Journal of Non-Linear Mechanics, 38:173-199, 2003.

[58] R. LIND, M. BRENNER - *Robust Aeroservoelastic Stability Analysis: Flight-Test Applications*. Volume Chaps. 8, 9. Advances in Industrial Control, Springer-Verlag, London, 1999.

[59] M. LOKATT - *Aeroelastic Flutter Analysis Considering Modeling Uncertainties.* Journal of Fluids and Structures, 74:247-262, 2017.

[60] X. MA, N. ZABARAS - *An Efficient Bayesian Inference Approach to Inverse Problems Based on an Adaptive Sparse Grid Collocation Method*. Inverse Problems, 25(3):035013, 2009.

[61] A. MANAN, J. E. COOPER - *Prediction of Uncertain Frequency Response Function Bounds using Polynomial Chaos Expansion.* Journal of Sound and Vibration, 329(16):3348-3358, 2010.

[62] S. MARELLI , B. SUDRET - *UQLab: A Framework for Uncertainty Quantification in Matlab*. Vulnerability, Uncertainty, and Risk, Proc. 2nd Int. Conf. on Vulnerability, Risk Analysis and Management (ICVRAM2014), Liverpool, United Kingdom, 2554-2563, 2014.

[63] Y. M. MARZOUK, H. N. NAJM - *Dimensionality Reduction and Polynomial Chaos Acceleration of Bayesian Inference in Inverse Problems*. Journal of Computational Physics, 228(6):1862-1902, 2009.

[64] R. E. MELCHERS - *Structural Reliability Analysis and Predictions*. Wiley, New York, 1999.

[65] D. R. MILLMAN - *Quantifying Initial Conditions and Parametric Uncertainties in a Nonlinear Aeroelastic System With an Efficient Stochastic Algorithm*. Technical report, PhD. Dissertation, Air Force Institute of Technology, september 2004.

[66] D. R. MILLMAN, P. I. KING, P. S. BERAN - *Airfoil Pitch-and-Plunge Bifurcation Behavior with Fourier Chaos Expansions*. Journal of Aircraft, 42(2):376-384, 2005.

[67] M. D. MINICH, C. C. CHAMIS - *Analytical Displacements and Vibrations of Cantilevered Unsymmetric Fiber Composite Laminates.* AIAA, ASME, and SAE, Structures, Structural Dynamics, and Materials Conference, Denver, Colorado, January 1975.

[68] J. P. MURCIA, P.-E. RÉTHORÉ, N. DIMITROV, A. NATARAJAN, J. D. SØRENSEN, P. GRAF, T. KIM - *Uncertainty Propagation through an Aeroelastic Wind Turbine Model using Polynomial Surrogates*. Renewable Energy, 119:910-922, 2018.

[69] V. NAIR, S. SARKAR, R. I. SUJITH - *Uncertainty Quantification of Subcritical Bifurcations*. Probabilistic Engineering Mechanics, 34:177-188, 2013.

[70] M. NAVARRO, J. WITTEVEEN, J. BLOM - *Polynomial Chaos Expansion for General Multivariate Distributions with Correlated Variables*. Technical report, Centrum Wiskunde & Informatica, 2014.

[71] L. W. T. NG, M. S. ELDRED - *Multifidelity Uncertainty Quantification using Non-Intrusive Polynomial Chaos and Stochastic Collocation*. 53rd AIAA Structures, Structural Dynamics, and Materials Conference, AIAA, pp. 1-17, April 2012.

[72] M. NIKBAY, P. ACAR - *Robust Aeroelastic Design Optimization of Wing/Store Configurations Based on Flutter Criteria*. 14th AIAA/ISSMO Multidisciplinary Analysis and Optimization (MAO) Conference, September 2012.

[73] C. NITSCHKE - *Quantification of Aleatory and Epistemic Uncertainties in the Prediction of Aeroelastic Instabilities*. PhD thesis, UNIVERSITÉ PIERRE ET MARIE CURIE, Feb. 2018.

[74] C. T. NITSCHKE, J.-C. CHASSAING - *Acceleration of Bayesian Calibration for Predictive Uncertainty Quantification in Aeroelastic Flutter.* ECCOMAS Congress, June 5-10, Creete, Greece, 2016.

[75] C. T. NITSCHKE, J.-C. CHASSAING, P. CINNELLA, D. LUCOR - *Quantification of Model-Form Uncertainty in Nonlinear Aeroelasticity.* WCCM XI, Barcelona, Spain, 20-25 July, 2014.

[76] C. T. NITSCHKE, J.-C. CHASSAING, P. CINNELLA, D. LUCOR - *Bayesian Calibration and Uncertainty Analysis for Airfoil Flutter Predictions*. UNCECOMP 2015, 25-27 May, Crete Island, Greece, 2015.

[77] C. T. NITSCHKE, P. CINNELLA, D. LUCOR, J.-C. CHASSAING - *Model-Form and Predictive Uncertainty Quantification in Linear Aeroelasticity*. Journal of Fluids and Structures, 73:137-161, 2017.

[78] C. T. NITSCHKE, A. VINCENTI, J.-C. CHASSAING - *Uncertainty Quantification in the Vicinity of Mode Switches in the Flutter Response of a Composite Cantilevered Wing*. International Forum on Aeroelasticity and Structural Dynamics, IFASD 2017, 25-28 June 2017 Como, Italy, 2017.

[79] S. OLADYSHKIN, W. NOWAK - *Data-Driven Uncertainty Quantification using the Arbitrary Polynomial Chaos Expansion*. Reliability Engineering and System Safety, 106:179-190, 2012.

[80] M. PAFFRATH, U. WEVER - *Adapted Polynomial Chaos Expansion for Failure Detection*. Journal of Computational Physics, 226(1):263-281, 2007.

[81] I. PARK, H. K. AMARCHINTA, R. V. GRANDHI - *A Bayesian Approach for Quantification of Model Uncertainty*. Reliability Engineering and System Safety, 95:777-785, 2010.

[82] J. A. PAULSON, E. A. BUEHLER, A. MESBAH - *Arbitrary Polynomial Chaos for Uncertainty Propagation of Correlated Random Variables in Dynamic Systems*. IFAC-PapersOnLine, 50(1):3548-3553, 20th IFAC World Congress, 2017.

[83] F. PEDREGOSA, G. VAROQUAUX, A. GRAMFORT, V. MICHEL, B. THIRION, O. GRISEL, M. BLONDEL, P. PRETTENHOFER, R. WEISS, V. DUBOURG, J. VANDERPLAS, A. PASSOS, D. COURNAPEAU, M. BRUCHER, M. PERROT, E. DUCHESNAY - *Scikit-learn: Machine Learning in Python*. Journal of Machine Learning Research, 12:2825-2830, 2011.

[84] C. L. PETTIT - *Uncertainty Quantification in Aeroelasticity: Recent Results and Research Challenges*. Journal of Aircraft, 41:1217-1229, 2004.

[85] C. L. PETTIT, P. S. BERAN - *Effects of Parametric Uncertainty on Airfoil Limit Cycle Oscillation*. Journal of Aircraft, 40(5):1004-1006, 2003.

[86] V. M. RAO, A. BEHAL, P. MARZOCCA, C. M. RUBILLO - *Adaptative Aeroelastic Vibration Suppression of a Supersonic Airfoil With Flap*. Aerospace Science and Technology, 10:309-315, 2006.

[87] A. RESMINI, J. PETER, D. LUCOR - *Sparse Grids-Based Stochastic Approximations with Applications to Aerodynamics Sensitivity Analysis*. International Journal for Numerical Methods in Engineering, 106(1):32-57, 2016.

[88] M. E. RILEY, R. V. GRANDHI - *Quantification of Model-Form and Predictive Uncertainty for Multi-Physics Simulation.* Computers and Structures, 89:1206-1213, 2011.

[89] M. E. RILEY - *Quantification of Model-Form, Predictive, and Parametric Uncertainties in Simulation-Based Design*. PhD thesis, Wright State University, 2011.

[90] R. SANDHU, M. KHALIL, A. SARKAR, D. POIREL - *Bayesian Model Selection for Nonlinear Aeroelastic Systems using Wind-Tunnel Data*. Computer Methods in Applied Mechanical Engineering, 282:161-183, 2014.

[91] R. SANDHU, C. PETTIT, M. KHALIL, D. POIREL, A. SARKAR - *Bayesian Model Selection using Automatic Relevance Determination for Nonlinear Dynamical Systems*. Computer Methods in Applied Mechanics and Engineering, 320:237-260, 2017.

[92] R. SANDHU, D. POIREL, C. PETTIT, M. KHALIL, A. SARKAR - *Bayesian Inference of Nonlinear Unsteady Aerodynamics from Aeroelastic Limit Cycle Oscillations*. Journal of Computational Physics, 316:534-557, 2016.

[93] S. SARKAR, J. A. S. WITTEVEEN, A. LOEVEN, H. BIJL - *Effect of Uncertainty on the Bifurcation Behavior of Pitching Airfoil Stall Flutter.* Journal of Fluids and Structures, 25(2):304-320, 2009.

[94] C. SCARTH, J. E. COOPER, P. M. WEAVER, G.H.C. SILVA - *Uncertainty Quantification of Aeroelastic Stability of Composite Plate Wings using Lamination Parameters*. Composite Structures, 116:84-93, September 2014.

[95] H. SHAH, S. HOSDER, S. KOZIEL, Y. A. TESFAHUNEGN, L. LEIFSSON - *Multi-Fidelity Robust Aerodynamic Design Optimization under Mixed Uncertainty*. Aerospace Science and Technology, 45:17-29, 2015.

[96] I. M. SOBOL - *Global Sensitivity Indices for Nonlinear Mathematical Models and their Monte Carlo Estimates.* Mathematics and Computers in Simulation, 55:271-280, 2001.

[97] C. SOIZE, R. GHANEM - *Physical Systems with Random Uncertainties: Chaos Representations with Arbitrary Probability Measure*. SIAM Journal on Scientific Computing, 26(2):395-410, January 2004.

[98] B. K. STANFORD, S. J. MASSEY - *Uncertainty Quantification of the Fun3d-Predicted Nasa Crm Flutter Boundary*. AIAA Paper No. AIAA-2017-1816, 2017.

[99] O. STODIECK, J. E. COOPER, P. M. WEAVER, P. KEALY - *Improved Aeroelastic Tailoring Using Tow-Steered Composites.* Composite Structures, 106:703-715, December 2013.

[100] M. A. TATANG, W. PAN, R. G. PRINN, G. J. MCRAE - *An Efficient Method for Parametric Uncertainty Analysis of Numerical Geophysical Model*. Journal of Geophysical Research Atmospheres, 102(18):21925-21932, September 1997.

[101] M. T. THANUSHA, S. SARKAR - *Uncertainty Quantification of Subcritical Nonlinear Aeroelastic System using Integrated Interpolation Method and Polynomial Chaos Expansion*. Procedia Engineering, 144:982-989, 2016. International Conference on Vibration Problems 2015.

[102] T. THEODORSEN - *General Theory of Aerodynamic Instability and the Mechanism of Flutter.* Technical Report 496, National Advisory Committee for Aeronautics, 1935.

[103] J. P. THOMAS, E. H. DOWELL, K. C. HALL - *An Investigation of the Sensitivity of F-16 Fighter Flutter Onset and Limit Cycle Oscillations to Uncertainties*. Volume 5 of AIAA/ASME/ASCE/AHS/ASC Structures, Structural Dynamics and Materials Conference, pp. 3137-3144, 2006.

[104] A. J. TORII, R. H. LOPEZ, L. F. F. MIGUEL - *Probability of Failure Sensitivity Analysis using Polynomial Expansion.* Probabilistic Engineering Mechanics, 48:76-84, 2017.

[105] H. A. TRAN, C. G. WEBSTER, G. ZHANG - *A Sparse Grid Method for Bayesian Uncertainty Quantification with Application to Large Eddy Simulation Turbulence Models.* ArXiv e-prints, 2015.

[106] S. W. TSAI, H. T. HAHN - *Introduction to Composite Materials*. Technomic Publ, Lancaster, Pa., 1980.

[107] U.S. DEPARTMENT OF DEFENSE - *Composite Materials Handbook.* U.S. Department of Defense, June 2002.

[108] P. VANNUCCI - *Plane Anisotropy by the Polar Method*. Meccanica, 40(4-6):437-454, December 2005.

[109] J. C. VASSBERG, M. A. DEHAAN, S. M. RIVERS, R. A. WAHLS - *Development of a Common Research Model for Applied CFD Validation Studies.* AIAA Paper No. 2008-6919, 2008.

[110] R. VEPA - *Finite State Modeling of Aeroelastic Systems.* Technical Report CR-2779, National Aeronautics and Space Administration, Langley Research Center, 1977.

[111] G. VERCHERY - *Les invariants des tenseurs d'ordre 4 du type de l'élasticité.* Comportement Méchanique des Solides Anisotropes, Volume 115, pp. 93-104, Villard-de-Lans, 1979. Éditions du CNRS, Paris.

[112] R. W. WALTERS - *Towards Stochastic Fluid Mechanics via Polynomial Chaos*. AIAA Paper 2003-413, 2003.

[113] X. WAN, G. E. KARNIADAKIS - *An Adaptive Multi-Element Generalized Polynomial Chaos Method for Stochastic Differential Equations.* Journal of Computational Physics, 209:617-642, 2005.

[114] X. WAN, G. E. KARNIADAKIS - *Multi-Element Generalized Polynomial Chaos for Arbitrary Probability Measures*. SIAM Journal of Scientific Computing, 28(3):901-928, 2006.

[115] N. WIENER - *The Homogeneous Chaos*. American Journal of Mathematics, 60(4):pp. 897-936, 1938.

[116] J. A. S. WITTEVEEN, H. BIJL - *An Alternative Unsteady Adaptive Stochastic Finite Elements Formulation based on Interpolation at Constant Phase*. Computer Methods in Applied Mechanics and Engineering, 198(3-4):578-591, 2008.

[117] J. A. S. WITTEVEEN, H. BIJL - *An Unsteady Adaptative Stochastic Finite Elements Formulation for Rigid-Body Fluid-Structure Interaction*. Computers and Structures, 86:2123-2140, 2008.

[118] J. A. S. WITTEVEEN, H. BIJL - *A Tvd Uncertainty Quantification Method with Bounded Error Applied to Transonic Airfoil Flutter*. Communications in Computational Physics, 6:406-432, 2009.

[119] J. A. S. WITTEVEEN, A. LOEVEN, S. SARKAR, H. BIJL - *Probabilistic Collocation for Period-1 Limit Cycle Oscillations*. Journal of Sound and Vibration, 311(311):421-439, 2008.

[120] J. A. S. WITTEVEEN, S. SARKAR, H. BIJL - *Modeling Physical Uncertainties in Dynamic Stall Induced Fluid-Structure Interaction of Turbine Blades Using Arbitrary Polynomial Chaos*. Computers and Structures, 85(11):866-878, 2007. Fourth MIT Conference on Computational Fluid and Solid Mechanics.

[121] J. R. WRIGHT, J. E. COOPER - *Introduction to Aircraft Aeroelasticity and Loads*. Wiley, Chichester, 2. ed edition, 2015.

[122] C. WU, H. ZHANG, T. FANG - *Flutter Analysis of an Airfoil with Bounded Random Parameters in Compressible Flows via Gegenbauer Polynomial Approximation.* Aerospace Science and Technology, 11:518-526, 2007.

[123] D. XIU, G. E. KARNIADAKIS - *The Wiener-Askey Polynomial Chaos for Stochastic Differential Equations.* SIAM Journal on Scientific Computing, 24:619-644, 2002.

[124] D. XIU, J. S. HESTHAVEN - *High-Order Collocation Methods for Differential Equations with Random Inputs.* SIAM Journal on Scientific Computing, 27(3):1118-1139, 2005.

[125] J. Y. GAN, H.-S. IM, X. Y. CHEN, G.-C. ZHA, C. L. PASILIAO - *Delayed Detached Eddy Simulation of Wing Flutter Boundary using High Order Schemes*. Journal of Fluids and Structures, 71(Supplement C):199-216, 2017.

[126] Z. ZHANG, S. YANG, F. LIU, D.M. SCHUSTER - *Prediction of Flutter and LCO by an Euler Method on Non-Moving Cartesian Grids with Boundary-Layer Corrections.* AIAA Paper 2005-0833.

Jean-Camille Chassaing received his M.S. degree in fluid mechanics from the *Ecole Nationale Supérieure d'Ingénieurs de Constructions Aéronautiques* (Toulouse, France) in 1997. He obtained a PhD degree in mechanical engineering from the *Université Pierre et Marie Curie* in 2002. After a postdoctoral stay at the Vibration University Technology Centre of the Imperial College in 2003, he was given an academic position as Assistant Professor at the *Université Pierre et Marie Curie* (France). He obtained his accreditation to supervise research (*Habilitation à Diriger des Recherches*) in 2012 in the field of uncertainty quantification in aeroelasticity and took part in the French research project CAPCAO, dedicated to the development of fast methods for the prediction of turbomachinery flutter. His research interests include fluid–structure interactions, probabilistic aeroelasticity, data assimilation and high-order numerical methods for computational fluid dynamics. He is currently an Full Professor at the Institute Jean Le Rond d'Alembert of the Sorbonne University and associate editor of the Mechanics & Industry Journal.

Christian Nitschke is a postdoc researcher in mechanics and applied mathematics at Paul Sabatier University in Toulouse. He graduated in mechanics from a double Master program at Karlsruhe Institute of Technology and *Arts et Métiers ParisTech* in 2015. At the beginning of 2018, he obtained a PhD degree at Sorbonne University for his work on the quantification of aleatory and epistemic uncertainties in aeroelasticity. He then returned to *Arts et Métiers ParisTech*, where he further developed his work on combined uncertainty quantification problems. Currently, Christian Nitschke works at the Clément Ader Institute in Toulouse, where he is investigating applications of artificial intelligence in the prediction of material fatigue. Throughout his career, he has been invested in questions of the use of data in engineering applications, especially within the context of machine learning and uncertainty quantification.

Didier Lucor is currently a research director at the French National Research Agency (CNRS) who received his MSc (2000) and PhD (2004) degrees in applied mathematics from Brown University, USA, under the supervision of Prof. G. Em Karniadakis. He was a postdoctoral fellow (2004-2005) in the department of Ocean Engineering at MIT, in the USA. He has received a French national award "*Chaires d'Excellence*" and funding from French Ministry of Research (2004). He was given a permanent position as fluid mechanics research scientist at the CNRS (2005), at the d'Alembert Institute of the *Université Pierre et Marie Curie* (UPMC) in Paris, France. He has been yearly involved with teaching at MSc and BSc levels at the UPMC (since 2005), and was an elected member of the UPMC governing board (2012-2015). He obtained his accreditation to supervise research (*Habilitation à Diriger des Recherches*) at the UPMC (2011). He became a senior research scientist at the CNRS (2015), and moved to the Computer Science Laboratory for Mechanics and Engineering Sciences (LIMSI) in Orsay, France. He is the coordinator of the special interest group on Uncertainty Quantification of ERCOFTAC. His research and teaching activities are related to the fields of predictive and stochastic modeling in computational mechanics, uncertainty quantification, data assimilation and robust optimization with particular focus on fluid-structure interaction problems with applications in biofluids, aerodynamics or environmental flows.

Paola Cinnella is a full professor in Fluid Mechanics at *Ecole Nationale Supérieure d'Arts et Métiers* (ENSAM), France. She graduated *summa cum laude* in Mechanical Engineering from the *Politecnico di Bari* (Italy) in 1995. In 1999, she obtained a PhD degree in Fluid Mechanics (summa cum laude) from ENSAM, where she also worked as a lecturer in Fluid Dynamics, from 1999 to 2000. After a postdoc at *Politecnico di Bari* (2000-2001), she joined the Faculty at the University of Salento (Italy) as an Assistant Professor from 2001 to 2008. In September 2008, she moved back to Paris, after obtaining a position of full professor at ENSAM. She has been a member of the Fluid Dynamics Laboratory (DynFluid) since then. She was the Head of DynFluid from 2011 to 2013. She was also the chairman of the Master of Science "Fluids and Energy Systems" program from 2010 to 2013, and a member of the Scientific Board of ENSAM from 2013 to 2017. She is the Vice-President of the board of directors of *Arts et Métiers ParisTech* since January 2018. P. Cinnella has been doing research for more than 20 years on high-fidelity methods for Computational Fluid Dynamics (CFD), focusing on high-order numerical schemes for compressible flows and uncertainty quantification. She has published more than 100 scientific papers, mostly peer-reviewed journal articles or international conference proceedings. She has been the investigator or principal investigator in many research projects in France and in Italy, including the FP7 project IDIHOM (industrialization of high-order methods) and the French projects UFO (Uncertainty quantification for flow optimization) and TRENERGY (TRain ENergy Efficiency via Rankine-cycle exhaust Gas heat recovery, involving a task in uncertainty quantification and robust optimization). She supervises or has supervised 20 PhD candidates and about 45 Master of Science candidates.
She has given invited lectures in the USA, France, Italy, the Netherlands, and Chile. She is a member of several scientific committees of international conferences and a referee for most major journals and conferences in CFD. She is a member of the Aerodynamics Panel of the French Association of Aeronautics and Astronautics.

Angela Vincenti is an Associate Professor in Solid and Structural Mechanics at the Sorbonne University, in Paris (France). She graduated in Mechanical Engineering from the *Università di Pisa* (Italy) in 1999, and in 2002 she obtained a PhD in Mechanics at the *Université de Bourgogne* (France) with her work on the optimization of composite laminates. After a one-year post-doctoral position at the University of Reading (UK) working on the design of composite structures, and a short research experience at BOKU University in Vienna (Austria) studying the mechanical behavior of wood glued assemblies, she joined the *Université Pierre et Marie Curie* (Paris 6, former name of the Sorbonne University) in September 2004 as Assistant Professor and was confirmed as Associate Professor in 2005. She is a member of the *Institut d'Alembert*, the research institute in Mechanics at the Sorbonne University. She teaches courses in solid and structural mechanics, composite materials and optimization at the Sorbonne University. Her research activities are related to the development of advanced methods for the design and optimization of composite materials and structures, both in the linear and nonlinear domains. Her recent projects have been focused on the study of multistable structures (she obtained the Young-Researcher grant from the *Agence Nationale de la Recherche* in 2013) and aeroelastic behavior of composite aeronautical structures.

C. Stephan, G. Pennisi
(ONERA)

G. Michon
University of Toulouse
(ICA, CNRS, ISAE)

E-mail: cyrille.stephan@onera.fr

DOI: 10.12762/2018.AL14-08

Vibration Mitigation Based on Nonlinear Absorbers

The design of vibration absorbers is a challenging task for complex real-life structures. Although several technological solutions have now reached maturity, a need for better efficiency in terms of added mass, broadband frequency range and level of reduction requires the study of new ideas and concepts coming from nonlinear dynamics. In this paper an introduction to a class of absorbers called Nonlinear Energy Sinks (NES) is proposed to highlight their potential for vibration mitigation. After a reminder of the different categories of vibration control, some principles of NES and their relationship with linear absorbers are presented. Two experimental NES prototypes are studied and the results have shown interesting capacities for vibration mitigation.

Introduction

During their operation, aeronautical structures often endure strong dynamical excitations and their vibrations can reach high levels. This has many undesirable consequences: shorter lifetime of structures, less user comfort in terms of the vibrations felt (and even vibroacoustics), and penalized controllability of trajectories (aircraft, missiles). For all of these reasons, the study of technological solutions that can mitigate vibrations is still an active and open research subject.

Indeed, several ways have already been investigated and the mitigation methods can be classified into three main categories.

- Active control methods have been widely developed over the last decades [1]. The principle is to reduce undesirable vibrations by generating an out-of-phase input. Active control usually gives good performance in terms of vibration reduction, but it requires an external energy supply. Since adding excitation to structures, even for their benefit, could seem tricky and perilous, active control has not achieved great success in industrial applications.
- Semi-active control methods using electro- and magneto-rheological fluids have been proposed [6], [1]. The particularity of these fluids lies in their varying viscosity with respect to the electric or magnetic field in which they are immersed. Since no energy is transferred to the controlled system, these techniques are robust and reliable, while offering a vibration reduction level similar to that of active techniques. However, both the modeling of fluid behaviors and the development of the controller represent major challenges that still complicate the use of the systems for real-life structures.
- Passive control methods reduce vibrations by adding to the structure a dissipative material [16] or a Dynamical Vibration Absorber (DVA) [1], [5]. Given that this can be achieved by using only mechanical components, this technique is an important alternative to the previous methods. DVAs can behave linearly or nonlinearly, with the latter case being the main subject of this article.

Indeed, nonlinear absorbers, also called NES (Nonlinear Energy Sinks), have drawn the attention of many laboratories in recent years, since their performance and robustness are very promising. However, relying on nonlinear dynamics for vibration mitigation is also very challenging, because almost all concepts coming from linear dynamics no longer apply for these devices. In this paper, we aim to present the basic principles of NES and their potential for industry. In a first part, we will introduce the concept of NES and its link to linear absorbers. The second part will be devoted to two experimental NES prototypes developed in our facilities.

Reminder of the concept of linear absorbers

Before presenting nonlinear absorbers, a reminder of the linear version should be instructive, since it preceded them historically. The Tuned Mass Damper (TMD) is probably the most popular device for passive vibration mitigation of mechanical structures. Thanks to its linear behavior and the well-established mathematical theory that it relies on, the TMD is widely implemented in various areas, such as civil buildings (e.g. Millennium Bridge, Taipei 101 skyscraper, Burj-el-Arab Hotel), electromechanical engineering structures (cars and high-tension lines), and aircraft (especially helicopters). Despite being widely used in industrial applications, the design of such absorbers can still be a challenging problem when it is coupled to complex structures.

In 1911, Frahm initiated the TMD with a patent describing his ideas. He considered a small mass m_2 coupled to a linear oscillator (LO) by a linear spring k_2. In his works, the LO is itself made of a mass m_1 and a linear spring k_1, the LO is forced by a harmonic excitation, and damping terms are skipped in computations. If the natural angular frequencies of both masses ω_1 and ω_2 are set to be equal, then it can be shown that the movement of a large mass is minimized when the LO is excited at its natural frequency. Hence, designing a TMD is basically tuning the eigenfrequency of a small mass to the critical frequency of a structure.

Considering damping terms c_1 and c_2 complicates the reasoning. Ormondroyd and Den Hartog [17] first proposed a damped version of the absorber by adding c_2 to the design parameters. An optimization process is then undertaken by means, for example, of the H_∞ technique or, more commonly now, the Den Hartog method, called the fixed-point theory [5].

Unfortunately, when the damping term c_1 of the LO is also taken into account, the fixed-point theory can no longer be used. Nevertheless, several solutions have been proposed, based on the Chebyshev min-max criterion [18], control theory [24] [25], perturbation techniques [1] [8] and nonlinear programming [13] [14].

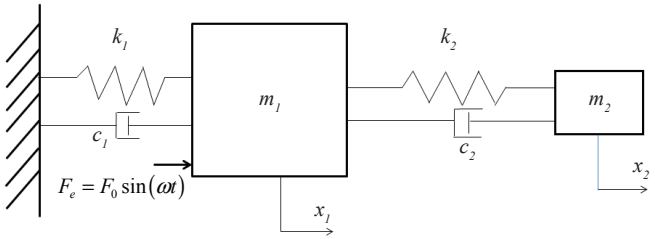

Figure 1 – A Tuned Mass Damper coupled to a linear oscillator (LO)

Although the design of TMD is now known and well mastered, it still has two main drawbacks. First, by definition, a TMD needs to be tuned to the natural frequency of an undesirable mode. Thus, its efficiency is strongly related to the actual closeness $|\omega_2 - \omega_1|$. However, if ω_1 is itself badly known or changing (lack of experimental testing, evolution over time, or influence of nonlinear components), the expected degree of closeness cannot be easily fulfilled, and the efficiency of the TMD drops drastically. Furthermore, since the TMD has to be tuned to one specific frequency, it is difficult, or even impossible, to damp several modes of a multiple-degree-of-freedom system with the same device.

Secondly, it can be shown that the efficiency of a TMD also depends on the mass ratio $\varepsilon = m_2/m_1$. In general, the order of magnitude ε is about 10%, even though lower values can be obtained for particular applications. However, it represents a significant added mass, which is highly undesirable in certain domains, such as aircraft.

Principles of Nonlinear Absorbers

The evolution from linear to nonlinear absorbers has been driven by the need to find an answer to the two previously mentioned drawbacks of TMD: the lack of robustness and, in a less important aspect, the significant added mass. The first studies focusing on using nonlinearities in vibration mitigation date back to the 50s [22] [20] [1]. In 1982, a first practical nonlinear absorber using a softening stiffness was presented [12].

A nonlinear absorber can be outlined as a mass m_2 that is coupled to a structure by a link F_{nl}. The device mass-link behaves nonlinearly as a function of its relative (or sometimes absolute) movement. In the specialized literature, the dynamical law $F_{nl}(\ )$ of this link is generally called a "restoring force" [28].

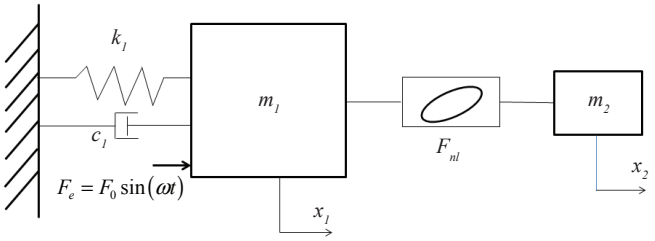

Figure 2 – A nonlinear absorber coupled to a linear oscillator

For a nonlinear absorber, the restoring force can take many forms (polynomial, friction, hysteretic, impacts, etc.), with the notable exception of the linear one. If the coefficients of the purely nonlinear part of F_{nl} are minor compared to its linear part, the restoring force can be approximated by its linear and nonlinear components

$$F_{nl}(x,\dot{x}) = kx + c\dot{x} + other\ minor\ nonlinear\ terms \qquad [1]$$

The dynamics of the small mass m_2 are then close to the behavior of a TMD, except that it depends on amplitude. In fact, it does not show solutions specific to nonlinear dynamics.

When the dynamics of the primary mass m_1 are not purely linear (*i.e.*, k_1 and c_1 are not constant), a relevant solution consists in designing an absorber whose restoring force is tuned according to the restoring force of the primary system. Such an absorber is called a Nonlinear Tuned Vibration Absorber (NTVA) [11].

Nevertheless, let us assume now that the dynamics of the primary system are linear, and that the nonlinear part is only due to the restoring force of the absorber. When the nonlinear restoring force of m_2 has no linear stiffness part, *i.e.*, $dF_{nl}/dx = 0$, then this DVA belongs to a specific category called "essentially nonlinear absorbers", because it cannot be approximated for small displacements by a linear spring.

Essentially, nonlinear absorbers captured the attention of researchers especially, because of their ability to "adapt" themselves to the primary system that they are attached to without being tuned to a specific frequency. Since they do not have a preferential resonant frequency, they are able to interact with the primary system over a broad range of frequencies and then to be effective on all of the modes within that range. Nonlinear Targeted Energy Transfer (TET or energy pumping) was observed by Gendelman [9], who studied a 2-DOF system composed of a linear oscillator nonlinearly coupled to an oscillator with zero linear stiffness. Not having a linear stiffness is a crucial point in order to not have a preferential frequency of oscillation. In [26] it was shown that when the energy of the LO is above a certain threshold, a localized periodic motion of the nonlinear oscillator is excited so that the energy is transferred from the LO and finally dissipated. A nonlinear absorber exhibiting this kind of behavior is called a Nonlinear Energy Sink (NES).

Furthermore, if the linear stiffness coefficient decreases further and becomes negative, there are two points of equilibrium instead of one. The resulting bi-stable absorber could be much more reactive

because the TET activation threshold is lower [15]. In any case, creating a negative linear stiffness requires more imagination, and elegant technological solutions based on magnets have been proposed in [3].

In the following sections we will present two NES prototypes: the cubic stiffness NES and the Vibro-Impact NES. For each case, the experimental and analytic study of the NES coupled to a harmonically forced Linear Oscillator (LO) will be carried out. The systems will be analyzed both analytically and experimentally. Finally, their vibratory behaviors will be explained through the analytical models.

Experimental Case No. 1: the cubic stiffness NES

The inspiration for the first NES comes from the literature [26] [27]. The LO is composed of a moving mass of 63.2kg (see Figure 3), attached to the ground by 4 springs. The LO can translate along one direction only. Its natural frequency is 5.05 Hz. The LO is excited by one modal shaker, with a cell force between the LO and the shaker. A lighter moving mass of 0.61 kg is installed on the top of the LO: it is the NES. Through linear bearings, the NES can move along two shafts. The restoring force of the NES is generated by 4 springs that can rotate and lengthen to follow the translation of the NES (see Figure 4). The NES/ LO mass ratio is 0.97%.

A sketch of the NES displacement is given in Figure 5. We assume that the length of the springs is l_0 at rest (totally free, not yet installed on the LO) and l when it is installed with zero-translation of the NES $(x=0)$. For a translation x, its extension $\sqrt{l^2+x^2}$ is given by a simple geometrical projection. Thus, the restoring force is (here only the conservative part):

$$f_{nl}(x) = 2k\left(\sqrt{l^2+x^2}-l\right) \qquad [2]$$

where k is the stiffness coefficient of two parallel springs. Using a Taylor series development, the nonlinear relationship between the displacement and the restoring force can be approximated by a 3rd degree polynomial

$$f_{nl}(x) \approx k_1 x + k_3 x^3 \qquad [3]$$

With the stiffness coefficients given by

$$\begin{cases} k_1 = \dfrac{2P}{l} + 2k\left(1-\dfrac{l_0}{l}\right) \\ k_3 = \dfrac{kl_0}{l^3} - \dfrac{P}{l^3} \end{cases} \qquad [4]$$

where P is the preload of two parallel springs. As can be noticed by the expression of k_1, the linear part of f_{nl} depends on the level of preload P and on the relative extension of the springs installed l_0/l. For a pure cubic restoring force, k_1 set to null requires $P=0$ and $l=l_0$.

Zero-preload cannot be guaranteed by extension springs: in fact, by design, extension springs always have a certain amount of preload P. This is the reason why here compression springs were selected for the NES, even though they are used extended (see Figure 4). Given that their coils are non-contiguous, they guarantee a regular Hooke law, even for a small extension of the springs, and then have a preload P that is almost negligible.

Experiments were performed to ensure the nonlinear relationship between displacement and force. The static force is identified by blocking the movement of the LO and by attaching weights to the NES. The static displacements due to weights were successively measured by a Laser sensor (see Figure 6). The curve obtained shows the typical inverted S shape of a cubic stiffness force. Furthermore, a polynomial was curve-fitted on data and computed

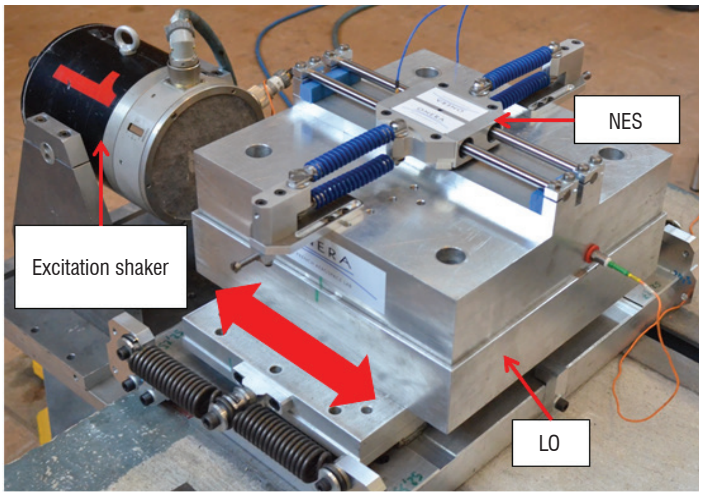

Figure 3 – A cubic stiffness NES on a LO

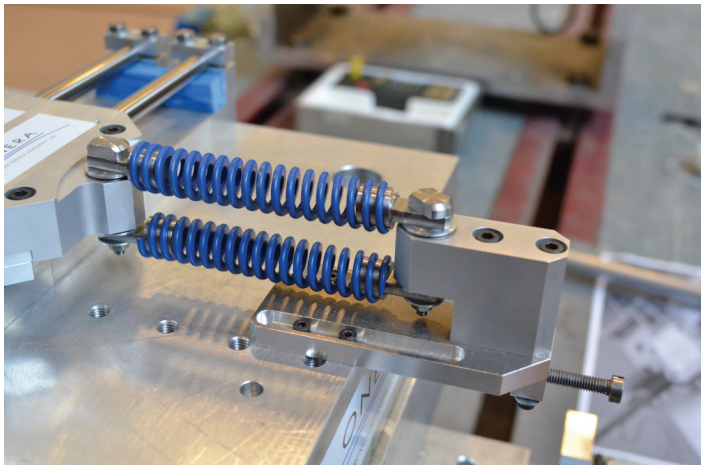

Figure 4 – The NES attached by springs to the LO

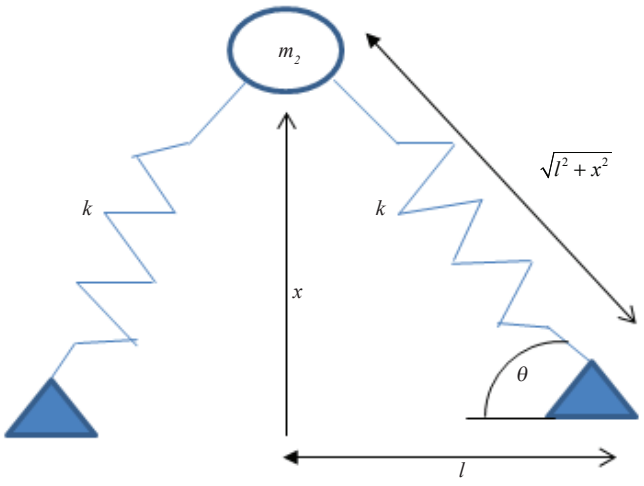

Figure 5 – Simplified movement model of the NES

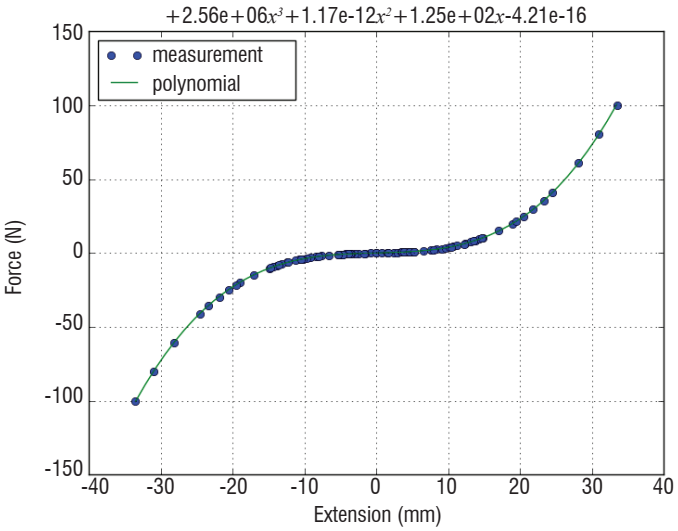

Figure 6 – Static force identified with weights

coefficients (top of Figure 6) ensuring that the cubic part is predominant over the linear part.

Finally, the restoring force F_{nl} comprises the nonlinear conservative part F_{nl}, which has just been derived, and a dissipative part. For the sake of simplicity, this dissipative part is modeled here by a viscous damping $c_a\dot{x}$. Hence, the restoring force F_{nl} is given by

$$F_{nl}(x,\dot{x}) = c_a\dot{x} + f_{nl}(x) \qquad [5]$$

Hopefully, in this case, the conservative and dissipative parts are clearly distinct, making the following dynamical analysis easier. It should be noted that, in general, nonlinear oscillator equations are more complicated and formulae usually involve entangled displacement x and speed $\dot{x}$ terms.

Dynamical equations of the coupled system (Figure 2) can now be derived by considering x_s, the displacement of the LO and x_a, the displacement of the NES.

$$\begin{cases} m_s\ddot{x}_s + c_s\dot{x}_s + k_s x_s + f_{nl}(x_s - x_a) &= F_e\sin(\bar{\Omega}t) \\ m_a\ddot{x}_a + c_a(\dot{x}_a - \dot{x}_s) + f_{nl}(x_a - x_s) &= 0 \end{cases} \qquad [6]$$

Equations clearly show the dependency of the restoring force as a function of the relative displacement $x_s - x_a$. Let us now introduce the following change of variables

$$\varepsilon = \frac{m_2}{m_1},\ \omega_0^2 = \frac{k_1}{m_1},\ K = \frac{k_2}{m_2\omega_0^2},\ \lambda_1 = \frac{c_1}{m_2\omega_0},$$
$$\lambda_2 = \frac{c_2}{m_2\omega_0},\ \Omega = \frac{\bar{\Omega}}{\omega_0},\ \tau = \omega_0 t,\ \frac{dx}{dt} = \omega_0\dot{x}, \qquad [7]$$
$$\frac{d^2x}{dt^2} = \omega_0^2\ddot{x},\ F = \frac{F_e}{\varepsilon m_1\omega_0^2}$$

And the following change of coordinates

$$v = x_s + \varepsilon x_a,\ w = x_s - x_a \qquad [8]$$

Thus, the system of dynamical equations [6] becomes

$$\begin{cases} \ddot{v} + \dfrac{\varepsilon}{1+\varepsilon}\lambda_1(\dot{v}+\varepsilon\dot{w}) + \dfrac{1}{1+\varepsilon}(v+\varepsilon w) &= \varepsilon F\sin(\Omega\tau) \\ \ddot{w} + \dfrac{\varepsilon}{1+\varepsilon}\lambda_1(\dot{v}+\varepsilon\dot{w}) + \lambda_2(1+\varepsilon)\dot{w} & \\ \quad + \dfrac{1}{1+\varepsilon}(v+\varepsilon w) + K(1+\varepsilon)w^3 &= \varepsilon F\sin(\Omega\tau) \end{cases} \qquad [9]$$

The cubic term in the second equation prevents the system from being resolved analytically. In any case, approximated periodic solutions can be sought through a combination of the Complexification-Averaging method and the Multiple Scales method [1]. First, complex variables are introduced

$$\begin{aligned} \psi_1 &= \dot{v} + i\Omega v, \quad \psi_2 = \dot{w} + i\Omega w \\ \psi_1 &= \phi_1 e^{i\Omega\tau}, \quad \psi_2 = \phi_2 e^{i\Omega\tau} \end{aligned} \qquad [10]$$

noting that

$$\begin{aligned} v &= \frac{1}{2i\Omega}(\psi_1 - \psi_1^*), & w &= \frac{1}{2i\Omega}(\psi_2 - \psi_2^*) \\ \dot{v} &= \frac{1}{2}(\psi_1 + \psi_1^*), & \dot{w} &= \frac{1}{2}(\psi_2 + \psi_2^*) \\ \ddot{v} &= \dot{\psi}_1 - \frac{i\Omega}{2}(\psi_1 + \psi_1^*), & \ddot{w} &= \dot{\psi}_2 - \frac{i\Omega}{2}(\psi_2 + \psi_2^*) \end{aligned} \qquad [11]$$

Thanks to complex variables, fast oscillations of the system at the excitation frequency Ω can be separated from slow modulations of complex amplitudes. The following system is obtained

$$\begin{cases} \dot{\psi}_1 - \dfrac{i\Omega}{2}(\psi_1 + \psi_1^*) + \dfrac{\varepsilon}{1+\varepsilon}\lambda_1\left[\dfrac{1}{2}(\psi_1 + \psi_1^*) + \dfrac{\varepsilon}{2}(\psi_2 + \psi_2^*)\right] & \\ \quad + \dfrac{1}{2i\Omega(1+\varepsilon)}\left[\dfrac{1}{2}(\psi_1 + \psi_1^*) + \dfrac{\varepsilon}{2}(\psi_2 + \psi_2^*)\right] &= \varepsilon F\sin(\Omega\tau) \\ \dot{\psi}_2 - \dfrac{i\Omega}{2}(\psi_2 + \psi_2^*) + \dfrac{\varepsilon}{1+\varepsilon}\lambda_1\left[\dfrac{1}{2}(\psi_1 + \psi_1^*) + \dfrac{\varepsilon}{2}(\psi_2 + \psi_2^*)\right] & \\ \quad + 2\lambda_2(1+\varepsilon)(\psi_2 + \psi_2^*) & \\ \quad + \dfrac{1}{2i\Omega(1+\varepsilon)}\left[\dfrac{1}{2}(\psi_1 + \psi_1^*) + \dfrac{\varepsilon}{2}(\psi_2 + \psi_2^*)\right] & \\ \quad + (1+\varepsilon)\dfrac{iK}{8\Omega^3}(\psi_2 - \psi_2^*)^3 &= \varepsilon F\sin(\Omega\tau) \end{cases} \qquad [12]$$

In a second step, equations [12] are averaged over the fast scale, *i.e.*, keeping terms only of $e^{i\Omega\tau}$. Then, terms of ψ_i are replaced by $\phi_i e^{i\Omega\tau}$ and, hence, equations are simplified to

$$\begin{cases} \dot{\phi}_1 + \dfrac{i\Omega}{2}\phi_1 + \dfrac{\varepsilon\lambda_1}{2(1+\varepsilon)}(\phi_1 + \varepsilon\phi_2) & \\ \quad - \dfrac{i}{2\Omega(1+\varepsilon)}(\phi_1 + \varepsilon\phi_2) + \dfrac{i\varepsilon F}{2} &= 0 \\ \dot{\phi}_2 + \dfrac{i\Omega}{2}\phi_2 + \dfrac{\varepsilon\lambda_1}{2(1+\varepsilon)}(\phi_1 + \varepsilon\phi_2) - \dfrac{i}{2\Omega(1+\varepsilon)}(\phi_1 + \varepsilon\phi_2) & \\ \quad + \dfrac{\lambda_2}{2}(1+\varepsilon)\phi_2 - (1+\varepsilon)\dfrac{i3K_3}{8\Omega^3}|\phi_2|^2\phi_2 + \dfrac{i\varepsilon F}{2} &= 0 \end{cases} \qquad [13]$$

It is important to remember that ϕ_1 and ϕ_2 are the slow evolutions of amplitudes for a 1:1 resonance. Thus, the temporal evolution of the

LO-NES couple is governed by the previous system of equations [13], under the assumption of a periodic movement of both oscillators at frequency Ω.

In a third step, the method of Multiple Scales is used to obtain approximated solutions [1]. The idea is to break down the time scale τ into several time subscales that depend on τ and ε. Derivation is performed through a series of partial derivatives

$$\frac{d}{d\tau}=\frac{\partial}{\partial\tau_0}+\varepsilon\frac{\partial}{\partial\tau_1}+\varepsilon^2\frac{\partial}{\partial\tau_2}+\ldots,\ \tau_k=\varepsilon^k\tau,\ k=0,1,2,\ldots \quad [14]$$

Solutions ϕ_1 and ϕ_2 are written as polynomials of ε

$$\begin{aligned}\phi_1 &= \phi_{10}+\varepsilon\phi_{11}+o(\varepsilon), & \frac{d\phi_1}{d\tau} &= \frac{\partial\phi_{10}}{\partial\tau_0}+\varepsilon\left(\frac{\partial\phi_{11}}{\partial\tau_0}+\frac{\partial\phi_{10}}{\partial\tau_1}\right)+o(\varepsilon)\\ \phi_2 &= \phi_{20}+\varepsilon\phi_{21}+o(\varepsilon), & \frac{d\phi_2}{d\tau} &= \frac{\partial\phi_{20}}{\partial\tau_0}+\varepsilon\left(\frac{\partial\phi_{21}}{\partial\tau_0}+\frac{\partial\phi_{20}}{\partial\tau_1}\right)+o(\varepsilon)\end{aligned} \quad [15]$$

Furthermore, the excitation frequency is assumed to be close to the natural frequency of the LO

$$\Omega=1+\varepsilon\sigma \quad [16]$$

where σ denotes a small variation around the natural frequency.

By approximating the system of dynamical equations [13] through this derivation, we can group the terms proportional to ε^0:

$$\varepsilon^0:\begin{cases}\dfrac{\partial\phi_{10}}{\partial\tau_0} &= 0\\ \dfrac{\partial\phi_{20}}{\partial\tau_0}+\dfrac{\lambda_2}{2}\phi_{20}+\dfrac{i}{2}\left(\phi_{20}-\phi_{10}\right)-\dfrac{3}{8}iK\left|\phi_{20}\right|^2\phi_{20} &= 0\end{cases} \quad [17]$$

At the first time scale $\tau_0=\varepsilon^0\tau$, amplitude modulations do not depend on the force amplitude F. In fact, F appears at the slower time scale $\tau_1=\varepsilon^1\tau$. Then, the dynamical system [17] at scale τ_0 is written in polar form

$$\phi_{10}=N_{10}e^{i\theta_{10}},\ \phi_{20}=N_{20}e^{i\theta_{20}} \quad [18]$$

Introducing these polar forms into the dynamic equations [17] at scale ε^0, after separating the real and complex parts, we obtain

$$\begin{cases}\dfrac{\partial N_{10}}{\partial\tau_0} &= 0\\ \dfrac{\partial N_{20}}{\partial\tau_0} &= -\dfrac{\lambda_2}{2}N_{20}+\dfrac{N_{10}}{2}\sin\left(\theta_0\right)\\ \dfrac{\partial\theta_0}{\partial\tau_0} &= \dfrac{N_{10}}{2N_{20}}\cos\left(\theta_0\right)-\dfrac{1}{2}+\dfrac{3}{8}K_3N_{20}^2\end{cases} \quad [19]$$

with $\theta_0=\theta_{20}-\theta_{10}$. At equilibrium, this phase is given by

$$\begin{cases}\sin\left(\theta_0\right) &= \lambda_2\dfrac{N_{20}}{N_{10}}\\ \cos\left(\theta_0\right) &= \dfrac{N_{20}}{N_{10}}\left(1-\dfrac{3}{4}KN_{20}^2\right)\end{cases} \quad [20]$$

By squaring both expressions [20] and adding them, the fixed points of the system [19] satisfy the equation

$$\left(\lambda_2^2+1\right)Z-\frac{3}{2}KZ^2+\frac{9}{16}K^2Z^3=N_{10}^2,\ \text{ with }\ Z=N_{20}^2 \quad [21]$$

This equation defines the invariant manifold of the coupled system: it means that it gives a relation between the main parameters of the system that can characterize its amplitude evolution. For a fixed value of the amplitude N_{10}, this 3rd degree polynomial can be solved analytically: for each value of N_{10}, either 1 or 3 solutions can be found for N_{20}.

To know the nature of the solutions given by this invariant manifold, we need to study the eigenvalues of the stability matrix

$$M_{\varepsilon^0}=\begin{bmatrix}0 & 0 & 0\\ \dfrac{\lambda_2N_{20}}{2N_{10}} & -\dfrac{\lambda_2}{2} & \dfrac{N_{20}}{2}\left(1-\dfrac{3}{4}KN_{20}^2\right)\\ \dfrac{1}{2N_{10}}\left(1-\dfrac{3}{4}KN_{20}^2\right) & -\dfrac{1}{2N_{20}}+\dfrac{9}{8}KN_{20} & -\dfrac{\lambda_2}{2}\end{bmatrix} \quad [22]$$

This matrix was computed by considering small perturbations of the previous system of dynamical equations. It can be observed that the stability matrix is independent of the phase difference θ_0.

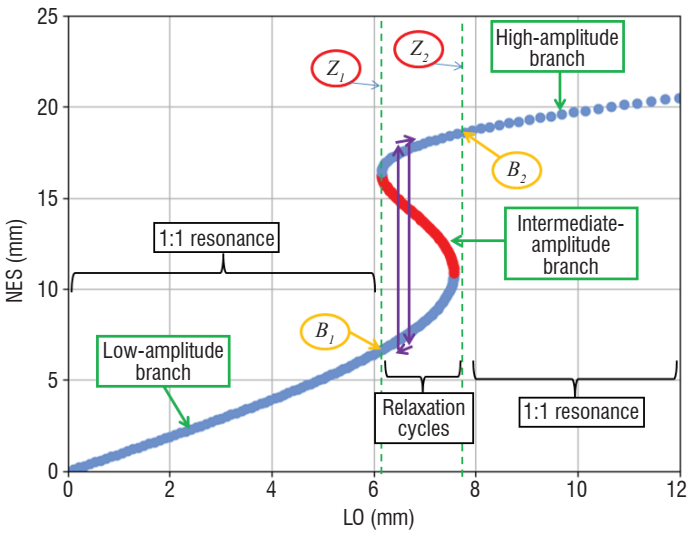

Figure 7 – Invariant manifold (blue circles: stable solutions, red circles: unstable solutions)

An example of an invariant manifold is presented in Figure 7. In this figure, each circle represents a possible solution for the movement. To understand this manifold, let us look at a particular point. For instance, if the periodic amplitude of the LO is 4 mm, then there is only one corresponding amplitude at 4.1 mm for the NES.

In the whole plot, solutions can be grouped into three distinct branches, depending on the NES amplitude: the low-amplitude branch (blue), the intermediate-amplitude branch (red) and the high-amplitude branch (blue). For a movement of the LO below 6.2 mm, only one stable branch of solutions exists for N_1 and N_2. A 1:1 resonance, also called a Constant Response Amplitude (CAR), can be observed: the NES has almost the same amplitude as the LO, but with a phase difference of 180°. In this zone, the NES is inactive because it only follows the LO movement.

Between 6.2 and 7.6 mm, a first bifurcation point B_1 is reached. In this zone, there are three solution branches: two stable ones on either side of an unstable one. These three solutions are differentiated by the NES amplitude: the low-amplitude one and the high-amplitude one for stable solutions, and the intermediate-amplitude one for the unstable solution. This particular configuration is called a "cusp catastrophe" in nonlinear dynamics literature ([23], [10]) and is at the origin of a special movement called "relaxation cycles", which can be observed both numerically and experimentally. For one value of the LO amplitude, the system is first attracted by a low-amplitude solution of the NES, but fast jumped to the high-amplitude branch. Being on this branch, the NES dissipates much more energy through viscous damping c_2. Thus, the whole system loses energy and jumps back to a low-amplitude solution. Of course, being back on this branch, the system receives vibratory energy again and its amplitude increases, until its jump to the high-amplitude solution is repeated. This strange behavior is due to the presence of an unstable solution, which makes the jumps appear constantly. This phenomenon, also called a Strongly Modulated Response (SMR), will be illustrated in the following by experimental tests.

Above 7.6 mm, a second bifurcation point B_2 is crossed: there is again a single stable solution for the LO-NES couple. It is characterized by a very high magnification of the NES compared to the LO, and then by a high dissipation of energy by the NES. However, contrary to the previous zone, here the dynamical system is simply locked in a 1:1 resonance (CAR).

As displayed in Figure 7, the invariant manifold has three zones that are delimited by two points of inflexion. These points can be analytically computed by deriving the invariant manifold expression and equaling the resulting equation to zero

$$Z_1 = \frac{9}{4K}\left(2-\sqrt{1-3\lambda_2^2}\right),\quad Z_2 = \frac{9}{4K}\left(2+\sqrt{1+3\lambda_2^2}\right) \qquad [23]$$

With $Z = N_{20}^2$. Two remarks should be made on these points. First, they both depend on the cubic stiffness coefficient K and on the NES damping λ_2. From Z_1, a condition of existence for relaxation cycles is $\lambda_2 < 1/\sqrt{3}$. It means that the NES damping should not be higher than this threshold; otherwise, no energetic relaxation cycles could appear.

Secondly, the NES activation threshold depends on the inverse of the cubic stiffness coefficient K. Thus, a low threshold would be obtained for a high value of K, which implies a high value of the spring stiffness coefficient k. Therefore, contrary to common sense when looking at Figure 3, it is better to select very stiff springs when a high NES amplitude is sought. In fact, softer springs would not be able to create strongly nonlinear dynamics, and thus achieve efficient vibration mitigation.

After having presented the analytical model and the mathematical methods that gave approximated solutions, all inputs are now gathered to analyze data coming from the experimental demonstrator (Figure 3). As a reminder, the natural frequency of LO is 5.05 Hz. Swept-sine tests were performed between 4 and 6 Hz at a slow rate of 0.05 oct/min and at 7 levels of force, regularly spaced between 17.2 and 23.1 N. The response of the LO is shown in Figure 8. Two kinds of response can be observed. As long as the LO movement has not reached a certain amplitude level, it behaves like a classical linear oscillator. Once this threshold is exceeded, relaxation cycles appear (see Figure 9). They are characterized by a strong irreversible transfer

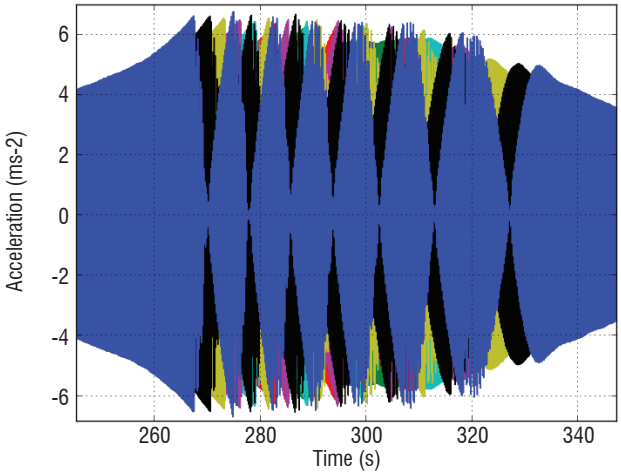

Figure 9 – Zoom on relaxation cycles

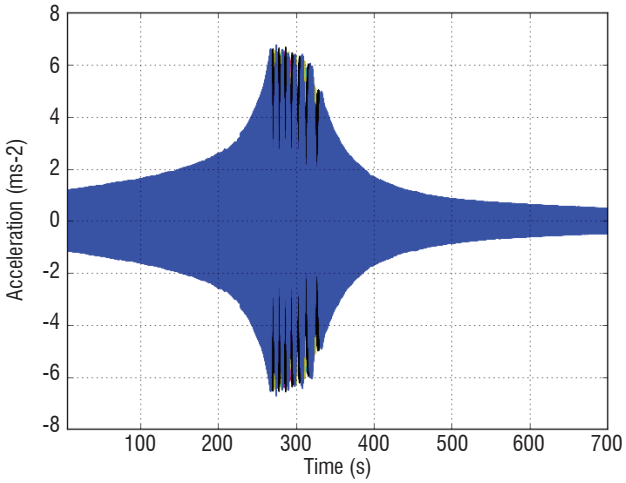

Figure 8 – Response of the LO in the temporal domain

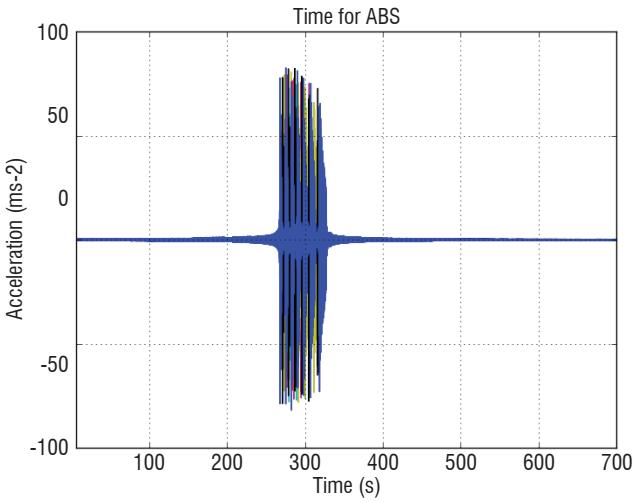

Figure 10 – Response of the NES

Caption for the three figures: 7 curves for 7 levels of force (17.2 to 23.1 N), sweep-sines from 4 to 6 Hz, sweep rate of 0.05 oct/min

of energy between the LO and the NES. Consequently, we can see in Figure 10 that the NES moves significantly only when these cycles are activated. Outside this regime, the NES movement only follows the LO oscillations: therefore it can be considered as inactive.

The LO and NES spectra are also instructive. The NES prevents the structure from exceeding a certain level of vibration (Figure 11 and Figure 12). The more the excitation force increases, the more broad-band the frequency range is, since relaxation cycles are increasingly

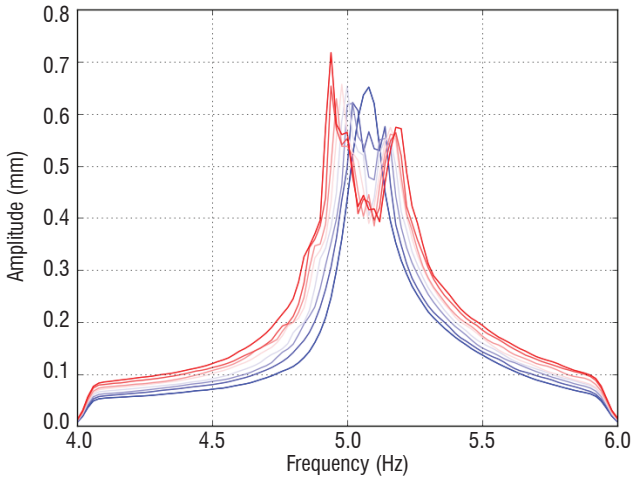

Figure 11 – LO spectra

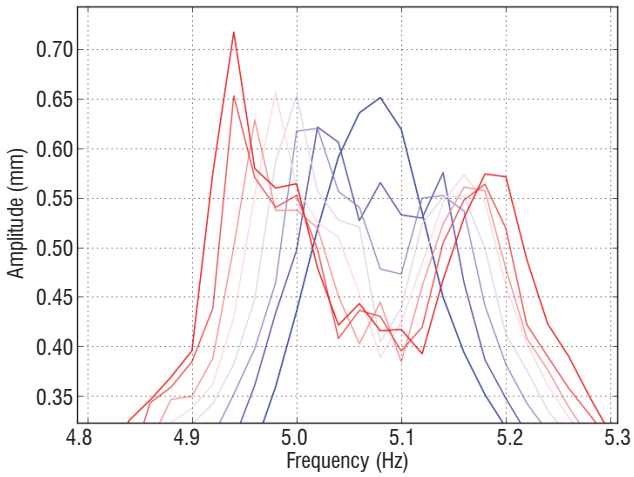

Figure 12 – Zoom on the primary structure spectra

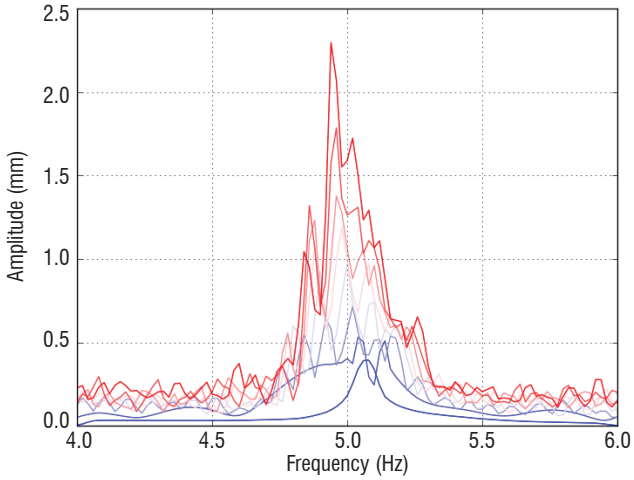

Figure 13 – NES spectra

Caption for the three figures: 7 curves for 7 levels of force, from dark blue (17.2 N) to dark red (23.1 N)

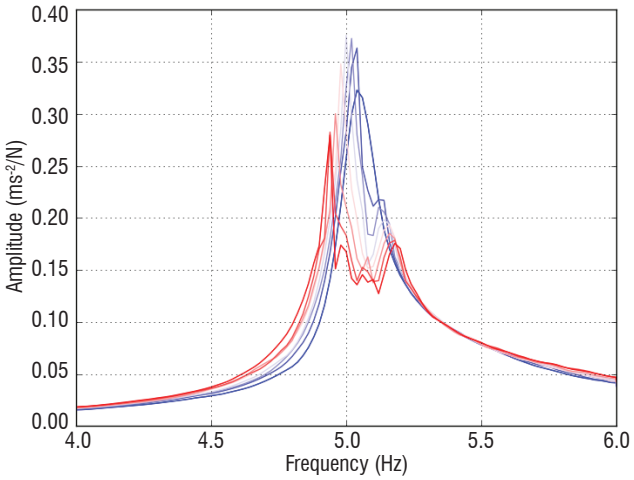

Figure 14 – LO FRFs

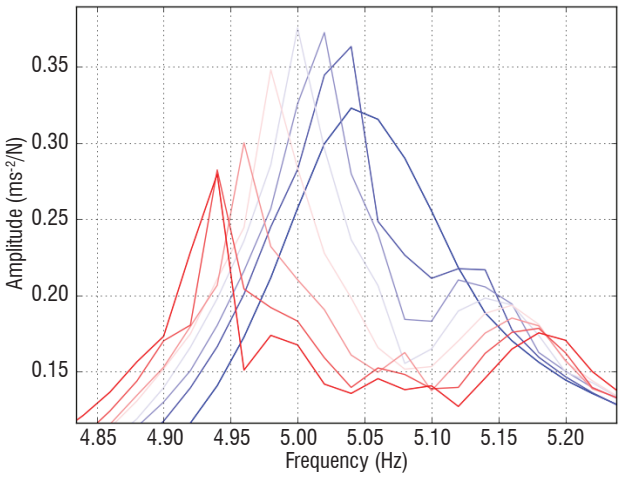

Figure 15 – Zoom on FRFs

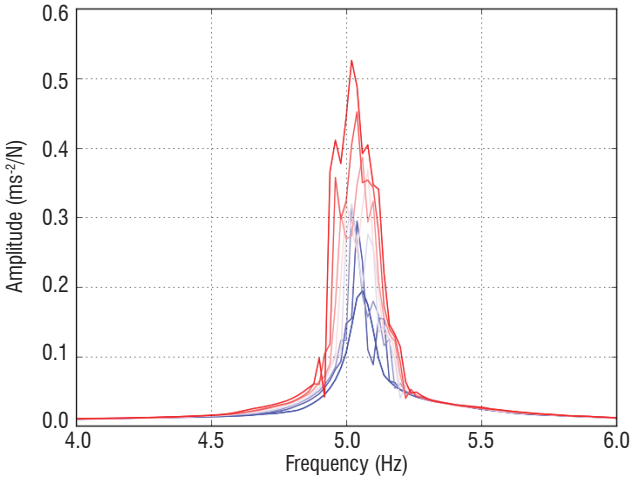

Figure 16 – NES FRFs

Caption for the three figures: 7 curves for 7 levels of force, from dark blue (17.2 N) to dark red (23.1 N)

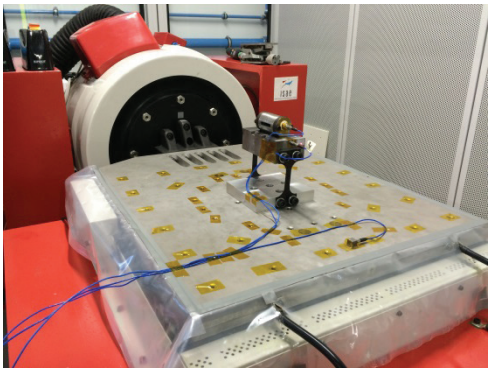

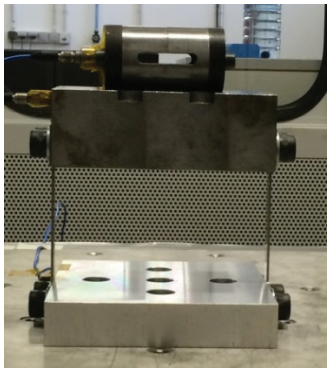

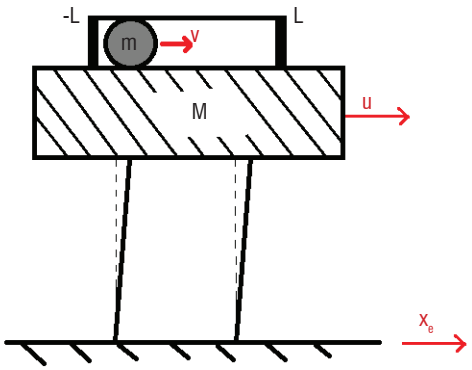

Figure 17 – LO coupled to a VI-NES: the system placed on the vibrating table (left), the LO and VI-NES (center) and its schematic diagram (right)

present. This clearly demonstrates that the efficiency frequency range does not depend on the excitation frequency (at least not on the first order), but rather on the level of excitation. The NES spectra are very disturbed, and it is difficult to interpret them (see Figure 13). It can only be noticed that, when the NES is active, its amplitude level increases as a function of the force level.

Strictly speaking, Frequency Response Functions (FRFs) are not appropriate tools for studying highly nonlinear systems [28]. In any case, they can still be useful to qualify the deviation of a system from a classical linear one. FRFs are computed by taking the cell force as a reference. FRFs of LO are presented in Figure 14. The FRF at the lowest level can easily be found (dark blue curve): it is the only smooth one and there are no relaxation cycles. Indeed, since relaxation cycles are a manifestation of a highly nonlinear behavior, the spectral content during these cycles is very rich. It affects FRFs and gives them a noisy appearance. Furthermore, when the force level was increased, two peaks appeared instead of one, as if the FRFs were cut at their summits (Figure 15). The FRFs of the NES clearly show that this resonance phenomenon suppression is due to the activation of the NES (Figure 16).

Experimental case No. 2: the Vibro-Impact NES (VI-NES)

The experimental study has been conducted with the aim of observing the behavior of the system and of exploring the different types of response that the system can exhibit. The relationship between the regimes and the external forcing, in terms of magnitude and frequency, is of particular interest.

The experimental setup is shown in Figure 17 and comprises a primary single-degree-of-freedom linear oscillator (LO), to which the VI-NES is attached. The LO is harmonically forced by an electrodynamic shaker.

The system is forced by a swept-sine external force with constant amplitude and the primary mass displacement is measured by means of a Laser Doppler Vibrometer.

f_0 [Hz]	K [N/m]	C [N/ms]	ξ [%]	M [kg]	m [kg]	$\varepsilon = m/M$ [%]
21.18	67421	8.566	0.8	3.807	0.032	0.84

Figure 18: Modal parameters of the primary system and mass value of the primary system M, of the VI-NES m and their ratio ε

The modal parameters of the LO and the mass values are shown in Figure 18. It is important to notice the very small mass ratio between the VI-NES and the primary system, *i.e.*, less than 1%.

Figure 19 (left) shows the displacement spectra for the system with and without VI-NES. We can observe that two types of qualitatively different responses exist when the VI-NES is active and, depending on the magnitude and the frequency of the external forcing, either one or the other may appear.

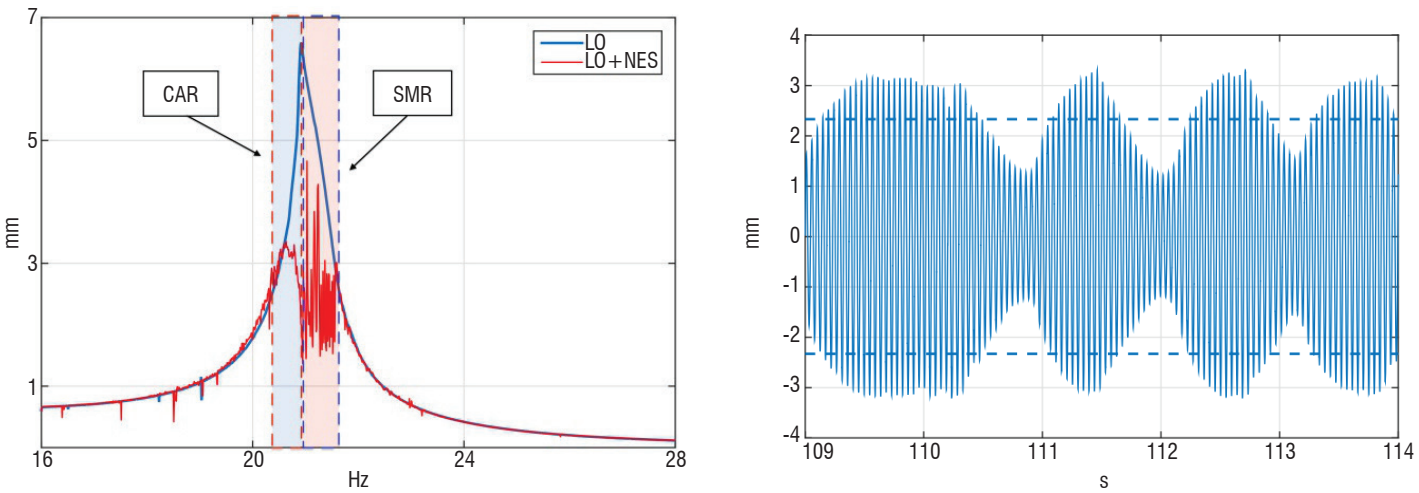

Figure 19 – Left: experimental spectra of the primary mass displacement with (red) and without (blue) the VI-NES. Right: recorded time signal of a SMR, the dashed lines indicate the amplitude of the LO without the VI- NES under the same forcing conditions.

We can classify the responses as:

- Strongly Modulated Response (SMR): the primary system goes through alternatively increasing and decreasing amplitude cycles and then the fast oscillations appear to be modulated. This behavior is caused by a repeated activation/deactivation of the VI-NES (Figure 19 right).
- Constant Amplitude Response (CAR): the VI-NES is stably active and the amplitude of the primary mass displacement remains constant.

The VI-NES seems to accomplish its task as a vibration absorber well, since the response amplitude is reduced near the resonance of the primary system. This is the proof that a Targeted Energy Transfer occurs from the LO towards the VI-NES and that the energy is dissipated by the impacts. It is important to emphasize that this goal has been achieved, despite a proper sizing process not having been carried out and with a significantly small mass ratio $\varepsilon = 0.84\%$. This result proves that the VI-NES is able to automatically tune itself to the primary system. This is a relevant general feature of nonlinear absorbers caused by the absence of a natural frequency for these devices.

By looking at the spectrum in Figure 19, one can draw the conclusion that a criterion exists on the primary mass displacement to activate the VI-NES. In fact, an amplitude/energy threshold is observed, beyond which the VI-NES is active.

The schematic diagram of the model is presented in Figure 17 (right). We define the variables u, v and x_e as the displacements of the primary mass M, of the NES mass m and of the base, respectively. We model the shocks as instantaneous impacts by using the basic concepts of Newtonian mechanics:

$$\begin{aligned} \dot{u}\left(t_j^+\right) - \dot{v}\left(t_j^+\right) &= -r\left(\dot{u}\left(t_j^-\right) - \dot{v}\left(t_j^-\right)\right) \\ M\dot{u}\left(t_j^+\right) + m\dot{v}\left(t_j^+\right) &= M\dot{u}\left(t_j^-\right) + m\dot{v}\left(t_j^-\right) \end{aligned} \qquad [24]$$

Where t_j^+ and t_j^- are the time instants after and before the j^{th} impact, respectively. The first equation provides a relation for the relative velocity of the two colliding masses after and before the impact, by using the restitution coefficient $0<r<1$. This allows the impact to be characterized from completely elastic $r=1$ to completely plastic $r=0$.

The second equation expresses the momentum conservation throughout the impact. Then, the motion equations are:

$$\begin{cases} \ddot{u} + 2\omega_0\xi\dot{u} + \omega_0^2 u + \dfrac{m(1+r)}{m+M}\displaystyle\sum_j \dot{w}^-\delta_j^- &= \omega_0^2 x_e + 2\omega_0\xi\dot{x}_e \\ \varepsilon\ddot{v} - \dfrac{m(1+r)}{M+m}\displaystyle\sum_j \dot{w}^-\delta_j^- &= 0 \end{cases} \qquad [25]$$

where $\omega_0^2 = \dfrac{K}{M}$ and $2\omega_0\xi = \lambda/M$.

The previous system [25] can be studied by means of the Multiple Scales method [26], which allows us to separate the various dynamic behaviors of the problem, happening at different time scales.

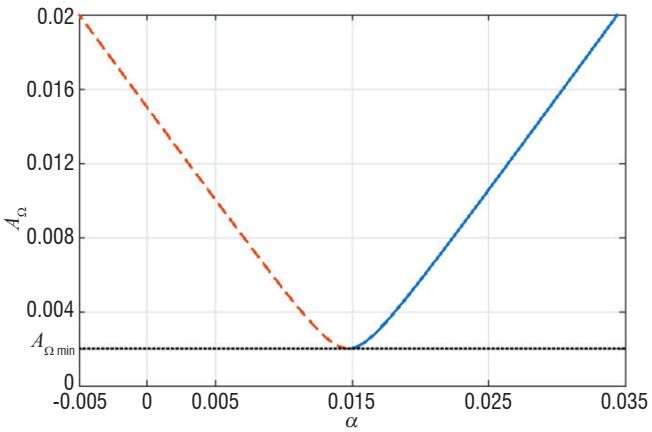

Figure 20 – Slow Invariant Manifold - $r = 0.65$, $L = 15$ mm

For the sake of conciseness, all mathematical steps are not detailed like in the previous section; they are given in [19]. We directly go to the important result that the analytic study provides us with: the Slow Invariant Manifold (SIM) of the problem, a mathematical tool that gathers all of the possible solutions that the system may exhibit. Under the condition of two impacts per oscillation, the SIM, shown in Figure 20, can be expressed by the following equation, where A_Ω and α are two variables that are strictly related to the displacements X and w.

$$\alpha = \frac{L \pm \sqrt{1+\sigma^2}\sqrt{A_\Omega^2 - A_{\Omega_{min}}^2}}{1+\sigma^2} \qquad [26]$$

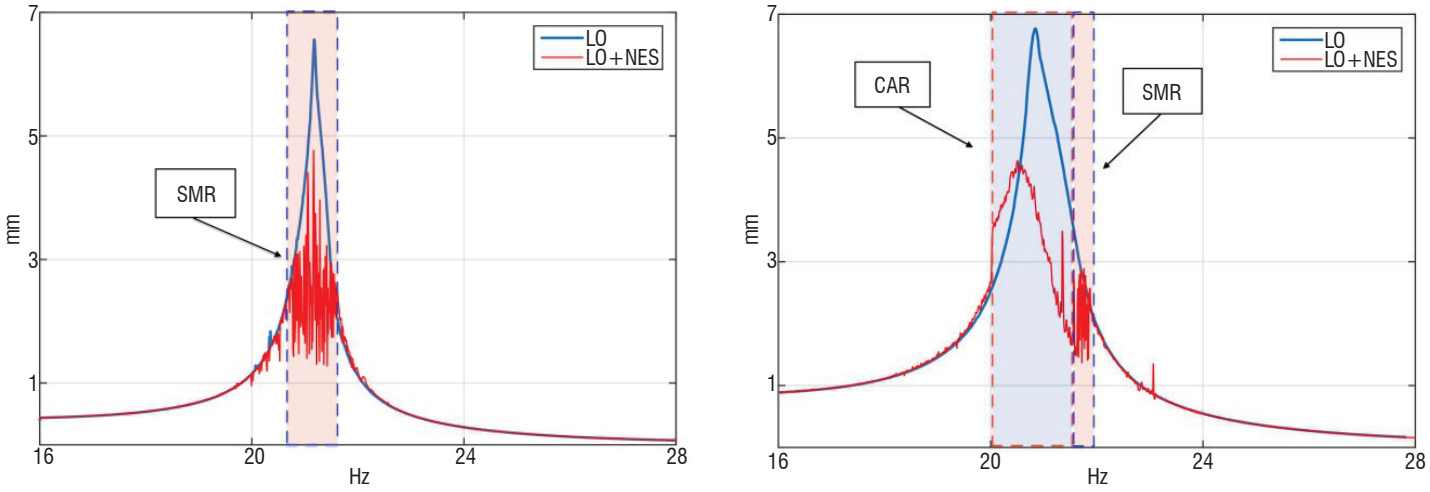

Figure 21 – Spectra of the primary mass displacement with and without VI-NES for F = 0.2g (left) and F = 0.4g (right).

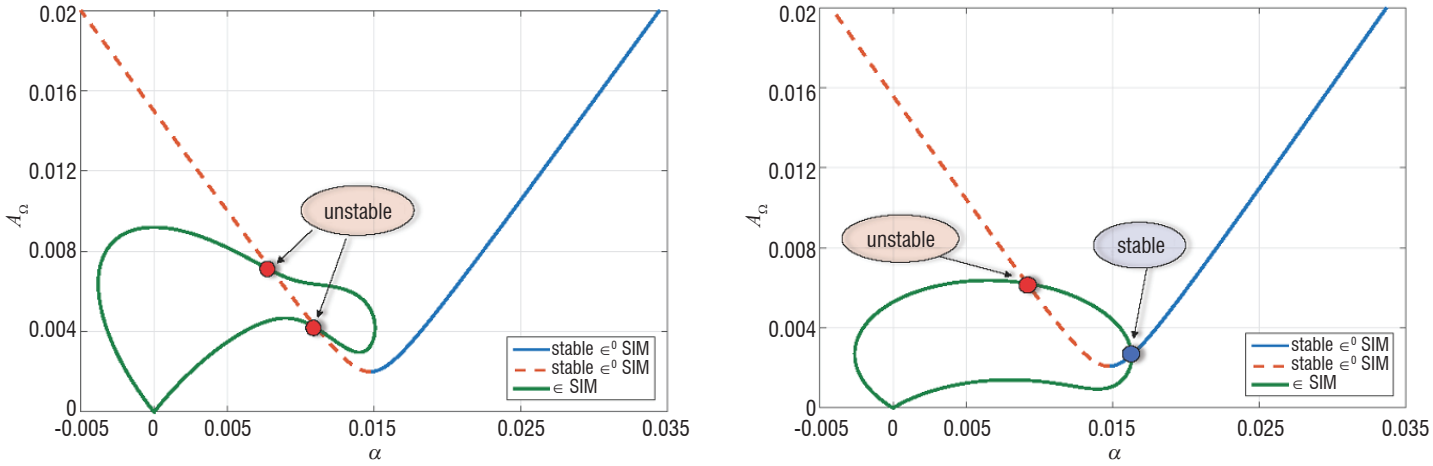

Figure 22 – SIM and fixed points for an external force level of F=0.2g and $\Omega = \frac{\omega}{\omega_0} = 1$ (left) and F = 0.4g and $\Omega = \frac{\omega}{\omega_0} = 1.02$ (right).

with $\sigma = \frac{2(1-r)}{\pi(1+r)}$ and where $A_{\Omega_{min}} = \frac{\sigma L}{\sqrt{1+\sigma^2}}$ is a minimum value of amplitude A_Ω for solutions to exist.

Some important information that the SIM contains is that a minimum A_Ω must exist for solutions to appear. This point mathematically represents a saddle-node bifurcation. Starting from this bifurcation point, two solution branches appear: one stable and one unstable.

Once the SIM has been obtained, we can take our analysis further and study the previous system of dynamical equations at the next order. Similarly, we reach an expression relating A and α (not reported here for the sake of conciseness), which represents the fixed points of the problem. The intersections between the SIM and the fixed points represent the solutions of the problem.

Figure 21 shows the experimental spectra of the primary mass displacement with and without the VI-NES attached. The two different kinds of regime, constant amplitude and strongly modulated responses (CAR and SMR), have been highlighted. We can see that for F=0.2g, *i.e.*, for a low level of external force, the only type of response observed is the strongly modulated response, whereas when the external forcing increases, the constant amplitude response appears and the transition from one type of regime to another is a function of the forcing frequency.

Figure 22 shows the SIMs for two different cases of external force amplitude and frequency. For the lower level (Figure 22 left), the only fixed points attainable are unstable points for any frequency Ω. The only type of possible response is then the strongly modulated response. This result is in perfect agreement with the experimental observations.

For the higher level of the external force (Figure 22 right) the behavior of the SIMs is different. As Ω grows, the system goes from a state of no solution (no impacts) to a state where two fixed points exist: one stable and one unstable. The stable one is reached and the system presents a CAR. When Ω increases further, just before the disappearing of solutions, the two intersections of the SIMs are both unstable points. Thus, the system exhibits a SMR. This behavior is also in perfect agreement with the experimental observations in Figure 21.

Conclusion

In this work, the vibration mitigation based on nonlinear absorbers has been explored. The links and differences between linear and nonlinear absorbers have been discussed. Two experimental cases of NES have been carried out. For each NES, approximated solutions of the nonlinear dynamical equation system were obtained by a combination of the Complexification-Averaging method and the Multiple Scales method. Fixed points of the approximated system were computed and, consequently, the invariant manifold was computed with its stability matrix. It was shown that different regimes could occur, depending on the LO response amplitude. When an amplitude threshold is reached, very energetic solutions appear and the NES is active because it dissipates a significant amount of energy. In conclusion, a NES is able to significantly reduce the level of vibrations, and even to suppress the resonance peak phenomenon, for a very small mass ratio below 1%. Furthermore, it can be active over a wide frequency range, since its behavior mainly depends on the amplitude level of the LO. It is believed by the authors that the NES can be an effective solution for vibration mitigation, especially for aircraft embedded equipment. In the future, several technologies could be explored and adapted to industrial applications ■

Nomenclature and Acronyms

x	Displacement at one location of a structure
$\dot{x}$	Velocity at one location of the structure
$\ddot{x}$	Acceleration at one location of a structure
NES	(Nonlinear Energy Sink)
LO	(Linear Oscillator)
TMD	(Tuned Mass Damper)
DVA	(Dynamical Vibration Absorber)
FRF	(Frequency Response Function)
SMR	(Strongly Modulated Response)
CAR	(Constant Amplitude Response)
SIM	(Slow Invariant Manifold)

References

[1] F. R. ARNOLD - *Steady-State Behavior of Systems Provided with Nonlinear Dynamic Vibration Absorbers*. Journal of Applied Mechanics, 22, pp.487-492, 1955.

[2] T. ASAMI, O. NISHIHARA, A. M. BAZ - *Analytical Solutions to H1 and H2 Optimization of Dynamic Vibration Absorbers Attached to Damped Linear Systems*. Journal of Vibration and Acoustics, 124, pp.284-295, 2002.

[3] S. BENACCHIO, A. MALHER, J. BOISSON, C. TOUZE - *Design of a Magnetic Vibration Absorber with Tunable Stiffnesses*. Nonlinear Dynamics, 85, pp.893-911, 2016.

[4] S. B. CHOI, W. K. KIM - *Vibration Control of a Semi-Active Suspension Featuring Electrorheological Fluid Dampers*. Journal of Sound and Vibration, 234, pp.537-546, 2000.

[5] J. P. DEN HARTOG - *Mechanical Vibrations*. Dover Books on Engineering, 4th edition, 1985.

[6] S. J. DYKE, B. F. SPENCER, M. K. SAIN, J. D. CARLSON - *Modeling and Control of Magnetorheological Dampers for Seismic Response Reduction*. Smart Materials and Structures, 5, pp.565-575, 1996.

[7] H. FRAHM - *A Device for Damping Vibrations of Bodies*. 1911.

[8] Y. FUJINO, M. ABE - *Design Formulas for Tuned Mass Dampers Based on a Perturbation Technique*. Earthquake Engineering and Structural Dynamics, 22, pp.833-854, 1993.

[9] O. V. GENDELMAN - *Transition of Energy to a Nonlinear Localized Mode in a Highly Asymmetric System of Two Oscillators*. Nonlinear Dynamics, 25, pp.237-253, 2001.

[10] J. GUCKENHEIMER, P. HOLMES - *Nonlinear Oscillations, Dynamical Systems, and Bifurcations of Vector Fields*. vol. 42, Springer-Verlag New York, 1983.

[11] G. HABIB, T. DETROUX, R. VIGUIE, G. KERSCHEN - *Nonlinear Generalization of Den Hartog's Equal Peak Method*. Mechanical Systems and Signal Processing, vol. 52-53, pp.17-28, 2015.

[12] J. B. HUNT, J. C. NISSEN - *The Broadband Dynamic Vibration Absorber.* Journal of Sound and Vibration, 83, pp.573-578, 1982.

[13] I. N. JORDANOV, B. I. CHESHANKOV - *Optimal Design of Linear and Nonlinear Dynamical Vibration Absorbers*. Journal of Sound and Vibration, 123, pp.157-170, 1988.

[14] I. N. JORDANOV, B. I. CHESHANKOV - *Optimal Design of Linear and Nonlinear Dynamical Vibration Absorbers, Reply*. Journal of Sound and Vibration, 132, pp.157-159, 1989.

[15] B. P. MANN, B. A. OWENS - *Investigations of a Nonlinear Energy Harvester with a Bistable Potential Well*. Journal of Sound and Vibration, vol.329, pp.1215-1226, 2010.

[16] B. C. NAKRA - *Vibration Control in Machines and Structures Using Viscoelastic Damping*. Journal of Sound and Vibration, 211, pp.449-465, 1998.

[17] J. ORMONDROYD, J. P. DEN HARTOG - *The Theory of the Dynamical Vibration Absorber*. ASME Journal of Applied Mechanics, 50(7), pp.9-22, 1928.

[18] E. PENNESTRI - *An Application of Chebyshev's Min-Max Criterion to the Optimal Design of a Damped Dynamic Vibration Absorber*. Journal of Sound and Vibration, 217, pp.757-765, 1998.

[19] G. PENNISI, C. STEPHAN, E. GOURC, G. MICHON - *Experimental Investigation and Analytical Description of a Vibro-impact NES Coupled to a Single-Degree-of-Freedom Linear Oscillator Harmonically Forced*. Nonlinear Dynamics, vol.88, pp.1769-1784, 2017.

[20] L. A. PIPES - *Analysis of a Nonlinear Dynamic Vibration Absorber*. Journal of Applied Mechanics, 20, pp.515-518, 1953.

[21] A. PREUMONT - *Vibration Control of Active Structures 3rd Edition*. Springer, 2011.

[22] R. E. ROBERSON - *Synthesis of a Nonlinear Dynamic Vibration Absorber*. Journal of the Franklin Institute, 254, pp.205-220, 1952.

[23] R. THOM - *Structural Stability and Morphogenesis: An Outline of a General Theory of Models*. Reading, MA: Addison-Wesley, 1989.

[24] A. THOMPSON - *Auxiliary Mass Throw in a Tuned and Damped Vibration Absorber*. Journal of Sound and Vibration, 70, pp.481-486, 1980.

[25] A. THOMPSON - *Optimum Tuning and Damping of a Dynamic Vibration Absorber Applied to a Force Excited and Damped Primary System*. Journal of Sound and Vibration, 77(3), 1981.

[26] A. F. VAKAKIS, O. V. GENDELMAN, L. A. BERGMAN, D. M. McFARLAND, G. KERSCHEN, Y. S. LEE - *Nonlinear Targeted Energy Transfer in Mechanical and Structural Systems I*. Springer, New York, 2008.

[27] A. F. VAKAKIS, O. V. GENDELMAN, L. A. BERGMAN, D. M. McFARLAND, G. KERSCHEN, Y. S. LEE - *Nonlinear Targeted Energy Transfer in Mechanical and Structural Systems II*. Springer, New York, 2008.

[28] K. WORDEN, G. R. TOMLINSON - *Nonlinearity in Structural Dynamics: Detection, Identification and Modelling*. CRC Press, 2000.

AUTHORS

Cyrille Stephan After having graduated from the ENSMM (*École Nationale Supérieure en Mécanique et Microtechniques*) in 2004, Cyrille Stephan obtained his PhD in Sciences for Engineering at the University of Franche-Comté in 2009. He then joined ONERA and is currently in charge of developing methods for structural dynamics, especially for signal processing and nonlinear dynamics.

Giuseppe Pennisi Having graduated in 2012 with a MS in Aerospace Engineering from the *Politecnico di Milano* and a MS in Aerospace Engineering from the *Institut Supérieur de l'Aéronautique et de l'Espace* (ISAE) in Toulouse, Giuseppe Pennisi obtained his PhD in Mechanical Engineering in 2016, working within the context of a collaboration between ONERA and ISAE. He then jointed ENSTA ParisTech as a Postdoctoral Researcher. Dynamics and Control, Vibrations, and Nonlinear Dynamics are among his main research interests.

Guilhem Michon Having graduated from INSA Lyon in 2002, Guilhem Michon obtained a PhD from the University of Lyon in 2006. Since 2007, he has been a Professor at ISAE-Supaero, conducting his research in nonlinear dynamics at the Clément Ader Institute (UMR CNRS 5312).

E. Garrigues
(Dassault Aviation)

E-mail: eric.garrigues@dassault-aviation.com

DOI: 10.12762/2018.AL14-09

A Review of Industrial Aeroelasticity Practices at Dassault Aviation for Military Aircraft and Business Jets

Aircraft structure design is a complex industrial process that requires multidisciplinary analyzes and considerations in fields as diverse as aerodynamics, structure, materials and systems, as well as the right compromise between the constraints imposed by these different fields, in order to meet the overall performances required for aircraft.
In the field of business jets and military aircraft, given the research into ever more efficient aerodynamic formulas, the constant desire to design "as light as possible", and the increase in fuselage sizes, aircraft flexibility has increased considerably over the last few decades. This has required the consideration of increasingly complex aeroelastic coupling phenomena that are present in the flight envelope from the very first phases in aircraft development. The challenge goes far beyond the domain of aerostructural performance alone, since aeroelasticity can also have a significant impact on related domains, such as aircraft performances, handling qualities, or system design. It has merely reinforced the potentially major impacts of aeroelasticity on the risks, costs and deadlines for new aircraft programs: aeroelasticity is now seen as one of the main disciplines in design, and as one of the "critical" processes in the aircraft development logic.
This highly-challenging context has been the source of major and constant modifications in the field of aeroelasticity since the 1990s at Dassault Aviation. Today, this trend continues, and aeroelasticity will have to tackle a series of entirely new challenges and needs, and continue to reinvent itself at the same pace if it is to avoid hampering innovation and future technological breakthroughs.
In this perspective, this article gives an overview of the current best industrial practices in terms of aeroelasticity in the military aircraft and business jet domains at Dassault Aviation. The main aspects of this challenging and exciting field are covered: the numerical methods and tools, the experimental validation process, the aircraft program expectations and aspects relating to human organization. It discusses the principles and guidelines rather than details about the basic equations and methods. The last part presents the future industrial challenges in the field of aeroelasticity for Dassault Aviation.

Introduction

The design of aircraft structures is a complex industrial process that requires multi-disciplinary analyses and considerations in fields as diverse as aerodynamics, structure, materials or systems, as well as the need to find the right compromise between the constraints imposed by these different fields, in order to meet the overall performances required for aircraft.

In the field of business jets, given the research into ever more efficient aerodynamic formulas, the constant desire to design "as light as possible" and the increase in fuselage sizes, the flexibility of aircraft has grown considerably over the last few decades. This has required the consideration of increasingly complex aeroelastic coupling phenomena that are present in the aircraft flight envelope from

the very first phases of development. The challenge goes far beyond the domain of aerostructural performance alone, since aeroelasticity can also have a significant impact on related domains, such as aircraft performances, handling qualities or system design.

In the military domain, the promotion of existing platforms in terms of the ability to carry multiple under-wing external store configurations, and the adaptation of these configurations to the needs and multi-role missions of customers, is also reflected by an increase in the aeroelastic phenomena present on the aircraft. The challenge is therefore to develop and certify new configurations by keeping major design modifications to a minimum (or, better yet, avoiding them), while preserving all of the performances of the existing aircraft. Aeroelasticity can motivate modifications to structures, upgrades to fly-by-wire (FBW) standards, or modifications to the architecture of aircraft systems.

Although in the early 1990s we may have thought that the domain of aeroelasticity for aircraft was one that we mastered well, and that really only required the tools and methods already envisaged in the 1960s to 1980s to be brought to maturity and industrialized in the future, the new challenges progressively imposed at Dassault Aviation at the end of the 2000s and at the start of the 21st century (design of the RAFALE air/ground standards, the FALCON 7X/8X/5X aircraft and the military nEUROn UAV) have placed aeroelasticity at the very heart of the aircraft design process, with major potential impact on the duration and costs of the various development phases and, more generally, the cost of the programs (and the associated risks). In preparing for the future, aeroelasticity has also become an indispensable factor for innovation.

This situation has been the source of major modifications to the field of aeroelasticity, in terms of the methods used, the calculation processes and the organization of human skills over the last 20 years, and, more specifically, over the last decade. Today, this trend continues, and aeroelasticity will have to tackle a series of entirely new challenges and needs, and continue to reinvent itself at the same pace, if it is to avoid hampering innovation and the setup of future technological breakthroughs.

In this context, this article gives a complete overview of the current best industrial practices in terms of aeroelasticity in the military aircraft and business jet domains at Dassault Aviation. The main aspects of this challenging and exciting field are covered: the numerical methods and tools, the experimental validation process, the program expectations and aspects relating to human organization. It discusses the principles and guidelines, rather than details about the basic equations and methods (more information about aeroelastic methods can be found in the list of references and extensive research literature). The final paragraph presents the future challenges in the field of aeroelasticity for Dassault Aviation.

The Growing Importance of Aeroelasticity Issues in Aircraft Projects

Since the end of the 1960s, aeroelasticity equations had already been well established, and the associated phenomena had already been experimentally studied in many publications. Due to a lack of computing power, engineers merely had to content themselves with simplified, and sometimes very conservative, methods to analyze this phenomenon.

Between the end of the 1960s (MIRAGE F1) and the end of the 1980s (FALCON 900, MIRAGE 2000, MIRAGE 4000 and the first RAFALE demonstrator; also CONCORDE at Sud-Aviation), the rapid growth of numerical aeroelasticity and the analysis of complex configurations, which had been difficult to obtain through analysis up until that point, were facilitated by a large number of projects at Dassault Aviation, the acquisition of the first scientific computers and, in parallel, the development of structural finite-element dynamic analyses [1]. Above all, the development of steady and unsteady linear aerodynamic numerical methods with interactions between lifting surfaces, such as the Doublet-Lattice Method (DLM) [2], [3], [4] contributed to this. A typical example is that of the delta/canard formula without stabilizer on the RAFALE.

Also over that same period, the development of in-flight instruments, telemetry and signal-processing techniques made it possible to observe and quantify the aeroelastic phenomena, and validate the associated models (or readjust them) using wind tunnel tests on flexible mock-ups or flight tests [5]. However, we should remember the accident that occurred on the first MIRAGE F1 prototype following horizontal stabilizer flutter at $M = 0.91$, at a low altitude. This accident occurred on May 16, 1967 during a training flight for a demonstration at the Paris Le Bourget airshow. It was a dark day in the history of Dassault Aviation, leaving René Bigand, the test pilot of the aircraft, no chance at all.

During this blossoming period for aeroelasticity, full of draft projects and tests on real structures (sometimes difficult), the growth and maturity of the various numerical and experimental techniques has been substantial at Dassault Aviation, and many of these techniques continue to be a point of reference, even to this day. This, to such an extent that we thought at the start of the 1990s that the field of aeroelasticity for aircraft was one that was mastered, and in the future would only require that the tools and methods already envisaged in the 1960s to 1980s reach maturity and be industrialized.

The experience of the following period between 1990 and 2020 (RAFALE, FALCON 2000/7X/8X/5X and nEUROn) and the conclusions that are drawn from it today show that, quite on the contrary, under the influence of the market and the competition, aeroelastic engineers continue to face constantly-evolving challenges today, due to the constant quest for innovative technological breakthroughs (unconventional architectures, complex configurations, introduction of composite materials, etc.), to increasingly efficient aerodynamic formulas, and to a constant desire to design "as light as possible" at reduced costs and with shorter deadlines, as well as to the increased flexibility of the aircraft and flight envelopes used and the increased importance of systems and their interaction with the aerostructure.

Aeroservoelasticity ("which adds servo in equal proportions to the other three fundamental disciplines in conventional aeroelasticity: elasticity, aerodynamics and dynamics" [82] is clearly a perfect illustration of these new challenges and of the way in which they have changed our way of looking at our practices in the field of aeroelasticity. This is a field that has been constantly evolving for more than 20 years and has witnessed exponential growth with the arrival

of the first aircraft with fully digital Fly-By-Wire (FBW) controls: the RAFALE and the FALCON 7X. Today, this branch of aeroelasticity continues to develop at a fast pace, given the new system architectures and the increased power of the controllers, new sensor and actuator technologies and innovative control surface architectures. It is also based on the fact that the aircraft, its handling qualities and aerostructural performances, are increasingly dependent on these systems.

Initial work in the field of aeroservoelasticity mainly consisted in filtering, as much as possible, the aircraft's flexible mode shapes in flight, which are "seen" by the digital FBW sensors attached to the structure, in order to decouple the rigid aircraft displacements of these flexible mode shapes, thereby avoiding aeroservoelastic instability phenomena. We are now seeking to build upon this discipline to control "flexible" aircraft and improve the aircraft's aerostructural performances. In particular, we will look in more detail later on at the potential of active control technologies on loads and flutter using the digital FBW system, which are completely changing the way we look at the design process for modern business jets and military aircraft. Simply note at this stage, that the development of aeroservoelasticity as a new branch of aeroelasticity has been accompanied over the last 10 years by a lot of new work in the following areas:

- the production of "reduced" aeroelastic models suited to the design of control laws,
- the coupling of flight mechanics with structural dynamics,
- experimental techniques (wind-tunnel and in-flight tests) and the identification of systems and aeroelastic models using real test data,
- the active control of loads and flutter,
- the integration of the interaction between systems and aerostructures in certification procedures (nominal configurations and failure cases).

The example of aeroservoelasticity is just one example, amongst others, and clearly an important one, of the new challenges in modern aeroelasticity and the abundance of scientific and industrial research in this field. We could have also mentioned the evolution in steady and unsteady CFD (Computational Fluid Dynamics) codes to predict loads and flutter, non-linear aeroelasticity, aeroelastic optimization, aeroelasticity of highly-deformable structures, aerothermoelasticity, and so on. We will return to some of these new aeroelasticity branches later on to describe their scope of application at Dassault Aviation.

However, the wealth of the field of aeroelasticity cannot only be expressed from the point of view of the discipline; it must also be examined with respect to the development process of modern aircraft and the challenges associated with the aircraft project: the "program" challenges.

In the design process for modern aircraft, mastering aeroelasticity has now become a key point and a design driver. It concerns all stages of the aircraft development phases, from the design and definition phases (Phase "A", the "feasibility phase" to obtain the general configuration; Phase "B", the "preliminary design phase" to obtain the overall aircraft definition; through to Phase "C" for the detailed definition of parts), to the justification phases that are essentially centered on demonstrating the means of compliance in relation to the applicable regulations (Phases "D" and "E", including flight tests).

The experience of the most recent projects at Dassault Aviation (FALCON 7X/8X/5X, nEUROn) clearly shows that, by going as far back as possible in the development of risk reduction linked to aeroelastic requirements, this helps to avoid major (and costly!) redesigning in the more advanced phases of aircraft design that are required to ensure the project viability.

A significant limitation to this logic is, of course, the availability and stability of the "input" data available at time "t" in the project to perform the various aeroelastic loops: typically, the status of the overall definition of the external shapes (including control surfaces), the internal architecture of the structure (*i.e.*, "ribs and panels"), the structural and non-structural masses, the system definitions, etc. The more this data is variable and uncertain, the more aeroelastic loops there are that require a lot of interpretation and engineering judgment in order to roll them out and transpose them to the entire design space, which remains still very large. This is typically the case during the feasibility phases, in which several designs and trade-offs have been assessed and in which some definition data is not fully known, or is clearly variable. Therefore, the compromise that must be found in this case, relates to the speed of obtaining the aeroelastic analysis (and the robustness of the analysis) with respect to the importance of this analysis in relation to the design process and the risks incurred by the lack of knowledge about aeroelastic phenomena in this field.

At this point in the paper, we are looking at one of the major future challenges with respect to the construction of the aircraft project: that of adapting the aeroelasticity tools and practices at the rate and short duration of the multidisciplinary design loops in the feasibility phases. Several studies are currently in progress in this field at Dassault Aviation (projects "OSANGE", "OSAVP", etc. See [6]). The challenge that clearly emerges is that of adapting the "traditional" aeroelasticity tools and practices (*i.e.*, those that were calibrated to provide the precise quantitative data needed for the safety of the flight envelope opening and to draw up certification and substantiation documents) to the logic of the feasibility phase, in which we want to prioritize the speed of analysis, and the "agility" of the tools and practices to rapidly issue qualitative derivatives and trends in "order of magnitude".

Figure 1, simplified for the sake of comprehension, summarizes all of the main aeroelastic analyses performed in the various development phases of any new civilian or military aircraft at Dassault Aviation.

The expected outcomes of the main aeroelastic loops are thus summarized as follows:

- **In Phase A – "Feasibility phase"**, as soon as an initial external shape of the aircraft and an internal structural architecture are set ("ribs and panels"):
  - Calculation of the flexible aircraft aerodynamic center and the deformed shape of the wings at different flight points during fast-cruise or long-range flight ➔ this can have a direct impact on the longitudinal position of the wings, and the jig shape of the wings.
  - Calculation of the global flexible coefficients of the aircraft and its control surfaces (aerodistortion and effectiveness) ➔ this enables the construction of the first reference aerodynamic databases (longitudinally and laterally) and an initial assessment of the aircraft handling qualities ➔ it can have a direct

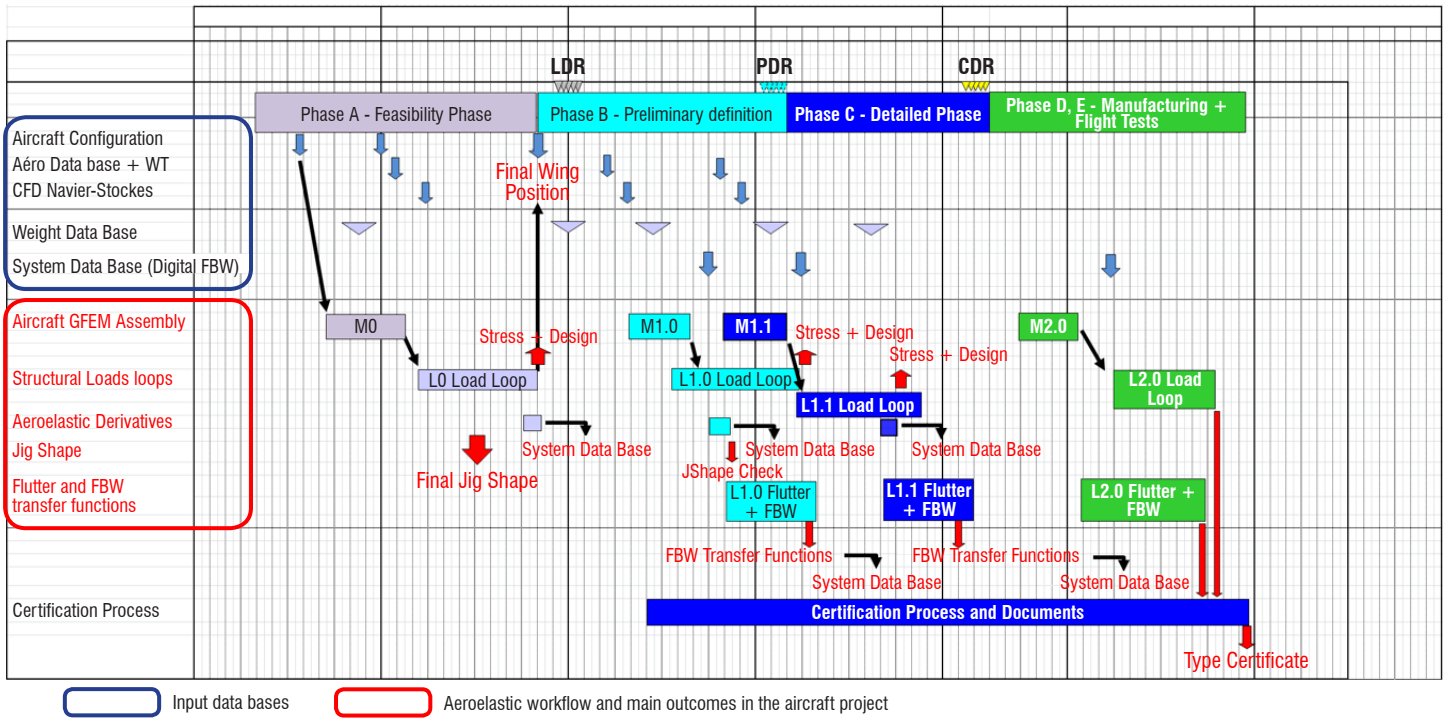

Figure 1 – Typical overall development logic for a new aircraft and the related aeroelastic analyses

impact on any redefinition of the external shapes of the aircraft (wing surface, vertical and horizontal stabilizer) and a direct impact on the surfaces or architecture of the control surfaces.
  - Calculation of the loop "L0" pre-design loads ➔ this contributes to an initial assessment of the structural mass of the aircraft in the feasibility phase, after the wing, vertical and horizontal stabilizer panels have been sized at these loads. These loads will also be used at the very start of Phase "B", as initial preliminary loads in the structural design.

- **In Phase B – "Preliminary design phase":**
  - Calculation of the "L1.0" structural design loads. These loads are used to provide an initial consolidated estimate of the sizing of all of the primary structural parts (*i.e.*, panels, stiffeners, spars, frames, etc.).
  - Calculation of the flutter speeds. This estimate is done using the structure sampled in the previous step. It is used to define the delta mass to be added to the L1.0 load sized structure to meet the aeroelastic stability objectives.
  - Calculation of the flexible response of the aircraft excited by control surface deflection at the digital FBW sensors ➔ this is used to define the best position for the digital FBW sensors in the aircraft: as near as possible to the vibration modal nodes likely to be excited by the control surfaces.
  - Final assessment of the position of the flexible aerodynamic center and the overall flexible coefficients of the aircraft and its control surfaces ➔ at this stage in the project, since the overall architecture is frozen, this data will be used to draw up the aerodynamic databases and the aircraft handling qualities, but can no longer result in architectural modifications (with no major impact on the costs and deadlines of the overall aircraft project)

- **In Phase C – "Detailed definition phase"** (aim of the end of Phase C = freezing of the definition of all structural parts in the aircraft and delivery of this definition to manufacturing for industrialization):
  - Calculation of the final "L1.1" structural design loads. These loads enable a final convergence of the sizing of all of the parts in the primary structure.
  - Verification of the flutter speeds.
  - Calculation of the flexible response of the aircraft excited by control surface deflections by the digital FBW sensors ➔ this is used to define the notch-filters that will be programmed in the digital FBW controls loops.

- **In Phases D and E – "Aircraft manufacturing, flight tests and certification phase":**
  - Calculation of the "L2.0" certification loads. These loads are the loads retained for structural strength certification. They are validated on the basis of flight tests performed on the first production aircraft specifically instrumented for the purposes of this validation.
  - Flutter and vibration synthesis. This synthesis is based on both the theoretical flutter predictions and the ground and flight vibration tests performed on the first production aircraft specifically instrumented for the purposes of certification.

All of these analyses in the perspective of the program organization call for the following comments:

- Even though flutter stability is of the utmost importance in aircraft design and certification, it is the analysis of the aerostructural loads that will be used as a baseline to size the structure. We will then try to minimize the additional structural mass to be added to this baseline, in order to satisfy the flutter requirements (given that these additions in mass for flutter are typically likely to increase the aircraft loads due to the stiffness increment that they induce through lower aeroelasticity or the dynamic effects that they can have on gust or ground loads).

The load calculation process is, therefore, certainly one of the most challenging processes in the development of an aircraft and, as such, is the attention focus of all programs.

- Each of the loads and flutter loops significantly contribute to the program expected outcomes. Indeed, these loops, which can represent several months of analysis, are needed to provide the loads that will enable the sizing of each structural part. They are, therefore, on the critical path of the program schedule for the design, manufacturing and certification of the structure. An incorrect estimate of the loads can have serious consequences on the drawing of the parts, and can result in considerable additional delays and costs. Even though load verification steps are possible during development, the ultimate load check through flight testing of the overall structure takes place at a very late stage in the program, and can be a source of major re-design risks. Therefore, one can easily see the crucial importance of predictive calculation methods for aeroelastic loads, which:
  - increase the accuracy of the assessment of structural sizing loads, directly related to the design mass,
  - are progressively enriched with partial tests during the program (wind-tunnel tests, systems tests, partial-stiffness tests, etc.) to minimize the risk of having to rework these loads at a very late stage in aircraft development.

- In the past, structural design methods were deemed conservative. Nowadays, the many improvements made to structural predictive tools, such as the finite-element method, and the improvements in drawing up structural strength criteria, have helped to reduce the margins that were traditionally adopted in design practices. Inaccuracies in the load calculation process are, therefore, more difficult to compensate for by the structural margin policy, whereas the constant innovation in the aerodynamic shapes of "modern" aircraft (for improved performance) has increased these sources of inaccuracies.

- Each of the loads and flutter loops previously mentioned are performed in conjunction with the other aircraft design disciplines, which in turn interact with the aeroelasticity and load results: typically, the drawing and the layout of the structure, the structural sizing, the aerodynamic databases and handling qualities, and the digital FBW system. These loops are therefore embedded in a more overall multidisciplinary/multi-trade process, which is complex to plan for, both from a human resources point of view, as well as from that of the calculations and associated tests. This entire process is one of the "critical" processes in aircraft design. It is a core part of the aircraft manufacturer's know-how.

The Industrial Numerical Approach to Aeroelasticity

General Principles

The development of aeroelasticity tools and methods at Dassault Aviation has been done in successive stages. It is materialized in the form of the *ELFINI* © proprietary platform developed for aircraft design needs ([7], [8], and [9]), which combines the main aerostructural analysis branches around a core of finite-elements solvers (see Figure 2 hereafter):

- calculations of static linear and non-linear stresses,
- thermomechanics,
- calculation and management of design loads (ground and flight),
- calculation of vibration modes,
- static and dynamic aeroelasticity,
- calculation of transitory dynamic and forced responses.

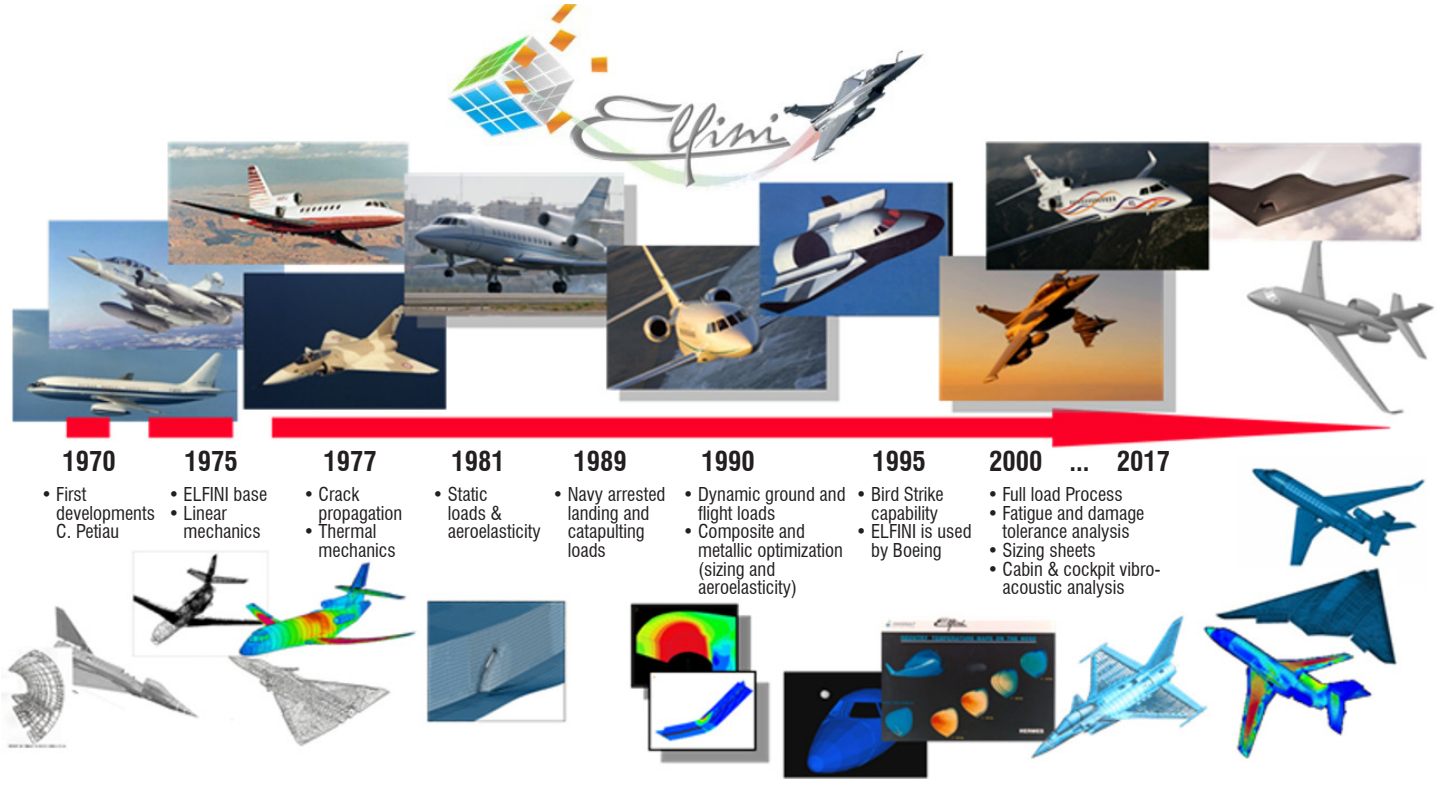

Figure 2 – *ELFINI* ©: over 45 years of experience in aircraft structure design

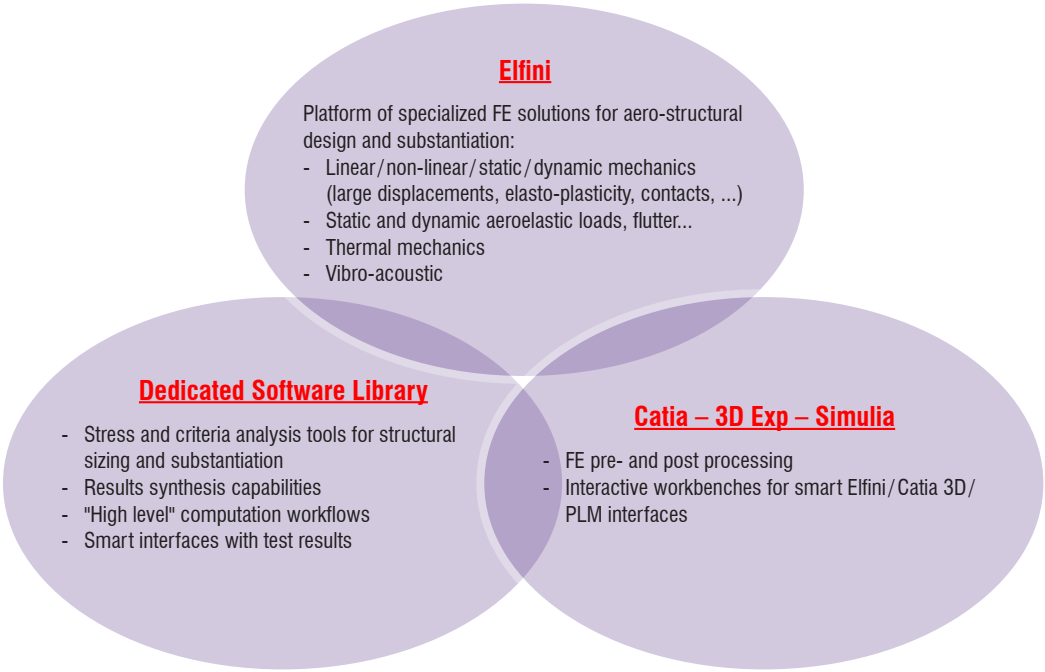

Figure 3 – *CATIA*© / *ELFINI*© cooperative platforms

As is often the case in the aeronautical industry, the main evolutions in the field of numerical aeroelasticity, and more generally in the field of structural calculations, have been mainly brought about by new aircraft programs. By imposing new challenges in terms of new technologies, the scope of use of the aircraft, industrial cooperation strategies, the organization of human and IT (Information Technologies) resources, and so on, these new programs have been formidable drivers that have quite literally propelled the advances in methods and IT architectures (see Figure 2).

A key point and an undeniable strength for all Dassault Aviation aeroelastic tools are the close links between the *ELFINI*© platform with the geometric modeler *CATIA*©, its finite-element pre/post-processor and its PLM (see Figure 3). We will see, in particular, how the parameterization of the aircraft geometry and its "inheritance" in the *ELFINI*© "computation workflow" have helped to revolutionize the practices of aeroelastic engineers in terms of calculation management, as well as in the field of aerostructural optimization.

Similarly, the traceability of models, input conditions and calculation results that are essential to the certification process, but no less vital in the design stages of the aircraft development cycle, has been greatly strengthened and made much easier in terms of its management thanks to the integration in the *CATIA*© PLM of the structural finite element, aerodynamic and aeroelastic models as well as the aircraft geometric definition models.

Over the years, the desire to mostly keep linear solvers was one of the main priorities that drove the development of tools and methods in the field of aeroelasticity at Dassault Aviation. When aeroelastic phenomena of a non-linear nature (with the non-linearity being either of aerodynamical or mechanical origin) needed to be modelled, piecewise-linear methods were preferred. This "linear" culture for aeroelastic analysis (almost a philosophy at Dassault Aviation) has indeed proved its effectiveness in the industrial domain, both in design and in certification, in terms of:

- the management of calculations and the effectiveness of the numerical processes,
- the architecture of tools and their coding,
- the understanding of calculation results, their validation by engineering judgment and their interpretation with respect to the phenomena encountered on the aircraft,
- the validation of models and their readjustment through experience,
- the communication and discussions with other aircraft design disciplines (aerodynamics, handling qualities, etc.), in which the "condensing" of the aeroelasticity field in the form of linear operators proved highly effective and industrially relevant.

Figure 4 below gives the general aeroelastic analysis process (and the associated mathematical models), as used these days by Dassault Aviation aeroelastic engineers in the *ELFINI*© environment.

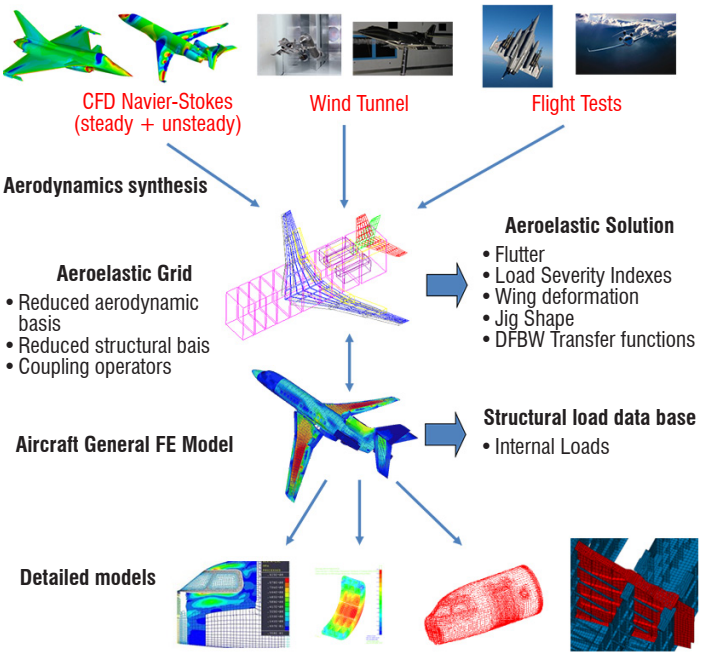

Figure 4 – Loads and aeroelasticity numerical process

The main characteristics of this process are detailed in the following chapters. However, at this stage, we can highlight the specific features that constitute its originality and its effectiveness from an industrial point of view:

- **The use of a single aerodynamic database, supported by the *ELFINI*© "aeroelastic grid" entity**, which synthetizes all of the aerodynamic information that will contribute to the aerostructural load calculations for the aircraft in flight. This information is available in the form of pressure fields on 2D grids (lifting surfaces typically) or in the form of aerodynamic field tensors "by zone" (called "boxes" in ELFINI© terminology: fuselage, high-lift devices, winglets, excrescences, etc.). At the start of the project, the aerodynamic database is mostly composed of theoretical information from the CFD calculations, readjusted by wind-tunnel tests. At the end of the project, these fields are enriched with flight-test results. It should be noted that the aerodynamic database contains both the quasi-steady part and the unsteady part of the aerodynamic field (recorded separately), which facilitates the adjustment of these two quantities independently from one another. The density of the 2D grid elements and the "boxes" is determined independently from the CFD mesh density. It is by physical consideration adjusted to enable sufficient discretization of the loads with respect to the structural sizing goal. This has the advantage of not being linked to the numerical mesh density convergence criteria of the CFD solvers, and thus of reducing the CPU calculations and processing, done within the aerodynamic database for the load calculation.

- **The use of a single structural load database, formalized by the aircraft's Global Finite-Element Model (GFEM).** The GFEM is the database of all cases of loads that the aircraft structure is subjected to. It is this same model that is also used by stress engineers to extract the internal flows inside the aircraft, which correspond to the various load cases that will be used to size the structural parts. The use of a single model shared by stress engineers and aeroelastic engineers has made it possible to eliminate redundant models, significantly reduce calculation cycles and avoid the time spent (and the resulting errors) transferring information between structural models and aeroelastic models.

- **Effective model-reduction techniques:**
  - For the structural part [10]: the finite-element displacements are reduced to a "generic" load basis, which consists of a few hundred displacements statically solved on the complete aircraft GFEM (> 100000 dof) by the loads obtained from: pressure cases projected from the "aeroelastic grid" individual pressure elements, cases of inertia loads and cases of some chosen individual interface loads (typically at the landing gear fasteners and engine or external store interfaces).
  - For the aerodynamic part [10]: the available aerodynamic quantities (pressure coefficient fields or aerodynamic load tensors per area) are linearly condensed in the form of operators that give the linearized variation of those aerodynamic quantities for unitary analytical displacements of the "monomial polynomial" type, in which the normal displacement $N(M)$ of a point $M(X,Y,Z)$ from a given lifting surface is defined in the analytical form: $N(M) = X^{\alpha}Y^{\beta}Z^{\gamma}$ (where α, β, γ are the degrees of the exponents of the "monomial" considered). This monomial base of displacements is used to represent global rigid displacements of the aircraft (plunge, pitch, roll, etc.) or partial rigid deflection of the control surfaces using 0 or 1-degree monomials, as well as analytical flexible displacements of the structure using monomials with degrees greater than 1. Note that, when drawing up the aerodynamic database and "reducing" it to the monomial basis, the definition of monomial is completely separated from the flexible displacements of the complete aircraft GFEM. Several hundred monomials are typically used for a complete aircraft, distributed in a typical manner over the aircraft wings, fuselage and stabilizers.

- **An effective organization of the coupling between the structural domain and the aerodynamic domain,** in which the aim is to perform "complex" and "heavy" calculation operations on the aircraft GFEM and in the aerodynamic database, independently from one another (these operations can be done in parallel by two different teams) and, above all, independently from all of the flight configurations and mass distributions to be considered. Only after a reduction in the structural and aerodynamic databases of only a few hundred degrees of freedom each (see previous point), can the aeroelastic coupling be solved and analyzed.

Box 1 below illustrates the main key equations, general principles and organization of the aeroelastic analyses, as performed at Dassault Aviation with the *ELFINI*© platform. The technical details of the equations and associated numerical approaches, in particular the projection operators for the pressure fields from the aerodynamic database to the aircraft GFEM, or the projection of the structural displacements from the aircraft GFEM onto the aerodynamic CFD meshes, which are today problems that have been fully mastered, can be found in References [7], [10] and [11].

Multiplicity of the Aeroelastic Calculation Conditions

One characteristic of aeroelastic analyses in the context of aircraft design and certification is the multiplicity of configurations and calculation conditions to be taken into account. It needs to cover:

- all aircraft configurations (wings in clean configuration or with high-lift devices or landing gear extended, for example),
- the entire Mach and altitude flight envelope,
- all of the internal mass distributions possible (payload configurations, tank filling, etc.),
- all external store configurations or sub-configurations for military aircraft,
- all of the maneuvers possible and external solicitations (discrete gust, continuous turbulence, etc.),
- all of the possible cases of system failures (including failures in the digital FBW control system, anti-icing system, pressure system, etc.).

In all, several hundreds of thousands of aeroelastic calculation conditions (nearly a million!) are needed to cover the design and justification of a civilian aircraft of the type FALCON 8X or 5X.

The trend over the last few years continues to be an increase in the number of cases to be considered, given the (fully understandable) desire to not overlook a critical condition, and to avoid late redesigns, as well as to reduce margins as much as possible, so that unnecessary structural mass is not allocated.

Box 1 - Organization of aeroelastic analyses with "Load" and "Aerodynamic shape" basis reductions

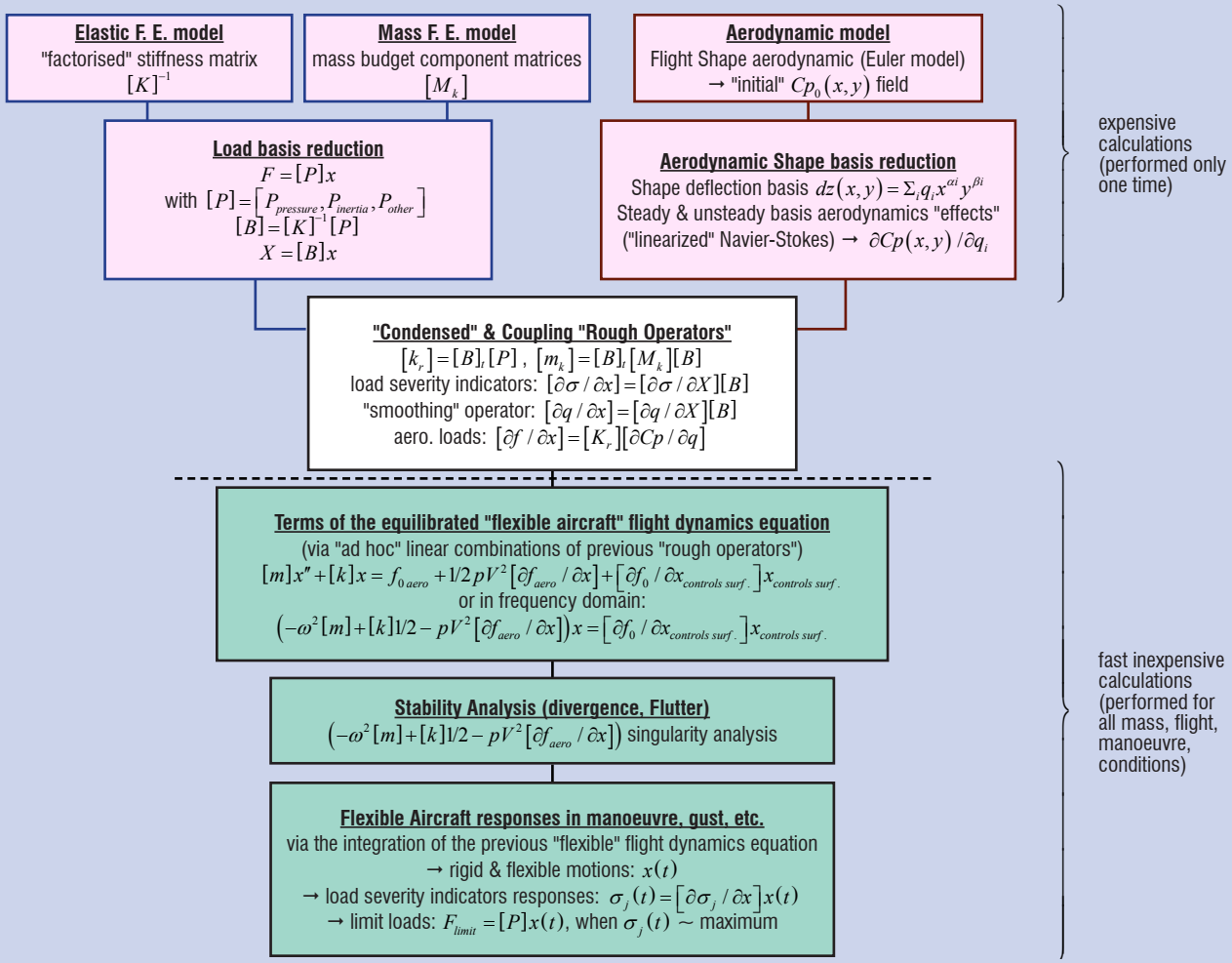

One element that also contributes to this trend towards ever more calculation conditions is the effectiveness of the analysis process itself. It gives the aeroelastic engineer the impression that having a lot of calculation cases does not significantly affect the analysis process as a whole. When this drift stems from this impression, it absolutely needs to be tackled because it tends to completely hinder the aeroelasticity engineer's intuition. Since they are fully occupied with managing the pre- and post-processing stages of the analysis results and the sheer amount of data, aeroelasticity engineers can no longer intuitively discern the most critical calculation conditions (since they forget to use their physical intuition, for example), nor are they able to focus all of their attention on these conditions, which are nonetheless of the utmost importance for the structural design and mass.

Model Organization and Implementation

As already discussed, all of the architecture in the aeroelastic analysis process at Dassault Aviation has been built and arranged in such a way as to reduce analysis cycles as much as possible, on the critical path of structural design (and therefore of the manufacture of the first series-production aircraft). With this aim, the definition of structural, aerodynamic and aeroelastic models is essential to enable each domain to be expressed with known quantities that are necessary and sufficient, as well as to avoid model redundancy and reduce information transfers from one field to another.

The fineness and density of these models to the "just enough" amount are also important issues. Especially so when there is a very large amount of calculation cases to be considered for the aeroelasticity analysis.

Another basic principle was also to build a calculation process that is similar throughout the aircraft design and certification cycle, and to apply the changes in definition, throughout the aircraft development, to just the models and not the calculation process itself. The aim of this is to minimize calculation workflows and tool variants and, consequently, the risk of handling errors and construction errors in these workflows.

To tackle the large volume of aeroelastic analyses and calculations, we have in the past opted for simplicity, by using a finite-element "stick model" (also called "beam models") to represent elasticity and the distribution of aircraft masses, and to project the aeroelasticity equations. The elastic part of this model thus resulted from the beam theory. In this case, configuration scanning was inexpensive, and the analysis of results and empirical corrections was simple. For a long time, these advantages have concealed the weaknesses in terms of the quality of the stick model representativeness: we tried to compensate for this shortcoming through stick-model calibrations on test results, or on more sophisticated calculation results.

The "topological" inability to represent the delta wings of military aircraft using stick models have led to the direct use of the GFEM for

the complete aircraft and to link it directly to the aerodynamic models available via what is called the "aeroelastic grid" in the *ELFINI* © organization (see the illustration in Figure 5). The challenge was, therefore, to find an organization to solve aeroelasticity that was almost as flexible as the one using stick models.

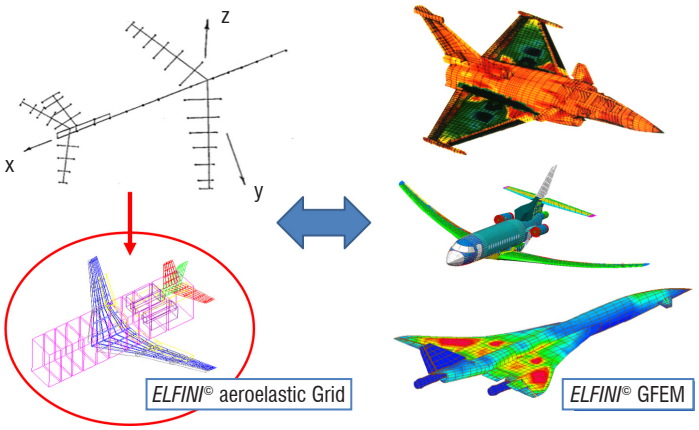

Figure 5 – From stick model to the use of an aeroelastic grid in the *ELFINI* © load and aeroelastic process

This organization is now based on 3 types of model:

- **The structural GFEM and the aerodynamic CFD model for the aircraft**, which are complex in nature and for which the definition could evolve in stages, according to the project definition status (see Figure 6 below).

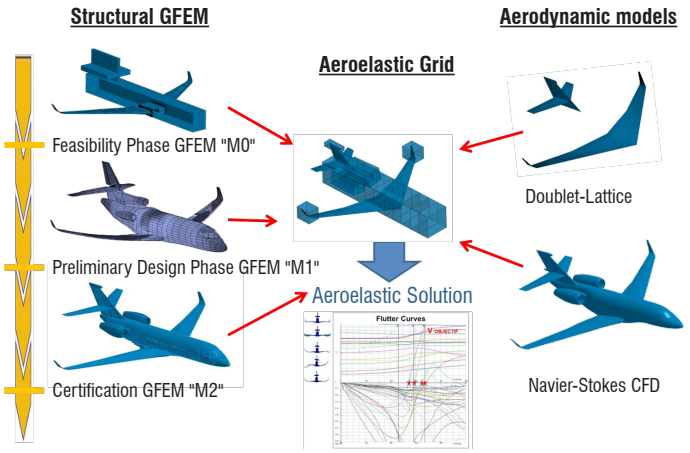

Figure 6 – The aeroelastic grid as the backbone of the ELFINI© aeroelastic analysis process

- **The "aeroelastic grid"**, which, in the spirit of the stick model, will be at the heart of aeroelastic solving. The "aeroelastic grid" is a conceptual entity used to:
  - manage the fineness of the reduced load database and the reduced monomial displacement base for aerodynamic calculations,
  - include all condensed and reduced operators, containing the only data involved in aeroelastic coupling. These operators are calculated using the aerodynamic CFD model and the aircraft GFEM:
    - reduced stiffness and mass matrices in the load basis,
    - smoothing operators of the finite-element displacements by the monomial analytic displacements,
    - reduced structural monitored quantities in the load basis: reactions to interfaces, general loads, flows and local stresses, etc. These monitored quantities will make it possible to determine the severity of loads on the structure sizing (see the notion of Load Severity Indexes detailed hereafter in this paper),
    - aerodynamic projection operators: used to either go from pressure field coefficients on CFD meshes to "peak" pressure fields centered on each node of the "aeroelastic grid" or "box" resultants; or go from pressure fields on the "aeroelastic grid" to finite-element node loads of the aircraft GFEM.

In this organization, the "aeroelastic grid" is the sole recipient for all of the aeroelastic solutions produced: the analysis of dynamic and static loads, flutter, aeroservoelasticity, control surface effectiveness and global flexible coefficients.

A very important aspect, in terms of the previously-described challenges, is that the definition of the "aeroelastic grid" (density, pressure zones, "boxes") will only change very little (or better yet, not at all, which is the aim) throughout the aircraft project. This will enable highly-similar aeroelasticity solutions, with the same granularity regardless of the mesh density and the level of precision of the aircraft GFEM or the CFD model.

Another important aspect is that the "aeroelastic grid" density is determined by "physical" representativeness criteria for structural loads from a structural sizing point of view. These criteria are completely independent from the criteria that govern the aircraft GFEM mesh density, or those of the aerodynamic CFD mesh cells, which are, in essence, dictated by numerical convergence criteria. When uncorrelated from all "numeric" density criteria, "aeroelastic grid" handling becomes much easier and uses far less CPU resources than the aircraft GFEM does, or than that of the aerodynamic CFD model.

Once the design loads have been calculated in the reduced load basis, they can be restored to the aircraft GFEM for analysis by the stress engineers who are designing the structure and who share the same finite-element model for the aircraft as the aeroelastic engineers. The "model cascade" technique (see Figures 4 and 7), which is now "a classic", is used to go from the representation of internal load flows in the aircraft to local stresses located at critical points in the structure panels (hole edges, assemblies, stiffener stops, etc.) or to the buckling stability analysis of critical aircraft structural elements

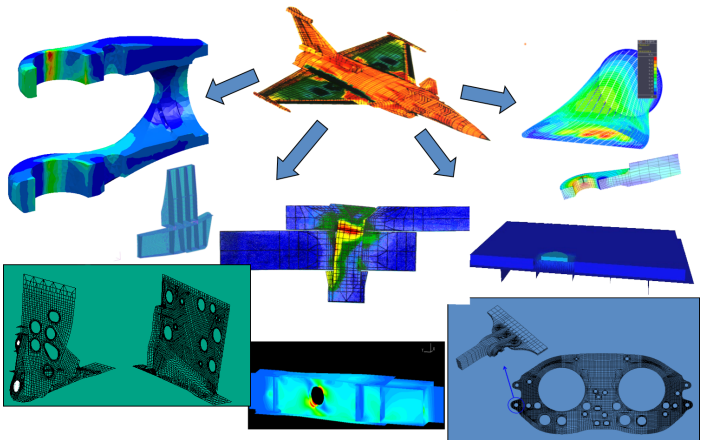

Figure 7 – Model cascade: from global internal loads to local critical stress analysis

(panels, stiffeners, etc.). To do so, the aircraft GFEM is used to define balanced load conditions on "isolated" refined finite-element models of structural parts or sections of the aircraft, which, given their mesh densities, are used to precisely discretize the geometry and any structural damage (see the damage tolerance analysis).

The Great Potential of CFD Aerodynamic Modelling

One of the greatest advances over the last 20 years at Dassault Aviation in the field of aeroelasticity was the progressive replacement of Doublet-Lattice linear aerodynamic modelling with steady and unsteady aerodynamic CFD codes.

These "high-fidelity" codes have the crucial advantage of capturing viscous phenomena and the effects of compressibility, whether steady or unsteady, even for highly-complex configurations, such as heavily armed military aircraft or FALCON high-lift configurations (see Figure 8 hereafter), without losing precision in the subsonic or supersonic regimes with respect to the Doublet-Lattice method.

At Dassault Aviation, the introduction and use of CFD for aeroelastic analysis has been done in stages: firstly, by the introduction of the Full Potential method, the Euler method and finally the Navier-Stokes method ([13] to [21]). The change involved first using the CFD codes to calculate rigid effects, while keeping the Doublet-Lattice modelling for flexible aeroelastic effects. Then CFD progressively took hold to model aeroelasticity as well.

Nowadays, the standard reference CFD for aeroelasticity, used as part of the development and certification of the latest aircraft produced by Dassault Aviation (FALCON 7X/8X/5X and the most recent RAFALE standards), is the Navier-Stokes CFD AETHER code, for steady and unsteady computations [21]. This code was developed internally at Dassault Aviation by the Aerodynamics department. The Doublet-Lattice method does, however, continue to be used as a backup for CFD, given its extensive use in the aeroelastic design practices for the previous aircraft method and the experience accumulated in flight tests. All of this makes it a reference method at Dassault Aviation, which we would not wish to abandon completely.

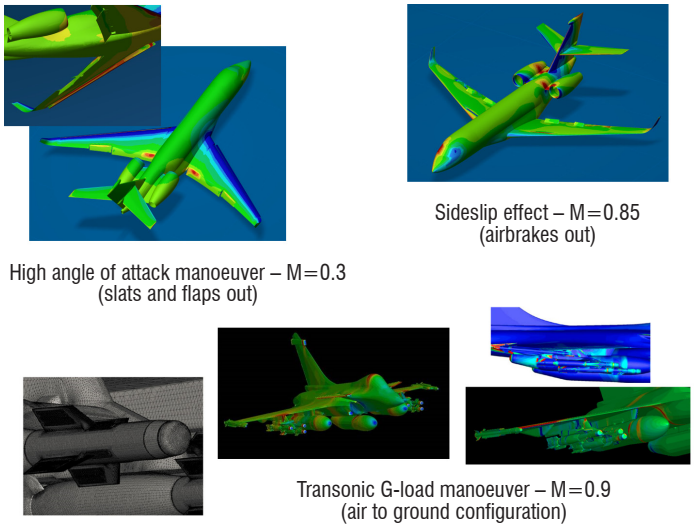

Figure 8 – Example of typical CFD Navier-Stokes analyses for structural load predictions in complex configurations

The introduction of a Navier-Stokes CFD code in the aeroelastic analysis process has raised a range of difficulties in practice:

- From the point of view of numerical techniques, the use of this code within the framework of aeroelastic analysis poses new problems with respect to the CFD calculations done "classically" for aircraft performance studies (drag, max Cz, buffeting, etc.):
  – the aeroelastic deformations of the aircraft structure can lead to aerodynamic mesh deformations with unacceptable element volumes or topological distortions in aerodynamic mesh elements,
  – the modelling of turbulence in the steady and unsteady regimes (Spalart-Allmaras, K-ε, K-ω, K-ℓ, K-KL, etc.) can have a considerable impact on the results of the aeroelastic behavior calculations for the aircraft, particularly in the case of strong aerodynamic interactions or separations.

- The preparation time for CFD models and the associated resolution times can be highly prohibitive with respect to the Doublet-Lattice method.

- The Navier-Stokes equations are non-linear in nature. It is not naturally easy to solve and process these equations within the efficient linear aeroelasticity organization designed and implemented for decades at Dassault Aviation in the *ELFINI* © platform.

- Even though this code has been relatively well validated in the steady regime in the past, based on the many wind-tunnel tests on pseudo-rigid mock-ups (for aspects related to drag predictions in particular), it lacks experimental validations in the unsteady domain.

It was quickly decided that the top priority should be to solve the 3rd point detailed above and to adapt the use of CFD to aeroelasticity in an organization that is just as flexible and effective as the one that we have with traditional linear methods. To do so, the method adopted for aeroelasticity was to solve the steady and unsteady Navier-Stokes linearized equations for small structural displacements.

Many publications describe in detail this work, which has resulted in the production of a linearized Navier-Stokes CFD code for aeroelasticity applications at Dassault Aviation (with [18], [19], [21] as typical references). These developments have been achieved thanks to support from the DGA and DGAC ([22], [23], and [24]). They would not have been completed so efficiently without the close cooperation between Dassault Aviation and ONERA. ONERA has played a crucial role in R&D, and in the numerical and experimental validation of these new approaches. This theoretical work has also helped to solve the numerical difficulties linked to the first point in the previous list.

It is also noted that one of the major benefits of the exact linearization of Navier-Stokes equations lies in the fact that complex aerodynamic calculations can be performed only once, at the start of the project, on the basis of monomial analytical displacement shapes, regardless of the knowledge of aircraft structural modes and displacement cases under load conditions. The aerodynamic fields resulting from any structural mode shape or from any displacement case under load conditions can then be obtained, for a marginal additional cost, by combining these "basic" pressure fields via the smoothing operator for a structural flexible displacement in the monomial basis. This

property distinguishes the "exact" linearization method of the Navier-Stokes equations adopted by Dassault Aviation from the time-domain harmonic balanced linearization methods that can be found in some publications ([25], [26]): in the case of time domain harmonic balanced methods, the derivatives for the aerodynamic quantities are numerically obtained with an accuracy linked to the numerical residual. When these residuals are recombined through the monomial displacement smoothing operator, they may completely ruin the precision of the recombined aerodynamic field, rendering it very inaccurate.

In parallel to these developments, substantial investments have been made at Dassault Aviation to experimentally validate these methods, again thanks to the support from the DGA and DGAC and in active collaboration with ONERA (including the use of the ONERA Modane wind-tunnel facilities). These validation campaigns were performed using flexible mock-ups, designed, manufactured, instrumented and implemented in wind tunnels by ONERA. The details of these validation campaigns are given in "Experimental validations and model-calibration methods".

Finally, we note that specific "direct coupling" tools in the time domain for structural and aerodynamic steady and unsteady equations have also been developed (full CFD-CSM codes coupled in the time domain, *i.e.*, "big game"). These tools, which are "beyond" the normal industrial process itself, given their prohibitively high costs and the fact that highly-specialized skills are required to handle them, are reserved for cases of extremely non-linear and highly-complex coupling between the structure and the aerodynamics, like those of the B-1 bomber [27] or of the F16 in heavy under-wing external store configuration [28]. If these cases are encountered during the development of an aircraft, the policy adopted by Dassault Aviation (where possible) is to deal with the aerodynamic design of the aircraft as a priority and to regularize the phenomena first, in order to avoid ever having to use such a tool for the aeroelastic analysis. It could, therefore, be thought that the simple analysis of the aerodynamic field (*i.e.*, position of separations, position of any shock waves, etc.) for imposed structural mode shapes would suffice to make designers think carefully about modifications in the aerodynamic design, without needing to model the complexity of coupling between the structure and the aerodynamics. Past experience has shown that the aerodynamic design criteria taken from the military domain (subsonic and supersonic) for designing the external aerodynamic shapes of Dassault Aviation aircraft have made it possible to prevent this type of phenomenon from occurring. This is true even in the business-jet domain, which was able to benefit from these aerodynamic design rules derived from the know-how in the military domain.

The "Global" Approach for Selecting Critical Load Cases

Given the millions of load cases that must be considered to size and certify the structure (see §"Multiplicity of aeroelastic calculation conditions"), it is inconceivable that they will all lead to detailed stress analyses. Otherwise, the analysis capabilities would be saturated, designers would be unable to focus their attention on the most critical cases, and the costs for the project and the lead times for each aeroelastic analysis "loop" would increase excessively.

The approach adopted at Dassault Aviation consists in using the notion of Load Severity Indexes (LSI) along the resolution of aeroelasticity and for load calculations. This is only possible because the aircraft GFEM is unique and shared by the aeroelastic and stress engineers who are sizing the structure.

LSI are defined as a set of finite-element operators (called "gages" or "monitored quantities" in *ELFINI* © jargon) that apply to the aircraft GFEM displacements, and are used to produce quantities ("indexes") that will monitor the rupture modes for a complete section or part of the aircraft structure. The LSI will, therefore, be used to check the severity of a load case by applying this operator to the solved displacement case for this load case on the aircraft GFEM, and by comparing the value obtained with respect to a limit value in relation to the structural strength of the section considered.

Note that this approach is a "global" one and not a "local" one:

- The LSI are properly defined on the aircraft GFEM (shared by the stress engineers and aeroelastic engineers), and not in a detailed finite-element model of a structural section. This will enable their reduction in the reduced-load basis used to solve aeroelasticity (see the equations in Box 1).

- The LSI are not intended to give an indication that is directly comparable to a strength allowable locally (therefore, it alone cannot judge the structural strength with respect to a load case); it is intended to give a global evaluation of the severity of a load case with respect to another one over an entire structural area/section of the aircraft.

Figure 9 illustrates the example of a typical set of LSI used to ascertain the severity of FALCON load cases on the various structural sections: wing, fuselage sections, horizontal and vertical stabilizer. On a FALCON wing, which is close to a beam behavior, the LSIs typically used are general loads over approximately twenty pre-defined cuts.

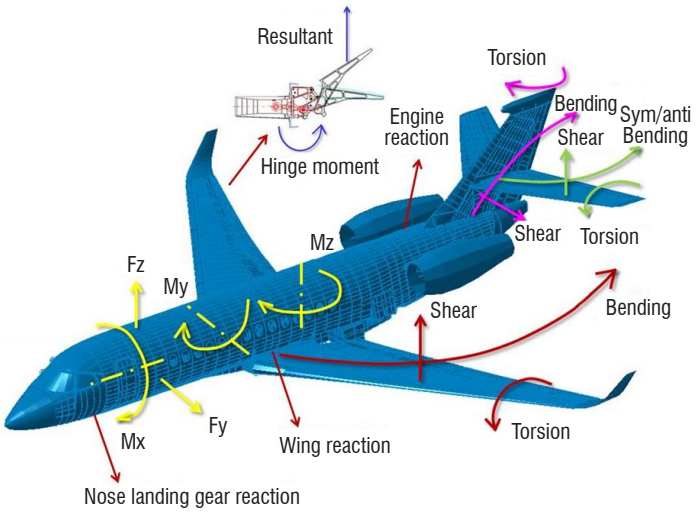

Figure 9 – Typical Load Severity Indexes (LSI) on a generic Falcon

Once all of the LSI have been reduced in the reduced load basis used to solve the aeroelasticity (see Box 1 above), it is calculated very quickly and can be done for all of the multiple calculation conditions to be considered in the aircraft load analysis. The analysis of the LSI values thus obtained is used to select the most critical load cases for each aircraft section. We typically go from a million load cases calculated for the load analysis to a few dozen critical-load cases. These are the critical cases known as "envelope-load cases" (or "sizing-load cases"), which are returned to the aircraft GFEM

and are subject to a precise structural strength analysis by the stress engineers. Figure 10 given below illustrates the few typical "envelope-load cases" that are well-known to size the wing of a generic FALCON.

For digital FBW aircraft (FALCON 7X/8X/5X, nEUROn and RAFALE), the LSI approach is also used to adjust the flight-control system gains and demonstrate that, regardless of the flight conditions, the FBW system keeps the aircraft within its structural design domain (*i.e.*, "carefree handling" philosophy). For this, the aeroelastic model is introduced into the simulation models used to design the FBW system. The LSI thus enable the "FBW system engineers" to check the effect of the FBW system gains on the structural loads induced by the pilot and the internal control loops of the system itself.

During the first part of the development phase of a new aircraft, this method has the advantage of being able to reach compromises between the aircraft performance delivered by the digital FBW system and the level of the design loads (therefore, the structural mass needed to size the aircraft) in a simple and optimal manner. In the more advanced project phases, this helps to ensure that every time a new digital FBW standard is set (and some can occur at a very late stage in the project), the aircraft design loads are not affected.

To be correctly implemented, note that this approach calls for a high degree of consistency between the aircraft's aerodynamic flexible global coefficients used to compute the structural loads and those used in flight mechanics to determine the digital FBW control laws.

Linear Flutter

The preferred method to solve linear flutter at Dassault Aviation is the P-K method modified by J. P. Brevan in the 1970s and incorporated since then in *ELFINI* ©. Its essence relies on the matched-point algorithm ([7], [29]).

Since its initial development up to the current day, flutter solution has not changed very much in terms of its theoretical principles. The main changes concern:

- **The introduction of digital FBW laws in formulating the flutter** eigenvalue problem to be solved; the implementation of the P-K method, meanwhile, remains identical. Two variants are possible [30]:
  - either the impedance of the digital FBW system is formulated in the frequency domain, and introduced into the flutter solution in a similar fashion to that of the general aerodynamic force matrix; therefore, we only monitor the evolution of the elastic poles coupled with aerodynamics, according to the flight point,
  - or we have a formulation of the digital FBW system laws in a state-space form (state-space model), and the flutter equation is "increased", alongside the general structural elastic degrees, to introduce the additional degrees of freedom coming from the internal digital FBW system variables. This variant is useful to be able to monitor the change in the digital FBW system poles coupled with aerodynamics according to the flight point, in the same manner as elastic poles. However, as the size of the aeroservoelastic system to be solved increases with respect to the first variant, the flutter resolution times using the P-K method are longer.

- **The use of a representation of the generalized aerodynamic forces in a state-space form.** To achieve this, the general aerodynamic forces are rationalized in the Laplace domain, using the Roger method [31] or the Karpel method [32]. The Karpel method is used, with a lesser degree of precision, to conduct a minimum-state method in terms of internal degrees of freedom. Once this operation is performed, the flutter equation can be formulated under a "state-space" form, with the degrees of

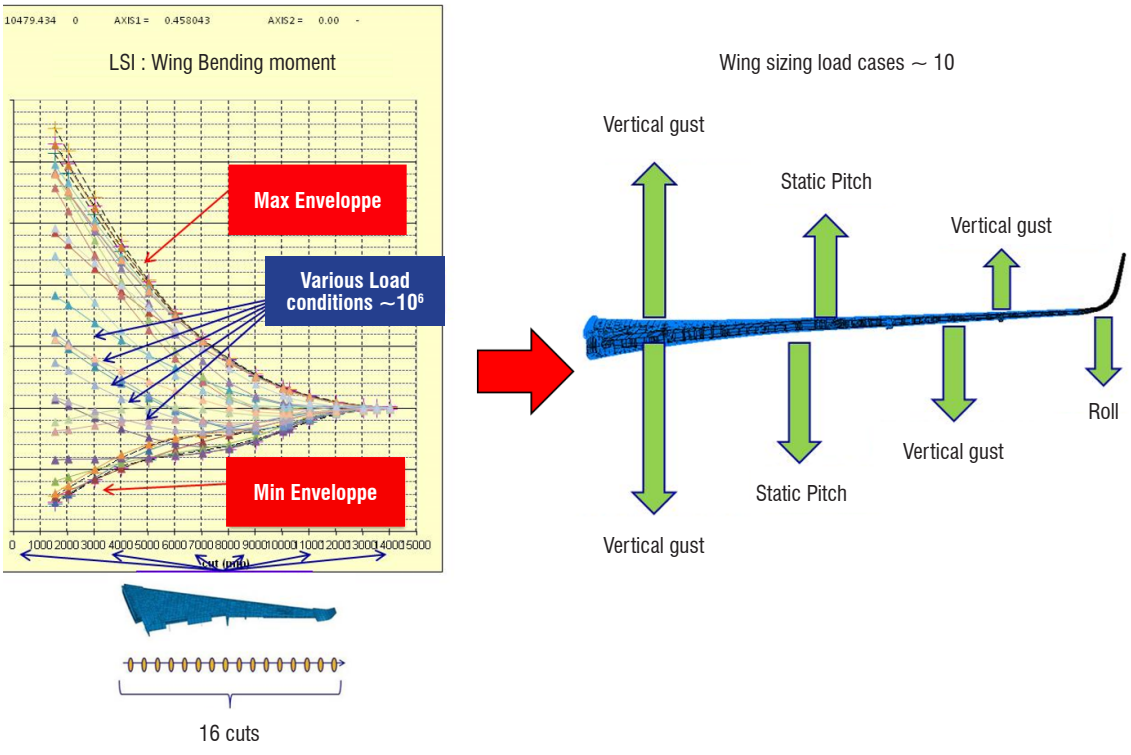

Figure 10 – Typical application of LSI for the selection of the wing envelope (sizing) load cases on a generic FALCON

freedom still being the concatenation of elastic degrees and "aerodynamic" degrees coming from the aerodynamic rationalization. The eigenvalue problem can then be resolved by classical methods like the QR algorithm, using the Hessenberg matrix form [33]. The advantage of this representation for the generalized aerodynamic forces is that:

– The specific flutter value equation can be solved by a "direct" non-iterative method, unlike the P-K method, making it possible to avoid some of the convergence issues arising from the P-K method if the modal density for the structure is high.
– It "naturally" enables the introduction of the digital FBW system in the same ways as in the 2nd variant of the previous point. The flutter equation solution therefore enables the monitoring of elastic, aerodynamic and digital FBW system poles in the flight envelope.

The progress made over the last 10 years in linear flutter analysis at Dassault Aviation has mainly been in the development of dedicated post-processing tools, which will help the aeroelastic engineers to have a better "physical" understanding of the flutter mechanisms for which the numerical solution remains highly mathematical in nature (*i.e.*, solution of an eigenvalue equation):

- calculation of the complex mode shapes at the flutter points (see Video 1 of a typical flutter displacement mechanism computed on the RAFALE in air-to-ground configuration, far away from the flight-domain envelope),
- calculation of the energy exchanges between the modes involved in the flutter mechanisms,
- automatic reduction and simplification (on energy principles) of the flutter mechanism to the main contributing modes (with variable energy threshold criteria used to refine this reduction to a greater or lesser extent),
- calculation of the power flows at the flutter points used to discern the dissipating lifting surfaces from the lifting surfaces contributing to the instability mechanisms (see Figure 11) [20],
- automatic plotting of the response surfaces of the instability speeds according to multiple structural parameters (rigidity and mass of the structural parts involved in the flutter mechanism modes), aerodynamic parameters (for example: pressure coefficients due to wing tip/winglet interactions or wing tip/missile interactions), external shapes (winglet sweepback or dihedral,) or "system" parameters (control surface servo-actuator stiffness, typically).

These flutter post-processing tools have proven to be essential in many design situations to better understand the flutter instability

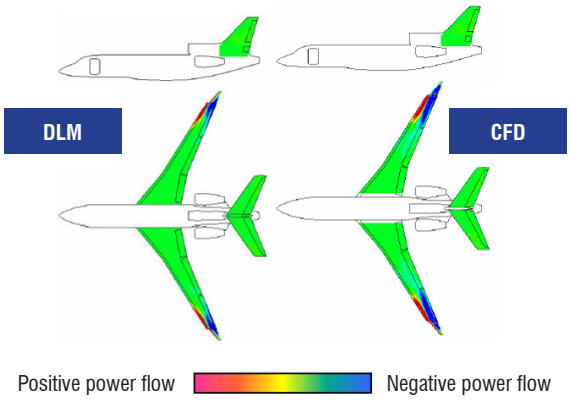

Figure 11 – Aerodynamic power flow on a flutter point of a generic FALCON

mechanisms, physically-speaking, particularly in the case of FALCON business jets, or in the case of heavily-armed configurations for military aircraft, given the major complexity of the flutter mechanisms encountered (resulting from the increased flexibility of the structures, the high modal density, and the potential coupling between the various lifting surfaces). These tools have provided a greater understanding, which has successfully guided the designers in the various modifications possible to the structural design, where the experience of a designer alone, without an effective analysis tool, may not have sufficed and could have led to excess mass over an area certainly far larger than necessary, and the risk that flutter stability objectives would not be met.

Aeroservoelasticity

On both military and civilian aircraft, the introduction of digital FBW controls (RAFALE, nEUROn, FALCON 7X/8X/5X) and their major interaction with handling qualities and aircraft performances, have reinforced the need to also analyze possible couplings between the domains of digital FBW control and aeroelasticity.

One of the reasons for this is that, when designing FBW control laws, "system" engineers consider the aircraft to be a "quasi-rigid" aircraft. However, the increased flexibility of structures (FALCON 7X vs. FALCON 900 or RAFALE vs. MIRAGE 2000), and the heavily loaded configurations with multiple external stores in the case of military aircraft, such as the RAFALE, mean that the structural modes have frequencies that are getting closer and closer to the frequencies of flight mechanics "modes" (angle of attack oscillation, Dutch roll, etc.). The current strategy used at Dassault Aviation, therefore consists in filtering the flexibility information measured by the digital FBW sensors attached to the structure, using notch-filters, before determining the control surface order via the digital FBW system, on the basis of this information.

In the 1980s to 1990s, the design of the notch-filters was mostly based on the ground and flight measurements of the flexible transfer functions between the FBW sensors and control surface excitation. This was done using pole extraction and identification techniques on those tests. There were many drawbacks to this strategy:

- Very "heavy" ground and flight test campaigns that comprised many flight points and multiple configurations.

- The risk of having to rework notch-filters at a very late stage in the aircraft development, at the time of the first ground or flight tests. This could have significant consequences if these filter modifications, given the dephasing that they could induce at low frequencies, were to be the source of delays in the digital FBW control loops, and these delays themselves could be the cause of deteriorated handling qualities of the aircraft.

- In the case of military aircraft, there was the risk of building flight-test programs that would be unable to measure the "worst" configurations with respect to the flexible transfer functions at the FBW sensors, given the large amount of configurations and sub-configurations to be considered (multiple external stores and fuel consumption in internal or external fuel tanks, etc.).

Over the last 15 years, the major challenge presented by aeroservoelasticity at Dassault Aviation was therefore to rely more and

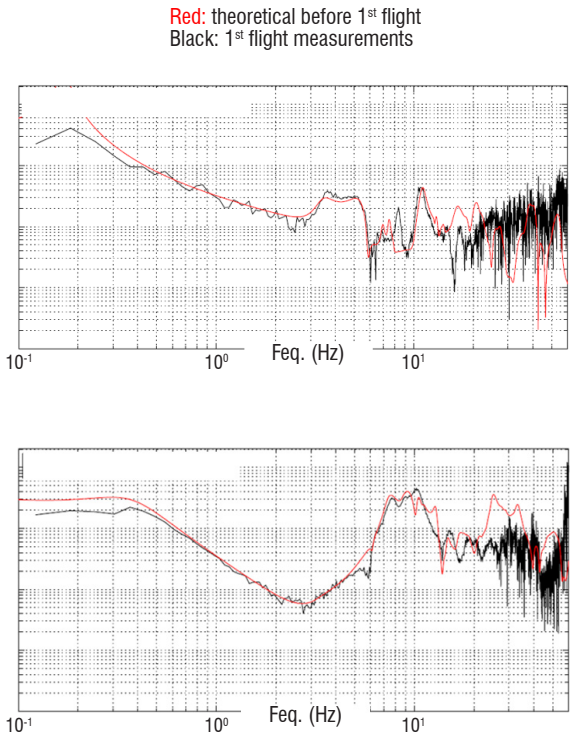

Figure 12 – Comparison of theoretically predicted and measured (very first flight) digital FBW transfer functions on F7X

more on dynamic aeroelastic predictions and to introduce it in the notch-filter design cycle as early as possible in the aircraft development, to reduce the disadvantages listed above. The efforts made in modelling and the associated investments (drafting of "specific" modelling rules and practices based on prior experience, introduction of linear Navier-Stokes CFD models in the aeroelastic tools, recalibration tools on the basis of partial or complete ground and flight tests, specific pre- and post-processing tools, etc.) have been enormous given the stakes, but also due to the fact that the modelling of aeroelastic flexible transfer functions at digital FBW sensors needs to be much more precise for the purposes of aeroservoelasticity (and the design of notch-filters) than in the case of other dynamic aeroelastic analyses.

As an illustration, Figure 12 gives the precision of the predictions for some of the digital FBW sensor transfer functions obtained by the aeroelastic model before the first flight of the FALCON 7X and the comparison with the very first results obtained subsequently during the first flights of this aircraft.

On the RAFALE, this strategy of using the aeroelastic model for aeroservoelasticity was also successfully applied in the development and certification of the "F2" air-to-ground standard [83]. Particularly to:

- Calculate several tens of thousands of external store configurations and sub-configurations for this standard and to only keep a few dozen of the most critical configurations with respect to the aeroservoelastic stability of the aircraft.

- Only rework the preceding standard "F1" (preceding the "F2" standard) notch-filters on the longitudinal or lateral axes and frequency domains to just the right amount with respect to the information given by the theoretical aeroelastic model, in order to minimize the impact on the aircraft handling qualities.

- Build flight test programs limited solely to the configurations (and sub-configurations) identified as being the most critical by aeroelastic calculations, with respect to the aeroservoelastic stability (see first point above).

Figure 13 gives an illustration of some of these calculations in the case of two asymmetric air-to-ground configurations of the RAFALE, including a comparison with flight-test measurements.

Figure 14 shows how the introduction of CFD with respect to the Doublet-Lattice method has contributed to the assessment of an aeroservoelastic transfer function.

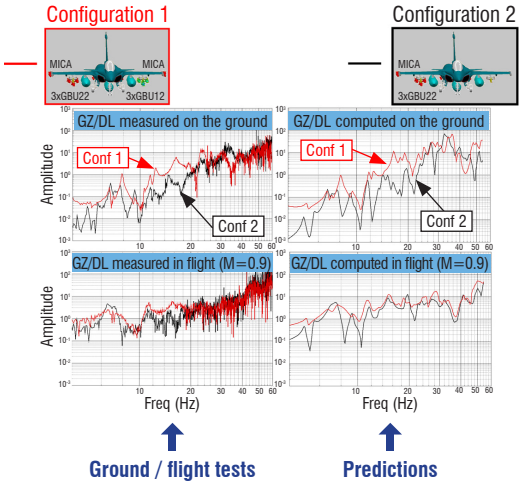

Figure 13 – Comparison of predicted and measured digital FBW transfer functions "Gz/sym elevons" on two asymmetrical air-to-ground configurations of the RAFALE

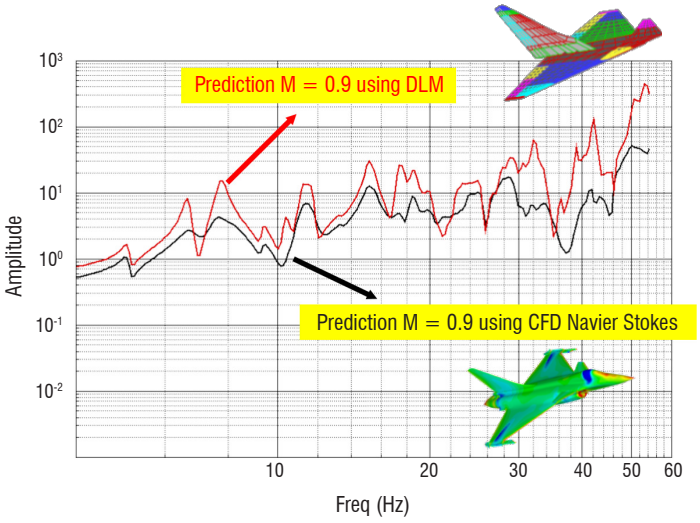

Figure 14 – Comparison of predicted digital FBW transfer functions "Gz/sym elevons" computed with Doublet-Lattice Method and CFD Navier-Stokes for configuration 1 of Figure 13

Figure 15 gives an estimate of the number of flights "saved" by using the aeroelastic model for aeroservoelasticity studies with respect to the initial estimate made by applying the conventional strategy of producing and validating notch-filters through ground and flight test campaigns [83].

As we can see in Figure 15 hereafter, the gain is over 150 flights, representing several months of flight-test activities. These savings alone justify the investments made to develop, debug and validate the computing aeroservoelastic approaches implemented, which also include the additional tests that were needed to recalibrate and gain confidence in the aeroelastic models.

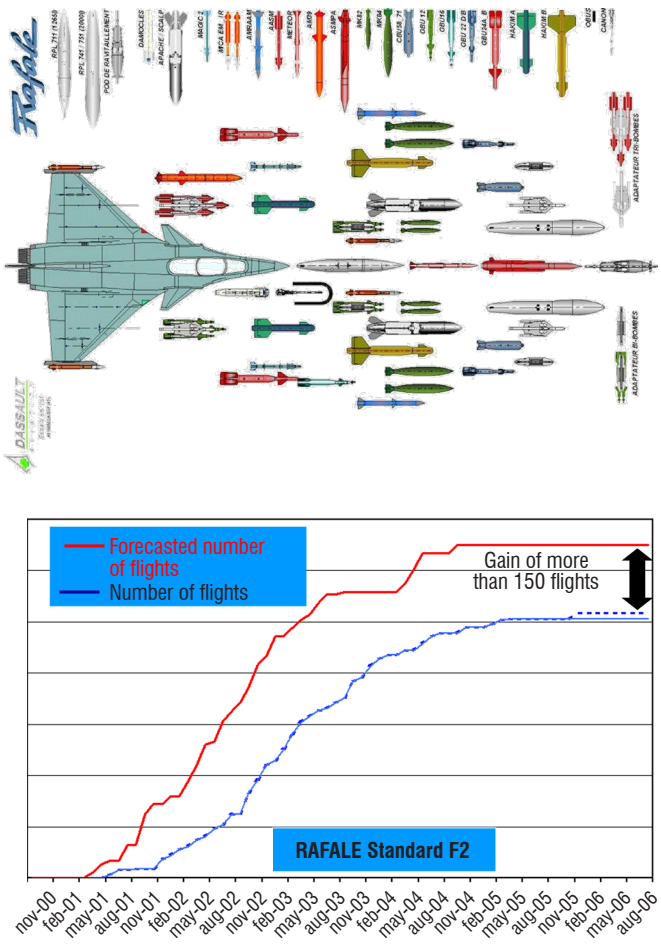

Figure 15 – RAFALE F2 "air-to-ground" standard: gain in number of flights obtained by using the aeroelastic prediction tool for aero-servo-elastic stability clearance

Non-Linear Aeroelasticity and Limit Cycle Oscillations (LCO)

The sources of aeroelastic non-linearity mostly encountered on military aircraft and business jets are either of an aerodynamic nature:

- transonic regime,
- static and dynamic load non-linearities due to large angles of attack or sideslip angles of the aircraft, or due to large control surface deflections,
- unattached flows,
- stalling,
- turbulent-laminar flow transition,
- etc.,

or of a mechanical nature:

- contact non-linearities linked to the clearance possibilities included in a "dormant" secondary fail-safe load path, or due to the effects of wear or failure cases in the systems that "release" mechanical clearances (typical case of the start of a fire, which, due to increased temperature, causes the destruction of flexible elastomer suspensions at the engine mounts),
- non-linearities in the behavior of systems: hydraulic servoactuator non-linearities on the control surfaces; etc.,
- geometric non-linearities, such as local membrane effects that can have an impact on the dynamic properties,
- etc.

In the presence of an aeroelastic instability, non-linear behavior can lead to an asymptomatic limitation of the instability in the form of Limit Cycle Oscillations (LCO). This limitation can be due to either a non-linear variation in the aeroelastic stiffness, which, by modifying the frequency or aeroelastic mode shapes, periodically "destroys" the instability mechanism (typical case of mechanical contact non-linearities), or a dissipation phenomenon caused by the non-linear behavior of the aeroelastic system (typical case of a "fluid damper" type non-linearity), or to a non-linear effect which reduces the aerodynamic work in the flexible-mode shapes when the amplitude of the modal displacement increases (typical case of aerodynamic-based non-linearities). Even though an LCO phenomenon is less of a cause for concern than aeroelastic instability like flutter, it is to be studied in detail and to be precluded, if possible, since it can be a source of premature wear and fatigue in structures, and can result in serious human factors among pilots, such as discomfort, or an inability to read the instruments or maneuver the aircraft controls properly.

As regards non-linearities of an aerodynamic nature, the current practice at Dassault Aviation is to perform an aeroelastic analysis that is "linearized by parts", based on the linearized Navier-Stokes CFD calculations, and enriched with wind-tunnel measurements and flight tests (when this information is available). Whether in the military domain, and more specifically the certification of configurations laden with multiple underwing stores, or in the business jet domain, there are no cases that we know of today in which this kind of "linear by parts" approach would not be able to explain the nature of a non-linear aerodynamic phenomenon encountered and, possibly, the flight domain areas in which this non-linearity would degenerate either into instability or into LCO.

In some typical cases where the LCO is linked to an aerodynamic work limitation with increased structural displacement amplitude, the linearized Navier-Stokes approach could be no longer sufficient to provide the amplitude of the LCO. Time domain harmonic balanced approaches [36], [37] may therefore be used. Those tools are specific tools beyond the normal industrial process itself, either for structural sizing or certification purposes, and would require highly specialized skills. Again, the preferred strategy at Dassault Aviation would be to use, instead, the linearized Navier-Stokes CFD tools to only predict the LCO areas in the flight domain (without seeking a precise prediction of the LCO amplitude), to "physically" understand the mechanism of this LCO and to guide the design to "push" those LCO areas "outside" the aircraft required flight domain. The literature is rich with examples where this strategy has been successfully applied in the aeroelastic domain for various industrial applications [68], [69].

Some other cases of LCO, the origin of which seems to be a strong non-linear aerodynamic behavior in the presence of a strong aero-structural

coupling, are discussed in detail in publications ([27] for example), and are known for only being able to be analyzed by highly advanced coupling of CSM (Computational Structural Mechanics) and CFD tools in the time domain (*i.e.*, "big game"). Even though this type of tool is available at Dassault Aviation, they are still in the prototype phase, and it is hard to make use of them in an industrial process and achieve certifiable approaches. The analysis of these cases gives us reason to think that, when this type of tool needs to be used, the design is not very robust and the associated non-linear aeroelastic phenomena are highly uncertain, with a lot of variability from one aircraft to another in the same series. In such a case, we recommend focusing on the aerodynamic design of the aircraft as a priority to regulate the underlying non-linear aerodynamic phenomenon and avoid implementing this type of analysis.

As regards mechanical non-linearities, there are two processes that are essentially equivalent in terms of results which are commonly used at Dassault Aviation according to the type of non-linearity (with a preference for the first):

- **First harmonic linearization of the mechanical non-linear behavior for a varying number of structural displacement amplitudes** and the calculations in the frequency domain with these linearized characteristics of flutter curves by the standard PK- method (see §"Linear flutter"). This approach is mostly used if the mechanical non-linearities only concern a few localized degrees of freedom or limited aircraft areas, which are the majority of cases encountered on military and business jet aircraft (localized free-play or servoactuator non-linearities, typically). The linearization amplitude for which the flutter curve is stable in behavior, unlike the lesser amplitudes that resulted in instabilities, corresponds to the amplitude of possible LCO. In the case of geometric non-linearities, first harmonic linearization can be replaced with an exact calculation of the tangential stiffness matrix of the structure (typical output of a non-linear module such as that of *ELFINI* ©). The entire aeroelastic computation workflow (reduced load basis, vibration modes and flutter curves) is, in this case, performed using this tangential stiffness.

- **Direct time integration of the non-linear aeroelastic dynamic equilibrium equation of the structure.** Working in the time domain is problematic in terms of formulating unsteady aerodynamic forces in this domain (unsteady aerodynamic calculations are performed 'natively' in the frequency domain by the linearized Navier-Stokes CFD method). The general aerodynamic forces are therefore rationalized in the form of state-space models in the Laplace domain using the Roger method [31] or the Karpel method [32]. The Karpel method is used, with a lesser degree of precision, to conduct a minimum-state method in terms of internal degrees of freedom. Once the generalized aerodynamic forces have been formulated in a state-space model, the linear degrees of the aeroelastic system can be condensed without difficulty at the boundaries of the non-linear degrees of the structure, in the form of "super aeroelastic elements". This allows the non-linear equilibrium of the structure to be resolved in the time domain for the non-linear degrees of the structure only, which are often limited. Classical time-stepping approaches can be used, such as the Houbolt, Newmark or Runge Kutta methods [38].

[39], [40] give details of the method and equations that are implemented as part of the time integration method for an aeroelastic system, including mechanical non-linearities. These references also present the cases for industrial application of this method, in aeroelastic prediction of LCO on a FALCON aircraft, as illustrated in Figure 16.

[34], [35] detail the method and results obtained during the aeroelastic stability analysis of thermal protection tiles in the HERMES project, for which non-linearity is related to "structural membrane" behavior.

[41] shows the equivalence of the two previously explained methods (frequency resolution after first harmonic linearization of the non-linearity, and "direct" full non-linear time resolution) within the framework of the aeroelastic behavior study on a generic FALCON, for which the rudder is coupled to a hydraulic servoactuator equipped with a passive non-linear anti-flutter system. Figure 17 offers an illustration of those results.

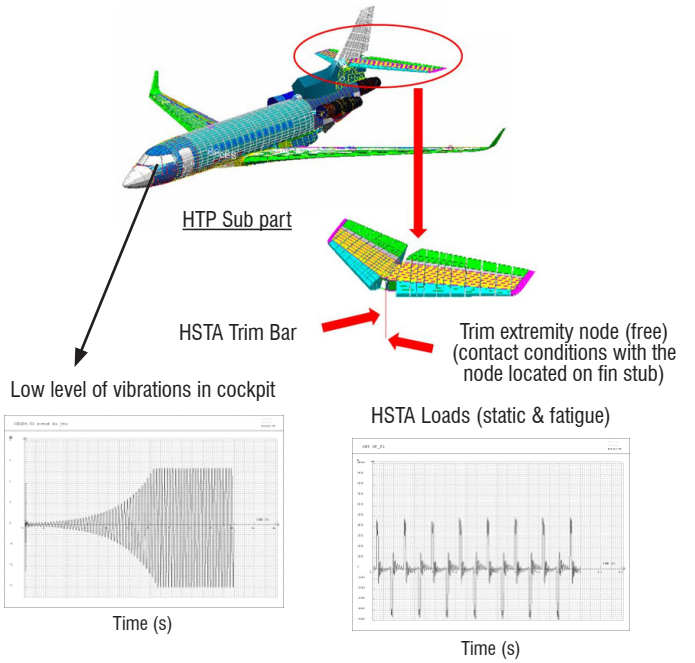

Figure 16 – LCOs prediction in the case of a Horizontal Stabilizer Trim Actuator (HSTA) in fail-safe condition (presence of free-plays) – direct time non-linear integration (from [39]).

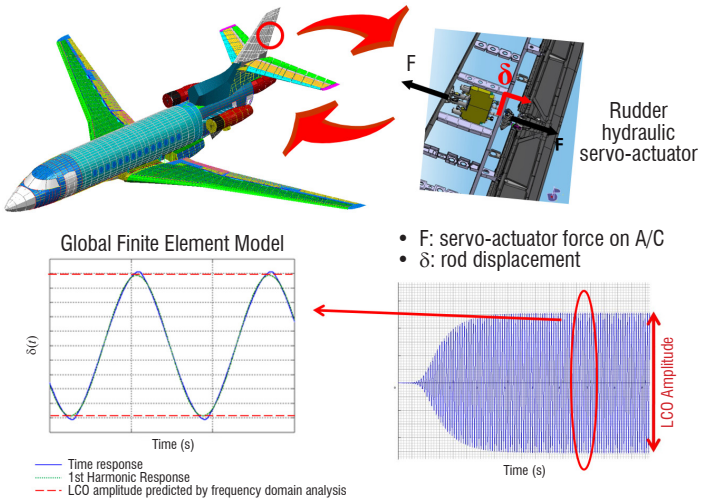

Figure 17 – Comparison of direct full non-linear time resolution and 1st harmonic linearization methods for the prediction of the LCOs of a rudder under an anti-flutter condition (from [41]).

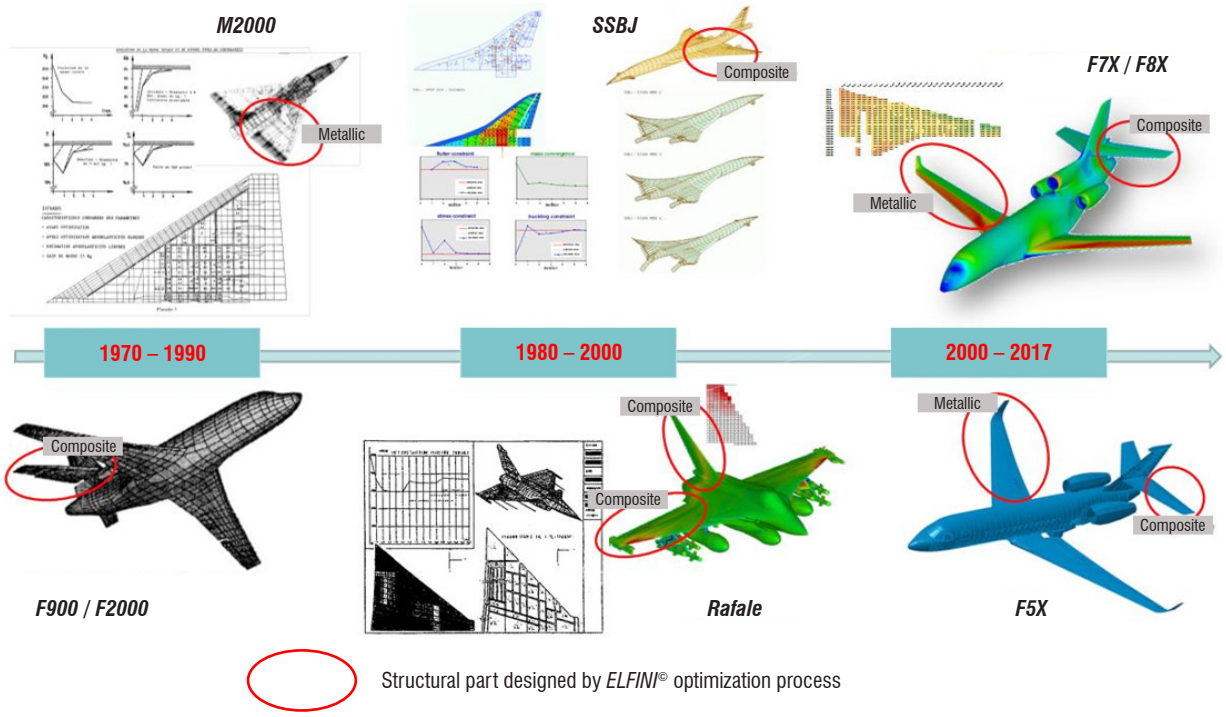

Figure 18 – Applications of *ELFINI* © aero-structural optimization on Dassault Aviation aircraft

Aerostructural Optimization

The means to analyze aeroelasticity that have just been presented in the previous chapters are of great use for the analysis and verification of a specific airframe drawing. However, the complexity of the aeroelastic phenomena is such, that no simple and rational rules can be given that would enable the designer to offer solutions that satisfy both the aeroelasticity criteria and the other design constraints. Despite the analysis tools, the designer may encounter difficulties, in certain cases, in "thinking intuitively" about the right changes to make to drawings to control complex phenomena, like aerodistortion, static control surface reversal or flutter.

Historically, the aeroelastic design process could only work with a good measure of intuition and, above all, the experience of the designers. This, in itself, could be problematic and particularly limiting when it came to innovating and moving away from the experience already gained. We can specifically mention the introduction of composite materials for large structural parts (typically the wing panels for the RAFALE or horizontal stabilizers for the FALCON 900), which was a true technological breakthrough compared to the use of metal parts.

At Dassault Aviation, the need to supplement the traditional design process with more effective aerostructural optimization tools has rapidly taken hold. It was strengthened by the integration of ever more complex aeroelastic phenomena in the design, as well as increased use of composite materials in airframes (see Figure 18 above).

This type of tool has been described in great depth in [42], [43], and [44] and, more recently, in [66]. They are based on the core of *ELFINI* © finite-elements solvers and the various branches of analysis of this platform (including the "Aeroelastic" branch), which provide an exact or approximate assessment of the derivatives for the calculated quantities (load flow, critical buckling load, modal mode shapes and frequencies, control surface efficiency, flutter speeds, etc.), with respect to the "design parameters" to be optimized, which the overall structural mass depends on: in practice, the skin and stiffener thicknesses in metal structures, or the number of plies in each direction for composite-material elements. The kernel of the *ELFINI* © finite-element tool also naturally provides the influence matrix for the structural mass with respect to the various design parameters considered.

In this calculation environment, the aerostructural optimization process aims to "drive" the following global iterative process (illustrated in Figure 19 below) [43]:

- definition of design parameters on the aircraft GFEM and their initial values,
- definition of the design constraints to be respected to enable the aircraft to reach the intended levels of performance (structural strength criteria, buckling stability, minimum required flutter speeds, maximum level of aerodistortion, etc.),

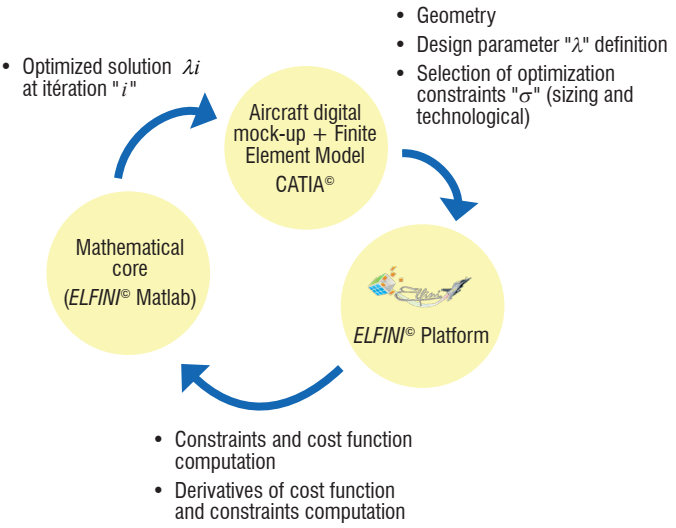

Figure 19 – Dassault Aviation global aero-structural optimization process

- definition of the "technological constraints" to be respected, so that the optimization process solution meets the design office drawing rules and constraints and can be manufactured,
- finite-element analyses (including aeroelasticity) in the structure for a given set of design parameters; calculation of the tangential derivatives of these analyses with respect to the design parameters,
- resolution of the optimization problem: minimization of the structural mass cost function under constraints and determination of the optimal design parameters. In *ELFINI*©, the algorithm used to solve this constraint optimization problem is a mathematical solver commonly used in the mathematical optimization domain, which operates by using the combined projected gradient method.

The developments over the last ten years in the field of aerostructural optimization at Dassault Aviation have mainly consisted in making the most of both the significant progress made in linearized Navier-Stokes CFD and the just as significant progress in the *ELFINI*© finite-element platform, in terms of:

- reinforcing the link with the digital mock-up and the CAD geometry definition (within the *CATIA*© environment),
- automating and facilitating elementary finite-element analyses,
- taking advantage of the increasing computing power (processor CPUs and multiple-core parallelization),
- ergonomics and specific control tools for the optimization workflow and the post-processing of results.

In comparison, the progress made in the algorithmic and methodological "mathematical core" of the optimizer has been relatively minor in nature.

In passing, we highlight once again the benefit of using linear CFD, which greatly facilitates the use of the latest generation of "high-fidelity" aerodynamic modelling (*i.e.*, the Navier-Stokes AETHER code at Dassault Aviation) in an aerostructural optimization process. The aeroelastic optimization process, as performed at Dassault Aviation, therefore uses the same level of structural and aerodynamic modelling as the rest of the aeroelastic analyses.

Once the aerostructural optimization process has been industrialized in the *ELFINI*© calculation tool platform, there are many optimization "sub-products" that offer an array of benefits. Take the example of the automatic plotting of response surfaces in Figure 20, which gives the evolution of an optimization constraint according to one, or several, design parameters.

At Dassault Aviation, the latest evolutions of the aerostructural optimization tool concern the introduction, within the framework of structures with composite materials, of new technological constraints linked to the optimization of a single lay-up table, as illustrated in Figure 21 [45]. We can also cite the introduction of geometric design parameters alongside structural design parameters in the optimization process [6]. This most recent evolution toward a future full topological-optimization capability is facilitated by the now very close links between the parameterized geometric definition (as proposed by the CATIA CAD tools) and the pre-processing tools for the finite-element codes.

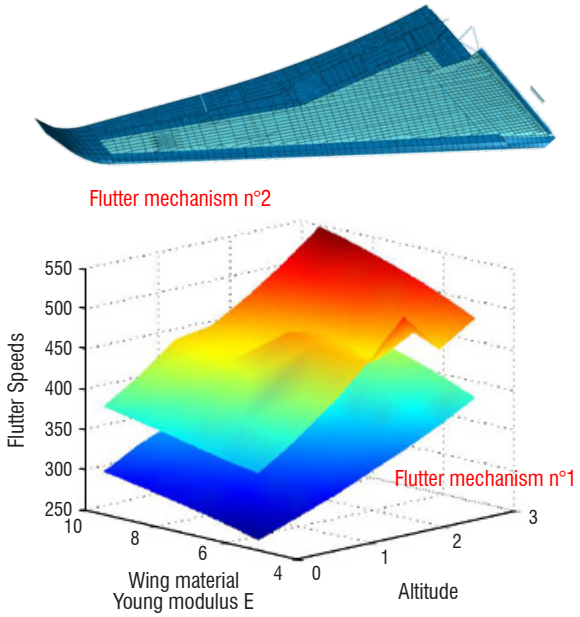

Figure 20 – Example of automatic response surface generation: flutter speed as a function of the wing stiffness.

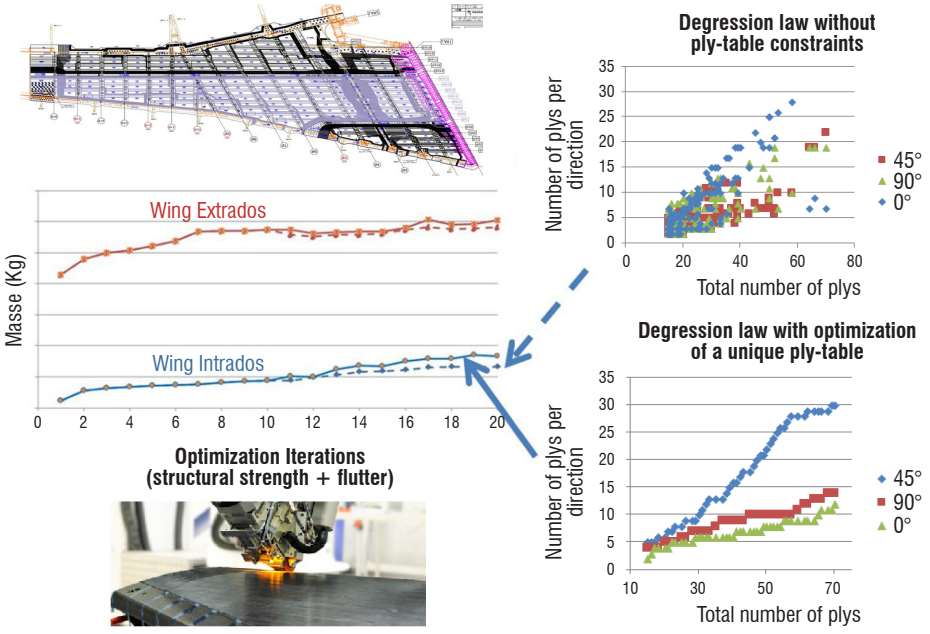

Figure 21 – Example of a composite wing optimization (static strength and flutter) with a single optimized ply-table

Experimental Validations and Model Calibration Methods

As we have seen in the previous sections, the use of aeroelastic tools and theoretical predictive models in the context of a military or civilian program is very challenging, in terms of risk and cost control. This challenge cannot be met if progress is not also made in parallel with the experimental techniques and adjustment tools that will be used to validate the methods, adjust the computational procedures and calibrate the associated models.

In the domain of experimental validation, the strategy currently adopted at Dassault Aviation is generally as follows:

- *With regard to aeroelastic method validation:* use of flexible mock-ups in wind-tunnel tests for the validation of CFD methods, CFD to CSM coupling procedures, tools and computational processes used for aeroelastic analyses.

- *With regard to aeroelastic certification model validation:* use of full-size ground and flight tests on aircraft, and calibration tools for the adjustment of the aeroelastic models used within aircraft projects.

Note that those 2 types of validation are recommended (or required) in the certification process for military and civilian aircraft ([86] for example).

Another important aspect that needed to be covered at Dassault Aviation was the training of young aeroelasticity engineers, and the renewal of the experience. Thirty years after the explosion of numerical aeroelastic modelling techniques, the generation of great experts who brought aeroelasticity to life, nurtured it, and participated in the aeroelastic design of famous aircraft such as the MIRAGE F1, RAFALE or the FALCON 900 (J. C. Hironde, C. Petiau, J. P. Brevan, B. Schneider, C. Geindre, G. Menard) have gradually taken leave from the professional world. Major efforts needed to be made (and must continue) to preserve the aeroelasticity techniques. The test specification on real structures, whether in a wind tunnel or in flight, and the monitoring of these tests and their correlation with theoretical calculations, has proven to be a key vector in training young aeroelastic engineers, which has actively contributed to a widened sphere of knowledge and the development of skills and creativity.

Experimental Validation of Aeroelastic Methods and Computational Procedures using Wind-Tunnel Tests on Flexible Mock-Ups

Since the beginning of aeroelasticity, the use of wind-tunnel tests on flexible mock-ups has proven to be a major factor in the aeroelastic analysis strategy for aircraft structures. Between the 1960s and the 1980s, these tests were mainly performed on flexible mock-ups that were "dynamically similar" to the aircraft being designed, mainly to validate the flight envelope for this aircraft with respect to aeroelastic instability phenomena before the flight tests. See Video 2 of a typical flutter test on a "MIRAGE F1 with a dynamically-similar flexible mock-up".

With the ramp-up in numerical aeroelastic analysis methods, the ultimate aim of these tests has changed at Dassault Aviation. The main objective is now to validate new aeroelastic methods and the associated calculation procedures. The difficulty is no longer to dynamically represent a specific aircraft through "similarity" using a mock-up and to study its aeroelastic behavior in the wind tunnel, but rather to design a flexible mock-up that highlights certain "generic" phenomena that may be encountered on the aircraft. The mock-up is therefore designed as a real "demonstrator of aeroelastic phenomena"; its instrumentation is defined to control the tests to be performed, with to the aim of maximizing the ability to observe the phenomena studied and collecting as many measurements as possible, which will be correlated with calculation previsions. We have clear evidence from the past that the use of results from real tests have made it possible to move forward and validate analysis techniques and methodology, by identifying difficulties that could not be detected in the case of purely numerical validations.

Over the last 20 years, this type of wind tunnel test on flexible mock-ups have enabled Dassault Aviation to validate, calibrate and develop aeroelastic analysis tools and methods in the following domains:

- **Steady and unsteady CFD aeroelasticity tools,** whether in the military domain [47] or civilian domain ([20], [21]). For this purpose, flexible mock-ups with flutter mechanisms, typically studied during the aircraft development phases at Dassault Aviation (*i.e.*, mechanisms that couple the bending/torsion modes of lifting surfaces or lifting surface bending/control surface rotation modes), were designed and heavily instrumented then tested in

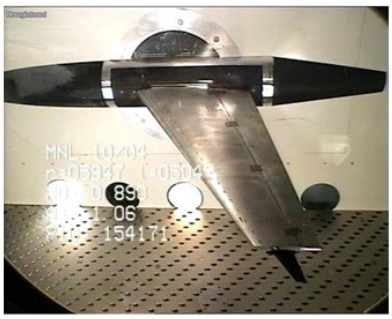

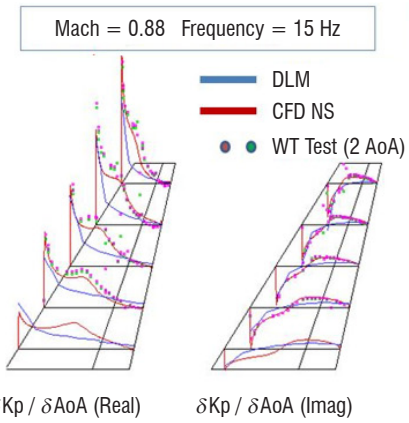

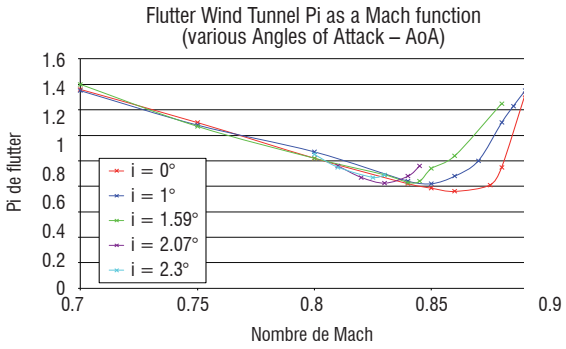

Figure 22 – Example of a wing flexible mock-up tested in ONERA S2-Modane (steady / unsteady aerodynamic + flutter tests) in subsonic and transonic regimes for aeroelastic methods validation

the ONERA S2 Modane wind tunnel under subsonic and transonic conditions in 1995 and 2005, as seen in Figure 22 ([46], [48]). Figure 23 shows an example of the pressures and flutter speed measured during WT testing, compared with the previsions obtained by the latest version of the Dassault Aviation linearized Navier-Stokes tools, with and without linearized turbulence.

- **Non-linear aeroelasticity in the presence of mechanical free-plays and contacts ([46], [53]).** Based on a flexible mock-up representing the planform of a horizontal stabilizer and integrating an elevator, the aeroelastic behavior of this mock-up in the presence of mechanical free-play in its control surface kinematics was measured in the ONERA Modane S2 wind tunnel (see Figure 24). The stability and instability areas could thus be observed in the wind tunnel, together with the conditions leading to LCO phenomena. In this second case, the amplitude of the LCO was measured and correlated with provisional calculations [53] (see Figure 24).

- **Aeroelasticity in complex or non-conventional aerodynamic configurations.** In the military domain, a flexible wing mock-up integrating a missile on the wing tip and two large under-wing stores was designed and measured in the ONERA Modane S2 wind tunnel in the subsonic and transonic domains in 2005 [47], [48] (see Figure 25 left and Video 3 of a wind-tunnel flutter test on a military wing in complex configuration near the flutter point, before and after the flutter instability is detected and the automatic security system activated). In the civilian domain, a flexible mock-up of an innovative configuration for a U-shaped stabilizer (see Figure 25 right), that could also represent a wing configuration with a very large winglet, was tested in 2016 at the S2 Modane in the subsonic and transonic domains [49], [50], [51]. The main aim of these tests was to validate unsteady linearized CFD tools for flutter applications on complex and innovative configurations with large aerodynamic interactions. Figure 26 presents some calculation results compared with the measurements taken. They show a satisfactory correlation between the calculations and the tests. Since tests on the U-shaped stabilizer mock-up are recent (end of 2016), they continue to be subject to work in progress [50].

Even though each mock-up is subject to specific instrumentation, they have all been equipped with a large number of steady and unsteady pressure sensors (a few hundred or so), to enable an in-depth correlation between the CFD calculations and the measurements and to gain a better understanding of the aerodynamic phenomena encountered in the wind tunnel. Similarly, these mock-ups are equipped with accelerometers, strain-gauges and optical equipment to obtain the structural behavior from the point of view of steady and unsteady flexible displacements and internal loads. In general, these tests are carried out in two parts [49]:

- The first part, mostly oriented towards the "aerodynamic domain", in which we measure aerodynamic data (mainly by pressure sensors), on the basis of steady and unsteady globally-rigid (or partially-rigid) displacements of the mock-up (angle of attack, sideslip, control surface deflection), in a configuration where the mock-up is not subject to flutter for the various aerodynamic regimes studied.

- The second part, oriented towards the "flutter domain", where we vibrate the mock-up for variable aerodynamic regimes (Mach and dynamic pressure) in configurations, in which the

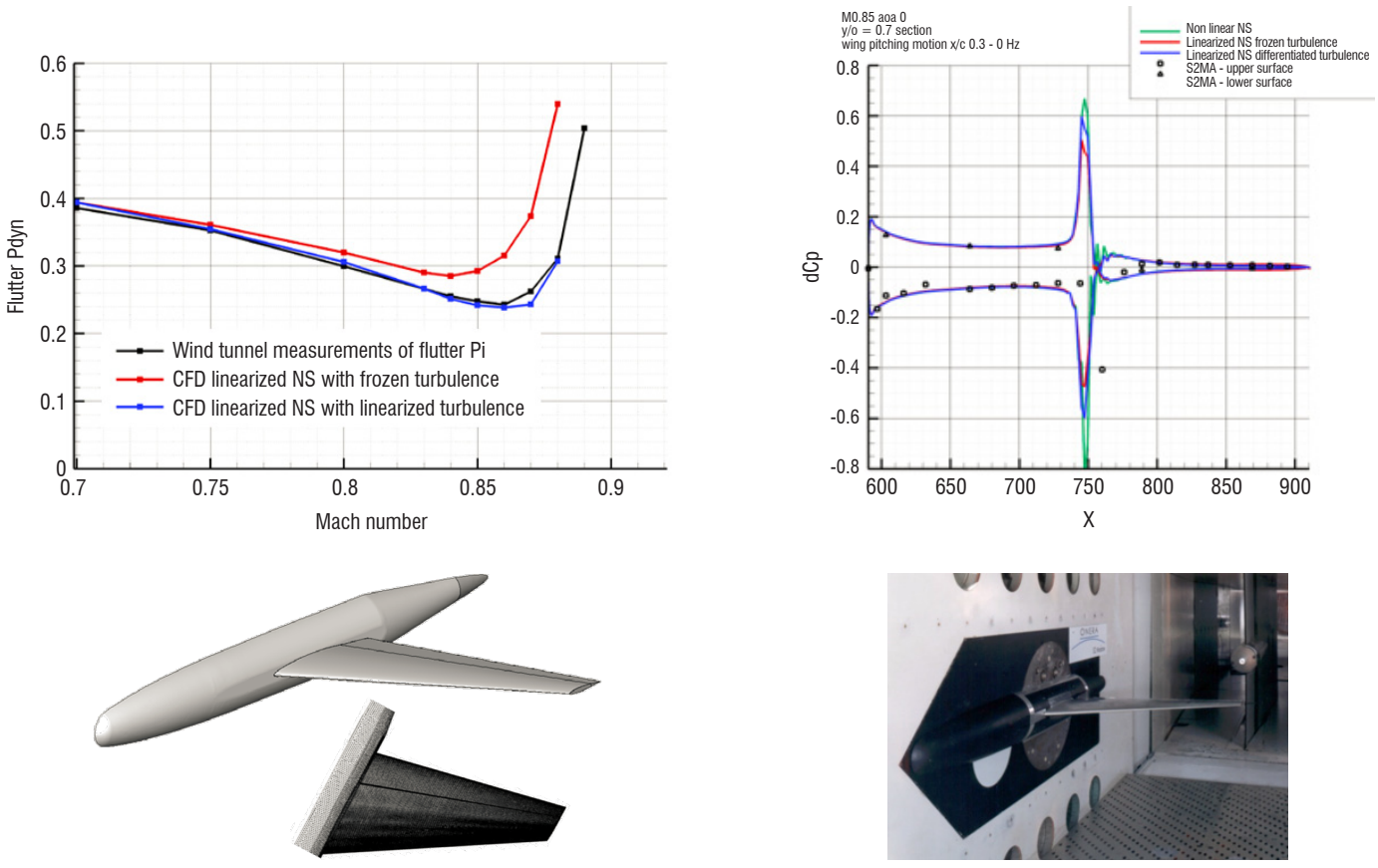

Figure 23 – Example of unsteady CFD validation for flutter prediction by wind-tunnel tests on a flexible mock-up (steady / unsteady aerodynamic + flutter tests).

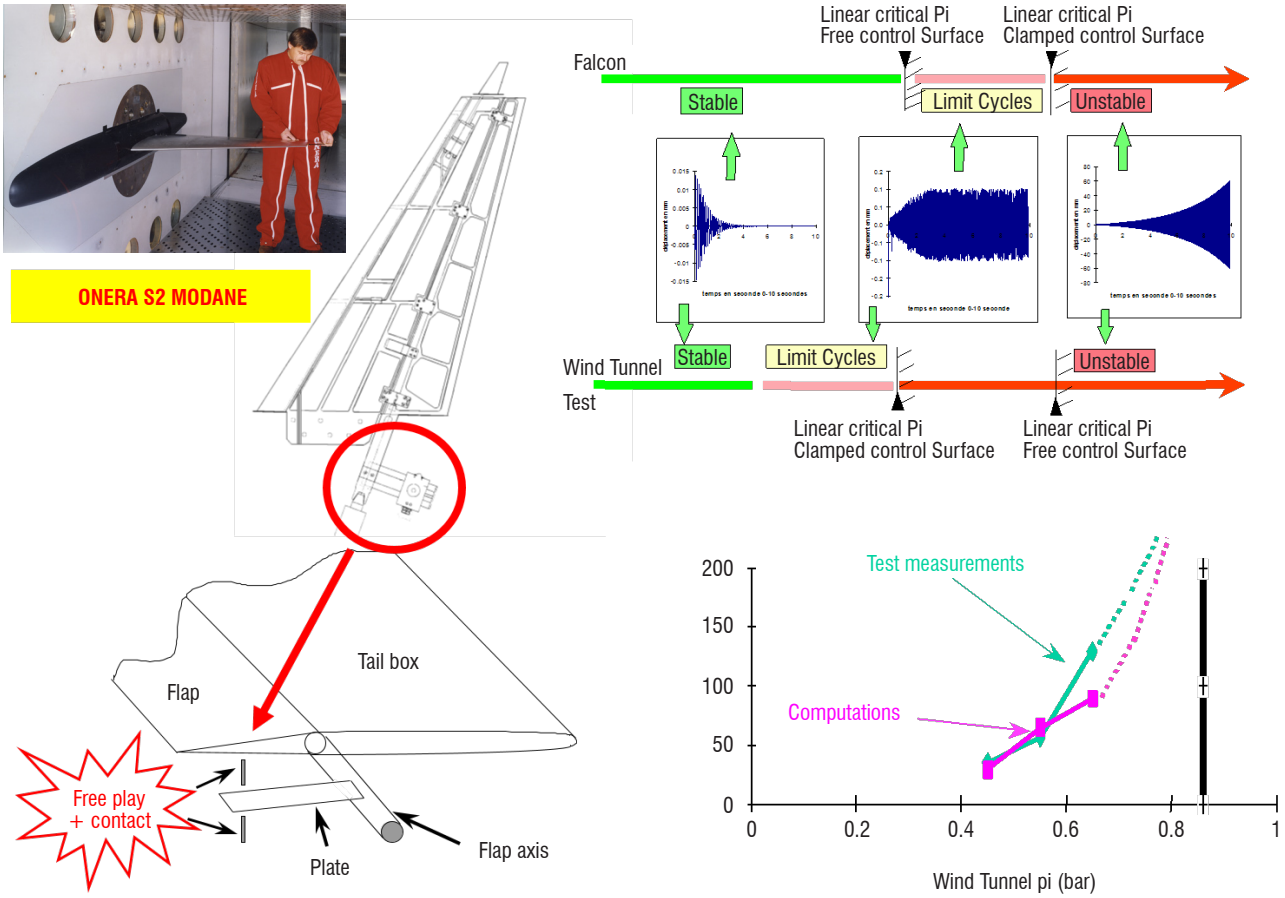

Figure 24 – Wind-tunnel validation of non-linear aeroelastic methodologies in the presence of mechanical free-plays (instability regions + LCO)

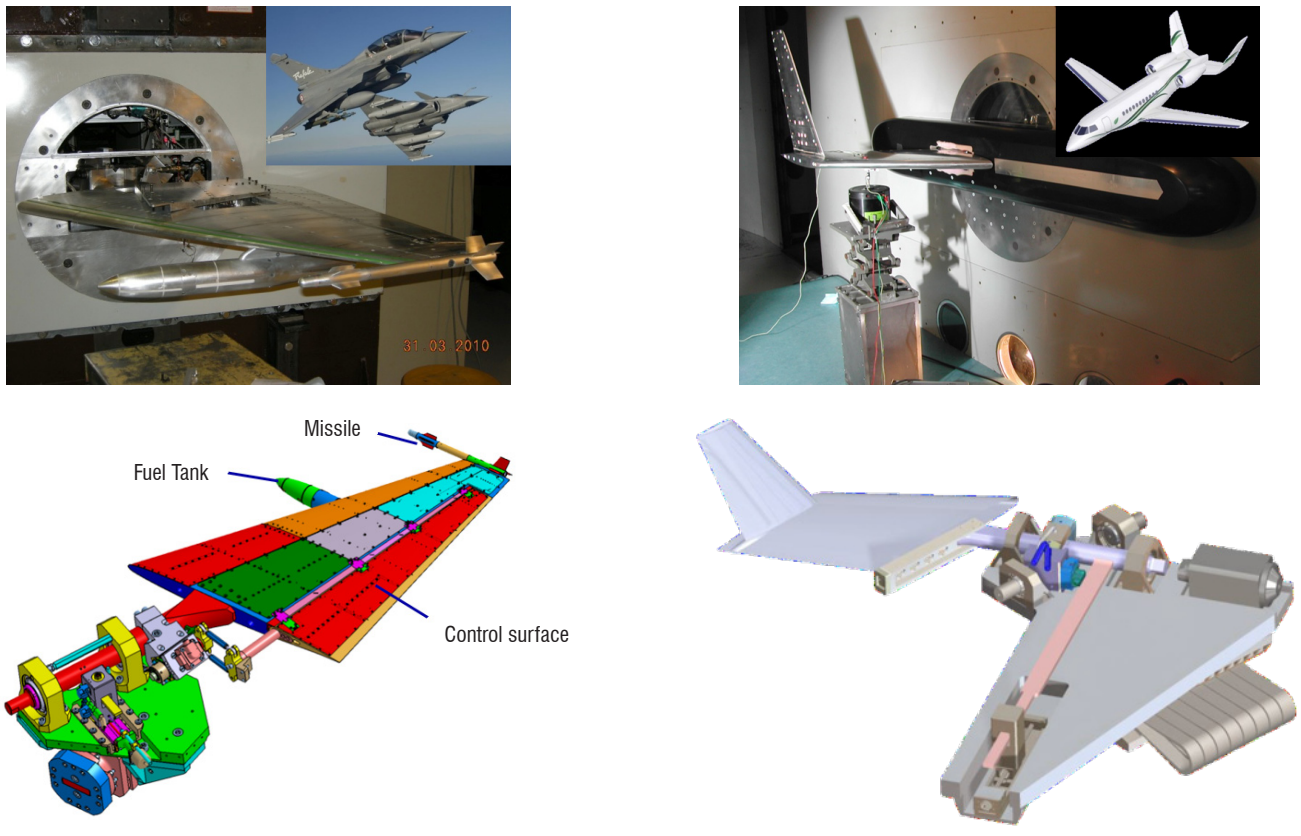

a) Military Aircraft

b) Civilian Aircraft

Figure 25 – Wind-tunnel validation of unsteady NS CFD applied to aeroelastic complex configurations: Test setup.

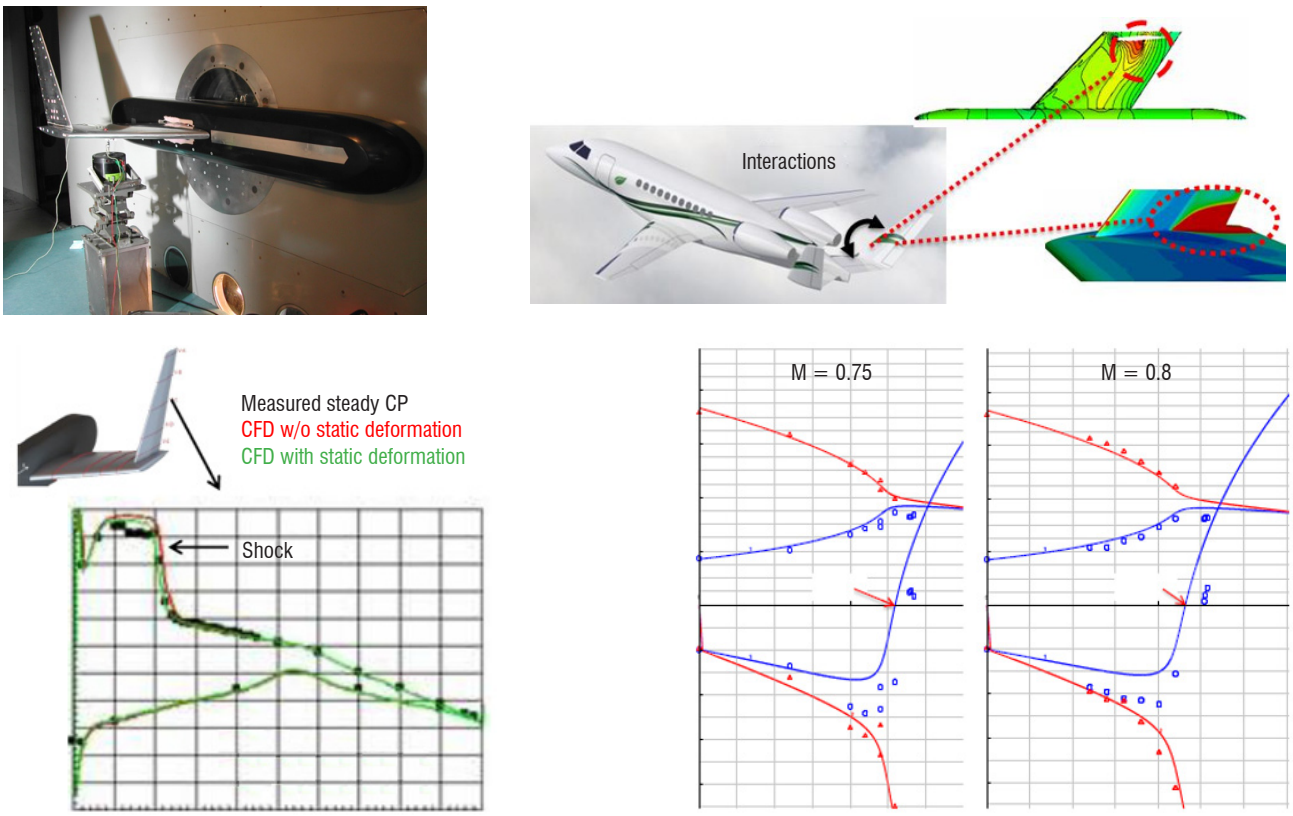

Figure 26 – Wind-tunnel validation of unsteady NS CFD applied to aeroelastic complex configurations: measurement / computation comparisons.

mock-up is subject to flutter. We measure and identify its aeroelastic modal behavior in the wind using techniques similar to those used during ground or flight vibration tests on aircraft [53]: identification by measuring the frequencies, damping and mode shapes of structural modes coupled with aerodynamics. During these "flutter tests", the measurements from the entire aerodynamic installation (pressure sensors, mainly) are also acquired, synchronously to with the structural measurements, for an improved correlation between the aerodynamic fields measured, the consequences of these fields on the aeroelastic behavior of the mock-up and the provisional calculations.

It is important to note that all of these mock-ups are equipped with a safety system that makes it possible to approach flutter points in complete safety in the wind tunnel (without running the risk of destroying the mock-up) [49]. In this manner, we can maximize the observations and measurements taken on the mock-up when the instability phenomenon is truly in place, and check that the critical flutter speeds calculated do indeed correspond with those observed in tests. All of this is not possible in real life during flight testing for aircraft programs, unless there is a major technical contingency or a highly-specific research program [54].

Finally, it must be emphasized that all of these test campaigns in wind tunnels on flexible mock-ups, which have given rise to significant advances in the field of aeroelasticity, would not have been possible without a close collaboration between Dassault Aviation and ONERA and the latter's know-how in terms of design, instruments and the implementation of this type of mock-up and testing.

ONERA, a key partner of Dassault Aviation for this type of study, is also in charge of the structuring, documenting, traceability, provision and data logging of the experimental databases that were built following these test campaigns. This is an important point and a crucial challenge for the future, given that these tests and the large volume of data that they generate (*i.e.*, dynamic phenomena over a large number of sensors) can lead to years of exploitation with a lot of feedback back and forth between the tool-development and validation activities and the measurement post-processing.

Lastly, we note that these wind-tunnel tests, which are intended to be methodological validations (and therefore, very well instrumented), are very costly and it is difficult for a single industrial manufacturer to bear such costs alone. These tests were made possible thanks to the support from the DGA, DGAC and the European community (the Clean Sky program in particular), as well as cooperation between the industrial players (Airbus, ONERA, RUAG, etc.).

Aircraft Ground and Flight Tests

These tests are used to calibrate and validate the aircraft aeroelastic models used during new military or civilian programs, for certification and substantiation purposes. The tests are performed on selected aircraft configurations, chosen from among the basic and most critical configurations. It is then accepted that the aeroelastic model, when calibrated, can represent other configurations that are not ground or flight tested.

Aircraft ground tests (static or vibration) are designed to calibrate the aircraft GFEM (*i.e.*, the "elastic part of the aeroelastic model") by measuring the strain gauge responses for a given set of static load conditions and by identifying the modal characteristics (frequencies and shapes) of the complete aircraft for dynamic excitations such as

shaker forces, hammer impacts or control surface sine-sweep, or white noise excitation (as illustrated in Figure 27). They are also one of the inputs needed to open the flight envelope to facilitate monitoring by flight-test engineers and thus ensure the aircraft safety: the Ground Vibration Test (GVT) is, in some senses "seen" as the first flight point measured for the entire flight envelope. The fact that GVT is very well instrumented and that it allows "clear pictures" of the frequencies and mode shapes to be identified means that it is possible to keep only a minimal onboard Flight Test Instrumentation (FTI) in the aircraft to monitor the rest of the points in the flight envelope. Moreover, aircraft ground tests (static or vibration) are a means of compliance, as required by the CS/FAR 25, to determine the accuracy of the aircraft GFEM and validate its use in calculating loads and flutter.

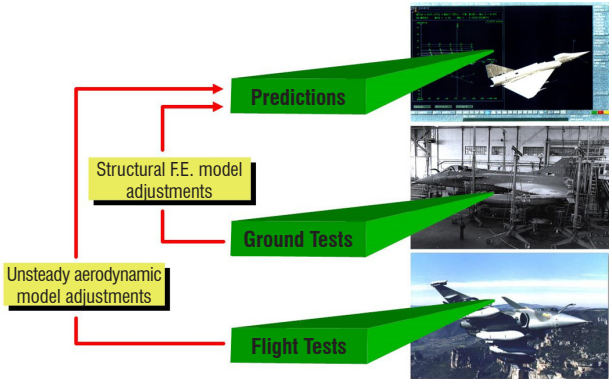

Figure 27 – Ground and flight test strategy to adjust aeroelastic models

Given that these tests are on the critical path for the first flight authorization of the first "prototype", there is a lot of work that needs to be done to adapt the ground test methods and organization, in order to reduce the time spent on the aircraft, achieve the required measurement precision, and prepare the future work on the correlation between all data obtained during those tests and the theoretical models. One of the major advances made by Dassault Aviation over the last decade was to propose a fully-integrated test team that reinforces the synergy between the test provider (SOPEMEA for Dassault Aviation), flight-test engineers, aeroelastic engineers and digital FBW control engineers, in areas such as experimental analysis tools, aircraft operations, result databases, pre- and post- processing, etc. (see Figure 28 for a typical installation). Studies are also in progress relating to the methods used to identify aircraft modal properties (on the basis of the Phase-Resonance Method [55] or the Phase-Separation Method [56]), to try to reduce their costs at iso-precision, and create hybrids of them using theoretical models or identification techniques that will be used also for flight tests.

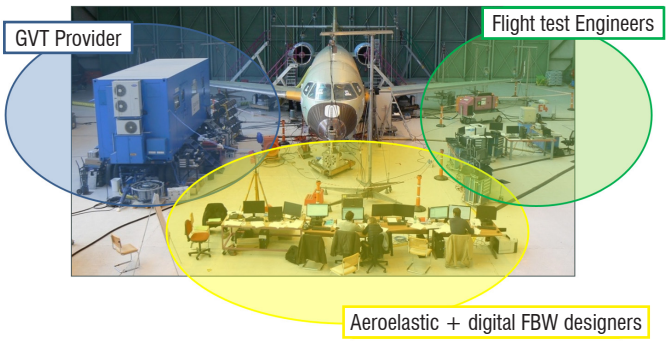

Figure 28 – Ground Vibration Test typical collaborative installation

Flight tests (maneuvers and control surface sine-sweep or white noise excitation) are used to calibrate the "aerodynamic part" of the aeroelastic model (as illustrated in Figure 27), by measuring the flight parameters, global aircraft parameters and aircraft structure responses (strain gauges and accelerations). They are a necessary means of compliance for the certification process of new military or civilian aircraft. The progress made at Dassault Aviation over the last decade in terms of aeroelasticity flight testing has mostly concerned Flight Test Instrumentation (FTI), the recording and onboard telemetry equipment and the post-processing of measurements, mainly with a dual objective:

- **During flights:** to allow flight-test engineers to improve their ability to analyze the aeroelastic behavior of the aircraft in real time, and to authorize progress in the flight domain during the flight tests, without having to land the aircraft for additional analyses and interrupt the flight. The progress made in this field has made it possible to drastically reduce the number of flights needed to open the flight envelope for aspects related to loads, flutter and aeroservoelasticity. Among the means implemented: Dassault Aviation's ability to run "light" aeroelastic models in real time in flight-monitoring rooms. These models are enriched by and re-calibrated in real time with measurements taken during the previous flight points, which allow the flight-test engineers to have a real-time adjustment of the 'best prediction' of the aeroelastic behavior of the aircraft for the remaining flight points. As an illustration of this point, Figure 29 gives the flight forecast for the

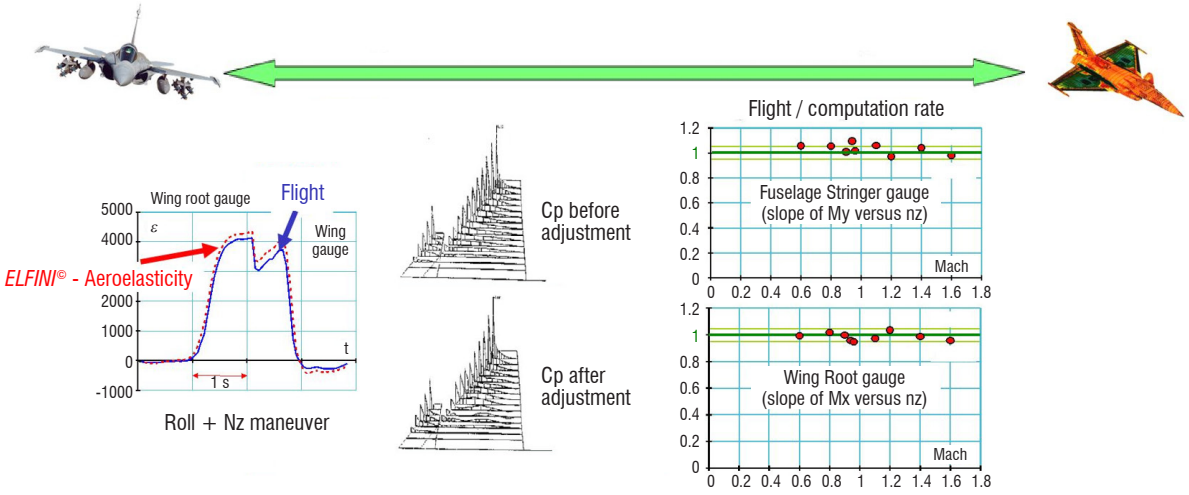

Figure 29 – Wing root load computed and measured during a combined "Roll + G" manoeuver on the RAFALE

RAFALE wing root loads during a combined "roll + G" maneuver superimposed in real time, in a flight-monitoring room, with the aeroelastic model forecast.

- **Once the flights are over:** to allow the flight-test engineers, in collaboration with the design engineers, to gain more confidence in the measurements taken, to identify trends and, above all, to understand the origin and the physics of the aeroelastic phenomena observed in flight on the aircraft. For this, the latest technologies in deformation measurement sensors (mainly optical sensors), load gauges and steady and unsteady pressure gauges were deployed on the most recent Dassault aircraft (F8X/F5X/nEUROn and RAFALE), which made it possible to noticeably increase the amount of information collected during flights. A specific "OCTAVE©" tool, whereby one of the modules is specialized in the analysis of aeroelastic vibrational phenomena and structural loads, was also developed internally at Dassault Aviation to process all measurements from flight tests. In addition to proposing a vast array of measurement processing functions, modal identification and post-processing tools specific to aeroelasticity, this tool makes it possible to easily compare many calculation results taken from the *ELFINI*© database with the test results, in an environment specific to aeroelasticity (see Figure 30).

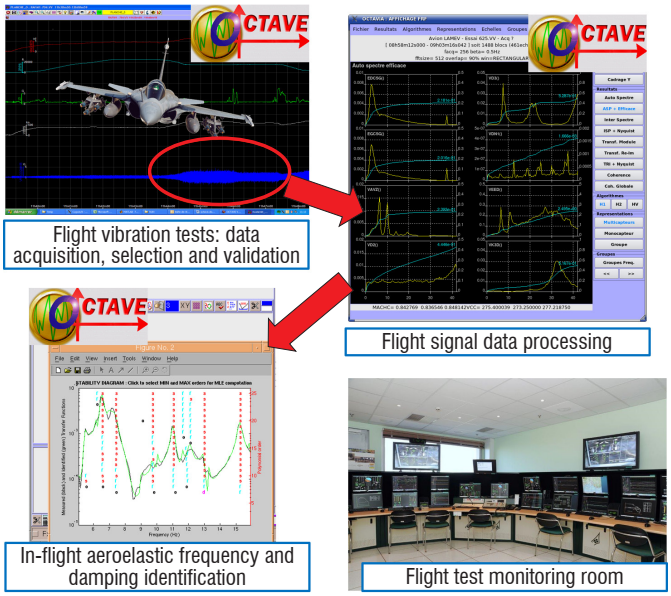

Figure 30 – Dassault Aviation OCTAVE© tool for flight-test vibration measurement processing (real-time and delayed-time)

Mathematical Calibration and Adjustment of Aeroelastic Models Based on Ground and Flight Tests

For the elastic and dynamic structural parts of the aeroelastic model, the adjustment techniques and tools were developed and fully integrated into *ELFINI*© during the 1980s for adjustment of the aircraft GFEM based on the strain-gauge information collected during static-calibration tests or on the vibration modes identified during GVT. An example of the application of such tools on a MIRAGE III/NG is given in [58]. In this case of structural finite-element model adjustments, the tuning parameters are physical characteristics of the structure through their representation in the finite-element model: thickness and area of structure-element sections, interface stiffnesses, material characteristics, etc.

During the 1990s, the main efforts at Dassault Aviation have been concentrated on tools to adjust the steady aerodynamic parts [57] to flight-test measurements and, more, recently the unsteady aerodynamic parts ([60], [61]) of aeroelastic models.

The mathematical "core" of the adjustment method that is used is an original identification technique [58], [59], which is based on "searching" tuning parameters "λ" (unknowns of the adjustment problem) as close as possible to their nominal (or presumed) values given by the theoretical aeroelastic model, with the requirement that the measurements be met by the model at a given accuracy "ε".

Applied to aerodynamic model adjustments in the scope of aeroelasticity (Figure 31):

- The adjustment parameters λ are either generalized steady or unsteady aerodynamic forces, or are directly the steady and unsteady components of the pressure field on the aeroelastic grid.

- The cost functions to be met are the model restoration with a given precision ε of the measured strain gauges during maneuvers or the aeroelastic modal frequencies and damping factors measured during flight vibration sequences.

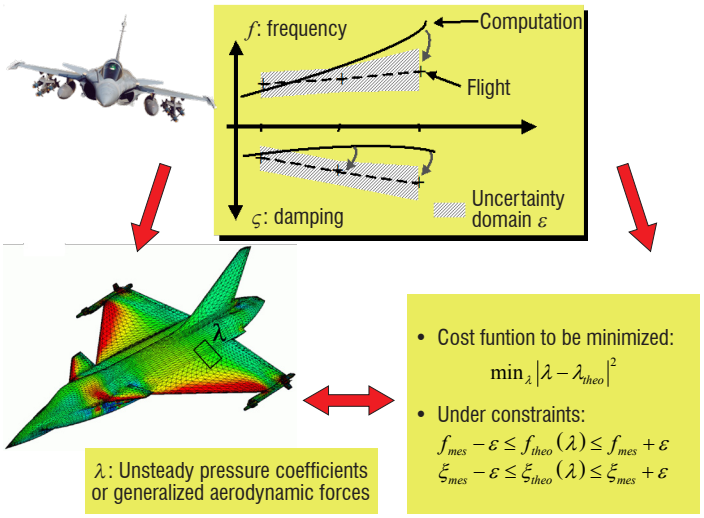

Figure 31 – Unsteady aerodynamic adjustments using flight-test data (aeroelastic frequency and damping values identified during flight tests): theoretical principles

This problem is then solved by a sequence of quadratic optimization problems.

Unlike the classic least mean square methods that solve minimization problems for cost functions, which is the distance between the aeroelastic model outputs and measurements, this approach has the considerable advantage of being "insensitive" to parameters under observation and trying to "stick" as close as possible to the "physics" of the theoretical aeroelastic model. If the bias of the model is too great, there is a clear statement by the method that it is impossible to reconstruct measurements by the model.

The true value of this method lies in the ability to detect potential critical flight envelopes or maneuver situations, far removed from the "quiet" calibrated test points. It has been proven that this procedure

leads to a drastic reduction in the number of flight tests, as well as improvements in their safety.

To illustrate the application and the results obtained with this method for steady pressure field adjustments on the aeroelastic grid, an example of the adjustments made after a flight-test campaign on the RAFALE is given in Figure 29 above.

Another example of the application of this adjustment method for flutter analysis is illustrated through the adjustment of unsteady aerodynamic forces on the MIRAGE F1. This case study is well known at Dassault Aviation: it is currently used as a benchmark to validate new methods in the field of aeroelasticity. It should be noticed that, for the purposes of this case study, the dynamic elastic model is completely derived from an experimental modal base identified during a dedicated GVT, and then believed to be perfectly correlated with the elastic dynamic behavior of the "real" aircraft.

Historically, theoretical flutter predictions in the transonic domain ($M = 0.9$) were made for this aircraft using the traditional Doublet-Lattice method. The flutter results are given in the left-hand side of Figure 32 hereafter, and compared with the flight-test results:

As can be seen, theoretical flutter analyses give a critical speed that is substantially greater than the speed for the test. To improve the situation, the frequency and damping measurements for the first three flight points, for which the speeds are substantially below the critical flutter speeds, are used to adjust the steady and unsteady aerodynamic forces of the aeroelastic model. Flutter analysis using this adjusted aerodynamic model is shown in the right-hand part of Figure 32 hereafter. It is noted that the critical speed calculated with the adjusted model is now superimposed on the one approached during the flight tests.

Industrial Future Areas of Focus in Aeroelasticity R&D

The future areas of focus in R&D aeroelasticity at Dassault Aviation are primarily aimed at fostering innovation in all design and manufacturing domains (participating in the development of future technologies to better respond to customer and market needs), improve aircraft quality (performances, costs, safety, etc.) and to increase the reliability and efficiency of the calculation processes and methods used in design and certification. These areas of focus are strategic for a company such as Dassault Aviation and cannot easily be described in detail in an article of this kind.

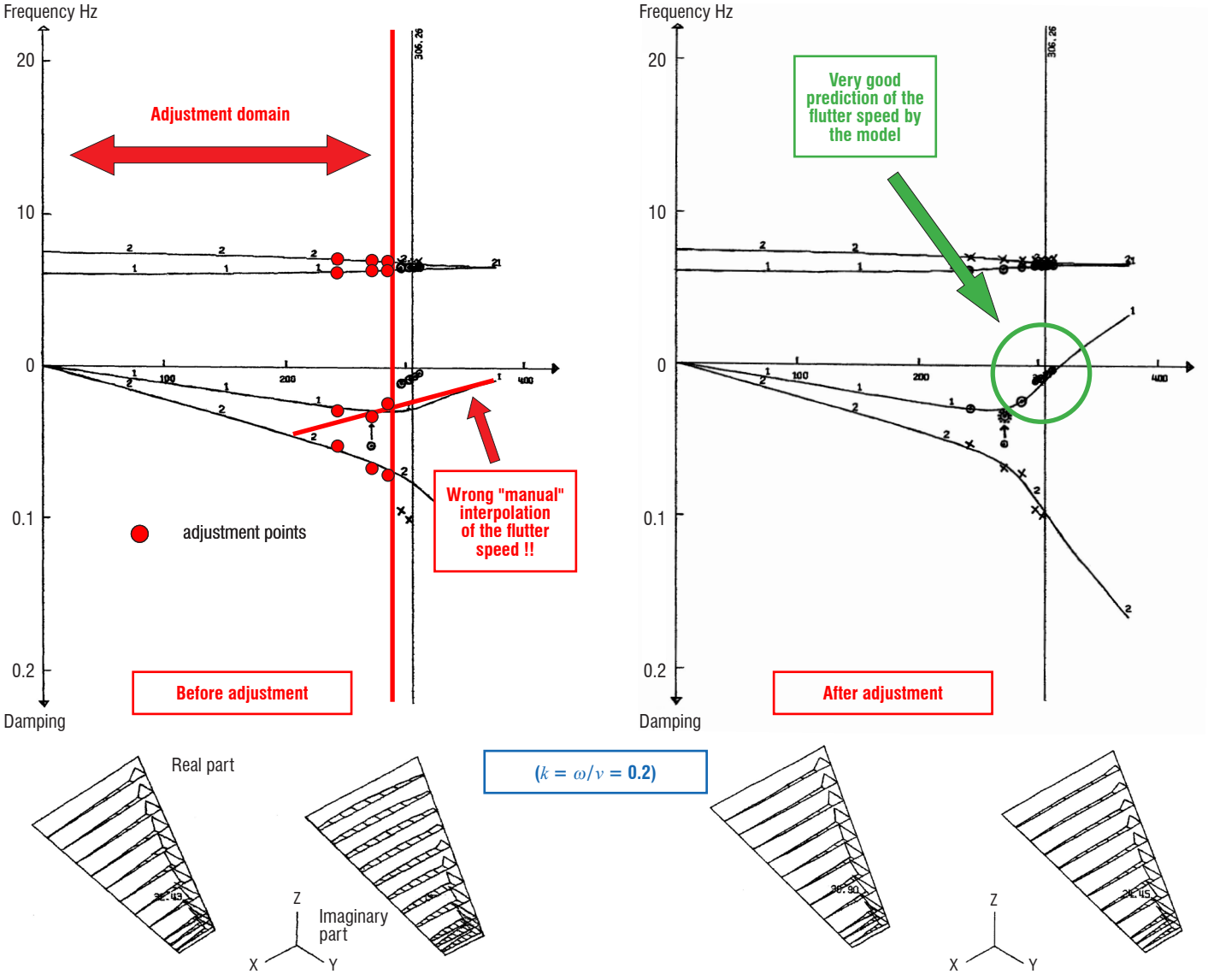

Figure 32 – Unsteady aerodynamic adjustments using flight-test data (aeroelastic frequency and damping values identified during flight tests): application to the MIRAGE F1 flutter analysis

In the following pages, a few select areas of focus in R&D are discussed in brief, and are not intended to be exhaustive. They mainly illustrate the importance of the challenges of aeroelasticity when preparing for the future.

Continuation of the CFD Development Plan for Aeroelastic Analysis

The improvements in the precision, effectiveness and applicability of the CFD aerodynamic prediction tools in the field of aeroelasticity remain THE key area of focus for future R&D developments in aeroelasticity.

While the use of Navier-Stokes CFD in aeroelastic analysis has truly taken off over the last ten years, with a host of advantages (see § "The great potential of CFD aerodynamic modelling"), a lot of work still remains to be done in understanding the characteristics of these tools and improving our use of them for real structure and industrial applications.

Many sensitivity studies (turbulence models, mesh density, etc.) have yet to be completed and summarized, based on simulations in the case of multiple applications in the civilian and military domains, or based on correlations with real test data (wind-tunnel or flight-test data). The aim is to clearly identify the areas of use and the limitations of the CFD tools in the industrial context of the aeroelastic analysis. The known limitations can give rise to additional developments to extend the applicability of CFD.

Given the "natural" increase in computing power, the ability of CFD to model complex flows around complex configurations will also be improved and therefore needs to be investigated. Non-linear aerodynamic phenomena on the angle of attack or Mach domain limits may be better captured, and this could give rise to new methodological studies and validation campaigns on the basis of real tests.

Finally, the arrival of new unsteady aerodynamic calculation codes linked to new approaches, such as the Detached Eddy Simulation (DES) [62], [63] (see Video 4 of a typical DES load computation on a Falcon with interaction between wing and horizontal tail plane at a high angle of attack) or the Field Velocity Method (FVM) [84] should give rise to a rigorous course similar to that already taken for Navier-Stokes CFD, based on their potential within the context of aeroelastic analysis (with respect to the other CFD methods). It is also the case for new turbulence models, which will continue to be enhanced and adapted for various aeroelastic computation and analysis "situations". While the potential for these new methods and models is great, they will need to be adapted to industry practice requirements in terms of aeroelasticity, so that their use in the aircraft project is industrially and reasonably permissible with respect to the calculation costs and analysis efforts.

In conjunction with these theoretical developments in the area of CFD, the in-flight measurement techniques, the calibration and adjustment techniques in the steady and unsteady aerodynamic fields must also be adapted to continue to enrich the theoretical aerodynamic predictions for real test results (wind tunnel and flight), which will be obtained through programs. However, we can reasonably assume that the improvements made to the precision of CFD tools would enable a future reduction in the number of tests needed to design and certify new aircraft.

Aeroelasticity of Laminar Wings

The integration of turbulent-laminar transition in CFD codes has been one of the key issues over the last few decades. The integration of transition in aerodynamic calculations makes it possible, firstly, to determine the drag coefficient in a rigorous manner and, secondly, to gain significant insight into the optimization of the aerodynamic design to reduce the surface friction drag on the aircraft: this is the wing concept known as laminar wings.

Nowadays, even though the design, industrialization and implementation of laminar profiles still pose a range of industrial and conceptual constraints on aircraft, there are now many demonstrators that are starting to appear (see the Clean Sky Project "BLADE" [87] or "ALFA" [88]), which are paving the way for the possible use of this technology in the future of commercial aircraft and business jets.

Recently, [64], [65] presented the results of a test campaign performed in a wind tunnel on a laminar profile. It was possible to measure the effects of the transition from the laminar flow to the turbulent flow on the aeroelastic behavior of the mock-up, and discuss and compare them with the behavior of the mock-up in a configuration in which the transition was fixed.

From an aerodynamic point of view, the measurements taken show that, in relation to the wing angle of attack, the lift coefficients have behaviors that are completely different when the transition is free (laminar wing), compared to when the transition is fixed. When the transition is free, the lift coefficients have a range of non-linearities according to the angle of attack, unlike the configuration in which the transition is fixed. The Mach evolutions of the lift polar curves are also extremely different between the cases in which the turbulent-laminar transition is free with respect to those in which it is fixed.

From a flutter point of view, these differences in aerodynamic behavior are reflected by [64], [65]:

- the appearance of additional flutter mechanisms on the "laminar" wing,
- the worsening of flutter mechanisms already present on the fixed transition wing at the "laminar" wing.

Given that these results show an atypical aeroelastic behavior of the laminar profile, we could have reason to believe that, in preparing for the future of laminar wings, improvements will need to be made with regard to:

- the predictability of CFD tools (particularly in the unsteady domain), to enable modelling of the aeroelastic behavior of these wings, which is just as robust as for "conventional" wings,
- the execution of wind-tunnel campaigns on flexible mock-ups to validate the aeroelastic calculation method for generic "laminar" profiles,
- the adaptation of the test procedures for flight-envelope opening to take into account the atypical aeroelastic behavior of these "laminar" profiles with respect to prior experience.

Analysis of the Aeroelastic Behavior in the Feasibility Phase

This important topic is given here as a reminder because it has been sufficiently discussed before in this paper in the context of the aircraft program objectives. The clear challenge here is to adapt "traditional" aeroelasticity tools and practices (*i.e.*, those that were calibrated to provide the precise quantitative data needed for aircraft commissioning, for the safety of the flight envelope opening and for drawing up certification and substantiation documents) to the "multidisciplinary" logic of the feasibility phase. In this regard, we want to prioritize the speed of

analysis, the "agility" of the tools and practices in order to rapidly give trends and qualitative derivatives in "order of magnitude".

We note that this topic is closely linked to aerostructural optimization, with which it shares a certain number of objectives. In particular, the automated management of a lot of calculations with design parameter variations and their parallelization, as well as the analysis of these calculations in the form of response surfaces. This very rich multi-disciplinary environment in the feasibility phase is also a key matter in terms of the aerostructural optimization developments that we are aiming for (*i.e.*, multi-disciplinary optimization).

Aerostructural Optimization

Structural optimization is often seen as a design improvement approach which, for a given calculation cost, significantly improves a nominal drawing taken from a classic design process. When aerostructural optimization is applied to aeroelasticity, and in particular as part of the implementation of composite materials, it is a vital tool in finding a feasible optimum, without which design office know-how alone would be unable to find a solution that meets all of the specified constraints.

While optimization tools are now already industrially used at Dassault Aviation, and in fields as specialized as aeroelasticity, we are far from being able to use them without a minimal amount of understanding and practice. This also implies that, to implement these tools, the specialists in the field concerned need to be involved: design engineers and aeroelasticity engineers to formulate the problems and the detailed analyses; production engineers for their know-how; and optimization experts and code developers to build effective tools. We are still far from a "black box" process that is frozen in a recurrent application method and fully referenced: each set of problems will once again require, in the future, the implementation of adapted suitable resolution strategy and the development of reliable, and often specific tools. The optimization method must also continue to be enriched and adapted in line with the technological advances in materials and assemblies, as well as the manufacturing and machining processes. Therefore, in the future, we will need to retain a high level of agility and skills in order to develop, reconfigure and assemble the tools as per the user needs.

It is also essential to develop geometric aerostructural optimization in the future, both from an external aerodynamic shape point of view (planform variation, position and surfaces of the control surface, definition of the control surface rotational axes, winglet shapes, etc.), and from an internal architecture point of view (position and size of the main structural elements, such as ribs and stringers, for example). To do so, we could certainly take a great advantage from the ever closer links between finite-element modelling and the digital mock-up of the aircraft and the possibilities now offered by modern CAD software such as *CATIA*© in terms of geometric parameterization and the PLM database. Despite this, some technically difficult "local" problems need to be solved, such as the calculation of the steady and unsteady load sensitivity to any planform variations, and the use of geometric optimization for aeroelastic analysis, meanwhile, remains a challenge.

Introducing robustness considerations in optimization also seems of utmost importance and would involve taking into account the influence of uncertainties on optimization results. In general, the uncertainties raise questions about the appropriateness of real structures in relation to their specifications and theoretical models to reality. Converging towards an optimized drawing that satisfies the constraints in a "robust manner", while bearing in mind the uncertainties, also seems to be of key importance for the future of the aerostructural optimization field. This would imply an additional calculation cost and must, therefore, also be accompanied by a continuing research into improvements to the performance of calculation tools. The research literature is full of examples of the application of robust optimization methods for complex dynamic systems [67], which could be transposed to aeroelastic analysis in an industrial environment.

Finally, the aim is to integrate structural optimization into a wider optimized multidisciplinary design process (illustrated in Figure 33), extended to all aircraft design disciplines, for which it will be necessary to think about the most relevant strategy to exchange and integrate knowledge about the physics and constraints of interaction

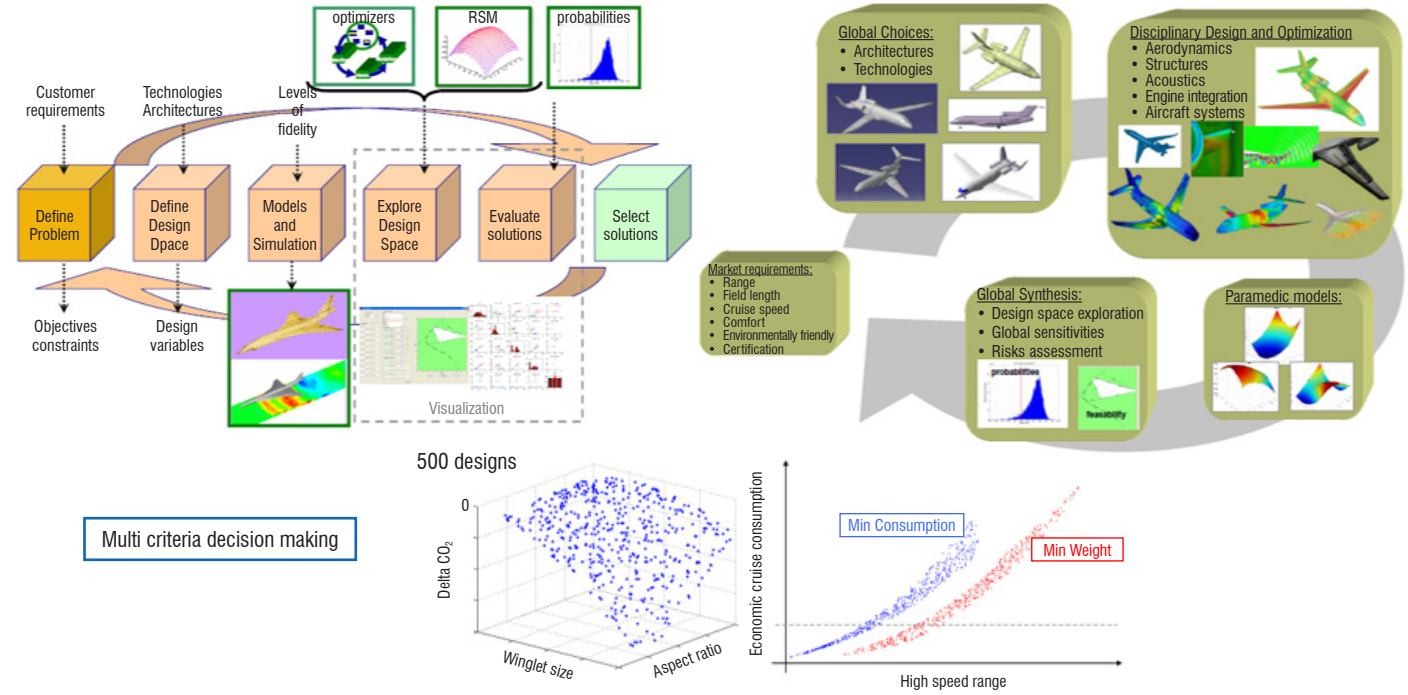

Figure 33 – Multi-Disciplinary Optimization: outline of the global process

domains: reduced models, condensed operators, meta-models ("surrogate" models), response surfaces, and so on. What should the use be? Which multi-level implementation strategies should be used? Which tools should be used to control the whole process and the convergence quality? The specialist literature is full of proposals and views for the future in this field.

Active Control of the Flexible Aircraft

As described before, the current practices in the field of aeroservoelasticity at Dassault Aviation mainly concern the design of notch-filters in the digital FBW control loops, in order to filter the flexibility information measured by the FBW sensors attached to the aircraft structure.

However, we note that the developments made over the last decade in the field of control system technology have been as important as those performed in the structural or aerodynamic domain. They concern sensor technologies, control law design/implementation methods, actuator technologies, modelling tools, etc.

This progress now offers promising perspectives for the future in fields as varied as: the "spatial" filtering of flexible modes into digital FBW control loops (when, for example, the flexible modes and the flight-mechanic frequencies overlap), the elimination of conventional lifting surfaces, load alleviation during maneuvers or when in turbulence or in discrete gust, the active aeroelastic damping augmentation system, or the improvement to the vibrational comfort when cruising. The example of the nEUROn and the lateral stabilization of this aircraft without vertical fin, using the digital FBW system, shows that some of these technologies are now attainable as part of aircraft programs.

We can reasonably think that the use of load alleviation techniques in the earliest phases of aircraft development should enable significant mass gains associated with improved performance. On aircraft that already exist, the implementation of FBW control laws to actively increase the aeroelastic damping should make it possible to avoid mass from being added that would have been necessary to stabilize the new configurations for a military aircraft heavily laden with external stores ([69, [70]) or to improve the vibration comfort during cruise or the aeroelastic stability of new version of business jets [70] to [73].

Given these potentials, Dassault Aviation has started to carry out prospective studies in the field of flexible aircraft control, with support from the DGA, DGAC and the European Community ([74], [75]). Among the challenges that were considered, the following stand out:

- The acquisition, as from the advanced phases of aircraft development, of aeroservoelastic models that are sufficiently precise and compact, and suitable for designing control laws. The readjustment of these models on the basis of ground and flight tests when these tests are available.
- The spatial filtering of flexible modes in overlap situations (or extreme proximity situations) between the aeroelastic modal frequencies of the structure and the frequencies of the flight mechanics.
- Control actuator and sensor modelling (including any non-linear or dynamic effects).
- The integration of a wide variety of flight conditions and aircraft configurations, as well as any uncertainty linked to aeroservoelastic modelling of an actively controlled aircraft; the analysis of the robustness of the envisaged control solutions regarding this variability.
- Research into new control architectures and also architectures for the corresponding equipment.
- The development of a Technology Readiness Level (TRL) ramp-up strategy, on the basis of demonstrators tested in a laboratory on digital test benches, in the wind tunnel or in flight.
- The certification methods of the implemented control technologies.

As an illustration of the first technical elements obtained, Figure 34 shows the gains attained by Dassault Aviation in a wind tunnel on an active aeroelastic damping augmentation system demonstrator whose purpose is to increase the flutter margin of a flexible wing on a heavily-armed military aircraft.

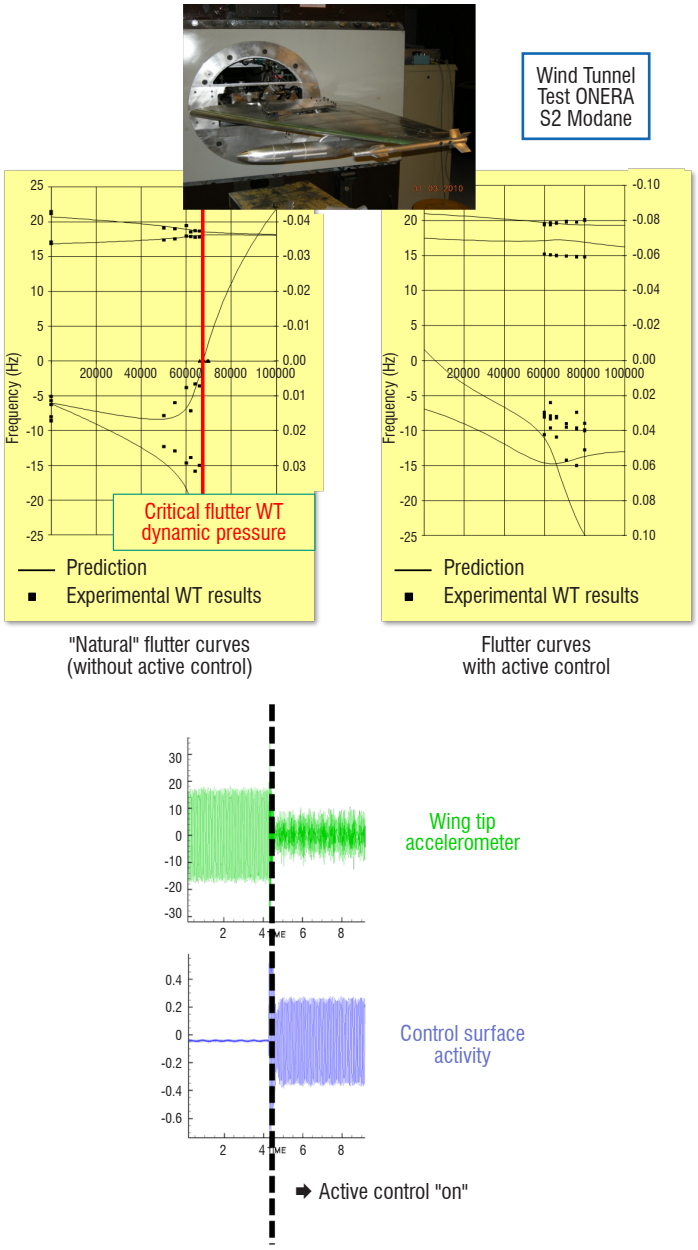

Figure 34 – Wind-tunnel demonstrator of a military wing active aeroelastic damping augmentation system

Figure 35, meanwhile, shows the reduction in pilot vibrations in the cockpit achieved during a real flight test by an active control system of a business jet using a combined elevator and aileron control system.

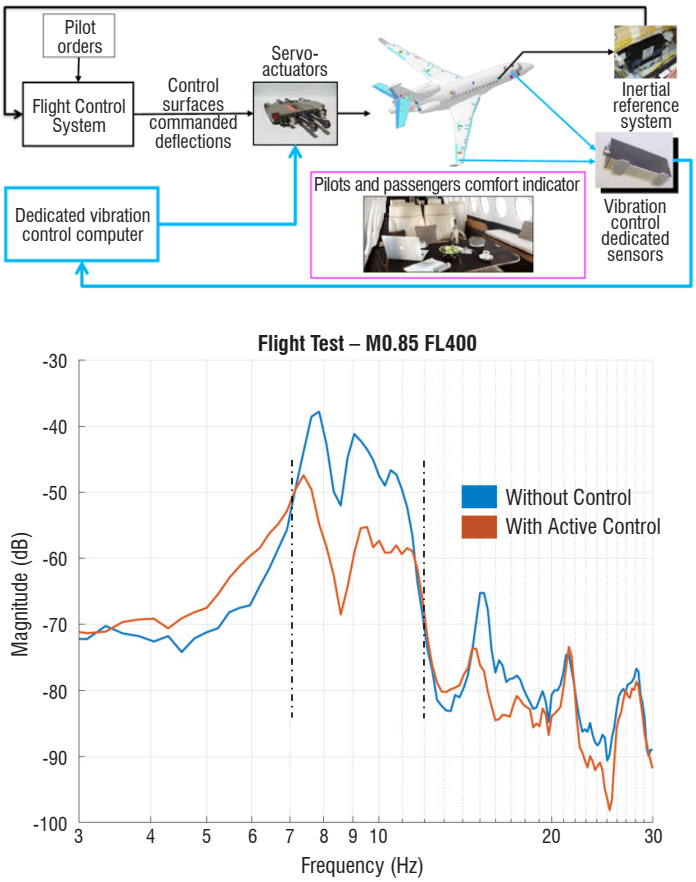

Figure 35 – Flight-test demonstrator of a FALCON active cockpit vibration control

Cooperation between universities and industrial partners is also a very important aspect to be taken into account in the field of active control for flexible aircraft, in terms of the new fundamental scientific aspects that it implies, the multidisciplinary nature of this field, and the need to effectively draw on skills existing in the academic and industrial world. The sharing of costs inherent in introducing design methods, validating them and demonstrating them on the basis of real tests in a wind tunnel or in flight is also a strong argument that speaks in favor of strengthening cooperation.

Integration of Uncertainties in Aeroelastic Analyses

It is generally acknowledged that the integration of uncertainties in aircraft design is part and parcel of "good design" rules. It makes it possible to provide rational arguments in the risk assessment and may be a pertinent guide in the decision-making for the fields of aircraft design and certification. It also contributes to the definition of a margin policy in the design method, to safeguard against complex and potentially hazardous phenomena, such as the stability of aeroservoelastic coupling or flutter.

The integration of uncertainties in the design process can also have an impact on the manufacturing quality control policy and on the maintenance procedures for in-service aircraft, to ensure minimal variation of the structural "key characteristics" from one aircraft to another (or at least to restrict these variations so that they remain within the limits considered during the design).

The notion of "robust design" (*i.e.*, less sensitive to uncertainties) is fully in line with this objective, as illustrated previously in the fields of aerostructural optimization and the active control of flexible aircraft.

When we speak of uncertainties for aeroelastic analysis, we are above all referring to the input data to build models: data that includes a scatter range either because it is naturally variable, random or misunderstood, or because it results from calculation inaccuracies in the upstream models. We can, for example, think of the material properties (particularly in the field of composites), geometric manufacturing tolerances, pressure fields, characteristics in terms of the mass, centering and inertia of external stores, the distribution of fuel in tanks and the characteristics of junction elements or assembly elements that are often non-linear and poorly understood or hard to model. Critical situations may therefore only appear for specific combinations of these parameters in this variation space. This is especially true for the flutter phenomenon [76].

Since the 1990s at Dassault Aviation, one approach for the integration of uncertainties has been to use optimization techniques and to have effective tools to automatically research potential critical configurations ("worst case configurations") in a space of uncertain parameters limited to predefined intervals [85]. In this approach, only the interval of variation limits for uncertain parameters are assumed, and there is no assumption made about the law of probability of the distribution inside these limits. The aim is to be protected against the "worst case configurations" using design actions, regardless of the probability of encountering these "worst case configurations", which may seem a highly-conservative approach.

This approach can be classified as belonging to the family of "robust" aeroelastic analysis methods, for which the μ-analysis method explained in Reference [77] is also included, and is often used in the industry for robust flutter analysis in its initial form or in a most refined one [79]. It is now industrialized and applied to the RAFALE when opening new external store configurations, or in the design of new FALCON aircraft.

One of the future areas for development in the domain of integration of uncertainties at Dassault Aviation, is to complete the methodology that is currently in place with a "probabilistic" uncertainty approach, which takes into account not only the limits of uncertain input parameter variations, but also the laws of probability of the distribution of these parameters within their interval of variations. The propagation of these laws of probability via the aeroelastic model must therefore make it possible to obtain the laws of probability for aeroelastic quantities as an output of the aeroelastic analyses.

There is a wealth of literature about the methods that could be applied in this context: Monte Carlo Simulation, Polynomial Chaos Expansion, Global Sensitivity Analysis, etc. [78], [80], [81]. The implementation of these methods within an industrial context will, of course, pose the question of obtaining laws of probability for uncertain input parameters using measured or simulated data. This is particularly the case for uncertain parameters relating to pressure fields [78], structural damping or the presence of non-linearities.

Another important topic is that of the construction of "light" metamodels using detailed aeroelastic models, in order to use uncertainty propagation methods with calculation costs that are permissible in the design cycle.

Control of Future Non-Conventional Configurations

The past and recent history of the latest developments in terms of new projects (see Figure 36) are sufficiently rich for us to readily believe that aeroelasticity will continue to play a key role in the future in promoting the design and certification of new unconventional configurations.

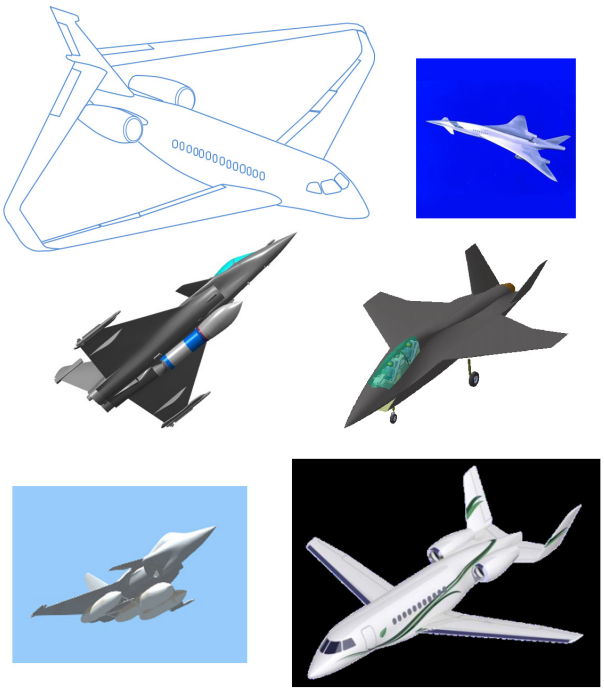

Figure 36 – Examples of future potential unconventional configurations that should be validated to check the expected aeroelastic behavior

If we want aeroelasticity to continue to play its role efficiently and not hamper innovation, then the methods, tools and procedures for numerical and experimental aeroelastic analyses will need to continue to evolve, as well as the corresponding human organization and skills. This is so that we can anticipate the technological breakthroughs being prepared in the field of materials, new structural and aerodynamic architectures, and in the field of sensors and control systems, which will be the precursor of the appearance of entirely new configurations for the aircraft of the future.

Conclusions

This paper presents a review of the industrial current practices at Dassault Aviation in the field of aeroelasticity for military aircraft and business jets.

It shows, in particular, how the issues relating to aeroelasticity have continued to take an ever more decisive role in the design process for aircraft over the last few decades, in light of the research into aerodynamic, structural and systems architectures that are more and more innovative, which has merely reinforced the potentially major impacts of aeroelasticity on the risks, costs and deadlines for new aircraft programs. Aeroelasticity is now seen as one of the main disciplines in design, and as one of the "critical" processes in the aircraft development logic.

This highly-challenging context has been the source of major and constant modifications in the field of aeroelasticity since the 1990s at Dassault Aviation. This is both in terms of industrial practices, the numerical and experimental methods used, the calculation process, model adjustment and validation strategies, as well as the human organization of skills. This paper has looked at the principles and key ideas drawn from some industrial cases of application in the military and business jet domain.

There are a few points that deserve to be highlighted given their importance:

- The time and effort required by each aeroelastic analysis loop (load determination, flutter analysis, etc.) significantly contribute to the total aircraft design and certification cycle. They stem mostly from the examination of a very large number of calculation cases. This has directed the development and introduction of new methods primarily directed towards linear or linearized methods, which help to reduce the calculation costs, facilitate the entry into a global and modular process that can be parallelized, and thus conserve maximum efficiency in the resolution of large aeroelastic analysis loops.

- The introduction and generalization of the linearized Navier-Stoke steady and unsteady CFD tool in all aeroelastic analysis branches has enabled significant gains in precision with respect to the traditional Doublet-Lattice methods, notably for complex configurations or specific aerodynamic regimes, all the while conserving the effectiveness of the global industrial analysis process. The use of CFD has massively contributed to minimizing the risks of underestimating loads, and reduces the efforts to readjust steady and unsteady pressure fields on the basis of wind-tunnel tests or flight tests on the aircraft, at a late stage in the programs.

- The growing importance of active control technologies and of the "servo" in the aero-servo-elastic domain, at each stage of the aircraft project. Introduced early in the program, these technologies should enable significant mass gains associated with improved performance in the future. On in-service military or civilian aircraft, they should make it possible to avoid mass from being added or aircraft architecture modifications that would have been necessary to stabilize new evolutions of existing configurations.

- We are now seeking to adapt the aeroelastic tools and practices to the specific environment, according to the rate and short duration of "multi-disciplinary" design loops in the feasibility phases. This is to take into account aeroelastic derivatives as soon as possible, in the early stages of the design, and to analyze the consequences for the aircraft performance and the relevance of the various architectures and trade-offs envisaged. During the upstream design phases, the use of tools such as aerostructural optimization has already proven to have many advantages.

- In parallel to the calculation processes and methods, it will be necessary to continue to develop the experimental techniques (ground, wind-tunnel, or in-flight techniques) that will continue to play a key role in the future in validating methods and models.

In the future, aeroelasticity must continue to evolve at the same rate if it is to avoid hampering innovation, and if it is to remain one of the means of innovating and seeing the technical breakthroughs of the future reach maturity.

To conclude, we must remember how important inter-industrial and academic cooperation are in the field of aeroelasticity, together with the support of Governmental or European agencies, with respect to the new scientific and fundamental aspects that they involve, the multi-disciplinary nature of this field, and the need to use existing skills effectively. The sharing of costs inherent to the introduction of new analysis methods, their validation and their demonstration on the basis of real tests in wind tunnels or during flights is also a major argument that speaks in favor of increased cooperation between industrial manufacturers ■

Acknowledgements and Contributors

Many of the works mentioned in this paper have been supported by the French Direction Génerale de l'Aviation Civile (DGAC), the French Direction Générale de l'Armement (DGA) and the European Community.

All my thanks also to my Dassault Aviation colleagues for the development of some of the ideas described here, and for their support through illustration pictures and videos.

Special thanks to the aeroelastic team of I. Barber and G. Broux, without forgetting M. Mallet and L. Daumas from the CFD aspect, for their kind cooperation and help.

My profound and personal thanks to "La CASETA", this secret magic place in Spain where this paper was written. It was the perfect place to mature this article surrounded by beauty and peace.

References

[1] J. F. IMBERT - *Analyses des structures par éléments finis*. Cépadués Editions, 1995.

[2] H. G. KUSSNER - *Allgemeine Tragflächen Theorie*. Luftfahrt-Forschung 17, 370-378, 1940.

[3] R. DAT - *Vibrations aéroélastiques*. École Nationale Supérieure de l'Aéronautique et de l'Espace, 1978.

[4] E. H. DOWELL - *A Modern Course in Aeroelasticity*. Sijthoff et Noordhoff, 1980.

[5] R. MAZET - *Mécanique vibratoire*. Dunod, Paris, 1966.

[6] P. HARDY - *OSAVP – Rapport technique de synthèse – Convention DGAC n°2010.93.0805*. Dassault Aviation internal document DGT 142.275, 2014.

[7] PH. NICOT, C. PETIAU - *Aeroelastic Analysis using Finite Element Models*. Proceedings from Europeen Forum on Aeroelasticity and Structural Dynamics, Aachen, Germany, 1989.

[8] CATIA-ELFINI Solver, Release 1, Modification Level B, Corp. Poughkeepsie, NY, 1997.

[9] C. PETIAU - *Structural Optimization of Aircrafts Practice and Trends*. ICAS Proceedings, 1990.

[10] C. PETIAU, S. BRUN - *Trends in Aeroelastic Analysis of Combat Aircraft*. AGARD conference Proceedings n°403, Athens, 1986.

[11] C. PETIAU, E. GARRIGUES - *Progresses in Aeroelasticity & Structural Dynamics during the Last Decade, at Dassault Aviation*. Proceedings from International Forum on Aeroelasticity and Structural Dynamics, Amsterdam, 2003.

[12] C. PETIAU, B. STOUFFLET, PH. NICOT - *Aeroelasticity and CFD*. Proceedings from AGARD RTO Workshop on numerical unsteady aerodynamics and aeroelastic simulations, Aalborg, 1997.

[13] S. GUILLEMOT, J. P. ROSENBLUM - *Modélisation d'écoulements Instationnaires par une approche potentielle non-conservative en différences finies*. Dassault Aviation internal Document DGT n°36.172, Paris, 1995.

[14] G. D. MORTCHELEWITCZ, A. S. SENS - *Solution of 3D Euler Equations with Unstructured Meshes for Aeroelasticity Problems*. Proceedings from International Forum on Aeroelasticity and Structural Dynamics, 1993.

[15] T. FANION - *Etude de la simulation numérique des phénomènes d'aéroélasticité dynamique: Application au problème du flottement des avions*. Ph.D. thesis, Université Paris Dauphine, 2001.

[16] R. THORMANN, M. WIDHALM - *Linear-Frequency-Domain Predictions of Dynamic-Response Data for Viscous Transonic Flows*. AIAA Journal Vol. 51, No. 11, 2013.

[17] M. LESOINNE, M. SARKIS, U. HETMANIUK, C. FARHAT - *A Linearized Method for the Frequency Analysis of Three-Dimensional Fluid/Structure Interaction Problems in all Flow Regimes*. Computational Methods Applied Mechanics Engineering, Vol. 190, pp. 3112-3140, 2001.

[18] C. LIAUZIN, E. CANONNE, G. D. MORTCHELEWICZ - *Flutter Numerical Computations Using the Linearized Navier-Stokes Equations*. Advanced Methods in Aeroelasticity, RTO-MP-AVT-154; NATO Science and Technology Organisation, pp. 8-1-8-12, Neuilly-sur-Seine, 2008.

[19] F. CHALOT, L. DAUMAS, N. FORESTIER, Z. JOHAN - *Industrial Use of Linearized CFD Tools for Aeroelastic Problem*. Proceedings from International Forum on Aeroelasticity and Structural Dynamics, Seattle, 2009.

[20] L. SCHMITT - *Transonic Aeroelasticity based on Linearised CFD Codes*. Proceedings from International Forum on Aeroelasticity and Structural Dynamics, Stockholm, 2007.

[21] L. DAUMAS, N. FORESTIER, A. BISSUEL, G. BROUX, F. CHALOT, Z. JOHAN, M. MALLET - *Industrial Frequency Domain Linearized Navier-Stokes Calculations for Aeroelastic Problems in the Transonic Flow Regime*. Proceedings from International Forum on Aeroelasticity and Structural Dynamics, Como, 2017.

[22] L. SCHMITT, L. DAUMAS, N. FORESTIER - *PEA Étude de l'aéroélasticité des avions de combat – Convention n°02/81 008 00470 75 88 – Rapport de synthèse*. Dassault Aviation internal document DGT n°108.595, Paris, 2006.

[23] G. BROUX, L. DAUMAS, N. FORESTIER - *PEA FAERELAC – Convention DGA n° 2007 0908 470 88 00 00 – Thème B – Rapport de synthèse*. Dassault Aviation internal document DGT n°123591-A, Paris, 2010.

[24] G. BROUX, L. DAUMAS, N. FORESTIER - *ER ASPI – Aérodynamique pour l'aéroélasticité de Surfaces Portantes Intersectées – Convention DGAC n°2012.93.0803 – Rapport technique de synthèse du lot 8*. Dassault Aviation internal document DGT n°152899-A, Paris, 2015.

[25] P. J. THOMAS, E. H. DOWELL, K. C. HALL - *A Harmonic Balance Approach for Modeling Three-Dimensional Nonlinear Unsteady Aerodynamics and Aeroelasticity*. ASME International Mechanical Engineering Congress and Exposition, Paper n°IMECE2002-32532, pp. 1323-1334, New Orleans, 2002.

[26] F. BLANC, F. X. ROUX, J. C JOUHAUD - *Harmonic-Balance-Based Code-Coupling Algorithm for Aeroelastic Systems Subjected to Forced Excitation*. AIAA journal, 2010.

[27] P. M. HARTWITCH. S. K. DOBBS, S. K. ARSLAN, S. C. KIM - *Navier-Stokes Computations of Limit-Cycle-Oscillations for a B-1 like Configuration*. Journal of Aircraft, Vol. 38, n° 2, pp. 239-247, 2001.

[28] L. CRYSTAL, J. PASILIAO, A. DUBBEN - *CFD Based Determination of Transonic Flow Field Characteristics of F-16 Wing Associated with LCO*. Proceedings of 47th AIAA Aerospace Sciences Meeting, Orlando, 2009.

[29] J. R. WRIGHT, J. E. COOPER - *Introduction to Aircraft Aeroelasticity and Loads, 2nd Edition*. Aerospace Series, Wiley Edition, 2015.

[30] Y. REVALOR - *ELFINI V9 – Développements et validations pour la prise en compte des systèmes de commandes de vol dans le calcul de flutter*. Dassault Aviation internal document DGT n° 354271, Paris, 2011.

[31] K. L. ROGER - *Airplane Math Modeling Methods for Active Control Design*. CP-228, AGARD, 1977.

[32] M. KARPEL, E. STRUL - *Minimum-State Unsteady Aerodynamics with Flexible Constraints*. Journal of Aircraft, Vol. 33, n° 6, pp. 1190-1196, 1996.

[33] D. S. WATKINS - *QR-Like Algorithms for Eigenvalue Problems*. Journal of Computational and Applied Mathematics, Vol. 123, pp. 67-83, 2000.

[34] AL. GEORGES - *Aeroelastic Nonlinear Study for Hermes Shingles*. Proceedings from Europeen Forum on Aeroelasticity and Structural Dynamics, Strasbourg, 1993.

[35] C. PETIAU, A. PARET - *Aeroacoustic Qualification of Hermes Shingles*. AGARD, Conference Proceedings n° 549, Lillehamer, 1994.

[36] W. YAO, S. MARQUES - *Prediction of Transonic Limit Cycle Oscillations using an Aeroelastic Harmonic Balance*. AIAA Journal, Vol. 53, pp. 2040-2051, 2015.

[37] E. H. DOWELL - *Some Recent Advances in Nonlinear Aeroelasticity: Fluid-Structure Interaction in the 21th century*. Proceedings of the 51st AIAA Structures, Structural Dynamics and Material Conference, Orlando, 2010.

[38] W. L. WOOD - *A Further Look at Newmark, Houbolt, etc., Time-Stepping Formulae*. Numerical Methods in Engineering, Volume 20, Issue 6, pp. 1009-1017, Wiley Edition, 1984.

[39] T. PERCHERON - *Etude de réponses dynamiques aéroélastiques en présence de non-linéarités mécaniques, Marché SPAé n°84.95.019, Lot n°3*. Note de Structure n° 26251, Paris, 1984.

[40] G. BECUS, C. PETIAU, PH. NICOT - *Influence of Mechanical Nonlinearities on Flutter – Analytical and Computational Aspects*. Proceeding of the AIAA Aircraft design and operations conference, Seattle, 1989.

[41] S. HUET, G. BROUX, E. GARRIGUES - *Aeroelastic Behavior of a Falcon Business Jet in Case of a Failed Servo-Actuator*. Proceedings from International Forum on Aeroelasticity and Structural Dynamics, Stockholm, 2007.

[42] C. PETIAU, G. LECINA - *Elements Finis et Optimization des Structures Aéronautiques*. AGARD, Conference Proceedings n° 280 on the use of computer as a design tool, Munich, 1978.

[43] G. LECINA, C. PETIAU - *Optimization of Aircraft Structure*. Foundations of structural optimization: a unified approach, Chap. 12, Edited by A.J. Morris, Wiley Edition, 1982.

[44] C. PETIAU - *Optimization of Aircraft Structure in Composite Material*. Proceeding of the ICCM/7 conference, Beijing, 1989.

[45] S. MELDRUM, L. COLO, G. BROUX, E. GARRIGUES - *A New Dassault Industrial Approach for Aero-Structural Optimization of Composite Structures with Stacking Table Constraints*. Proceedings from International Forum on Aeroelasticity and Structural Dynamics, Como, 2017.

[46] P. VIGUIER - *Wind Tunnel Test of a Non-Linear Flutter Model*. Proceedings from International Forum on Aeroelasticity and Structural Dynamics, Amsterdam, 2003.

[47] N. MOREAU - *Specification of the Aeroelastic Fighter Model Project (AFMP)*. ONERA report n° RT 9/05284 DDS, Paris, 2001.

[48] A. GEERAER, D. LE BIHAN - *Flutter Control During Wind Tunnel Tests in Transonic Conditions*. Proceedings from International Forum on Aeroelasticity and Structural Dynamics, Paris, 2011.

[49] A. GEERAERT, A. LEPAGE, P. STEPHANI, D. FELDMANN, W. HÄBERLI - *Wind Tunnel Flutter tests of a U-Tail Configuration, Part 1: Model Design and Testing*. Proceedings from International Forum on Aeroelasticity and Structural Dynamics, Como, 2017.

[50] H. MAMELLE, G. BROUX, E. GARRIGUES - *Wind Tunnel Flutter Tests of a U-Tail Configuration, Part 2: Experimental and Numerical Results*. Proceedings from International Forum on Aeroelasticity and Structural Dynamics, Como, 2017.

[51] A. GEERAERT, H. MAMELLE, G. BROUX, M. JANKA - *Flutter Testing of Innovative Noise Shielding Empennage Concepts for Business Jets*. Proceedings from 3AF Greener Aviation conference, Brussels, 2014.

[52] C. PETIAU, B. JOURNEE, E. GARRIGUES - *Flutter Analysis Method in Presence of Mechanical Play and Experimental Verification*. Proceedings from RTO MEETING n°36 on Structural Aspects of flexible aircraft control, Ottawa, 1999.

[53] P. GUILLAUME, P. VERBOVEN, S. VANLANDUIT, H. VAN DER AUWERAER, B. PEETERS - *A Poly-Reference Implementation of the Least-Squares Complex Frequency-Domain Estimator*. Proceedings from IMAC conference, pp. 183-192, 2003.

[54] R. LIND, D. VORACEK, R. TRUAX, T. DOYLE, S. POTTER, M. BRENNER - *A Flight Test to Demonstrate Flutter and Evaluate the Flutterometer*. The Aeronautical Journal, 2002, pp. 577-588, Vol. 107, 2003.

[55] E. BALMÈS, C. CHAPELIER, P. LUBRINA, P. FARGETTE - *An Evaluation of Modal Testing Results Based on the Force Appropriation Method*. Proceedings from IMAC conference n°13, 1995.

[56] M. BÖSWALD, D. GÖGE, U. FÜLLEKRUG, Y. GOVERS - *A Review of Experimental Modal Analysis Methods with Respect to their Applicability to Test Data of Large Aircraft Structures*. Proceedings from ISMA conference on Noise and Vibration Engineering, Leuven, 2006.

[57] C. PETIAU, M. DE LA VIGNE - *Analyse aéroélastique et identification des charges en vol*. Proceedings from AGARD conference n° 375 Operational loads data, Siena, 1984.

[58] C. PETIAU, PH. NICOT - *A General Method for Mathematical Model Identification in Aeroelasticity*. Proceedings from International Forum on Aeroelasticity and Structural Dynamics, Manchester, 1995.

[59] C. PETIAU - *Problèmes d'identification de modèles dans le processus de conception des structures aéronautiques*. Proceedings from A3F thematic day – Structural Group, Paris, 1997.

[60] C. PETIAU, E. GARRIGUES, PH. NICOT - *Method of Mathematical Identification of Unsteady Airloads from Flight Measurements, Experimental Validation*. Proceedings from RTO MEETING n°36 on Structural Aspects of flexible aircraft control, Ottawa, 1999.

[61] E. GARRIGUES, PH. NICOT - *New Trends in Aeroelasticity for Modern Military Aircraft and Business Jet Design at Dassault Aviation*. Proceedings from International Forum on Aeroelasticity and Structural Dynamics, Madrid, 2001.

[62] F. CHALOT, V. LEVASSEUR, M. MALLET, G. PETIT, N. REAU - *LES and DES Simulations for Aircraft Design*. Proceedings from 45th AIAA Aerospace Sciences Meeting and Exhibit, Reno, 2007.

[63] H. MAMELLE, Y. REVALOR, J. M.HASHOLDER, J. J. VALLEE, E. GARRIGUES - *A New Methodology for the Estimation of Structural Load Level due to Complex Unsteady Aerodynamic Excitation*. Proceedings from International Forum on Aeroelasticity and Structural Dynamics, Bristol, 2013.

[64] A. HEBLER - *Experimental Assessment of the Flutter Stability of a Laminar Airfoil in Transonic Flow*. Proceedings from International Forum on Aeroelasticity and Structural Dynamics, Como, 2017.

[65] L. TICHY, H. MAI, M. FEHRS, J. NITZSCHE, A. HEBLER - *Risk Analysis for Flutter of Laminar Wings*. Proceedings from International Forum on Aeroelasticity and Structural Dynamics, Como, 2017.

[66] E. GARRIGUES – *Applications industrielles de l'optimisation structurale au flottement sur avions civils d'affaire*. Proceeding from "Entretiens de Toulouse" conférences, Toulouse, 2017.

[67] I. TARTARUGA, J. E. COOPER, M. H. LOWENBERG, Y. LEMMENS - *Reliable & Robust Optimization of a Landing Gear*. Proceedings from International Forum on Aeroelasticity and Structural Dynamics, Como, 2017.

[68] C. GOODMAN, M. HOOD, E. REICHENBACH, R. YURKOVICH - *An Analysis of the F/A-18C/D Limit Cycle Oscillation Solution*. AIAA Paper 2003-1424, 2003.

[69] W. B. HAYES. K. SISK - *Prevention of External Store Limit Cycle Oscillations on the F/A-18E/F Super Hornet and EA-18G Growler Aircraft*. NATAO STO Document Release n°SPR-08-247.265, 2008.

[70] E. LIVNE - *Aircraft Active Flutter Suppression – State of the Art and Technology Maturation Needs*. Proceedings from the 58th AIAA Structure, Structural Dynamics and Material Conference, Grapevine, 2017.

[71] EASA - *Proposed Special Condition for Installation of Flutter Suppression System – Boeing 747-8/-8F*. Special Condition C18 Publication.

[72] FEDERAL AVIATION ADMINISTRATION - *Special Condition: Boeing 747-8/-8F Airplane, Interaction of Systems and Structures*. Department of Transportation, Special Condition n° 25-388A-SC.

[73] FEDERAL AVIATION ADMINISTRATION - *Special Condition: The Boeing company model 787-10 Airplane; Aeroelastic Stability requirements, Flaps-Up Vertical Modal-Suppression System*. Department of Transportation, Special Condition n° 25-16-05-SC, 2016.

[74] G. BROUX, C. MEYER, O. CANTINAUD, L. GOERIG, E. GARRIGUES - *Aeroelastic Stability Augmentation by the Flight Control System on Heavy Loaded Fighter Aircraft*. Proceedings from International Forum on Aeroelasticity and Structural Dynamics, Paris, 2011.

[75] C. MEYER, G. BROUX, J. PRODIGUE, O. CANTINAUD, C. POUSSOT-VASSAL - *Demonstration of Innovative Vibration Control on a Falcon Business Jet*. Proceedings from International Forum on Aeroelasticity and Structural Dynamics, Como, 2017.

[76] C. CHUNG, S. SHIN - *Worst Case Flutter Analysis of a Stored Wing with Structural and Aerodynamic Variation*. Proceedings from the 51th AIAA Structure, Structural Dynamics and Material Conference, Orlando, 2010.

[77] R. LIND, M. BRENNER - *Robust Flutter Margins of an F/A-18 Aircraft from Aeroelastic Flight Data*. Journal of guidance, control and dynamics, Vol. 20, N°3, pp. 597-603, 1997.

[78] S. WU, E. LIVNE - *Alternative Aerodynamic Uncertainty Modeling Approaches for Flutter Reliability Analysis*. AIAA journal, June, 2017.

[79] S. HEINZE, U. RINGERTZ, D. BORGLUND - *Assessment of Uncertain External Store Aerodynamics Using mu-p Flutter Analysis*. Journal of Aircraft, Vol. 46, N°3, pp 1062-1068, 2009.

[80] C. SCARTH, J. E. COOPER, G. H. C. SILVA - *Aeroelastic Stability of a Composite Wing Box with Uncertainties in Material Properties*. Proceedings from the 16th European Conference on composite materials, Seville, 2014.

[81] R. G. COOK, C. J. A. WALES, A. L. GAITONDE, D. P. JONES, J. E. COOPER - *Uncertainties Quantification in Gust Load Analysis of a Highly Flexible Aircraft Wing*. Proceedings from International Forum on Aeroelasticity and Structural Dynamics, Como, 2017.

[82] E. LIVNE - *Future of Airplane Aeroelasticity*. Journal of Aircraft, Vol. 40, N°6, pp. 1066-1092, 2003.

[83] E. GARRIGUES - *What's Going on at Dassault Aviation? A Brief Overview of the Last Five Years in the Structural Dynamics and Aeroelasticity Field Advanced Combat and Civilian Aircraft*. Proceedings from International Forum on Aeroelasticity and Structural Dynamics, Stockholm, 2007.

[84] C. WALES, D. JONES, A. GAITONDE - *Prescribed Velocity Method for Simulation of Airfoil Gust Responses*. Journal of Aircraft, Vol. 52, N°1, pp. 64-76, 2015.

[85] E. JACOB - *PEA Aéroélasticité des futures configurations d'emports – Convention DGA n° 2002 0607 456 45 00 00 – Recherche des configurations " les pires "*. Dassault Aviation internal document DGT n°122227, Paris, 2002.

[86] European Aviation Safety Agency - *Certification Specifications and Acceptable Means of Compliance for Large Aeroplanes - CS-25 - Amendment 13*. 2015.

[87] *BLADE makes significant progress towards Natural Laminar Flow wing technology*. Cleansky.tmab.eu website.

[88] *JTI-CS2-2015-CFP02-LPA-01-06 – Laminar Horizontal Tail Plane full scale demonstrator*. cordis.europa.eu website.

AUTHOR

Eric Garrigues has been a professional engineer at Dassault Aviation since 1988. He is currently Head of the Load and Stress Department of the Aerostructure Division, which covers structural strength substantiation and certification, flight and ground load computations, and aeroelastic, flutter, vibration and interior vibro-acoustic analyses. He participated in several projects on military (RAFALE, nEUROn) and business jet aircraft (Falcon F7X, FALCON F8X, Falcon F5X) and is currently a Compliance Verification Expert for the certification process of those aircraft in the field of Loads and Flutter.
Eric Garrigues is additionally a member of the Structural Commission of the *Association Aéronautique et Astronautique de France (3AF)* and is also a member of the Program Committee of the "International Forum on Aeroelasticity and Structural Dynamics (IFASD)".

C. Liauzun, D. Le Bihan, J.-M. David, D. Joly, B. Paluch
(ONERA)

E-mail: cedric.liauzun@onera.fr

DOI: 10.12762/2018.AL14-10

Study of Morphing Winglet Concepts Aimed at Improving Load Control and the Aeroelastic Behavior of Civil Transport Aircraft

Morphing is today widely studied in order to improve aircraft performance and thereby decrease their environmental footprint. This paper deals with the preliminary study of several morphing winglet concepts aimed at improving load control and aeroelastic behavior. The first step consisted in building and validating low-CPU-time-consuming but accurate aeroelastic models able to take into account aerodynamics, structural dynamics and flight mechanics, in order to handle free flexible aircraft. Aeroelastic state-space models have therefore been built from a structural modal reduction and from a rational function approximation of the aerodynamic forces based on the Roger formulation. They have been validated through comparisons with high-fidelity fluid-structure (CFD-CSM) coupling simulations. The flight mechanics has been taken into account by coupling these models with the AVL software. The second step consisted in designing a realistic reference wing equipped with a conventional winglet. Then, four morphing winglet concepts were assessed: a flapping winglet, a winglet whose deformation in torsion is controllable, a winglet able to rotate around an axis along its span and a winglet equipped with a trailing edge flap. The latter concept was found to be the most promising in terms of load control, in particular when used in conjunction with the aileron. Finally, a technological study was performed in order to ensure the feasibility of the concepts. This study was pursued up to the drawing phase, but stopped before a demonstrator was manufactured. Nevertheless, it demonstrated the feasibility of a winglet equipped with a trailing edge flap, at both the demonstrator and real aircraft scales.

Introduction

Flight transport has greatly increased over these last years, which has entailed a great number of technological developments to make aircraft increasingly larger and more performant. However, recent events, such as the increase in oil prices in 2008, or even in the '70s, and the compelling need to combat global warming led the EU to define new objectives for the aeronautic community, in order to drastically decrease the aerial transport environmental footprint (VISION2020 and FLIGHTPATH2050 [1]). In order to meet such challenges by at least reducing fuel consumption, both the aircraft structural weight and its aerodynamic performance – especially drag – must be significantly improved.

Aerodynamic performance has been greatly improved by the use of winglets. Such wingtip devices, patented for the first time by F. W. Lanchester in 1897, were developed and made popular by R. Whitcomb [29]. He showed that winglets yield better lift to drag ratios and lead to a decrease in induced drag by diminishing the trailing-edge-induced vortex intensity. They therefore enable the aircraft range to be increased. Nowadays, all aircraft manufacturers have carried out, or are currently carrying out, studies to improve this device and mount it on most aircraft (e.g., Gulfstream business jets, the Boeing blended winglet, the Airbus Sharklet, and the Spiroid winglet by Partner Aviation Inc., among others).

Another way of improving aerodynamic performance is by morphing, that is, the capability of an aircraft to adapt its geometry to the flight conditions. Two of the most famous examples are the Grumman F14 Tomcat fighter aircraft, able to change its wing sweep angle according to the flight speed, and the droop nose of the Concorde aircraft, whose fuselage nose could be deflected downwards, not to improve the aerodynamic performance, but rather to make landings possible. Discussions about the definition of "morphing" and its challenges are given in [25] and [18], and potential benefits are shown in [20]. This kind of technique, inspired by numerous examples provided by Nature (birds, fish, and insects), is not recent (see C. Ader's "Eole" aircraft built in 1890, and the Wright Brothers' wing wrapping used to control the Wright Flyer in 1903), but recent technological advances in terms of materials (composites, rubber or highly-flexible materials, and smart materials), actuators (piezoelectric, electromechanical, shape-memory alloy), sensors, computers, controllers, and computational techniques, have allowed new morphing ideas and technologies to be developed [8]. Some of them consist in modifying the upper surface, in order to delay downstream the laminar-turbulent transition location according to the flight conditions, and thereby decrease drag and fuel consumption [21], through changing the wing trailing edge camber using a three-hinge device to improve the lift-over-drag ratio, or drag [19]. This is, of course, far from being exhaustive and a review of morphing technologies can be found in [5]. A recent overview of what morphing implies for aeronautics can be found in [9].

Both previous ways of decreasing drag and weight have also been combined. Several morphing winglet concepts have indeed been patented [23] [6] [26], or have been studied or assessed. Different kinds of morphing have been considered. Control surfaces at the leading or/and trailing edges have been added to the winglet to control vortices under high-lift conditions [3], or to improve the lift-to-drag ratio and the gust-load alleviation [28]. A winglet with a trailing edge flap has been designed and assessed in terms of both aerodynamic performance and loads, taking into account the certification requirements within the framework of the European Union project SARISTU [27] [17]. Another morphing winglet based on a chiral-type internal structure has been designed, enabling cant, twist and camber control throughout the flight envelope [10].

The main motivation for developing morphing winglet concepts is, most often, to improve the aerodynamic performance. The goal of this study is to assess the potentiality of such a device to improve load alleviation, and therefore the aircraft aeroelastic behavior.

The first part of the paper gives a brief description of the four morphing winglet concepts that are assessed. The second part, dedicated to the aeroelastic models used for the evaluation, presents the theoretical aspect, the preliminary results and their validation by comparisons with CFD simulations. The third part is devoted to the evaluation of the concepts, used alone or in combination with a conventional aileron. The last part focuses on the technological point of view to demonstrate the feasibility of the most promising concept.

Morphing Winglet Concepts

The main idea consists in adding a new control surface on the winglet, or making it moveable, in order to improve load control. The latter is assessed as the capability to decrease the wing root bending moment in cases where critical and sizing loads are applied. This bending moment decrease would thus allow the structure weight to be reduced. Several concepts are evaluated with that goal, as well as with the constraint of not altering drag (Figure 1). The first concept consists in applying torsion around an axis along the winglet span, and then driving the toe angle and modifying the apparent incidence. Such a morphing shape can be achieved by replacing winglet ribs with actuators to drive the position of the spars relative to one another thereby creating a kind of shear deformation of the sections. The second concept can be seen as a limit case of the previous one, and consists of a rotation of the whole winglet around a span-wise axis. The third one is a kind of flapping, thereby allowing the cant angle to be driven. The last concept considers a trailing edge equipped with a single-hinged flap.

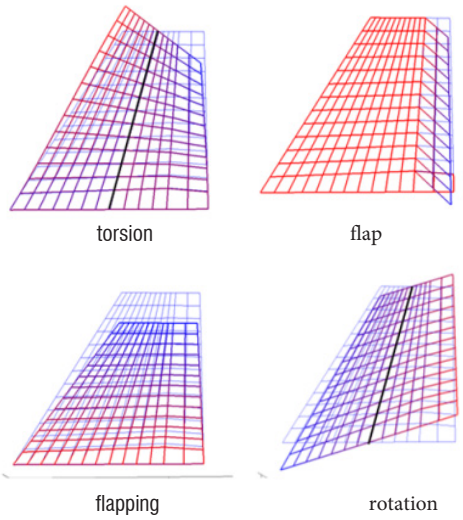

Figure 1 – Morphing winglet concepts

These morphing concepts are evaluated for a transport aircraft whose top level requirements and wing geometry were provided by Alenia within the framework of the European project SARISTU [30]:

- Npax: 130
- Range: 3,000 NM
- MTOW (Maximum Take Off Weight) = 60,000 kg
- MLW (Maximum Landing Weight) = 55,000 kg
- Design cruise speed = Mach 0.75 at 35,000 ft

The geometrical characteristics are:

- Reference surface = 111 m^2
- Span = 34.14 m
- Dihedral angle = 3.5°
- Sweep angle at the leading edge = 18°
- Mean aerodynamic chord = 3.7457 m

The efficiency of these concepts is evaluated for cruise flight conditions.

Aeroelastic Models

Aeroelastic Reduced Model

The winglet concept efficiency is assessed using a reduced aeroelastic model aimed at computing loads, the global aerodynamic lift coefficient, aerodynamic forces and structural deformations. The model is based on a fluid-structure state-space model. It is built, on the

one hand, from a structural model classically projected onto a modal basis to compute the dynamic behavior and, on the other hand, from a reduced aerodynamic model to obtain the aerodynamic forces.

The main advantage of state-space models lies in their simplicity, since they are able to provide any physical quantity (displacements, forces, moments, twist angle, etc.) from linear relations. They are also very useful and convenient for the control-surface controller law determination. The state-space model is indeed expressed in the time domain as

$$\begin{cases} E\dot{x}(t) &= Ax(t)+Bu(t) \\ y(t) &= Cx(t)+Du(t) \end{cases} \quad (1)$$

where x is the state vector, y is the vector of quantities of interest and u is the command (input) vector. u is, in the case of morphing winglet evaluation, the vector of the control-surface deflections. It can also be a turbulence perturbation in the case of load alleviation assessment, or rigid mode coordinates in the case of flight mechanics. E, A, B, C and D are matrices that are independent of time, x and u, but can depend on other parameters (e.g., flight characteristics, such as the flight speed V and the air density ρ). In the case of aeroelastic models, these matrices are built from structural mass, damping and stiffness matrices, or their projection onto a modal basis. The structural model is enriched with the aerodynamic force representation resulting from a Rational Function Approximation (RFA) model [24]. Such a model assumes that the aerodynamic forces are proportional to the structural motion and that the proportionality coefficient, also called the Aerodynamic Influence Coefficient (matrix $\frac{1}{2}\rho V^2 A$), can be written in the Laplace domain, with s being the Laplace variable, as

$$A(s) = D_0 + D_1 s + D_2 s^2 + \sum_{i=1}^{n_a} E_{i+2}\frac{s}{s-\lambda_i} \quad (2)$$

where D_0 D_1 and D_2 denote the aerodynamic stiffness damping and inertia, and n_a is the number of aerodynamic states. The denominator zeros λ_i are the lag coefficients. With each lag term or partial fraction can be associated an aerodynamic state η_i defined as

$$\eta_i = s\left[(s-\lambda_i)I\right]^{-1} E_{i+2}x$$

The latter relation can be expressed in the time domain as

$$\dot{\eta}_i = E_{i+2}\dot{x} + \lambda_i \eta_i$$

The RFA model then allows an aeroelastic state-space model to be built. If the structure mass, damping and stiffness are modeled by the matrices M, C and K, the aeroelastic model can be written as

$$\partial_t \begin{pmatrix} x \\ \dot{x} \\ \eta \end{pmatrix} = \begin{bmatrix} I & 0 & 0 \\ 0 & M-\frac{1}{2}\rho V^2 D_2 & 0 \\ 0 & 0 & I \end{bmatrix}^{-1} \begin{bmatrix} 0 & I & 0 \\ -\left(K-\frac{1}{2}\rho V^2 D_0\right) & -\left(C-\frac{1}{2}\rho V^2 D_1\right) & \frac{1}{2}\rho V^2 \begin{bmatrix} I & \cdots & I \end{bmatrix} \\ \begin{bmatrix} 0 \\ \vdots \\ 0 \end{bmatrix} & \begin{bmatrix} E_3 \\ \vdots \\ E_{n_a+2} \end{bmatrix} & \begin{bmatrix} \lambda_1 I & \cdots & 0 \\ \vdots & \ddots & \vdots \\ 0 & \cdots & \lambda_{n_a} I \end{bmatrix} \end{bmatrix} \begin{pmatrix} x \\ \dot{x} \\ \eta \end{pmatrix} \quad (3)$$

The RFA model used for the assessment of the morphing winglet was that proposed by Roger [22]. In order to reduce the number of states, the structure is usually projected onto a rather small -eigen-mode basis. The number of aerodynamic states is then equal to the number of these structure modes times a number of lag terms (n_L), which has to be determined as a compromise between the requirement of a small number of total states and an accurate approximation of the Generalized Aerodynamic Forces (GAF, aerodynamic forces projected onto the structural modes). Computation of the RFA matrices is performed in such a way that the best approximations of tabulated known GAF data are determined using a least square algorithm. These tabulated data are obtained using an unsteady aerodynamic code able to compute the aerodynamic pressure or force variation due to a purely oscillatory motion at prescribed frequencies. The lag coefficients are determined from an optimization process aimed at minimizing the angular variation between the aerodynamic force components (GAF_{ij}) resulting from the RFA model and from the tabulated data.

$$\min\left[1-\frac{\left(\mathrm{GAF}_{ij}^{\mathrm{RFA}},\mathrm{GAF}_{ij}^{\mathrm{tab}}\right)^2}{\left\|\mathrm{GAF}_{ij}^{\mathrm{RFA}}\right\|^2\left\|\mathrm{GAF}_{ij}^{\mathrm{tab}}\right\|^2}\right]$$

The evolutions of the damping and frequencies resulting from the state-space model are strongly dependent on this GAF smoothing process. That is why the optimization process has to be carried out taking into account the following parameters: number of tabulated frequencies to be able to catch the GAF loop-like evolutions in the complex plane, the number (n_L) and type of the lag coefficients (real or imaginary), and the range within which they are selected. A first guess of the latter parameter is given by a flutter analysis using the classical double scanning p-k method and only the tabulated GAF.

The system (3) represents the first equation of the aeroelastic state-space model (1) and can be enriched by an observation equation expressing the expected quantity (bending moment, lift coefficient, displacement, etc.) as a function of the unknown states, thus representing the second equation of (1). Nevertheless, if the structure is modelled by a modal representation, the state-space model is used to compute the deformation of the wing. The latter deformation is then transferred (through interpolation or smoothing) to the aerodynamic grid, thereby updating the geometry, which can be used as input for a fast aerodynamic code to provide integrated forces, such as the lift force or the bending moment at the wing root. Another way to compute them consists in calculating the integrated forces for each mode using the aerodynamics code and in combining them linearly with the generalized coordinates as coefficients.

First Evaluation of the Concepts

In a first step, a preliminary finite-element model of a wing with a conventional winglet has been built, taking into account classical wing

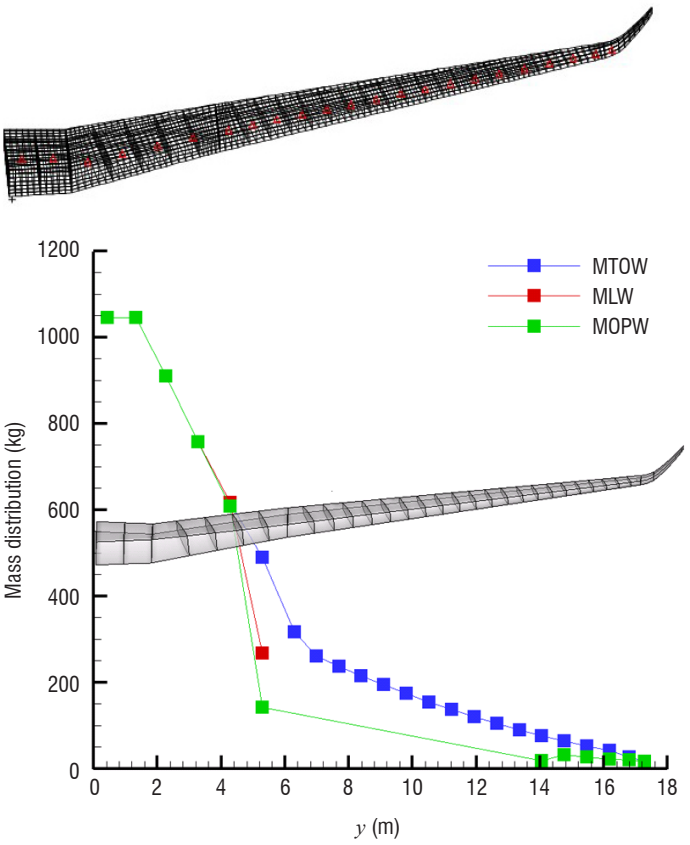

Figure 2 – Wing preliminary finite-element model and fuel mass distribution along span

architecture (spars, ribs, stringers, mass penalty for the leading edge trailing edge and equipment) and primary structures (spars, ribs, stringers and skin). The model is made out of a composite material and has been sized according to two symmetric load cases with load factors equal to 2.5 and –1. It has been validated with respect to flutter and buckling. Kerosene has been added to this model as one-node elements connected to the wing box with rigid elements, according to the distribution shown in Figure 2. Furthermore, the winglet has been modeled as a continuity of the wing and not as a separate device that can be plugged into it.

In the second step, aimed at morphing winglet concept assessment, an aeroelastic state-space model has been built from first structural elastic modes, rigid modes, control surface commands (winglet concepts, aileron and inner flap) and generalized aerodynamic forces (GAF), whose dependency on the frequency is computed using the Roger formulation [22] described above. The tabulated aerodynamic forces used as input for the Roger model are computed at some oscillation frequencies using the Doublet Lattice Method (DLM) [2], which is based on the assumption of linear subsonic aerodynamics. This panel method actually computes the local unsteady pressure variations and then the force variations due to a harmonic motion at a given frequency. This motion can be due to rigid modes, elastic deformation modes of the wing or a rotation of a control surface. Since DLM is a linear formulation, those variations are, in fact, the derivatives of the pressure or forces (after integration) with respect to the lifting surface motion.

Such a model has been built from the first seven structural elastic deformation modes of the preliminary finite-element model (Figure 3), from the control surface command highlighted in light blue (winglet)

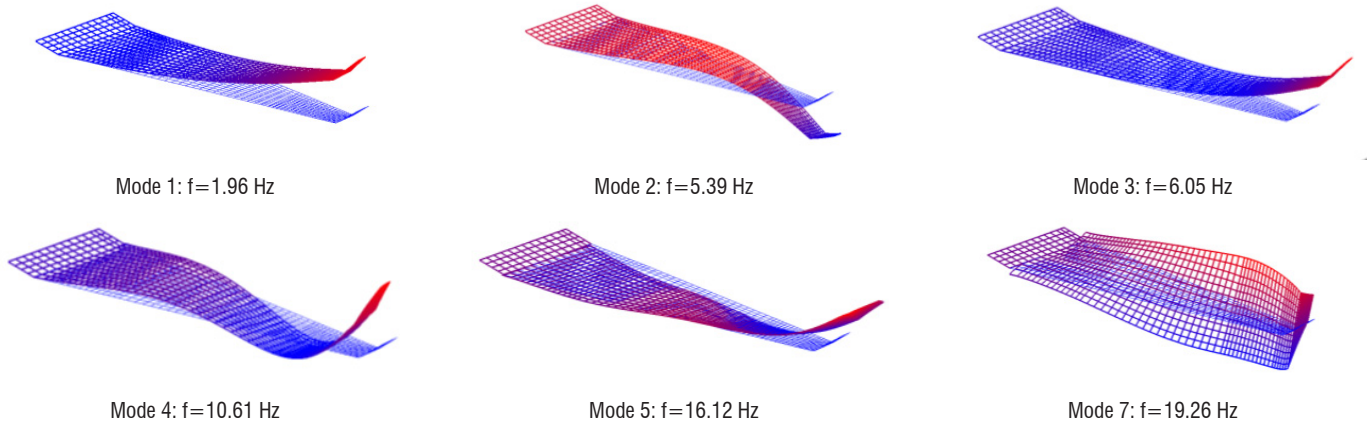

Figure 3 – Structural eigen-modes of the wing preliminary finite-element model (clamped root)

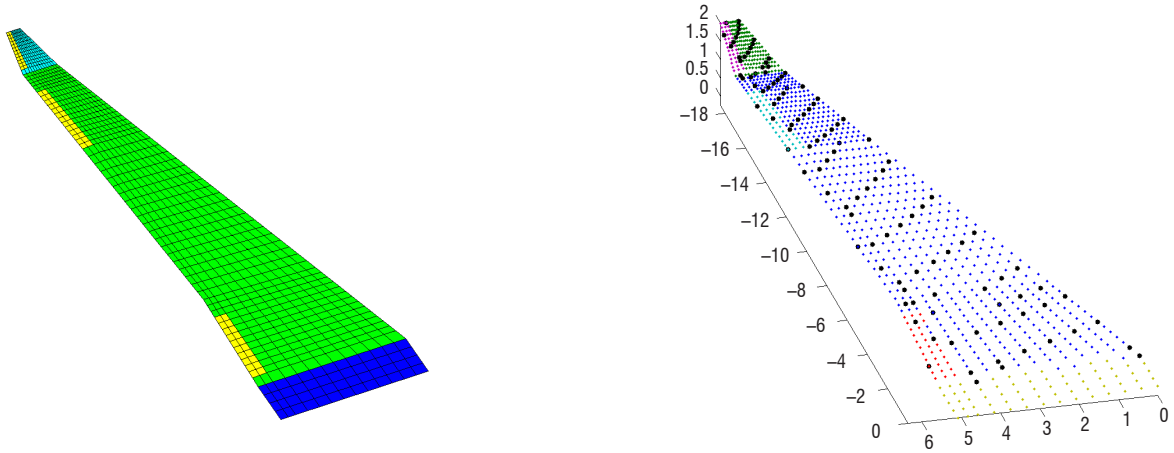

Figure 4 – Panel mesh for aeroelastic force calculation using DLM (left) and measurement locations (right) for the state-space model

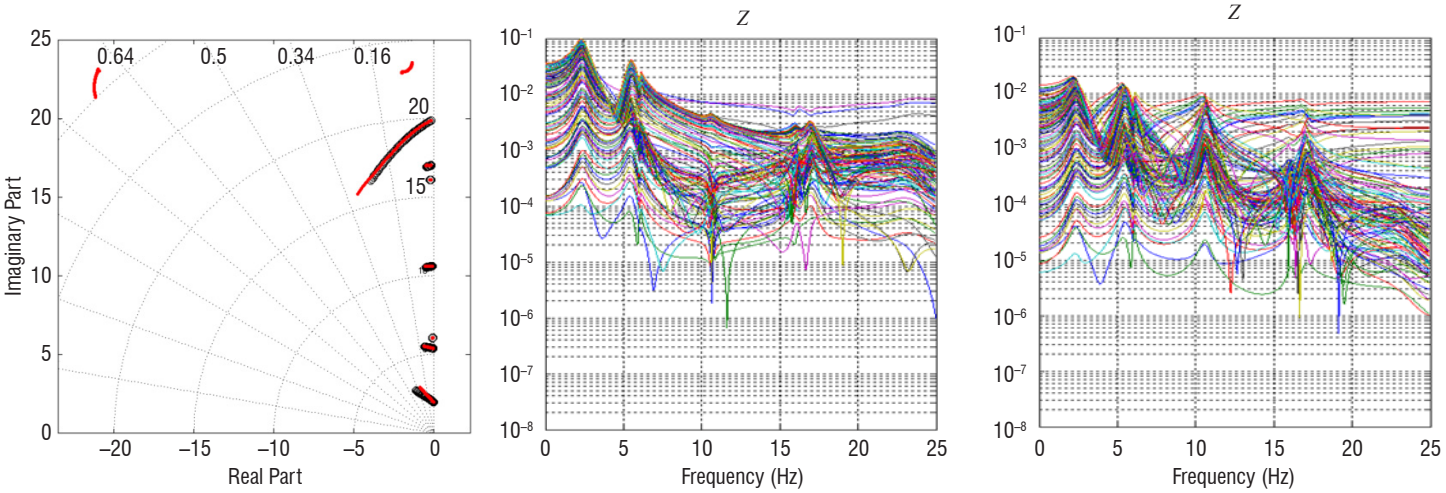

Figure 5 – Eigen-values of the aeroelastic system resulting from both the state-space model and a classical flutter analysis using a p-k method (left); displacement FRF due to the aileron deflection (middle) and to the deflection of the deformable-in-torsion winglet (right)

and yellow (aileron, inner flap and winglet flap) in Figure 4, from the plunge and pitch flight mechanics modes, and from a cylindrical turbulence mode. The aerodynamic computations providing the tabulated GAF used to build the RFA model have been performed at the cruise Mach number.

The GAF smoothing has been validated by comparing the evolution of the fluid-structure system complex eigen-values resulting from the state-space model and from a flutter analysis using the p-k method (Figure 5 left). Figure 5, middle and right, show the vertical displacement FRF of all observation points (Figure 4 right) in response to the aileron (middle) and to the deformable-in-torsion winglet (right) deflections. A displacement 5 times greater can be noticed when the aileron is deflected.

In a third step, every winglet concept has been assessed using this reduced aeroelastic model. Table 1 gives the vertical force variation at the wing root resulting from the different input commands at null frequency (quasi-static computations): pitching flight mechanics mode, turbulence, wing internal flap deflection, aileron deflection, rotation of the whole winglet around an axis along its span, torsionally-deformable winglet deflection, and winglet trailing-edge-flap deflection. As expected at the cruise Mach number, the effectiveness loss due to the structural flexibility is higher for the winglet and aileron commands. Furthermore, the impacts on the vertical effort of the torsional winglet and of the winglet flap are significantly higher than the impacts of

	pitching motion	turbulence	internal flap	aileron	winglet rotation	torsional winglet	winglet TE flap
rigid wing	120102	125994	–9693	–7930	73	839	–1033
flexible wing	110420	118178	–8818	–3265	–4	284	–139
ratio (%)	8	6	9	59	105	72	86

Table 1 – Vertical effort variation (in Newton) at the wing root for 7 input static commands

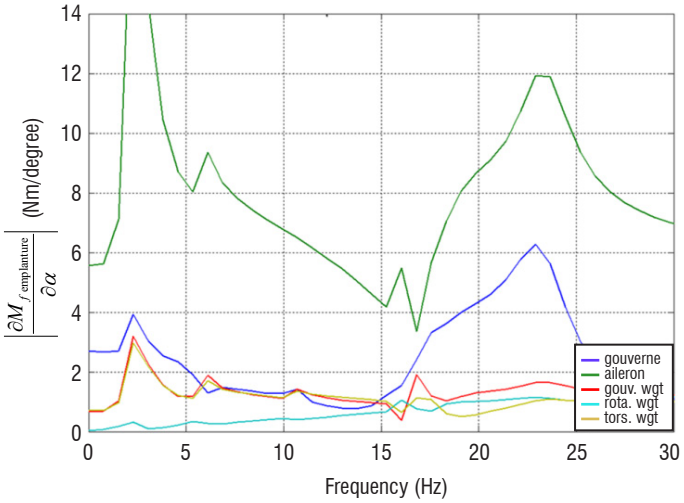

Figure 6 – Bending moment variation at the wing root for the deflection of the internal flap (blue curve), aileron (green), winglet TE flap (red), whole winglet (rotation) (light blue) and torsional winglet (yellow)

the other morphing winglet concepts. The wing root bending moment variation for non-zero frequencies has also been investigated, taking into account the structure flexibility (Figure 6). The effectiveness of the aileron is significantly higher than that of the other commands for the entire frequency range considered. The morphing winglet concepts, like the aileron, are most efficient at a frequency matching the first structural bending eigen-frequency.

Comparisons with High-Fidelity Fluid-Structure Coupling Simulations

The previous aeroelastic model has been built from a DLM formulation for the aerodynamic forces, which does not take into account either the fluid viscosity or the flow discontinuities like shocks or flow separation. In order to validate the latter model, high-fidelity fluid-structure coupling simulations have been carried out for both the deformable-in-torsion and the trailing-edge-flap winglet concepts. Such simulations model the fluid behavior with RANS CFD and the structure with the preliminary finite-element model. They have indeed been performed using the in-house CFD software

elsA [7] [14] associated with the aeroelastic module Ael [15] [16] for the two winglet concepts, as well as for the aileron (Figure 7). The control-surface static deflections have been carried out by mesh deformation, as can be seen in Figure 8. The control-surface effectiveness has been computed for cruise conditions (Mach=0.75, C_L=0.52, altitude=35,000 ft).

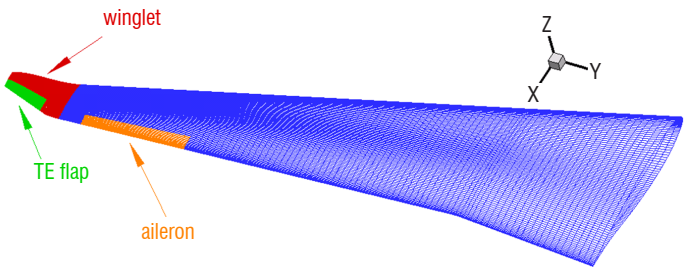

Figure 7 – Wing surface CFD mesh with the movable surfaces in orange, red and green

Such fluid-structure coupling simulations, like the ones using the reduced aeroelastic model, allow the impact of a control surface deflection on the aerodynamic performance to be investigated, as well as the impact on the aeroelastic wing deformations and on load alleviation. The efficiency loss due to the structural flexibility of the wing can also be assessed by comparing simulations carried out with a flexible structure (fluid-structure coupling simulations, named "AEL" in the following figures) and with an infinitely rigid wing (only fluid computations named "CFD" in the figures). First of all, the behavior of all control surfaces remains linear throughout the entire deflection range, except for the winglet trailing-edge-flap, whose linearity deflection range goes up to 5°. This checks that the case of this wing under the considered cruise flight conditions is within the validity range of the DLM formulation. From the aerodynamic performance point of view, unlike the aileron, a positive (downwards) or negative (upwards) deflection of the whole winglet, or of the winglet trailing edge flap, yields a drag increase (Figure 9 middle). This is indeed expected, since the simulations have been performed for cruise conditions, for which the shape of the transport aircraft wing and winglet is optimized. Nevertheless, the lift-over-drag ratio can be slightly increased, which shows the great potentiality of morphing winglet to improve the performance during at least the whole cruise. The second point is that an important loss of control-surface effectiveness (defined as the lift variation over the deflection variation, or as the slope of the lift evolution with respect to the deflection angle, Figure 9 left) due to the structural flexibility can be noticed, except for the torsionally-deformable winglet (Table 2).

Control surface	Rigid effectiveness (/°)	Flexible effectiveness (/°)	Effectiveness loss (%)
aileron	0.0063	0.0034	46
torsional winglet	0.0005	0.000375	25
winglet TE flap	0.0016	0.00073	54

Table 2 – Effectiveness of three control surfaces: aileron, deformable-in-torsion winglet and winglet trailing edge flap

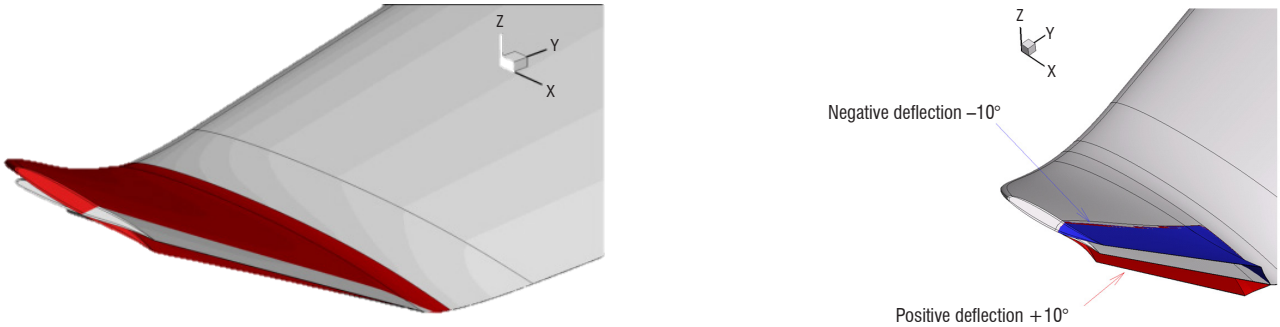

Figure 8 – CFD mesh surfaces on winglet: deformable-in-torsion winglet on the left, and trailing-edge-flap on the right

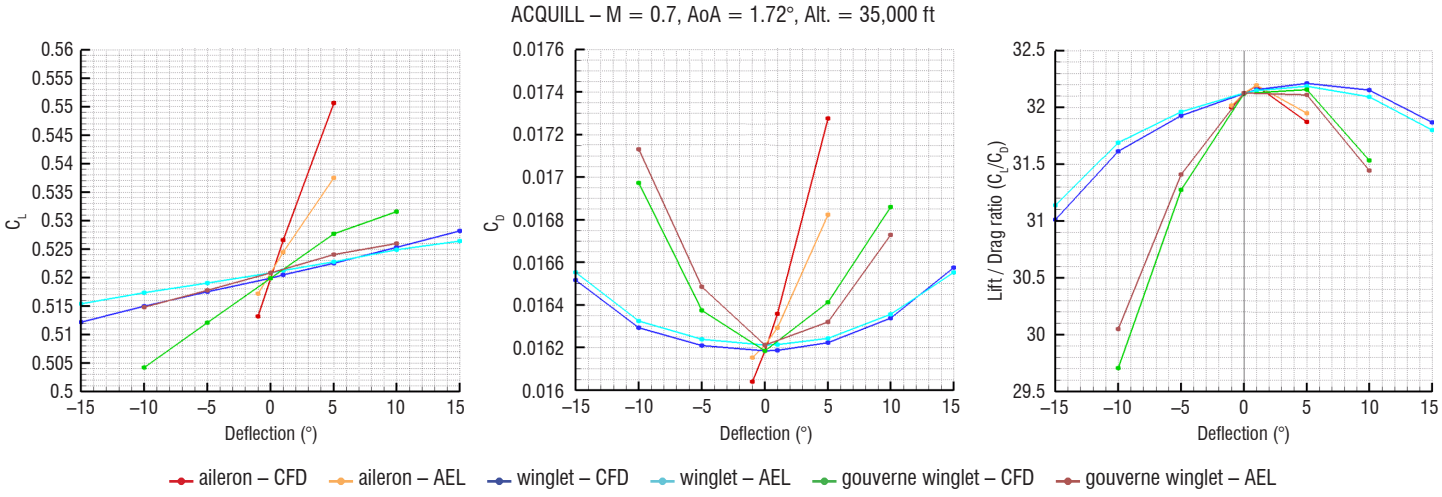

Figure 9 – Lift, drag and lift-over-drag evolution with respect to the control surface (aileron, deformable-in-torsion winglet and winglet TE flap) deflection

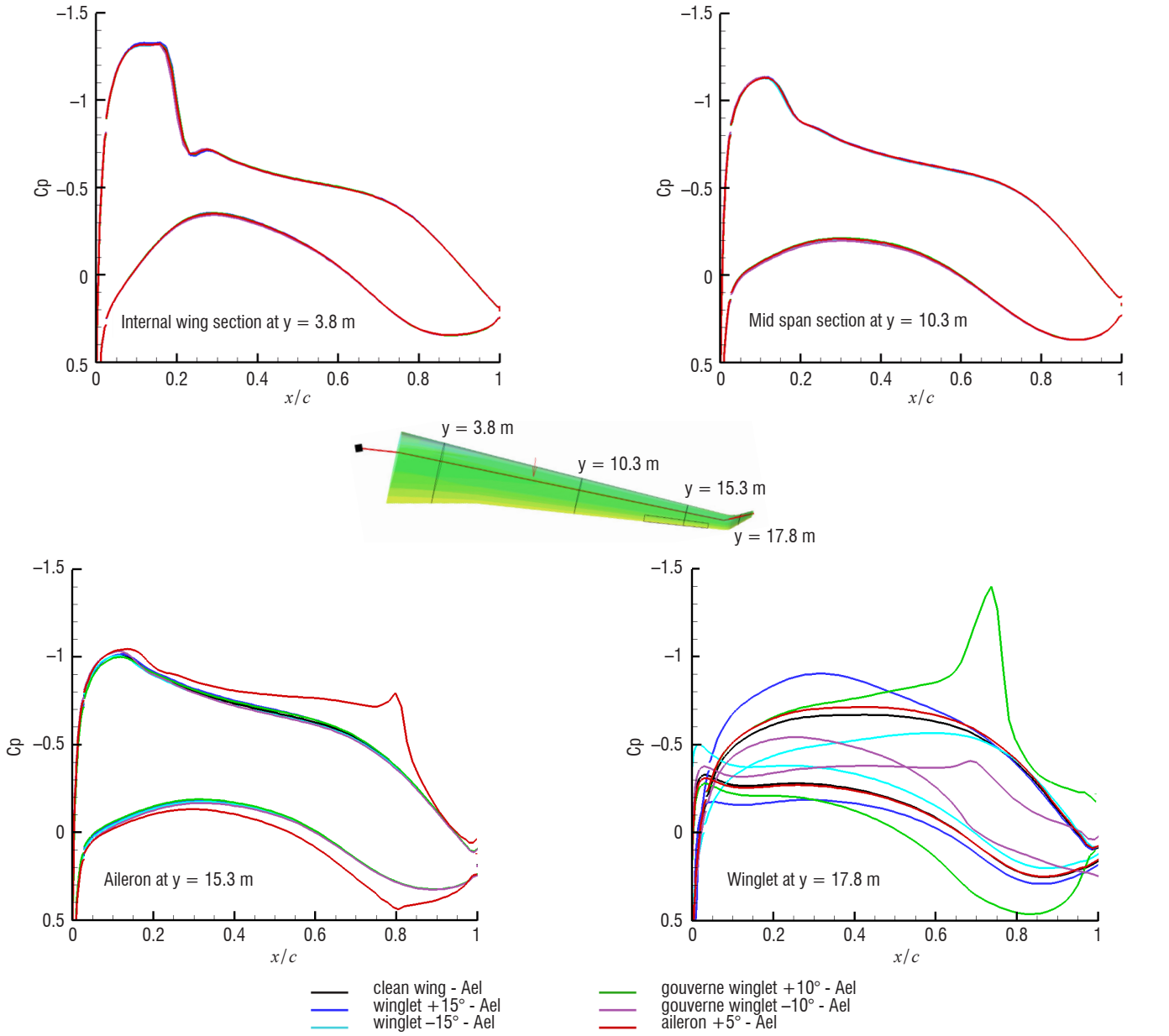

Figure 10 – Pressure distributions on 4 wing sections

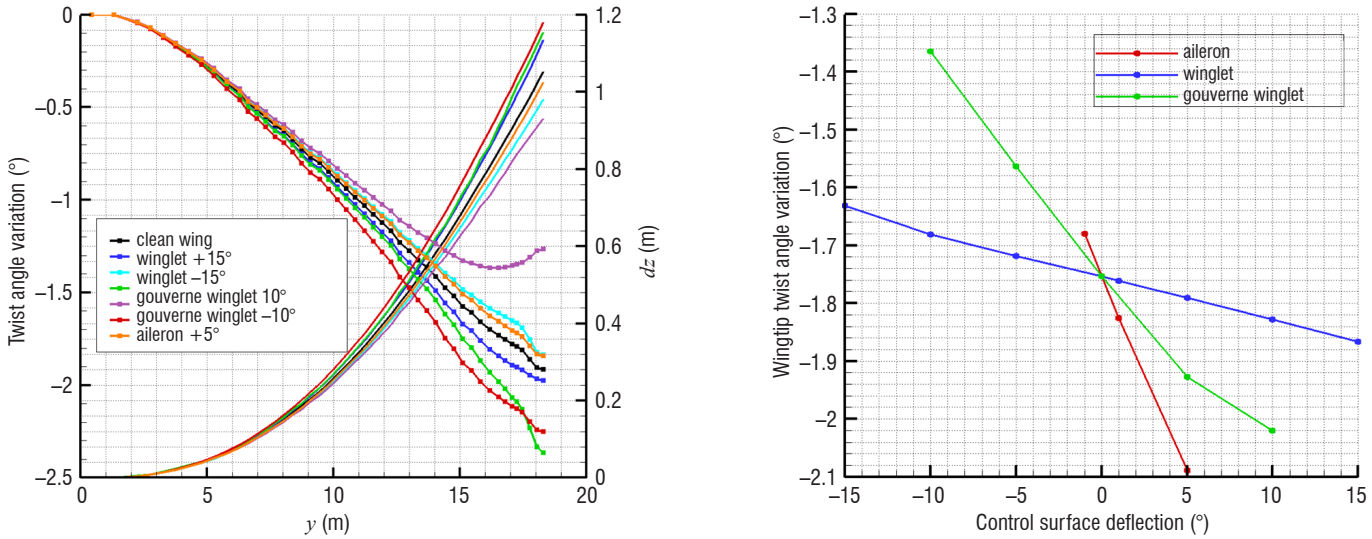

Figure 11 – Aeroelastic deformations due to control surface deflection (aileron: red and orange curves, torsional winglet: blue and cyan curve, winglet TE flap: green and purple curves) with respect to the span coordinate (left) and deflection angle (right)

From an aeroelastic point of view, Figure 11 shows the aeroelastic deformations (twist angle variation and vertical displacements along the span) of the wing thanks to aileron and morphing winglet deflections. The figure also shows (plot on the right) the twist angle of the wing tip with respect to the deflection of the three control surfaces. Even if the pressure perturbations due to the deflection remain local (see Figure 10), particularly if the control surface is the winglet itself or its flap, the impact of the deflection on the twist angle variation along the span is significant for both the aileron and the winglet trailing edge flap.

In terms of loads, the impact of morphing winglet deflections can be seen in Figure 12. The middle and right-side plots indeed show the span-wise distribution of the local bending moment induced by the pressure integration along the only chord for fixed sections. The plot on the left represents the span evolution of the bending moment integrated along the span.

The reduced aeroelastic model and the high-fidelity fluid-structure coupling modelling were then compared. A good agreement was noticed with regard to the qualitative behavior of the control surfaces in terms of aerodynamic load alleviations, even though the levels are slightly different, as can be seen in Table 3.

	$\Delta C_L / °$	
control surface	*elsA*-Ael	state-space model
aileron	0.0034	0.0025
torsional winglet	0.0004	0.00025

Table 3 – Lift variation induced by aileron or torsional-winglet deflection

Morphing Winglet Concept Evaluation

Design of a Realistic Reference Wing

CFD computations have shown the validity of the reduced aeroelastic models based on a state-space formulation for the aerodynamic conditions of interest in this study. In order to assess the innovative morphing concepts, such reduced models have to be built from a structural model of a wing, which should be the most representative possible of a real wing, at least from a structural point of view. The latter wing is called a "reference wing" in the following and has been designed by optimizing the preliminary finite-element model using the solvers SOL200 (optimization solver) and SOL144 (static aeroelastic solver) of the MSC/NASTRAN software, and taking into

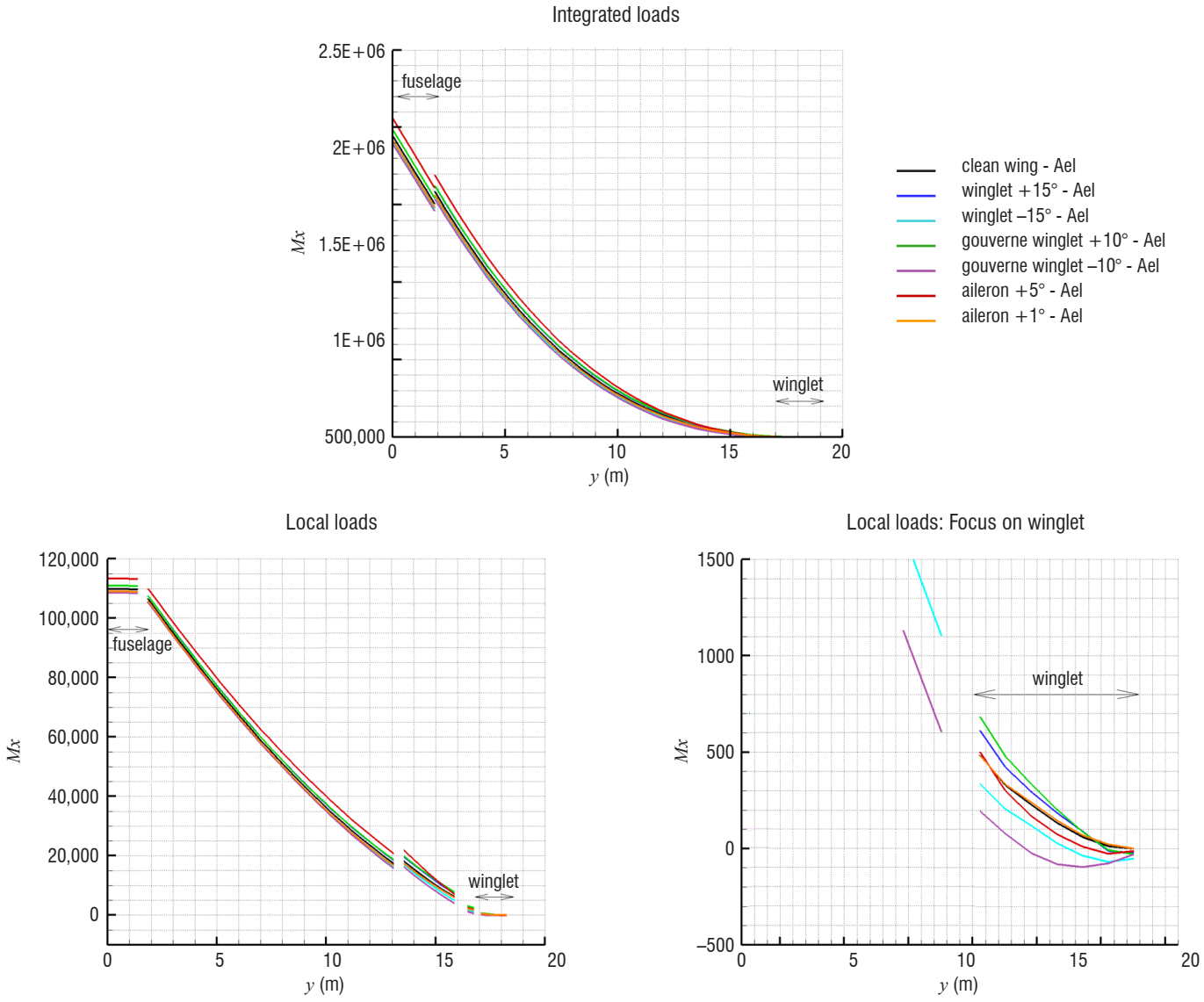

Figure 12 – Bending moment distributions along span

account both symmetric (2.5 g pull-up maneuver, gust load) and antisymmetric load cases (roll maneuver) resulting from balanced maneuvers. Aerodynamic loads have been computed using fluid-structure coupling simulations with a full free-free aircraft model. The fuselage and tail have been considered as rigid and the aircraft mass and inertia have been represented by a one-node element (CONM2) at the center of gravity of the aircraft (Figure 13 left). The optimization has been performed considering as design parameters the thickness of the skin spars and ribs of the wing box, taking into account the constraints of 3.2×10^{-3} maximal deformations in the composite shells (Figure 13 right).

Flutter stability has been checked for several flight speeds and mass configurations (MTOW, MLW and one intermediate configuration for which fuel mass is concentrated in the outer wing, which is a configuration named MOPW, see Figure 2). The resulting optimized wing is then realistic and will be used as reference for morphing winglet concept evaluations.

Morphing Winglet Assessment Based on the Reference Wing

The evaluation of the morphing winglet concepts has been performed taking into account the whole free-free aircraft described in the previous section, equipped with the optimized reference wing. Two mass configurations have been considered: MTOW (60 tons) and the intermediate configuration (called MOPW), for which fuel mass is mainly located in the fuselage and in the outer wing (Figure 2).

Two reduced aeroelastic models were then built from the first eight deformation eigen-modes, a pitching rigid mode and a "phugoid" mode (combination of plunge and pitch), a cylindrical turbulence mode, a GAF model built using a Roger approach and six control-surface deflections: deformable-in-torsion winglets, rigid rotation of the winglets, winglets with trailing edge flaps, winglets flapping, ailerons and horizontal tail planes (HTP). In order to be able to design controllers and to synthetize control laws, the number of states have been reduced to 78 using a robust algorithm available with control toolboxes (Robust Control Toolbox working with Matlab).

The latter aeroelastic models allow the effectiveness of the six control surfaces to be assessed in terms of lift variations. These effectiveness data are given for both mass configurations in Table 4. One can note that the impact of the structure flexibility on the lift variation is high for the MOPW configuration, especially for the morphing winglet concepts. This discrepancy is significantly less for the MTOW configuration, thus showing a high influence of the mass distribution on the control surface effectiveness. Moreover, and as expected from the results of the computations with the preliminary finite-element model

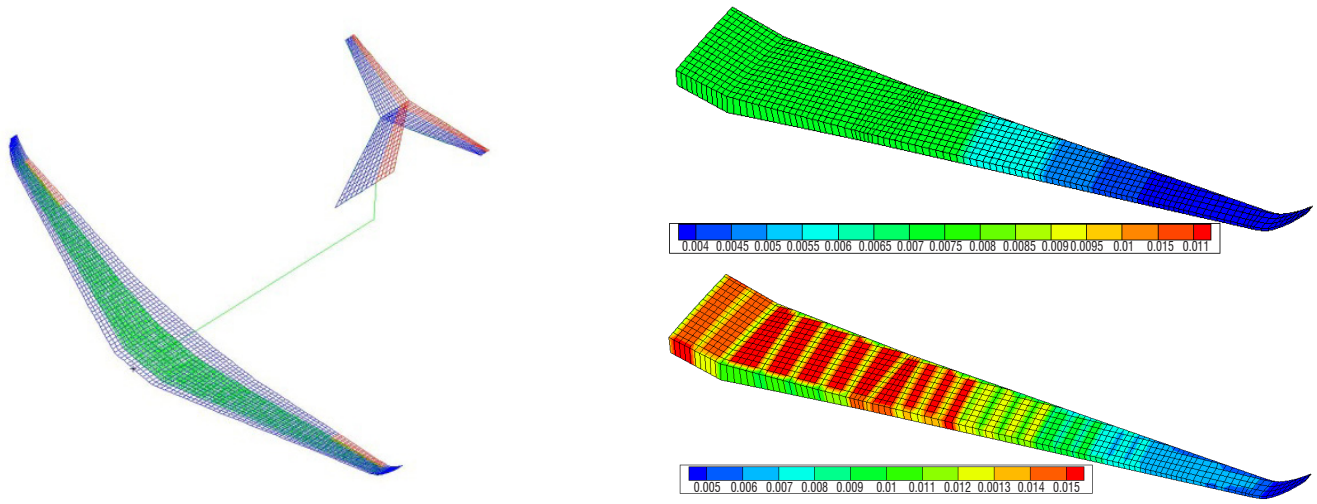

Figure 13 – Whole aircraft aeroelastic model (structure finite elements in green, aerodynamic panels in blue and control-surface aerodynamic panels in red), and shell-thickness distributions before (top right) and after (bottom right) optimization

Command	MOPW			MTOW		
	Rigid/flexible	$\partial Cz/\partial\alpha$ (/deg)		Rigid/flexible	$\partial Cz/\partial\alpha$ (/deg)	
		Rigid	Flexible		Rigid	Flexible
Torsional winglet	2.22	1.42e–04	6.41e–05	1.44	1.42e–04	9.89e–05
Aileron	1.59	2.36e–03	1.48e–03	1.25	2.36e–03	1.89e–03
Winglet flap	2.22	3.02e–04	1.36e–04	1.44	3.02e–04	2.10e–04
Winglet flapping	2.10	–2.14e–05	–1.02e–05	1.41	–2.14e–05	–1.51e–05
Winglet rigid rotation	2.12	–5.98e–04	–2.83e–04	1.41	–5.98e–04	–4.24e–04
HTP	0.98	5.01e–03	5.13e–03	0.98	5.01e–03	5.14e–03
Pitch	1.12	1.13e–01	1.01e–01	1.05	1.13e–01	1.07e–01
Phugoid	1.03	1.13e–01	1.09e–01	1.01	1.13e–01	1.11e–01
Turbulence	1.03	1.13e–01	1.09e–01	1.01	1.13e–01	1.11e–01

Table 4 – Impact of commands on lift (frequency = 0Hz)

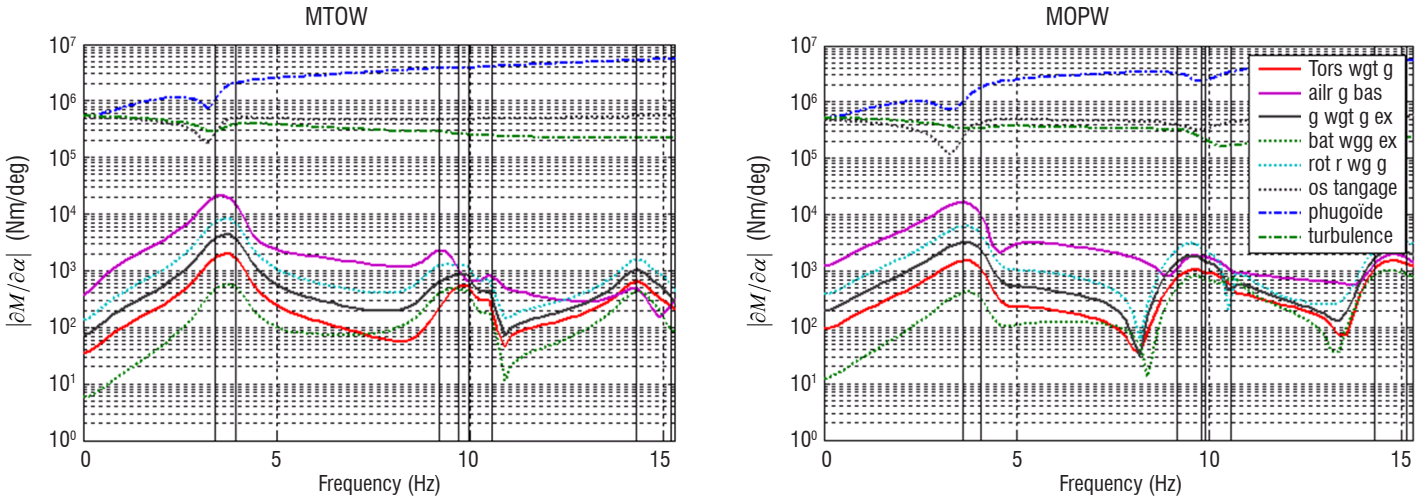

Figure 14 – Bending moment variations at the wing root vs. frequency response to the commands: winglet flapping (dotted green curve), torsional winglet (red curve), winglet flap (black curve), winglet rigid rotation (cyan curve), aileron (purple curve), turbulence (green dashed-dotted curve), pitching motion (gray dotted curve) and phugoid (dashed-dotted dark blue curve)

and using both reduced and high-fidelity fluid-structure models, one can note the greater effectiveness of the winglet flap compared to that of the torsional winglet. Furthermore, the structure flexibility induces an increase in the moment variations for all commands when their frequency is close to the structural eigen-frequencies. Similar conclusions can be drawn for the bending moment variations at the wing root (Figure 14).

The four morphing winglets presented in Figure 1 have thus been assessed in terms of variations of lift and bending moment at the root. The effectiveness of the flapping winglet has been found to be significantly lower than that of the other control surfaces. The previous simulations have also shown a lower effectiveness of the torsional winglet than that of the winglet equipped with a flap and, of course, of the aileron (Table 4 and Figure 14). This can be partly explained by geometric considerations. Taking indeed into account the surfaces of the control surfaces and their projection onto a horizontal plane, the effective surface of the torsional winglet is decreased due to its cant angle of about 50° compared to a horizontal aileron. Furthermore, the deflection of the torsional winglet is, for technological reasons, progressive according to a quadratic function ranging from 0° at the root to the wanted deflection at the tip. At last, the chord decreases also along the span to reach its minimum when the maximal deflection is applied. Those three factors lead to a loss of 2/3 of the initial surface and finally to an effective surface of 1/4 of the aileron surface.

The rotation of the winglet around an axis along the winglet span is a concept that would yield a too high mass penalty to be considered as feasible from the technological point of view. However, it can be considered as a limit case of the torsional winglet, thus allowing the highest potential of such a morphing concept to be evaluated.

Strategy of the Command of the Winglet with Flap Combined with the Aileron

The winglet with a trailing edge flap seems to be the most efficient in terms of load control from the previous evaluations. It has therefore been further investigated by assessing its load alleviation capabilities, taking into account a trimmed aircraft in flight. The reduced aeroelastic model built as described above is not able to compute the trim parameters. It has therefore been coupled with the AVL software developed by M. Drela and H. Youngren [13]. This code, based on a Vortex Lattice Method to compute aerodynamic forces, is able to compute the trim parameters (incidence, and control-surface deflection angle) for balanced static maneuvers of a rigid aircraft. Furthermore, it also computes drag, using the Trefftz formulation [4] and lift taking into account the mean chord curvature, thus allowing the evaluation of the lift at null incidence. The coupling with the reduced aeroelastic model leads then to the trim computation of a flexible aircraft. It is performed using a classic iterative method:

- Trim computation using AVL, whose outputs are the incidence, HTP deflection angle, pressure distribution on the wing surfaces and integrated pressure forces and moments at the wing root.
- Transfer of the pressure distribution onto the DLM mesh used to build the state-space aeroelastic model, and computation of the resulting generalized aerodynamic forces.
- Computation of the wing deformations using the aeroelastic state-space model.
- Translation of these deformations into AVL inputs. The vertical displacements and rotation of the mean chord of some wing sections are indeed deduced from the wing deformation.
- If no convergence is achieved, return to Step 1.

This coupling procedure has been applied to the aircraft for cruise flight conditions (load factor $n_z = 1$), in order to investigate the effect of both aileron and winglet flap deflections. The trim has been computed taking into account plunge and pitch rigid motions. Convergence has been reached after 7 iterations for every aileron and winglet flap deflection configuration, as can be seen in Figure 15, which represents the evolution of four quantities: trim parameters, *i.e.*, incidence and HTP control-surface deflection (top left), drag representing the aerodynamic performance and computed using the Trefftz formulation (top right), the bending moment at the wing root (bottom left) and a combination of both the load and aerodynamic performance (bottom right), which is a quantity that can be used for

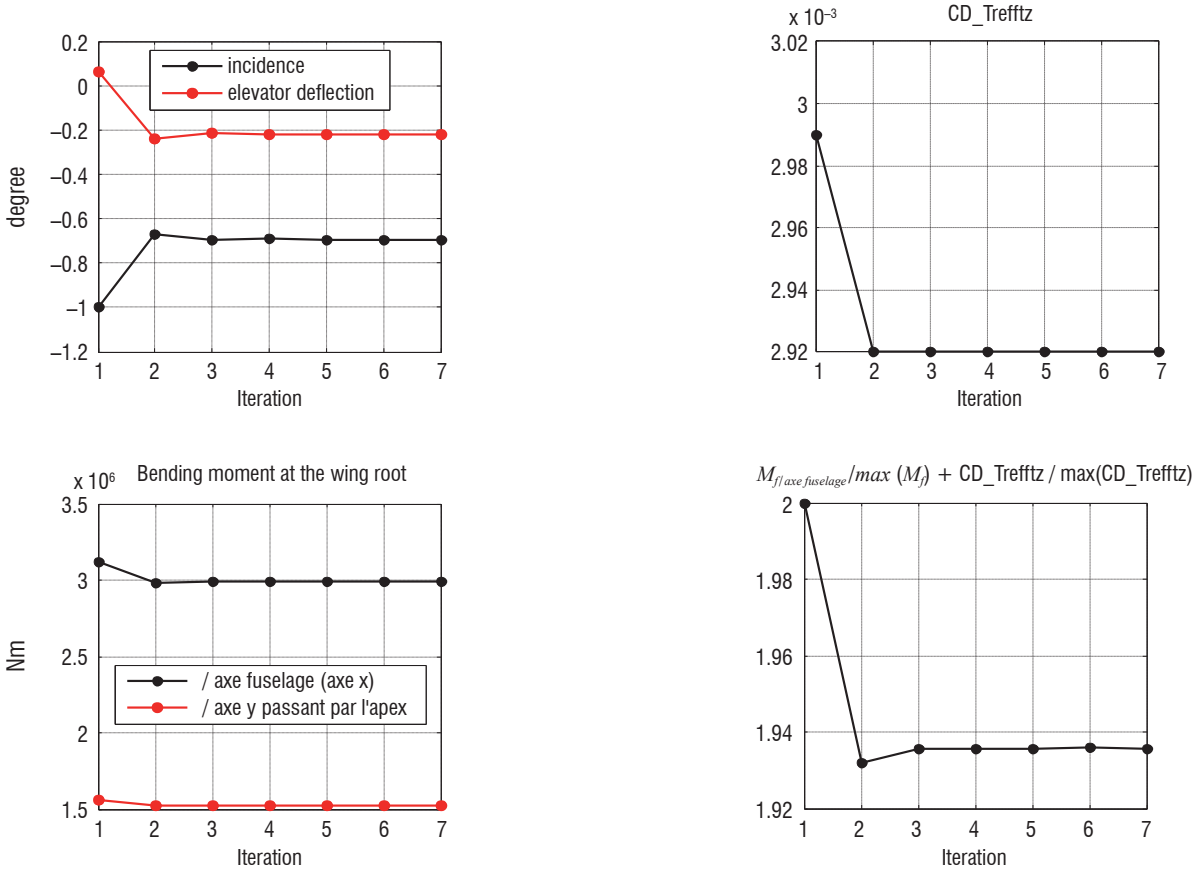

Figure 15 – Flight mechanics – elasticity coupling convergence

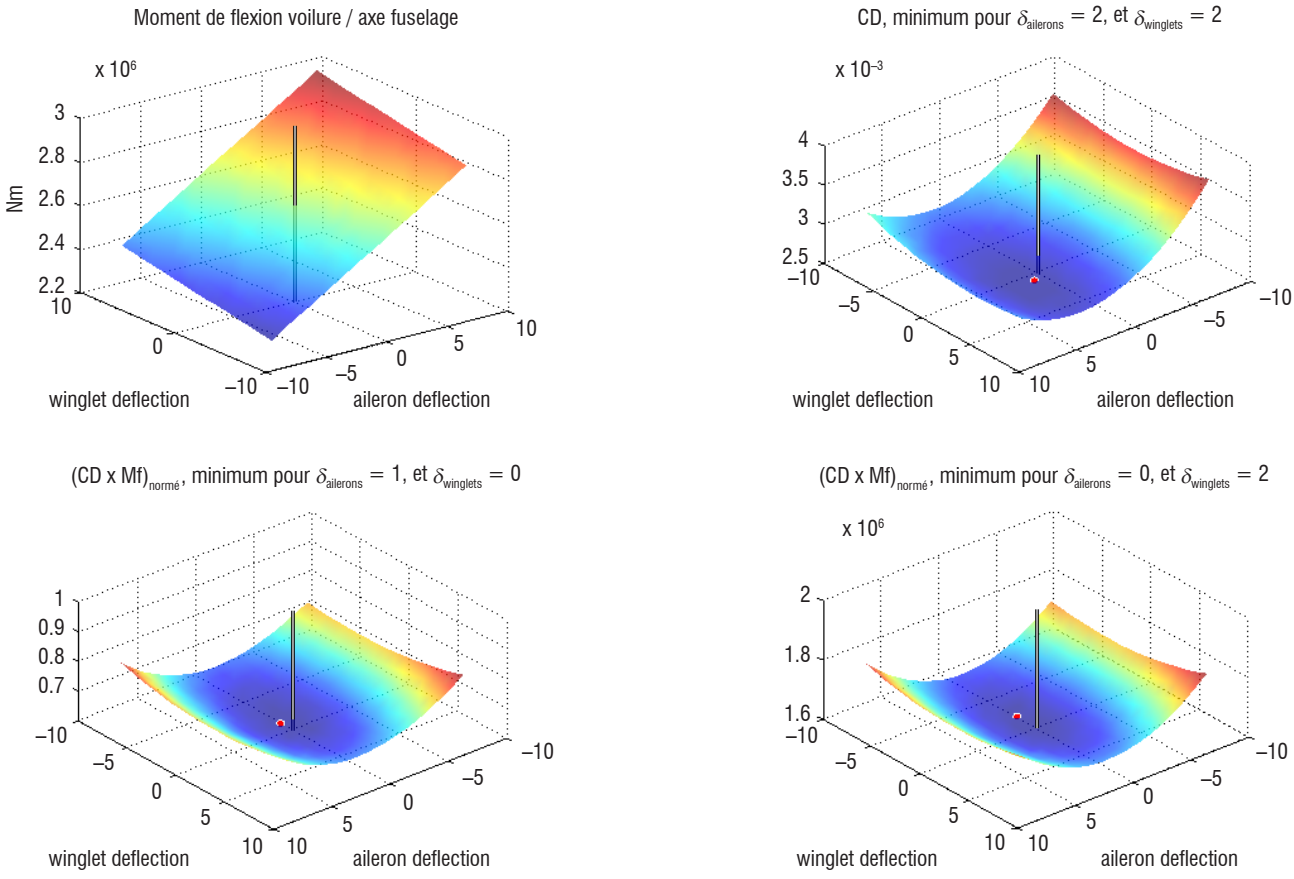

Figure 16 – Bending moment at the root (top left), drag (top right), and the product (bottom left) and sum (bottom right) of both for several aileron-winglet flap deflection configurations.

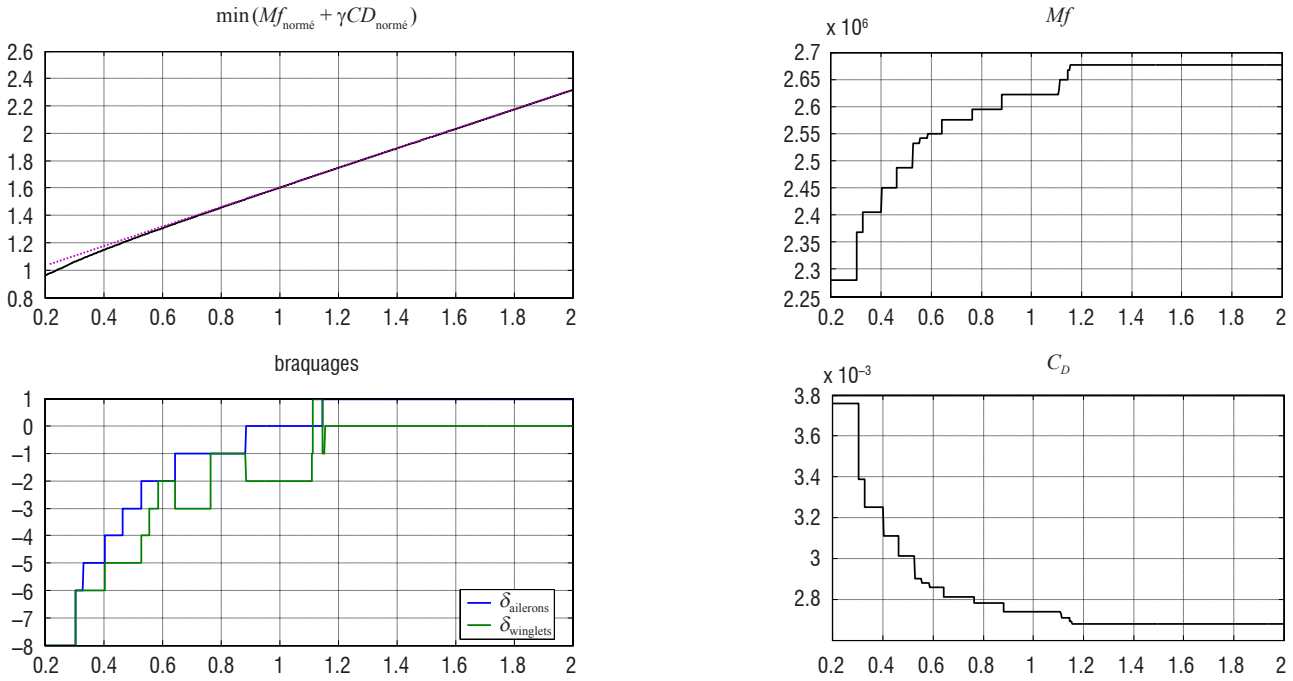

Figure 17 – Optimal objective function, bending moment, aileron and winglet flap deflection and drag with respect to the drag weighting coefficient γ in the objective function expression (bending moment + γ drag)

aero-structure optimization or for control-surface function optimization. The response surfaces of the bending moment, drag, sum of these and product of these have therefore been determined in a reasonable time for aileron and winglet flap deflections ranging from –8° to 8° (Figure 16). One can note that the minima of the drag and the quantities involving drag are reached for deflections close to 0 but not null. Furthermore, the curvature of the drag behavior with respect to the aileron deflection is higher than that with respect to the winglet flap deflection, thus showing a significantly stronger impact of the aileron on the drag than that of the winglet flap.

A preliminary study has been carried out to compute the optimal deflections of both the aileron and the winglet flap according to an objective function built from both the load (bending moment at the wing root) and the aerodynamic performance (drag) contributions:

$$\min\left[Mfx/Mfx_0 + \gamma\, C_D/C_{D0}\right]$$

In order to make the objective function coherent and thus make the bending moment and the drag coefficient dimensionless, the latter variables have been divided by reference values (Mfx_0 and C_{D0} matching the maximal values in the top sketches of Figure 16). Furthermore, the drag coefficient is deduced only from the Trefftz formulation, without any CFD result contribution. Only the induced drag is therefore considered for the optimization process. A weighting coefficient γ has been applied to the drag contribution, in order to investigate the influence of one contribution on the other. An optimization problem has thus been solved for values of this weighting coefficient ranging from 0.2 to 2. The optimal deflections of both the aileron and the winglet flap are plotted in Figure 17 – Optimal objective function, bending moment, aileron and winglet flap deflection and drag with respect to the drag weighting coefficient g in the objective function expression (bending moment + γ drag). The latter shows that the optimal deflection of the winglet flap is similar to that of the aileron for the entire range of γ. The winglet flap used in association with the aileron therefore has a significant efficiency for load alleviation, while having lower impact on the drag. Future works will be dedicated to finding the optimal aileron-winglet flap deflection configurations for several flight conditions, in order to assess the real gain in structure weight and fuel consumption.

Technological aspects

Additional work has been performed to ensure the feasibility of the trailing-edge-flap winglet concept. Nevertheless, the aim of the previous study was just to prove that it is possible to design a demonstrator using current technologies. In this context, we did not pay particular attention to certification requirements, as presented in [17] for the winglet adaptive trailing edge development carried out within the framework of the European project SARISTU. Aerodynamic calculations showed that the proposed control surface should have the following performances:

- Hinge moments: 67 mN, 13 mN and 28 mN at +10°, –10° and 0° flap deflection respectively.
- Maximal flapping frequency of 5 Hz.
- Ability to operate at cruise flight conditions, *i.e.*, Mach = 0.7 and an altitude of 35,000 ft (this flight altitude imposes an operating temperature of –55°C for the actuator).

Preliminary calculations showed that it was not possible to find actuators and a hinge geometry able to ensure the required hinge moments for flap deflections of +/–10° at 5 Hz. Consequently, the initial requirement regarding the flap amplitude has been reduced to +/–5°.

The first problem that arose was the implementation of a movable control surface of about 30% of chord at the trailing edge. Starting

from the initial finite-element mesh, the winglet spar ribs and skins have been redesigned to take into account a straight flap hinge (red line in Figure 18 left). The most suitable area to implement an actuator was the winglet root, where the available room is the widest (Figure 18 middle). These conditions lead to a slight modification of the initial finite-element mesh, as shown in Figure 18 right.

The second step has consisted in selecting an actuator satisfying all of the constraints (geometry, forces, operating temperature, dynamics and energy consumption). Taking into account the cruise aerodynamic conditions, a deflection ranging from –10° to 10° yields a maximal aerodynamic moment of 67 Nm. The actuator should be able to apply this moment with a moment arm measuring less than 42 mm, since it has to be located in a reduced volume. The most suitable actuator has to have the following characteristics: maximal effort of 10,000 N for a displacement amplitude of 20 mm. The dynamic operating speed has therefore been deduced from the required displacement and from the specified deflection amplitude and frequency. Owing to the cruise altitude, the actuator should also be able to operate at low temperatures of about –55°C. An electrical actuator seems to be the most suitable, but it also has to satisfy additional constraints, such as low energy consumption and the ability to use a power supply system compatible with that of the aircraft (voltage lower than 400 V). Some commercial actuators meet all of these specifications, as can be seen in [11]. It is important to note that only cruise conditions have been taken into account and other conditions such as "off-design" (take off, climb, descent, and landing) should also be considered to achieve the feasibility of the demonstrator. Unfortunately, this leads to greater loads requiring a specific actuator design to meet all certification requirements, as has been performed in [12].

The next step consisted in studying the implementation of the actuator and flap in the winglet. Figure 19 shows a planform view of the flap, the actuator location, the hinge axis and the kinematic connections. A more detailed view of the installation of the actuator in the winglet box and its connection with the flap is given in Figure 20. The initial finite-element model has therefore been modified to represent the morphing system as accurately as possible.

The additional mass of the actuator, connecting rods and ball joints is 13.18 kg and that of the flap is 2.925 kg. The flap spars and stiffeners are made of an aluminum alloy and the flap skin is made of the same composite material as that of the wing. Finite-element computations have also been performed based on the aerodynamic forces deduced from the specifications. A first static simulation was carried out applying pressure forces to the flap skin (Figure 21 left) and a second simulation was carried out applying forces deduced from the maximal effort of the actuator (9600 N) to the actuator fixation nodes (Figure 21 right). These simulations have shown a maximal displacement of 0.458 mm at the winglet and a maximal stress of about 21 Mpa, which are values lower than the admissible ones.

This technological work is obviously not sufficiently complete to manufacture a high TRL demonstrator, but was aimed solely at demonstrating the feasibility of the concept of the morphing trailing-edge winglet. It has indeed shown that a flap could be mounted on a winglet

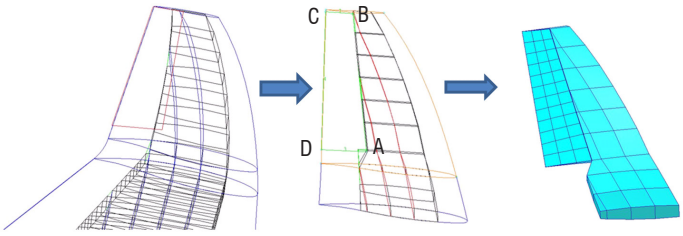

Figure 18 – New winglet box design and modified finite-element model

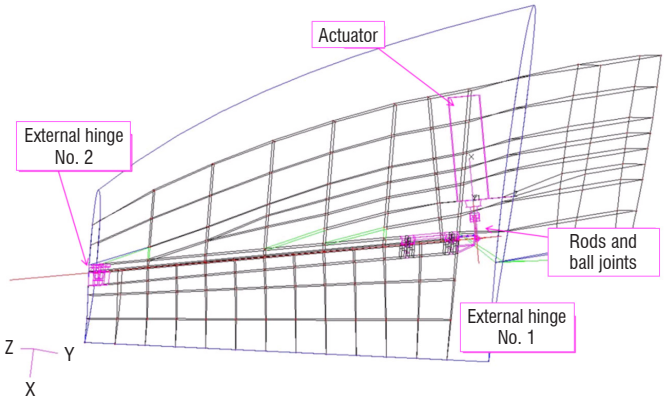

Figure 19 – Implementation of a flap and an actuation system in the winglet

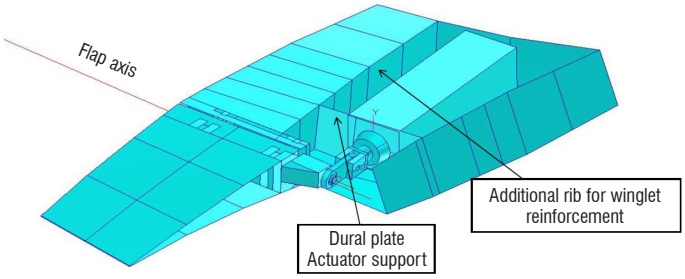

Figure 20 – Focus on the actuator and its installation in the central box

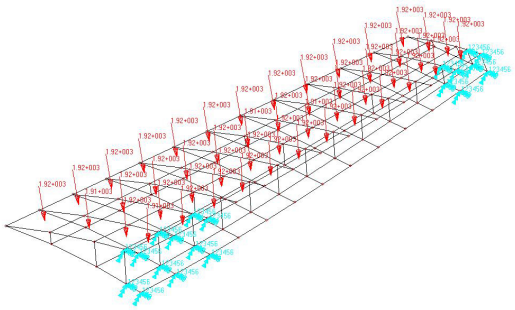

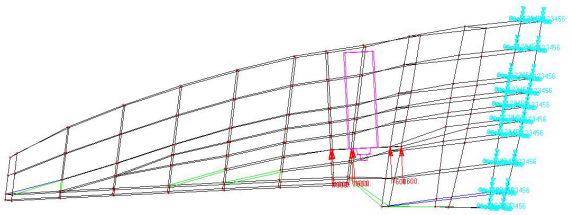

Figure 21 – Sizing static simulation boundary conditions and applied loads

using commercial actuators, even though no demonstrator has been built. Moreover, the problem of designing a skin covering the entire winglet allowing smooth flap deflections has not been addressed in this study. Furthermore, improvement could be envisaged in the case of a full scale winglet, by optimizing the actuator location to increase its travel and to improve its efficiency, and by optimizing the connecting rod angles to increase the moment arm.

Conclusions

One priority for the aeronautic community is now to significantly decrease the environmental footprint of aircraft. One possible way is to improve aerodynamic load control and alleviation, while improving, or at least not altering the aerodynamic performance, in order to decrease the structure weight. In this context, several morphing winglet concepts have been evaluated from the load control point of view.

The first step consisted in developing a numerical simulation tool able to accurately capture most physical phenomena, while remaining reasonable in terms of computational time. This software is based on coupling the publicly available static flight mechanics software AVL with an aeroelastic reduced model able to take into account the structure dynamics, structural deformations and unsteady aerodynamics. This reduced model is based on a state-space model built from a set of structure deformation modes and from a rational function approximation of aerodynamic forces, according to the Roger formulation. This state-space model has been validated by comparisons with CFD and high-fidelity coupling fluid-structure (CFD-CSM) for the aerodynamic conditions of interest (high subsonic flight). The coupled aeroelastic model is then able to assess the performance of a flexible free-free aircraft, which is trimmed for a specified maneuver. This performance can be seen from the aerodynamic (lift or drag), load control (bending or torsion moment, vertical effort) and aeroelastic (vertical displacement, twist variation, control surface efficiency) points of view. Furthermore, since the model is low-CPU-time-consuming, it can be used in an optimization process for control-surface design, as well as for designing a control surface driving strategy.

The second step consisted in the determination of a reference wing, which has to be the most representative of a real aircraft equipped with a winglet. Such a wing has been designed from the wing specifications and geometry of a regional aircraft determined within the EU project SARISTU [30] and from several sizing load cases (both symmetric and asymmetric maneuvers) extracted from the certification standard documents (CS 25). The aeroelastic stability has also been checked.

In a third step, four morphing winglet concepts were assessed in terms of aerodynamic performance and load control for subsonic-cruise-like conditions: flapping winglet (rotation of the winglet around the wing-tip chord axis), rotation of the whole winglet around its spanwise axis, torsional winglet (controllable torsion deformation) and a trailing edge control surface. The winglet with trailing edge flap was found to be the most efficient in terms of load control, in particular when used in conjunction with the aileron. This morphing concept indeed has significant efficiency, though less than that of the aileron, but has a weaker impact on drag.

The last step consisted in investigating the technological feasibility of such a morphing concept. This study did not lead to the building and testing of a demonstrator, as in the work by Wildschek *et al.* within the framework of the EU project SARISTU [30 Part III] [27], but it proved that the concept could be implemented in both a demonstrator and a real aircraft ■

References

[1] ACARE - *Strategic Research & Innovation Agenda (Volume 1)*. www.acare4europe.org/sites/acare4europe.org/files/attachment/acare-strategic-research-innovation-volume-1-v2.7-interactive-fin.pdf.

[2] E. ALBANO, W. RODDEN - *A Doublet-Lattice Method for Calculating Lift Distributions on Oscillating Surfaces in Subsonic Flow*. AIAA Journal 7(2), pp. 279-285, 1969.

[3] A. ALLEN, C. BREITSAMTER - *Investigation on an Active Winglet Influencing the Wake of a Large Transport Aircraft*. 25th International Congress of the Aeronautical Sciences ICAS2006, Hamburg, 3-8 September 2006.

[4] J. D. ANDERSON - *Fundamentals of Aerodynamics*. Mac Graw Hill, 2001.

[5] S. BARBARINO, O. BILGEN, R. M. AJAJ, M. I. FRISWELL, D. INMAN - *A Review of Morphing Aircraft*. J. Intel. Mat. Syst. Str. 22, 823-877, 2011.

[6] W. BRIX - *Subsonic Aircraft with Backswept Wings and Movable Wing Tip Winglets*. US patent no. US 6,345,790 B1, 12 February 2002.

[7] L. CAMBIER, S. HEIB, S. PLOT - *The ONERA elsA CFD Software: Input from Research and Feedback from Industry*. Mechanics & Industry 14(3) pp 159-174, doi: 10.1051/meca/2013056, 2013.

[8] I. CHOPRA - *Review of Sate of Art of Smart Structures and Integrated Systems*. AIAA Journal 40(11) 2145-2187, 2002.

[9] A. CONCILIO, I. DIMINO, L. LECCE, R. PECORA - *Morphing Wing Technologies Large Commercial Aircraft and Civil Helicopters*. 1st Edition, Elsevier, 19 October 2017.

[10] J. E. COOPER, I. CHEKKAL, R. C. M. CHEUNG, C. WALES, N. J. ALLEN, S. LAWSON, A. J. PEACE, R. COOK, P. STANDEN, S. D. HANCOCK, G. M. CAROSSA - *Design of a Morphing Wingtip*. AIAA Journal of Aircraft, Vol. 52 No 5, September 2015.

[11] DIAKONT - *Actionneurs electro-mécaniques (EMA) Séries DA*. SNT catalog.

[12] I. DIMINO, G. AMENDOLA, B. DI GIAMPAOLO, G. IANNACCONE, A. LERRO - *Preliminary Design of an Actuation System for a Morphing Winglet*. 8th International Conference on Mechanical and Aerospace Engineering (ICMAE), Prague, 2017.

[13] M. DRELA, H. YOUNGREN - *AVL*. http://web.mit.edu/drela/Public/web/avl/.

[14] M. GAZAIX, A. JOLLES, M. LAZAREFF - *The elsA Object-Oriented Computational Tool for Industrial Applications.* 23rd Congress of ICAS Toronto Canada, 8-13 September 2002.

[15] P. GIRODROUX-LAVIGNE - *Progress in Steady/Unsteady Fluid-Structure Coupling with Navier-Stokes Equations*. International Forum on Aeroelasticity and Structural Dynamics, Munich Germany, 28 June – 1 July 2005.

[16] P. GIRODROUX-LAVIGNE - *Recent Navier-Stokes Aeroelastic Simulations using the elsA Code for Aircraft Applications.* International Forum on Aeroelasticity and Structural Dynamics, Stockholm Sweden, 18-20 June 2007.

[17] C. HEINEN, A. WILDSCHEK, M. HERRING - *Design of a Winglet Control Device for Active Load Alleviation*. International Forum on Aeroelasticity and Structural Dynamics (IFASD), Bristol UK, 2013.

[18] S. J. MILLER - *Adaptive Wing Structures for Aeroelastic Drag Reduction and Loads Alleviation*. University of Manchester, PhD thesis, September 2010.

[19] R. PECORA, F. AMOROSO, G. AMENDOLA, A. CONCILIO - *Validation of a Smart Structural Concept for Wing-Flap Camber Morphing*. Smart Structures and Systems, Vol. 14 Issue 4, pp. 659-678, 2014.

[20] F. PETER, E. STUMPF, G. CAROSSA - *Morphing Value Assessment on Overall Aircraft Level (Chapter XI)*. Wolcken PC, Papadopoulos M (eds) Smart Intelligent Aircraft Structures (SARISTU) (Proceedings of the final project conference), Berlin, Heidelberg: Springer-Verlag, pp. 859-872, 2015.

[21] A. V. POPOV, T. L. GRIGORIE, R. M. BOTEZ, Y. MERBAKI - *Real Time Morphing Wing Optimization Validation Using Wind-tunnel Tests*. Journal of Aircraft 47(4), July 2010.

[22] K. L. ROGER - *Airplane Math Modeling Methods for Active Control Design.* CCP-228, AGARD, August 1977.

[23] M. M. K. V. SANKRITHI, J. B. FROMMER - *Controllable winglets*. US patent no US 2008/0308683 A1, 18th December 2008.

[24] S. H. TIFFANY, W. M. ADAMS Jr - *Nonlinear Programming Extensions to Rational Function Approximation Methods for Unsteady Aerodynamic Forces*. NASA-TP-2776, July 1988

[25] T. A. WEISSHAAR - *Morphing Aircraft Technology - New Shapes for Aircraft Design*. NATO meeting proceedings RTO-MP-AVT-141, 2006.

[26] A. WILDSCHEK, R. MAIER - *Winglet with Autonomously Actuated Tab*. Patent no EP 2233395 A1, 29 September 2010

[27] A. WILDSCHEK, S. STORM, M. HERRING, D. DREZGA, V. KORIAN, O. ROOCK - *Design, Optimization, Testing, Verification, and Validation of the Wingtip Active Trailing Edge.* "Smart Intelligent Structures (SARISTU)", pp. 219-255, Springer 2016.

[28] A. WILDSCHEK, S. STORM, J. KIRN - *Wingtip Active Trailing Edge for Loads Alleviation*. ECOMAS Congress 2016.

[29] R. T. WHITECOMB - *A design Approach and Selected Wind-tunnel Results at High subsonic Speeds for Wing-Tip Mounted Winglets*. NASA TN D-8260 July 1976.

[30] P. C. WOLCKEN, M. PAPADOPOULOS Editors - *Smart Intelligent Aircraft Structures (SARISTU) Proceedings of the Final Project Conference*. Springer.

AUTHORS

Cédric Liauzun graduated from the *Ecole Nationale Supérieure de Mécanique et d'Aérotechniques* (ENSMA) in 1996, and has about 20 years of experience as a member of the Numerical Aeroelasticity team at ONERA, where his activity is mainly devoted to the development of numerical simulation methods for aeroelasticity and fluid-structure coupling.

Dominique Le Bihan has been a Research and Test Engineer for the Aeroelasticity and Structural Dynamic Department, at ONERA, in Châtillon, France, since 1980. He was involved in technical support for wind tunnel test facilities and, a few years later, became active in linear control law design, mainly applied to the reduction of internal vibration and acoustics in aircraft and helicopters. He is currently involved in flutter and dynamic response reduction, and load alleviation on wind-tunnel mock-up and aircraft models. His current research interests include the dynamics of structures (modeling and identification), and fluid-structure coupling by mean of an aeroelastic state-space model and numerical aerodynamic tools.

Jean-Michel David graduated from the "*Ecole Nationale Supérieure de Mécanique de Nantes*" in 1981. He received a PhD in Acoustics from the "*Ecole Doctorale de Lyon*" in 2005. He worked for a long time as a research engineer in Acoustic Discretion and Vibroacoustics for ONERA's Structural Department in Chatillon, since 2009. He is now involved in aircraft and turbomachinery numerical aeroelasticity in the Aerodynamics, Aeroelasticity and Acoustics Department (DAAA), where his knowledge and experience in Structural Dynamics are strongly appreciated.

Didier Joly has been a Research and Test Engineer for the Material and Structural Department, ONERA-Lille, since 1981. He has worked on helicopter blade design for 20 years. His activity is now devoted to the study, design, and technological development of new blade and aircraft structure concepts.

Bernard Paluch graduated from engineering school in 1983, and has about 30 years of experience at ONERA in various fields, such as composite materials, numerical simulations and aircraft structural design. His main activity is now devoted to structural concept evaluation in association with Multi-Disciplinary Analysis and Optimization tools developed at ONERA for Hybrid Propulsion Aircraft, Blended Wing Body, and reusable space launchers.

E. Deletombe, D. Delsart
(ONERA)

E-mail: eric.deletombe@onera.fr

DOI: 10.12762/2018.AL14-11

Highly-Nonlinear and Transient Structural Dynamics: a Review about Crashworthiness of Composite Aeronautical Structures

This paper is a bibliographic review dealing with composite aircraft and rotorcraft crashworthiness. The paper focuses on structural aspects of large composite aircraft or rotorcraft parts (fuselage parts, barrels or larger parts). Material topics, such as the experimental characterization and numerical modelling of the dynamic behavior of composite materials, of composite joints (details) and of energy-absorbing components (elementary parts) are mentioned but not discussed in detail. More information about this topic can be found, for instance, in another bibliographic review. The first section of the paper deals with work performed in various labs since the early '90s. The second section describes the global strategy of the French Aerospace Lab in the matter of studying composite aircraft or rotorcraft crashworthiness over the same period, following a quite different strategy. Lessons learnt from all of these works are discussed in detail, which can be derived into best practices for young engineers or researchers working in this field. Indeed, the complexity of the composite materials, and hence the structure behavior under crash conditions, is so great (due to potentially very versatile rupture behaviors) that great care must be taken when studying their crash response. As a conclusion of the review paper, the need for a numerical/experimental building-block approach up to the barrel level is clearly evidenced, which should not be done without well-assessed V&V (verify and validate) strategies for the virtual part of the process.

Introduction

Aviation is one of the safest public transport modes today. To reach such performance, aircraft safety mainly relies on experience feedback and on a set of constantly evolving rules that concern the flying products and operations. In the course of events that punctuate the aeronautics history, aircraft certification rules progressively improved. This is especially the case in the field of crash and survivability, which is identified as a specific topic, for instance, in the CS25 (large civil aircraft) document, and where highly-nonlinear and transient structural dynamics is concerned.

An advisory international group – which Airbus Aircraft was involved in – was set up in the USA in the early 2010s by the FAA, to address the question and identify beneficial research activities in the field of civil aircraft crashworthiness. Among the initial objectives of this advisory group, one could find: (1) the evaluation of the interest and feasibility of future regulation evolutions, (2) the standardization/harmonization of (absolute) crash performance criteria for whole aircraft or parts of it, some of them being still quite de-correlated from the others, (3) the validation and standardization of the building-block approach used for the aircraft static design demonstration, as an acceptable way forward to deal with crash certification, and (4) the consideration of more representative crash scenarios, in particular, at the full-scale level.

In parallel, some European aircraft manufacturers also proposed to the French CORAC organization (Council for Civil Aviation Research) to unite efforts in order to also better cover possible future regulation evolutions in the domain of crash safety. A transverse "Crash and Survivability" theme was introduced in 2013 within the CORAC overall roadmap. Once completed, the results of the discussions were presented to the French DGAC (French General Civil Aviation Directorate), which defined clear objectives for such research: (1) to analyze the full-aircraft numerical simulation to better cover the crash domain (to avoid a costly experimental approach), and (2) to develop

and standardize advanced experimental means of characterization for nonlinear material models from quasi-static to dynamic loadings, to optimize and reduce the number, types, and costs of required tests. Considering these objectives, several themes of transversal interest for the various European aircraft and rotorcraft manufacturers have been identified, which have an upstream, general and prospective character. The French DGAC then contracted the French Aerospace Lab (ONERA) to conduct some of these research studies for the benefit of the aeronautic community as a whole, meaning to increase its capability to better understand, analyze and improve the aircraft behavior in the event of crash situations (which is the purpose of this review paper).

The four-year PHYSAFE 2015-2019 research project funded by the French DGAC is straight online with the transverse CORAC "Crash and Survivability" roadmap. It is aimed, on the one hand, at experimentally studying and characterizing various phenomena that may have a noticeable influence on aircraft passenger safety in the event of a crash. On the other hand, it is aimed at developing the numerical finite-element code capabilities to predict the crash response of composite aircraft structures and their consequences in terms of passenger survivability. The corresponding research activities are being conducted by ONERA according to the following general line of research: (1) the development of test means and facilities to characterize the dynamic behavior, rupture and abrasion of composite aircraft primary structure materials, (2) the study and development of dynamic behavior and rupture models for organic matrix composite materials and crashworthiness numerical analysis.

This paper is a bibliographic review dealing with composite aircraft and rotorcraft crashworthiness. Its main objective is to contribute to the definition and dissemination of best practices in designing such aircraft. It complements a previous bibliographic report and paper [31] limited to work on metallic aircraft crashworthiness [1][31]. Since general questions, besides the nature of the materials used to design the aircraft, were already discussed in more or less detail in these previous report and paper (standards, test means, seats and dummies, numerical methods, etc.), this paper only focuses on the structural aspects and composite structures. It also only focuses on large composite aircraft or rotorcraft structures (fuselage parts, barrels or larger parts): specific topics, such as the experimental characterization and numerical modelling of the dynamic behavior of composite materials, composite joints (details) and energy-absorbing components (elementary parts), can be found elsewhere, e.g., [2][3][4][33][34]. A review of the work performed in other labs is presented and analyzed in the second part of this paper. In the third section, the expertise of the ONERA Design and Dynamic Resistance research unit is summarized to shed light on the global strategy of the French Aerospace Lab in the matter of studying composite aircraft or rotorcraft crashworthiness.

Literature Review on Composite Aircraft and Rotorcraft Crashworthiness

Compared to the crashworthiness of metallic airframes [1][31], research work on composite structures appeared later in the open literature, in the '90s. Concerning the experimental works, the same crash test facilities and philosophies as those previously used for the metallic airframes were naturally used, without any real modification of the test facilities being necessary. Although the FE explicit codes were really starting to spread, hybrid tools were already well developed and used – combined with a component-based testing approach – to study the crashworthiness of full-scale aircraft or rotorcraft structures, and all the more preferred for composite structure analysis, since the complexity of composite material behaviors and their potentially associated FE computing costs were high compared to those of metals. A first set of reviewed papers gathers those that dealt with such hybrid models for composite structures, one way or another. Hybrid models (based on component test results) were first used by Jackson *et al.* [5] to study the crash behavior of a general aviation composite aircraft section (Lear Fan). A first simplified structural model (added masses set on seat rails instead of seats and passengers) was developed (no laminate description or material data available in the paper) for the initial aircraft design: a quasi-static crush test was used to determine the ground and underfloor spring characteristics to be used in the hybrid model, and the composite material rupture criterion was calibrated according to the crash test result. A retrofitted design was then studied (this time with seats and dummies) with the initial underfloor structure being replaced by composite energy-absorbing beams (Kevlar and foam-based sandwiches). Again, a post-test hybrid model was developed with (1) the composite frame stiffness being first calibrated using a preliminary quasi-static linear elastic analysis, and (2) the non-linear hybrid spring characteristics, being characterized through a quasi-static crush test of the underfloor structure. The same composite material rupture criterion as that used for the first version of the model was used, making it possible to obtain the rupture of the composite frames as in the test (the underfloor energy-absorbing structure remained undamaged during the crash test). A third model was then proposed (without any test being done) to evaluate a new design concept for the fuselage section, where the composite frame integrity was ensured *a priori* by design. Here, the underfloor energy-absorbing composite sandwich structure virtually turned to crush properly, which increased the crash performance of the structure compared to the two previous cases. One of the first reported purely FE crash simulations of a composite aircraft structure was performed by Vincente *et al.* [6]. It was limited to a coarse FE model of a composite commuter sub-floor structure, which was later compared to the full-scale crash test result performed within the framework of the EU project CRASURV [7]. To limit the computing costs for the full structure, the authors' choice was to use simple shell elements and calibrated nonlinear isotropic material models based on FE simulations of tests performed on simple parts and components, in a way very similar to that of the previous hybrid approach. The material models needed to be seriously calibrated again once the full-scale test results were known, to reach a good correlation level. In the same period, a MSC-DYTRAN FE model of a Sikorsky composite helicopter underfloor structure was developed by Lyle *et al.* [8], starting from an existing NASTRAN model (initially developed for structural dynamic analysis). The size of the crash FE model was constrained by the CPU costs, which were targeted to be less than 1 day: important assumptions and simplifications in the FE description of the complex underfloor keel beams (geometry, materials, etc.) then needed to be done. With the idea of combining hybrid and FE methods, the crash-model loading conditions were deduced from both the full scale Sikorsky crash test result and the associated KRASH [32] hybrid model of the helicopter. The crash simulation was simplified, using a falling mass (representing the remaining helicopter mass, except for the subfloor) onto the subfloor FE model, with a kinetic energy (and hence velocity) estimated from the crash test and KRASH numerical results. Since no dynamic crash data were locally recorded during the test relative to this subfloor structure, only a post-mortem analysis (maximum crush displacement) was proposed for comparison and discussion of the MSC-DYTRAN dynamic numerical results.

The lessons learnt from this first set of papers are as follows: Jackson *et al.* proved in [5] that hybrid models can be efficient, but need many test results at the component level – as for metallic airframes – to be used properly. If the materials used are not dependent on the strain rate (e.g., aluminum and quasi-isotropic carbon fiber laminates) quasi-static tests are enough to build the hybrid model of the airframe. However, composite energy-absorbing underfloor structures cannot be properly designed if the load introduction scenario is misunderstood, with the risk of the driving energy-absorbing mechanisms not developing/ triggering as wanted. The use of rigid added masses instead of deformable (with complex kinematics) seats and passenger/dummy systems to design the underfloor structure was proven to lead to the overestimation of local input inertial loads, which can then lead to unwanted experimental ruin modes. By using the FE method in the same way as the hybrid one (model development based on sub-component testing), the results in [6] also prove that the building-block approach cannot be applied with confidence whatever the numerical tool when excessively simple models are used for composite structures and highly-nonlinear crash behaviors. Lyle *et al.* list several difficulties concerning the FE model development and study of the crash behavior of composite aircraft (helicopters) in [8]. First, only partial information and a partial description can be derived straightforwardly from standard structural dynamics FE models (e.g., NASTRAN) into crash FE models, and a significant effort is then needed to achieve a satisfying FE crash model. Starting from a CAD (geometry) model would have lessened the effort, using, for instance, the NASTRAN data cards just to obtain some of the composite laminates and material parameters. Second, a full-structure physical crash test alone with KRASH numerical analysis appear to be of limited interest to validate the FE crash models and explicit codes (applied here to the subfloor structure only). Since component tests have been performed to develop the KRASH model crush springs, some of these tests (even the static ones) could have been used (with great care, see the previous paragraph) in a Building-Block-like Approach, to progressively assess the subfloor FE crash model and then increase confidence in the FE dynamic numerical result analysis. The inverse path, starting from the top of the pyramid of experiments to assess numerical tools for intermediate level structural components, clearly seems not to be the appropriate way to proceed.

Among a second set of papers dealing with crashworthiness and FE methods, Fasanella *et al.* presented a full-scale crash test and post-test numerical simulation of a composite helicopter with its landing gears [9]. A coarse FE model and a simple composite material model were used. The results of the test and numerical simulation were analyzed and quantitatively compared up to 150 ms, in terms of filtered accelerations at several locations. The experimental local accelerations had, somehow, quite different shapes, here and there, whereas the numerical ones had more similar (harmonic) shapes, but the acceleration orders of magnitude were correctly predicted. The tail break (observed in the physical test) seemed not to be predicted well, but the acceleration response was anyway mainly driven by the dynamic response of the landing gears, which was almost properly modelled. Fasanella *et al.* retried the same work in [10], meaning that the post-test simulation of the Sikorsky ACAP helicopter full-scale crash test, with the main effort of the work being this time dedicated to propose an engineering methodology that would permit the full crash test event to be computed more efficiently (CPU costs). Besides the fact that a still quite coarse mesh (7,350 finite elements, developed from a NASTRAN model (thus needing to track and remesh areas with very small FE elements) was used to model the helicopter airframe, a simplified landing gear modelling methodology was proposed. To save more CPU time, the simulation was split into two phases: in the first step (45 ms, during which the rear landing gears only interact with the ground) the helicopter FE model was forced to behave rigidly, and final positions and initial velocities of all of its nodes were recorded. These data were then used in the second step as initial input data to start a flexible-model crash simulation (with gravity being taken into account), to be able to capture the tail break (as known from the test), to simulate the contact (no friction was modelled) of the main helicopter body with the ground and the final deformation of the subfloor structure. As previously mentioned, in terms of crash analysis, no dynamic data were experimentally available/recorded to compare with local subfloor dynamic numerical responses: the test and simulation were again globally compared through post-mortem observations, to major event chronology recorded by videos, and dynamic data from accelerometers (60 Hz filtered) located at some floor, engine, gear and bulkhead locations. Following this work, due to the cost of full-scale structure crash tests, and considering the previously described limitations in numerical simulations, Jackson *et al.* proposed a crashworthy composite fuselage design strategy in [11] based on a concept definition step (starting from engineering and analytical considerations), followed by a 1/5th scale model manufacturing and testing step to select best EA concepts. The performance of the final selected concept was then extrapolated to the full scale using scaling rules and simple empiric static material laws. The scale-model test results were also used to assess numerical FE (MSC-DYTRAN) tool capabilities (post-test). The full-scale manufacturing and crash testing of the selected concept was performed in following works [12], where Jackson *et al.* studied the improved full-scale composite general aviation fuselage section concept (selected among 5 possibilities), both experimentally (2 drop tests) and numerically (using MSC-DYTRAN). The fuselage concept was based on a protective composite sandwich shell (cabin), together with an energy-absorbing subfloor structure partly made of Rohacell foam blocks. A coarse FE crash model (18,250 shell elements) was developed with different nonlinear material behavior laws (with rupture criteria) being used for the E-glass composite material and Rohacell foam. Carbon fiber composite laminates and sandwich foam cores for the protective fuselage shell were modelled as linear elastic. All of the different parts were modelled as perfectly bonded (no possible debonding). Gravity was not taken into account in the simulation, with just the initial velocity (kinetic energy) being applied. The same cabin fuselage shell was used for two drop tests (0° and 15° roll angles), with only the subfloor part, including the Rohacell foam, being replaced after the first test (0°). The results of this 1st test (both experimental and numerical) were quite satisfying and comparable. The structure behaved as predicted, except that the experienced G-levels were higher than expected from the 1/5th scale study, and all the more for the FE model, which seemed to be stiffer than the physical structure (a small debonding developed within the cabin sandwich shell during the test, which could not be simulated). This damage was not repaired before the second test (15°), during which major ruptures occurred in the cabin shell. The large difference between this second test and its FE simulation was then explained not to be due to the change in test conditions (15°), but rather to the initial damage after the 1st physical test, which was missing in the virtual test. In the continuity of these works, Fasanella *et al.* studied the numerical simulation (30,000-finite-element model) and comparison with the test of a new crashworthy fuselage demonstrator, including composite parts and Rohacell foam in its underfloor structure for business jet or helicopter airframes (#2 m fuselage

diameter) [13]. The crash test was performed on a rigid surface, and the attention was paid to the comparison with the simulation in terms of several filtered acceleration measurements at rail positions, and several dummy pelvis acceleration and lumbar load measurements. The main energy-absorbing concepts introduced in the tested fuselage section were Rohacell foam blocks in the subfloor part, and energy-absorbing seats in the cabin. The other parts of the structure (stiff fuselage section and floor) were made of a sandwich material (no frames or beams) with glass-epoxy face sheets and Rohacell core, which was expected to keep safe (almost no energy absorbed there). Thus, the sandwich material was modelled using shell elements for the composite sheets (simple bi-linear elastic-plastic behavior), and brick elements for the Rohacell core (linear elastic behavior). The order of magnitude of the predicted acceleration levels was quite good, with noticeable differences being nevertheless pointed out. No detailed analysis of the damage and rupture of the composite skins (2nd order influence on accelerations compared to the Rohacell blocks and energy-absorbing seats) was given in the paper. The same composite structure was used again by Fasanella *et al.* (several demonstrators were manufactured) to compare test (and numerical) results for vertical impacts on rigid surface, soft soil (sand) and water [14]. The composite material in the 30,000-FE simulations was still simply modelled using a linear orthotropic elastic material law, and laminated shell elements were used, because of the first-order influence of Rohacell material on the nonlinear response of the very specific tested structure (as proven in the previous works). Filtered acceleration results were compared between tests and simulations with a quite good agreement.

In this second set of papers, as shown by Fasanella *et al.* in [9] [10], coarse FE models can be used to predict the crash response of full structures, even composite ones, if the driving phenomena are global ones (e.g., the landing gear response) and not local ones (sub-component ruptures). Due to the coarse model used to describe the subfloor structure, and due to missing dynamic local information (only few post-mortem comparisons are given) it is difficult in these papers to conclude whether deviations compared to the test results stem from modelling approximations/inaccuracies or from other FE model limitations. Following the same general idea, the deterministic design (stiff and strong frame/fuselage/cabin design, no windows, etc.) with no joints, etc., proposed by Jackson *et al.* in [11] prevents complex damage/failure modes to develop during tests: simple elastic static composite material models are then enough to properly catch the fuselage response using FE models. Thanks to such a well-controlled scenario, an energy-absorbing concept can be selected among others (using 1/5th scale models), with a FE model comparison with the test being done, which only requires a sufficiently accurate absorber model to be used in the FE structure model to achieve a very satisfying comparison with the experiment (e.g., accelerations at floor level, in several locations). Considering the study of the full scale demonstrator of the selected 1/5th concept [12], the interesting results come from the first test/simulation comparison. First, the scaling exercise (from 1/5th to 1/1th) seems pretty successful, except for the added lead mass (which has been overestimated and turned out to be the reason for the G-levels that were 20 percent higher than expected). These higher G-levels can be the reason for the unexpected damage to the cabin shell structure during the first test (which then deviated from the initial deterministic design scenario and had a dramatic consequence for the second test). Pre-test simulations would probably have helped to detect and to correct this deviation. Whatever the case, the post-test simulations show that the local damage and ruin phenomena cannot be captured (very few comments about this) because of the use of excessively simple nonlinear material models and rupture criteria and – above all – the perfect bonding model without rupture set between the various parts of the structure. Note that it was reported that, although gravity is not taken into account, the simulation results can miss the contribution of potential energy (which may be non-negligible even for the crash response of a lightweight structure). The second design described by Fasanella *et al.* in [13] is again made in order for no composite failure to occur along the stiff composite cabin fuselage and floor. With such a deterministic design, as long as the crushing behavior of the underfloor Rohacell foam blocks and energy-absorbing seats are properly modelled, the main collapsing phenomena can be captured and the accelerations and dummy loads well predicted, even with a quite coarse FE model (30,000 elements). Last, for the different studied cases presented by the major contributors to this field in [14], impacts on rigid surfaces are shown to be the most severe ones (higher acceleration levels), but this conclusion could possibly be contradicted if horizontal velocities are considered, with plowing forces (soft soil or water) probably changing the crash scenario and results. In order to achieve a good agreement with the tests, the sand and foam materials must be accurately modelled, especially their rate-dependent behavior (foam), their zero Poisson ratio (sand), and their unloading dissipative "crushable" behavior (nonlinear hysteresis), if one wishes to avoid any non-physical rebound in the simulation. Last but not least, the use of quite coarse FE models – once validated with some full-scale crash tests – proves in the end to be acceptable for numerical parametric crash justifications (in the sense that hybrid models were).

Then, very few works were reported in the literature after these works by Fasanella, Jackson, and Lyle *et al.* until recent years. In 2012, Zou *et al.* published a purely numerical study of the crash performance of a hybrid metallic/composite fuselage section [15]. The only composite part of the virtual fuselage section was its skin (given thickness); all of the other parts were made of aluminum. The parametric study focused on the influence of the metallic strut angle and section on the crash performance of the fuselage section, according to an academic vertical crash condition. The behavior of the composite material was modelled as orthotropic elastic brittle (multi-layered shell elements) behavior with no possible energy absorption (in the skin). No test result was available/presented to be compared with the numerical simulations in this paper. In 2013 (about 10 years after Fasanella's last paper), Heimbs *et al.* presented this time a building-block-type exercise, including the comparison of dynamic test results and numerical simulations of composite parts of different increasing complexity: from simple plates and riveted T-joints up to complete frames [16]. Although the numerical simulations fitted well for simple plates, noticeable differences appeared when more complex structural tests were studied. The differences were claimed to be due to complexities that could still not be properly tackled by numerical FE methods: boundary conditions, load-introduction issues, etc. Note that the paper did not comment about the possible nonlinearity or strain rate sensitivity of the composite materials, since very simple (elastic brittle) material models were used (quasi-isotropic laminates). The numerical tool was then used to compute the macroscopic behavior (super-element) of some details that could not be accurately represented in a full 2-frame composite barrel structure, which was then crash-simulated. The lack of experimental results at the barrel scale prevented any estimation of the error propagation in the FE model (from coupons to full scale) to be made. The last of the series of papers reviewed here, a CFRP composite (sandwich design) fuselage response was investigated by

Sturm *et al.*, with respect to crashworthiness [17]: the development of a "plastic" hinge in the airframe has been identified for a long time as a key and favorable mechanism in the crash response of metallic commercial airframes. The purpose was, here again, to study composite integral (sandwich) fuselage concepts (no frame) that could develop such hinges at pre-determined locations, in order to ensure a satisfying crash scenario (proper load introduction in struts and energy-absorbing components). The studied concept was based on a honeycomb core trigger to pre-determine hinge locations. Experimental and numerical works were done separately: a FE numerical model at the fuselage level was used to identify the load (compression and bending) conditions to be supported by a fuselage panel under crash situations. These loads were used to design the experiment at the sandwich panel level. The numerical tool was also used to perform a parametric sensitivity study about the core trigger concept efficiency, with only the honeycomb core being modelled (not the CFRP skins). Then, different sandwich solutions were fabricated and tested. No comparisons were made in the end in this paper between sandwich panel test results and simulations.

Among this last set of more recent works, Zou *et al.* [15] has shown that the composite part (only the skin in this paper) has very little influence on the crash scenario of the hybrid metallic/composite fuselage design that is numerically studied (the crash performance is controlled by the metallic parts, including the struts). In reality, true manufacturing would rely on setting up many riveted fasteners (which are not modelled in this virtual test): the EU TIM-CRASH project results in 1995 [18] suggested that devil key rupture mechanisms might be in such structural details in terms of crash behavior even of metallic structures. All the more as like recently shown by Heimbs *et al.* [16], despite many improvements in the FE explicit codes in terms of computing costs and modelling accuracy (finite elements, material models, etc.) the building-block approach for composite structures is still not straightforward when the crash simulation of composite airframe structures (prediction or simply justification) is concerned: numerical models still have to be assessed/calibrated by tests at every level of the design pyramid. Last, Sturm *et al.* once more remind the composite structure designers that the crash response of a full airframe needs to be studied experimentally in the end, since unpredicted rupture in the fuselage frame, for instance, would clearly endanger survivability [17]. In that sense, these works are complementary to those of Fasanella *et al.*

ONERA Background in Crashworthiness of Composite Aeronautical Structures

Composite rotorcraft crashworthiness is a particularly important topic at ONERA, insofar as military helicopter structures must fulfill crash specifications: indeed, Airbus Helicopters chose many years ago to develop a full composite combat helicopter because of the weight benefits and marine environment specificities. In [19][20], research works aimed at improving the crash resistance of the Tiger helicopter (thanks to the use of composite underfloor energy-absorbing sinewave beams) are presented, with the ONERA CRD Research Unit being involved in the '90s in the development and validation of a FE model (Radioss) of the central composite section of the helicopter, including the main rotor mass, the weapon supporting wings, the fuel tanks and the under-floor energy-absorbing components. The overall objective of the research was, in fact, to assess modeling methodologies for the prediction of composite helicopter crashworthiness and to demonstrate the feasibility of calculations for full-scale structures. Compared to other research teams and at that time, ONERA took the gamble and made the choice to develop very detailed FE crash models from the very beginning of its involvement in this field (no hybrid methods/models). For the Tiger case, the works led to the definition of a FE model that was finally made up of 180,000 shell elements (see Figure 1) and 60,000 volume elements (mainly for the fuel), which means ten times more than the models used by Fasanella *et al.* In order to evaluate the prediction capability of such a model, experimental data obtained from a crash test conducted on the considered section in 1998 at the CEAT (French crash test center, now DGA TA) were available for comparison with the numerical results. Various kinds of data were recorded at various points of the structure, including acceleration measurements on the main additional masses (rotor, wing weapons, etc.), gauges on structural panels, and pressure measurements in fuel tanks.

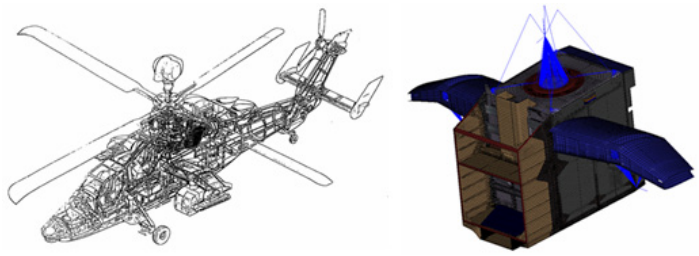

Figure 1 – Broken view (left) and FE model (right) of the Tiger central composite structure

Besides the intrinsic difficulty of modeling composite structures, the major issue in simulating such a complex event was, in the fact, that the structural ruin mechanisms are strongly interdependent. These mechanisms essentially concern the in or out-of-plane loading of unsymmetrical sandwich panels, the resistance of riveted or bounded assemblies, the crushing of energy-absorbing components and finally, the response of the fuel tanks (the structure included 2 flexible fuel tanks partly filled by more than 1 ton of fuel, representing three quarters of their total capacity). The latter point appeared to be one of the most influential phenomena in the ruin scenario, since the expansion and increase of pressure in the tanks directly control the out-of-plane loading of the structural panels and the vertical loading of the composite underfloor beams. Two methods were mainly investigated in order to evaluate which would be the most appropriate to correctly model the pressure load transfer to the panels and under-floor beams: several methods were analyzed (which is not the purpose of this paper) with some of them yielding satisfactory results in terms of robustness, CPU costs and correlation with experimental results. This point being solved, a very fine mesh size (4x4mm multi-layered shell elements) and a new composite material law developed and validated in the Radioss code were used to model the composite energy-absorbing components. The material model – describing the composite material at the ply level – is orthotropic with a rate dependent yield stress and nonlinear behavior, and proposes a set of rupture criteria to describe the different material failure modes (tension, compression, maximum dissipated energy, etc.). Using these advanced functionalities and after a calibration step based on subcomponents test comparisons, the simulated energy-absorbing underfloor structure turned out to correctly approach the global deformation of the physical under-floor system during the test, with a progressive crushing of the trapezoidal and sine-wave

beams obtained (see Figure 2). Finally, the calculations conducted at a full-scale level (including fuel tanks) achieve a satisfactory level of prediction with an acceptable computational cost.

The next steps in the 2000s focused on the dynamic characterization and modelling of composite riveted joints, since in the previously described FE simulations, kinematic relations (tied interfaces) were mostly used to model the assembly of the various parts of the fuselage structure. Other works done by ONERA in the field of helicopter crashworthiness have dealt with ditching situations: the most recent numerical formulations proposed to deal with fluid/structure interactions were, here again, analyzed to establish the current numerical capabilities of explicit commercial codes (e.g., Radioss). For instance, a Euler/Lagrange coupling interface implemented in the Radioss code was evaluated to cope with the modelling of fluid/structure interactions [21] (see Figure 3).

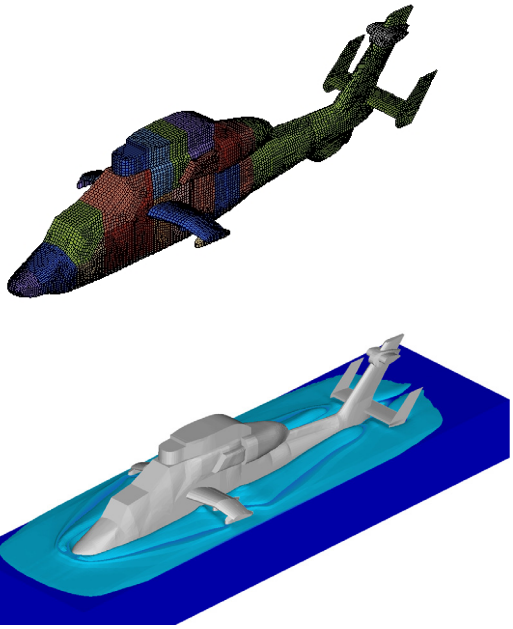

Figure 3 – FE model of a full-scale rigid helicopter model (up) and ditching simulation (vertical and horizontal speed) using Radioss CEL formulation – final stage: 300ms (bottom)

From the works presented in [19][20] it was proven that the explicit FE codes could be used to study crashworthiness for very complex composite structures (C3-C4 composite helicopter structure). However, a lot of preliminary works were necessary before such a satisfying result (French reports) could be achieved. These preliminary works started in 1993 with the numerical simulation of the crash behavior of underfloor composite beams using state-of-the-art

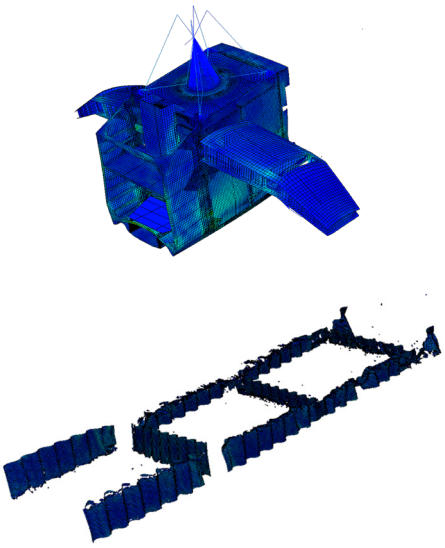

Figure 2 – Global response of the composite airframe (up) and final crushing state of composite underfloor beams (bottom)

models and FE tools and continued till 1998 with the dynamic characterization of composite materials and the development and identification of enhanced composite material laws for brick and shell [7] elements. The final successful exercise constituted the required demonstration before the industry partner started to develop its skills and to use this kind of FE explicit tool for composite helicopter crashworthiness analysis.

In the field of composite commercial aircraft, the objectives of the EU CRASURV project (1997-2000) [7] were to develop the technology for the design of composite airframes (commuter and large transport aircraft) with maximum safety with respect to potentially survivable crash scenarios. ONERA first contributed to the dynamic characterization of composite materials, and the development and identification of a dynamic material law for composite multi-layered shell elements [22]. The new material law implemented in the Radioss explicit FE commercial code was verified, and applied to the post-test simulation of a sub-cargo floor composite structure (half-moon), which was previously drop-tested at the French DGA-TA test center (see Figure 4) [23][24]. Note that separate reports are dedicated in the PHYSAFE project to the various topics of the dynamic bulk behavior characterization and modelling of Organic Matrix Composite (OMC) materials [2][4].

ONERA also used its test facilities (crash tower, hydraulic jack) [1] [31] in the EU CRASURV project for the crash-testing of sub-cargo floor energy-absorbing components [22] and the dynamic testing of composite riveted joint specimens manufactured by other partners. A summary of the ONERA CRASURV works is presented in [25].

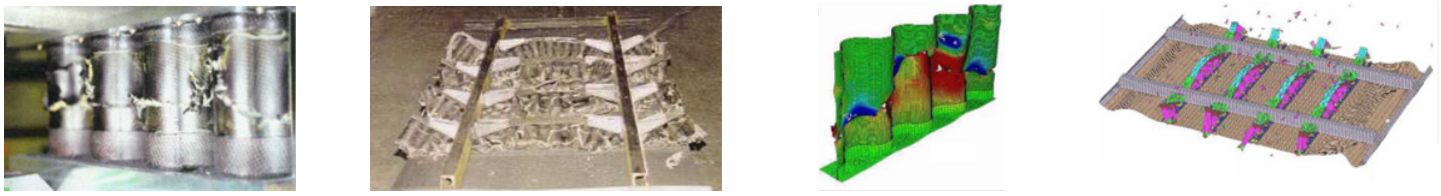

Figure 4 – Various crash tests of composite components and corresponding FE simulations (EU CRASURV)

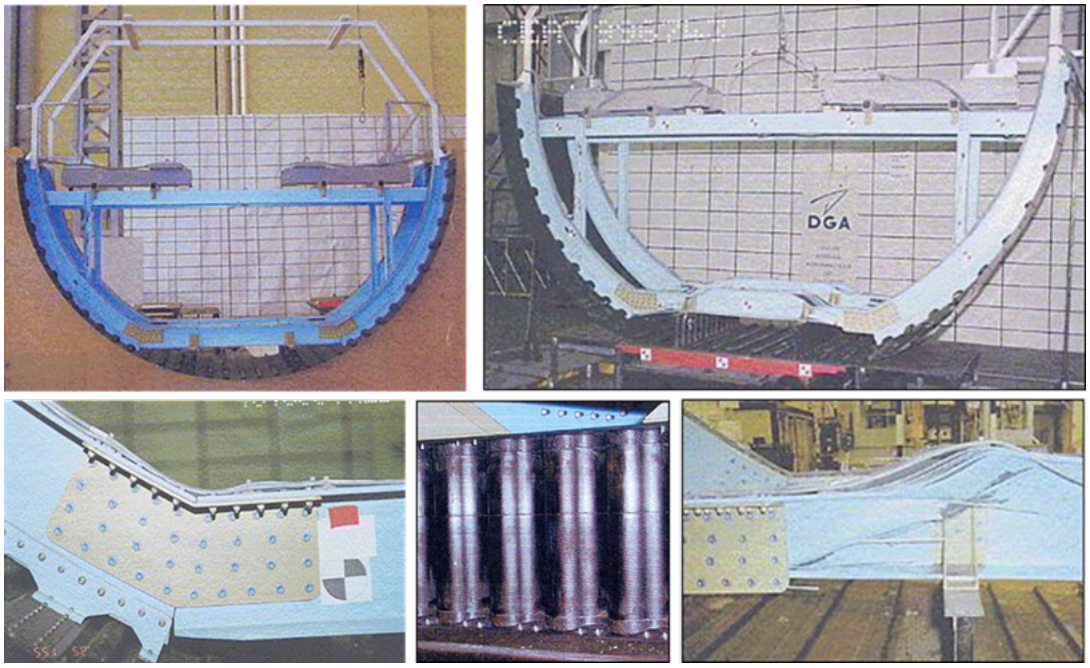

Figure 5 – EU CRASURV composite A/C half-fuselage demonstrator before and after the crash test (DGA TA test center)

Despite the experimental-numerical Building-Block Approach, which was implemented up to the half-moon component level and followed by a crashworthy pre-test numerical simulation of the designed composite half-fuselage structure, the physical test of the composite half-fuselage demonstrator did not quite go as expected, with the cargo-floor beams breaking before the sinewave energy-absorbing beams started to crush and then failed to absorb any energy. The passenger composite floor beams remained safe, but the measured "passenger" acceleration levels exceeded 50 Gs (unsurvivable conditions). The explanation proposed for this unpredicted behavior was the embrittlement of the 2-part cargo floor beam junction in the metallic riveted fastener area (see Figure 5), where the rupture initiated (these fasteners were not taken into account in the numerical simulation of the final proposed composite half-barrel design). In the end, the test results revealed that the composite frames and main floor beams should have been reinforced (safety coefficient taken compared to the numerical design, which would have meant an extra mass penalty), in order to ensure that the energy-absorbing components would behave as expected. After the EU CRASURV project ended, a feedback (retour d'experience, REX) study was funded by the French DGAC (Civil Aviation General Directorate) [26][27], in order to precisely analyze the reasons why the EU CRASURV FE simulations failed to predict the composite half-fuselage final crash test result (see Figure 6) although the FE models of the half-moon structures had been properly calibrated (see Figure 4). The exercise mainly consisted in a numerical sensitivity study dealing with different parameters, such as the mesh size, laminate description, riveted joint models (kinematic constraints or beam-spring finite elements), the nonlinear material law and its

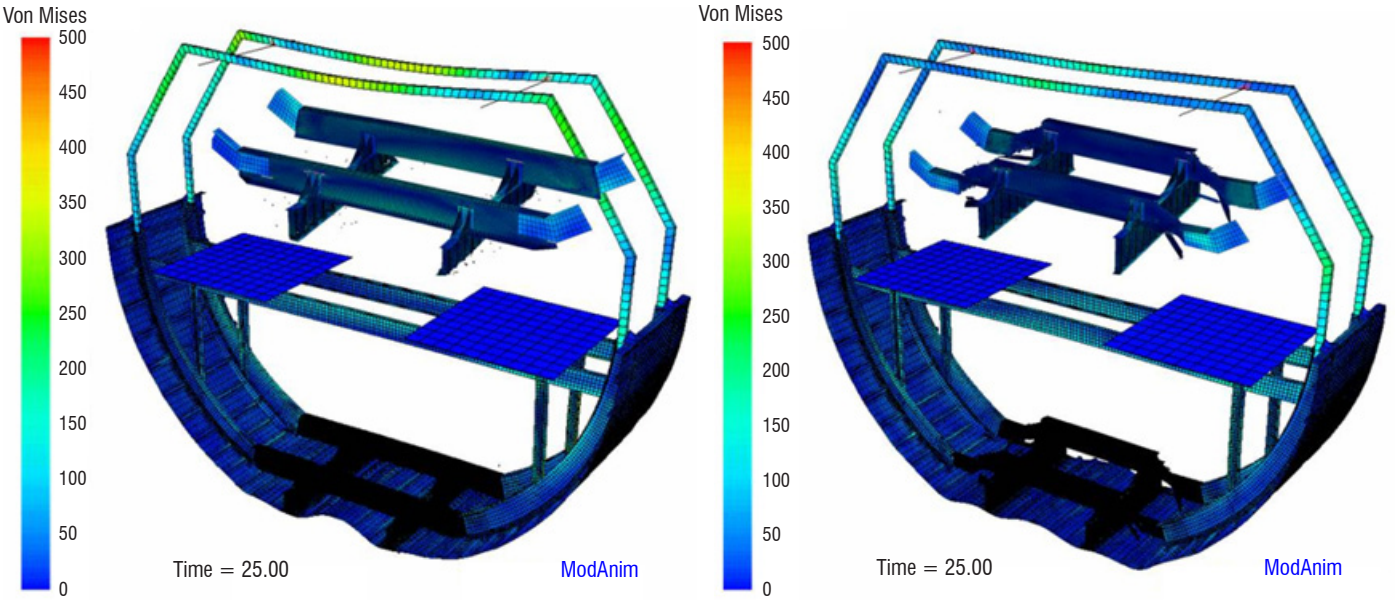

Figure 6 – Illustration of various numerical ruin scenarios obtained during the parametric REX study for the EU CRASURV fuselage structure, with either the crushing of the sinewave beams (left) or the rupture of the cargo beam (right)

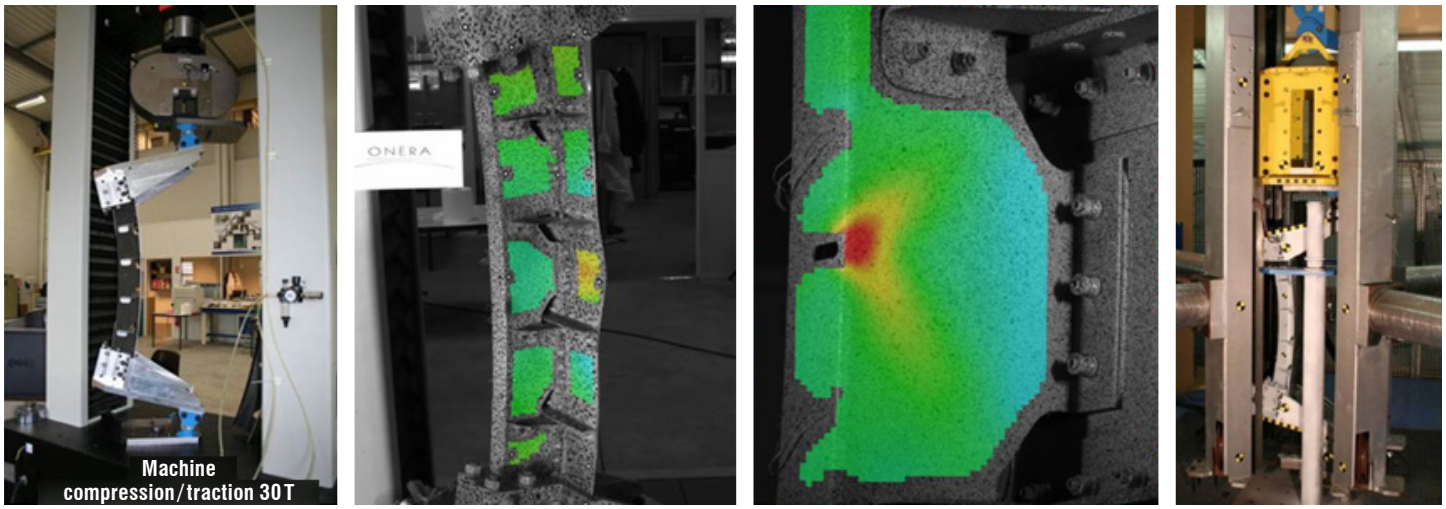

Figure 7 – Static (left) and dynamic (right) compression/bending tests on composite A/C fuselage frames with stereo-DIC analysis (middle) of the overall strain field (with zoom on the crack-starter area)

rupture criteria, and the introduction of some missing design details, such as, for instance, the "brackets" at the top and bottom of the sinewave beams. The objective of the study was to investigate their numerical influence on the global structural ruin mode and the rupture – or lack of it – of the composite sinewave beams and/or cargo floor beams (see Figure 6).

Concerning the EU CRASURV project, as already mentioned, despite the various developments and the (possibly too simple/quick) Building-Block Approach followed up to the half-moon composite structure, the pre-test FE simulations failed to predict the composite half-fuselage final crash test result. In the end, these results proved the higher-than-expected complexity of composite structure crash problems, where representative load transfer and boundary conditions between the various components of the full composite structures must be properly represented in the sub-component test program. Then, it was shown in the DGA funded REX study that all of the "numerical parameters" studied in [26][27] have an influence on the composite half-barrel structural ruin mode one way or another. However, the final conclusion of this REX study was that it was possible – whatever the value of the other parameters – to cover a large spectrum of ruin modes – including that observed during the physical test – just by "playing" with the ultimate rupture criteria of the composite multilayered shell elements in the various parts (frame, beam, sinewave) of the composite structure (see Figure 6). Last, as shown in [23][24] during the EU CRASUV project and also in [26][27] during the final REX study, post-test simulations based on knowledge-driven calibration of the ruin mode and scenario can yield a satisfying comparison with physical tests, but no certainty can be claimed that empirical (and not physically justified) calibrations could be predictive of higher level structures in the pyramid or different crash conditions (e.g., roll angle, forward velocity, etc.). It also means that any blind-test simulation based design should be decided only after a large parametric numerical study, leading at the end only to acceptable ruin scenarios, whatever the values of the uncertain parameters (in the CRASURV case: the ultimate rupture criterion of the multilayered shell elements).

From 2006 onwards, following this philosophy, ONERA took part in a series of national studies funded by the French Institutions and AIRBUS-DLR-ONERA (ADO) collaborative projects funded by AIRBUS industry. The objective of these works was to propose, study with FE crash codes, design and test different concepts that would lead to deterministic failure modes in composite fuselage frames under vertical crash conditions. The first step was to search for mechanical load transfer concepts that would guarantee a more robust crushing initiation process of the energy-absorbing beams. Within the ADO projects, the second idea was to study the possibility of introducing "kinematic joints" [17] and "crack starters" in the composite fuselage frames (to mimic plastic hinges found in metallic frames) that would fail at a prescribed load level and location, in order to avoid rupture in unexpected/unwanted areas, and would redistribute the loads in an appropriate way onto the crush/energy-absorbing components. Static (hydraulic machine) and dynamic (crash tower) tests were performed by ONERA to study the efficiency of such "crack starter" concepts (see Figure 7). The Digital Image Correlation technique was used to record more information (displacement and strain fields) from the tests, to improve analysis.

In this ADO project, a final A/C black fuselage demonstrator (half-moon) was finally designed and manufactured by AIRBUS Germany, numerically studied by the DLR and tested at the ONERA crash tower. The testing at the ONERA crash tower of this half-moon full composite sub-cargo structure representative of possible new-generation CFRP (carbon fiber reinforced polymer) commercial aircraft is presented in [28]. The demonstrator was based on a single aisle aircraft geometry and comprised 2 Integrated Cargo Units (ICU) equipped with Triggered Tube Segments (TTS) dedicated to energy absorption and CFRP stringer-stiffened skin. The crash concept was based on an integrated structural design, which used the "bend-frame-concept" where the cargo cross-beam acts as a bend frame and withstands the dynamic loads introduced by the TTS components. The testing configuration – loading system and instrumentation – was defined on the basis of numerical analysis performed by the DLR at the fuselage section level. For this purpose, a kinematic model with a 2-frame typical fuselage section and ICUs involving the "bend-frame" concept was numerically simulated,

with the main objective of identifying the loading conditions that apply at specific sections, notably those surrounding the ICU-frame coupling areas where the test fixtures were to be implemented. Since the outcomes of these numerical works show that bending/compression loading, at a specific ratio, must be targeted as a priority, the loading system accordingly designed by ONERA thus consisted of articulated rigs holding both ends of the demonstrator (see Figure 8). The testing was performed with the ONERA-Lille crash tower at 6.7m/s impact velocity, with a 1050 kg trolley mass. The acquisition system comprised a total of 48 channels, including force sensors (6), strain gauges (36), displacement laser sensors (5) and an accelerometer (1). In addition, 4 high-speed cameras were implemented to visualize the rupture phenomena likely to develop during the crash test. Finally, the compact half-moon structure was successfully tested.

About 15 years after the EU CRASURV project, the ADO project test results in 2016 confirmed the simulated and expected crash scenario (representative load transfer and boundary conditions for the half-moon composite structure have been numerically studied and the test rig has been designed according to the numerical results), with the bending of the composite half-moon sub-cargo cross-beams and the resulting progressive crushing of the TTS components. However, it should be noted that, in order to ensure the expected crash scenario, the beams and frames surrounding/supporting the energy absorption components had to be quite heavily reinforced, thus notably increasing the final mass of the structure. The first crack starter concepts (ply drop-off, notches, holes, etc.) were also abandoned because they penalized the static design (mass), and because of the difficulty in achieving truly predictive rupture simulations.

Last, very recently, the EU SMAES project (2010-2014) focused on the study of the ditching behavior of business jets and commercial aircraft [29]. Part of the ONERA work was dedicated to the testing and modelling of composite fuselage sub-structures (business jets), and more specifically to the buckling and crushing behavior of these sub-structures [30]. In order to make the tests more representative of ditching ones without having to deal with water wells or pools, an original concept was proposed with the use of substitute calibrated honeycombs (distributed pressure load with a prescribed peak pressure) instead of water (see Figure 9). Thanks to this, static and dynamic tests with different honeycombs (tailored compression strength) could be performed, to mimic the effect of different impact speeds (corresponding to different hydrodynamic pressures). Digital cinematography and an image correlation technique were used to globally instrument and analyze the tests. The different experiments have been modelled: most of the experimental data were correctly predicted by the FE models for the different loading conditions (compression, bending, and crushing on honeycomb). The global force displacement response was well predicted, as well as those of the strain gauges (located on the structure outside the area where non-linear geometrical and material phenomena develop).

Conclusions

Due to the more recent introduction of composite CFRP materials in primary fuselage structures, less works concerning crashworthiness of composite aircraft or rotorcraft are reported in the open literature compared to metallic ones. Nevertheless, these works benefited from more recent advances in the experimental and numerical fields, with more expertise having been built and confidence gained thanks to metallic studies.

The same building-block strategy was used as for metallic structures, but combining more experimental and numerical results (especially explicit FE simulations). Hybrid models were still used at the

Figure 8 – Drawing of the dynamic test rig set up on the 2mx2m test floor of the ONERA crash tower (left) and picture of the AIRBUS composite crashworthy Sub-Cargo demonstrator before testing (right)

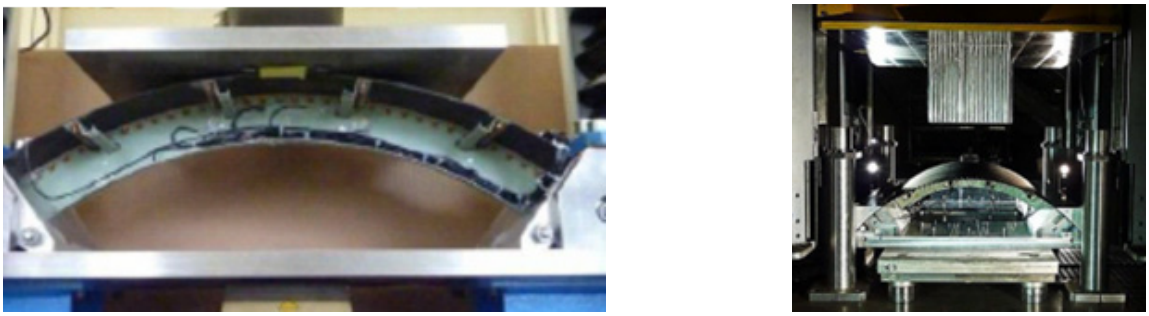

Figure 9 – Pictures of the ONERA test protocols used during the EU SMAES project for static buckling (left) and to mimic crash tests on water (ditching) using equivalent dynamic tests with calibrated honeycombs (right)

beginning of the composite story, but it rapidly gave way to explicit FE ones, especially in the design process, compared to the justification – to not mention the certification – process.

However, the complexity of the composite materials and the component behavior under crash conditions proved to be so high (and their rupture behavior so versatile, for instance, with respect to the way in which the external and internal loads and inertial forces are applied, with respect to the boundary conditions, etc.) that only two appropriate procedures were quickly established:

- either concentrating (thanks to a "simple" and robust design) the nonlinear absorbing and rupture mechanisms in pre-determined parts or components of the structure (e.g., parts made of more simple and less versatile metallic or foam materials), and designing the composite parts to keep completely safe of any rupture,
- or by increasing the complexity of the composite material laws and numerical FE models (leading to much greater FE models than those used for metallic structures), and by performing enough parametric studies by varying as many relevant parameters as possible to check their influence on the structural ruin scenario.

In the first case, hybrid or quite simple FE models (tens of thousands of finite elements) in a "coarse" building block philosophy can be used to calculate key criteria and support crash justifications, either together with composite fuselage barrel crash tests (e.g., for the Boeing B787) or with hybrid metallic/composite fuselage barrel FE crash simulations (e.g., for the Airbus A350). In this case, quite simple elastic composite material models and rupture criteria can be used. Note that scale models were even used in more prospective research works to partly reduce the experimental costs.

In the second case (e.g., the latest versions of the Airbus A350 aircraft), more steps in the test pyramid are needed (up to large full-scale components, such as half-moon sub-cargo floor structures if not full barrels), together with the development of clearly specific (different from the FE models used for standard static or dynamic analysis, e.g., using NASTRAN) and detailed (hundreds of thousands of finite elements) explicit FE models. Indeed, the FE codes still have many limitations and generally raise supplementary difficulties related, for instance, to (1) the need for complex nonlinear material models and rupture criteria, (2) the need for assessment of simplifications (e.g., joints) and approximations (e.g., geometry) and (3) the demonstration of numerical robustness and accuracy, etc. In this case, a much larger number of mechanical tests (including dynamic ones) also has to be performed, to identify the composite material law parameters and calibrate them at the composite detail level: this point is key for (and then is to be the subject of) the PHYSAFE research project, since no standards exist as yet for the dynamic mechanical characterization of composite materials and elementary joint behavior and rupture (including delamination).

In both cases, the need for an experimental and/or numerical building-block approach up to the full barrel level is evidenced, as well as an even more elaborate V&V (verification and validation) process for the numerical crash simulations, compared to metallic fuselage designs. In the end, the (exponential) complexity of FE crash simulation validation from the composite material level up to that of the composite structures still seems to be higher today than possibly expected initially. The intrinsic composite material behavior (and model) is not the only difficult point to be solved, in particular, since it cannot be as simply de-correlated from its "structural" environment in FE crash simulations as one would wish (e.g., materials that behave differently once they are used in structural details that cannot yet be modelled in the FE crash simulation for FE size limitations) ■

References

[1] E. DELETOMBE, PHYSAFE - *Introductory Bibliographic Review in the Field of Commercial Aircraft Safety and Crashworthiness of Commercial Aircraft*. ONERA-DADS Technical Report RT 2-23324, 2016.

[2] T. FOUREST, PHYSAFE - *Dynamic Characterisation of Unidirectional CFRP Composites: a Review*. ONERA Technical Report RT-3-233214, 2016.

[3] S. BELON, PHYSAFE - *Literature Review on the Modeling of Delamination and Debonding*. ONERA/DMAS Technical Report RT 4/23324, 2017.

[4] J. BERTHE, PHYSAFE - *A Review on Composite Material Laws for Crash Modelling*. ONERA Technical Report RT 5-23324, 2017.

[5] K. E. JACKSON - *Analytical Crash Simulation of Three Composite Fuselage Concepts and Experimental Correlation.* Journal of the American Helicopter Society, 7(3), 981-986, 1997.

[6] J. L. S. VICENTE, F. BELTRAN, F. MARTÍNEZ - *Simulation of Impact on Composite Fuselage Structures*. European Congress on Computational Methods in Applied Sciences and Engineering, 2000.

[7] CRASURV - *Design for Crash Survivability*. CEC DG XII, EU RTD BRITE-EURAM Project, BRPR-CT96-0207, 1996.

[8] K. H. LYLE, K. E. JACKSON, E. L. FASANELLA - *Development of an ACAP Helicopter Finite Element Impact Model*. Journal of the American Helicopter Society, 45(2), 137-142, 2000.

[9] E. L. FASANELLA, R. L. BOITNOTT, K. H. LYLE, K. E. JACKSON - *Full-Scale Crash Test and Simulation of a Composite Helicopter*. International Journal of Crashworthiness, 6(4), 485-498, 2001.

[10] E. L. FASANELLA, K. E. JACKSON, K. H. LYLE - *Finite Element Simulation of a Full-Scale Crash Test of a Composite Helicopter.* Journal of the American Helicopter Society, 47(3), 156-168, 2002.

[11] K. E. JACKSON, E. L. FASANELLA, S. KELLAS - *Development of a Scale Model Composite Fuselage Concept for Improved Crashworthiness*. Journal of Aircraft, 38(1), 95-103, 2001.

[12] K. E. JACKSON - *Impact Testing and Simulation of a Crashworthy Composite Fuselage Concept.* International Journal of Crashworthiness, 6(1), 107-121, 2001.

[13] E. L. FASANELLA, K. E. JACKSON - *Impact Testing and Simulation of a Crashworthy Composite Fuselage Section with Energy-Absorbing Seats and Dummies*. Journal of the American Helicopter Society, 49(2), 140-148, 2004.

[14] E. L. FASANELLA, K. E. JACKSON, K. H. LYLE, C. E. SPARKS, A. K. SAREEN - *Multi-Terrain Impact Testing and Simulation of a Composite Energy-Absorbing Fuselage Section*. Annual Forum Proceedings – American Helicopter Society, 2, 1535-1546, 2004.

[15] T. ZOU, H. MOU, Z. FENG - *Research on Effects of Oblique Struts on Crashworthiness of Composite Fuselage Sections*. Journal of Aircraft, 49(6), 2059-2063, 2012.

[16] S. HEIMBS, M. HOFFMANN, M. WAIMER, S. SCHMEER, J. BLAUROCK - *Dynamic Testing and Modelling of Composite Fuselage Frames and Fasteners for Aircraft Crash Simulations*. International Journal of Crashworthiness, 18(4), 406-422, 2013.

[17] R. STURM, Y. KLETT, C. KINDERVATER, H. VOGGENREITER - *Failure of CFRP Airframe Sandwich Panels under Crash-Relevant Loading Conditions*. Composite Structures, 112(1), 11-21, 2014.

[18] IMT-2002 - *Crashworthiness for Commercial Aircraft.* CEC DG XII, EU RTD BRITE-EURAM Project, 1992.

[19] D. DELSART, V. LASSUS, Y. CHAUVEAU - *Crashworthiness of Composite Helicopters: Towards Design Cost Reduction*. ICCE, 9th International Conference Computational Engineering, San Diego (USA), July 2002.

[20] D. DELSART, J.-F. SOBRY, J.-L. CHARLES, V. LASSUS, Y. CHAUVEAU - *Development of Cost Effective Tools for the Design of Crashworthy Helicopter Structures*. 59th Annual Forum of the American Helicopter Society, Phoenix (USA), May 2003.

[21] D. DELSART, B. LANGRAND, A. VAGNOT - *Evaluation of an Euler/Lagrange Coupling Method for the Ditching Simulation of Helicopter Structures*. Fluid Structure Interaction V, 105, 259-268, 2009.

[22] E. DELETOMBE, D. DELSART, CRASURV - *Commercial Aircraft Design for Crash Survivability*. ONERA Lille Task 1 Final report, ONERA-DMSE Technical Report RT 99-63, 1999.

[23] E. DELETOMBE, D. DELSART, CRASURV - *Commercial Aircraft Design for Crash Survivability.* ONERA Lille Final report, ONERA-DMSE Technical Report RT 99-64, 1999.

[24] E. DELETOMBE, D. DELSART, CRASURV - *Commercial Aircraft Design for Crash Survivability*. D3.4.7 Post-test simulation of the sub-cargo floor structure, ONERA-DMSE Technical Report RT 99-61, 1999.

[25] F. ARNAUDEAU, M. MAHÉ, E. DELETOMBE, F. LE PAGE - *Crashworthiness of Aircraft Composite Structures*. IMECE, ASME International Mechanical Engineering Congress and Exposition, New Orleans, USA, November, 2002.

[26] D. DELSART, D. JOLY, G. WINKENMULLER - *Evaluation of Finite Element Modelling Methodologies for the Design of Crashworthy Composite Commercial Aircraft Fuselage*. ICAS 24th International Congress of the Aeronautical Sciences, Yokoama, Japan, August-September, 2004.

[27] D. DELSART, D. JOLY - *Finite Element Analysis for the Design of Crashworthy Composite Fuselages.* ACMA International Symposium on Aircraft Materials, Agadir, Morocco, May, 2007.

[28] D. DELSART, G. PORTEMONT, M. WAIMER - *Crash Testing of a CFRP Commercial Aircraft Sub-Cargo Fuselage Section*. European Conference on Fracture – ECF 21, Catane (Italy), June, 2016.

[29] SMAES - *Smart Aircraft in Emergency Situations*. CEC DG XII, EU FP7-AAT-2010-RTD, CP-FP/ACPO-GA-2010-266172, 2010.

[30] B. LANGRAND, R. ORTIZ, J. FABIS, J.-F. SOBRY - *Smart Aircraft in Emergency Situations (SMAES)*. Final Report, ONERA-DADS Technical Report RT 4-17523, 2014.

[31] E. DELETOMBE, M. MAHÉ - *Credibility of 21st Century Numerical Simulations in A/C Crash and Impact Analysis*. 6th CEAS Conference, Bucarest (Romania), 2017.

[32] M. GAMON, G. WITTLIN, B. LABARGE - *KRASH 85 User's guide – Input/Output Format.* Final Report DOT/FAA/CT-85/10, 1985.

[33] P. FERABOLI, B. WADE, F. DELEO, M. RASSAIAN, M. HIGGINS, A. BYAR - *LS-DYNA MAT54 Modeling of the Axial Crushing of a Composite Tape Sinusoidal Specimen*. Composites Part A: Applied Science and Manufacturing, 42 (11), pp. 1809-1825 (2011).

[34] J. OBRADOVIC, S. BORIA, G. BELINGARDI - *Lightweight Design and Crash Analysis of Composite Frontal Impact Energy-Absorbing Structures*. Composite Structures, 94 (2), pp. 423-430 (2012).

AUTHORS

Eric Deletombe is Director of Scientific Industrial and Institutional Outreach for Northern France, and Senior Scientist (PhD supervision accreditation by the Valenciennes University) in the Materials and Structures Department at ONERA (The French Aerospace Lab). He was Head of the "Structural Design and Dynamic Resistance" Research Unit at the French Aerospace Lab (Office National d'Etudes et de Recherches Aerospatiales) from 1999 till 2009. He started work at ONERA in 1990 (having graduated from Sup'Aéro in 1988) as a Research Engineer, to work on modelling the crash behavior of metallic aircraft structures. His key research topics are: Metallic and Composite Materials, Joints, Behavior, Damage and Rupture, Transient Dynamic Loads (crash, impacts, etc.), and Fluid/Structure Interactions (HRAM, etc.).

David Delsart graduated from the Ecole Centrale de Lille in 1994. He then graduated from the University of Sciences and Technologies of Lille (with a Post-graduate diploma in Mechanics, in 1994). He has worked as a Research Engineer at ONERA in the Design and Dynamic Resistance Research Unit since 1997, specializing in the dynamic characterization of materials and assemblies, and in the development of dynamic mechanical models and Finite-Element explicit modelling (Radioss, Abaqus, and Europlexus). He is the manager and the person technically in charge of the ONERA/DLR/AIRBUS-Helicopters joint research program on the crashworthiness/vulnerability of helicopter structures.